1127-2/
1521

JOURNAL OF COLLOID SCIENCE

Editor-in-Chief

Victor K. La Mer, Columbia University, New York

Editors:

F. E. Bartell
T. R. Bolam
E. F. Burton
R. M. Fuoss
H. R. Kruyt
J. W. McBain
E. K. Rideal
William Seifriz
A. W. Thomas
Arne Tiselius
Robert D. Vold

Consulting Committee:

W. T. Astbury
J. J. Bikerman
W. Clayton
P. Debye
W. Feitknecht
Alexander Frumkin
William D. Harkins
Ernst A. Hauser
Wilfried Heller
Hans Jenny
S. S. Kistler
Herman Mark
J. N. Mukherjee
F. F. Nord
J. Th. G. Overbeek
R. Ruyssen
Robert Simha
The Svedberg

VOLUME 4

1949

ACADEMIC PRESS INC., PUBLISHERS
NEW YORK, N. Y.

Copyright 1949, by Academic Press Inc.
Made in United States of America

JOURNAL OF
COLLOID SCIENCE

Editor-in-Chief
VICTOR K. LA MER, Columbia University, New York

Editors:

F. E. BARTELL
T. R. BOLAM
E. F. BURTON
R. M. FUOSS
H. R. KRUYT
J. W. MCBAIN
E. K. RIDEAL
WILLIAM SEIFRIZ
A. W. THOMAS
ARNE TISELIUS
ROBERT D. VOLD

Consulting Committee:

W. T. ASTBURY
J. J. BIKERMAN
W. CLAYTON
P. DEBYE
W. FEITKNECHT
ALEXANDER FRUMKIN
WILLIAM D. HARKINS
ERNST A. HAUSER
WILFRIED HELLER
HANS JENNY
S. S. KISTLER
HERMAN MARK
J. N. MUKHERJEE
F. F. NORD
J. TH. G. OVERBEEK
R. RUYSSEN
ROBERT SIMHA
THE SVEDBERG

VOLUME 4

1949

ACADEMIC PRESS INC., PUBLISHERS
NEW YORK, N. Y.

Second Printing, 1968

Copyright 1949, by Academic Press Inc.
Made in United States of America

CONTENTS OF VOLUME 4

No. 1, February, 1949

G. King and J. A. Medley. D. C. Conduction in Swollen Polar Polymers. I. Electrolysis of the Keratin-Water System 1

G. King and J. A. Medley. II. The Influence of Temperature and Adsorbed Salts on the D. C. Conductivity of Polar Polymer Absorbate Systems 9

William Seifriz and Hans L. Pollack. A Colloidal Interpretation of Biological Stimulation and Depression 19

Leo Shedlovsky, John Ross and Conrad W. Jakob. The Effect of Certain Impurities on the Surface and Interfacial Tension of Aqueous Solutions of Sodium Dodecyl Sulfonate 25

O. Kratky and G. Porod. Diffuse Small-Angle Scattering of X-Rays in Colloid Systems 35

Takuzo Sakai and Akira Isihara. On the Statistical Theory of Rubber-like Elasticity 71

H. C. van de Hulst. Scattering of Light by Colloidal Solutions. Interpolation of the Oscillatory Functions 79

Letter to the Editors:

R. Matalon and J. H. Schulman. A New Method of Studying Mechanical Properties of Penetrated Monolayers 89

Book Review:

Victor K. La Mer. The Electron Microscope, Its Development, Present Performance, and Future Possibilities 91

No. 2, April, 1949

Marjorie J. Vold, Gopal S. Hattiangdi and Robert D. Vold. Crystal Forms of Anhydrous Calcium Stearate Derivable from Calcium Stearate Monohydrate 93

H. D. Landahl and R. G. Herrmann. Sampling of Liquid Aerosols by Wires, Cylinders, and Slides, and the Efficiency of Impaction of the Droplets 103

A. S. Buchanan and E. Heymann. The Electrokinetic Potential of Sparingly Soluble Sulfates. I. 137

A. S. Buchanan and E. Heymann. Electrokinetic Potential and Reversible Electrode Potential of Sparingly Soluble Sulfates. II. 151

A. S. Buchanan and E. Heymann. Determination of Electrokinetic Potentials in Concentrated Solutions by the Streaming Current Method. 157

Allen S. Kenyon and Victor K. La Mer. Light Scattering Properties of Monodispersed Sulfur Sols. I. Monochromatic Ultraviolet Angular Scattering. II. Effect of the Complex Index of Refraction upon Transmittance 163

No. 3, June, 1949

W. H. Markwood, Jr. The Bingham Medal-Society of Rheology, 1948 . . 185

J. H. Dillon. Introduction of Melvin Mooney as E. C. Bingham Medalist 187

M. Mooney. Speech of Acceptance 188

F. R. Eirich. Impressions from the International Rheological Congress, Scheveningen. 1948 189

Herbert Leaderman. Proposed Nomenclature for Elastic and Inelastic Behavior of High Polymers 193
Turner Alfrey, Jr., Norman Wiederhorn, Richard Stein and Arthur Tobolsky. Some Studies of Plasticized Polyvinyl Chloride 211
R. S. Spencer. Volume-Temperature-Time Relationships for Polystyrene 229
R. S. Spencer and R. E. Dillon. The Viscous Flow of Molten Polystyrene. II 241
G. J. Dienes. Flow Properties of Phenolic Resins 257
Welker G. Bechtel and Earl K. Fischer. The Measurement of Starch Paste Viscosity 265
Turner Alfrey, Jr., and Charles W. Rodewald. An Experimental Study of Thixotrophy in Bentonite Suspensions 283
D. C. Drucker. The Significance of the Criterion for Additional Plastic Deformation of Metals 299
W. E. Davis and J. H. Elliott. Present Status of the Intrinsic Viscosity Determination 313
F. S. Stow, Jr., K. H. Horowitz and J. H. Elliott. Application of the Rising-Column Capillary Viscometer to the High-Viscosity Range 321
J. G. Oldroyd. The Interpretation of Observed Pressure Gradients in Laminar Flow of Non-Newtonian Liquids Through Tubes 333
Charles Mack. A Theory of Anomalous Viscosity and Elasticity 343
C. B. Havens. Plasticizing Linear Polymers 347

No. 4, August, 1949

Mata Prasad and K. D. Venkatesha Doss. Scattering of Light During the Process of Gel Formation 349
William D. Harkins and Rose Mittelmann. X-Ray Investigations of the Structure of Colloidal Electrolytes. IV. A New Type of Micelle Formed by Film Penetration 367
J. W. McBain and Harriette M. Huff. Changes in Solubilizing Power with Concentration for Various Detergents 383
E. Heymann and I. J. O'Donnell. Physicochemical Investigation of a Cation Exchange Resin (Amberlite IR100). I. Resin Equilibria 395
E. Heymann and I. J. O'Donnell. Physicochemical Investigation of a Cation Exchange Resin (Amberlite IR100). II. Resin Conductance. 405
A. P. Brady. Surface Films of Soluble Detergents 417
Frank C. Collins and George E. Kimball. Diffusion-Controlled Reaction Rates 425
Letter to the Editors:
  M. Halwer and B. A. Brice. Molecular Weight of β-Lactoglobulin as Determined by Light-Scattering Measurements 439
Book Reviews:
  William Seifriz. Submicroscopic Morphology of Protoplasm and Its Derivatives 441
  R. N. Traxler. Plasticity as a Factor in the Design of Dense Bituminous Road Carpets 444

No. 5, October, 1949

H. K. Livingstone. The Cross-Sectional Areas of Molecules Adsorbed on Solid Surfaces 447
Ernst K. Goette. Theoretical Considerations of Detergency 459
M. L. Corrin, E. L. Lind, Adelle Roginsky and William D. Harkins. Adsorption of Long-Chain Electrolytes from Aqueous Solution on Graphite of Known Area and on Polystyrene 485
J. H. Schulman and J. A. Friend. Light Scattering Investigations of the Structure of Transparent Oil-Water Disperse Systems. II 497

B. A. Toms. Detection of a Wall Effect in Laminar Flow of Solutions of a Linear Polymer 511
Santi R. Palit. A Note on Mixed Solvent Effect in Solubilization 523
Koreo Kinosita. Sedimentation in Tilted Vessels. I 525
Letter to the Editors:
Lorraine Arkin and C. R. Singleterry. The Effect of Water on the Size and Shape of Soap Micelles in Benzene Solution 537
Book Review:
W. O. Baker. Principles of High-Polymer Theory and Practice 540

No. 6, December, 1949

Frank T. Gucker, Jr., and Chester T. O'Konski. An Improved Photoelectric Counter for Colloidal Particles, Suitable for Size-Distribution Studies 541
T. H. James. Loss of Developability of Photographic Emulsions Caused by Washing in Weak Silver Halide Solvents: A New Reversal Effect . . . 561
Elaine G. Shafrin and W. A. Zisman. Hydrophobic Monolayers Adsorbed from Aqueous Solutions 571
J. A. Erikson and E. C. Lingafelter. Ionic Effects in a Paraffin-Chain Salt Solution as Measured by the Primary Salt Effect 591
Letter to the Editors:
Eric Hutchinson. A Note on the Direct Determination of Adsorption from Solution 599
Book Reviews:
George Goldfinger. Elastomers and Plastomers, Their Chemistry, Physics and Technology. Volume III. Testing and Aanlysis; Tabulation of Properties 603
Emery I. Valko. Neue Verfahren in der Technik der chemischen Veredlung der Textilfasern (Hilfsmittel in der Textilindustrie). Vol. I 604
Victor K. La Mer. Surface Chemistry 605

D.C. CONDUCTION IN SWOLLEN POLAR POLYMERS. I. ELECTROLYSIS OF THE KERATIN-WATER SYSTEM

G. King and J. A. Medley

Wool Industries Research Association, Torridon, Headingley, Leeds, England

Received October 11, 1948

Introduction

The mechanism of D.C. conduction in partially swollen polar polymers has been the subject of speculation for some time. Marsh (1), following earlier investigators (2,3,4,5), favored the pore theory of conduction suggesting that, in the case of a wool fiber swollen by water, the electric current follows water channels in the fiber. Baxter (6), however, showed that, if this was the case, then the adsorbed water must be in a totally different state from that of free water, as the conduction process has a temperature coefficient several times as great as that for conductivity water.

The presence of such isolated channels of "liquid" water is also difficult to reconcile with present conceptions of the adsorbtion process in keratin-water systems (7). Over the greater part of the adsorbtion isotherm more than half the adsorbed water is distributed over the available low energy sites, the remaining mobile or "liquid" fraction being distributed over the occupied sites. Thus, the chance of getting even two associated "liquid" molecules is rather remote, except near saturation regains (8)

Because of the high value of the activation energy of the conduction process, and because keratin-methyl alcohol systems gave results similar to those for keratin-water systems, Baxter suggested that these conduction processes might be electronic. Alternatively, Fuoss (9) has suggested that the conducting process in such systems is ionic, and that the presence of a plasticizing agent facilitates the diffusion of ionizable impurities originally present in the polymer. This theory is supported by recent work in our laboratories on D.C. conduction in nylon-water and nylon-formic acid systems (10). It has been shown that the increase in conductivity per mole of adsorbate is greater in the latter case, when the more powerful swelling agent is adsorbed.

Recently, O'Sullivan (11) has shown the movement of ion boundaries in cellulose impregnated with various salts for water contents as low as 10%, using methods previously developed for gelatin gels. He was, however, unable to obtain a quantitative relation between the amount of electricity passed and the extent of electrochemical change, and could only conclude that for these systems the conduction process was chiefly ionic in nature.

It has been noticed in previous work on the electrical resistance of keratin-water-KCl systems, that, when the water content is high, and a relatively large direct current is passed through the system for some time, a slight but appreciable decrease in water content is obtained (12). O'Sullivan also mentions the liberation of gas at the electrodes during some of his experiments. These phenomena suggest that electrolytic decomposition of the adsorbed water occurs during the passage of the current. In the present work, this property of the keratin-water system has been investigated and a quantitative analysis of the evolved gases has been made.

EXPERIMENTAL

1. *Apparatus*

The general lay-out of the apparatus is shown in Fig. 1. The principles involved in its use follow very much along the lines of those developed by Langmuir (13) and others. In order to simplify procedure, vacuum stopcocks lubricated with silicone vacuum grease were used in place of mercury cut-offs, and gave no trouble within the range of pressures measured. The apparatus was made of soda glass throughout, each section being washed in chromic acid and distilled water prior to final assembly.

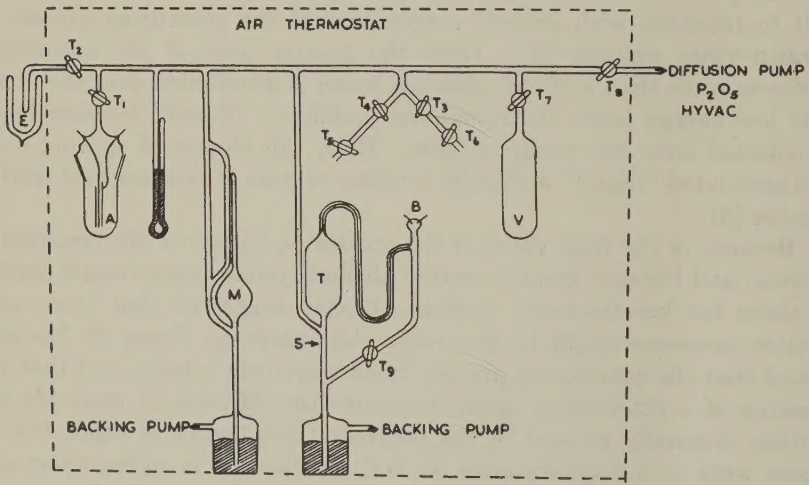

FIG. 1. Apparatus used.

The greater part of the system was housed in an air thermostat which could be maintained at either 20.5°C. or 41.5°C. The water reservoir and freezing trap, E, was maintained at either solid carbon dioxide or liquid air temperatures but this was found to have no appreciable effect on the pressure readings, the volume of E being a very small fraction of the total volume of the system

The electrode system, A, was similar to that used in previous work (4). The horn films used were washed in distilled water for 24 hr. and then coated with "Aquadag." The electrodes were of platinum foil and the whole was clamped between brass plates.

2. Occluded Gases

It was not possible to heat the keratin sample to a sufficiently high temperature to ensure the removal of all occluded gases. The use of soda glass also made it impossible to ensure that such gases would not be evolved during the course of the experiment, over and above any electrolysis effects. The major fraction of these gases is evolved during the time water vapor is being adsorbed by the keratin, *i.e.*, about 24 hr., and can only be taken into account by performing a "blank" analysis without electrolytic action taking place. During such a series of runs it was found that, at first, a relatively large amount of gas was evolved (measured with E surrounded by carbon dioxide paste), but after a few repetitions the pressure fell to a roughly constant value of about 0.015 mm. Hg., as measured by the McLeod gauge, M. Any evolution of gas occuring during the period of analysis was neglected, the time interval being of the order of 2 hr.

Finally, it should be mentioned that any possible evolution of gas due to heating of the keratin by the passage of the electric current was tested for by passing an equivalent alternating current through the sample with negative results.

3. Test Analysis

A preliminary test of the analyzing procedure was made by investigating the combustion of hydrogen and oxygen. Commercial hydrogen was passed through the system via T_6 and trapped between T_6 and T_3 at atmospheric pressure. In a similar manner, the space between T_5 and T_4 was used as an oxygen reservoir. The remainder of the system was then evacuated for 24 hr., after which a small quantity of hydrogen was introduced and adjusted to a suitable pressure with the mercury in the Toepler pump T brought up to a fixed reference point S and with T_2 open and E surrounded by liquid air. The hydrogen was then pumped into the combustion chamber B, and the procedure repeated using oxygen (in excess). After sparking the mixture in B, the remaining gases were returned to the system via T_9 and the final pressure read off. Typical results are shown in Table I.

TABLE I

Test Combustion of Hydrogen and Oxygen

Initial H_2 pressure	Initial O_2 pressure	Final O_2 pressure	Combined O_2 pressure
mm. Hg	*mm. Hg*	*mm. Hg*	*mm. Hg*
0.100	0.120	0.073	0.047
0.170	0.150	0.062	0.088
0.220	0.181	0.070	0.111

The results are given in the form of pressures as measured, which are, of course, proportional to the corresponding mass of gas at constant volume and temperature. The results deviate by about 6% from theoretical requirements.

4. Electrolysis

About 1 cc. of freshly distilled water was introduced into E, and, by alternate freezing with carbon dioxide paste under vacuum, and thawing, any remaining dissolved gases were removed. The keratin sample was then passed through a series of sorption-desorption cycles until the residual gas pressure reached a low value, after which the final water content of the sample was adjusted to a suitable value, generally not less than 15%, at the temperature of the thermostat. Then, after equilibrium had been established, T_1 was closed and E surrounded with carbon dioxide paste, when the residual gas pressure was measured.

A direct current was then passed through the keratin, the value being noted at regular intervals of time by means of a calibrated microammeter. The readings generally varied between 0.1 and 0.03 ma., the applied voltage being adjusted in steps from about 10 volts to 60 volts during the course of the experiment in order to maintain the current within these limits. The quantity of electricity passed was determined by graphical integration and was of the order of 0.2–0.5 coulombs.

After the passage of a suitable quantity of electricity, T_1 was opened and the new pressure measured with E surrounded with carbon dioxide paste. The non-"permanent" fraction of the gas was then removed by immersing E in liquid air and the new pressure determined. This free gas was pumped into B, sparked, and returned to the system, the change in pressure being noted. The gas was then returned to B together with a measured quantity of oxygen (in excess), sparked once more and the pressure of the remaining gas measured. This was repeated using excess hydrogen and, after again measuring the final pressure, all the residual gas was pumped away.

By replacing the liquid air surrounding E by carbon dioxide paste once more, the condensible fraction of the liberated gas was released and its pressure was measured. In all cases, it was found to be equal to the initial value determined by difference, which indicated that the above combustion processes had only produced water and that no carbon monoxide was present initially. The above form of analysis was then repeated but without combustion taking place either with hydrogen or oxygen, suggesting that this fraction consisted chiefly of carbon dioxide.

TABLE II

Analysis of Occluded Gas Evolved

Nitrogen *per cent*	Oxygen *per cent*	Non-permanent gas (CO_2 ?) *per cent*
50	15	30
60	20	20

In order to correct for the small amount of occluded gas initially present, two approximate analyses were carried out on "blank" runs and the mean of these used, Table II.

The corrected partial pressures of the constituent gases evolved during the passage of the direct current are given in Table III. The values have been reduced to those obtaining at 20°C.

TABLE III

Analysis of Gas Evolved during Passage of Direct Current

Expt. no.	Temp. sample	Water content sample	Quantity electricity passed	Total pressure gas evolved	Pressure H_2	Pressure O_2	Pressure CO_2(?)
	°C.	*per cent*	*coulombs*	*mm. Hg.*	*mm. Hg.*	*mm. Hg.*	*mm. Hg.*
1	20.5	16	0.26	0.100	0.070	0.005	0.030
2	20.5	20	0.37	0.150	0.106	0.010	0.038
3	41.5	18	0.51	0.208	0.140	0.012	0.050
4	41.5	15	0.33	0.136	0.098	0.008	0.031

5. *Estimate of Quantity of Electricity Passed*

According to Table III, simple electrolytic decomposition of the adsorbed water does not occur. However, assuming that hydrogen is the only electropositive gas evolved, one can still make a quantitative estimate of the amount of electricity passed. In this respect, the volume of the apparatus available to the gas during the pressure measurements is required, and this was estimated by measuring pressures with and without the known volume *V* connected, and applying Boyle's Law.

Thus, the mass of hydrogen liberated during each run was estimated, and from these values the corresponding values of the respective quantities of electricity passed were obtained. The estimated values are compared with the measured values in Table IV.

TABLE IV

Electrochemical Action and Quantity of Electricity Passed

Expt. no.	Quantity electricity (measured)	Pressure hydrogen (20°C.)	Quantity electricity (calculated)	Q. Calculated / Q. Measured
	coulombs	*mm. Hg.*	*coulombs*	*per cent*
1	0.26	0.070	0.230	88
2	0.37	0.106	0.345	93
3	0.51	0.140	0.455	89
4	0.33	0.098	0.318	96

DISCUSSION OF RESULTS

It will be seen that, according to Table IV, the amount of hydrogen liberated is electrochemically equivalent to the amount of electricity passed through the system. The results obtained have been limited to a range of water contents of 15% and over. This restriction has been imposed by the necessity of keeping the time of electrolysis as short as possible to minimize errors due to the evolution of occluded gases. However, the relation between the amount of electricity passed and the corresponding electrochemical action shows no appreciable trend with respect to the water content of the keratin and should remain constant over much wider limits.

From these results it is reasonable to assume that D.C. conduction in the keratin water system takes place by ionic migration. Furthermore, as will be shown in Part II of this paper, the D.C. conduction phenomena associated with the keratin water system are common to other polymer adsorbate systems which suggests that all such conduction processes are of an ionic nature. A conduction mechanism based on this principle is discussed in the following section of the paper.

SUMMARY

It has been shown that, when a direct current is passed through a keratin film containing at least 15% water, then the amount of hydrogen present in the gas evolved is always electrochemically equivalent to the amount of electricity passed. This is assumed to confirm the ionic nature of the conduction process. It is suggested that this is true of all such systems.

REFERENCES

1. MARSH, *Trans. Faraday Soc.* **29**, 173 (1933).
2. WILLIAMS AND MURPHY, *Trans. Am Inst. Elec. Engrs.* **48**, 568 (1929).

3. Murphy and Walker, *J. Phys. Chem.* **32**, 1761 (1928).
4. Murphy, *ibid.* **33**, 200 (1929).
5. Murphy, *ibid.* **33**, 509 (1929).
6. Baxter, *Trans. Faraday Soc.* **39**, 207 (1943).
7. Cassie, *ibid.* **41**, 450 (1945).
8. King, *ibid.* **43**, 601 (1947).
9. Fuoss, *J. Am. Chem. Soc.* **61**, 2329 (1939).
10. King and Medley, *Nature* **160**, 438 (1947).
11. O'Sullivan, *J. Textile Inst.* **38**, T285 (1947).
12. Medley, unpublished work.
13. Langmuir, *J. Am. Chem. Soc.* **34**, 1310 (1912).

II. THE INFLUENCE OF TEMPERATURE AND ADSORBED SALTS ON THE D.C. CONDUCTIVITY OF POLAR POLYMER ADSORBATE SYSTEMS

G. King and J. A. Medley

Wool Industries Research Association, Torridon, Headingley, Leeds, England

Received October 11, 1948

INTRODUCTION

A preliminary report (1) on D.C. conduction in swollen polymer systems has indicated that there exists a close correlation between conduction relations and associated plasticizing phenomena. This factor, together with the conclusions reached in Part I of this publication, suggests that Fuoss' conception of the D.C. conductivity as ionic migration facilitated by plasticizing processes appears to be essentially correct (2).

The origin of the ions is uncertain. Impurities in the polymer play a large part, for it is often possible to increase the electrical resistance to a great extent by electrodialysis, and alternatively to decrease the resistance by impregnating the polymers with salts (3, 4). The swelling agent may also contribute some ions.

The present work extends previous investigations of D.C. conductivity-sorption relations to the polymers keratin, nylon, and gelatin, using water and formic acid as adsorbates. The effect of adsorbate concentration on the temperature coefficient of D.C. conduction has been investigated and also the effect of impregnating some of the polymers with salts of high and low dissociation constant, such as potassium chloride and magnesium sulphate. It is shown that these conductivity relations are analogous to those for solutions of electrolytes in solvents of low dielectric constant. Bjerrum's (5) relation between the dielectric constant and dissociation constant is shown to describe the phenomena fairly quantitatively.

EXPERIMENTAL

Most of the conductivity measurements were made on graphite-coated polymer films clamped between electrodes and placed in a sorption system situated in an air thermostat which could be controlled at 25°C. or 40°C. as required. The general arrangement was identical with that used in previous dielectric constant measurements (6).

Specimens of keratin and nylon required, free from excess electrolytic impurities, were electrodialyzed (after coating) for 24 hr. between platinum electrodes which were separated from the film surfaces by pieces of filter paper through which distilled water was allowed to flow. The current density was maintained at about 0.5 ma./cm.^{2}. It was found that not only was the conductivity of the polymers decreased, but that more stable conductivity measurements were possible at low adsorbate concentrations when using these specimens. Gelatin films were electrodialyzed between layers of gelatin hardened with formalin, but were coated subsequently.

One keratin specimen was impregnated with potassium chloride, and one with magnesium sulphate by steeping in a solution of the appropriate salt for several days, followed by washing in distilled water to remove excess salt on the surface. The amount of adsorbed salt was estimated by repeated washing of the specimens in distilled water and measuring the conductivity of the washings. About 2% of either salt (estimated on the dry weight of the keratin) was adsorbed in each case. Gelatin films were prepared from sols.

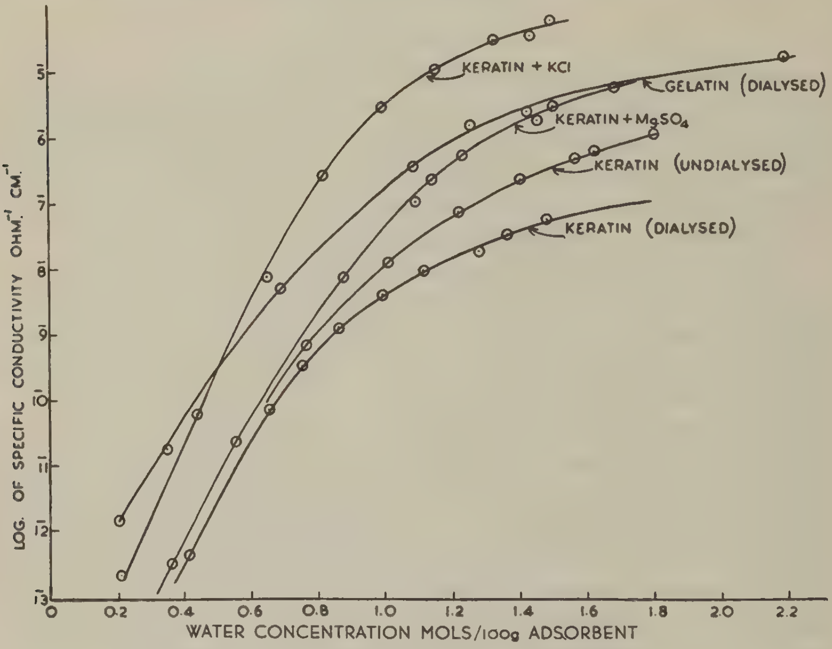

Fig. 1. Conductivity sorption relations at 25°C.

Owing to the extensive range of conductivities to be measured and the accompanying dielectric and electrolytic polarization effects, a variety of methods was used in this work. At low concentrations, over the range 10^{-14}–10^{-10} mhos, conductivities were obtained by observing the rate of decay of charge on a Lindemann electrometer, after an initial delay suffi-

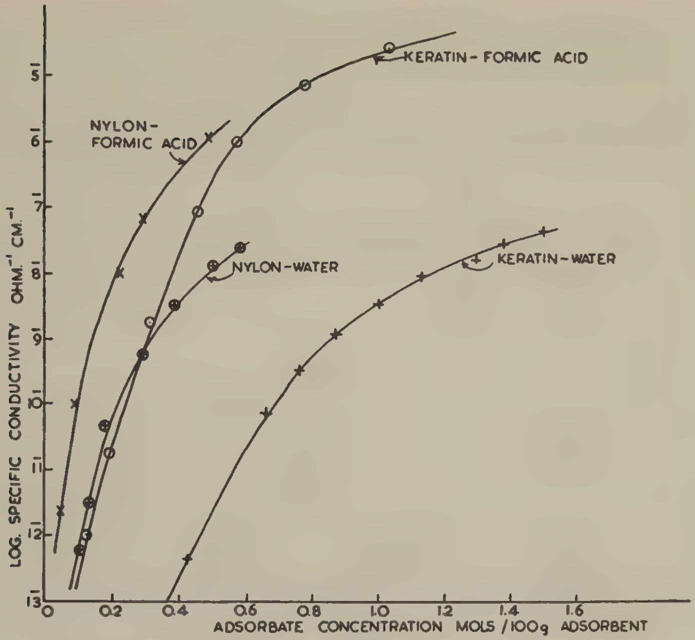

Fig. 2. Conductivity sorption relations at 25°C.

cient to allow the dielectric polarization to subside. Electrode guard rings were used to prevent surface leakages.

At higher conductivity values of about 10^{-9}–10^{-6} mhos, a sensitive d'Arsonval mirror galvanometer was employed in conjunction with suitable resistances and shunts. In this range, electrolytic polarization effects

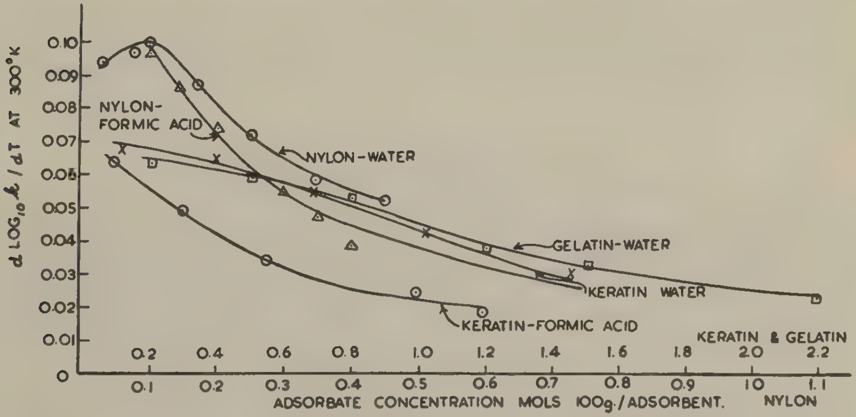

Fig. 3. Relations between sorption and logarithmic temperature coefficients of conductivity.

become apparent while dielectric effects show a rapid rate of decay and the initial galvanometer readings may be used.

In the range 10^{-5}–10^{-2} mhos, electrolytic polarization develops so rapidly as to demand methods of measurement capable of quick response. In this case, a Wheatstone bridge was used, employing a Lindemann electrometer as null point indicator.

The conductivity-adsorbate relations as measured at 25°C. are shown in Figs. 1 and 2, and the corresponding temperature coefficient-adsorbate relations are shown in Fig. 3.

Discussion

1. Results

The conductivity-adsorbate relations are of a similar type for all the polymers and adsorbates used, formic acid being more effective in increasing the conductivity than water. In agreement with the results of Marsh and others, small amounts of KCl greatly increase the conductivity in the case of the keratin-water system. The addition of $MgSO_4$ does not affect the keratin-water relation until relatively large water concentrations are reached, and this is also true of the result of electrodialysis in that it does not effect a reduction in conductivity except at the higher water concentrations (Fig. 1).

The temperature coefficients of conduction (Fig. 3) are shown to be greatest at low adsorbate concentrations, falling away to less than half this maximum value as the concentration of the adsorbate is increased. In the case of the gelatin-water and nylon-formic acid systems, the polymers will ultimately dissolve in the adsorbate so that the conditions will approach those for conduction in a solution for which the adsorbate becomes the solvent, and where relatively low temperature coefficients obtain. Both the nylon relations differ from the other polymers in showing values of temperature coefficient as much as 50% higher than the rest at low adsorbate concentrations.

2. The Conduction Process

If we compare the conductivity-adsorbate relations with the corresponding diffusion relations in the case of the keratin-water system, one finds that in both cases these are of a logarithmic nature, but whereas, in the former case, a range of about 10^5 is possible between water concentrations of 6% and 18%, the range of diffusion coefficient is less than 10^2 (7). It would, therefore, seem that the enormous conductivity range cannot be explained as entirely due to a reduction in the resistance of the polymer lattice to ionic migration, although this must have some noticeable effect analogous to the viscous restraint experienced in the case of conduction in liquids.

Conductivity-adsorbate relations of a similar nature have been observed in the case of borate and silicate glasses containing large amounts of dissolved oxides of alkali metals. In these latter instances, the increased conductivities have been associated with a reduction in the ionic dissociation energy due to an increase in the dielectric constant of the system caused by the presence of the polar adsorbate, an increase in dielectric constant from 4 to 12 corresponding to a change in conductivity of the order of about 10^6 (8).

The close relation between the D.C. conductivity and dielectric constant of swollen polar polymers has been stressed previously (1), and it would seem that the plasticizing action not only facilitates ionic migration but also the ionic dissociation of electrolytes in the polymer, through a rapid increase in dielectric constant of the system. This finds support in that O'Sullivan has shown that bi-bivalent electrolytes, such as calcium sulphate, which are not highly dissociated in dilute solution in water, show abnormally low conductivities in cellulose-water systems (4).

In the case of electrolytes in solvents of low dielectric constant, Fuoss and Kraus (9) have adequately described the variation in dissociation constant (and therefore the D.C. conductivity) with change in dielectric constant by applying Bjerrum's treatment of ionic dissociation (5) to the problem. Following Fowler and Guggenheim (10), the results of this theory may be briefly restated as follows:—

For small concentrations of an electrolyte in a medium of dielectric constant D the fraction, α, of associated ion pairs is:

$$\alpha = \frac{N\pm}{V}\int_a^q 4\pi r^2\cdot\exp\cdot\left(\frac{z^2\epsilon^2}{D\cdot k\cdot T\cdot r}\right)\cdot dr, \qquad (1)$$

where $\alpha \ll 1$.

$N\pm$ is the total number of ions of each type in a volume V.
z is the ionic valency (the ions are assumed to be equivalent).
ϵ is the electronic charge.
k is Boltzmann's constant.
T is the absolute temperature.
a is the closest distance of ionic approach.
q is the closest distance of approach for free ions.

When the condition $\alpha \ll 1$ fails, α may be obtained by treating the distribution as one of dissociation equilibrium between associated ion pairs and free ions. This takes the form,

$$\frac{(1-\alpha)^2}{\alpha}\cdot N = \frac{f_i\cdot f_j}{f_{ij}}, \qquad (2)$$

where f_i, f_j, and f_{ij} are the partition functions for the free ions and the associated pair, respectively. Only configurational factors can contribute to this ratio and it can be shown that

$$\frac{f_i \cdot f_j}{f_{ij}} = V \cdot \left[\int_a^q \exp \cdot \left(\frac{z^2 \epsilon^2}{D \cdot k \cdot T \cdot r} \right) \cdot 4\pi r^2 \cdot dr \right]^{-1} = \frac{(1 - \alpha)^2 \cdot N}{\alpha}, \tag{3}$$

if the electrostatic forces due to the distant ions are ignored, and other factors remaining constant, the conductivity will vary as $(1 - \alpha)$.

The integral has been evaluated as a function of $\left(\frac{\epsilon^2}{D \cdot a \cdot k \cdot T} \right)$ over a comprehensive range, so it is possible to determine the relation between $(1 - \alpha)$ and D after choosing a suitable value for "a," the mean ionic diameter. Now in the case of D.C. conduction in a salt-impregnated polymer the major part of the conduction must be due to the transport of ions of the adsorbed salt, and we may look upon this system as a solution of this salt in the swollen polymer, so that Bjerrum's theory should give a rough description of the conduction phenomena if ionic dissociation is the controlling factor.

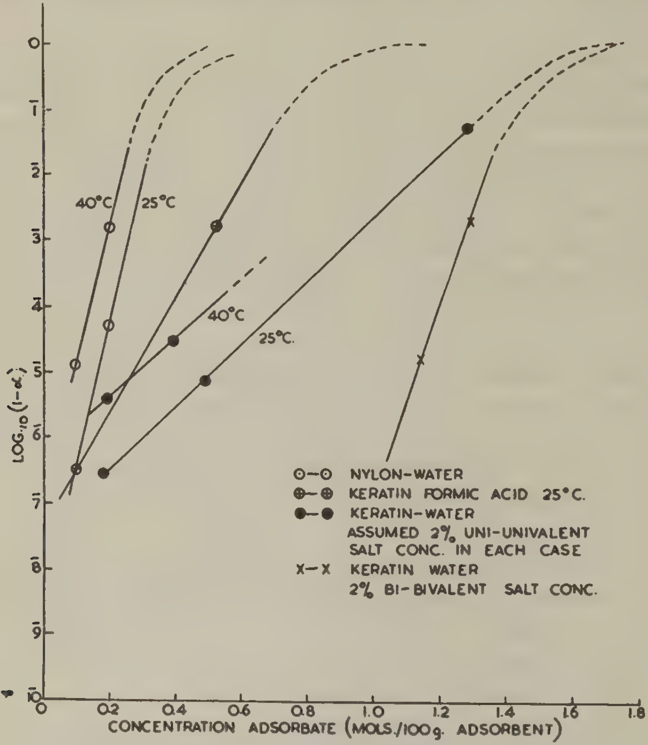

FIG. 4. Theoretical dissociation sorption relations.

The above treatment was applied to the keratin-water-potassium chloride system and the resulting relation between $\log_{10} (1 - \alpha)$ and the molar water concentration is shown in Fig. 4. The dielectric constant-adsorbate relations used were those obtained previously for the keratin-water system at a frequency of 10^4 cps (6). The parameter "a" was taken as 3.1 Å, the ionic distance in the potassium chloride crystal lattice, $\frac{N}{V}$ as the molar salt concentration in the keratin multiplied by Avogadro's number, and $T = 298°K$. It is seen that, between the water concentrations of 0.1 and 1.1 moles/100 g. keratin, a linear relation is obtained, after which the salt approaches complete ionization and $\log_{10}(1 - \alpha)$ tends to zero asymptotically, which explains the bend found in the conductivity relations at these concentrations. The slope of the linear portion of the $\log_{10}(1 - \alpha)$ relation is less than for the experimental conductivity curve shown in Fig. 1. It could be increased by using a smaller value of the parameter "a" or by using dielectric constant values measured at a lower frequency (zero frequency preferably) when the dielectric constant increases more rapidly with water concentration (11). This latter factor will be discussed later in the paper in the section on ionic hydration where it is suggested that the lower values used are more suitable, in which event one must ascribe the smaller slope of the theoretical relation as due to the fact that no account has been taken of the increased restriction of the polymer lattice to ionic migration at lower water concentrations.

Effect of Increasing Valency of Ions

A relation between $\log_{10}(1 - \alpha)$ and the molar water concentration in keratin has been determined for the case when the impregnated salt is the bi-bivalent electrolyte magnesium sulphate, assuming a mean ionic radius of 3.35 Å (12). The resulting relation Fig. 4 shows that the salt cannot modify the conductivity of keratin until the water concentration is of the order of 1.3 moles/100 g., which is in complete agreement with the observed results shown in Fig. 1.

Conductivity Relations for Different Polymers and Adsorbates

The gelatin-water conductivity relations are very similar to those for keratin-water systems, no doubt due to the similarity in the corresponding dielectric constant relations (11). In the case of the nylon-water system, a more rapid increase in conductivity is obtained with increased water content. This is also shown by the corresponding $\log_{10}(1 - \alpha)$ relation shown in Fig. 4, which was determined for a mean ionic radius of 3.1 Å and using dielectric constant relations measured at 10^4 cps. (6).

The $\log_{10}(1 - \alpha)$ relation for the keratin-formic acid system is also shown in Fig. 4. The slope is steeper than the corresponding keratin-water relation as found experimentally. In this system, the experimental curves not only show an increased slope, but much higher conductivity values both for nylon and keratin than those for the corresponding water systems. This will be partly due to the more effective plasticizing effect of the formic acid on the polymer lattice, but also due to increased dissociation of the formic acid itself at the high dielectric constants available for these adsorbate concentrations.

Temperature Coefficient of Conductivity

A change in temperature affects the value of $\log_{10}(1 - \alpha)$ both directly and also indirectly through the corresponding change in dielectric constant, the latter effect being by far the more important. To examine this, dielectric constant relations for keratin-water and nylon-water systems were determined experimentally at temperatures of 25°C. and 40°C. by methods previously described (6). They were limited to the lower adsorbate concentrations due to the increased power loss effects experienced at the higher temperature making further readings difficult. The results are shown in Fig. 5. They reflect the thermoplastic nature of nylon as compared with keratin for low water concentrations, in that the temperature coefficient of the dielectric constant at constant adsorbate concentration is greater in the former case. Using the dielectric constant relations measured at 40°C. the corresponding relations for $\log_{10}(1 - \alpha)$ were determined and are shown in Fig. 4. The temperature change has a greater effect in the case of nylon as was found experimentally for low adsorbate concentrations Fig. 3. The restrictive effect

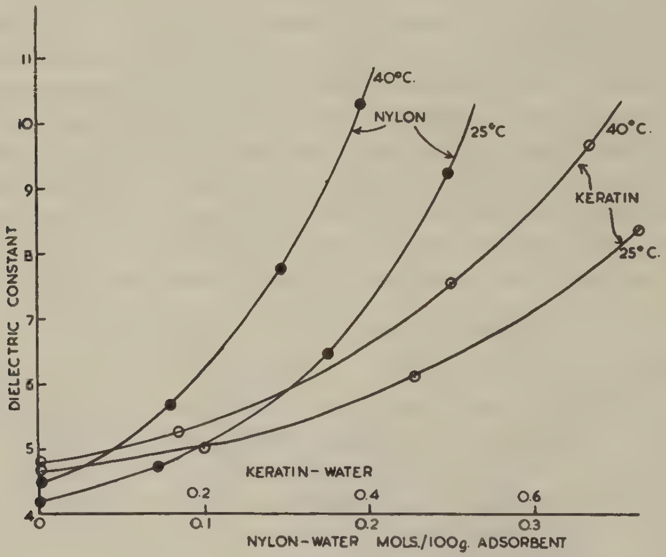

FIG. 5. Effect of temperature on dielectric sorption relations.

of the polymer lattice to ionic migration must also be more sensitive to temperature change in the case of nylon due to this temperature-plasticizing property, and will assist the above effect. At high adsorbate concentrations, as one approaches complete dissociation, a change in dielectric constant is less effective in altering the conductivity and the temperature coefficient will fall.

Hydration of Ions

In the above description of the conduction mechanism, no mention has been made of the possible reduction in the value of the effective dielectric constant below the corresponding macroscopic value, due to the saturation effect experienced in the presence of strong ionic fields (13). To some extent, this has been allowed for by employing dielectric constant values determined at relatively high frequencies. According to Guggenheim (14), however, in the case of ionic solution, the effect is corrected for by the association of the positive ions and the solvent molecules.

In the present instance, where we have swollen polar polymers, it is possible that the ions may become associated with the adsorbate molecules, and, indeed, this has been suggested as an explanation of the transport of water during the passage of D.C. currents through clays (15). However, in the case of nylon polymers, it is possible to increase the dielectric constant and D.C. conductivity over a wide range by an in-

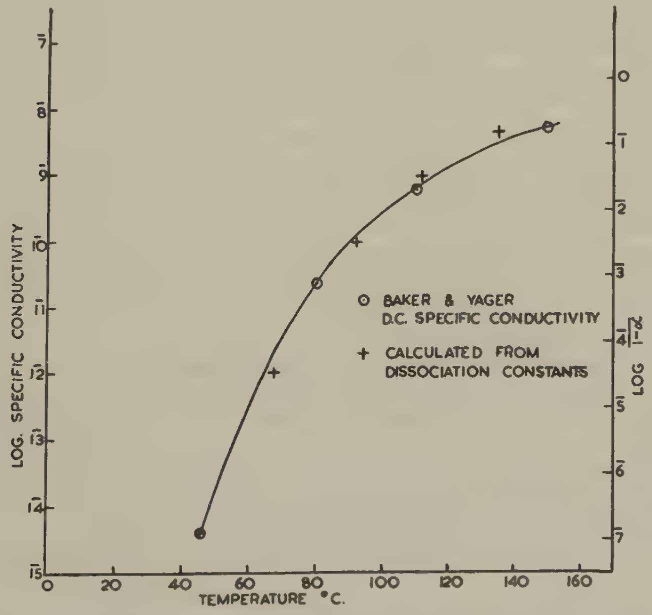

FIG. 6. Temperature conductivity relations (polyhexamethylene sebacamide).

crease in temperature alone. Both these relations are available in the case of polyhexamethylene sebacamide (16), so it is possible to apply Bjerrum's treatment to this system also. This has been done using a value of 3.0 Å for the parameter "*a*," and using the dielectric constant temperature relation for a frequency of 10^3 cps. (Fig. 6).

The excellent fit between $\log_{10}(1 - \alpha)$ and Baker and Yager's temperature-conductivity relation for polyhexamethylene sebacamide suggests that the equilibrium between free ions and ion pairs is not critically dependent on the hydration factor. "Solvation" of the ions on to polar groups in the polymer will not affect the conductivity since such ions become immobile.

SUMMARY

The D C. conductivity of polar polymer adsorbate systems has been measured for the polymers keratin, gelatin and nylon over a wide range of adsorbate concentrations, using water and formic acid as adsorbates. The effect of temperature changes and the presence of impregnated salts in the polymer has also been investigated. On the assumption that the conduction process is ionic in nature, it is shown that Bjerrum's relation for ionic dissociation gives an adequate description of the conduction phenomena.

ACKNOWLEDGMENTS

We are grateful to Mr. B. H. Wilsdon, Director of Research, for his continued interest in the work, to Dr. A. B. D. Cassie for discussion, and to the Council of the Wool Industries Research Association for permission to publish the results.

REFERENCES

1. KING AND MEDLEY, *Nature* **160**, 438 (1947).
2. FUOSS, *J. Am. Chem. Soc.* **61**, 2329 (1939).
3. MARSH, *Trans. Faraday Soc.* **29**, 173 (1933).
4. O'SULLIVAN, *J. Textile Inst.* **38**, T285 (1947).
5. BJERRUM, *Kgl. Danske Videnskab. Selskab, Mat.-fys. Medd.* **9**, 2 (1926).
6. KING, *J. Colloid Sci.* **2**, 551 (1947).
7. KING, *Trans. Faraday Soc.* **41**, 479 (1945).
8. FRENKEL, Kinetic Theory of Liquids. Clarendon Press, 1946, p. 434.
9. FUOSS AND KRAUS, *J. Am. Chem. Soc.* **55**, 2387 (1933).
10. FOWLER AND GUGGENHEIM, Statistical Mechanics. Cambridge Univ. Press, 1939, p. 411.
11. KING, *Trans. Faraday Soc.* **43**, 601 (1947).
12. FALKENHAGEN, Electrolytes. Clarendon Press, 1934, p. 256.
13. DEBYE, Polar Molecules. Reinhold, New York, 1929.
14. FOWLER AND GUGGENHEIM, Statistical Mechanics. Cambridge Univ. Press, 1939, p. 377.
15. MACLEAN AND ROLFE, *Phil. Mag.* **37**, 863 (1946).
16. BAKER AND YAGER, *J. Am. Chem. Soc.* **64**, 2176 (1942).

A COLLOIDAL INTERPRETATION OF BIOLOGICAL STIMULATION AND DEPRESSION

William Seifriz and Hans L. Pollack [1]

Botanical Laboratory, University of Pennsylvania, Philadelphia 4, Pa.

Received November 9, 1948

Introduction

Studies on the pharmacological action of depressants and stimulants (8, 9, 10) led us to the conclusion that depressants gelate, whereas stimulants solate, protoplasm. If the artificially produced gelation of protoplasm is reversible, the quiescent condition may be regarded as a state of anesthesia. Irreversible gelation or solation results in death.

Both reversible gelation and solation occur frequently during the normal activities of protoplasm.

The irreversible solation of protoplasm may be produced in lower organisms by stimulants (10). When produced by caffeine, the phenomenon is a striking one to observe; complete collapse of cellular organization takes place. The reversible gelation of protoplasm is accomplished by a variety of anesthetic agents (8). Irreversible gelation is produced by many poisonous substances which cause death.

Our studies on the effects of anesthetic agents on protoplasm included a large number and variety of agents, among them nitrous oxide, carbon dioxide, cyclopropane, cold, heat, and shock mechanically and electrically produced, all of which, without exception, reversibly gelate protoplasm. We had given little attention to substances which solate protoplasm, other than salts. Once the extraordinary effects of caffeine and other xanthines had been observed, the stimulation and solation of protoplasm became an intensive study. All xanthine derivatives studied stimulate, and all liquefy protoplasm (10). As a result of this work we developed an hypothetical graph in which the physiological state of the protoplasm served as abscissae, and the state of protoplasmic aggregation as ordinates (Fig. 1). The purpose of the present article is to present this curve, to add further proof of its validity, to correlate certain pharmacological and normal physiological activities with colloidal changes, and to consider the several possible states of molecular aggregation which exist in normal, gelated, and solated protoplasm.

---

[1] The authors wish to express their indebtedness to the Sloan-Kettering Institute and the Cancer Commission of the University of Pennsylvania for financial support.

MATERIAL

The living material on which the foregoing and the following observations were made is the plasmodium of the *Myxomycete* or *Mycetozoan*, *Physarum polycephalum*. This primitive organism is a non-cellular, multinucleate, relatively undifferentiated mass of protoplasm, commonly referred to as a slime mold. Its dual technical name indicates its plant and animal characteristics.

EXPERIMENTAL

Having advanced the general rule that stimulants solate and depressants gelate protoplasm, we sought further evidence in support of the hypothesis. Opiates next occupied our attention. The concentrations of the solutions varied with the desired magnitude and rapidity of action. Morphine sulphate of 0.04 M concentration disrupts protoplasm quickly. The first sign of injury is immediate, and death follows in 10–15 min. Lower concentrations of 0.01–0.02 M produce injury, but it is delayed.

To our surprise, morphine and heroin had a remarkable dispersing effect on protoplasm, similar to that of caffeine. The fluidity of the protoplasm is greatly increased, disruption of normal flow is rapid, and complete collapse follows, resulting in an outpouring of the protoplasm into large abnormal surface vesicles. The whole effect closely parallels that caused by the xanthine derivatives.

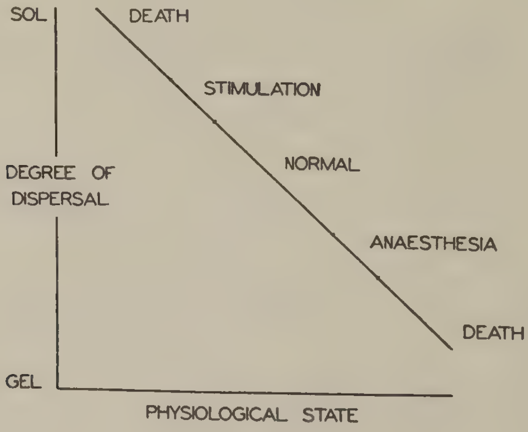

FIG. 1.

The action of morphine and heroin appeared to contradict our theory, illustrated in Fig. 1, that stimulants, such as caffeine, solate, and depressants, such as nitrous oxide, gelate protoplasm. The seeming contradiction rested, however, on a misconception, namely, our belief that morphine is a depressant. In a sense, and to a limited degree only, this is true, for morphine is described as analgesic, sedative, and a respiratory depressant. The same is said of heroin. As solation is the mark of a stimulant, we sought in medical literature for some substantiation of morphine as a stimulant. It was possible that the opiates function as does alcohol, first stimulation, then depression. The result of our search in the literature outdid our hope in regard to the possible stimulating effects of the opiates, for we read that "the phenanthrene alkaloids have both depressant and stimulating effects on the central nervous system" (5). On reading further, it was soon obvious that the stimulating effects of morphine and heroin, as indicated by the solation of protoplasm, are more characteristic of these alkaloids than are their depressing effects. The action of morphine on muscle is one of stimulation, resulting in contraction. Convulsions are produced by codeine to an even greater extent than by morphine. The effect of heroin on the central nervous system is one of excitation. Heroin is taken by the addict for euphoric stimulation long after tolerance to the depressant effect has been established. Animals clearly show the excitatory effects of morphine. In some, "this alkaloid causes almost pure stimulation, convulsions, and death by exhaustion"; in certain species, morphine causes mania and tonic spasms which last many hours and often end fatally (5).

From these quotations it is evident that morphine and its chemical relatives are highly stimulating, depression being a less frequent and a secondary result. That morphine should liquefy protoplasm is, then, to be expected, and experimentation showed this to be true. The graph in Fig. 1 is, therefore, in full agreement with known normal and pathological behavior.

The graph presents 5 major regions which depict normal, pathological, and lethal states of protoplasm. Stimulation lies to one, and depression to the other side of the normal condition. The graph terminates with death by solation at one end, and death by gelation at the other end. The central, normal region represents the great range in degree of fluidity through which active protoplasm may go. Obviously, the 5 regions grade imperceptibly into each other.

It is not our intention to extend the foregoing hypothesis further than the stimulation and depression of protoplasm caused by drugs, but the idea may have wider applicability. This is indicated by the work of Karrer (6), who suggests that the electric stimulation of muscle may be correlated with the thixotropic behavior of gels, *i.e.*, with thixotropic solation and thixotropic gelation. Karrer's interpretation of muscular activity is supported by Freundlich (3) who made much of thixotropy in biological reactions.

There is one feature of drug action which must constantly be borne in mind; it is well illustrated in the response of organisms to alcohol and ether. Many substances first stimulate and then depress, or they are stimulants in mild doses and depressants in heavy doses. Thus, a feeble electric current may activate protoplasm, as in the case of muscle, whereas a heavier current will depress or anesthetize protoplasm, as in the case of some experiments on slime molds (11).

THEORY

Protoplasm, in passing from one degree of fluidity to another coincident with changes in physiological state, must inevitably undergo changes in the degree of aggregation of its molecular or colloidal units. The primary structural units of protoplasm are fibrous protein molecules, or molecular aggregates of these, oriented and interlocked in such a way as to give to the active living substance both the elasticity and the fluidity of a soft jelly (4, 9). The physical state of the various degrees of colloidal aggregation, and the kinds of bonds existing between the structural units, are problems of as much significance to the study of protoplasm as they are to the study of elastic proteins, rubber, and polymers in general.

Numerous hypotheses of aggregation have been advanced in explanation of the solation and gelation of colloidal jellies. The interlocking of protein fibers is the basic mechanism of most of them. The micelles of Naegeli give no hint of structural continuity. The parallel alignment of molecular chains into grids, as postulated by Astbury (1), makes for rigidity, but not fluidity. Bungenburg de Jong (2) introduced the coacervate concept, which he thought best illustrates the physical state of many colloidal jellies, of muscle, and of protoplasm. The chief virtue of a coacervate as a model of living matter is the delicate balance existing between the forces of solvation and those of dehydration. But there is another feature of the living and non-living jellies which more truly represents the structural basis of sol-gel transformation: it is the continuity in structure which gives to protoplasm and to non-living jellies the fluidity of a sol and the elastic rigidity of a soft gel.

The colloid chemist may see in a coacervate the molecular mechanism which permits sol-gel transformation, and the protein chemist may regard denaturation as responsible for the change. In the latter case, the solation of protoplasm may be due to a loosening or a destruction of the lateral bonds of proteins, or to a complete cleavage of the protein chains, or, less likely, a curling or folding of molecular fibers, all of which mechanisms will partially or fully set free previously interlocked molecules. Increase in the viscosity of protein solutions is used as a criterion of denaturation. Without denying coacervation and protein denaturation as mechanisms involved in changes in protein fluidity, we believe that a better picture of what is happening in the sol-gel transformations of protoplasm is to be had from present-day concepts of loose, shifting, and fluid bonds.

Fibrous molecules, feebly interlocked by side chains with mobile bonds, permit flow in a semirigid structure. The nature of these intermolecular ties is the subject of much present-day colloidal literature, from the hydrogen bond discussed in full by Pauling (7) to the fluid joint postulated for rubber (12). It is these labile unions between linear molecules which make possible the pronounced, and often rapid, changes in the physical state of protoplasm, the sol-gel transformations which accompany stimulation and narcosis.

Whatever the precise mechanism of the sol-gel transformation in protoplasm may be, the experimental facts are clear, that there is a correlation between pathological change and the physical state of protoplasm, that aggregated protoplasm is characteristic of the depressed state, and dispersed protoplasm of the stimulated state. Anesthetic agents which suppress activity, gelate protoplasm; drugs such as morphine, heroin, and the xanthine dervatives which cause stimulation, disperse protoplasm. This deduction is to be expected for chemical reactions and, therefore, physiological activities are certain to occur at a lower rate in a gel than in a sol. This fact is well illustrated in the comparatively dry protoplasm of a resting seed, and even better in the so-called sclerotium of the organism on which the present research rests. This sclerotium is the resting or hibernating protoplasm of a slime mold. It is a xerogel and represents as dry and hard a form of living protoplasm as is known anywhere in nature.

SUMMARY

Protoplasm undergoes great changes in fluidity during its normal activity. This range is increased by pathological conditions. Stimulation by xanthines and opiates solate the living substance. Depression or anesthesia by certain drugs and other agents gelate protoplasm. An increase in activity is, therefore, correlated with a dispersal or "relaxing" of the protein units in protoplasm, whereas anesthesia or suppressed activity is coincident with an aggregation or tightening of the interlocking linear molecules of protoplasm. Excessive loosening or tightening of the fibrous structural units results in death.

REFERENCES

1. ASTBURY, W. T., in Essays on Growth and Form, Ed. by E. Clark and P. B. Medawar, p. 309. Oxford, 1945.
2. BUNGENBURG DE JONG, H. G., La coacervation, les coacervats, et leur importance en biologie, Vols. 1 and 2, Paris, 1936.
3. FREUNDLICH, H., The Structure of Protoplasm, a monograph, ed. by William Seifriz, p. 85. Ames, Iowa, 1942.
4. FREY-WYSSLING, A., Submicroscopic Morphology of Protoplasm, New York, 1948.
5. GOODMAN, L., and GILMAN, A., The Pharmacological Basis of Therapeutics, New York, 1941.

6. Karrer, E., *J. Rheology* **3**, 334 (1932).
7. Pauling, L., The Nature of the Chemical Bond, Ithaca, N. Y., 1940.
8. Seifriz, W., *Anesthesiology* **2**, 300 (1941).
9. Seifriz, W., The Structure of Protoplasm, Ames, Iowa, 1942.
10. Seifriz, W., and Pollack, H. L., Toxicity and Molecular Structure of the Xanthine Derivatives, in press.
11. Seifriz, W., *Anesthesiology*, in press.
12. Treloar, L. R. G., *Repts. Progress Phys.* **9**, 113 (1943).

THE EFFECT OF CERTAIN IMPURITIES ON THE SURFACE AND INTERFACIAL TENSION OF AQUEOUS SOLUTIONS OF SODIUM DODECYL SULFONATE

Leo Shedlovsky, John Ross and Conrad W. Jakob

From the Research and Development Department
Colgate-Palmolive-Peet Co., Jersey City, N. J.

Received November 26, 1948

INTRODUCTION

Many examples of dilute solutions which show a minimum in the surface tension-concentration and interfacial tension-concentration curves have been reported (1,2,3,4). According to Gibbs' adsorption Equation, the adsorption is proportional to the negative slope of the surface tension-activity curve. Where activity coefficients do not change with concentration, concentrations may be used instead of activities. On this basis no adsorption would be indicated at the concentration corresponding to the minimum. Miles and Shedlovsky (5,6,7) have shown the effects of small amounts of certain impurities which cause minima in *s.t.*-concentration and *i.t.*-concentration curves. (To avoid cumbersome repetition, the following abbreviations will be used: *s.t.* for surface tension and *i.t.* for interfacial tension.) Such curves have been used as a guide to the method for the purification of certain mixtures by selective adsorption at air-liquid interfaces (foam) or benzene-liquid interfaces (emulsion). These data may give criteria of purity not easily obtainable from the measurement of bulk properties.

It has been suggested (5,6) that both the appearance of minima and the concentration at which they appear should be re-examined with regard to the presence of small amounts of impurities. Recently, Brady (8) has repeated measurements of *s.t.* of aqueous solutions of purified sodium lauryl sulfate and of lauryl sulfonic acid.

Tartar and coworkers (9,10) have measured the *s.t.* and *i.t.* of aqueous solutions of sodium alkyl sulfonates. Their *s.t.*-concentration curves show pronounced minima. For sodium dodecyl sulfonate, they report a minimum *s.t.* about 9.3 dynes/cm. lower than the value reached at higher concentrations (throughout this report sodium docecyl sulfonate refers to sodium dodecane-1-sulfonate.) The sodium sulfonates which they used were prepared as described in previous papers (11,12) and analyzed by the determination of sulfur by oxidation of the sulfonate to sulfate, followed by precipitation and weighing as barium sulfate. Their analyses showed the sulfonate to have a purity within ± 0.2%. It will be seen later that 0.2% of certain impurities may have a considerable effect on the *s.t.* of the solutions.

It was found previously (5,6) that small amounts of certain impurities cause minima in *s.t.*-concentration curves of sodium alkyl sulfates. In order to find out whether the surface active properties of sodium alkyl sulfonates are susceptible to small amounts of impurities in a way which is analogous to that shown for sodium alkyl sulfates (5,6), we have measured the effect of adding certain materials on the *s.t.* and *i.t.* of aqueous solutions of purified sodium dodecyl sulfonate.

Experimental

Measurement of Surface and Interfacial Tension

The static *s.t.* and *i.t.* of the solutions were determined by the du Nouy method using a hydraulic jack to support the flask. Aging effects were found for many of the solutions, particularly in the more dilute range. This change was usually a decrease in surface or interfacial tension with time. The tension on the ring was set 0.1 dyne/cm. above the previous setting and the tension at which the film was ruptured was noted. One minute was allowed after each setting. Successive readings were taken in most cases over a period of half an hour and the lowest value recorded. Usually this half hour period was sufficient to obtain steady readings. Many repeated and independent measurements of this kind were made and the reproducibility was found to be ± 0.1 dyne/cm. For the *i.t.* measurements, the solution of the sodium dodecyl sulfonate was prepared in distilled water in a 500 cc. Erlenmeyer flask. Benzene was run down the side of the flask until a layer approximately $\frac{1}{4}''$ thick covered the surface of the aqueous solution. Dilutions were made directly in the flask by adding distilled water from an automatic buret, introducing the water below the benzene layer by means of a long capillary tube. The solution with the layer of benzene was stirred slowly with a magnetically operated stirrer so that an emulsion was not formed at the solution-benzene interface. The static values of *i.t.* were obtained for most solutions in about half an hour of slow stirring. For measurements at 40°C. the flask was immersed in a water thermostat. The temperature of the solution was maintained within ± 0.2°C.

For *s.t.* measurements, a 500 cc. Erlenmeyer flask was used, which had the neck paraffined inside and outside.

In all the measurements, the solutions were kept covered to avoid contamination.

Selective Adsorption in Foam

Sodium dodecyl sulfate to make 0.01 molal solution was weighed into a 500 cc. Erlenmeyer flask and 0.25% octadecanol (sodium dodecyl sulfate basis) was then added. The octadecanol was introduced by making an ethyl ether solution and the ether evaporated by first heating on a steam bath and finally by placing the flask in a desiccator under vacuum. The inside of the neck of the flask was paraffined after the ether was evaporated.

A column of foam was prepared from the solution in a cylindrical jacketed tube, 46 cm. long and 3.7 cm. in diameter, from another jacketed tube placed below the first one. The lower tapered tube was 17 cm. long and 2.8 cm. at the widest portion. Filtered air was bubbled through a stainless steel perforated cup "spinnerette" (40 holes, 0.0032 inches in diameter) at a manometer reading of 12.0 cm. of water.

Measurements of *s.t.* were made on 0.007 molal sodium dodecyl sulfate solutions, by dilution of the 0.01 molal solution after it had drained through the foam column. Ten minutes was allowed for this drainage.

In this case, dilutions were made directly in glass stoppered dishes (5.5 cm. diam.). After the *s.t.* had been determined, the dishes were stoppered and the solutions allowed to stand overnight at room temperature.

The foam was somewhat unstable and, therefore, approximately half a column of fresh foam had to be formed after each foam extraction due to coalescence and appearance of gaps in the column after drainage.

Selective Adsorption in Emulsion

A 0.006 molal aqueous solution of sodium dodecyl sulfonate was emulsified with benzene by vigorous stirring for 10 min. with a magnetic stirrer. One volume of benzene to two volumes of aqueous solution were used. Fifty cc. of the lower aqueous solution layer were withdrawn with a pipet, and transferred to a clean flask. Fresh benzene was added and the *i.t.* determined after aging for 2 hr. without stirring.

Materials. The sodium dodecyl sulfate was prepared according to the method described by Dreger and coworkers (13), and then recrystallized from methyl alcohol and extracted with diethyl ether.

The sodium dodecyl sulfonate was prepared[1] by a slight modification of the procedure outlined by Reed and Tartar (11). Dodecanol (b.p. 132–135°C. at 3.5 mm., n^{D}_{25} 1.4410) which was obtained by fractional distillation of lorol (commercial mixed alcohols derived from coconut oil fatty acids) was converted into 1-bromododecane by the method of Kamm and Marvel (14).

To a solution of 85 g. of sodium sulfite in 500 cc. water, 119 g. of 1-bromododecane was added, and the mixture placed in a liter stainless steel rocking bomb and heated at 180°C. for 7 hr. After cooling, the reaction mixture was removed, the crude sulfonate collected on a Buchner filter funnel and the filtrate discarded. The crude solid was washed twice with 1 l. portions of diethyl ether by slurrying with the solvent. It was then filtered and dried in a vacuum desiccator over calcium chloride. The dry powder was treated with 2 l. of hot 95% ethanol and the inorganic salts removed by filtration. The crystals of sulfonate which separated from the cooled filtrate were collected on a Buchner funnel and washed with diethyl ether. The yield was 84 g. This material was fractionally recrystallized from 2300 cc. of 95% ethanol, giving a total of 65 g. of sodium dodecyl sulfonate.

---

[1] The authors wish to express their appreciation to Dr. J. F. Gerecht of these laboratories for the preparation of this compound.

The water was collected directly from a Barnstead still and was free from surface active materials.

The benzene was C. P. grade.

Results

Portions of the *s.t.*-concentration curves for sodium dodecyl sulfonate where the solution was at 27°C. and 40°C. and for sodium dodecyl sulfate at 27°C. are shown in Fig. 1. At 27°C., neither the sulfonate nor the sulfate show any minimum.

An equimolar mixture of sodium dodecyl sulfate and sodium dodecyl sulfonate does not show a minimum in the curve (Fig. 1), and gives values intermediate between those for the sulfate and sulfonate.

Fig. 2 shows the effect of added materials on the *s.t.* of solutions of sodium dodecyl sulfonate. Curve A represents the data for the sulfonate at

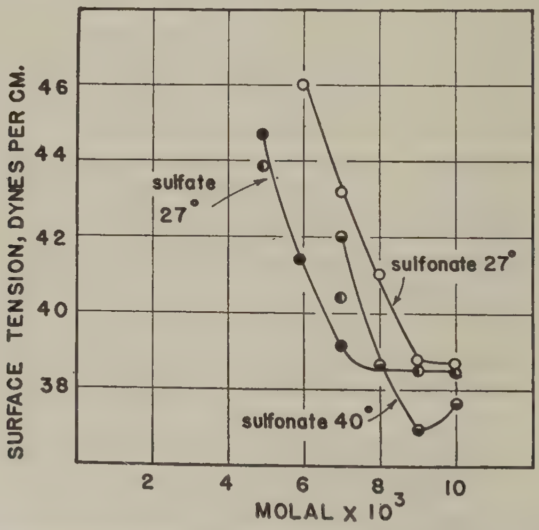

FIG. 1. Surface tensions of solutions. ○, sodium dodecyl sulfonate at 27°C.; ◒, at 40°C.; ●, sodium dodecyl sulfate at 27°C.; ◐, 1 mole of sodium dodecyl sulfonate + 1 mole sodium dodecyl sulfate at 27°C.

29°C., showing the relatively flat portion up to 0.02 molal, and Curve B at 40°C. Points (1) and (2) are obtained after foam extraction of solutions which originally had surface tensions indicated in Curve. B

Curve C (Fig. 2) indicates the effect of adding sodium hexadecyl sulfate and D, E, and F are the curves for the sulfonate with 0.05, 0.10, and 0.50% dodecanol (on the sulfonate basis) added, respectively. The dotted curve T corresponds to the data for sodium dodecyl sulfonate reported by Tartar and coworkers (9,10).

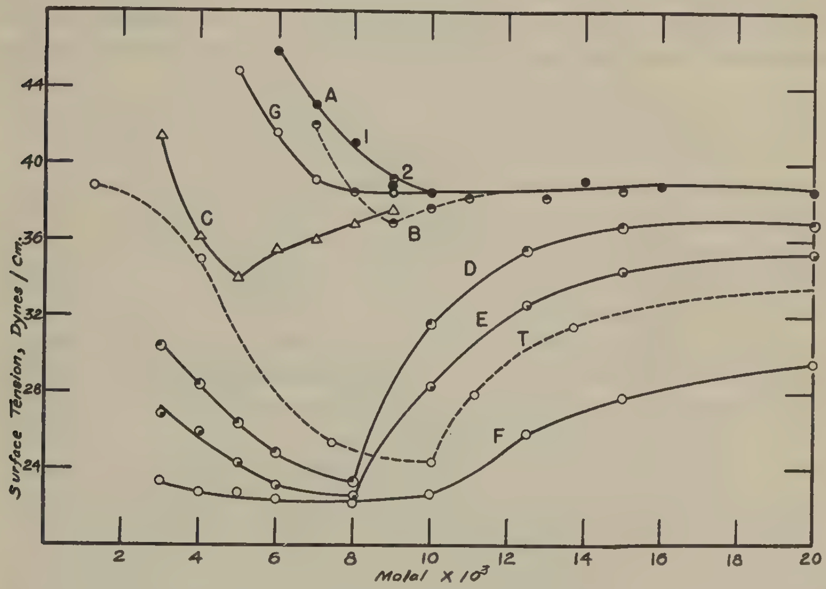

FIG. 2. Surface tension of solutions of sodium dodecyl sulfonate and effect of addition of dodecanol and sodium hexadecyl sulfate. (A) Sodium dodecyl sulfonate at 29°C. (B) Sodium dodecyl sulfonate at 40°C. Points (1) and (2), after foam extraction. (C) Sodium dodecyl sulfonate + 1% sodium hexadecyl sulfate (on sulfonate basis) at 29°C. (D) Sodium dodecyl sulfonate + 0.05% dodecanol (on sulfonate basis) at 26°C. (E) Sodium dodecyl sulfonate + 0.10% dodecanol at 27°C. (F) Sodium dodecyl sulfonate + 0.50% dodecanol at 30°C. (G) Sodium dodecyl sulfate at 27°C. (T) Sodium dodecyl sulfonate at 40°C. (From data of Tartar, Sivertz and Reitmeyer (9).)

Curve A (open circles) of Fig. 3 represents the *i.t.* of sodium dodecyl sulfonate (fourth crop of crystals) solutions against benzene. The half shaded circles (Curve A^1) represent the values for solutions of the sulfonate (third crop of crystals). Addition of 5% dodecanol (sulfonate basis) to solutions corresponding to Curve A^1 (third crop of crystals) gave essentially the same curve as A^1. If a 0.006 molal solution (Curve A^1) of sodium dodecyl sulfonate (*i.t.* of 4 dynes/cm.) is extracted with benzene, an *i.t.* of 5 dynes/cm. is obtained and this is slightly above the value for Curve A at this concentration. It appears from Curves A and A^1 that the third crop of crystals contains a very slight amount of impurity which is removed in the fourth crop.

Curve B of Fig. 3 shows the pronounced effect on *i.t.* of the solution of the sulfonate to which 1.3% of sodium hexadecyl sulfate (solids basis) had been added. The lowest value obtained in this case is 2.4 dynes/cm. at 0.0025 molal as compared with the lowest value of 4.7 dynes/cm. at 0.006 molal for the purified sulfonate.

A 0.004 molal solution of sodium dodecyl sulfonate plus 1.5% of sodium hexadecyl sulfate with an *i.t.* of 2.2 dynes/cm. was extracted with a benzene emulsion (1 volume of benzene to 2 volumes detergent solution). This extracted solution had an *i.t.* of 6.3 dynes/cm. After standing for 20 hr., the value obtained is 5.8 dynes/cm. On the basis of measurements of the electrolytic conductivity of the solutions for the above extractions with benzene emulsion, the bulk concentration of the sodium dodecyl sulfonate decreased by about 2% which is quite an insufficient change in concentration to explain the rise in *i.t.* of 3.6 dynes/cm.

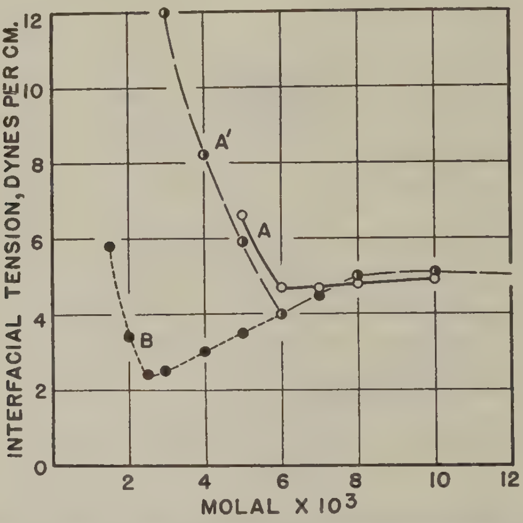

FIG. 3. Interfacial tension (water/benzene) of aqueous solutions of sodium dodecyl sulfonate with dodecanol or sodium hexadecyl sulfate added at 25°C. A = sulfonate (fourth crop of crystals); A^1 = sulfonate (third crop of crystals); B = sulfonate + 1.3% hexadecyl sulfate (solids basis).

DISCUSSION

Tartar and coworkers (9) report pronounced minima in *s.t.*-concentration and *i.t.*-concentration curves for solutions of sodium dodecyl and sodium tetradecyl sulfonate. For example, for 0.009 *M* solutions at 40°C., they find a *s.t.* of 24.1 dynes/cm., whereas, at 0.02 *M*, where the curve tends to flatten out, the value reaches 33.6 dynes/cm. It appears, from our investigation, that such minima may be attributed to the presence of as little as 0.2% of certain impurities, as reported in previous papers (11,12).

In our work, for 0.009 *M* solution at 40°C., the *s.t.* is 36.9 dynes/cm., and, at 0.015 *M*, the value is 38.6 dynes/cm. The relatively small dip in our curve at 40°C. (Figs. 1 and 2B) may be attributed to a minute contamination since it can be eliminated by selective adsorption in foam (Fig. 2, Points 1 and 2). Our curves (Fig. 1) at 27°C. and (Fig. 2A) at 29°C. do not show any minima and this is taken as an indication of the absence of impurities of the type of dodecanol in our preparation.

Reichenberg (15) emphasizes that minima in the *s.t.*-concentration curves should not be expected if the materials used are pure, and also adopts the explanation proposed by Miles (6) for the shape of the curves with minima. For example, with solutions of sodium dodecyl sulfonate (Fig. 2) or the corresponding sulfate containing relatively small amounts of dodecanol (6), the dodecanol is much more strongly positively adsorbed than the sulfonate or sulfate up to the concentration of the relatively flat portion of the curve. This is in accord with the fact that, in this range of concentrations, dodecanol can be removed from solutions of the sulfonate or sulfate by foam fractionation. At higher concentrations in the flat portion of the curve, dodecanol is not selectively removed in the foam. This means that the dodecanol is no longer positively adsorbed, and this can be attributed to the solubilization of the dodecanol.

The comments of Reichenberg (15) with regard to the work of C. Robinson (16) on *i.t.*-concentration curves with minima, and of Powney and Addison (1), however, do not seem to be supported by the available data. In our work with pure sodium alcohol sulfates (13) and sulfonates, the presence of small amounts of inorganic salts does not cause minima to appear in the *s.t.*- or *i.t.*-concentration curves. In the cases discussed by Reichenberg (15), it is probable that the minima in the curves reported by C. Robinson (16) and Powney and Addison (1) are primarily due to impurities such as higher homologs or alcohols present in the detergent or introduced into the solutions in some other way and not due to traces of salts present in distilled water. For *s.t.*- and *i.t.*-concentration curves, Miles and Shedlovsky (5,6) have shown examples of a quite different salt effect, where the inorganic salt is added in relatively large amounts (20 times the amount of the detergent).

A comparison of the effect on the *s.t.*-concentration curve of the addition of dodecanol to solutions of the pure salts shows that for the same amount of dodecanol added, the sodium dodecyl sulfonate gives much lower surface tensions covering a greater range in concentration than for sodium dodecyl sulfate. For example, for the sulfonate with 0.5% dodecanol added (Fig. 2F) for 0.01 *M* of the sulfonate, the *s.t.* is 22.6 dynes/cm., for 0.02 *M* it is 29.5 dynes/cm., whereas for the sulfate (5), at 0.01 *M* with 0.5% dodecanol added, the *s.t.* is 35.5 dynes/cm. This difference in behavior could be due in part to a larger degree of solubilization for the dodecanol by the sulfate than by corresponding concentrations of sulfonate. At present, no comparative solubilization data are available for these materials.

In Fig. 2, the minima in the *s.t.*-concentration curves approach a value somewhat less than for water saturated with dodecanol, which has a *s.t.* of 24.4 dynes/cm. at 27°C. For sodium dodecyl sulfonate plus 0.10% dodecanol at 27°C., at 0.008 *M* (Fig. 2E) the solution has a *s.t.* of 22.5 dynes/cm.

From Fig. 1, we have seen that equimolar concentrations of sodium dodecyl sulfate and sulfonate do not show a minimum in the *s.t.*-concentration curve. In Fig. 2C, for sodium dodecyl sulfonate plus 1.0% sodium hexadecyl sulfate, the curve is shifted toward much lower concentrations than that for the pure sulfonate, and shows a minimum about 5 dynes/cm. below the relatively flat portion of the curve. The *s.t.* of solutions of sodium hexadecyl sulfate (13) is considerably lower than that of sodium dodecyl sulfonate and the *s.t.*-concentration curves are similar to those reported for mixtures of sodium alcohol sulfates (5). The same explanation given previously could apply here, namely, that the lower part of the curve is due to a salt effect of the sodium dodecyl sulfonate on the sodium hexadecyl sulfate.

It appears that for *s.t.*-concentration curves of mixtures of sodium dodecyl sulfate and sulfonate where the polar groups are different, no minimum in the curve is obtained. The length of the paraffin chain anion is greater for the sulfate than for the sulfonate which is in accord with the considerably lower surface tensions obtained for the sulfate up to concentrations above 0.009 *M* (Fig. 1). At concentrations above 0.009 *M* the difference in *s.t.* is only slight. On the other hand, when the difference in the length of anions is increased sufficiently, minima in *s.t.*- as well as *i.t.*-concentration curves are obtained for mixtures of sodium alcohol sulfates as shown previously (5,6,7), as well as for sulfonate plus sulfate (Fig. 2C).

SUMMARY

The surface tension-concentration curves of sodium dodecyl sulfonate at 27°C. and 40°C., and the interfacial tension-concentration curve (water/benzene) at 25°C. have been determined. For purified materials, these curves do not show minima. It is demonstrated that this is another example where the data in the previous literature with pronounced minima in the corresponding curves can be attributed to certain impurities.

The surface tension-concentration curve for equimolar mixtures of sodium dodecyl sulfonate and sulfate does not show a minimum. This mixture has quite different surface properties from those of mixtues where the hydrocarbon chain lengths are different, such as sodium dodecyl sulfonate and sodium hexadecyl sulfate which show pronounced minima.

The effect on the surface tension-concentration curve of adding dodecanol to solutions of sodium dodecyl sulfonate has been shown.

The minima in surface tension-concentration and interfacial tension-concentration curves for sodium dodecyl sulfonate solutions containing impurities may be eliminated by selective adsorption of these impurities by foam extraction or emulsion extraction at concentrations of detergent at or near the minimum in the corresponding surface tension or interfacial tension curves.

REFERENCES

1. POWNEY, J., AND ADDISON, C. C., *Trans. Faraday Soc.* **33**, 1243 (1937).
2. LOTTERMOSER, A., AND STOLL, F., *Kolloid-Z.* **63**, 49 (1933).
3. McBAIN, J. W., AND WOOD, L. A., *Proc. Roy. Soc. London* A958, **174**, 286 (1940).
4. McBAIN, J. W., in Colloid Chemistry, Ed. by J. ALEXANDER **5**, New York, 1944, p. 116.
5. MILES, G. D., AND SHEDLOVSKY, L., *J. Phys. Chem.* **48**, 57 (1944).
6. MILES, G. D., *ibid.* **49**, 71 (1945).
7. SHEDLOVSKY, L., *Ann. N. Y. Acad. Sci.* **49**, 279 (1948).
8. BRADY, A. P., Twenty-second National Colloid Symposium, M. I. T., Cambridge, Mass. June 23–25, 1948.
9. TARTAR, H. V., SIVERTZ, V., AND REITMEYER, R. E., *J. Am. Chem. Soc.* **62**, 2375 (1940).
10. LINGAFELTER, E. C., WHEELER, O. L., AND TARTAR, H. V., *ibid.* **68**, 1490 (1946).
11. REED, R. M., AND TARTAR, H. V., *ibid.* **57**, 570 (1935); **58**, 322 (1936).
12. TARTAR, H. V., AND WRIGHT, K. A., *ibid.* **61**, 539 (1939).
13. DREGER, E. E., KEIM, G. I., MILES, G. D., SHEDLOVSKY, L., AND ROSS, J., *Ind. Eng. Chem.* **36**, 610 (1944).
14. Organic Synthesis, Coll. Vol. I, p. 27, 1932.
15. REICHENBERG, D., *Trans. Faraday Soc.* **43**, 467 (1947).
16. ROBINSON, C., Symposium on Wetting and Detergency, p. 137, 1937.

DIFFUSE SMALL-ANGLE SCATTERING OF X-RAYS IN COLLOID SYSTEMS

O. Kratky and G. Porod

Institute for Theoretical and Physical Chemistry, The University of Graz, Austria

Received May 26, 1948

MATERIAL INHOMOGENEITIES OF COLLOIDAL DIMENSIONS AS CAUSE OF THE EFFECT

The most important details on the historical development of the diffuse small-angle scattering of X-rays have already been reported. [1,2] It suffices to say that the discovery of the effect in itself is due to Krishnamurti, Mark and Hengstenberg, and Warren and Hendriks (3), whereas the quantitative interpretation has been initiated partly by Guinier (4) (scattering by individual particles), and partly by one of the authors (5) (scattering by a close packing of particles). In addition to a series of investigations carried out by these two authors and their collaborators during the subsequent period (6,7,8,9,10,11), some interesting papers by Hosemann (12), Fankuchen, Mark, Jellinek, Riley and Ruess (13), as well as the comprehensive reviews by Donnay, Shull and Nowacki (14) may be mentioned. Lately, papers by Bauer (15), Shull and Roess (16) have been presented.

This paper is intended to give, without adhering strictly to the historical course of the development, a rough outline, chiefly of our own investigations, which will be followed by the new conceptions and experiments.

The first problem to be treated will be that of the causes of the effect. They may be of manifold nature; confining ourselves to *coherent* and *diffuse* [1] scattering of X-rays under very low angles, as far as it is *not* due to the phenomenon of total reflection, we may mark *material inhomogeneities of colloidal dimensions* as the general cause of the effect.

The small-angle scattering produced by a single colloid particle, *e.g.*, a very small crystallite, can easily be understood from the example of a one-dimensional model. Considering a row of equidistant points of total length l with the incident beam normal to its direction (Fig. 1), the zero order of diffraction will have decreased to intensity zero at an angle

---

[1] The appearance of very large identity periods in crystals, or fibers of micellar structure, leads to *sharp* low-angle reflections which are not within the scope of this paper.

2ϑ[2] where

$$\lambda = l \cdot \sin 2\vartheta.$$

Hence the extension of the low-angle scattering range depends only on the quotient λ/l, *i.e.*, with fixed λ, on the length l of the scattering object. This is only slightly modified by an irregular distribution of the diffracting centers along the row l. With a sufficiently great number n of scattering points, the intensity of the diffracted rays will practically (although not exactly) have decreased to zero for the first time with the same angle 2ϑ, for in this direction n coherent waves will superpose, the phase differences of which are distributed statistically over the range from zero to one in the same way as the scattering centers are distributed along the row l. It is easily understood that, with n not too small, the superposition actually leads to the amplitude zero with the said angle.

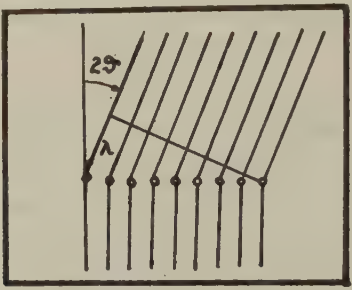

Fig. 1.

Both these cases, *i.e.*, the strictly periodic and the statistical distribution, differ only slightly, as far as the phenomenon in question is concerned, from a third case in which scattering elements are distributed uniformly and continuously along the distance l. Here again the amplitude (and the intensity) will have decreased exactly to zero when

$$2\vartheta = \text{arc} \sin \frac{\lambda}{l}.$$

There is one more case of some interest for the following: a region of definite electron density ρ is imbedded in another one of much greater (infinite) extension and of different electron density ρ_0. It is easy to see that the "background" causes no scattering of its own, and that only the difference $(\rho - \rho_0)$ is of inference for the small-angle scattering.

In principle, the above statement may be transferred also to a 3-dimensional particle. In the course of the study of low-angle scattering, it has actually become usual to consider the scattering matter as distributed continuously and uniformly in the above sense ("smeared out"). The justification of this way of proceeding has already been proved in a satisfactory manner by Guinier (4).

---

[2] Further on, we shall always denominate the angle of deflection as 2ϑ, conforming to the habit used in crystal analysis.

The existence of small-angle scattering, therefore, points (if total reflection is excluded) to material inhomogeneities of colloidal dimensions, and the resulting problem is to employ the effect for a qualitative and quantitative description of the colloid system. The theoretical treatment usually starts with composing the waves scattered by the volume-elements of a single particle, the variability in size, shape, and positions of the particles relatively to the beam causing the variety of the problem.

The second step is to carry out the superposition of the scattered intensities due to the single particles. It may become necessary in this step to take into account also mutual interference of the waves scattered by the single colloid particles. Such consideration leads, on grounds which will become evident at once, to an unconstrained classification of the small-angle scattering into three main types:

(1) "External" small-angle scattering;
(2) Scattering of "dilute" systems;
(3) Scattering of "densely packed" systems.

I. External Low-Angle Scattering

What has been said thus far is valid, at first, for a single colloid particle only. We succeeded in verifying the noticeable case that, from a single particle, a very intensive small-angle scattering could be obtained, which was well measurable. This particle has, however, macroscopic dimensions in one direction, microscopic ones in the other, and only in one dimension colloidal ones. If an X-ray beam falls on a cylindrical sample of a strongly absorbing substance, *e.g.*, on a capillary filled with mercury, the beam will penetrate only a thin outer segment, one dimension of which will be of colloidal order (Fig. 2). Calling D the diameter of

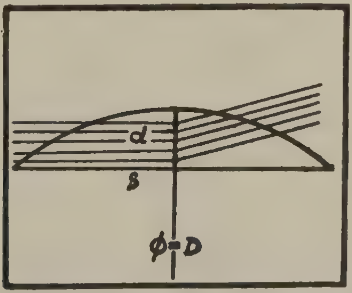

FIG. 2.

the sample, s the half width of the segment, and d its height, the following equation is known:

$$s^2 = d \cdot D.$$

In the mathematical treatment, however, we must take into account that the lightened layer is not sharply limited, and that the contributions of the lower layers decrease because of the increasing absorption. With the beam penetrating the segment at level d, we find for the scattered amplitude

$$A \propto 2se^{-\mu s}.$$

It is easily seen that this is the case of a linear body with variable scattering power which is given by the above expression and has a maximum at $s^* = 1/\mu$ or $d^* = \frac{1}{\mu^2 D}$. Introducing the "characteristic penetrating range" d^*, as unit length, and calling the relative lengths $x = d/d^*$ and $y = s/s^*$, we obtain the resulting amplitude as

$$A = \int_0^\infty \tfrac{1}{4}\sqrt{x}e^{-\sqrt{x}}e^{i\sigma x}dx, \qquad \sigma = \frac{4\pi}{\lambda}\, d^* \sin \vartheta.$$

The intensity is given as the square of the modulus of the amplitude. Since the exact evaluation of the said integral seems impossible, a mechanical procedure has been employed, giving the theoretical Curve 1, Fig. 3.

As may be seen at once, the agreement with the experimental points is satisfactory. (The experimental curve has been adjusted to the theoretical one by a linear transformation of coordinates.) From the theoretical curve, we get, for the absorption of mercury,

$$\mu = \frac{4.45}{\sqrt{\lambda}} \cdot 10^4 \qquad \lambda \text{ in Å},$$

which is a surprisingly large value. This seems to suggest that the phenomenon of external small-angle scattering is chiefly due to great wavelengths, as only these may penetrate a sufficiently thin segment. Discussing the result, we must consider that this can be regarded only as a rough estimation, as the experimental curve has been taken with polychromatic light. Investigations with monochromatic light are being carried out for further evidence. At any rate, our explanation is supported by the good agreement between the forms of the experimental and the theoretical curve.

The high absorption coefficient, as well as the smallness of the effective region suggest that a very thin layer of different material (*e.g.*, of occluded wax or anything of this kind) might be chiefly responsible for the effect.

To test this concept, the theoretical curve for a uniformly thin lamella was calculated (Curve 2, Fig. 3). Comparison shows that it does not satisfy the experiment nearly as well as the assumption of a scattering outer segment. Comparing the two curves (after adjusting to match their points at $\phi = \frac{1}{2}$), we may infer that the thickness of the lamella would have to be as low as $d = 11.6$ Å, which value seems difficult to understand, from a physical point of view.

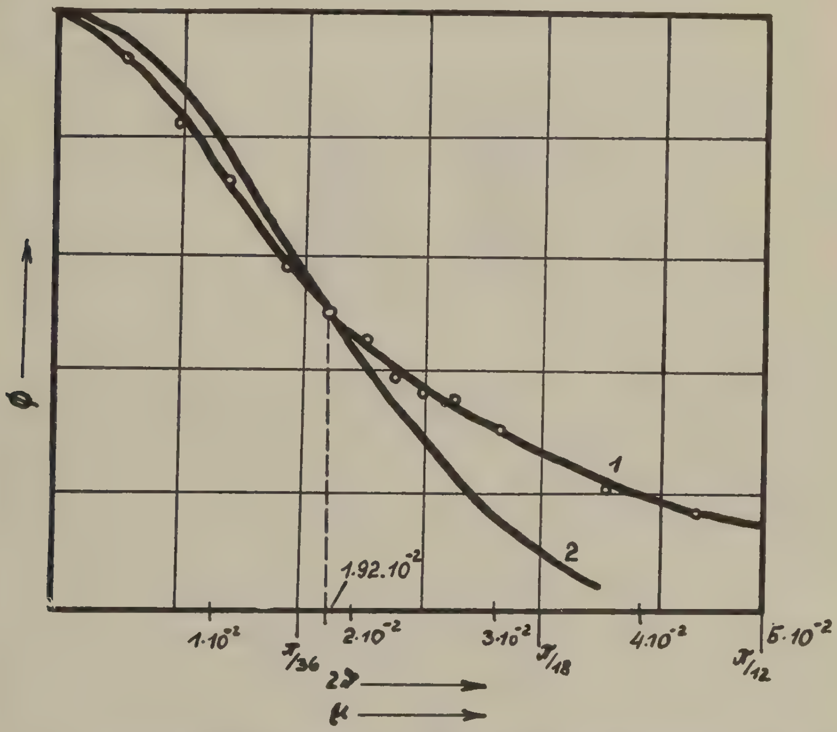

FIG. 3. External small-angle scattering from mercury-filled capillary. 1 = theoretical curve for outer segment of cylinder; 2 = theoretical curve for lamella (surface layer); ○○○ = experimental points.

We would suggest the name "External Low-Angle Scattering" for the phenomenon, because it depends on the external shape of the whole sample. It seems important to know the effect in itself, as it will always be found with strongly absorbing samples and might cause misunderstandings. In this connection, a phenomenon may be pointed out which seemed difficult to understand, at first. It is important, in taking low-angle X-ray graphs, to confine the beam by means of metal edges giving as low as possible a small-angle scattering themselves. It is found, then, that the steepest edges are best, although, as may be seen from Fig. 4, the possible scattering volume is of course larger than with obtuse ones. Obviously, however, the leading rôle is played by external small-angle scattering and this is noticeable only in obtuse edges. However, the actual circumstances are certainly more complicated than is expressed by Fig. 4, as the edge will never be exactly sharp, but somehow rounded off. It will be understood that, with obtuse angles, this pernicious region is more difficult to control than with sharp ones.

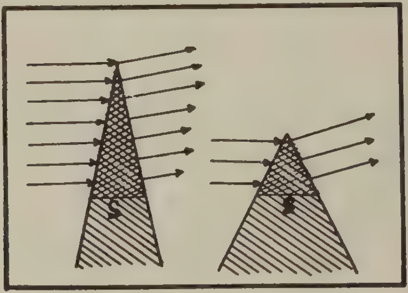

FIG. 4.

In some cases, a practical application of the external low-angle scattering may be thought of, *e.g.*, the measuring of very thin surface layers the electron density of which differs noticeably from that of their substratum. We may expect the effect also when the absorption is weak, and it is not material whether the layer or the substratum be of greater electron density.

II. Low-Angle Scattering of Dilute Systems

We shall call those systems dilute in which the distances between the individual particles are irregular and great as compared with the dimensions of the particles themselves. Here, the intensities due to the individual particles add, no doubt, in precisely the same way as in a gas (6). For the case of uniformly sized and shaped particles, we have only to carry out the summation over all possible situations in space.

As has been shown (8,1), the scattering effect of particles composed of spheres can easily be calculated by applying Debye's theory of the scattering function of the molecular gas. In previous papers, a series of scattering curves of this kind have been calculated so that a further detailed discussion may be saved here. In any case, the application of Debye's theory is generally advantageous for all bodies the shape of which may reasonably be approximated by composition of equally sized spheres. In particular, the remarkable result may be recalled that is given by an infinite row of spheres, *i.e.*, a straight-line composition of spheres. Such particles (which must, of course, be imagined as randomly situated to the

X-ray beam) give scattering curves with peaks whose situations yield the diameter of the spheres. In several proteins, this type of particle seems to come about through association of several globular bodies, and has been proven to be that of hemocyanine by one of the authors (9). Theoretical attempts by Jordan, as well as the very important results of Szent, György and Straub (18), and Astbury *et al.* (19) on the muscle protein actin, suggest that this type of particle occurs frequently in the chemistry of proteins. In the said papers the proposition is advanced that globular actin may pass to a fibrous form simply by an aggregation of the globular particles to fibers.

In attempting to reduce subtle concepts to the form of the particles, the task arises of exactly calculating scattering curves of as many and as variegated forms as possible. In previous papers (2,10), three paths to this objective have been communicated. The most expedient of these depends on the special shape for which the scattering curves are to be calculated. In this paper, we shall confine ourselves to a short sketch of the methods, referring to the quoted papers for further details.[3]

First of all, we can calculate the scattering amplitudes of one particle in one definite position, and then average the squares of the amplitudes of particles of all possible positions. It appears useful to consider the scattering as reflection from a fictitious reflecting plane. This plane has the quality that the phase differences between all its points are zero. Therefore, we may proceed as though the electron coating of each plane were concentrated into one point, thus reducing the problem to the one-dimensional case of a rod of varying scattering power which again is representible by varying cross-section. Thus we have:

$$A \propto \int F(l) \cos sl dl,$$

A = amplitude,
$s = \frac{4\pi}{\lambda} \sin \vartheta$,
l = coordinate in direction normal to plane, with origin at center,
F = cross-section at l.

This first step of the calculation yields the scattering amplitude of one particle in a distinct position. The actual scattering is the average over all possible positions in space. Practically, the calculation is possible only in a small number of special cases. For ellipsoids of rotation of axial ratio

---

[3] In a paper by Shull and Roess (34), received since, a method of calculating the scattering curves for one special type of particle, *i.e.*, ellipsoids, is given which is, in its chief part, identical with that given by us in 2 and 10 for that type.

v we obtain thus:

$$v = 1 \quad \phi = 1 - \frac{1}{10}\frac{\mu^2}{3!} + \frac{9}{70}\frac{\mu^4}{5!} - + \cdots f_n \frac{\mu^n}{(n+1)!} \cdots,$$

$$f_n = \frac{72}{(n+3)(n+4)(n+6)}.$$

$$v \lesseqgtr 1 \quad \phi = 1 - k_2 \cdot \frac{1}{10}\frac{\mu^2}{3!} + k_4 \cdot \frac{9}{70}\frac{\mu^4}{5!} - + \cdots k_n f_n \frac{\mu^n}{(n+1)!} \cdots;$$

the coefficients k_n being drawn from the following recursion formula:

$$v < 1 \quad k_2 = \tfrac{1}{3} \cdot (v^2 + 2), \qquad k_n = \frac{1}{n+1}(v^n + n k_{n-2}),$$

$$v > 1 \quad k_2 = \tfrac{1}{3}\left(1 + \frac{2}{v^2}\right), \quad k_n = \frac{1}{n+1}\left(1 + \frac{n}{v^n} k_{n-2}\right).$$

Fig. 5 shows the scattering curves thus obtained for a series of ellipsoids of rotation.

A second method goes back to the calculation of the scattering by accumulations of spheres. It will be seen immediately that a given body can be better approximated by spheres the smaller we choose them. At the limit of infinitely small spheres, we may consider volume-elements of any shape in their place. At the same time, the place of the single sphere-to-sphere distances is taken by a distance distribution function $\psi(x)$ which defines the scattering behavior.

The distance functions of three limiting cases may be given as examples:

(a) sphere $\quad \psi(x) = 12x^2(1 - x)^2(2 + x),$

(b) circular disk (two-dimensional) $\quad \psi(x) = \frac{16}{\pi} x(\arccos x - x\sqrt{1 - x^2}),$

(c) rod (one-dimensional) $\quad \psi(x) = 2(1 - x).$

The connection with the scattered intensity is given by

$$\phi(\mu) = \int_0^1 \psi(x) \frac{\sin \mu x}{\mu x} \, dx,$$

l = distance between two points within the particle,

L = maximal distance,

$x = l/L, \quad \mu = 4\pi \frac{L}{\lambda} \sin \vartheta.$

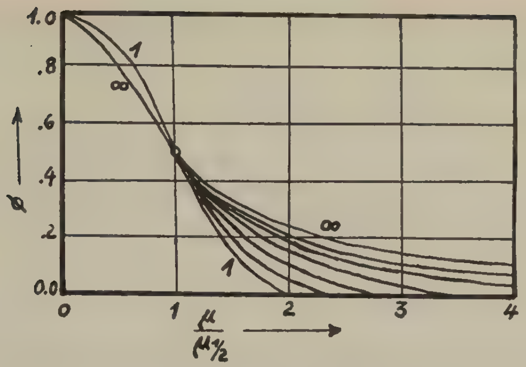

FIG. 5. Scattering curves of ellipsoids of rotation; axial ratios $v = 1, 2, 3, 4, 6, \infty$. Points $\phi = \frac{1}{2}$ made to fit by linear transformation of coordinates.

For the above examples we obtain (Fig. 6):

(a) sphere $$\phi = \left[3 \frac{\sin \mu/2 - \mu/2 \cos \mu/2}{(\mu/2)^3} \right]^2,$$

(b) disk $$\phi = \frac{8}{\mu^2} \left[1 - \frac{2}{\mu} \mathfrak{J}_1(\mu) \right],$$

(c) rod $$\psi = \frac{2}{\mu} \left[\mathrm{Si}\,\mu - \frac{1 - \cos \mu}{\mu} \right],$$

$\mathfrak{J}_1$ = 1st order Bessel function,
Si = integral sine.

This reduces the calculation of the scattering function to a purely geometrical problem, *i.e.*, the deduction of the distance function. The considerable difficulties cropping up in this may be overcome by extending

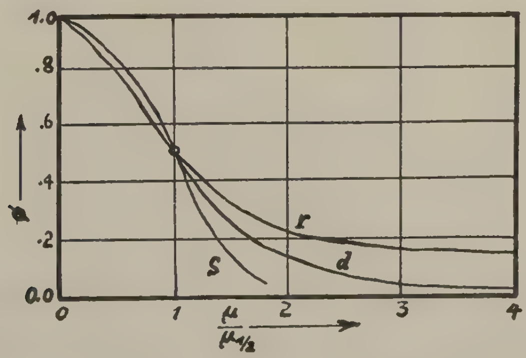

FIG. 6. Scattering curves of sphere, disk, rod. Points $\phi = \frac{1}{2}$ made to fit by linear transformation of coordinates.

the above integral to a series. Then we obtain the universal form of the scattering function:

$$\phi(\mu) = 1 - f_2 \frac{\mu^2}{3!} + f_4 \frac{\mu^4}{5!} - + \cdots f_n \frac{\mu^n}{(n+1)!} \cdots$$

in which only the coefficients f_n depend on the shape of the particles. They have a simple geometrical meaning:

$$f_n = \int_0^1 \psi(x) x^n dx,$$

being the mean values of the 2nd, 4th, *etc.*, powers of the relative distances. These characteristic coefficients can be found also without the introduction of the distance function, which opens a third way for calculating the scattering function. For further details, the reader is referred to the above-mentioned paper (11). Suffice it to quote some of the results:

cylinder (long):

$$\phi = \frac{2}{\mu}\left\{ \pi/2\Lambda_1(\sigma/2) - 1/\mu \left[2\Lambda_2(\sigma) - \frac{8}{\sigma^2}(1 - \Lambda_1(\mu)) \right] - \frac{\sin \mu}{\mu} \right\};$$

cylinder (flat):

$$\phi = \frac{8}{\mu^2}\left\{ \left(\frac{\sin \sigma/2}{\sigma/2} \right)^2 + \frac{1}{\mu} I_1(\mu) \cdot \frac{2}{\sigma} [I_0(\sigma) - 2\mathfrak{J}_1(\sigma)] - \Lambda_1(\mu) \right\};$$

rectangular disks:

$$\phi = \frac{2}{\mu}\left\{ \pi/\sigma \cdot \tfrac{1}{2} I_1(\sigma) - \left(\frac{\sin \sigma/2}{\sigma/2} \right)^2 - \frac{\sin \mu}{\mu^2} \right\}.$$

$$\mu = 4\pi \frac{L}{\lambda} \sin \vartheta,$$

$$\sigma = 4\pi \frac{D}{\lambda} \sin \vartheta,$$

$$\Lambda_n(x) = \frac{n!}{(x/2)^n} \mathfrak{J}_n(x),$$

$$I_n(x) = \int_0^x \Lambda_n(\xi) d\xi,$$

$$I_0 \rightarrow 1, \quad I_1 \rightarrow 2.$$

For cylinders and very long prisms we find, in first approximation:

$$\phi \propto \frac{1}{\sigma} \varphi(\sigma), \qquad \sigma = 4\pi \frac{D}{\lambda} \sin \vartheta, \qquad D = \text{diameter}.$$

$\varphi(\sigma)$ being a function characteristic for the cross-section which can be written in a form analogous to ϕ:

$$\varphi(\sigma) = 1 - f_2 \frac{\sigma^2}{2^2} + f_4 \frac{\sigma^4}{(2\cdot 4)^2} - + \cdots f_n \frac{\sigma^n}{(2\cdot 4\cdots n)^2} \cdots.$$

The basic function is, in this case, the zero order Bessel function, the coefficients f_n having the same meaning as before.

Circular cross-section: $\varphi(\sigma) = \Lambda_1^2(\sigma/2)$,

Linear profile (ribbon): $\varphi(\sigma) = \dfrac{I_1(\sigma)}{\sigma} \rightarrow \dfrac{2}{\sigma}$.

Leaflets of very large area give, regardless of shape,

$$\phi \propto \frac{1}{\sigma^2}\left(\frac{\sin \sigma/2}{\sigma/2}\right)^2.$$

Thus we must distinguish three types of particles:

(a) globular particles

$$\phi \doteq e^{-h^2\mu^2},$$

(b) rods (prevalent extension in one direction)

$$\phi \doteq \frac{1}{\mu} e^{-h^2\mu^2},$$

(c) leaflets (prevalent extension in two directions)

$$\phi \doteq \frac{1}{\mu^2} e^{-h^2\mu^2}.$$

The sign $\doteq$ is to mark that the analytical expressions are approximations of the types of the scattering curves.

It seems as though dilute protein were becoming the most important scope of application of low-angle scattering. Some experimental data in this line have already been presented (8,9,1); they have, however, been evaluated on the basis of the theoretical scattering curves of agglomerations of spheres. While this procedure, in the case of chain-like associations of nearly spheroidal molecules, leads to almost the exact scattering curves, it seems desirable to investigate cases in which considerable deviations from the spheroidal shape of the individual particle occur, on the basis of scattering curves that would better fit the supposed forms of the particles. This may be done when more experimental information is available.

III. Low-Angle Scattering of Density Packed Systems

If the distances between the scattering particles do not exceed their dimensions, mutual interference of the waves scattered by the individual particles must be taken into consideration. We call such systems densely packed, in contrast to the dilute system in which, because of the great and irregular distances of the particles, mutual interference may be neglected.

The nature of the subject implies that all transitions between dilute and densely packed systems are possible. We will draw a limit by calling a system densely packed in which the mutual interference is just noticeable. In many cases, other authors held the view that this mutual interference is not to be considered. Guinier's application of his formulae to cellulose (4) tacitly implies this assumption, and it was also put forward expressly by Hosemann (11). The view that dense systems required a consideration of mutual interference was put forward in previous papers of the authors (5,7). Subsequently, the influence of this particle-to-particle scattering shall be demonstrated mathematically in certain examples, as a further support of this view. There are so many possible varieties of densely packed systems that a general proof seems difficult to give. We shall, therefore, deal with three special cases only, which appeared typical to us and which, in fact, seem to rank among the most important cases occurring in physical practice:

(A) The packing of lamellae,
(B) The bundle of rods, and
(C) The accumulation of spheres of different sizes.

Subsequently to this,

(D) A comparative treatment of the systems (A), (B), (C) will be given.

A. THE PACKING OF LAMELLAE

1. Justification of the Choice of This Model

The consideration of this model was suggested by the study of cellulose. The pursuit of the deformation process of reprecipitated cellulose having made clear that the micelles (*i.e.*, the supermolecular units of structure that may be viewed as bundles of cellulose chains) must have a leaflet-structure (20), the smallness of the density difference between the macroscopic fiber and the actual micelle (the "crystal lattice") (21), as well as the low-angle scattering of cellulose threads of higher orientation (7), unreservedly lead to the idea that, within small regions, such leaflet-shaped micelles, packed in piles like the sheets of a book, must occur also in specimens without higher orientation, *e.g.*, samples of fibrous structure. This model was used for a first interpretation of the small-angle scattering of cellulose (5). It has been proved that such structures occur also in protein fibers, such as silk-fibroin (22) and keratin (23). Recalling, on top of all that, that the first leaflet-structured micelle has been found, by Mark and Susich (24), in rubber, we recognize that the packing of lamellae obviously is to be considered an idealized model of the supermolecular structure of a great number of substances. We would suggest the following structure for it: the lamellae lying in a pile like the sheets of a book; they must be assumed to vary in thickness statistically, the same as their distances from each other. The pile is, however, *not infinite,* but consists of a finite and defined number of single lamellae.

That variations in natural objects will occur, requires no argument. Also, the limitation of the size of the packing may be assumed to meet the actual conditions. With cotton fibers, for instance, according to most investigators, the histologic structure reaches far beyond the resolving limit of the microscope, *i.e.*, the rhythmical piling of the lamellae will be interrupted at times. Despite all this, there is, of course, no doubt that the above idea is modified by the existance of the "fringed micelle." As regards scattering at low angles, however, it should be possible to neglect this partial splitting of the crystalline regions in first approximation, for these fringed parts will generally, because of their small transverse dimensions, scatter at considerably greater angles, thus leaving the range in question untouched. We may, therefore, consider the packing of lamellae the model best fitting our object, in spite of the ideas of fringed micelles, transverse covalence chains, *etc.*

2. *Mathematical Treatment of the Lamella-Packing*

A particularly clear survey of the scattering phenomena is to be had by making use of the known reciprocity theorem of optics which states that the scattering of the system in Fig. 7a is identical with that of a system originating from the first by exchanging matter for empty space and *vice versa* (Fig. 7b, the dotted lines emphasize the fact that the extension of the system is greater than shown). The result is a series of parallel, very thin lamellae the distances of which are not, however, all equal. For the limit of very small fluctuations it will be recognized immediately that

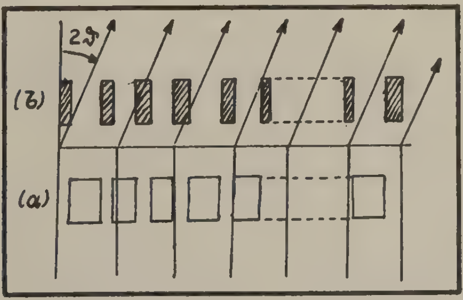

Fig. 7.

it would be fallacious to neglect, in this system, the particle-to-particle interference and proceed as though only the intensities of the individual micelles would add, for the form-factor of the single prismatic micelle gives a curve falling from $2\vartheta = 0$ on, and the superposition of the curves for micelles of different thickness must, of course, be of the same type, whereas the grid equivalent to the original system leads, at the limit, to a sharp interference at $2\vartheta = \arc \sin \frac{\lambda}{d}$.

For an exact treatment of the finite packing of lamellae we shall have to line up micelles of varying thickness parallel to each other, the intermediate lamellae (prismatic interstices) varying as well. Whereas we may reasonably assume the fluctuation in thickness of the micelles to follow a Gaussian curve, the distribution of the interstices is a more difficult problem. If we imagine only the interstices for themselves to be lined up, with omission of the micelles, their dimensions are equivalent to the problem of dividing a distance L' into n parts. Assuming, for instance, the subdivision to be due to mere coincidence, the distribution will be determined statistically. Difficulties arise in deducing the scattering of the *finite* packing of lamellae directly from this consideration. Yet we may find some other methods which contain the above assumptions on principle, taking, however, a slightly different starting point. A preliminary sketch shall be given of three possible ways of treatment as regards the assumptions implied in them.

(*i*) The fluctuation of the interstices shall follow a Gaussian distribution, so that also the central distances of the neighboring micelles show a Gaussian fluctuation consisting of the individual fluctuations of micelle diameter and interstice. This case has been treated in full by one of us (11), and an abstract will be given below. A certain roughness of this idea lies in the fact that the Gaussian curve extends to infinity so that the central distance would be assigned a certain probability of decreasing to zero or even to negative values. With a sufficiently narrow fluctuating range, this physically senseless component will become negligible because of the steep descent of the Gaussian curve, but, nevertheless, this circumstance puts a limit to the half fluctuation range, as compared with the mean central distance. Moreover, the idea of the interstices varying about one mean value is certainly reasonable for relatively small distances; with relatively great distances however (high degrees of swelling) the mean distance need not be the most probable one. Here the method reviewed below under (*ii*) is more practical.

(*ii*) Again, the diameters of the micelles are assumed to vary. Their mutual impenetrability is taken into account by choosing for two diameters d_1 and d_2, picked at random, a distribution function of the type of Curve 1, Fig. 8. The sense of this proposition is as follows: The minimum central distance is certainly given as the sum of the half diameters, $\frac{1}{2}(d_1 + d_2)$. In a dilute, infinitely expanded system, all greater distances would occur with equal probability (Curve 2). In a finite system, however, it is easily seen that a linear decrease from the original value at $\frac{1}{2}(d_1 + d_2)$ to zero at distance L is to be expected. Subsequently, we must sum all the combinations of micelle diameters. The scattering function is then obtained by adding to the mutual interference term the sum of the intensities scattered by the individual micelles. The relative amounts of these two components of the scattering function depend on the density of the whole system. The more dilute the system (the higher the degree of swelling), the smaller becomes the interference term. The advantage of this method is that the system, with high degree of swelling, passes continuously to the dilute system, contrarily to case (*i*) in which, even with very high degrees of swelling, the grid structure (although with fluctuations) will never fully disappear. On the other hand, type (*ii*) is not quite satisfactory with low degrees of swelling, because the distance function in Fig. 8 is too greatly simplified. This is easily recognized when considering the special case of equally thick micelles. Then the distance function must show (with low swelling degrees) the curling known from the structure of fluids (31,32), regardless of all other assumptions. *e.g.*, the double minimum distance $\frac{1}{2}(d_1 + d_2)$ will be realized with more probability than the 1.5 multiple, *etc.* The curling of the distance function will, of course, decrease when returning to the general case of varying micelle diameters, and the same influence is effected by increasing the degree of swelling, *i.e.*, approaching the dilute system. At any rate, however, the error due to neglect of the subtilities of the distance function will only *diminish* the difference from the dilute system.

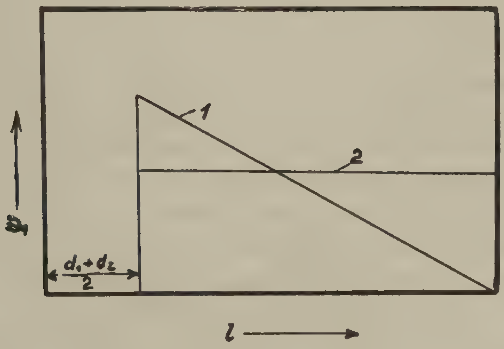

FIG. 8. Distance function of two lamellae of thickness d_1 and d_2; (1) for finite packing, (2) for infinite packing.

(*iii*) As a model for a fluid, Zernicke and Prins (25) calculated the scattering of a one-dimensional object of the following nature: rods of equal length are arranged in a line so as to let the distances of subsequent rods be determined by chance. If we substitute micelles for the rods—which does not noticeably complicate the calculation—the model corresponds to the general case mentioned at the beginning, as regards the interstices. Further, the nature of this consideration implies that the system be infinite. The treatment of this model is possible in close pursuance of the procedure given by Zernicke and Prins; here we shall confine ourselves to saying that broad maxima appear at angles connected with the mean distance of two subsequent micelles (micelle diameter + mean interstice) by about the Bragg equation. We could not content ourselves with this model, because it does not imply the two material points of our consideration, *i.e.*, the varying thickness of the micelles and the finiteness of the packing.

ad (*i*). In the following we shall give a short review of the exact deduction already published (10). We shall consider a system of n micelles and interstice-lamellae, taking the latter as the scattering bodies according to the theorem of reciprocity. Calling the mean distance (= micelle diameter + interstice) d_0, and the relative fluctuation of the distance between two neighboring lamellae δ, we assume the frequency distribution of the distances to obey a Gaussian curve. Then the mean distance between the ith and $(i + k)$th lamella must be $\bar{d}_k = kd_0$, with an average fluctuation $\delta\sqrt{k}$. The axis of the packing coinciding with the symmetry-axis of the beams, the scattering amplitude of the kth lamella may be written: $\mathbf{a}_k = F_k e^{i\varphi_k}$, F_k meaning the form-factor which may practically be neglected for our objects, and $\varphi_k = \dfrac{4\pi}{\lambda} d_k \sin\vartheta$ the phase difference against an arbitrary zero. The resulting amplitude then appears as the sum $\mathbf{a} = \sum_1^n \mathbf{a}_k$, and the intensity as the double sum

$$\mathfrak{J} \propto \mathbf{aa}^* = \sum_1^n nF_k^2 + 2\sum_1^{n-1} F_kF_{k+1}\cos\varphi_1 \cdots$$
$$+ 2\sum_1^{n-l} F_kF_{k+l}\cos\varphi_l \cdots + F_1F_n\cos\varphi_{n-1},$$

in which φ_l is used as the abbreviation for $\varphi_{k+l} - \varphi_k$. There are many such systems within one fiber, and their number is proportional to $1/n$, if the number of micelles is assumed to be constant. Neglecting the factors F_k as nearly constant and averaging, we obtain the scattering function

$$\phi = 1 + \frac{2}{n}\left[(n-1)\,\overline{\cos\varphi_1} + (n-2)\,\overline{\cos\varphi_2} + \cdots + \overline{\cos\varphi_{n-1}}\right].$$

Averaging gives, after short rearrangement:

$$\overline{\cos\varphi_k} = e^{-(\mu^2\delta^2/2)}\cdot\cos k\mu = k^k\cos k\mu, \quad \mu = \varphi_1, \quad k = e^{-(\mu^2\delta^2/2)}.$$

For small n, the above formula is well adapted for numerical calculation (see Fig. 9). Also the exact summation into one expression is possible, but this leads to an inconvenient formula. As shown by Fig. 9, the scattering curves are superimposed by waves which become more numerous with increase in n. Now we must consider that, practically, very short waves cannot occur, as they would always be "smeared out" by various influences (wide slit, irregularities in structure and position of the packings, *etc.*). This justifies the introduction of a smooth average $\bar{\phi}$ which is found from the deduction as

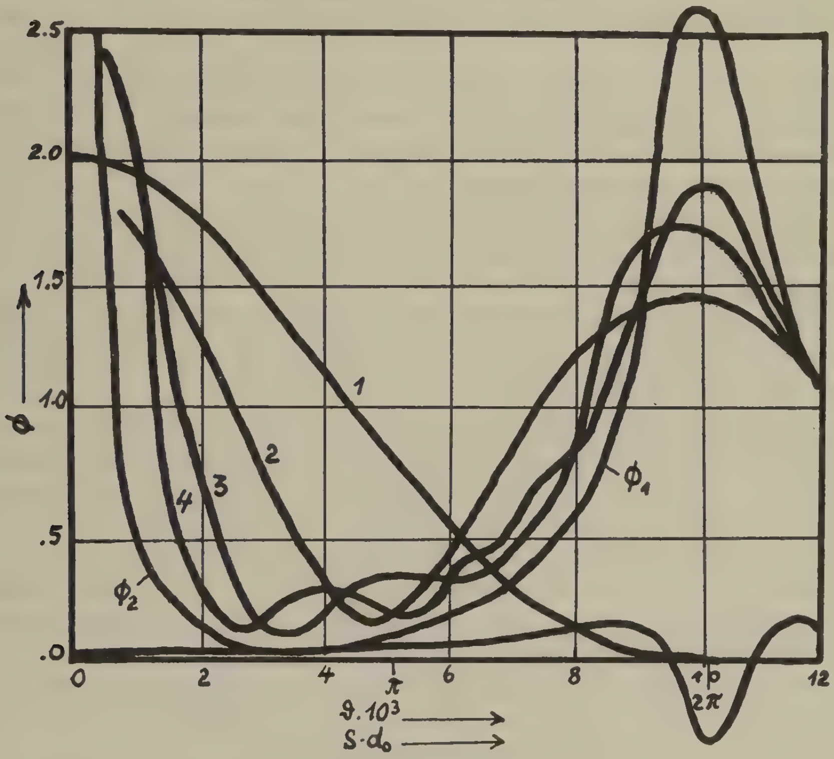

FIG. 9. Scattering of a packing of micelles, type (*i*), $\delta = 0.2$. 1 = single micelle, 2, 3, 4 = packing of 2, 3, 4 micelles, ϕ_1 = small-angle scattering, ϕ_2 = minimum-angle scattering, ϑ-scale for $d_0 = 50\lambda$.

$$\phi_1 = \frac{1 - k^2}{1 - 2k\cos\mu + k^2},$$

$$\bar{\phi} = \phi_1 + \frac{1}{n}\phi_2$$

$$\phi_2 = \alpha\frac{2k}{1 - 2k\cos\mu + k^2}, \qquad \alpha = \frac{1 - \cos\mu\,\mathrm{Cos}\,\mu^2\delta^2/2}{\mathrm{Cos}\,\mu^2\delta^2/2 - \cos\mu} \doteq 1.$$

So the partial curves ϕ_1 and ϕ_2 are no longer dependent upon n, although the ratio of their compositions is. It may be mentioned that the consideration of the form factors and the varying thickness of the interstices does not cause any material alteration. Irregularities in the orientation of the micelles in height, however, may have a considerable influence and must therefore be corrected for by a factor H. As has been shown elsewhere, H can be put $H \propto \frac{1}{\vartheta}$ at the limit to disappearing fluctuations, thus weakening the scattering with increasing angle. The essential results of the deduction can, therefore, be summed up by saying that the packing of lamellae gives two types of scattering:

(1) a *small*-angle scattering in the regions of the angles corresponding to the mean distance of the neighboring lamellae under Bragg's law in all low orders of reflection,

(2) a *minimum*-angle scattering which sets in with a fraction of the Bragg angle only ($\frac{1}{3}$ or $\frac{1}{4}$), and then rapidly increases to high values as the angle 2ϑ goes towards zero.

Let us compare this with the result found after neglect of the mutual interference, *i.e.*, let us proceed as though the intensities due to the single micelles would simply add (as has been done chiefly by Hosemann, on principle). Then we have simply to superimpose the form-factors of the single micelles. Fig. 9 shows the result, and we recognize that there is a fundamental difference depending upon the type of curve found under consideration of the mutual interference. A neglect of this particle-to-particle scattering must needs lead, therefore, to incorrect results.

ad (*ii*). Let us, at first, consider a system of equally thick lamellae of thickness d, which will be our unit length. According to the principles developed above, we find the distance function as

$$\psi(l) = (L - l), \qquad \int_1^L \psi(l)dl = \tfrac{1}{2}(L-1)^2.$$

The share of the mutual interference is then given by

$$\Psi = \frac{2}{(L-1)^2}\int_1^L (L-l)\cos\mu l dl$$

$$= -\frac{2}{L-1}\frac{\sin\mu}{\mu} + \frac{2}{(L-1)^2}\frac{\cos\mu - \cos\mu L}{\mu^2}; \quad \mu = \frac{4\pi}{\lambda} d\sin\vartheta.$$

Again, as in the case of (*i*), the formula consists of one term with a long period and one with a very short one, $\cos\mu L$. On the grounds explained above we may neglect the latter. The scattering function is then composed of the scattering of the single lamella $F^2 = \left(\frac{\sin\mu/2}{\mu/2}\right)^2$ and the mutual interference term Ψ which must be multiplied by $(n-1) \doteq n$. Introducing the coefficient $\epsilon = \frac{n}{L} \doteq \frac{n-1}{L-1}$ which measures the repletion of the space with micelles, we obtain

$$\phi = F^2 \left[1 - 2\epsilon \frac{\sin \mu}{\mu} + \frac{2\epsilon^2}{n} \frac{\cos \mu}{\mu^2} \right] = F^2 \left[\phi_1 + \frac{1}{n} \phi_2 \right].$$

The first term of this expression is due to the individual particle scattering, the second to mutual impenetrability, and the third to the influence of the finiteness of the packing of micelles. The first and second together correspond to the term ϕ_1 in type (*i*) and give a fluid-like curve, naturally without any periodicity, as nothing of like nature has been taken into account at the outset. The minimum-angle scattering is very similar to that deduced by the first method, which seems to prove that the effect is really rather independent of the structure of the packing. For $n \to \infty$, the minimum-angle scattering converges toward zero. With increasing delution, *i.e.*, $\epsilon \to 0$, the scattering curve passes continuously to that of the dilute system, *i.e.*, $\phi \to F^2$.

Now we are but left to consider the variation of the thickness of the micelles by introducing a frequency-function. Then the mutual interference term is given by the integral

$$\Psi = \iint H(x)F(x)H(y)F(y) \cdot x \cdot y \cdot \left[-2\epsilon \frac{\sin \mu(x+y)/2}{\mu} + \frac{2\epsilon^2}{n} \frac{\cos \mu(x+y)/2}{\mu^2} \right] dxdy$$
$$= -4\epsilon XY + \frac{2\epsilon^2}{n}(Y^2 - X^2),$$

if we introduce the following abbreviations:

$$X = \frac{1}{\mu} \int H(x)(1 - \cos \mu x)dx, \qquad Y = \frac{1}{\mu} \int H(x) \sin \mu x dx.$$

The assumption made for the frequency function is, within a wide range, arbitrary. On practical grounds, we shall assume equal frequency between two limits deviating from the mean value by $\Delta = \pm 0.5$. Then we obtain, by a simple calculation,

$$X = \frac{1}{\mu} \left[1 - \frac{\sin \Delta\mu}{\Delta\mu} \cos \mu \right], \qquad Y = \frac{\sin \mu}{\mu} \frac{\sin \Delta\mu}{\Delta\mu}.$$

The scattering of the single micelles gives a mean value of $\overline{F^2} = \frac{2}{\mu} X$. The total scattering curve which again consists of a small-angle and a minimum-angle scattering component is then given by the following expression:

$$\phi = \frac{2}{\mu} X - 4\epsilon XY + \frac{2\epsilon^2}{n}(Y^2 - X^2) \doteq \phi_1 + \frac{1}{n}\phi_2.$$

The result is represented in Fig. 10. Comparison with Fig. 9 shows that the characteristic features of the scattering curve of the micelle-packing have not been touched by our assumption, although this was completely different from that made under (*i*). The curve of the dilute system, F^2, has been drawn in this figure (Curve 1) for comparison; it shows an entirely different shape.

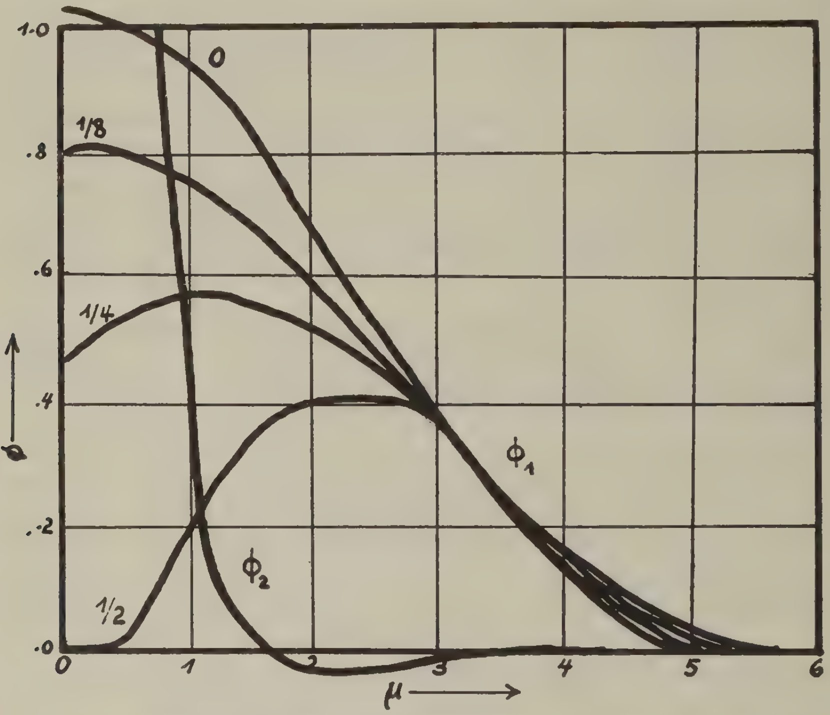

FIG. 10. Scattering of a packing of micelles, type (*ii*). ϕ_1 = small-angle scattering for $\epsilon = \frac{1}{2}, \frac{1}{4}, \frac{1}{8}, 0$, ϕ_2 = minimum-angle scattering for $\epsilon = \frac{1}{2}$.

3. Dependency of Scattering Intensity on Swelling Degree of the Lamella-Packing

(Test in reprecipitated cellulose)

An independent way of verifying the above-mentioned ideas about small-angle scattering is opened by the study of the dependency of the effect on the degree of swelling of reprecipitated cellulose.

Starting from the idea that the swelling process increases all distances equally, it becomes possible to calculate the dependency of the scattered intensity on the swelling. Considering the scattering intensities of differently swollen threads, at the same angle ϑ_0, the intensities correspond, barring other influences, to different points on the scattering curve for $q = 1$. For, as all distances are enlarged in the same ratio, a given swelling (*e.g.*, $q = 2$) causes a certain jigging of the scattering curve in the direction of the abscissa, in the ratio $1/q$ (*e.g.*, $\frac{1}{2}$). Calling the scattering function for $q = 1$ $\phi(\vartheta_0)$, the intensity with a given degree of swelling is $T \propto \phi(q\vartheta_0)$. At the same time, a displacement of the micelle-packings has taken place in the volume through which the beam is passing. Their number has decreased to n/q. Except for the form factor, the dependency of the intensity on the swelling is given by $T \propto \frac{1}{q}\,\phi(q\vartheta_0)$. To consider the influence of the varied form factors, we must introduce a special assumption. As will be shown below, it is reasonable to consider the scattering, in first approximation, as a superposition of micelle-packings of different mean micelle diameters (see p. 29), so that to each angle ϑ_0 there is one definite parcel with a mean central distance D_0 of the micelles. The form factor of the scattering interstices is given by

$$F^2 \propto q^2 \sin^2\left(\frac{\pi}{\lambda}\, D_0\vartheta_0\, \frac{q-1}{q}\right),$$

or, considering that the mean distance D_0 and the angle ϑ_0 must obey Bragg's law, by $F^2 \propto q^2 \sin^2 \pi \dfrac{q-1}{q}$. The connection between intensity and swelling degree is then given by

$$\mathfrak{J} \propto q \sin^2\left(\pi \frac{q-1}{q}\right) \phi(q\vartheta_0).$$

The curve intensity *vs.* swelling degree is thus determined by the orignal scattering curve ϕ and the angle ϑ_0 at which the comparative intensity measurements were taken. It seems reasonable to take for this the angle that corresponds to the most frequently occurring packing of micelles (*i.e.*, the value for which the scattering curve multiplied by ϑ^2 has a maximum (see p. 31)). As shown by Fig. 11, the agreement between the intensity curves found experimentally and the calculated ones is rather satisfactory; the curves do, at least, agree in type and have their maxima at about the same angle. With smaller degrees of swelling, the increase runs almost linear with the swelling, theoretically as well as experimentally. Asking for the intensity while neglecting the micelle-to-micelle interference, we find (with the intensities due to the single micelles at each degree of swelling simply additive) that the "dilution" of the micelles can cause only a decrease of the intensity with $1/q$, which forms a rude contrast to the initial increase (Fig. 11, Curve 2). It is, however, improbable, that with very great swelling degrees the interstices increase uniformly, *i.e.*, maintaining the ratios of the central distances of neighboring micelles. On the contrary, once they have exceeded a certain measure, the central distances will start varying more expressly so that the assumption of a Gaussian fluctuation about an average value is no longer justifiable. The actual conditions will be better met by method (*ii*). The calculation of the swelling dependency cannot, however, be given in a general manner, as it depends on the angle at which we measure the intensity. Anyway, a discussion on the basis of (*ii*) leads to the fact that there is some dependency with $1/q$, with greater angles, a behavior similar to that of the completely dilute system. In fact, the experimental curves are found to approach, for $q > 2$, the limit of the statistically varying packing, or of the dilute system. So we find that an approach to the behavior of the dilute system actually takes place only in those regions where it is to be expected from the standpoint of mutual interference.

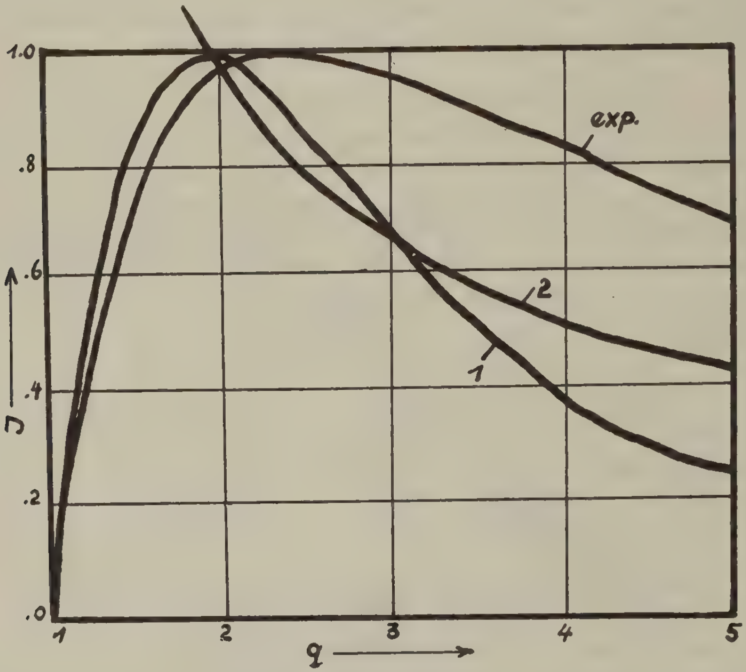

FIG. 11. Reprecipitated cellulose: Scattered intensity *vs.* swelling degree. 1 = theoretical curve for packing of micelles, type (*i*), 2 = theoretical curve for dilute system, type (*ii*).

With smaller degrees of swelling, experiments are convincing that *mutual interference* prevails in the determination of the phenomena.

In the following, an attempt shall be made to test whether or not, in the case of native cellulose and reprecipitated cellulose, the angular dependency of the intensity (with fixed swelling degree) might be understood from our theory of densely packed systems, too.

4. The Scattering of the Native Ramie Fiber

This native cellulose fiber was lightened with a bundle of beams of considerable convergence within the plane defined by the axes of the fiber and of the bundle, the latter being normal to the axis of the fiber.

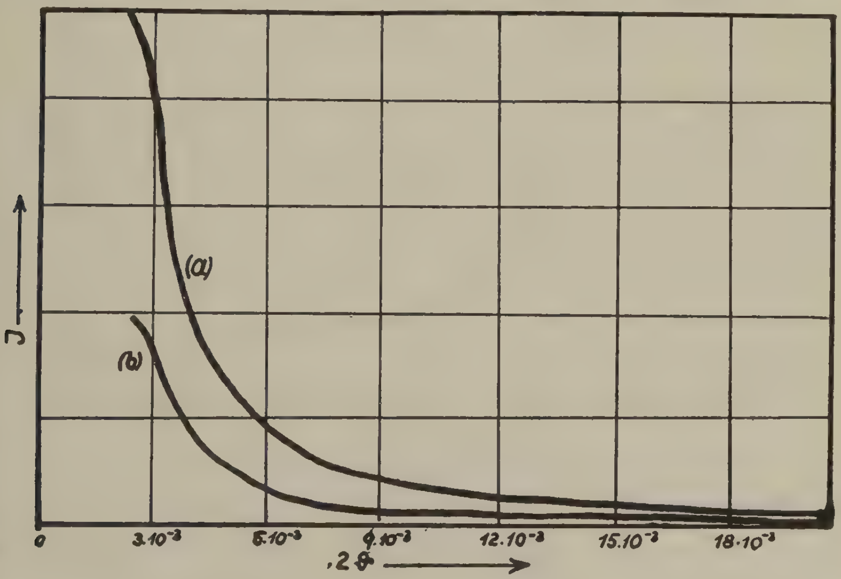

FIG. 12. Photometer curves of the small-angle scattering of ramie-fiber; (a) with nickel filter, (b) with cobalt filter.

This arrangement has proved to be practical for reasons of intensity (26). The obtained scattering curves, which are called "slit-distorted," are then slightly modified as compared with those obtained from a cylindrical beam, as has been shown in detail (1).

The photometer curves of the graphs obtained are shown in Fig. 12. According to the requirements of the filter difference method (27) used for obtaining monochromatic diagrams, we have made all exposures with nickel and cobalt filters, respectively; the photometer curves had to be transformed to intensities and then to be subtracted. The result is shown in Fig. 13. A quantitative comparison with the above calculations is not at once possible. Firstly, it was assumed there that the plane of the lamellae coincides with the axis of the beam, while in our case the planes of the lamellae may occupy all positions arising from rotation around the axis of the fiber. It may, however, be understood that with lamellae of greater width than length, all other positions than those with the beam in the plane of the lamellae will effect little influence on the total scattering, so that we may compare, in first approximation, with the curve in Fig. 9. It ought to be corrected for slit-distortion, whose effect upon the curve ϕ_2 is, however, hardly noticeable. Trying to interpret our results in this way, we may say that:

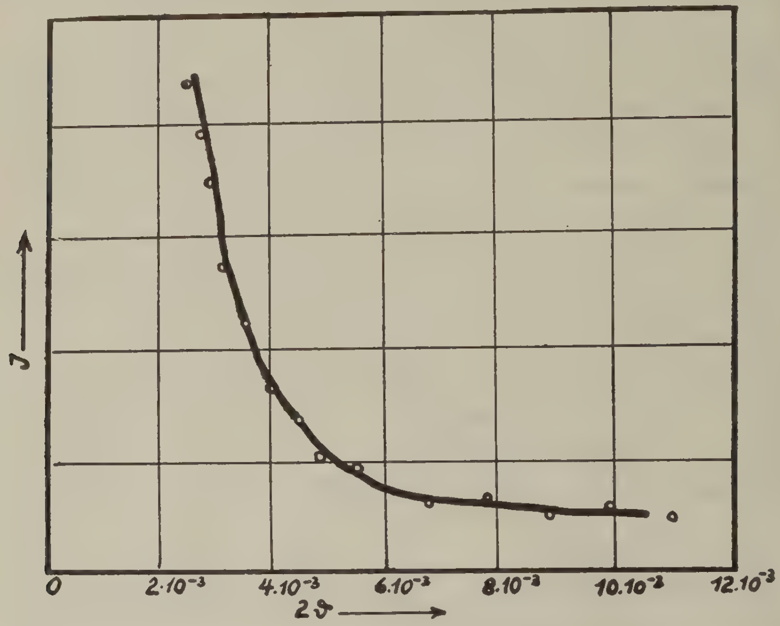

FIG. 13. Monochromatic small-angle scattering of ramie. ——— = theoretical curve (ϕ_2, minimum-angle scattering from Fig. 9), ○○○ = experimental points.

(a) There is a scattering rapidly increasing toward small angles which we would interpret as minimum-angle scattering in terms of the theory expounded above. A quantitative comparison gives rather satisfactory agreement of the curves in shape (Fig. 13). The following relation is found

$$2\vartheta = 4\cdot10^{-3}, \qquad \mu = 1,$$

whence we may infer

$$d_0 = 61\ \text{Å},$$

i.e., an average for lamella + interstice which may be considered reasonable also on the basis of other information, particularly the measurements of line-broadening by Hengstenberg and Mark (33). Interpretation under neglect of the mutual interference (Curve 2, Fig. 9) would lead to a value of about 200 Å, which is certainly much too high.

(b) The small-angle interferences theoretically to be expected (*i.e.*, maxima in the region of the Bragg angle) do not appear. A plausible explanation might be given as follows: According to the relation laid down on p. 22, the high intensity of the small-angle scattering points to smaller packings of lamellae which appear to be limited by their histological structure. It seems reasonable that the individual packings do not yet represent a total average as regards the mean diameter of the single micelles, so that each packing may have its small-angle maximum at another point. It might be assumed, then, if we consider the slit-distortion and the multitude of different positions of the lamellae, which also have a flattening influence, that there really results only a uniform background, increasing toward small angles.

This view is supported by the fact that there is, with sufficiently long exposure times and thicker beams, a considerable small-angle scattering also with greater angles, particularly with those angles for which Figs. 12 and 13 (Curve 1) already show a slight increase. If we assume, as above, that this part of the scattering is to be considered as the superposition of numerous maxima, we may deduce a frequency distribution of these interferences and, therefore, a frequency distribution of the different lamella diameters. We must, however, bear in mind that the interferences become crowded as the angle of deflection increases, for the interval of lattice-plane distances covered by a certain range of the half angle of deflection, $d\vartheta$, is the larger the smaller is the angle ϑ itself. This will be immediately recognized by forming $\frac{dD}{d\vartheta}$ from the equation $\lambda = 2D\vartheta$ which holds at least approximately for the position of the single maxima. Differentiation of this simplified Bragg law leads to

$$0 = D d\vartheta + \vartheta dD,$$

whence we infer

$$\frac{dD}{d\vartheta} = -\frac{D}{\vartheta} \propto \frac{1}{\vartheta^2}.$$

The range of lattice-planes which has to be assigned to a given interval of ϑ is thus found to increase with $1/\vartheta^2$. This crowding of the reflections toward small angles implies, of course, that the intensity given by the scattering curve for the different values of ϑ is not a direct measure for the frequency of the D values assigned to them by $\lambda = 2D\vartheta$. If we wish to obtain such a frequency curve for the different values of D, we obviously must plot the scattered energy $\mathfrak{J}_\vartheta d\vartheta$ belonging to each interval $d\vartheta$ in the corresponding interval dD:

$$\mathfrak{J}_\vartheta d\vartheta = \mathfrak{J}_D dD,$$

$\mathfrak{J}_\vartheta$ and $\mathfrak{J}_D$ meaning the intensity for the scattering curve and the "intensity" of the frequency curve, respectively. Now dD is proportional to $1/\vartheta^2$ under the above equation, thus

$$\mathfrak{J}_D \propto \mathfrak{J}_\vartheta \vartheta^2,$$

which means that we should have to multiply the $\mathfrak{J}_\vartheta$-curve by ϑ^2 and plot the intensity values thus obtained linearly *vs.* the corresponding values of D. Proceeding in this way, we always obtain curves with a maximum at $D \doteq 60$ Å (5) [4] which agree rather satisfactorily with the values calculated from the minimum-angle scattering so that the given deduction seems reasonable.

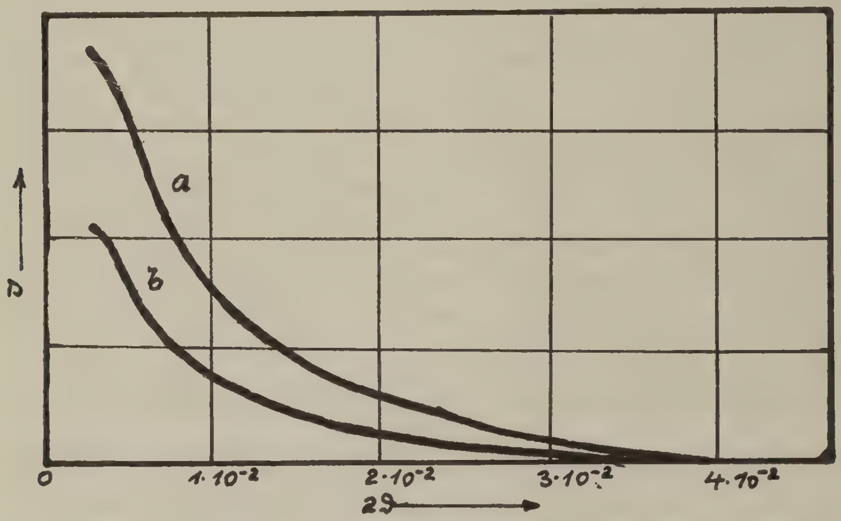

FIG. 14. Photometer curves of the small-angle scattering of reprecipitated cellulose; (a) with nickel filter, (b) with cobalt filter.

The above deduction [which has been given a long time ago (5)] seems to receive a better foundation from the exact theory of the packing of lamellae.

5. *Scattering of Reprecipitated Cellulose* (*Viscose*)

The experimental set is the same as with the experiments on ramie. The evaluation of the photometer curves (Fig. 14) leads to Fig. 15. Comparing with ramie, we find two fundamental differences:

(a) The small-angle scattering at relatively greater angles is more intense than with ramie, for about one order of magnitude (*cf.* Figs. 13, 15).

---

[4] As regards this experimental statement, Hosemann (10), too, agrees with us, although drawing completely different conclusions from this fact.

(b) The minimum-angle scattering, *i.e.*, the rapid increase towards very low angles, is missing. To understand this, we must consider two differences in the finer structure.

First, with reprecipitated cellulose, the interstices occupy a much greater percentage of the total volume. Whereas, in ramie, only 2 or 3% of the total volume is to be considered as interstices, we have to assume a figure of about 15 or 20% in the case of reprecipitated cellulose. Considering the interstices as the scattering centers under the law of reciprocity, we recognize immediately that we have to expect—*ceteris paribus*—a scattering about one order of magnitude more intense, with reprecipitated cellulose. It can be understood from what has been said above, about the swelling dependency of the intensity, that with interstices essentially smaller than the lamellae the intensity increases about linearly with the interstices (10).

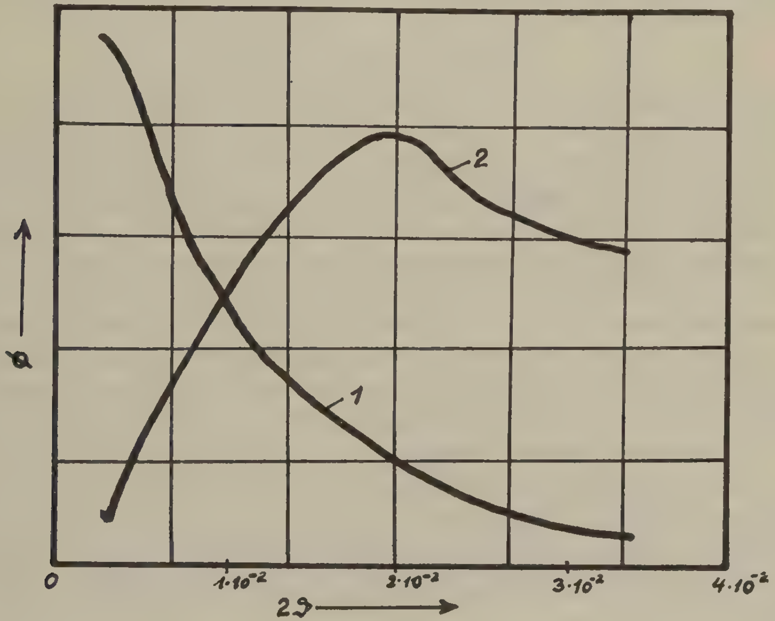

FIG. 15. Monochromatic small-angle scattering of reprecipitated cellulose; 1 = experimental, 2 = curve multiplied by ϑ^2.

Secondly, the ramie fiber is of very regular structure, as it has been grown by nature in contradistinction to the reprecipitated cellulose in which the piling of the individual, leaflet-shaped micelles is a statistical effect, determined chiefly by the form of the particles. Hence we have not, in the latter case, to expect distinguished groups, *i.e.*, definitely limited packings of lamellae. The packing covers, though less regularly constructed and with greater interstices, a much wider region. In the case of ramie, a space of the order of magnitude of a single micelle already causes an interruption of the packing, whereas with reprecipitated cellulose, because of its much "spongier" structure, the same interspace is, for statistical reasons, still of the order of magnitude of the ordinary interstices and thus does not affect the continuity of the packing. Thus, we have to expect a weak *minimum*-angle scattering with reprecipitated cellulose.

Evaluating the small-angle scattering after the same method as with ramie, we also find a curve with distinct maximum at about 80 Å. (Fig. 11).

Here, too, further experiments and theoretical work will have to test and complete this first interpretation.

6. *Scattering of Carbon Black*

According to the investigations of Warren (3), Riley (13), Fankuchen (13), and others, all sorts of soot give a small-angle scattering. Ruess (13) found a maximum at about 20 Å slowly decreasing toward higher angles. We believe that this may be interpreted as small-angle scattering in the above sense, the slow decrease being due, perhaps, to the superposition with maxima situated at higher angles. The conception of lamellae, however, seems not quite suitable to meet the actual conditions, as the single crystallites, according to precise measurements by Ruess, have to be considered as about prismatic, of almost equal height and diameter. Thus, approximation by spheres or flat lamellae would seem almost equally justified. We will, therefore, come back to this object when dealing with the aggregation of spheres, below.

It seems interesting to investigate whether or not there is also a *minimum*-angle scattering with carbon black, *i.e.*, a second increase of the intensity with much smaller angles than those examined by Ruess. The experiments so far made by Ruess do not allow for a decision of this question.

B. THE BUNDLE OF RODS

A very rough consideration has made clear that a bundle of rods should give rise to small-angle interferences very similar to those of the packing of lamellae. In this paper, we shall omit the exact deduction which is a bit complicated, and mention only an experimental result which makes clear the typical behavior. Exposing a bundle of myosin fibers to the ray, three diffuse small-angle maxima are found besides a minimum-angle scattering, as shown by Fig. 16 [from a paper by one of the authors, A. S. Sekora, and H. H. Weber (28)]. Thus, small-angle scattering and minimum-angle scattering are found at the same time. As has been reported in the said paper, the maxima correspond to "lattice-plane distances" of 33, 42, and 66 Å. Now, according to the electron microscope

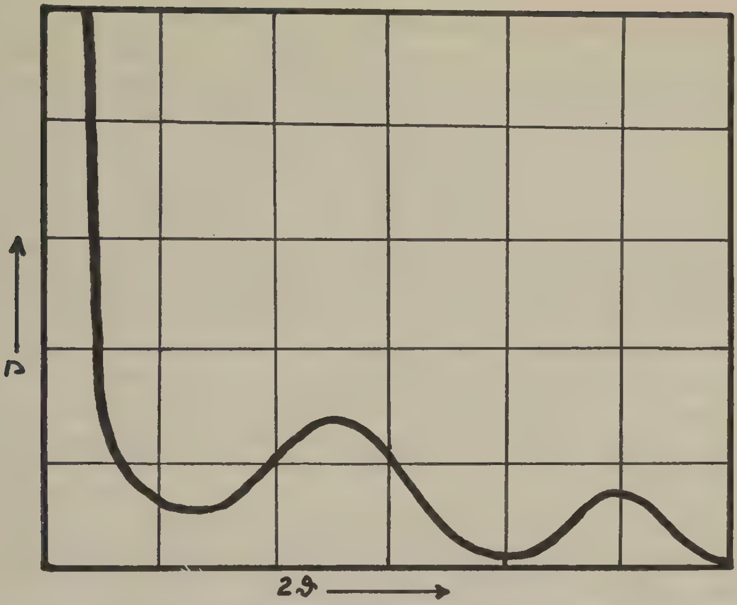

FIG. 16. Scattering curve of expanded actomyosin.

investigations carried out by H. H. Weber and v. Ardenne (29), dissolved myosin consists of rods of about 50–60 Å diameter. Threads drawn out in precipitating show, according to X-ray results, a fibrous structure, thus obviously being an aggregation of such particles in parallel arrangement. The appearance of interferences corresponding to distances of about the size of the diameter may be interpretable in two ways:

(a) the particles of the myosin have "crystallized," *i.e.*, they have associated to a "super-crystal," at any rate, to an aggregation in which the longish rods are regularly arranged when looked at "edge on." Then equatorial interferences might be expected within the range in which they are actually found.

(b) There is no completely regular arrangement; the thread is to be considered as a more or less regular bundle of rods. The individual rods are of equal diameter, but their mutual distances vary a little. This system gives, as can be shown by a consideration similar to that made with the packing of lamellae, diffuse small-angle interferences—*i.e.*, such as have actually been found—and a minimum-angle scattering which starts increasing at $\frac{1}{3}$ or $\frac{1}{4}$ of the angle of the inmost small-angle reflection, again in agreement with observation.

To us, the latter interpretation appears more probable. It abandons the assumption of a superlattice (which, in other cases, has been found to exist, *e.g.*, in that of the tobacco mosaic virus according to Bernal and

Fankuchen (30), but is unproved in this case), and gives an unconstrained explanation of the minimum-angle scattering. Assuming supercrystals, the minimum-angle scattering could be explained chiefly by holes between those, but it would then have to lie much more inside than observed.

C. THE ACCUMULATION OF SPHERES

It has already been pointed out, when dealing with the packing of lamellae, that the neglect of mutual interference may be proved absurd by using the theorem of reciprocity. Now the argument might be raised against such consideration that the packing of lamellae is a special case, as treated by Hosemann and others, and that additional examination should be required to decide whether we could not neglect the mutual interference with globular particles. The aggregation of spheres seems an apt object for this further examination. We shall base the calculation on the following assumptions:

(1) Picking out pairs of immediately touching spheres, we find the combinations of a sphere of given diameter with spheres of all other sizes determined by the overall frequency of the given diameter.

(2) All distances greater than the minimum distance between two spheres of given sizes (which is the sum of the radii) shall be realized with equal probability. The distance function of two spheres of given sizes with radii r_1 and r_2, respectively, has then a constant value from that minimum distance on (Curve 2, Fig. 8). Thus the wave character of the probability curve to which we are accustomed from the structure of fluids (31) has not been regarded.

As concerns this second (not exactly true) assumption, it may be noticed that the mere existence of spheres much different in size would certainly flatten the waves of the distance function of, say, one-atomic fluids. Should this neglect influence our result at all, then it would be only in the way of neglecting a part of the mutual interference. That is to say, in our deduction only the mutual impenetrability of the spheres has been taken into consideration. The introduction of an exact distance function, however, could only increase the mutual interference effect, but never weaken it!

We assume the frequency distribution of the radii of the different spheres to be of Maxwellian type: $H(x) = \frac{4}{\sqrt{\pi}} x^2 e^{-x^2}$, $x = r/r_0$ meaning the radius expressed in terms of the most frequent radius r_0. It is advantageous to approximate the form factor of the sphere as suggested by Guinier (4):

$$F(x) = e^{-1/10\mu^2 x^2}, \qquad \mu = 4\pi \frac{r_0}{\lambda} \sin \vartheta.$$

The scattering consists of three components which may be calculated separately:

(1) The scattering ϕ_0 of the single spheres, *i.e.*, a superposition of the intensities which will obviously give a Gaussian curve.

(2) The mutual interference of all spheres, which must give zero if the volume is assumed to be filled at random, none of its parts being particularly favored.

(3) The intensity due to the interferences of those combinations of spheres which are excluded by their mutual impenetrability. The share of two spheres with radii x and y, respectively, in this term, is then given by

$$\frac{v_0}{V}(x+y)^3F(x+y), \qquad v_0 = \frac{4\pi r_0^3}{3}.$$

Because of its complicated form, the deduction will be given in principle only:

$$\phi_0 \propto \int_0^\infty NH(x)v_0^2x^6F(x)dx = Nv_0^2\cdot\frac{3\cdot5\cdot7}{8}(1+0.2\mu^2)^{9/2}$$

$$\phi_1 \propto \int_0^\infty\int_0^\infty NH(x)v_0x^3F(x)\cdot NHyv_0y^3F(y)\cdot\frac{v_0}{V}(x+y)^3F(x+y)\,dxdy$$

$$= Nv_0^2\cdot\frac{3\cdot5\cdot7}{8}\frac{200}{7\sqrt{\pi}}N\frac{v_0}{V}\left(1+\frac{0.02\mu^2}{5+\mu^2}\right)(1+0.3\mu^2)^{-7}(1+0.2\mu^2)^{-\frac{1}{2}}.$$

To normalize the curves for the value $\phi_0(0) = 1$, we divide by the factor $Nv_0\cdot\frac{3\cdot5\cdot7}{8}$ and put

$$\phi_0 = (1+0.2\mu^2)^{-\frac{9}{2}}, \quad \phi_1 = \left(1+\frac{0.02\mu^2}{5+\mu^2}\right)(1+0.3\mu^2)^{-7}(1+0.2\mu^2)^{-\frac{1}{2}};$$

$$\phi = \phi_0 - \frac{200}{7\sqrt{\pi}}N\frac{v_0}{V}\phi_1 \qquad \text{(Fig. 17).}$$

The coefficients of the second term may be brought into a more evident form by the introduction of an average impenetrability volume Ω and the coefficient $\epsilon = \frac{\Omega}{V}$. Ω shall be defined as the sum of all spheres of impenetrability surrounding a sphere on the average.

$$\Omega = Nv_0\frac{16}{\pi}\int_0^\infty\int_0^\infty (x+y)^3x^2y^2e^{-x^2}e^{-y^2}dxdy = \frac{26}{\sqrt{\pi}}Nv_0.$$

Then we obtain

$$\phi = \phi_0 - \frac{100}{91}\epsilon\phi_1, \qquad \frac{100}{91} = 1.10.$$

Fig. 17 shows the resulting scattering curves for several values of ϵ.

From this result, it seems to be evident that, also in the case of the *aggregation of spheres*, mutual interference must *not* be neglected because of the density of the packing.

Returning, once more, to carbon black, we recognize that the behavior found by Ruess (13) could be immediately explained as the interference of a dense aggregation of spheres. At any rate, there is one common feature in both interpretations, as aggregations of spheres and as packing of lamellae, *i.e.*, that the mean dimension of the sphere of impenetrability may be roughly inferred from the angle of maximum intensity under Bragg's law, as has already been assumed by Ruess.

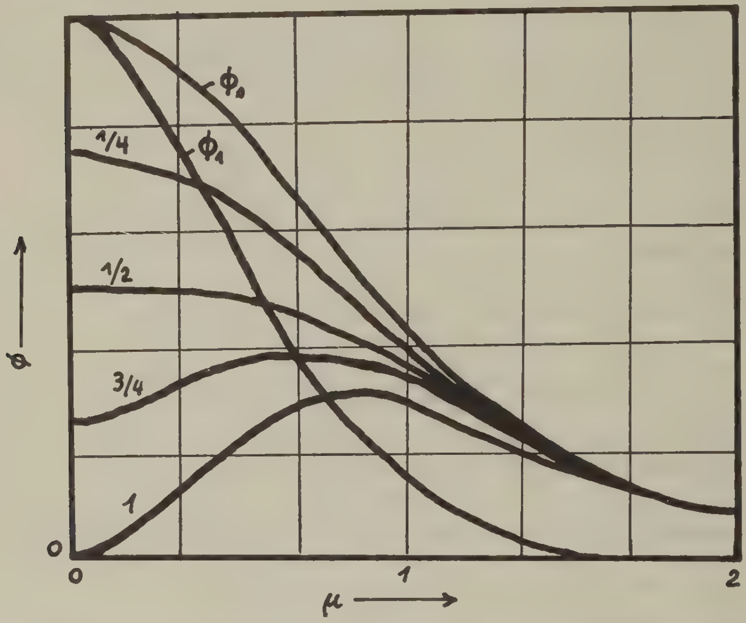

FIG. 17. Theoretical scattering curves of the aggregation of spheres at different degrees of space-repletion; $\epsilon' = 50/7$. $\epsilon = \frac{1}{4}, \frac{1}{2}, \frac{3}{4}, 1$.

D. COMPARATIVE TREATMENT OF DENSELY PACKED SYSTEMS

The above investigations on densely packed systems prove that there are fundamental differences from the dilute system. Thus in addition to the scattering of the individual particles which will always be present and forms, in itself, the scattering of the dilute system, a component appears due to mutual interference the intensity of which corresponds to the density of the packing. Three effects must be distinguished in this mutual interference component:

1. The Effect of Mutual Impenetrability. It is due to the fact that no central distances smaller than the sum of the diameters of the scattering bodies can occur. This effects a diminishing influence upon the scattering curve; hence the characteristically small intensities given by fluids at small angles (*cf.* Figs. 9, 10, 17).

2. The Effect of Regular Arrangement. With a dense packing of any kind of particles, certain distances must occur in a particularly distinguished measure, others being highly improbable. There is a certain analogy to the structure of fluids in this (quasicrystalline arrangement), and therefore the angles of maximum intensity are found to obey Bragg's law. Contrarily to the first effect, this second one need not invariably appear. It is favored by uniform size and shape of the particles (*cf.* the packing of micelles).

3. The Effect of Finiteness. The existence, within a colloid system, of definitely limited aggregations of particles of not too great extension gives rise to a scattering with still lower angles ("minimum-angle scattering," *cf.* the packing of micelles, Figs. 9 and 10).

A minimum-angle scattering appears in the calculations of Debye (32); this is, however, dependent upon the total dimensions of the system and moves toward smaller angles as the total extension of the system increases, whereas our minimum-angle scattering is, in first approximation, dependent only on the size of the individual particle and not on that of the whole system (diameter of the packing of micelles or rods). Only the intensity varies with the size of the whole system, *i.e.*, oppositely to it.

Whereas, with the dilute system, the shape of the scattering curve is directly connected with the shape and size of the individual particle, the scattering curve of the densely packed system gives evidence chiefly of the arrangement of the particles and one of their mean dimensions, their shape effecting only a secondary influence upon the curve. Indirectly, however, clear statements may of course frequently be made as to shape, since the type of the system itself is dependent on the form of the particles (packing of lamellae, aggregation of spheres, *etc.*).

If particles deviating from the ideal spheroidal form are oriented (*e.g.*, in the case of a fibrous structure or leaflet-shaped micelles in higher orientation—foil structure), their shape may be deduced directly from the different scattering behavior of the system with different directions of the incident beam. A good example is offered by reprecipitated cellulose in higher orientation (7).

SYNOPSIS

It is shown that the general cause of diffuse small-angle scattering of X-rays, considering only coherent scattering and barring total reflection, are material inhomogeneities of colloidal dimensions. Three types are distinguished: External small-angle scattering, scattering of dilute systems, and scattering of densely packed systems. External scattering is found, *e.g.*, when a beam penetrates only a thin outer segment (or surface layer) of cylindrical samples, because of strong absorption. It is to be considered as the "small-angle scattering of the single particle." Small-angle scattering of dilute systems is spoken of when the individual particles have distances from each other great as compared with their own dimensions. The theoretical problem lies in the calculation of the intensity scattered by the single particle, and the summation over all angular positions, in case of nonspheroidal particles. A short review is given of three methods allowing for the exact calculation of the scattering curves for differently shaped particles. Low-angle scattering of densely packed systems is spoken of when the distances of the particles from each other are of the same size as, or smaller than, the particles themselves. Then, contrary to the view held by several authors, the mutual interference of the waves scattered by the individual particles must be considered. The importance of this mutual interference is proved in three examples, *i.e.*, the packing of lamellae, the bundle of rods and the aggregation of spheres. A packing (limited in its total extension) of lamellae with varying thickness and distance, which is certainly realized approximately in many natural fibrous substances (cellulose, silk-fibroin, keratin, *etc.*) leads, theoretically, to a flat maximum at about the Bragg angle that would correspond to the average central distance of two neighboring micelles (small-angle scattering), and furthermore to a minimum-angle scattering setting in at still much smaller angles and then rapidly increasing toward the primary beam. The dependency of the scattered intensity on the swelling degree found experimentally can be interpreted on this basis (initial increase proportional to the degree of swelling, maximum with swelling of about 100% and slow decrease beyond that), whereas, if the mutual interference is neglected, the curves should decrease with the reciprocal swelling degree from the very beginning. Data on the angular dependency of the scattering in ramie fibers and reprecipitated cellulose may be understood from this standpoint. It is assumed that the superposition of numerous sharp maxima in the small-angle range leads to a slow increase. It is possible, on this basis, to derive a rough frequency distribution of the micelle diameters which agrees, on the one side, approximately with the values suggested by other measurements, and with the minimum-angle scattering found experimentally, on the other. Here, again, the interpretation is made with neglect of the mutual interference which would lead to incorrect results. Also the measurements of Ruess on carbon black might be interpretable in this way. The finite bundle of rods suggests similar results. Previous experiments of the authors with myosin threads show, at the same time, a minimum-angle scattering and diffuse small-angle maxima. The interpretation as bundles of rods is discussed. Also the mathematical treatment of the infinite aggregation of spheres makes recognizable an influence of the mutual interference in a weakening of the scattering with very low angles.

A comparison of the behavior of all these types of densely packed systems shows that, in all cases, the mutual interference causes three kinds of effects:

(1) The effect of the mutual impenetrability of the particles (weakening of the intensity with small angles, possibly leading to a maximum at medium angles).

(2) The effect of orderly arrangement (may lead to maxima at about the Bragg angles).

(3) The effect of the finiteness of the whole system (leading to minimum-angle scattering, the angular dependency of which gives evidence of the size of the *particles*, the intensity increasing with decreasing extension of the *whole system*).

REFERENCES

1. KRATKY, O., *Monatsh.* **76**, 325 (1947); *J. Polymer Sci.* **3**, 195 (1948).
2. KRATKY, O., AND POROD, G., *Acta Phys. Austriaca* **2**, 133 (1948).
3. KRISHNAMURTI, P., *Indian J. Phys.* **5**, 473 (1930); MARK, H., Physik und Chemie der Zellulose, p. 139. Springer, Berlin, 1932; HENDRICKS, S. B., *Z. Krist., Mineral. Petrog. A* **83**, 503 (1932); WARREN, B. E., *J. Chem. Phys.* **2**, 551 (1934); *Phys. Rev.* **49**, 885 (1936).
4. GUINIER, A., Thèses Serie A, Nr. 1854, Univ. Paris, 1939; Compt. rend. **204**, 1115 (1937); *Ann. Physik* **12**, 161 (1939).
5. KRATKY, O., *Naturwissenschaften* **26**, 94 (1938); **30**, 542 (1942).
6. GUINIER, A., *J. chim. phys.* **40**, 133 (1933); BUSSET, H., DEVAUX, J., AND GUINIER, A., *Compt. rend.* **216**, 152 (1943).
7. KRATKY, O., SEKORA, A., AND TREER, R., *Z. Elektrochem.* **48**, 587 (1942); KRATKY, O., Kolloidchem. Taschenbuch, p. 132. Akad. Verl. Ges., Leipzig, 1943. Remarks to a lecture by R. HOSEMANN, *Z. Elektrochem.* **46**, 535 (1940).
8. KRATKY, O., AND SEKORA, A., *Naturwissenschaften* **31**, 46 (1943).
9. KRATKY, O., SEKORA, A., AND FRIEDRICH-FREKSA, H., *Anz. Akad. Wiss. Wien, Math.-naturw. Klasse*, Mar. 7 (1946).
10. KRATKY, O., AND WURSTER, A., *Z. Elektrochem.* **50**, 249 (1944).
11. POROD, G., Ph.D. Thesis, Univ. Graz, 1947; *Acta Phys. Austriaca*, 4th and 5th commun., in press (since Sept. 1947).
12. HOSEMANN, R., *Z. Physik* **113**, 751 (1939); **114**, 133 (1939); *Z. Elektrochem.* **46**, 535 (1940).
13. FANKUCHEN, I., AND MARK, H., *J. Applied Phys.* **15**, 364 (1944); JELLINEK, M. H., AND FANKUCHEN, I., *Ind. Eng. Chem.* **37**, 158 (1945); JELLINEK, M. H., SALOMON, E., AND FANKUCHEN, I., *Ind. Eng. Chem.* **18**, 172 (1946); JELLINEK, M. H., AND FANKUCHEN, I., *Phys. Rev.* **67**, 201 (1945); SALOMON, E., AND JELLINEK, M. H., *Rev. Sci. Instruments* **15**, 348 (1944); RILEY, D. P., Proc. Conference Ultrafine Structure of Coals and Cokes, p. 232. B.C.U.R.A., London, 1944; RUESS, G. L., *Monatsh.* **76**, 253 (1947).
14. DONNAY, J. D. H., AND SHULL, C. G., *Am. Soc. X-Ray Electron Diffraction* **1**, 111 (1946); NOWACKI, W., *Schweiz. Chem.-Ztg. u. Tech.-Ind.* **29**, Nr. 14/15 (1946).

15. Bauer, S. H., *J. Chem. Phys.* **13**, 450 (1945).

16. Shull, C. H., and Roess, L. C., *J. Applied Phys.* **18**, 295 (1947); Roess, L. C., *J. Chem. Phys.* **14**, 695 (1946).

17. Jordan, P., Eiweiβmoleküle. Wissenschaftl. Verlagsges., Stuttgart, 1947.

18. Szent Györyi, Chemistry of Muscular Contraction. Academic Press, Inc., New York, 1947.

19. Astbury, W. T., *Proc. Roy. Soc. London* **134B**, 303 (1947); *Nature* **160**, 388 (1947); Astbury, W. T., Perry, S. V., Reed, R., and Spark, D. C., *Biochim. et Biophys. Acta* **1**, 370 (1947).

20. Burgeni, A., and Kratky, O., *Z. phys. Chem.* **4B**, 401 (1928); Kratky, O., and Mark, H., *ibid.* **36B**, 129 (1937); Baule, B., Kratky, O., and Treer, H., *ibid.* **50B**, 255 (1941).

21. Kratky, O., *Kolloid-Z.* **68**, 347 (1934); P. H. Hermans, Contribution to the Physics of Cellulose Fibers. Elsevier Pub. Co., Inc., New York, 1946.

22. Kratky, O., *Z. phys. Chem.* **5B**, 297 (1929); Kratky, O., and Kuriyama, S., *ibid.* **11B**, 363 (1931).

23. Astbury, W. T., and Sisson, W. A., *Proc. Roy. Soc., London* **150A**, 533 (1935); Nowotny, H., and Zahn, H., *Z. phys. Chem.* **51B**, 265 (1942).

24. Mark, H., and Susich, G. v., *ibid.* **4B**, 431 (1929).

25. Zernicke, F., and Prins, J. A., *Z. Physik* **41**, 184 (1927).

26. Kratky, O., *Z. Krist., Mineral. Petrog.* **76A**, 261 (1930).

27. Ross, P. A., *J. Optical Soc. Am.* **16**, 433 (1928); Wollan, E. O., *Phys. Rev.* **43**, 955 (1933); Hoffmann, K., *Physik. Z.* **39**, 695 (1938); Kratky, O., *Naturwissenschaften* **31**, 325 (1943).

28. Kratky, O., Sekora, A., and Weber, H. H., *ibid.* **31**, 91 (1943).

29. Ardenne, M. v., and Weber, H. H., *Kolloid-Z.* **97**, 322 (1941).

30. Bernal, J. D., and Fankuchen, I., *J. Gen. Physiol.* **25**, 11, 147 (1941).

31. Prins, J. A., *Z. Phys.* **56**, 617 (1929); Mark, H., *ibid.* **54**, 505 (1929); Debye, P., and Menke, H., *Physik. Z.* **31**, 797 (1930); Menke, H., *ibid.* **33**, 393 (1932).

32. Debye, P., and Menke, H., Ergebnisse der techn. Röntgenkunde, Vol. II, p. 1. Akad. Verl. Ges., 1931.

33. Hengstenberg, J., and Mark, H., *Z. Krist., Mineral., Petrog.* **69**, 271 (1928).

34. Roess, L. C., and Shull, C. G., *J. Applied Phys.* **18**, 295, 308 (1947).

Mathematical symbols used in the text are in conformance with the tables by Jahnke-Emde, 3rd Ed., B. G. Teubner, Leipzig-Berlin, 1938.

ON THE STATISTICAL THEORY OF RUBBER-LIKE ELASTICITY

Takuzo Sakai and Akira Isihara

From the Faculty of Science, Tokyo University, Tokyo, Japan

Received June 28, 1948; revised December 3, 1948

INTRODUCTION

According to the theories initiated by Kuhn (1), and later elaborated by himself (2) and others (3), the modulus of elasticity of a rubber-like substance at the beginning of elongation is given by

$$\epsilon_0 = f\rho RT/M, \tag{1}$$

where ρ is the density of the substance, R the gas constant, T the absolute temperature, M the molecular weight of one of the elementary chains which constitute the network of the substance, and f a numerical factor which is equal to 3 in ordinary cases. But it was pointed out by James and Guth (4), and independently by one of the present authors (5), that there is another theory according to which the modulus is given by

$$\epsilon_0 = 3\rho RT\lambda_0^2/m, \tag{2}$$

where λ_0 is the original distance between the two ends of a chain divided by the length of the chain, and m the molecular weight of a kinetic unit (or an effective link) of the chain. λ_0 is effectively equal to the natural length divided by the greatest stretched length of the sample. Taking $\rho = 1$, $\epsilon_0 = 10$ kg./cm.^{2}, $T = 300°$K., and $\lambda_0 = 1/8$, we get $m = 120$. This value for m means that the kinetic unit consists of about 2 isoprenes in the case of rubber, and seems plausible. Moreover, the theoretical stress-strain relationship and other results explain the experiments fairly well.

But our theory cited above is not completely satisfactory, since the orientations of the chains are one-dimensional. The case in which there are varying orientations of the chains has been treated by Oti (6), also giving the above result (Eq. 2). But the junctions of the network are assumed to be fixed in space in this theory. The dynamics of the network is developed by James (7) on the assumption that the position of one end of the chain relative to that of the other obeys the Gaussian law of distribution. His result is essentially the same as the above formula (Eq. 2). We shall show here another method, which is based on the principles of statistical mechanics, making no use of the Gaussian law of distribution.

The results are the same as those obtained by James. Discussion of the status of the various theories will be found at the end of this paper.

MATHEMATICAL THEORY

Let r_a be the position vector of the a-th junction. The chain connecting the a-th and the b-th junctions is composed of N_{ab} kinetic units. These kinetic units have various orientations in space. Let $n_{ab}(\omega)$ be the number of those kinetic units, the orientations of which are contained in the solid angle $\Delta\omega$. If we assume that each kinetic unit can take various orientations freely, the number of the complexions of the chain is given by

$$G_{ab} = N_{ab}!\prod_{\omega}(\Delta\omega)^{n_{ab}(\omega)}/\prod_{\omega} n_{ab}(\omega)!, \tag{3}$$

where

$$\sum_{\omega} n_{ab}(\omega) = N_{ab}, \qquad \sum_{\omega} n_{ab}(\omega)\boldsymbol{l}(\omega) = r_b - r_a. \tag{4}$$

Here $\boldsymbol{l}(\omega)$ means the vector which represents the kinetic unit of length l and with the direction belonging to the solid angle $\Delta\omega$. Thus, when the junctions have the positions $r_1, r_2, \cdots, r_a, \cdots$, the number of the complexions of the network is given by

$$G = \prod_{ab} G_{ab}. \tag{5}$$

The product is to be taken over all chains.

Following the usual principles of statistical mechanics, the entropy of the network is given by

$$S = k \ln G. \tag{6}$$

In the case of thermodynamic equilibrium, G takes the maximum value with respect to the variations of $n_{ab}(\omega)$'s and the positions of the free junctions.

Let us first consider the problem of variation with respect to $n_{ab}(\omega)$'s, the junctions being kept fixed in space. By the usual method we obtain

$$n_{ab}(\omega) = \exp(\lambda_{ab}\cos\theta + \mu_{ab})\cdot\Delta\omega \tag{7}$$

from Eqs. 3 and 4. Here θ is the angle between $\boldsymbol{l}(\omega)$ and $r_b - r_a$, λ_{ab} and μ_{ab} are indeterminate multipliers, being determined by the relations:

$$\left.\begin{aligned} |r_b - r_a|/(N_{ab}l) &= \coth\lambda_{ab} - 1/\lambda_{ab}, \\ 4\pi\exp\mu_{ab} &= N_{ab}\lambda_{ab}/\sinh\lambda_{ab}, \end{aligned}\right\} \tag{8}$$

which follow from Eq. 4. Here $l = |\boldsymbol{l}(\omega)|$, the length of the kinetic unit. When $|r_b - r_a|/(N_{ab}l) \ll 1$, λ_{ab} is also small. Thus, we get:

$$\left.\begin{aligned} \lambda_{ab} &= 3|r_b - r_a|/(N_{ab}l) + 0[|r_b - r_a|^3/(N_{ab}l)^3], \\ \mu_{ab} &= \ln N_{ab} - \lambda_{ab}^2/6 + \cdots \end{aligned}\right\} \tag{9}$$

from the above equations.

Substituting Eq. 7 in Eq. 6, we get

$$S = k \sum_{ab} \{N_{ab} \ln N_{ab} - \lambda_{ab} | r_b - r_a | / l - N_{ab}\mu_{ab}\}. \tag{10}$$

The summation is to be taken over all chains.

This equation takes the form:

$$S = -k \sum_{ab} 3 | r_b - r_a |^2 / (2l^2 N_{ab}) + \cdots \tag{11}$$

in the case of Eq. 9, neglecting small quantities.

Now, in the case of thermodynamic equilibrium, the above quantity should take the maximum value with respect to the variations of the positions of free junctions. Thus, we get

$$\sum_b (x_b - x_i)/N_{ib} = 0, \tag{12}$$

and similar equations with respect to y and z coordinates. The summation is to be taken over the junctions which are connected by a single chain to the i-th junction. Here r_i means the position vector of the i-th free junction. Following James (7), the above equation can be written in the form:

$$\sum_j \gamma_{ij} x_j = - \sum_\alpha \gamma_{i\alpha} x_\alpha, \tag{13}$$

where

$$\gamma_{ii} = \sum_{b' \neq i,} 1/N_{ib}, \qquad \gamma_{ij} = -1/N_{ij}, \qquad \gamma_{i\alpha} = -1/N_{i\alpha}. \tag{14}$$

Here i or j designates the number of the free junctions, α that of the fixed junctions, and a or b that which is common to free and fixed junctions. By means of Eq. 12, the equilibrium positions of the free junctions are determined by those of the fixed junctions. The results are the same as those obtained by James on the assumption of the Gaussian law of distribution of the distance between the two ends of the chain.

The physical importance of the fixed junctions is such that they represent the shape of the sample when it is deformed. Actually, the fixed junctions are situated on the surface of the sample. In this sense, it is preferable to call them boundary junctions. They are external parameters, like the volume in the theory of gases.

Let the unit cube of a sample be deformed into a rectangular parallelepiped, the length of its sides being L_x, L_y, and L_z. The coordinates of the boundary junctions are changed proportionally to L_x, L_y, and L_z. As Eq. 3 is linear with respect to x_j and x_α, the free junctions are displaced in the same way as the boundary junctions. It is to be noted that this linear relation holds only to the first approximation, even in the present ideal case.

If the original position of the a-th junction is denoted by the coordinates ξ_a, η_a, and ζ_a, it is displaced into the position $x_a = \xi_a L_x$, $y_a = \eta_a L_y$ and $z_a = \zeta_a L_z$. The entropy per unit volume can be written in the form:

$$S = -k \sum_{ab} 3\{(\xi_b - \xi_a)^2 L_x^2 + (\eta_b - \eta_a)^2 L_y^2 + (\zeta_b - \zeta_a)^2 L_z^2\}/(2l^2 N_{ab})$$

by Eq. 11, where the summation is to be taken over all the chains contained in the unit volume. If we take those chains, each of which consists of the same number of kinetic units, their orientations in space will be distributed uniformly in the original state. Then $(\xi_b - \xi_a)^2$, $(\eta_b - \eta_a)^2$, and $(\zeta_b - \zeta_a)^2$ will be replaced by $r_{ab}^2/3$ in the above summation, where r_{ab} means the original distance between the two ends of the chain consisting of N_{ab} kinetic units. Thus S takes the form:

$$S = -k(L_x^2 + L_y^2 + L_z^2) \sum_{ab} r_{ab}^2/(2l^2 N_{ab}). \tag{15}$$

Now following James and Guth (3), we take into consideration the internal pressure. Assuming the internal energy $U(L_x L_y L_z)$, which depends only on the volume $L_x L_y L_z$, the stress per unit original cross section is given by the equation:

$$\sigma_x = \frac{\partial U}{\partial L_x} - T\frac{\partial S}{\partial L_x} = kTL_x \sum_{ab} r_{ab}^2/(l^2 N_{ab}) - L_y L_z \varphi, \tag{16}$$

where $-\varphi$ means the first derivative of U with respect to $L_x L_y L_z$, and represents the internal pressure. Similar equations hold with respect to the y and z directions. Take the case of a sample stretched uniformly along the x-direction by the amount $L_x = L$, the other sides being free. If we assume that no change in volume occurs, then $L_y = L_z = 1/\sqrt{L}$ and we get:

$$\varphi = kT/L \sum_{ab} r_{ab}^2/(l^2 N_{ab})$$

from the equations concerning σ_y and σ_z similar to Eq. 16. Thus, the tension σ_x becomes

$$\sigma_x = kT(L - 1/L^2) \sum_{ab} r_{ab}^2/(l^2 N_{ab}). \tag{17}$$

Of course, Eq. 16 refers to the principal axes of the stress and strain. We can write the equation in any other system of coordinates. For instance, using the equilibrium equation for the stress, the difference of the internal and external pressures of a thin spherical rubber balloon is expressed by the equation:

$$\Delta p = \frac{2h\epsilon_0}{3\gamma}(1 - 2/\Lambda^4 + 1/\Lambda^6)/\Lambda,$$

where γ is the original radius of the balloon, h its thickness, Λ the ratio of the radius of the expanded sphere against the original radius, and ϵ_0 is the modulus of elasticity defined by Eq. 2.

If m means the molecular weight of the kinetic unit, and ρ the density of the sample, Eq. 17 is written in the form:

$$\sigma_x = \frac{\rho R T \lambda^2}{m}(L - 1/L^2), \tag{18}$$

where

$$\lambda^2 \sum_{ab} N_{ab} = \sum_{ab} [r_{ab}{}^2/(l^2 N_{ab})]. \tag{19}$$

Discussions

(*1*). *Gaussian Distribution.* As shown above, it is not necessary to use the Gaussian law of distribution of the chains as long as we treat the problem as a thermodynamic equilibrium. Gaussian law comes into the problem as the fluctuation of the entropy just as in ordinary problems in statistical mechanics. This is evident from Eqs. 11 and 6. If we suppose that the kinetic units assume the equilibrium configuration but the junctions a nonequilibrium one, then the number of complexions G takes the form:

$$G = \exp[-\sum_{ab} 3|r_b - r_a|^2/(2l^2 N_{ab})], \tag{20}$$

which represents the Gaussian law of distribution of $|r_b - r_a|$. In the paper of James (7), this law is assumed as a starting point. But it is to be noted that this law is the result of the fact that the kinetic units of the chain already have the equilibrium configuration.

(*2*). *Statistical Method.* We wish to make a remark concerning the method of treating the problem, because some confusion seems to exist. Here we have applied Boltzmann's method, the external parameters being the positions of the boundary junctions just as the volume in the theory of gases. In the sense of Gibbs' statistical mechanics, the above method corresponds to the method of the canonical ensemble or, rigorously, the canonical ensemble at constant strain (or volume in the theory of gases). But we can also use the method of canonical ensemble under constant stress (or pressure in the theory of gases). In the latter method, the external parameter is the stress but the strain is variable. Now, when we derived Eq. 2, we used the method of the canonical ensemble at constant strain just as in the present paper, while the method of James and Guth (4) corresponds to the case of the canonical ensemble under constant stress. In general, the two methods give the same thermodynamical functions. James and Guth seem to believe that their treatment corresponds to the case of large elongation, but we think that there is no reason why their results should not be applicable to small elongations.

(*3*). *Kuhn's Theory.* We shall call those theories Kuhn's which lead to formulas of the type of Eq. 1 in the introduction. The characteristic point of this theory is that the molecular weight of the chain enters the formula. We wish to make clear the difference between his theory and ours.

For the sake of simplicity, we take the case that each chain consists of the same number of kinetic units. The factor λ^2 defined by Eq. 18 becomes

$$\lambda^2 = \sum_{ab} r_{ab}^2/(\nu l^2 N^2), \tag{21}$$

where ν means the number of chains per unit volume.

Now r_{ab} is determined by the positions of the boundary junctions in the case of the unloaded state. For instance, r_{ab} is the same for all chains when the network is of regular cubic lattice (7). If the substance is homogeneous and isotropic in the unloaded state, each chain will be equally qualified and r_{ab} will be the same for all chains. Thus, making $r_{ab} = r_0$, λ takes the form

$$\lambda = r_0/(lN), \tag{22}$$

and is equal to λ_0 in Eq. 2.

But in Kuhn's theory there is assumed various kinds of chains which have different values of r_{ab}. The number of that kind of chains which have the value r_{ab} is given by the weight function of the type

$$P(r_{ab}) = A \exp\left[-3r_{ab}^2/(2l^2N)\right]. \tag{23}$$

This number is assumed to be always preserved when the sample is stretched or contracted. The sample is, so to speak, an assemblage of different kinds of molecules. The summation of r_{ab} in Eq. 21 will then be expressed by

$$\sum_{ab} r_{ab}^2 = \nu \int P(r_0) r_0^4 dr_0 / \int P(r_0) r_0^2 dr_0 = l^2 N.$$

The tension defined by Eq. 17 becomes

$$\sigma = \frac{\rho RT}{M}\left(L - \frac{1}{L^2}\right), \tag{24}$$

and the initial modulus is given by Eq. 1.

But, in the present theory, there is no reason to introduce a weight function of the type shown in Eq. 22. r_{ab} is determined by the coordinates of the boundary junctions in the unloaded state, and it is most probable that r_{ab} is the same for all chains. Indeed, it will be true that the chains obey some law of distribution at the moment when the sample is newly prepared. However, after a time lapse, in particular, after the elongations and contractions were repeated in order to obtain the reversible condition, the heterogeneity of the kind mentioned above will disappear by dint of the micro Brownian motions of the kinetic units, and all the chains will be equally qualified. A chain which has a value of r_{ab} at one time will take equally well other values of r_{ab} at other times. This fluctuation may be described by the function defined by Eq. 20, but it does not come into question as long as we treat the problem in thermodynamic equilibrium. It is a matter different from the assumption of heterogeneous constitution expressed by the weight function such as that of Eq. 3. If we can prepare the samples which have a different number of junctions per unit volume, the experimental verification between the two theories will be given.

Acknowledgment

In conclusion we wish to express our hearty thanks to Prof. Victor K. LaMer for his kindness in acquainting us with the pertinent literature and for making suggestions in preparing this paper.

References

1. Kuhn, W., *Kolloid-Z.* **76**, 258 (1936).
2. Kuhn, W., *J. Polymer Sci.* **1**, 380 (1946); **2**, 527 (1947). These papers are not yet accessible to us in Japan. We can only infer their general idea from the following paper. James, H. M., and Guth, E., *J. Chem. Phys.* **15**, 669 (1947).
3. Mark, H., *Chem. Revs.* **25**, 121 (1939); Wall, F. T., *J. Chem. Phys.* **10**, 132, 485 (1942); **11**, 527 (1943); James, H. M., and Guth, E., *J. Chem. Phys.* **11**, 455 (1943); Kubo, R., *Proc. Phys.-Math. Soc. Japan* **17**, 273 (1943).
4. James, H. M., and Guth, E., *J. Chem. Phys.* **11**, 455 (1943).
5. Sakai, T., *Proc. Phys.-Math. Soc. Japan* **17**, 226 (1943).
6. Oti, Y., *Proc. Phys.-Math. Soc. Japan* **2**, 182 (1947).
7. James, H. M., *J. Chem. Phys.* **15**, 651 (1947).

SCATTERING OF LIGHT BY COLLOIDAL SOLUTIONS. INTERPOLATION OF THE OSCILLATORY FUNCTIONS

H. C. van de Hulst

From the Astronomical Observatory, Leiden, Holland

Received November 9, 1948

I. The Use of Complex Amplitudes

If a parallel beam of light is thrown on a colloidal solution, part of it is scattered. In addition, true absorption takes place if the colloidal particles have a finite conductivity, the energy thus absorbed being converted into heat. The scattered light is thrown in all directions, with different intensities and different degrees of polarization forming a characteristic pattern. This *scattering pattern* depends on the relative refractive index, m, of the particles in the medium and on their size with respect to the wavelength. The latter is expressed by the parameter $x = \frac{2\pi r}{\lambda}$. Here, r is the radius of the particles and λ is the wavelength in the surrounding medium (mostly water or air).

Different values of x give different scattering patterns. Consequently, experiments made with polydisperse sols or with light of different wavelengths (*e.g.*, white light) give diffuse patterns. Only recently, with carefully prepared monodisperse sols, have the intricate maxima and minima of the scattering pattern been studied experimentally (1). La Mer calls them higher-order Tyndall spectra.

Theoretically, the problem had been solved in 1908 by Mie and by Debye. It is a straightforward problem in Maxwell's electromagnetic theory of light. A complete analytical solution was given, and has since been repeated by many authors using slightly different notations (2). The solution has a very complicated form, involving Bessel functions and spherical harmonics. It is still a big operation, therefore, to compute the numerical results for one m and x. The same operation must be repeated for any other combination of m and x. The most extensive tables have been computed by Lowan (3); others by Blumer (4) and Holl (5). They give the scattered intensity for scattering angles at intervals of 10° and for several combinations of m and x.

Although great effort has been expended in the construction of these tables, they are by no means complete. Frequently, a particular value is needed that has not been computed, and this must be found by interpolation between the known values. This interpolation is difficult because most scattering patterns show wild intensity fluctuations. The main subject of this paper is to explain a device by which a reliable interpolation can be made.

The important point is that the scattered light has not only a certain intensity but also a certain phase. This is true for any wave motion, like sound, light, alternating current, *etc.* Let us take water waves as an example: their *amplitude* is half the difference in height between a crest and a valley, and their *phase* tells whether we find a crest, a valley, or some intermediate stage at a certain point and time. The amplitude and the phase together are often represented in one complex number, the *complex amplitude.* It is graphically represented as a vector in a plane. In Fig. 1, S is the amplitude and σ the phase. The complex amplitude is the vector OA; its real part is OB $= S \cos \sigma$, and its imaginary part is OC $= S \sin \sigma$. The same complex amplitude is written in one formula as

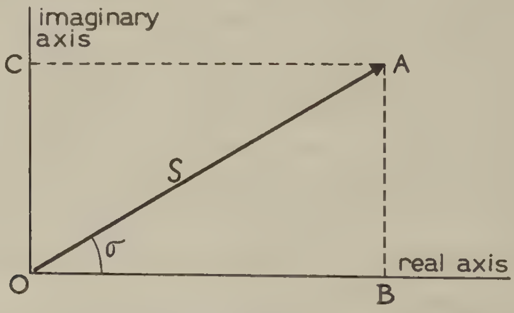

Fig. 1. Graphic representation of a complex amplitude.

$$\Sigma = S\,e^{i\sigma} = S \cos \sigma + iS \sin \sigma. \tag{1}$$

Here e is the base of the natural logarithm (= 2.718 ···) and i is the imaginary unit.

Since light is a transverse wave motion we need two such complex amplitudes, one for each direction of polarization. The publications referred to above give only the *intensities* of the scattered light. The intensities for both directions of polarization are

$$i_1 = S_1^2 \qquad \text{and} \qquad i_2 = S_2^2, \tag{2}$$

i.e., the squares of the amplitudes. Instead, we shall now employ the *complex amplitudes*

$$\Sigma_1 = S_1\,e^{i\sigma_1} \qquad \text{and} \qquad \Sigma_2 = S_2\,e^{i\sigma_2}. \tag{3}$$

The theory of Mie, being a complete solution, gives these complex amplitudes as well as the intensities. Usually, only the intensities are published and the phases neglected. By using the phases also we can make much more reliable interpolations, or discussions of theoretical results, than by using intensities only.

II. Application to Scattered Light

1. *Interpolation with Angle*

As an example of this problem, Fig. 2 gives the curves for $m = 1.33$ and $x = 4.00$. The values of Σ_1 and Σ_2 (*i.e.*, their real parts and their complex parts) were computed for intervals of 10° of the scattering angle, θ. They are represented by circles and dots and the value of θ is written with them. The circle and dot for $\theta = 0°$ (forward scattering) coincide; those for $\theta = 180°$ (back scattering) are opposite with respect to O.

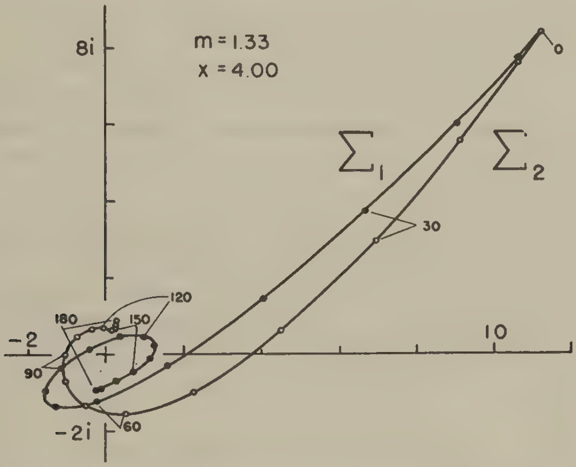

FIG. 2. Theoretical scattering diagram for $m = 1.33$ (refractive index) and $x = 4.00$ $(= 2\pi r/\lambda)$. The complex amplitudes for both directions of polarization are plotted as a function of the scattering angle (0°–180°).

Circles and dots are connected by smooth curves. It is now easy to estimate the points corresponding to any intermediate scattering angle on these curves. Once such a point is found, the square of the distance to the origin is the corresponding intensity, i_1 or i_2.

2. *Red-Green Ratios*

A further illustration is given in Fig. 3. This was constructed in connection with experiments made by Kenyon and La Mer (6). The data in this figure refer to i_1 only. The authors had noticed that the intensity i_1 had the more pronounced maxima and minima of i_1 and i_2. This effect is also seen in Fig. 2: the Σ_1-curve has the more elongated loops of the two curves. The intensity i_1 is measured when a Nicol prism transmitting

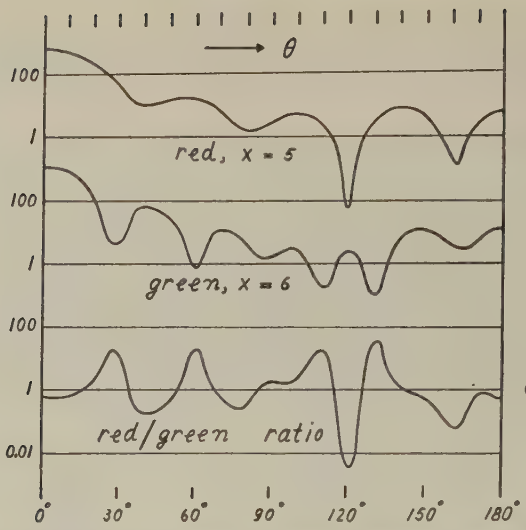

FIG. 3. Diagram showing the scattered intensity (log-scale) *vs.* the scattering angle, for $r = 0.376\mu$, and $m = 1.44$. The distance between two lines represents a factor 10 in S_1, *i.e.*, a factor 100 in i_1.

only vertical vibrations is placed in the incident, or in the scattered beam, or in both beams (both beams being horizontal).

La Mer elected, for practical reasons, to measure the ratios of the scattered intensities in green light ($\lambda = 5240$ Å) and red light ($\lambda = 6290$ Å).

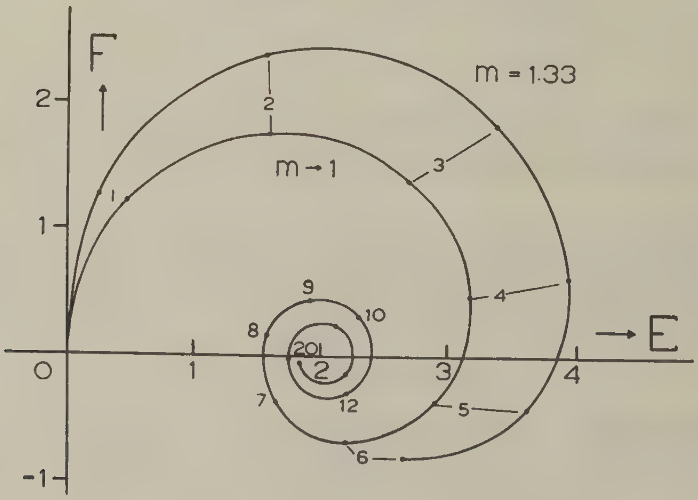

FIG. 4. Curves showing the complex attenuation factor, $E + iF$, as function of the size. Dotted curve: $m = 1.33$; solid curve: m close to 1. Along the curves, values of $2x(m - 1)$.

Since the ratios of these wavelengths is 1.2, there is one size, $r = 0.376\ \mu$, for which $x = 5$ gives the red scattering, while $x = 6$ gives the green scattering. Note that the relation between r and x contains the wavelength in water, which is ⅔ of that in air. The curves of $\log i_1$ for these two values of x are shown in Figs. 3a and 3b, respectively. They have been constructed by using graphs like Fig. 2. The minima are as sharp as the maxima on this logarithmic scale; in a plot of direct intensities only sharp maxima are seen. There was a suspicion that the maxima in green would coincide with the minima in red. This suspicion proves incorrect. The curve of the red/green ratios, obtained by simple subtraction of Fig. 3b from Fig. 3a, is shown in Fig. 3c. Most of its maxima correspond to minima of the green-curve rather than maxima of the red-curve.

3. The Scattering of Incident Polarized Light

The usual experiments are made with incident natural light; i_1 and i_2 are, then, the intensities scattered in the two directions of polarization, and the phases of Σ_1 and Σ_2 are unimportant. However, if the incident beam is plane-polarized, the light scattered in an *arbitrary* direction contains both Σ_1 and Σ_2. In general, elliptical polarization occurs, unless the phase difference, $\sigma_1 - \sigma_2$, is a multiple of π (*i.e.*, 0° or 180°). This result is contained in the Mie solution. We may use a diagram like Fig. 2 to judge how strongly elliptical the light scattered in a certain direction will be. We see there, for example, that no elliptical polarization occurs near $\theta = 80°$ but a fairly strong one near $\theta = 120°$. It is not difficult to derive also the quantitative expressions for the Stokes parameters of the scattered light.

4. Scattering by Large Particles

For particles that are large compared to the wavelength ($x \gg 1$), we can frequently use the laws of geometrical optics. This rule is not quite general. Strictly, we must distinguish 3 regions of the scattering diagram.

(a) A small region near $\theta = 0°$ contains the coronae caused by diffraction around the scattering particle. They depend only on the size, not on the material of the particle. In this region Σ_1 and Σ_2 are equal in amplitude and phase (7).

(b) The further pattern, until close to 180°, follows from geometrical optics. Classical formulae give both the amplitude and the phase, if due account is taken of the phase differences introduced by focal lines in the beams. The result is in complete accordance with the asymptotic forms of the Mie formulae (8). The rainbow theory can be developed in the same way (9). The scattering by fairly large particles has important applications in meteorology and astronomy (10), but many details are still obscure. Here also the complex amplitudes might be used to advantage.

(c) The region near 180° may be described as the region of the glory, or anti-coronae. Here the curve of Σ_2 takes a sudden twist: while the phases σ_1 and σ_2 remained close together for all other angles, they finish at $\theta = 180°$ in exactly opposite directions. Strong polarization effects occur in this region. A classical theory for this region has been given (11), but the quantitative effects are not well understood. Again, the use of complex amplitudes might clarify this problem.

III. Application to the Attenuation

1. *Exact Expression for the Efficiency Factor*

Both the scattering and the absorption by the colloidal particles result in an attenuation of the incident beam. We express the same by saying that the incident beam suffers a certain extinction. The net effect is that each particle screens E times the amount of light that can be screened by its geometric cross-section, πr^2. We call E the efficiency factor of the particle for attenuation (or extinction) and the product $E \cdot \pi r^2$ its attenuation cross-section.

The theory of Mie gives E as a function of m and x. Its formula can be written in the form:

$$E = \frac{4}{x^2} \operatorname{Re}[\Sigma(0)]. \tag{4}$$

Here $\Sigma(0)$ is the common value of Σ_1 and Σ_2 for $\theta = 0$, and the symbol Re means that the real part of this complex number must be taken.

I have found no physical interpretation of this surprising relation between the complex amplitude for forward scattering and the attenuation. It is correct for conductive and non-conductive particles of any size. We can use it to advantage in many problems.

2. *Interpolation in the m-x-Plane*

Each single computation based on Mie's formulae gives the value of E for a single combination of m and x. This combination represents an isolated point in the m-x-plane. The interpolation between these points is difficult since E shows strong and irregular fluctuations. As a general rule, we may state that the use of the complex numbers,

$$E + iF = \frac{4}{x^2} \Sigma(0),$$

enables us to make much more sense of these fluctuations than the use of E alone does.

The particular procedure can be chosen to convenience, depending on the particular part of the m-x-plane (12). Fig. 4 shows the most convenient presentation for the interesting case of small m and fairly large x. The curve of $E + iF$ as a function of the size is here a spiral, spiraling to the final point, $E = 2$ and $F = 0$, for very large particles. The figure shows the spiral for the asymptotic case of m close to 1 and also the beginning of the spiral for $m = 1.33$ (water droplets). In accordance with the theory (13), the running parameter written along the curves is not x but $2x(m - 1)$. The values of the efficiency factor, E, are simply the abscissae of the points on these curves. We read directly that

$$\left.\begin{array}{l} E \text{ has a maximum near } 2x(m-1) = 4.0, \\ E \text{ has a minimum near } 2x(m-1) = 7.5, \textit{ etc.} \end{array}\right\} \tag{6}$$

These formulae are approximately correct for any value of m between 1 and 2, but for $m = 1.50$ (sulfur drops in water), or larger, secondary effects are noticeable. It is clear that Fig. 4 is only an illustration. With more data it can be made into an accurate construction graph permitting exact interpolation and an adequate discussion of the secondary effects.

3. E-Factors for Complex Values of m

Conductive materials in the electromagnetic theory of light have a complex refractive index. The formulae of Mie hold unchanged for conductive particles, but their numerical evaluation becomes even more difficult. It is now—in principle—possible to avoid all calculations with complex values of m until one has derived the values of the complex function, $E + iF$. This function is a so-called analytic function of m (14). By a well-known theorem, the values of this function for any complex value of m can be found, once its values for real values of m are known. The exact procedure is again a matter of convenience, but in practice one may say that any approximation by which $E + iF$ is expressed in an analytic formula for real values of m holds also for complex values of m. All we need, therefore, is some curves like those of Fig. 4, and the rest is a matter of mathematical technique. Lowan and Horenstein (15) developed this method with power series as an approximation. Van de Hulst (16) computed the exact extinction curves for complex values of m close to 1 by essentially the same method.

IV. FORMULAE FOR THE AMPLITUDES

The preceding sections have been written with emphasis on the physical meaning and application, and with omission of most mathematics. In order to avoid confusion I repeat here briefly the formulae by which Σ_1 and Σ_2 are computed. The notation used is that of Ref. 2, parts I and II.

The coefficients, a_n and b_n, are computed by means of I, Eq. 2.7:

$$\begin{aligned} a_n &= \frac{x\psi_n'(y)\psi_n(x) - y\psi_n'(x)\psi_n(y)}{x\psi_n'(y)\zeta_n(x) - y\zeta_n'(x)\psi_n(y)}, \\ b_n &= \frac{y\psi_n'(y)\psi_n(x) - x\psi_n'(x)\psi_n(y)}{y\psi_n'(y)\zeta_n(x) - x\zeta_n'(x)\psi_n(y)}, \end{aligned} \tag{7}$$

where ψ_n, ζ_n, ψ_n', and ζ_n' are the so-called spherical Bessel functions and their derivatives in a conventional notation (I, Eq. 2.8) and $y = mx$.

The complex amplitudes are:

$$\Sigma_1 = \sum_{n=1}^{\infty} \frac{2n+1}{n(n+1)} \{a_n \pi_n(v) + b_n \tau_n(v)\},$$
$$\Sigma_2 = \sum_{n=1}^{\infty} \frac{2n+1}{n(n+1)} \{b_n \pi_n(v) + a_n \tau_n(v)\}. \tag{8}$$

Here $v = \cos\theta$ and π_n and τ_n are the spherical harmonics first introduced by Mie (I, Eq. 2.10):

$$\pi_n(v) = \frac{1}{\sin\theta} P_n^1(v),$$
$$\tau_n(v) = v\pi_n(v) - (1 - v^2)\pi_n'(v). \tag{9}$$

$\Sigma(0)$ is found by the substitution of $\pi_n(1) = \tau_n(1) = \frac{1}{2}n(n+1)$; E follows by means of Eq. 4 (*cf.* I, Eq. 8.5).

Lowan uses Blumer's notation, which in turn is an adaptation of Mie's original formulae. This is, in some respects, an unfortunate choice. The main difference is that the angle γ is measured from the backward direction, while throughout the present paper (as in I and II) we reckon θ from the forward direction. Lowan's choice causes a somewhat confusing alternation in the signs of the coefficients. Further, the factors $(2n+1)/n(n+1)$ plus a factor i or $-i$ were included with Blumer's coefficients. This again obscures some simple properties of a_n and b_n (see I, p. 9 *ff.*).

Let us temporarily mark Lowan's notations by an asterisk (17). Lowan writes α^* instead of our x. By the different choice of angle we have $\gamma^* = 180° - \theta$, so $x^* = -v$; consequently, $\pi_n^* = (-1)^{n+1}\pi_n$ and $\tau_n^* = (-1)^n\tau_n$. Further, the coefficients are

$$A_n^* = \frac{2n+1}{n(n+1)} i^{2n+1} a_n,$$
$$P_n^* = \frac{2n+1}{n(n+1)} i^{2n-1} b_n. \tag{10}$$

Now we find, by comparison with the formulae given above, that the sums computed by Lowan are:

$$\text{first sum} = \sum_{n=1}^{\infty} \{A_n^*\pi_n^* + P_n^*\tau_n^*\} = -i\,\Sigma_1,$$
$$\text{second sum} = \sum_{n=1}^{\infty} \{A_n^*\tau_n^* + P_n^*\pi_n^*\} = +i\,\Sigma_2. \tag{11}$$

For details about notations of other authors see I, p. 13.

Finally, it may be noted that the complex amplitudes Σ_1 and Σ_2 defined in this paper are not identical with those following from the classical formulae of Kirchhoff and Fresnel (for large particles). The latter have an extra factor $-i$ (I, pp. 27 and 35).

SUMMARY

The paper describes a mathematical device useful in the theory of light scattering by colloidal particles. This device is the use of complex amplitudes. It can be applied in many variations, both to simplify computations and to clarify their physical meaning.

The applications treated are: intensity and polarization as a function of the scattering angle, scattering of polarized light, scattering by large particles, attenuation by conductive and nonconductive particles.

The complete formulae are given at the end.

REFERENCES

1. LA MER, V. K., AND BARNES, M. D. *J. Colloid Sci.* **1**, 79 (1946); **2**, 349 (1947); *J. Phys. Colloid Chem.* **52**, 65 (1948); JOHNSON, I., AND LA MER, V. K. *J. Am. Chem. Soc.* **69**, 1184 (1947).
2. A general review (English) of the subject was given by the author in: Recherches Astronomiques de l'Observatoire d'Utrecht, Vol. **11**, parts I (1946) and II (in press). These publications will be referred to as I and II. Some copies of I have been distributed as a separate thesis with the title "Optics of Spherical Particles."
3. LOWAN, A. N., Scattering Functions for Spherical Particles, *Natl. Bur. Standards, (U. S.) Applied Math. Ser.*, 1949. Part of these tables were published earlier in the mimeographed *O.S.R.D. Rep. No.* **1857** by V. K. La Mer.
4. BLUMER, H., *Z. Physik* **32**, 119 (1925); **38**, 304 (1926).
5. HOLL, H., *Optik* **1**, 213 (1946).
6. KENYON, A. S., AND LA MER, V. K., *J. Colloid Sci.*, in press.
7. See Ref. 2, I, pp. 26 and 27.
8. See Ref. 2, I, pp. 34 and 35.
9. VAN DER POL, B., AND BREMMER, H., *Phil. Mag.* **21**, 141, 825 (1937).
10. See KUIPER, G. P., AND others, Planetary Atmospheres, Chapter 3B. University of Chicago Press, 1949.
11. VAN DE HULST, H. C., *J. Optical Soc. Am.* **37**, 16 (1947).
12. See Ref. 2, I, p. 15.
13. See Ref. 2, I, pp. 43–51.
14. *E* alone is not an analytic function, because of the symbol Re in Eq. (4). Hence, the method cannot be applied to *E* alone.
15. LOWAN, A. N., AND HORENSTEIN, unpublished (see Ref. 6).
16. See Ref. 2, II, Section 10.
17. The notations are those of the mimeographed report, see Ref. 3.

A NEW METHOD OF STUDYING MECHANICAL PROPERTIES OF PENETRATED MONOLAYERS

The general use of Langmuir's method (1) of studying mechanical properties of monolayers, is based on the fact that one part of the surface A (Fig. 1) is exerting a pressure on a float, while the other side B, is always kept clean and unchanged during the whole time necessary to carry out the experiments. Therefore, compression curves of insoluble monolayers spread on water can readily be obtained. The mechanical conditions however, are altered when pressures arise on both sides of the float, as always happens in penetration studies.

The interaction of the insoluble monolayer with substances in the underlying solution is generally followed by a rise of pressure P_A of the mixed film at constant area (2), the ejection process of the mixed film at constant pressure P_A, or the compression curve of the mixed film (3). All these experiments require an accurate knowledge of the film pressure P_A.

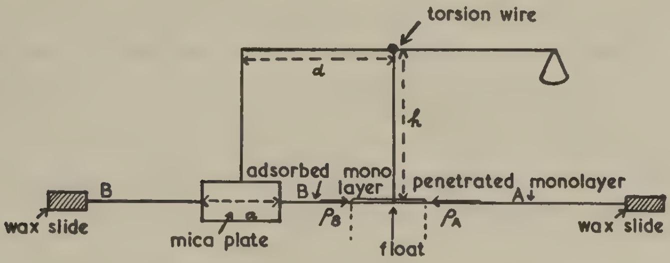

Three methods can be used to allow for the pressure in B due to the adsorbed monolayer of the solute:

(a) Sweeping several times the area B behind the float by waxed slides, so as to remove the adsorbed film of the injected solute. This process is stopped when the movement of the slide toward the float does not alter the position of the latter as shown by the light image on the scale.

(b) Substituting a constant pressure in B to the changing pressure with time of the adsorbed film. This is achieved by the spreading of a piston oil which does not interact with the solute, and the pressure of which is greater than the equilibrium surface pressure of the adsorbed compound in solution.

(c) Measurement of the total pressure acting on the float $P_A - P_B$ and measurement of P_B by a ring or plate attached to a chainomatic balance. From these two measurements pA can be obtained at any moment.

A new method has now been devised which allows for an automatic compensation of the pressure acting on B so that pA can be obtained with penetrated monolayers as readily as with insoluble monolayers on pure water.

To the standard Langmuir apparatus a beam (Fig. 1) is attached to the center of the torsion wire normal to it and in the same horizontal plane. On one side, the beam carries a mica plate cut to the required shape, and treated to make its surface porous, to ensure instantaneous and complete wetting in all solutions. This plate is dipping in the surface B, while on the other side of the beam is set a pan on which weights can be placed to equilibrate the moment of the two forces acting on each side of the beam. When the surface of the trough is perfectly clean $P_A = P_B = 0$.

If the length of the mica plate in contact with the surface is a, its distance to the torsion wire d, w the width of the trough, h the distance between the float and the torsion wire, the system will be in equilibrium for any value of P_B when: $2\,ad = wh$. No pressure will be acting on the float from B when impurity or adsorbed film is present in B, so that the measurement of the pressure of the mixed film or penetrated film, could be carried out by the standard method as used with insoluble monolayers.

A more detailed work will be published on the application of this new method to an investigation of the "penetration" phenomena. The authors are indebted to Mr. L. Saggers for technical assistance in designing and constructing the apparatus.

REFERENCES

1. ADAM, N. K., The Physics and Chemistry of Surfaces. 3d ed., 1941, p. 27.
2. SCHULMAN, J. H., AND RIDEAL, E. K., *Proc. Roy. Soc. London* **122B**, 38 (1937). MATALON, R., AND SCHULMAN, J. H., *Trans. Faraday Soc.* **43**, 479 (1947).
3. SCHULMAN, J. H., STENHAGEN, E., AND RIDEAL, E. K., *Nature* **141**, 785 (1938). SCHULMAN, J. H., AND STENHAGEN, E., *Proc. Roy. Soc. London* **126B**, 364 (1938).

Department of Colloid Science,
The University,
Cambridge, England.

R. MATALON [1]
J. H. SCHULMAN

Received December 10, 1948.

---

[1] Oliver Gatty Student, Cambridge University.

BOOK REVIEW

The Electron Microscope, Its Development, Present Performance, and Future Possibilities. By Dr. D. GABOR, Engineer, British Thomson-Houston Co., Ltd., Research Laboratory, Rugby. Published by Chemical Publishing Co., Inc., Brooklyn, New York, 1948. 164 pp., 50 figs. Price $4.75.

"This monograph is an amplified version of a lecture, delivered on the 4th of March, 1943, before the Cambridge University Physics Society. In its present form it intends to be both an introduction to the electron microscope and a critical contribution to its theory."

The present American edition has been extended to include a number of more recent photographs, and a note of de Broglie's current work on the proton microscope has been added. The chapter headings, "Geometrical Electron Optics," "Electron Wave Optics," "Electron Microscopes without Lenses," "Electron Microscopes of the Transmission Type," "Contrast by Scattering," "The Resolution Limit," "Description of Commercial Electron Microscopes," "Achievements," "The Scanning Microscope," "Possibilities," "Diffraction Theory," indicate the subject matter treated. The book is well written. The author's comment: "the fundamental development of the instrument has now reached a stage beyond which progress is likely to be slow and difficult." It is recommended to those who wish a compact and useful treatment of the theory and uses of this most valuable instrument.

VICTOR K. LAMER, New York, N. Y.

CRYSTAL FORMS OF ANHYDROUS CALCIUM STEARATE DERIVABLE FROM CALCIUM STEARATE MONOHYDRATE [1]

Marjorie J. Vold, Gopal S. Hattiangdi [2] and Robert D. Vold

From the Chemistry Department, University of Southern California, Los Angeles, Calif.

Received December 27, 1948

INTRODUCTION

Calcium stearate, prepared either by direct neutralization of stearic acid with either an excess or a deficiency of calcium hydroxide, or by metathesis between sodium or potassium stearates and calcium chloride, washed free of impurities and dried to constant weight at 105–115°C., has been shown by standard analytical procedures to consist of 100% normal soap, formula $Ca(C_{17}H_{35}CO_2)_2$. Nevertheless, various preparations differ considerably in X-ray diffraction pattern. All of the patterns so far obtained can be resolved into 3 types or mixtures thereof. Two of these are sharp line patterns while the third appears to belong to a relatively noncrystalline structure. It is the purpose of this paper to report the experimental factors leading to the production of each of these states, and to offer a tentative explanation—or rationalization—of the phenomena observed.

EXPERIMENTAL

Materials

Calcium stearate was prepared in this laboratory from 8 independent samples of stearic acid; characterizing analytical data are given in Table I. Over 50 separate samples of calcium stearates were made in investigating the effects of preparative variables. The following procedure was finally adopted as the most satisfactory for preparing pure anhydrous crystalline calcium stearate: To a 5 wt.-% solution of stearic acid in boiling, CO_2-free, 95% ethanol, add sufficient 5% aqueous carbonate-free NaOH to just neutralize the acid to phenolphthalein, and then reacidify with stearic acid solution to give about a 0.5% excess. Add a 5% aqueous solution of $CaCl_2$ (in CO_2-free water) in amount slightly less than required for complete conversion of sodium stearate to calcium stearate, stirring rapidly to prevent local excess of calcium ion, and filter at once. Wash the precipi-

---

[1] This work is part of a project "Phase Studies of Greases" supported by the Office of Naval Research, Contract No. N6-onr-238-T0-2; NR057057.

[2] Present address: National Bureau of Standards, Washington, D. C.

TABLE I

Stearic Acids Used to Prepare Calcium Stearate

Sample no.	Source	Iodine no.[e]	M.P.	Equiv. wt.
			°C.	
A	This laboratory[a]	0.05	68.8–69.5	284.0
4	Neo-fat 1–65[b]	4.5	65–66	287
5	Neo-fat 1–65[b]	4.6	64–66	285
E	Eastman Kodak No. 402	3.0	64–66.5	284
5R1	From Neo-fat No. 1–65 sample 5[c]	0.2	67.5–68	—
5R3	From Neo-fat No. 1–65 sample 5[c]	0.34	—	286.5
5R4	From Neo-fat No. 1–65 sample 5[c]	0.35	69–70	—
6	Technical triple-pressed stearic acid[d]	6.8	—	—

[a] Sample purified from E by Dr. L. L. Lyon, as described in Ref. 4, p. 340.

[b] Acid No. 4 was a 1 lb. sample sent for inspection. Acid No. 5 was a 50 lb. purchase (Armour Chemical Co.).

[c] Samples 5R1, 5R3, and 5R4 were independent purifications of sample 5 by recrystallization from acetonitrile at room temperature, suggested to the authors by Dr. A. W. Ralston, Armour Chemical Co.

[d] Purchased from the Mefford Chemical Co.

[e] Wijs method.

tate with hot water until the filtrate shows no turbidity whatsoever upon addition of $AgNO_3$. Then place the soap in an extraction thimble and steam it at 100°C. for at least 8 hr. Wash off excess water, first with acetone and then with ether, and air dry the product at room temperature. This product is calcium stearate monohydrate. It may be dehydrated (weight loss 2.88%) by heating to constant weight (in air or vacuum) at 90–115°C. to yield the anhydrous soap. If desired, the product may be recrystallized from a solvent containing 15% propylene glycol and 85% chloroform (1) (solubility *ca.* 5% at 50°C., negligible at room temperature, but crystal formation is slow).

Instrumental Techniques

X-ray diffraction patterns for all preparations of anhydrous soap and most hydrates were obtained with a Norelco X-ray spectrometer as described in a previous paper (4). Differential heating curves were obtained on several preparations at a heating rate of 1.5°/min. against white mineral oil (Nujol) as a reference material using the calorimeter also described elsewhere (3,4).

RESULTS

The Existence of $CaStr_2 \cdot H_2O$

The existence of this hydrate had been reported previously (4). However, it was confirmed by regenerating the hydrate by steaming anhydrous calcium stearate and analyzing the air dry product for water content. Found, 2.78–2.99 in six trials; theory 2.88%.

The Polymorphism of $CaStr_2 \cdot H_2O$

All samples of calcium stearate hydrate gave exactly the same X-ray diffraction pattern in so far as the position of the principal lines is concerned. Up to 9 orders are obtained of a spacing somewhat less than twice the length of two stearate ions. This spacing has the numerical value 49.85 ± 0.15 Å for all reasonably pure acids but may be as low as *ca.* 47 Å for technical "stearates" containing significant amounts of palmitate (5). Additional peaks are found, both for pure and technical samples, at *d/n* values of 4.40 ± 0.02 Å, 4.13 ± 0.03 Å, 3.88 ± 0.02 Å, and 3.41 ± 0.02 Å with relative intensities (peak heights) of approximately 1: 0.8: 0.5: 0.4, respectively. A sample diffraction curve is given in Fig. 1, Curve I. In addition, there are many lines of lower intensity which need not be considered for present purposes.

Despite the X-ray diffraction results, there seem to be two varieties of calcium stearate hydrate, since the differential heating curves show a

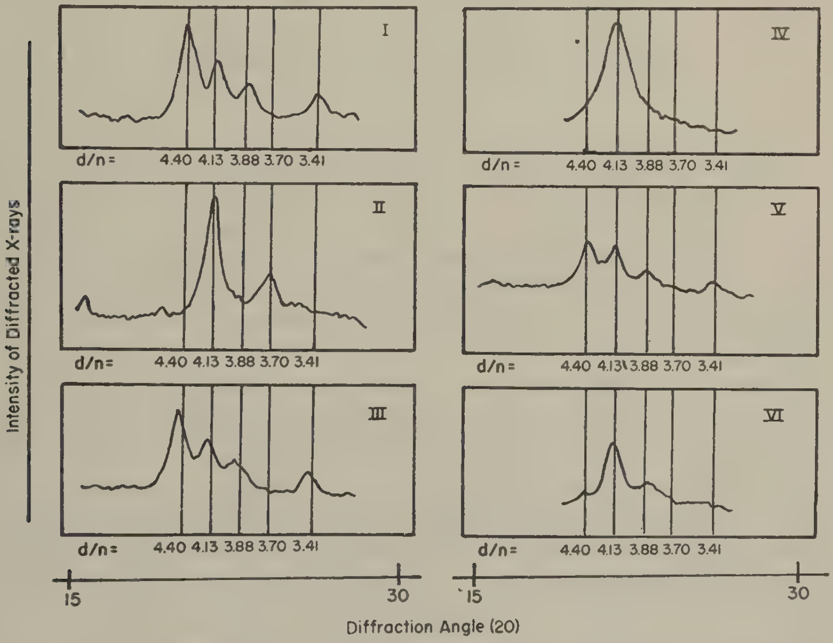

FIG. 1. X-ray diffraction patterns of calcium stearate hydrate and various anhydrous calcium stearates. I. Calcium stearate hydrate. II. Calcium stearate VIA. III. Calcium stearate VIH. IV. Calcium stearate VIN. V, VI mixed patterns. Sample III (made from stearic acid 6 of Table I) has somewhat larger (0.04–0.1 Å) numerical values of the side spacings than are found with samples made from less crude acids.

second order transition [3] at 48°C. for some preparations and not for others. Fig. 2 shows differential heating curves for two preparations of calcium stearate hydrate both made from stearic acid 5R4. One of these (Curve I) exhibits a transition of the second kind (increase in heat capacity) at 48°C. Both undergo a further transition (also accompanied by vaporization of water) at 125° ± 2°C.

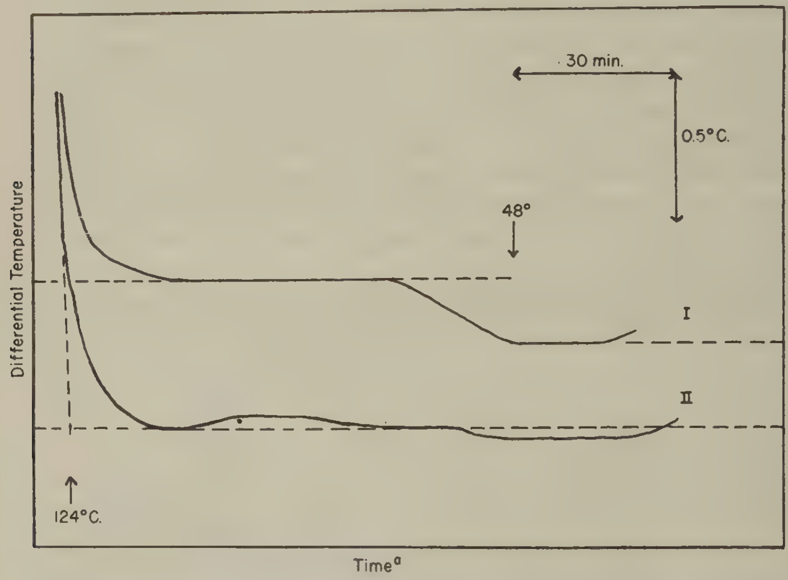

FIG. 2. Differential heating curves of calcium stearate hydrates. I. Sample yielding anhydrous calcium stearate VIA. Note second order transition at 48° as well as first order transition at 124°. II. Sample yielding anhydrous calcium stearate VIH.

a. Proportional to sample temperature, which is read off an auxiliary automatic record.

The designation of 48°C. as the temperature of a second order transition in calcium stearate hydrate from Curve I of Fig. 2 follows unambiguously from the theory of differential thermal analysis developed by one of us (3). The temperature difference at steady state conditions between two materials of the same heat conductivity is proportional to their difference in heat capacity. When the heat capacity of the sample changes abruptly, as in the present case at 48°C., a new steady state temperature difference is established. The differential heating curve consists of two flat segments. The sample temperature where the change from one to the other begins on heating is that of the second order transition. The sample temperature when the new steady state becomes established depends on the thermal characteristics of the calorimeter and the heating rate, and is not a property of the sample itself.

---

[3] The term second order transition is used in its original sense as one for which the latent heat is zero but for which a finite change in heat capacity occurs at the given temperature.

X-ray Diffraction Patterns of Anhydrous Calcium Stearate

The dehydration of calcium stearate monohydrate in air at 110°C. to form anhydrous calcium stearate leads to materials giving a diffraction pattern like Curve III of Fig. 1, which is substantially identical with the pattern of the hydrate, or like Curve II of Fig. 1, or like mixtures of the two exemplified in Curves V and VI of Fig. 1. The long spacing is slightly increased (*ca.* 0.5 Å) in samples which show a change of pattern upon dehydration.

Recrystallization of anhydrous calcium stearate from a mixture of 15% propylene glycol in chloroform leads to materials giving a pattern like Curve II.

It is proposed to designate these two crystalline forms of anhydrous calcium stearate obtainable at room temperature as calcium stearate VIA (Form VI of reference 4, pattern like Curve II of Fig. 1) and calcium stearate VIH (pattern like Curve V of Fig. 1, or Curve I, the hydrate pattern). It is unfortunate that calcium stearate hydrate was designated VIH in Ref. 4. This substance is a compound of calcium stearate and water and should not be referred to as a "form" of calcium stearate. The pattern of calcium stearate VIA differs conspicuously from that of calcium stearate VIH in that the former contains an intense peak at 3.70 Å in place of the set at 4.40, 3.88, and 3.41 Å, and in that the peak at 4.13 Å is relatively more intense.

The two forms of dry calcium stearate seem to have nearly identical differential heating curves, although the varying degrees of "premelting" accompanying varying purity of the samples, and the fact that the present technique of differential thermal analysis is not precise (reproducibility ±2°C.), make this conclusion open to some question. In particular, the most nearly pure preparation of calcium stearate VIA shows a transition of the second kind at 65°C. in samples which have never been subjected to temperatures in excess of 125°C. This change in heat capacity at this transition is much smaller than in the case of the second order transition of the hydrate at 48°C. It is absent from preparations of calcium stearate VIH, but its presence in all samples of calcium stearate VIA was not definitively established.

Occasionally anhydrous calcium stearates were obtained which showed an X-ray diffraction pattern in which the long spacing peaks are weak and diffuse and greatly shortened in magnitude (as low as 48.5 Å) in samples made from stearic acid from which calcium stearate VIA (long spacing 49.9) could also be prepared. The shortened long spacing is accompanied by a single wide halo centering at 4.14 Å and replacing or obscuring all additional side spacings in this region (Curve IV, Fig. 2). Although this pattern is similar to that of the transparent glassy form obtained by quenching anhydrous calcium stearate from temperatures of the order of 250°C., the samples are not glassy in appearance and do not rehydrate in air at room temperature as does the glassy form. For purposes of discussion this state is described as calcium stearate VIN (for noncrystalline).

In so far as tested, samples of calcium stearate hydrate showing the second order transition at 48°C. yield calcium stearate VIA upon dehydration while samples not showing this transition yield calcium stearate H, or mixtures of the VIA and VIH form or calcium stearate VIN.

Effect of Preparative Variables on the Formation of Calcium Stearates VIA, VIH, or VIN

At the beginning of the present investigation of the phase behavior of calcium stearate in cetane, 150 g. of "calcium stearate" was prepared from stearic acid A of Table I by metathesis between calcium chloride and potassium stearate in aqueous alcohol. This preparation was subsequently found to be the monohydrate and yielded calcium stearate VIA upon dehydration. Later on, another batch was prepared from stearic acid 4 of Table I, which is a much cruder acid, by the same procedure and also yielded calcium stearate VIA. Meanwhile the X-ray diffraction pattern of calcium stearate VIH had been published by Smith and Ross (2). Since this pattern was identical with that of calcium stearate hydrate, the conclusion that Smith and Ross had not adequately dried their material seemed obvious. However, almost simultaneously, a preparation (made in India by G.S.H.) of calcium stearate was found to give the VIH pattern after even exhaustive drying. Thereupon an investigation was begun into the factors responsible for the production of one form or the other. Calcium stearate VIN was produced when some preparations of calcium stearate hydrate were extracted with benzene and acetone in an effort to remove possible adsorbed stearic acid, and then dehydrated. At first, the form of dry calcium stearate which resulted appeared to be a matter of chance, and upwards of 50 preparations were made in an effort to identify the significant variables, which appear to be the following.

1. Purity of the Stearic Acid Used. From the purest acids (A of Table I) calcium stearate VIA was usually obtained in samples made by metathesis between sodium or potassium stearate and calcium chloride without special care as to the concentration of reactants or exhaustive washing beyond that necessary to eliminate the residual chloride ion. From stearic acids containing appreciable amounts of either unsaturated acids or saturated acids of different chain length, any of the three forms may result, but calcium stearate VIA is difficult to achieve, and with stearic acid 6 (the technical triple pressed "stearic acid" of commerce) attempts to prepare calcium stearate VIA were unsuccessful.

2. Metathesis or Direct Neutralization. Other conditions being the same, metathesis between calcium salts and sodium stearate favors the production of calcium stearate VIA, while direct neutralization of the stearic acid with $Ca(OH)_2$ tends to form calcium stearate VIH.

3. Concentrations and Temperature. These variables play no important role, except in so far as adequate mixing is impaired by the thick mushy nature of the precipitate from highly concentrated solutions, or by temperatures and concentrations such that sodium stearate forms alcogels. However, in metathetic reactions it is important whether sodium stearate or calcium chloride is in excess. A preparation of calcium stearate hydrate giving a mixture of VIA and VIH upon dehydration was washed with lime water (followed with pure water) and found then to yield almost pure VIH. A second sample was washed with a 1% sodium stearate solution (followed by hot water) and found to yield almost pure VIA.

4. Washing Procedure. Exhaustive washing of precipitated calcium stearate hydrate favors the production of calcium stearate VIA. The material is fluffy and not easily wet by water. To secure good contact between precipitate and wash liquid it is convenient to use aqueous acetone or aqueous alcohol and to mix the solid with a small volume of wash liquid to form a concentrated slurry before diluting with the remaining volume of wash liquid. More than 25% of organic solvent in the water, temperatures above room temperature, and vigorous agitation of the concentrated slurry, all tend to result in the formation of calcium stearate VIN from samples in which calcium stearate VIH results in the absence of these variables. Steaming the hydrate tends to result in the formation of calcium stearate VIA.

5. Drying Procedure. Slow dehydration favors the production of calcium stearate VIA. If the formation of calcium stearate VIN is to be avoided, the wash solvents, particularly acetone, alcohol, ether, *etc.*, should be removed from the hydrate at temperatures below 50–60°C. before subjecting it to the more elevated temperatures of 90–110°C. required to decompose the hydrate at an appreciable rate.

6. Recrystallization. Although calcium stearate is insoluble in most solvents, steaming the hydrate is perhaps equivalent to a recrystallization from water. The dry soap may also be recrystallized from the mixed solvents suggested by Palit and McBain (1). This procedure yields calcium stearate VIA.

7. Aging. A large (100 g.) batch of calcium stearate hydrate was prepared from a relatively pure acid (5R3 of Table I) in an effort to obtain a stock supply of calcium stearate VIA. When first prepared, it yielded a mixture of VIA and VIH, dominantly VIH, upon dehydration. After several months standing at room temperature it was found to be non-uniform, yielding mostly calcium stearate VIA, but with traces of VIH still present in one out of three 10 g. batches dried.

Behavior of Calcium Palmitate

Calcium palmitate appears to exhibit the same behavior as calcium stearate. An H type pattern was obtained from a technical quality soap by Vold and Hattiangdi (5). Subsequently an A type pattern was obtained (by M. J. Vold) for a sample made from Eastman palmitic acid.

DISCUSSION

In view of the influence of preparative variables (particularly 1, 4, 6, and 7) upon its preparation, it seems likely that calcium stearate VIA is the stable crystal modification of anhydrous calcium stearate. In its formation from the hydrate, considerable rearrangement in the packing together of the calcium stearate molecules is indicated to be involved by the accompanying changes in X-ray diffraction pattern.

The mechanism of the change in structure may involve rotation or partial rotation of the calcium stearate molecule about its long axis. It is reasonable to suppose that this change could then be inhibited by the presence of impurities in the stearic acid which would pack irregularly—such as unsaturated fatty acids or shorter or longer chain saturated acids. It would also be inhibited by adsorption of foreign materials into or onto the hydrate lattice, as indicated by the finding that inadequate washing of the hydrate leads to calcium stearate VIH or VIN rather than VIA. The formation of calcium stearate VIH or VIN on rapid dehydration of samples which yield dominantly calcium stearate VIA upon slower dehydration is also in accord with this explanation. Calcium ion appears to be particularly tenaciously adsorbed. The production of calcium stearate VIA from a hydrate formerly yielding calcium stearate VIH, after washing with sodium stearate, could be due to conversion of adsorbed calcium salts to calcium stearate.

This explanation receives further support from the finding that the second order transition of calcium stearate hydrate at 48°C., which could be due to development of free rotation in the lattice, is absent in samples which yield calcium stearate VIH upon dehydration.

On the basis of the above explanation, calcium stearate VIN is believed to result from an intermediate state in which the regularity of the calcium stearate hydrate crystallites is sufficiently perfect for the structural inversion to begin, but not sufficient for the molecules, dislodged from their equilibrium arrangement in the hydrate, either to fall into the regular arrangement characteristic of the stable anhydrous crystal, or to return to the arrangement characteristic of the hydrate.

In addition to its intrinsic interest, and the possible utility of the observations in the as yet unsolved problem of a complete structure determination for these materials, the circumstance that anhydrous calcium stearate may show a diffraction pattern identical with that of calcium stearate hydrate is of importance in phase studies of calcium greases (ternary systems of calcium soap, oil and water) in the identification of the phases present by means of X-ray diffraction.

SUMMARY

Anhydrous calcium stearate can be obtained at room temperature in any one of three forms, or mixtures thereof, by dehydration of calcium stearate monohydrate. Calcium stearate VIA is believed to be the stable modification. Calcium stearate VIH is an anhydrous crystalline powder having the same X-ray diffraction pattern as calcium stearate monohydrate. Calcium stearate VIN is relatively amorphous with respect to interchain spacings although it exhibits a crystalline long spacing.

Samples of calcium stearate hydrate which yield calcium stearate VIH upon dehydration lack a second order thermal transition at 48°C. characteristic of calcium stearate hydrate samples which yield calcium stearate VIA upon dehydration. Evidence is presented supporting the interpretation that transformation of the hydrate type structure to the anhydrous type is inhibited by impurities in the calcium stearate, particularly adsorbed calcium salts and foreign fatty acid anions.

REFERENCES

1. PALIT, S. R., AND MCBAIN, J. W., *J. Am. Oil Chemists' Soc.* **6**, 190 (1947).
2. SMITH, G. H., AND ROSS, S., *Oil & Soap* **23**, 77 (1946).
3. VOLD, M. J., accepted for publication by *Anal. Chem.*
4. VOLD, R. D., GRANDINE, J. D., 2ND, AND VOLD, M. J., *J. Colloid Sci.* **3**, 339 (1948).
5. VOLD, R. D., AND HATTIANGDI, G. S., accepted for publication by *Ind. Eng. Chem.*

SAMPLING OF LIQUID AEROSOLS BY WIRES, CYLINDERS, AND SLIDES, AND THE EFFICIENCY OF IMPACTION OF THE DROPLETS

H. D. Landahl and R. G. Herrmann

From the University of Chicago Toxicity Laboratory,[1] *Chicago, Illinois*

Received July 23, 1948; revised November 24, 1948

INTRODUCTION

In many types of field experiments it is desirable to determine wind velocity, particle size, and concentration in a cloud. For example, the effectiveness of an insecticidal aerosol depends on the various properties of the aerosol cloud (1,2,3,4). A method is presented which relies on the measurement by chemical analysis of the amount of material deposited by the cloud on selected surfaces; thus, a source of power to operate the samplers is not needed. This is much simpler than preparation of samples for microscopic examination, and the laborious measurement which follows. It is the purpose of this report to present data obtained using wires, cylinders and slides for the collection of airborne particles in a wind tunnel and to consider the interpretation and evaluation of the results obtained.

THEORETICAL CONSIDERATIONS

General

If a wire or rod, of length L and diameter D cm., or a flat surface of length L and width D, is suspended perpendicular to the direction of the wind, then it presents a surface area $D \times L$. Suppose that all the airborne particles which strike this surface are retained. If the mass is found to be M g., then the amount of material which would have passed per unit area, the area dose A, may be computed as $A = M/DL$ g./cm.^{2}. If some of the aerosol particles are not impacted and retained, the area dose may be calculated from $A = M/EDL$, provided that the efficiency of collection, E, is known. The collection efficiency of an object depends principally upon the size of the particles, particle density, wind speed, adherence to the object, and the object diameter.

---

[1] The work described in this paper was done under contract between the Medical Division, Chemical Corps, U. S. Army and the University of Chicago Toxicity Laboratory. Under the terms of the contract, the Chemical Corps neither restricts nor is responsible for the opinions or conclusions of the authors.

If the wind speed U is also known, the average concentration C of the aerosol multiplied by the time t of passage of the cloud may be calculated as $Ct = A/U = M/EDLU$. The quantity Ct is a useful and commonly used concept. If the time is also known, the concentration C can be calculated.[2]

The two principal factors with which we shall be concerned are settling due to gravity, and the slippage of a particle relative to the air due to its momentum when the velocity of the air is non-uniform, as, for example, in the neighborhood of objects. The former is fairly complex, due to turbulence, except near objects where the effect of turbulence is small. When the flow is smooth, Stoke's law is adequate in describing the rate of fall for particles in the size range of approximately 1–80 μ. For small particles, the Cunningham correction (5) can be applied, while for larger particles the Oseen correction (6) may be applied. With respect to the slippage of particles, and the resulting impaction on objects, one can apply the theories of impaction discussed subsequently (7,8,9).

Unless otherwise specified, c.g.s. units will be implied in all equations. By field units we shall mean that the mass is in mg., time in min., and lengths in m., except particle diameters which are measured in μ, the object dimensions in cm., and the density in g./cm.^{3}.

Collection by Wires

The following expression roughly represents the calculated efficiency of impaction of spherical droplets on cylindrical objects (*cf.* Appendix I):

$$E_v = \frac{\alpha(\rho d^2U/D)^3}{a + (\rho d^2U/D)^2 + \alpha(\rho d^2U/D)^3} + \frac{d}{D}, \qquad (1)$$

where d is the particle diameter, D is the cylinder diameter, ρ is the density, U is the wind speed, and $\alpha = 400$ cm. sec./g. and $a = 3 \times 10^{-6}$ g.^{2}/cm.^{2} sec.^{2}. Eq. (1) approximates the description of the Sell theory (7) curves if $a = 0$ and $d \ll D$ and if $\alpha = 600$ c.g.s. units, whereas the data to be given subsequently are consistent over a wide range with $\alpha = 150$ and $a = 3 \times 10^{-6}$ in c.g.s. units, or with $\alpha = 60$ and $a = 0$ when the efficiency is not less than about 5%. Other data (4) would suggest that α is considerably less, about $\frac{1}{6}$ of that calculated by Sell. The term d/D enters, since the particle only needs to graze the wire to be retained.

---

[2] More precisely, if the concentration is not constant, we have

$$A = \int_{t_1}^{t_2} C(t)U(t)dt \equiv \bar{U}\int_{t_1}^{t_2} C(t)dt = \bar{U}Ct,$$

in which the interval t_1 to t_2 is the time for which $C(t)$ is greater than zero, i.e., the time during which the aerosol cloud is passing. Generally, $\bar{U}$ will be nearly equal to the average wind speed during the passage of the cloud.

Particle Diameter from Weight Deposited on Vertical Slides

In the following few paragraphs we shall, for convenience, set $a = 0$ in Eq. (1), neglect the term d/D, assume unit density, and take $\alpha = 130$ c.g.s. units. Suppose a cloud of particles of diameter d passes two wires at a speed U, one wire of D_1 cm. diam. and another D_2 cm. The efficiencies are E_1 and E_2 given by Eq. (1). Let the actual area dose of the cloud be A and the actual amounts collected on the wires divided by the *projected* cross sectioned area by M_1 and M_2. Then

$$M_1 = AE_1 \qquad \text{and} \qquad M_2 = AE_2, \tag{2}$$

and if the ratio $r = M_1/M_2$

$$r = \frac{D_2 + \alpha U d^2}{D_1 + \alpha U d^2}. \tag{3}$$

For a given wind speed, the ratio r depends on d, so conversely, d may be estimated by the experimental value r. For $D_1 = 0.08$ cm. and $D_2 = 0.9$ cm., and $U = 1$, 3, and 8 m.p.h., the $d(r)$ relationship is shown in Fig. 1. As is to be expected, the estimation of d from r can only be made for a certain range of values of r. If, for example, r is approximately unity, this implies that $M_1 \doteq M_2 \doteq A$, whereas, if the ratio r is approximately equal to D_1/D_2, then $M_2D_2/D_1 \doteq M_1 \ll A$, the actual area dose.

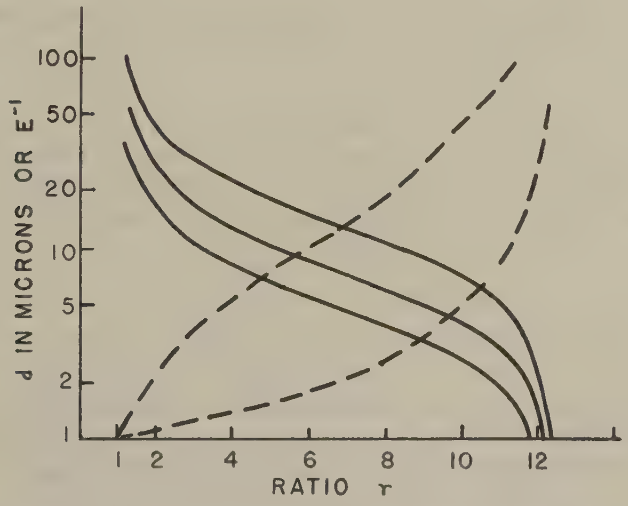

FIG. 1. Curves for a homogeneous cloud of particles calculated from Eqs. (3) and (4). Abscissa—r, the ratio of area dose M_1 to M_2. Ordinate for solid curves—d in μ for 1 (highest curve), 3, and 8 m.p.h. wind speeds. Ordinate for broken curve—E^{-1}, factor from which to obtain area dose from amount collected on 0.1 (upper curve) and 0.008 cm. wires.

Area Dose from Weight Deposited on Vertical Slides

If d can be estimated as above, then one has

$$A = \frac{M_1(D_1 + \alpha U d^2)}{\alpha U d^2} = M_1 E_1^{-1}, \tag{4}$$

so that the cloud area dose A can be determined if U is known. Using the same numerical values as above, one obtains the ascending curve in Fig. 1, which gives $E_1^{-1}(r)$, the factor by which the amount of material/cm.^{2} collected on wire 1 (M_1) is to be multiplied to obtain the cloud area dose A. Note that E^{-1} is independent of U and d in this particular case, U and d having been eliminated by Eq. (3). If the quantity d/D is not neglected, E^{-1} as calculated will not necessarily be independent of d. Furthermore, it may be less than unity for small values of r; *i.e.*, for large d and small D the amount collected/cm.^{2} may exceed the area dose A.

If $r \doteq 1$, then evidently A can be estimated readily but d cannot be estimated, although $d \gtrsim \sqrt{D_2/\alpha U}$. But if $r \doteq D_1/D_2$, then neither A nor d can be estimated although $d \lesssim \sqrt{D_1/\alpha U}$ and $A \gtrsim 3E_1$. In the first case, the use of a larger diameter wire is required, while in the latter case a smaller diameter wire must be used to estimate both d and A.

Since one does not work with homogeneous clouds, one can not expect quite so simple or exact results. However, one could expect similar relationships to occur, so that calibration of a set of wires would seem feasible.

Estimation of Wind Speed from Comparison of Deposits on Vertical and Horizontal Surfaces

In some field situations measurement of wind speed may not be practicable or the measurements attempted may have been lost. Some index of the wind speed from the deposition of the cloud on vertical and horizontal surfaces may be useful. For intermediate values of the quantity $\rho U d^2/D$ one has the approximate relation (1) (*i.e.*, neglecting the first and last term in the denominator of Eq. (1))

$$M_v \equiv \alpha_0 \rho U d^2 A/D = \alpha \rho U d^2 A/D + \cdots \tag{5}$$

for the amount deposited per unit area (projected), the numerical value of the coefficient α in this equation being somewhat different from its value in Eq. (1). The impaction coefficient α_0, defined by Eq. (5) will be used subsequently. The amount which settles is given by the product of the area dose A and the ratio of the settling speed, V, to the wind speed, U. If Stoke's law (6) is used, $V = \beta \rho d^2$ so that

$$M_H = \beta \rho d^2 A/U \tag{6}$$

for d in the interval about 1–80 μ. The quantity β is $g/18\eta$, where g is the value of gravity and η the viscosity of air, 1.8×10^{-4}. Thus, $\beta = 3.0 \times 10^5$

c.g.s. units (cm.^{2}/g. sec.). From this it is to be expected that, over an intermediate range

$$\frac{M_v}{M_H} = \frac{\alpha U^2}{\beta D} + \cdots \doteq \frac{U^2 \text{ (m.p.h.)}}{3D \text{ (cm.)}}, \tag{7}$$

so that the ratio of vertical to horizontal contamination would vary with the square of the velocity and be almost independent of the particle size, the coefficient depending inversely as the vertical object diameter or width. Thus, the velocity would be proportional to the square root of the ratio, being rather insensitive to errors of measurement in either M_v or M_H. For very large ratios, the ratio would become more nearly linear with the wind speed, while for very small wind speeds the relation should be more nearly cubic.

Assessment of Cloud by Microscopic Observation of Particles on Vertical Surfaces

For each particle of size d, only a fraction $E_v(d)$ given by Eq. (1) impacts. Thus, to estimate the area dose of the original cloud the number of particles $f(d)$/cm.^{2} in the size range, of which the average is d, should be increased by $1/E_v(d)$. The number distribution in the cloud is thus $f(d)/E_v(d)$. Hence, one should estimate A by

$$A = 0.52\rho \sum f(d)d^3/E_v(d) \text{ g./cm.}^2. \tag{8}$$

For particles in an intermediate range of sizes we may use Eq. (5) and obtain $E_v = \alpha\rho U d^2/D$ so that

$$A = \frac{0.52D}{\alpha U} \sum f(d)d, \tag{9}$$

and the cloud mass median diameter (MMD) is given by (10)

$$\sum_0^{MMD} f(d)d = \tfrac{1}{2} \sum_0^{\infty} f(d)d, \tag{10}$$

which is a special case of the general relationship defining the MMD:

$$\sum_0^{MMD} f(d)d^3/E_v(d) = \tfrac{1}{2} \sum_0^{\infty} f(d)d^3/E_v(d). \tag{11}$$

If we substitute E_v from Eq. (1) in Eq. (8), we have (neglecting d/D),

$$A = \frac{0.52aD^3}{\alpha\rho^2 U^3} \sum f(d)/d^3 + \frac{0.52D}{\alpha U} \sum f(d)d + 0.52\rho \sum f(d)d^3. \tag{12}$$

For very large particles, or high wind speeds, the third term then dominates and the equation simply states that the area dose is approximately equal to the amount collected per cm.^{2}.

Assessment of Cloud by Microscopic Observations of Particles on Horizontal Surfaces

We may define E_H analogously to E_v as the ratio of M_H to A, *i.e.*, the ratio of the horizontal contamination per unit area to the area dose. Then from Eq. (6)

$$E_H = \frac{\beta\rho d^2}{U}. \tag{13}$$

Again the number of particles in the size range, of which the average is d, occurring per unit area on the horizontal surface is only the fraction $E_H(d)$ of that in the cloud passing through space per unit area perpendicular to the wind direction. Thus, the number density of the particles of size d in the cloud is the observed number divided by E_H or $f(d)/E_H(d)$. Thus, the cloud area dose is given by

$$A = 0.52 \sum \frac{f(d)d^3}{E_H(d)} \text{ g./cm.}^2 \tag{14}$$

or, for d from 1 to 80 μ

$$A = \frac{0.52U}{\beta} \sum f(d)d, \tag{15}$$

and the cloud *MMD* is given again by Eq. (10). If too many large particles are present, E_H must be corrected for by the Oseen correction term. In this case, for d from 1 to 400 μ

$$E_H = \frac{\sqrt{1 + 5.6\beta\rho d^3} - 1}{2.8dU}. \tag{16}$$

Essentially the same values have been given graphically elsewhere (11). If U is in m/min., d in μ, $f(d)$ is the count/cm.², and if only a small fraction of the mass is contained in particles over 100 μ in diam., then

$$A = 0.0029U \sum f(d)d \text{ mg./m.}^2, \tag{17}$$

and

$$Ct = 0.0029 \sum f(d)d \text{ mg. min./m.}^3. \tag{18}$$

EXPERIMENTAL PROCEDURES

The experiments were carried out in a wind tunnel, the diameter of which was 18″, the working section 4′ in length. The flow was turbulent and the concentration was nearly the same at every point in the working section. The wind speed was quite constant over a period of time. It was generally measured before and after each experiment, and often during passage of the aerosol.[3]

---

[3] In this latter case the pressure difference between the inside and outside of the tunnel was measured with a velometer; this had been previously calibrated against the wind speed as measured by a precision anemometer.

The material atomized was *n*-butylphthalate with 1 or 5% phenyl-α-naphthylamine as a characterizer for analysis (12). For the small cloud an impinger type atomizer was used. For the other clouds a modified Bink's nozzle was used. For fixed settings, the size distribution of particles in the cloud was fairly reproducible. Cascade impactors (13) were used in almost every experiment to check the cloud *MMD*. For a given type of cloud, the *MMD* of each cloud fraction was estimated from microscopic observations of the cascade impactor slides. The *MMD* of the whole cloud was determined using these values (14). The distribution of particle sizes is illustrated in the following table.

Sample Distribution of Particle Sizes for Clouds of Various Particle Sizes

Per cent[a]	Diam. in μ		
	Small particle cloud	Medium particle cloud	Large particle cloud
5	(0.8)	1.8	5
10	1.0	2.9	8
50	4.0	13	28
90	12	40	58
98	(20)	55	75

[a] Per cent of mass less than stated diameter.

The various sampling devices were placed as near to the center of the tunnel and as far back as was consistent with keeping the various objects separated sufficiently to minimize interference. The filters were always operated approximately isokinetically[4] by fitting glass tubes of various diameters to the filter. The inside of the tubes were washed and included in the analysis. The flow rates were maintained by calibrated critical pressure orifices. In general, for long experiments (except for very large cloud *MMD* at low wind speed) the nominal area dose was in fair agreement with the filter area dose, as well as with that given by the cascade impactor.

The vertical slides (1″ × 3″ × 0.05″) were mounted by placing them against a small, flat, sticky surface at the end of a bent rod. Thus, both sides could collect adequately. The horizontal slides were set flush into a metal plate having a sharpened leading edge. The forward slide was $\frac{3}{4}$″ from the leading edge and there was $\frac{1}{2}$″ between slides. The forward slide generally contained slightly more material.

---

[4] By isokinetic sampling is meant that the average velocity in the sampling tube is the same as the velocity in the air stream. If the velocity in the sampling tube is much greater than the velocity in the stream, then some of the large particles that should have entered will fail to enter the orifice of the sampling tube. If the sampling velocity is much too low, too many of the large particles will be forced into the orifice of the sampling tube due to their momentum.

The data relating to the wires were obtained by placing a rectangular metal frame, with the various wires stretched across it, in the tunnel. Several methods were used for holding the wires in place. We shall describe only the final one. This was a rectangular frame made from $\frac{1}{8}'' \times \frac{3}{8}''$ steel strip, 10 × 27 cm. inside width. Two cylindrical brass tubes 9 mm. outside diameter and 10 cm. long were used both as supports and collectors. Three 1 mm. wires [5] 10.3 cm. long alternated with the tubes and were set into shallow holes in the frames. These could be removed by bending the wires slightly with small forceps. Two smaller sized wires were used, one 0.25 mm. and 0.08 mm. These were wound over the frame, grooves in the frame keeping them spaced. These were again alternated; a total of three pairs each. For tunnel work this random spacing is not very important, but for field sampling in a very non-uniform cloud this may be important. Wherever quantities of material are given, it will be in terms of the sampler described. Even though a different number of wires was actually used in a particular experiment, the observed quantities collected are multiplied by the ratio of the wire length in the standard frame to the length actually used. In general, however, one is only interested in the amounts per unit area, which are independent of the number of wires used in the sampling.

Every experiment, unless otherwise stated, was run in duplicate and the average given. Unless dilutions were anticipated, the wires or slides after being removed from the frame or holder were washed in 8 cc. ethanol and then removed before color development. The color was developed by adding 1 cc. of 50% HCl solution and 1 cc. of diazotized sulfanilic acid reagent. A transmission of 50%, using a Coleman spectrophotometer at a wavelength of 560 mμ, corresponds to approximately 10 γ of characterizer in 10 cc. of the final solution.

In another set of experiments, the various sized particles on the vertical and horizontal slides and vertical cylinders were counted with the aid of a microscope, after which the amounts of material on the various surfaces were ascertained by chemical analyses. One tube was a 9 mm. diameter glass tube sealed and rounded at one end, the other two were test tubes 1.8 cm. in diameter with the tops cut off. In each case the tubes were set on holders, the rounded ends up, and so held that the tube rested on another of the same diameter to reduce edge effects.

EXPERIMENTAL RESULTS

Data from the Wires

The results of the experiments employing wires (and cylinder) are presented in Table I. Horizontal slides were included but no counts were made. The values given are the percentages of the amounts collected per

---

[5] The 1 mm. wire was chosen as approximately representing a mosquito body.

TABLE I

Per Cent Area Dose

Amounts of material collected by various objects in wind tunnel

Cloud *MMD* (microns)	0.08 mm. Wire	0.25 mm. Wire	1.0 mm. Wire	9 mm. Cylinder	Horizontal slides	Eq. flow rate[a] l./min.
0.9 m.p.h.						
3.3	5.3	1.9	0.53	0.20	0.27	0.3
7	34	18	8.6	1.37	1.4	2
10	52	32	13	2.0	3.0	4
15	75	50	25	4.3	4.4	6
3 m.p.h.						
3.7	34	20	8.4	0.70	0.095	7
7.5	69	47	25	2.6	0.45	20
13	89	69	40	7.6	0.85	30
27	93	85	54	15	1.7	50
8 m.p.h.						
3.7	46	31	16	2.1	0.041	30
7.5	65	57	42	11	0.24	90
13	87	73	53	19	0.23	140
27	100	84	64	28	0.89	190

[a] This represents the rate of flow necessary to collect an amount of material equal to that collected by all the surfaces perpendicular to the wind.

cm.^{2} relative to the cloud area dose measured by amount collected on the filter. The last column indicates the actual amounts collected. This is represented by the flow rate through a filter necessary to collect the same amount as collected by the wires and tubes. At high wind speeds and large cloud *MMD*'s the amounts collected are equivalent to the amounts collected at high flow rates. The value of the *MMD*'s of Table I were obtained by using the cascade impactor as described above.

Perhaps the chief source of error [6] is the non-uniformity of the cloud.

---

[6] The effect of orientation to the wind was investigated by one experiment in which one frame was perpendicular to the wind and the other at an angle of about 45°. The per cent area doses from small to large diameter were 71, 58, 31, and 6, for the usual position, and 69, 33, 20, and 4, for the frame oriented at an angle to the wind. Experiments at two different cloud sizes and wind speeds in which the wires in one frame were horizontal and the other vertical showed a negligible difference in the amounts collected. At low wind speed and large particle cloud size one might expect some settling to occur when the wires are horizontal. Unless specified, the results are from wires in the horizontal position.

The concentration from point to point at any particular instance may vary greatly. In general, very short experiments show great variability. Furthermore, the wind speed varies both temporally and spatially. Since the characterizer decomposes slowly on exposure to air (rapidly in sunlight), the samples were analyzed as quickly as possible.

Some experiments at high wind speeds were carried out for demonstration purposes. These were not repeated. The results are given in the first three columns of Table II. The values for which the per cent area dose is very small are not too reliable, since the amount of material was inadequate for accurate chemical analysis. Several experiments were carried out in a miniature wind tunnel with a wind speed of 45 m.p.h. using glycerol droplets (Table II). The cloud in this case was much more homogeneous than the others used. The 5, 25, 75, 95, and 99% diams. were, respectively, 1, 1.7, 3.7, 5.0, and 5.6 μ. Microscopic counts were made on the 4 mm. tubes. The *MMD* of the impacted material was 4.0 μ; the cloud *MMD* from Eq. (10) was 3.5 μ. The amount deposited is correctly given by Eq. (5) if $\alpha = 40$ c.g.s. units.

TABLE II

Per Cent Area Dose

Collection efficiency for various objects in wind tunnel

Sampler	Cloud *MMD*: 2 μ	4 μ	16 μ	2.7 μ
	Velocity: 15 m.p.h.	14 m.p.h.	14 m.p.h.	45 m.p.h.
0.08 mm. wire	33	64	106	95
0.25 mm. wire	22	46	87	49
1.0 mm. wire	5.4	20	87	20
4.0 mm. rod	—	—	—	3
9.0 mm. rod	1.6	2.2	31	—
Four horizontal slides	0.02	0.045	0.7	—
Eq. flow rate (l./min.)	28	80	340	—

Procedure for Estimating Wind Speed, Cloud Area Dose, and Cloud Particle Size by Means of Analysis Only

Wind Speed. If adequate direct values are not available, the wind speed may be estimated from the data collected from the 9 mm. rod and the horizontal slides. In Fig. 2 are shown the results of a (log − log) plot of the ratio of the area dose on a vertical tube 9 mm. in diameter to the mass per unit area on horizontal slides against the wind speed for heterogeneous sprays of 4 different sizes. The results are fairly consistent with Eq. (7) if α is set equal to 115 c.g.s. units.

Area Dose. In a previous section it was pointed out that the reciprocal of the impaction efficiency may be employed as a factor for determination

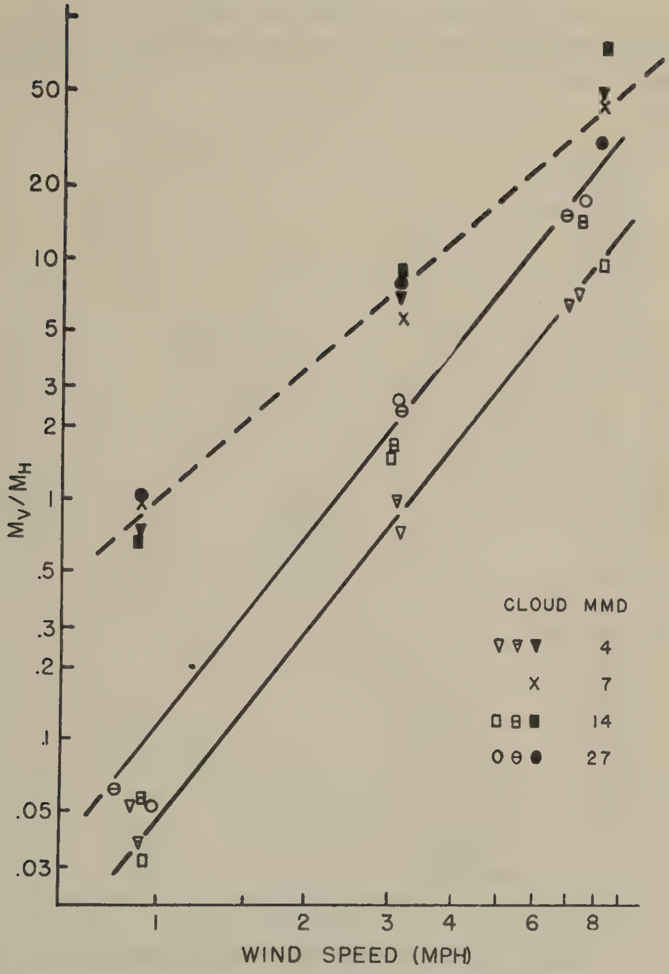

FIG. 2. The effect of wind speed on the ratio of impaction on surfaces perpendicular to direction of wind to settling on horizontal surfaces. Abscissa—wind speed in m.p.h. Ordinate: broken curve—ratio of area dose for 9 mm. cylinder (brass) to that on horizontal slide (Table I, *cf.* Eq. 7); solid curves—ratio of area dose on vertical slide (1″ × 3″) to that on horizontal slide (Tables VI and VIII).

of area dose. In Fig. 3 are shown the results of plotting the area dose factor for an 0.08 mm. wire against the ratio of the area dose for the 0.08 mm. wire to the 0.25 mm. wire, and a similar plot using the wires of 0.08 and 1.0 mm. diam. (*cf.* Fig. 1). Experiments were carried out at 3 wind speeds and sprays of different particle size (the smaller ordinate at any wind speed is obtained with the larger sized cloud). The plot is nearly independent of wind speed and particle size. Only a very rough estimate of the wind speed is sufficient to make the estimations.

Determination of Ct. When the wind speed and area dose have been determined the Ct is obtained from the area dose divided by wind speed, using appropriate units.

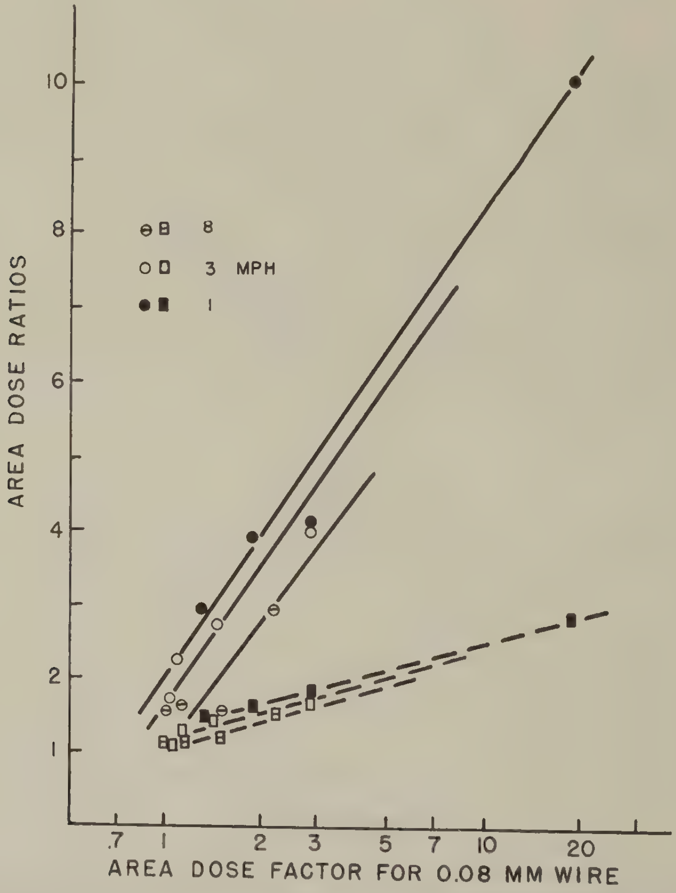

FIG. 3. Curves for the estimation of the area dose factor E^{-1} for the 0.08 mm. wire from which to obtain the cloud area dose. Abscissa—area dose factor. Ordinate—ratio of area dose on 0.08 mm. wire to area dose on 0.25 mm. wire (broken curves) or to area dose on 1.0 mm. wire (solid curves). Data obtained from Table I.

Estimation of the Mass Median Diameter of Cloud. Having obtained the area dose, the per cent area dose of the wire may be computed. From this the mass median diameter (MMD) of the cloud may be determined.

In Fig. 4 is a plot of per cent area dose *vs.* cloud MMD for wind speeds of 1, 3, and 8 m.p.h. using a 0.25 mm. wire and a 9 mm. rod. It is to be noted that, if the MMD is large or the wind speed higher than 1 m.p.h., the curves are too flat for reliable calculations. The 0.08 mm. wire would

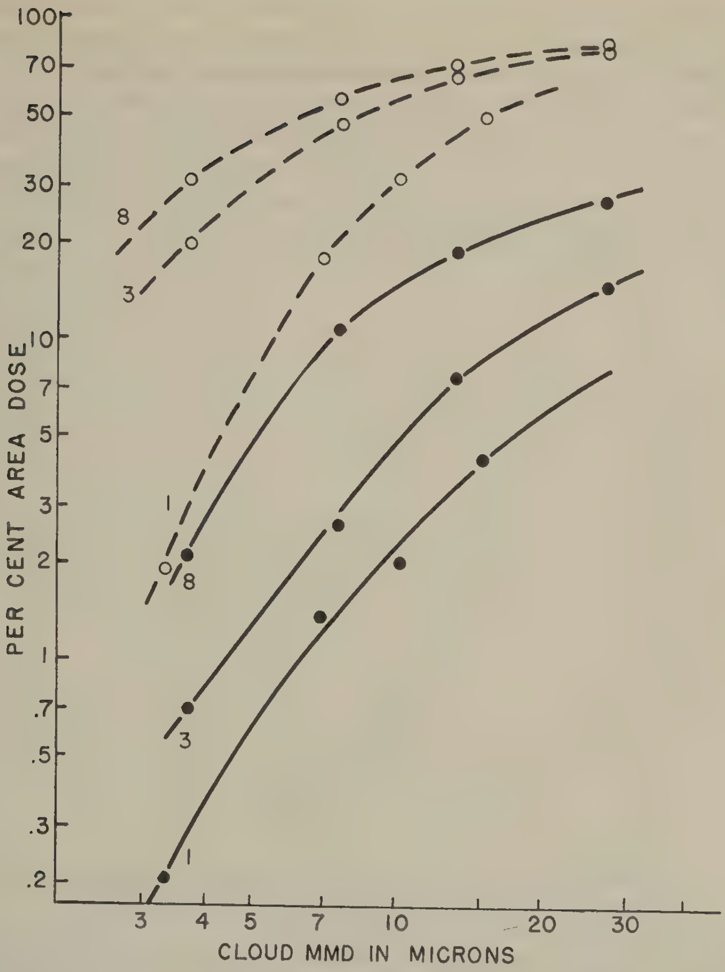

FIG. 4. Per cent area dose collected by 9 mm. cylinder (solid) or 0.25 mm. wire (solid) as a function of cloud *MMD* in μ for various wind speeds (Table I).

be of use only for very small *MMD*'s and low wind speeds (figure not shown).

Since the determinations of wind speed and area dose by the methods lescribed above are practically independent of the *MMD* of the cloud hey are also fairly independent of the shape of the size distribution curve. But determination of the *MMD* is necessarily dependent on the size disribution to some extent.

Alternate Procedure for MMD Determination. The above procedure is nost satisfastory for high wind speeds and large particles. An alternate rocedure is satisfactory for wind speeds of 3–8 m.p.h. This utilizes the type of relationship shown in Fig. 1 in which the *MMD* is plotted against the ratios of the area doses on the various wires. This is illustrated graphically in Fig. 5. Intermediate wind speeds require interpolation.

Vertical Deposition. The deposition on the wires may be used directly to give an estimate of the contamination to be expected on fairly smooth vertical surfaces. For objects larger than the cylindrical tube, one may expect that the contamination would be very roughly inversely proportional to the diameter. In some instances a knowledge of this factor may be of primary interest.

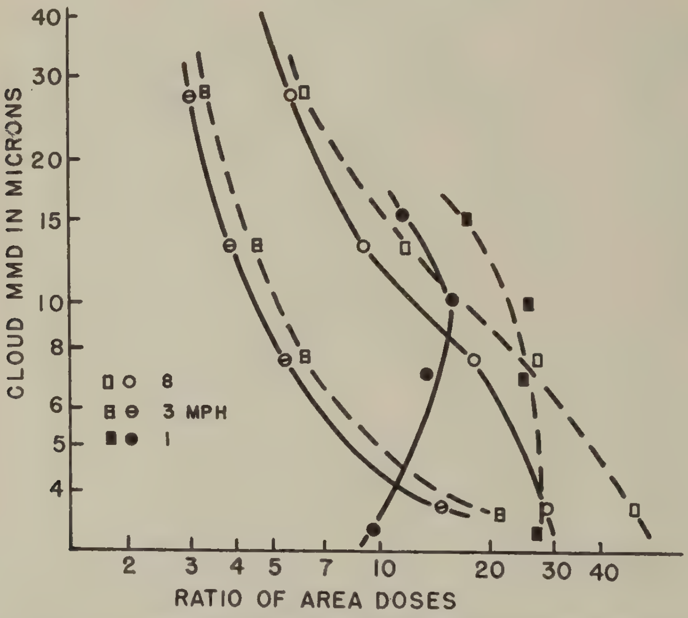

Fig. 5. Curves for estimating *MMD* of cloud from ratio of area dose of 0.25 mm. wire (solid) or of 0.08 mm. wire (broken) to area dose on 9 mm. cylinder. Data from Table I.

Ground Contamination. For some purposes this may be of primary interest. Evidently, the horizontal slide area dose at ground level is a direct measure of this quantity. Similarly, the horizontal slide measurements at any other level are direct measures of horizontal deposition on horizontal objects at the corresponding height, provided that the size of the object is not too large or too small as compared to the slide holder used.

Illustration of the Use of Wires for the Assessment of a Cloud of Particulates. Two examples are given in detail to illustrate the procedure and to indicate the amounts of material analyzed chemically. Data and results of computations are given in Tables III and IV. In Run A no cascade

TABLE III

Amounts Collected by Various Surfaces under Two Experimental Conditions, Used to Illustrate the Assessment of a Particulate Cloud without Microscopic Observations

Sampling surface	Run A[a]			Run B[b]		
	Mg. collected	mg./cm.^{2}	% filter area dose	Mg. collected	mg./cm.^{2}	% filter area dose
0.08 mm. wire	0.96	2.00	91	0.22	0.458	104
0.25 mm. wire	2.80	1.87	85	0.67	0.447	101
1.0 mm. wire	3.81	1.27	58	0.98	0.326	74
9 mm. tube	1.61	0.226	11	0.93	0.103	24
2 horizontal slides	0.26	0.0068	0.31	0.35	0.0052	1.8
Filter (17 l./min.)	2.8	2.20	—	0.46	0.44	—
Nominal	—	2.65	—	—	0.64	—
Cascade	—	—	—	0.56	0.53	—

[a] Wind speed 5 m.p.h., cloud *MMD* 8–10 μ, filter *Ct* 165 mg. min./m.^{3}, area dose 2.2 mg./cm.^{2}, 1% characterizer.

[b] Wind speed 4.8 m.p.h., cloud *MMD* 19–23 μ, filter *Ct* 34 mg. min./m.^{3}, area dose 0.44 mg./cm.^{2}, 5% characterizer.

TABLE IV

Assessment of the Two Clouds of Table III by Graphical Method without Microscopic Observations

	Run A		Run B	
Calc. wind speed	6.8 m.p.h.		5.1 m.p.h.	
Calc. area dose[a]	1.9 mg./cm.^{2}	2.2	0.34 mg./cm.^{2}	0.44
Calc. area dose[b]	1.8 mg./cm.^{2}		0.49 mg./cm.^{2}	
Calc. area dose[c]	2.8 mg./cm.^{2}		0.49 mg./cm.^{2}	
Calc. average *Ct*	120 mg. min./m.^{3}		32 mg. min./m.^{3}	
MMD of cloud[d]	12	10 μ	27	24 μ
MMD of cloud[e]	10		24	
MMD of cloud[f]	8		22	

[a] From area dose factor for 0.08 mm. wire *vs.* ratio of area dose on 0.08 to that on 0.25 mm. wire (Fig. 3).

[b] From area dose factor for 0.08 mm. wire *vs.* ratio of area dose on 0.08 to that on 1.0 mm. wire (Fig. 3).

[c] From area dose factor for 0.25 mm. wire *vs.* ratio of area dose on 0.25 to that on 1.0 mm. wire.

[d] From per cent area dose on 9.0 mm. rod *vs.* *MMD* of cloud (Fig. 4).

[e] From *MMD* of cloud *vs.* ratio of area dose on 0.08 mm. wire to that on 9.0mm. rod.

[f] From *MMD* of cloud *vs.* ratio of area dose on 0.25 mm. wire to that on 9.0 mm. rod (Fig. 5).

impactor was used. The atomizer was set to give a cloud whose *MMD* was from 8 to 10 μ. In Run B the percentages of material collected on slides A to D of the cascade impactor were 63, 31, 3, 3, and 0 on the impinger, only the first two figures having an adequate amount of material to analyze chemically. This indicates a cloud *MMD* of 19–23 μ in Run B. A longer run at the same settings gave a *MMD* of about 19 μ. In Run A, the wind speed was set shortly before the run, while in Run B a number of readings were taken at intervals just before and after the passage of the aerosol cloud.[7]

To check the effect of a more heterogeneous cloud, one may assume that Runs A and B were made in succession, and that the samplers collected from both clouds. The following results were obtained, assuming that Run B was 4 times as long, so as to get roughly equal amounts from each cloud. Thus, the average wind speed was 4.84 m.p.h., the area dose 4.0 mg./cm.^{2}, the cloud *MMD* 14 μ and *Ct* about 300 mg. min./m.^{3} The corresponding calculated averages are 5.5, 4.3, 15, and 290.

Computed Impaction Efficiencies of Wires. The impaction efficiencies of the several wire sizes have been given in Table I. Using impactor data for the size distribution and the measured wind speeds, the theoretical efficiencies have been computed from Eq. (1), using $a = 0$ and $\alpha = 100$ c.g.s. units. Since the wires are small enough for the particles to be of comparable size, the term d/D is used, where d is the particle diameter and D the wire diameter. This assumes that any particle touching a wire is retained.

Comparing the values in Table V with those in Table I, one finds satisfactory agreement, except for the small cloud at the low wind speed. Computations for the horizontal slides, using Stoke's law with Oseen's correction and assuming non-turbulent settling, are also included.

Data on Slides, Test Tubes, and Rods Involving Microscopic Observations and Chemical Analysis

Horizontal slides, vertical slides, and vertical tubes were placed in the wind tunnel and clouds of various sizes were set up at each of 3 wind speeds. Microscope slides were used, since they are readily available in the field, while the test tubes (1.80 cm. diam.) and rods, also fairly available and not too difficult to count microscopically, were used since they need not be oriented to the wind. A number of trials indicated that the amount deposited on a vertical slide does not change much if it is oriented within 30° to the wind.

---

[7] It may be pointed out that in Run B only one wire size collected less material than the filter or cascade, the total collected on the wires being 6 times that on the filter (17 l./min.). The smaller the cloud size and the less the wind speed, the less the wires collect relative to the filter. The per cent of the filter area dose is listed for completeness in Table III, but the values are not used in the computation given in Table IV.

TABLE V

Per Cent Area Dose Calculated from Eq. (1) with $\alpha = 100$ c.g.s. Units and $a = 0$ or from Stoke's Law

(Data in Table I)

Cloud *MMD* in μ	At several wire diameters				Horizontal slides
	0.08	0.25	1.0	9.0	
0.9 m.p.h.					
3.3	21	7	2	0.25	0.4
7.0	43	19	6	0.8	1.4
10	53	30	13	2	4
15	62	37	19	4	6
3 m.p.h.					
3.7	34	20	5	0.9	0.15
7.5	60	37	17	3	0.6
13	81	56	31	8	2
27	(101)	74	46	19	6
8 m.p.h.					
3.7	42	25	12	1.8	0.06
7.5	67	42	26	6	0.26
13	86	57	40	16	0.9
27	105	72	54	26	3

Each pair of slides and test tubes was counted when possible. Focal length ratios were determined for each slide (13). An attempt was made to collect enough material to analyze without overloading the slide. The 9 mm. tube was generally too heavily loaded to be counted, so short (time) samples were taken. At the low wind speeds, the vertical samplers were run about 10 times as long as were the horizontal slides, to get enough material to analyze (runs 16–21, 1 m.p.h.). This is indicated by the numbers in parentheses in Table VI under "time of run." Cascade impactor samples were taken for most runs. The *MMD*'s from these are listed in the table. Values in parentheses are nominal values.

The area dose in mg./cm.^{2} as determined from the filter sample (isokinetic sampling), cascade impactor, and from the amount put out by the atomizer (nominal), are listed in Table VI. In the columns headed "per cent analytical" are given the ratios in per cent of mg./cm.^{2} collected to the filter area dose. Samples for which the transmission readings were above 85% are listed to one significant figure. The last two columns of Table VI will be discussed subsequently.

TABLE VI

Per Cent Area Dose

Amounts of material collected by various objects in wind tunnel

Run no.	Cloud *MMD*	Wind speed m.p.h.	Horizontal slide		Vertical slide		Test tube		Vert. rod	Area dose in mg./cm.²			Time of run	Calc. area dose[a] % F, C, N		
			% Anal.	% Count	% Anal.	% Count	% Anal.	% Count	% Anal.	Filter	Cascade	Noml.		H.S.	V.S.	T.T.
9	3.0	0.93	0.28 0.27	0.51	0.024	0.003	0.11 0.15	0.06	0.05 —	6.4	4.3	4.4	3′	78	(10)	—
10	(3.0)	0.87	0.25 0.19	0.08	(.01)	0.005	(.01) —	0.008	(.01) —	5.7	—	4.4	3′	44	(20)	35
11	(3.0)	0.93	0.22 0.23	—	0.010 0.019	—	0.028 0.039	—	0.038	67.2	—	29.4	20′	—	—	—
16	13	0.96	2.6 2.6	2.5	0.064	—	0.58 0.56	0.12	1.15 —	0.97	0.80	0.64	2.3′ (23′)	69	—	325
18	15	0.93	4.7 3.9	4.2	0.06 0.19	0.09 F 0.00 B	0.44 0.56	0.14	1.3	0.28	0.40	0.64	2.5′ (30′)	91	200	100
17	27	0.92	7.6 6.3	12.7	0.30	—	1.4 1.1	1.0	2.8	1.48	1.66	3.2	6″ 29 (60″)	106	—	44
19	18	0.98	5.2	4.4	0.25	0.001F	1.0	0.9	4.1	1.78	1.07	3.2	(7″) 34″	86	1.5F	37

Run no.	Cloud *MMD*	Wind speed m.p.h.	Horizontal slide		Vertical slide		Test tube		Vert. rod	Area dose in mg./cm.^{2}			Time of run	Calc. area dose[a] % F, C, N		
			% Anal.	% Count	% Anal.	% Count	% Anal.	% Count	% Anal.	Filter	Cascade	Noml.		H.S.	V.S.	T.T.
21	26	1.03	7.1 7.4	5.7	0.45	0.05 F 0.12 B	1.7 2.0	1.0	5.9	1.63	1.13	3.2	(6″) 27″ (56″)	89	4 F 92 B	33
5	4.2	3.15	0.14 0.10	0.09	0.080	0.04	0.087 0.080	0.05	0.27 —	1.61	5.0	4.4	3′	42	5	19
6	4.2	3.17	0.18 0.16	0.15	0.13	0.05	0.20 0.19	0.09	0.63	6.3	5.5	4.4	3′	64	3	32
1	11	3.16	2.4 2.3	0.80	1.2 1.2	1.4			7.9 7.9	2.28	1.39	3.26	30″	80	66	—
2	15	3.05	1.5 1.5	0.83	3.0 2.6	1.1	5.1 3.3	2.7	8.6 10.6	1.82	1.46	1.74	15″	67	44	20
20	15	3.02	0.81 1.01	—	1.5 1.8	—	3.3 2.8	—	7.8 —	2.42	2.02	2.56	9′	—	—	—
12	27	3.14	1.9 2.5	2.1	5.3 7.0	3.0	9.9 5.8	3.6	11.4 —	2.0	1.14	1.27	14″	91	86	52

TABLE VI—*Continued*

Run no.	Cloud *MMD*	Wind speed m.p.h.	Horizontal slide		Vertical slide		Test tube		Vert. rod	Area dose in mg./cm.²			Time of run	Calc. area dose[a] % F, C, N		
			% Anal.	% Count	% Anal.	% Count	% Anal.	% Count	% Anal.	Filter	Cascade	Noml.		H.S.	V.S.	T.T.
13	26	3.15	1.6 2.2	3.6	5.1 2.7	2.7	7.6 8.7	3.5	29.1	1.70	0.96	1.27	14″	112	73	70
7	4.0	7.2	0.079	0.07	0.44 0.44	0.36	0.57 0.45	0.28	1.45	5.3	4.7	2.94	2′	54	15	6
8	(4.0)	7.5	0.04 0.035	0.07	0.34 0.38	0.15	0.50 0.38	0.23	1.32	6.0	—	2.94	2′	107	12	10
3	14	8.3	0.24 0.39	0.08	2.6 2.8	1.7	3.0 3.2	1.8	5.8	1.31	0.45	0.32	5″	51	100	34
4	10	8.2	0.41	1.3	4.3 3.7	2.6	3.9 3.4	1.8	8.8 —	0.56	0.36	0.26	5″	44	98	45
14	30	7.6	1.10	0.72	24 16	21	18 28	14	34 —	1.0	0.70	0.85	10″	95	153	72
15	30	7.7	0.94	1.5	16.9 16.6	16	26 19	8.4	40 —	0.99	0.88	0.85	10″	124	145	56

If the flow is smooth in the immediate vicinity of the horizontal slide (set flush in a metal plate), then the *Ct* (and hence area dose times wind speed) should be the same for any wind speed. For homogeneous clouds, the amount collected should be proportional to the settling rate, which, in turn, is proportional to the square of the particle diameter. Since these clouds, as would generally be the case in field trials, are not homogeneous, the relationship need not be quite parabolic. In Fig. 6 are shown the values from Table VI, with per cent area dose times wind speed plotted

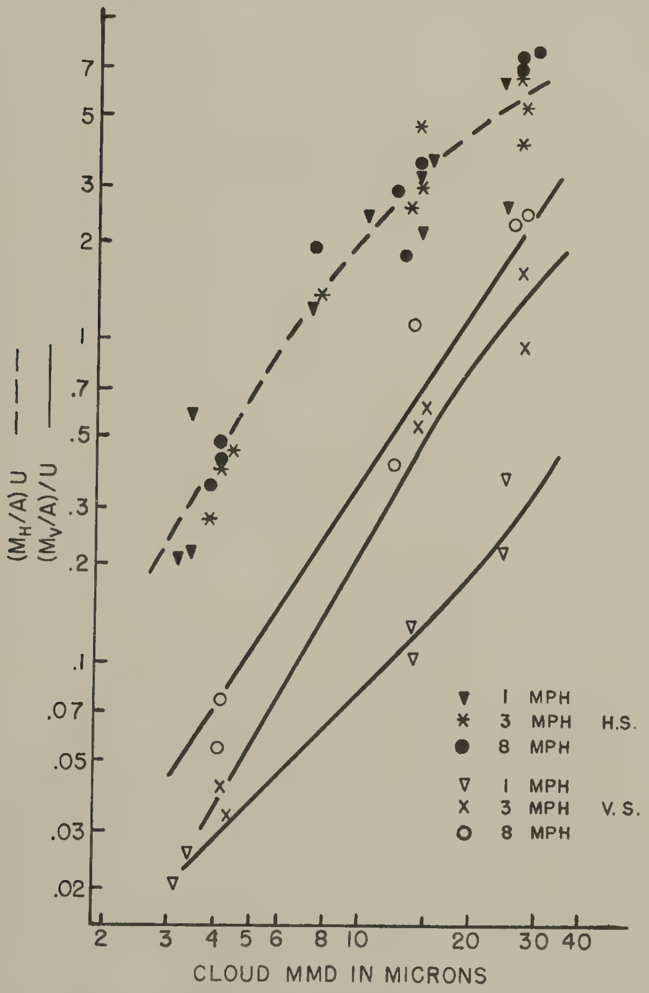

FIG. 6. Ordinate—broken curve, per cent area dose on horizontal slides times wind speed in m.p.h. (Tables I, VI, and VIII); solid curves, ratio of area dose on vertical slides to wind speed in m.p.h. (Tables VI and VIII). Abscissa—*MMD* cloud in μ.

against cloud *MMD*. The results of duplicate experiments are averaged and, to some extent, weighted by the duration of the experiment. One will notice considerable variability, but no marked trend with wind speed. Included in this figure, are also values given in Table I as well as data from Table VIII, to be discussed subsequently.

Also shown in Fig. 6 are similar data from the vertical slides (from Tables VI and VIII), except that the ordinate in this case is the per cent area dose divided by the wind speed. The ratio increases with the wind speed for each cloud size. This can be accounted for qualitatively by Eq. (1) since, for a small per cent impaction, the ratio should increase with wind speed.

TABLE VII

MMD of Impacted Material and Estimated MMD of Cloud
For data of Table VI

Run no.	Cloud *MMD*	Wind speed m.p.h.	*MMD* of material deposited				*MMD* of cloud calc. from deposit (Eq. (10))			
			Horizontal slide	Vertical slide	Test tube	Vertical rod	Horizontal slide	Vertical slide	Test tube	Vertical rod
9	3.0	0.93	19	15	7	—	5.5	3.3	1.0	—
10	(3)	0.87	9.5	14	11	8	3.6	3.9	3.0	4
16	13	0.96	36	—	28	41	17	—	13	21
18	15	0.93	27	−B, 34F	38	—	14	17	26	—
17	27	0.92	45	—	46	—	26	—	34	—
19	18	0.98	31	35B, 57F	50	48	22	24	38	39
21	27	1.03	(35)	27B, 58F	48		(22)	19	44	—
5	4.2	3.15	21	33	30	—	5.4	15	26	—
6	4.2	3.17	24	38	34	17	5.3	28	24	2
1	11	3.16	34	47	—	—	14	30	—	—
2	15	3.05	33	43	54	25	18	34	39	22
12	27	3.14	48	55	54	—	28	49	45	—
13	26	3.15	56	58	49	32	31	48	39	25
7	4	7.2	19	34	31	18	9	22	18	13
8	(4)	7.5	21	29	26	—	8	21	17	—
3	14	8.3	22	19	38	19	14	24	23	18
4	10	8.2	29	21	28	—	15	23	17	—
14	30	7.6	43	77	61	—	24	50	40	—
15	30	7.7	54	68	48	31	27	42	33	21

TABLE VIII

Per Cent Nominal Area Dose

Nominal cloud size in μ	Wind speed m.p.h.	Horizontal slide	Vertical slide	Test tube	Nominal AD	Time of run (min.)	Ratio $\frac{VS}{HS}$
3.3	0.93	0.58 0.68	0.012 0.035	0.083	22	15	0.037
14	0.94	2.00 2.52	0.12	0.24	6.4	26.4	0.053
24	0.84	2.84 3.30	0.21 0.15	0.59 0.64	6.4	1.3	0.059
4	3.11	0.14 0.11	0.14 0.11		22	15	1.00
14	3.08	1.03 0.86	1.68 1.62	3.35 4.22	6.4	29	1.7
27	3.19	1.1 1.4	3.7 2.3		6.4	1.2	2.4
4	7.0	0.075 0.065	0.48 0.48	0.80 0.81	22	15	6.9
14	7.1	0.47 0.52	8.27 7.49		6.4	29	16.0
27	7.0	0.91 1.23	15.5 17.1		3.2	0.5	15.1

VS—Vertical slide. HS—Horizontal slide. Nominal AD—Output area dose in mg./cm.^{2}

The data from the test tubes can be similarly graphed. Unlike the data from the vertical slides, the effect of wind speed is not apparent. This may in part be due to settling on the rounded top of the tube which would be greater at low wind speeds. If one obtains ratios of per cent impaction on test tubes to that on vertical slides it will be found that the ratios increase with wind speed (roughly 0.3, 0.6, 0.9 for 1, 3, and 8 m.p.h.). However, this effect does not enter into the microscopic counts and should be taken into consideration when comparing the amounts on the test tubes as estimated from the microscopic counts with the amount determined by chemical analysis.

In Table VII are listed the *MMD*'s of the material on the slides and cylinders as well as the *MMD* of the cloud estimated, assuming Stoke's law of settling, and assuming that the impaction efficiency is proportional to $\rho U d^2/D$. The horizontal slide gives a fair estimate of cloud *MMD*, though it is somewhat large for the cloud with the smallest particles. This may in part be due to evaporation of the very small droplets, as well as to the tendency to overlook very small droplets in counting. On the other hand, the other estimates are generally very high. If Eqs. (12) and (11) are used, but with $\alpha = 150$, the agreement is much improved. In all cases, as expected, the *MMD* of the collected material is considerably greater than that of the cloud. It may be pointed out that, if MgO or carbon coated slides were used, the interpretation of the results would be especially difficult since in $\sum fd$, the small particles contribute considerably.

If one plots the ratio of material on the vertical slide to that on the horizontal slide (Table VI), one finds a marked dependence upon wind speed, but a relatively minor dependence upon the particle size of the cloud. This relationship is included in Fig. 2. Since there were a considerable number of objects in the wind tunnel, and the vertical and horizontal slides were not too close together, another set of runs was made, in which the vertical slides were directly behind the horizontal slides and about 1–1.5 in. above and behind the latter. These were not counted, so that considerably longer runs were possible. Generally, in longer runs, the filter and nominal are almost equal, except for a cloud of very large particle size at low wind speed. No filters were used, so that all values (Table VIII) are in per cent of the nominal. These ratios are also given in Fig. 2, differentiated from the former by bars through the points. The value of α from Eq. (7) which is most consistent with these data is 60 c.g.s. units. However, it varies with wind speed and cloud *MMD*, increasing with both.

In Table V are listed also the area doses as determined from the counted mass. The two duplicates were computed as a unit, except where the focal length ratios differed considerably. These values are very erratic, indicating the difficulty of estimating the mass by counts. This is to be expected, since all errors in measurement of the diameter are cubed. Furthermore, since a few large particles appreciably influence the mass, the sampling errors are serious. For most slides about 200 or more particles were counted, and an attempt was made to sample a considerable number of fields in various parts of the slide in a regular manner. In the case of the test tubes, and rods, it was necessary to count a complete ring around the tube. Only a few such annuli were taken; in some cases, only one. To increase the stability of the count without appreciably increasing the effort and time, two (or generally many more) times as many fields were counted to estimate the droplets larger than an estimated *MMD*. The primary area counted generally was about 10–50 mm.^{3}. In most instances there were from 20 to 30 class intervals. Precautions were taken to avoid overloading the surfaces. The vertical cylindrical tube (9 mm.) was most likely to have too great a density of particles.

The vertical slides were mounted so that there was practically no obstruction in the rear. In most cases, only the front surfaces of the vertical slides were counted. However, at 1 m.p.h., there was a considerable mass on the back surface, necessitating separate counts from both front and back. At 3 m.p.h., a small amount could be noticed on the back. The amount was too small to affect the mass estimated by microscopic counts or the slide *MMD*, but it could have some effect on the estimated cloud *MMD*. This point will be discussed in the subsequent section. For Runs 9 and 10, there is no record as to whether the surface counted was the front or back.

In the third from the last column of Table V are given the area dose as determined by Eq. (15), as a per cent of the area dose obtained by averaging the results from the filter, cascade impactor, and nominal (% *F*, *C*, *N*). Actually $\sum fd$ was determined from $\sum f(c)c.\ g$ where $f(c)$ represents the actual counted frequencies of apparent diameters equal to a circle number c (Patterson graticule) and g is the product of the focal length factor times the number of microns in the diameter of the unit circle.

In the last two columns are given the values computed from Eq. (9) using the vertical slide and test tube data. For the slides, α was set equal to 30 c.g.s. units and for the test tube α was set equal to 50 c.g.s. units (see below). The results suggest that the small particles should be given even greater weight than is given by Eq. (9). Even if Eq. (1) is used with modified coefficients, the small particles are not sufficiently weighted in many cases. However, one should keep in mind that, in counting a wide distribution of particles, the small particles tend to be overlooked.

It may be pointed out that, at either high or low wind speed, the vertical or horizontal slides may be overloaded, but not likely both. Thus, generally one or the other will be satisfactory for counting.

If the area dose and wind speed are known, then Fig. 6 enables a fairly good estimate of the cloud *MMD* to be made without microscopic counts.

Distribution of Material on Slides. The values in Table IX for the per cent of material on the back of the vertical slide from a limited number of experiments indicate how the material is distributed. Each figure for relative amounts was determined from the average of three slides. Inspection of individual slides shows even more marked variations. The figures are generally averaged from several slides unless a range is given.

Impaction and Settling Coefficients α_0 *and* β *Calculated from Data or Vertical and Horizontal Slides.* The quantity α in Eq. (1) may, in general, depend on any of the variables, but, according to the Sell theory, depends only on shape unless the efficiency becomes too large, since $E_v < 1.00$ except for very small objects. Using the data from the cascade impactor,

TABLE IX

Distribution of Material on Back and Front of Vertical Slides

Approximate cloud size	4	14	25
% Mass on back 1 m.p.h.	72–90	70–80	37–66
3 m.p.h.	22	4	1.4
Slide *MMD* 1 m.p.h.	14 B	22 B	31 B[a]
	13 F	43 F	58 F[a]
	14 T	24 T	40 T
3 m.p.h.	13 B	19 B	24 B
	40 F	45 F	57 F[a]
	35 T	44 T	57 T
Cloud *MMD* 1 m.p.h.	4.4 B	16 B	19 B
	5.1 F	32 F	50 F
	4.6 T	18 T	22 T
3 m.p.h.	7 B	16 B	16 B
	27 F	32 F[a]	30 F[a]
	22 T	31 T	30 T

B—Back. F—Front. T—Total.

[a] These values are also given in Table VII.

the size distribution of particles in a cloud was determined. From the microscopic counts on the sampling devices and the chemical analysis for the total material collected, the distribution of particle sizes collected on a vertical slide was determined. From these two distributions the ratio of the amounts of material in a given size range is the impaction efficiency for the vertical slide. From this ratio, α_0 in Eq. (5) was determined. This process was repeated for each size interval of each type of cloud and wind speed. The results are given in Table X for the data from the vertical slides. Similar results for the vertical cylinders (test tubes, 1.8 cm. diameter) are given in Table XI. The rather large values of α_0 for small diameters at 1 m.p.h. may be due to diffusion. The results for the 0.9 cm. vertical rod were more variable because the analyses were not run in duplicates, the counts were less complete, and many of the computed samples were short samples in separate runs. The results (not shown) were very similar to the data from the 1.8 cm. glass cylinders.

According to the calculations of Sell, a flat plate should collect more efficiently than a cylinder by an appreciable amount. The results here would indicate that the efficiency is slightly less. Arithmetic averages for α_0 from vertical slides, test tubes, and vertical rods are 5×10^{-7}, 8×10^{-7}, and 12×10^{-7} in field units, or 30, 50, and 70 c.g.s. units.

In a similar way the efficiency of collection of the horizontal slides can be estimated. In this case the efficiency, E_H, is defined as the ratio of the horizontal speed (wind speed) to the vertical falling speed. Using the cascade impactor data to determine the original cloud distribution, the counts and analysis to determine the slide distributions, the efficiencies for various intervals of sizes were determined. These are shown in Table XII. There seems to be no striking trend with respect to size or wind speed or original cloud *MMD*. An arithmetic average for β is 2.8×10^5 c.g.s. This is in satisfactory agreement with the expected figure, 3×10^5, from Stoke's law. The values of β are somewhat lower for small sizes. This may be due partly to evaporation and coalescence of small drops. Note that the computed *MMD*'s of the clouds given in Table VII were too high for

TABLE X

Calculated Values of α_0 in C.G.S. Units for Vertical Slides (2.54 cm.)

d in μ	1 m.p.h.			3 m.p.h.			8 m.p.h.		
	4	14	24	4	14	27	4	12	30
2	10	—	—	0.4	—	—	—	—	—
3	15	88	—	1	2	—	—	—	—
5	24	100	—	2	5	—	0.4	—	—
10	19	57	50	3	3	2	3	24	—
15	22	31	—	4	16	—	15	62	—
20	—	48	48	16	55	4	22	80	20
30	—	10	22	—	55	22	35	68	48
40	—	—	14	—	31	57	31	24	53
50	—	—	—	—	—	88	—	—	57

TABLE XI

Calculated Values of α_0 in C.G.S. Units for Vertical Glass Cylinders (1.8 cm.)

d in μ	1 m.p.h.			3 m.p.h.			8 m.p.h.		
	4	14	24	4	14	27	4	12	30
3	84	26	—	—	—	—	—	—	—
5	99	90	—	—	—	—	—	—	—
10	26	84	20	1	0.4	4	7	35	53
15	29	48	—	4	5	—	18	57	—
20	26	55	22	26	18	24	22	44	59
30	—	31	40	—	48	59	26	35	66
40	—	44	62	—	79	73	—	22	77
50	—	—	75	—	106	114	—	—	81

the cloud of small particles. The value of β in field units may be obtained from c.g.s. units by multiplying by 6.0×10^{-9}.

In the above calculations, the error for small particle size is chiefly due to the microscopic count, while, for large particles, it is largely due to uncertainty in the original distribution determined by the cascade impactor. In each case, at least one interval has been omitted at each extreme, but still the first and last entries given in Tables X–XII tend to be unreliable, even as to order of magnitude.

TABLE XII

Settling Coefficient $\beta \times 10^{-5}$ in C.G.S. Units from Horizontal Slides
(From Stoke's law $\beta = 3 \times 10^{5}$)

d in μ	1 m.p.h.			3 m.p.h.			8 m.p.h.		
	4	14	24	4	14	27	4	12	30
2	1.6	1.7	—	1.7	1.1	—	0.3	—	—
3	2.2	2.2	—	2.2	1.1	—	0.6	—	—
5	2.9	3.4	—	2.7	2.1	—	1.4	2.0	—
10	1.5	3.7	4.1	1.6	6.0	1.6	2.0	6.8	4.5
15	1.9	3.9	—	1.5	4.7	—	1.4	8.1	—
20	1.7	4.0	4.7	5.1	4.7	2.0	1.3	4.7	3.5
30	—	3.4	5.1	—	2.8	1.9	1.5	3.4	3.0
40	—	2.4	3.0	—	1.8	1.7	—	1.3	2.7
50	—	—	1.9	—	—	2.1	—	—	2.7
70	—	—	1.8	—	—	3.1	—	—	—

At 1 m.p.h., the variability from slide to slide is evident from inspection of the slides. In the case of the test tubes, an appreciable amount of material was present on the rounded top, a large part of which may be due to settling. This affects the chemical analysis. In the case of the vertical slides, a large fraction of the material is on the back surface. This is included in the figures in Table XII. Even at 3 m.p.h., this effect is appreciable with the cloud of the smallest particle size. Since the particles on the back are smaller, an estimation of cloud size from the front surface alone may be very faulty.

"Smallest" Particle Impacting. Some idea of the diameter of the smallest particles impacting is given in Table XIII. The size, below which there were 10 particles counted, was estimated for each slide and cylinder. Generally there were two slides or cylinders counted for each of two runs. The value for the second smallest is given in the table as the "smallest" particle impacted. Since generally about 250 particles were counted on each slide, this value corresponds to the twentieth particle out of one thousand or to the 2% of the number distribution. Included in the table are also the median diameters of the particles counted, and a measure of the mass distribution.

TABLE XIII

"Smallest" Particle Impacted on Vertical Slide or Cylinder at Various Wind Speeds

Wind speed m.p.h.	Cloud *MMD* in μ	"Smallest" particle diameter in μ		Smallest $\rho d^2 U/18\eta D$ in c.g.s. units		Median diameter in μ		Standard deviation,[a] cylinder or slide
		Vertical slide	1.8 cm. cylinder	Vertical slide	1.8 cm. cylinder	Vertical slide	1.8 cm. cylinder	
1	3	1	1	0.0001	0.0001	1.5	1	0.28
1	14	1	1	0.00005	0.0001	10	7	0.29
1	24	3	3	0.00005	0.0006	11	26	0.26
3	4	1	3	0.0002	0.002	7	18	0.23
3	13	15	15	0.004	0.05	27	34	0.19
3	27	20	17	0.07	0.07	45	34	0.16
8	4	4	3	0.008	0.006	16	15	0.21
8	12	11	7	0.06	0.03	18	21	0.20
8	30	14	9	0.09	0.05	36	24	0.20

[a] Standard deviation of the logarithm of the mass, a quantity approximately normally distributed. At 1 m.p.h. the curves were noticeably concave downwards when plotted on log—probability paper.

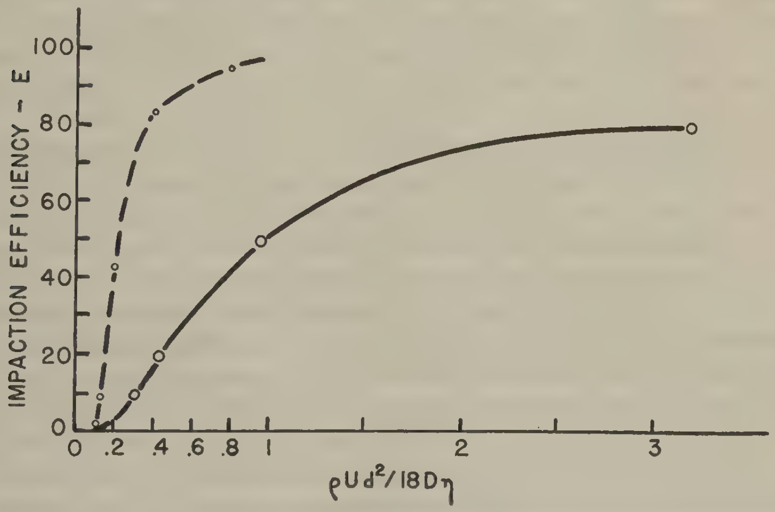

FIG. 7. Efficiency of impaction, E, of droplets on cylinders (solid curve) and in bent cylindrical tubes (broken curve) calculated as a function of $\rho d^2 U/18\eta D$.

SUMMARY AND CONCLUSIONS

Experiments have been carried out using wires, horizontal slides, vertical slides, cylindrical rods, and test tubes as devices for sampling liquid aerosols. By chemically analyzing the amounts of material collected by wires and horizontal slides in a wind tunnel, one is enabled, without microscopic observations, to estimate wind speed, area dose (and hence

Ct) and particle size in addition to contamination on horizontal and vertical surfaces. For wind speeds ranging from about 1 to 8 m.p.h., and clouds having mass median diameters in the range about 4–30 μ, the wind speed can be estimated fairly satisfactorily from the ratio of the amount impacting to that settling. If the wind speed is fairly high and the particle size of the cloud is large, the area dose can be obtained very satisfactorily, but the estimation of the particle size becomes inadequate. However, the method could probably be altered to increase the range. On the other hand, if the wind speed is very low and the *MMD* of the cloud is small, then both estimates are unsatisfactory and increasing the range would probably be difficult. In any case, the estimation of particle size depends to some extent on the actual distribution of particle sizes in the cloud.

To test the adequacy of sampling aerosols by microscopic observations alone, horizontal and vertical slides, and vertical cylinders were exposed, together with filter and cascade impactor samplers, to clouds of aerosols. After the microscopic counts were made, the material collected by the various samplers was chemically analyzed. The amount of material was calculated from the microscopic counts and this result compared with the chemical analysis. The agreement evidently depends upon the extent of the microscopic observations and the method of sampling. Unless fairly extended and careful observations are made, the calculated values for the amounts of material deposited will be accurate only to an order of magnitude.

From the number of various sized droplets found on a horizontal slide, one can calculate, using Stoke's law of settling, the area dose, the *Ct*, as well as the size distribution of the cloud. The area dose and the cloud *Ct* are very easily obtained from Eqs. (17) and (18), and the *MMD* of the cloud is obtained from Eq. (10) with very little additional computation. A knowledge of the wind speed gives the area dose. The wind speed may be estimated by calculating the amounts of material deposited on the horizontal slide and comparing that with the amount deposited on a vertical slide. The calculated amount on the horizontal slide referred to a unit area is a direct estimate of contamination on horizontal surfaces at the particular height used; *e.g.*, ground contamination if the slide is on the ground. In most instances the estimation of cloud *Ct* and cloud *MMD* was found to be fairly satisfactory.

If it is assumed that the fraction impacted on a vertical surface is given by $\alpha\rho Ud^2/D$ (α a coefficient, ρ the density, U the wind speed, d the particle diameter, and D the width of the vertical object) then the cloud area dose times wind speed and the cloud mass median diameter can be calculated from the microscopic counts. A knowledge of the wind speed then enables one to compute the area dose and the *Ct*. The latter will be subject to any error in the square of the wind speed. A comparison of values calculated in this manner with values measured directly indicates (with the exception of the cloud of smallest particle size) that the calculated area dose is rather inaccurate. The mass median diameter of the cloud is overestimated, especially at high wind speeds. At 1 m.p.h. the total amount of material deposited on a vertical slide is very variable, as is also the distribution between the back and front surface of the slide. With the cloud of smallest particle size, the cloud area dose is much too low and the cloud *MMD* is overestimated except at the lowest wind speed.

Calculations from the cylinders give results which are very similar to the results from the vertical slides.

Since the calculated results from the horizontal slides are in substantial agreement with the observed data, it may be concluded that particles over a wide range of sizes settle as though in quiet air even though the air is flowing turbulently. This is not unexpected if the flow immediately above the horizontal surface is smooth.

Since the calculated results from the vertical slides are not in satisfactory agreement with the observed data, the theory requires modification. If one excludes particles of sizes less than about 10 μ then most of the data are in fair agreement with the assumption that the fraction of particles, which would have passed through the projected area occupied by a vertical object which actually impact on the object (that is, the impaction efficiency), is given by $\alpha\rho Ud^2/D$, where α is about 60 c.g.s. units. A suitable modification, as in Eq. (1), must be introduced whenever the efficiency exceeds about one-half. However, for small particle sizes, the impaction efficiency is much less than that given by the above expression, and is qualitatively in agreement with the calculated values of Eq. (1). However, the calculated values of Eq. (1) are too high. When $\rho d^2U/D = 18$ for $a = 3 \times 10^{-6}$, the impaction efficiency is one-half according to the calculations, whereas the data would indicate an efficiency of about 20%. Thus, if, in Eq. (1), α is arbitrarily set equal to about 150, the resulting efficiencies are approximately correct, except perhaps for very small particles, in which case the quantity is underestimated at very low wind speeds.

ACKNOWLEDGMENTS

The authors are particularly indebted to Dr. W. L. Doyle, Director of the laboratory at the time the experiments were carried out, for his helpful suggestions and his interest in the work. The authors are also indebted to Mr. W. E. Steinmetz for technical assistance.

APPENDIX I

Calculation of the Efficiency of Impaction of Air-Borne Droplets on Cylinders and in Bent Cylindrical Tubes

Since the results given above showed impaction efficiencies lower than would be expected (7,8), the efficiencies of impaction were recalculated.

For the flow of air about the cylinder, values of the velocity as calculated by Thom (15) were used. These values were in satisfactory agreement with the results of his experiments. The case of a Reynold's number equal to 10 was chosen ($Ud\rho_a/\eta = 10$). Actually, a much larger number should have been used. However, the solution contains the viscosity, so that the velocity near the surface of the cylinder becomes small.

The calculations were made as follows: Let $b = 18\eta/\rho d^2$, V_x = velocity along x of the air stream at a point x, y, and dx/dt = velocity of the particle. Then, from Stoke's law,

$$d^2x/dt^2 = b(\bar{V}_x - dx/dt),$$

with a similar expression in y.

The calculations were started assuming $V_x = U$ at x equal to 6 times the value of the cylinder radius. The intervals, over which an average value $\bar{V}_x$ was estimated, were chosen so that bt was less than one-half except for the first few intervals, where the velocity change was small. In all cases the final value of x or y for each step, as obtained from the solution of the differential equation, was equal to the value obtained from multiplying one-half the sum of the initial and final velocity by the time, the error being a small number in the third place. From the path of the particle already calculated, the new path was extrapolated. From this path an average value of V_x, $\bar{V}_x$, for this interval was estimated and the calculations made. If the estimate was noticeably in error, the calculations were corrected. It was felt that the error in this estimation, that is, interpolating from the data by Thom, was the most serious.

For large enough particles, the Oseen correction term should be applied. This correction breaks down for Reynold's number of the particle ($\rho_a(U - V_x)d/\eta$) of about 4. This number contains V_x as a variable. It may be written as $\rho_a Ud/\eta$ times $(U - V_x)/U$. A rough calculation suggests that when $\rho_a Ud/\eta$ is about 4, the error in the impaction is not serious.

The results of the calculation are given in Fig. 7. The curve is that of Eq. (1) with $\alpha = 400$ and $a = 3 \times 10^{-6}$ in c.g.s. units. It will be noted that the efficiencies are lower than the previous estimates but are still not low enough. Since, for the data on the 1.8 cm. cylinder, the Reynold's number of the cylinder was from 600 to 5000 instead of 10, this is a likely source of the discrepancy.

The impaction efficiencies in the cascade impactor are in satisfactory agreement with estimates similar to that given above, even for a 50% impaction efficiency. The calculations for smooth flow through a bent cylindrical tube are relatively direct. The results of such calculations for parabolic velocity distribution, neglecting the Oseen correction term, show that, for a right angle bend, the values of $\rho d^2 U/18\eta D$ (U being the average velocity, $U_{\max}/2$, and D the inner diam.) corresponding to the percentages of impaction 95, 83, 50, 43, 9, 2, and 0, are 0.8, 0.4, .23, 0.2, 0.133, 0.114, and 0.10, respectively. Whether the radius of curvature of the central line is $D/2$ or $5D/2$ the results are not appreciably changed. It may be noted that, in either case, the first approximation, which is obtained by equating the slip into dead air for a particle originally at the center equal to a distance $D/2$, would give a value of 0.25. The corresponding value obtained by successive calculations is 0.20.

The above values were obtained from calculating several particle paths as outlined above. The particles within a prescribed area which impact are initially in an area approximately given by the intersection of circles of equal diameter. The particles were weighted by their initial velocity to obtain the final per cent impaction.

Using 8 mm. and 4 mm. tubes of curvatures $2.5D$ and $4D$, the per cent impacted for particle diameters of 1.0, 1.8, 3.3, 7.7, and 12 μ were, respectively, <3, <3, <3, 36, and 77, and <3, 16, 70, 99, and >99. The estimated values of the diameter for 50% are 9 and 2.7 μ. The average velocities in the tubes were respectively 590 and 2350 cm./sec. The density of the droplets (glycerol) was 1.26. The corresponding values for $\rho d^2U/18\eta D$ are thus 0.23 and 0.17, as compared with the calculated value of 0.23. Comparing a sharp and slow bend, indicated that the former was slightly more efficient. For the two cases $\rho_a DU/\eta$ equals 330 and 660, respectively. The orders of magnitude of $\rho_a d(U - V_x)/\eta$ are about 2 and 7. Simultaneously with the experiments at 45 m.p.h. or 2000 cm./sec., (Table II) the 4 mm. bent tube was used. The fraction of the total cloud removed was 50%. Note that the velocity toward the 4 mm. cylinder was 2000 cm./sec. while the average velocity in the 4 mm. tube was 2350 cm./sec. The former gave 3%; the latter gave 50%. From the calculations represented in Eq. (1), with $\alpha = 400$ and $a = 3 \times 10^{-6}$ in c.g.s. units, the value for the cylindrical rod should have been about 6%. If α is taken to be 150, then the calculated value is slightly less than 3%.

REFERENCES

1. LATTA, R., ANDERSON, L. D., ROGERS, E. E., LAMER, V. K., HOCHBERG, S., LAUTERBACH, H., AND JOHNSON, I., *J. Wash. Acad. Sci.* **37**, 397 (1947).
2. LAMER, V. K., HOCHBERG, S., HODGES, K., WILSON, I., FALES, I. A., AND LATTA, R., *J. Colloid Sci.* **2**, 539 (1947). Field data. BRESICA *et al. J. Econ. Entomol.* **39**, 698 (1947).
3. WINSCHE, W. E. (report not currently available in the open literature).
4. WINSCHE, W. E., AND JOHNSTONE, H. F. (report not currently available in the open literature). (Pertinent material of Refs. 3 and 4 were presented at Am. Chem. Soc. Aerosol Symposium, Chicago, April, 1948, and will appear in *Chem. Revs.* in 1949.)
5. DALLAVALLE, J. M., Micromeritics. Pitman Publishing Corporation, New York, 1943.
6. LAMB, H., Hydrodynamics. The University Press, Cambridge, England, 1932.

7. Sell, W., *Forsuchungsheft* **347**, 1–22 (1931).
8. Albrecht, F., *Physik. Z.* **32**, 38–56 (1931).
9. Langmuir, I., and Blodgett, K. B., *Army Air Forces Tech. Rept.* **5418** (1946). This reference was not issued at the time that the experiments here reported were carried out. The viscosity of air was neglected in the calculations of the stream lines about the cylinders.
10. Wilson, I. B., The Suitability of Vertical Slides as a Particle Size Measurement Method. *NDRC* 10.4–49.
11. Smith, L. W. (report not currently available in the open literature).
12. Snell, F. D., and Snell, C. S., Colorimetric Methods of Analysis, Vol. 2. D. Van Nostrand Co., Inc., New York, 1937.
13. May, K. R., *J. Sci. Instruments* **22**, 187 (1945).
14. Landahl, H. D., and Black, S., *J. Ind. Hyg. Toxicol.* **29**, 269–277 (1947).
15. Thom, A., *Proc. Roy. Soc. London* **141A**, 651–669 (1933).

THE ELECTROKINETIC POTENTIAL OF SPARINGLY SOLUBLE SULFATES. I

A. S. Buchanan and E. Heymann

Department of Chemistry, University of Melbourne, Melbourne, Australia

Received November 19, 1948

I. INTRODUCTION

We have suggested recently (1) that the ζ-potential of $BaSO_4$ in its saturated solution depends on the structure (geometrical and otherwise) of the surface. Ignited crystals of natural barite have a much lower positive potential than samples of precipitated $BaSO_4$ which were recrystallized from conc. H_2SO_4 and ignited afterwards. The former have very even surfaces while the latter have irregular surfaces. Our investigations have shown, further, that the ζ-potential of $BaSO_4$ in its own saturated solution cannot be explained solely by adsorption of Ba^{++} and $SO_4^{=}$ from solution, but is a characteristic of the crystal itself. It is suggested that the positive potential arises mainly from a preferential release of $SO_4^{=}$ from the crystal lattice; however, preferential ion adsorption becomes more important in electrolyte solution.

Meanwhile, Grimley and Mott (2) have published a theoretical discussion on the surface potential of AgBr in electrolyte solutions. In two important respects their conclusions appear to coincide with our deductions from the experimental material on $BaSO_4$.

In the first instance, the charge on the surface of the crystal in its own saturated solution is due to an inherent property of the crystal itself. Grimley and Mott consider the ζ-potential to be due to an excess of vacant lattice sites or interstitial ions in a region of the order of 10^{-6} cm. thick near the interface, while we have concluded that the degree of disorder (geometrical or otherwise) determines the magnitude of the potential assumed by the solid, the more disordered surface having a higher potential. Further developments of the work of Grimley and Mott may afford an explanation, in terms of lattice defects, of these results with $BaSO_4$.

Secondly, ions from solution, although undoubtedly changing the potential, are, according to Grimley and Mott, "not appreciably adsorbed actually on the surface of silver bromide." Our experimental results lead us to the conclusion that ions reversibly adsorbed from solution, and changing the potential of $BaSO_4$, are not permanently built into the lattice, but are held more or less loosely near the crystal surface and probably remain hydrated.

In our opinion, the contribution by Grimley and Mott is significant in that, for the first time, a theoretical treatment emphasizes the importance of properties of the solid, rather than of the solution, in determining the surface potential of an ionic solid.

We have extended our investigation to other sparingly soluble sulfates, *viz.*, $SrSO_4$, $PbSO_4$, $CaSO_4 \cdot 2H_2O$, and investigated solutions in water and in alcohol-water mixtures.

II. EXPERIMENTAL

The experimental technique of determining the streaming potential and resistance of the electrolyte in the porous plug has been described previously (1). Rigorous precautions were taken to exclude surface-active impurities. Perforated platinum electrodes coated with silver and silver chloride were used; with these electrodes there was no evidence of polarization in solutions of chlorides, nitrates and sulfates at concentrations below 10^{-3} N.

Recrystallized $BaSO_4$, $SrSO_4$, and $PbSO_4$ were obtained by dissolving precipitated samples of these compounds in hot concentrated sulfuric acid, from which they crystallize after concentration and cooling (*cf.* 1). The $BaSO_4$ and $SrSO_4$ were ignited at 700°C.; $PbSO_4$ was ignited at 520°C. in order to avoid decomposition. Crystals of up to 1 mm. in diameter may be obtained in this way.

Fairly large crystals (up to 0.5 mm. diameter) of $BaSO_4$ were also obtained by very slow precipitation at high dilution by adding very dilute H_2SO_4 from a dropping funnel to twice recrystallized $BaCl_2$ dissolved in N HCl at 90°C. $BaSO_4$ obtained by ordinary precipitation methods is unsuitable for investigation because the electrokinetic equations break down for plugs containing very fine particles (1), probably because of anomalous viscosity effects in narrow channels (3, 4).

The treatment of the natural samples of $BaSO_4$ and $SrSO_4$ was the same as that previously described for barite (1).

Natural gypsum, $CaSO_4 \cdot 2H_2O$, was investigated without any treatment except washing with warm conductivity water which was free from surface-active impurities. The crystals were analyzed using gravimetric and spectrographic methods. The sample contained 0.46% MgO, 0.11% CO_2 as carbonate, 0.1–0.2% SiO_2, and traces of Fe and Na. Precipitated gypsum was made by slowly adding dilute solutions of twice recrystallized calcium nitrate and sulfuric acid from dropping funnels to 3 l. of well stirred boiling water. In this way, thin needle-shaped crystals were obtained. Larger crystals required for retaining the finer crystals in the cell between the perforated electrodes were obtained by keeping a saturated solution of $CaSO_4$ in $N/10$ H_2SO_4 in a vacuum desiccator over conc. H_2SO_4. Crystals of 3 mm. length were obtained in this way.

All electrolyte solutions were made from chemicals of A.R. purity, recrystallized if necessary and analyzed spectroscopically. Double distilled water was used, $KMnO_4$ and a few drops of dilute H_2SO_4 being added during the second distillation to eliminate any organic surface-active impurities that may be present. Neglect of these precautions leads to variable results.

The cell constants of our plugs (*cf.* Section III) were determined from resistance measurements of plugs filled with $N/10$ or $N/50$ KCl solution. In the case of gypsum, 0.1 N solution of KBr in a 44.1% (wt.) alcohol-water mixture was used.

We estimate the overall accuracy of our ζ-potential measurements as 1.5% for $BaSO_4$, 3–4% for $SrSO_4$ and $PbSO_4$, and $\simeq$5% for gypsum. The accuracy decreases with increasing solubility of the solid, that is, increasing conductivity of the system.

III. Calculation of the ζ-Potential

For the calculation of ζ from measurements of the streaming potential and plug resistance the Helmholtz-Smoluchowski equation, as modified by Briggs, was used, *viz.*—

$$\zeta = \frac{4\pi\eta}{D} \cdot \frac{E\kappa'}{P}, \tag{1}$$

where η is the viscosity and D the dielectric constant of the solvent, E the streaming potential and P the pressure under which the liquid is forced through the porous plug, $\kappa' = C/R$ is the specific conductivity of the liquid contained in the porous plug and thus includes the bulk conductivity (κ) and the surface conductivity. C is the cell constant of the plug and R its resistance between the two perforated electrodes. Thus we obtain

$$\zeta = \frac{4\pi\eta}{D} \cdot \frac{EC}{RP}. \tag{2}$$

A comparison of κ' with κ was made in all experiments. With our systems, consisting of coarsely crystalline materials, the surface conductivity in no case amounted to more than 1–2% of the bulk conductivity and was usually less.

In all calculations we used the value of the dielectric constant of the respective solvent. However, the dielectric constant in the diffuse double layer may be different from that of the bulk of the solution. There is no possibility at present of correcting for this. If one is concerned with very dilute aqueous solutions only, the correction may have the same value in all cases, and ζ calculated in the manner outlined above, though its absolute value may be in error, may still be a useful means of characterization for comparative purposes. This appears to be a tacit assumption made by most investigators. Its justification may be doubted, however, if one wishes to compare results obtained in aqueous solutions with those for solutions in alcohol-water mixtures. In such cases it may be preferable, in accordance with a suggestion by Guggenheim (5), to use the electric moment of the double layer μ as a basis of comparison, *viz.*,

$$\mu = \frac{\zeta D}{4\pi}.$$

We have quoted our results in terms of ζ throughout this paper. In order to make a calculation of μ from our experimental values of ζ possible, we also give the values of D used in our calculations (Table I).

TABLE I

	D
Water 6°C.	85.5
Water 18°C.	80.8
Water 30°C	76.5
8.06% (wt.) alcohol in water 20°C.	75.6
20.88% (wt.) alcohol in water 20°C.	68.2

IV. DEPENDENCE OF THE ζ-POTENTIAL ON THE ORIGIN OF THE SOLID

Table II shows the ζ-potentials of a number of samples in their own saturated aqueous solution. All samples were ignited. The solid is positive in all cases.

All ζ-potential values are reproducible. Spectroscopic analysis revealed impurities, particularly in the case of the natural samples. However, the differences in impurity content between the natural and synthetic samples are not sufficiently marked to account for the large differences in ζ-potential. In the case of $BaSO_4$, it was shown previously (1) that incorporation of some of the common impurities of natural barite in the precipitated and recrystallized samples did not produce a ζ-potential similar to that of natural barite. We must, therefore, conclude that the differences between natural and synthetic samples are not due to chemical impurities.

With both $BaSO_4$ and $SrSO_4$, the natural samples with regular surfaces have a much lower ζ-potential than the precipitated and recrystallized samples possessing irregular surfaces. The irregularity of the recrystallized samples is presumably produced on ignition of the crystals which, before ignition, may have included some acid sulfate and sulfuric acid from the recrystallization process. That the high potential is due to surface irregularity and not to chemical impurities is further suggested

TABLE II

	ζ in mv. (20°C.)
Barium sulfate	
(1) Natural Barite (sample B), clear well-built crystals	5.3; 5.4
(2) $BaSO_4$, crystals (0.2–0.5 mm. diameter) obtained by slow precipitation at high dilution in N HCl	15.0
(3) $BaSO_4$, sample IV, precipitated and recrystallized from hot conc. H_2SO_4; crystals with very irregular surfaces (electron microscope)	26.6; 26.8
(4) Natural Barite (sample B), crystals wetted with conc. H_2SO_4 and ignited afterwards	27.0; 27.7
Strontium sulfate	
(1) Natural Celestite (Gloucestershire, England), slightly translucent well-formed crystals	1.4; 1.8
(2) $SrSO_4$, precipitated and recrystallized from hot conc. H_2SO_4, crystals with irregular surfaces	13.8; 14.4
(3) Natural Celestite, crystals wetted with conc. H_2SO_4 and ignited afterwards	15.0; 15.3
Lead sulfate[a]	
(1) $PbSO_4$, recrystallized from hot conc. H_2SO_4, crystals (0.2–0.5 mm. diameter) with irregular surfaces	16.0; 16.0

[a] Unfortunately, no samples of natural Anglesite of sufficient purity were obtainable, and therefore a comparison of the natural and synthetic materials could not be made.

by the fact that natural barite and celestite, having a small positive potential, on wetting with conc. H_2SO_4 and subsequent ignition, acquire a large positive potential, similar in magnitude to that of the recrystallized samples.

The geometrical surface irregularity of the samples which have a large ζ-potential has been established by optical and electron microscopy. We are indebted to Dr. A. L. G. Rees and to A. J. Hodge, of the Division of Industrial Chemistry of the Council for Scientific and Industrial Research, Melbourne, for this investigation. In the light of the ideas of Grimley and Mott (2), it would appear that the lattice defects in the layer immediately adjacent to the surface are operative in producing a higher charge density in a geometrically irregular surface than in an even one; or else the number of lattice defects may be greater in the recrystallized samples than in the natural ones.[1]

There may be some doubt as to whether theoretical conclusions from a comparison of the ζ-potential values of the 3 sulfates are justified in view of the limited experimental material available (Table III). Moreover, it is doubtful whether the ζ-values are suitable for comparative purposes, since the potential at the crystal surface is a function of the surface disorder, or surface lattice defects, and there is no certainty that.

---

[1] This explanation differs somewhat from the one given previously (1).

TABLE III

Origin	ζ mv. (all positive)		
	$BaSO_4$	$PbSO_4$	$SrSO_4$
Natural	5.3	—	1.5
Recryst.	26.7	16.0	14.0
Pptd. dil. HCl	15.0	—	—

for instance, all the recrystallized samples have even approximately the same degree of surface disorder.

Bearing these reservations in mind, it does appear, however, that, for samples of similar origin, the ζ-values are in the order of $BaSO_4 \gg PbSO_4 > SrSO_4$. The order of solubility is $SrSO_4 > PbSO_4 > BaSO_4$, and, therefore, the more soluble compound seems to have the smaller ζ-potential. A similar result is obtained for the ζ-potentials and solubilities of the three sulfates in alcohol-water mixtures (Table IV).

TABLE IV

ζ-Potentials (in mv.) in Alcohol-Water Mixtures (20°C.)
(All Positive)

	$BaSO_4$ (recryst.)	$PbSO_4$ (recryst.)	$SrSO_4$ (recryst.)
Water	26.6; 26.8	16.0; 16.0	13.8; 14.4
8.06% (wt.) alcohol	28.9; 28.9	—	—
20.88% (wt.) alcohol	28.9; 28.7	11.9; 11.6	10.6; 10.8

One cause of this influence of the solubility of the solid on the ζ-potential may be a reduction of the thickness of the diffuse double layer as the concentration of ions in solution increases. However, it appears from our experiments in concentrated solutions[2] that the influence of increasing electrolyte concentration on the ζ-potential is smaller than has often been assumed.

Solubility of an ionic solid depends on the lattice energy and on the energy of hydration of the ions concerned. One would expect the ζ-potentials of the 3 sparingly soluble sulfates to be related to these quantities also. A larger free energy of hydration should counteract preferential retention of the cation by the lattice, and thus the ζ-potential should decrease with increasing free energy of hydration of the cation. Actually, computations by Bernal and Fowler (6) suggest that the heat of hydration of Sr^{++} is about 10% greater than that of Ba^{++}, which would be compatible with the above reasoning; on the other hand, that of Pb^{++} is slightly greater than that of Sr^{++}. It must be borne in mind, however, that the difference between the heats of hydration of Ba^{++} and Sr^{++} is rather small to account for the large difference in ζ-potential. Furthermore, it is uncertain whether the order of heats of hydration is the same as that of the free energies of hydration; nevertheless, it appears that the entropies of hydration of the 3 cations in question are not very different (*cf.* 7).

---

[2] *Cf.* the third paper of this series.

V. THE TEMPERATURE COEFFICIENT OF THE ζ-POTENTIAL OF $BaSO_4$

Several authors determined temperature coefficients of ζ-potentials, but the systems chosen were rather complex (*e.g.*, cellulose, clay). Both decreases and increases of ζ as well as changes of sign were observed (8). It appeared desirable to determine the temperature coefficient for a simple system, such as $BaSO_4$ against its saturated solution. Fig. 1 shows that the ζ-potential increases with decreasing temperature, $d\zeta/dT$ being $\simeq -0.20$ mv./degree.

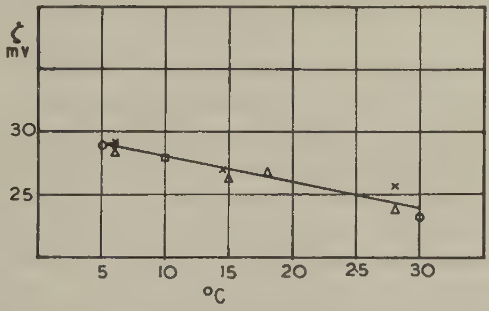

FIG. 1. ζ-potential (in mv.) of recrystallized $BaSO_4$ plotted against temperature in °C.

A variation of ζ with temperature may be related to the increasing thickness of the diffuse double layer with increasing temperature; this may, however, be counteracted by the fact that the saturation concentration increases somewhat with increasing temperature (2.10×10^{-3} g./l. at 5°C. and 3.0×10^{-3} g./l. at 30°C.). Another possibility is that preferential adsorption of Ba^{++} over $SO_4^{=}$ increases with decreasing temperature. Fig. 2 shows the variation of the ζ-potential (Δζ) with the concentration of $BaCl_2$ and Na_2SO_4 at two temperatures. Although both the increase of ζ due to $BaCl_2$ and the decrease of ζ due to Na_2SO_4 are greater at 30°C. than at 10°C., there is no marked change with temperature in the difference between these two quantities which may be regarded as a measure for the preferential adsorption of Ba^{++}. For instance, in N/50,000 solutions (which correspond roughly to the concentration of a saturated $BaSO_4$ solution) we have at 10°C. Δζ ($BaCl_2$): +8.5 mv. and

$\Delta\zeta$ (Na_2SO_4): -6.0 mv.; and at 30°C. $\Delta\zeta$ ($BaCl_2$): $+4.5$ mv. and $\Delta\zeta$ (Na_2SO_4): -2.5 mv. The difference between the effects of $BaCl_2$ and Na_2SO_4 is $\simeq 2$ mv. for both temperatures. There is thus no evidence that the variation of the ζ-potential with temperature is due to a variation in the preferential adsorption of Ba^{++} over $SO_4^{=}$.

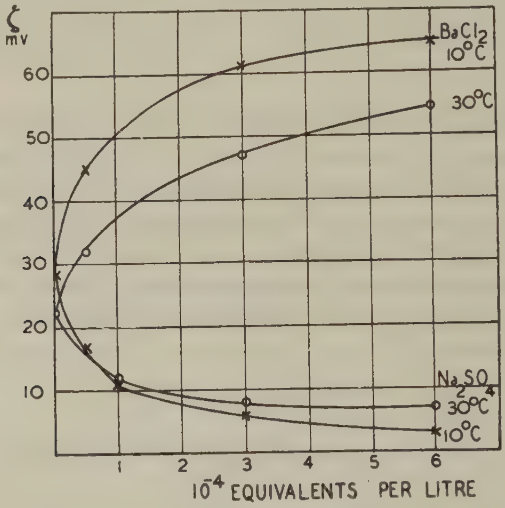

FIG. 2. Variation of ζ (in mv.) of recrystallized $BaSO_4$ with the concentration of electrolytes (in 10^{-4} equivalents at 2 temperatures.

VI. INFLUENCE OF THE SOLVENT AND OF ELECTROLYTES ON THE ζ-POTENTIAL OF $BaSO_4$, $SrSO_4$ AND $PbSO_4$

To compare the influence of electrolytes on the ζ-potential of the 3 sulfates, it is preferable to use, instead of water, an alcohol-water mixture as solvent, in order to reduce the solubility of $PbSO_4$ and $SrSO_4$, and thus the conductivity of the systems, sufficiently to make an accurate determination of ζ by the streaming potential method possible. The influence of alcohol on the initial ζ-potential is noticeable but not great (Table IV).

Fig. 3 shows the influence of electrolytes on the ζ-potential of $BaSO_4$ both in water and in 20.88% (wt.) alcohol-water mixtures. All electrolyte effects are reversible except some obtained with lanthanum salts, which exhibited slight irreversibility. In all cases in which electrolytes have a marked effect, such effects are greater in alcohol-water mixtures than in water.[3] This is probably due to a decrease in the attraction between the

---

[3] Similar results were obtained by Ruyssen (9) and by Reyerson, Kolthoff and Coad (10). However, these investigators employed fine precipitates of $BaSO_4$, which, for reasons mentioned previously (Section III), appear to us to be less suitable for electrokinetic investigation than recrystallized $BaSO_4$.

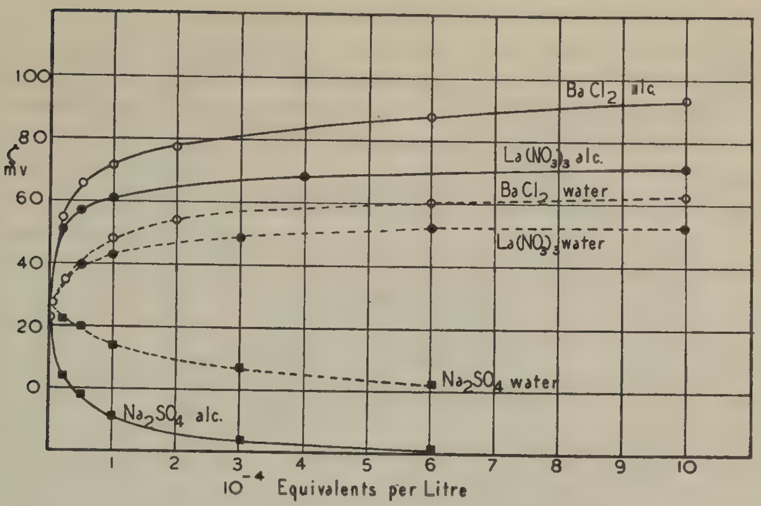

FIG. 3. Plot of the ζ-potential (in mv.) of recrystallized $BaSO_4$ against the concentration of various electrolytes (in 10^{-4} equivalents/l.) dissolved in water and in alcohol (20.88 wt.-%)—water mixtures (20°C.).

ions concerned and the solvent, on partly replacing water by alcohol, as a consequence of which adsorption on the crystal surface increases. That these effects are real and not due to the uncertainty about the value of the dielectric constant in the double layer (*cf.* Section III) is evident on comparison of the curves for sodium sulfate in water and in an alcohol-water mixture. While, in aqueous solution, Na_2SO_4 merely lowers the positive potential to small values, a change of sign occurs in the alcohol-water mixture ($\zeta = -19$ mv. at $6 \times 10^{-4}\ N$). This can only be explained by increased adsorption of $SO_4^=$ from the alcohol-water mixture.

Fig. 4 shows the change of the ζ-potential ($\Delta\zeta$) produced by addition of electrolytes for $BaSO_4$, $PbSO_4$, and $SrSO_4$ in 20.88% alcohol-water mixtures. The magnitude of the electrolyte effects, both positive and negative, is in the order of $BaSO_4 > PbSO_4 > SrSO_4$. Thus the influence of electrolytes on the ζ-potential of these 3 sparingly soluble sulfates decreases with increasing solubility of the sulfate.[4] On the basis of these experiments it seems probable that preferential adsorption is less strong on the surface of a moderatly soluble solid than on that of a sparingly soluble one.

[4] The order of solubilities in 20.88% alcohol-water mixtures is shown qualitatively by the specific conductivities at 20°C.: $BaSO_4$, 1.7×10^{-6}; $PbSO_4$, 3.3×10^{-6}; $SrSO_4$, 6.40×10^{-6} ohm.$^{-1}$ cm.$^{-1}$. The ionic mobilities of Ba^{++}, Pb^{++}, and Sr^{++} in the alcohol-water mixture are not known but are not likely to differ appreciably from one another. The corresponding specific conductivities in water are: $BaSO_4$, 3.8×10^{-6}; $PbSO_4$, 34.0×10^{-6}; $SrSO_4$, 117×10^{-6} ohm.$^{-1}$ cm.$^{-1}$, suggesting that the addition of alcohol reduces the solubility of $SrSO_4$ and $PbSO_4$ much more strongly than that of $BaSO_4$.

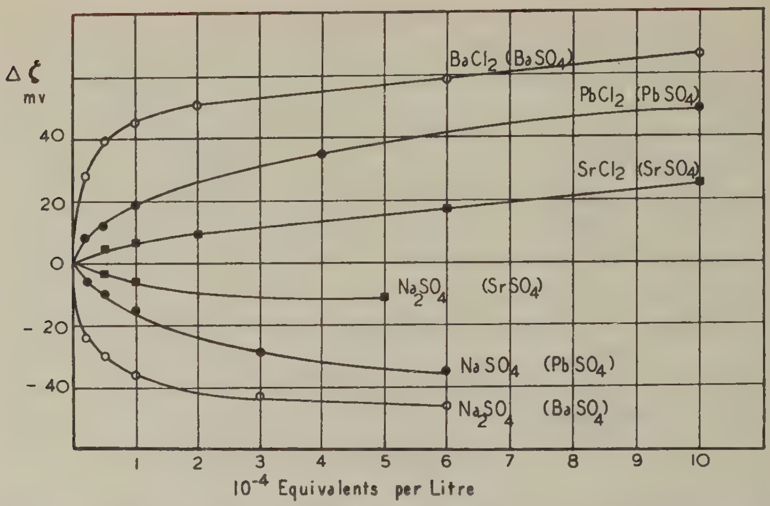

FIG. 4. Plot of the change of the ζ-potential (Δζ) in mv. produced by various electrolytes against the concentration (in 10^{-4} equivalents/l.) in alcohol (20.88 wt.-%)—water mixture (20°C.) for recrystallized $BaSO_4$, $SrSO_4$, and $PbSO_4$.

Solubility may be regarded as a measure of the stability of a crystal lattice in contact with the solvent (*cf.* Section IV). It seems possible that the solid possessing a higher solubility in which the ions are not held so firmly by the lattice should exhibit reduced preferential ion adsorption from solution. Unfortunately, no values for the lattice energy of the solids concerned are available.

The influence of lanthanum nitrate on the ζ-potential of $BaSO_4$, $SrSO_4$, and $PbSO_4$ is shown in Fig. 5. Lanthanum nitrate, in spite of the tervalency of La^{+++}, increases the potential of $BaSO_4$ less than $BaCl_2$

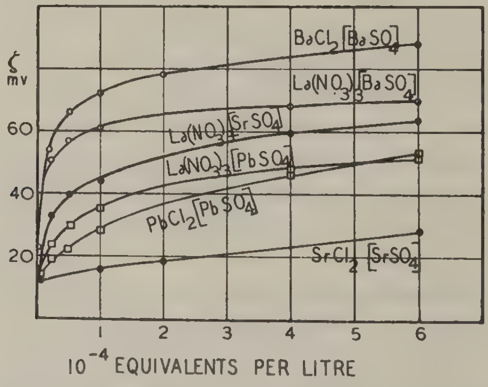

FIG. 5. Plot of the ζ-potential (in mv.) of recrystallized $BaSO_4$, $SrSO_4$, and $PbSO_4$ against the concentration of various electrolytes, including lanthanum nitrate, in alcoho (20.88 wt.-%)—water mixture (20°C.).

does, probably for reasons of geometry. In the case of $PbSO_4$, the influence of lanthanum nitrate is approximately equal to that of $PbCl_2$. With $SrSO_4$ the influence of lanthanum nitrate is very much greater than that of $SrCl_2$, probably due to a fairly close similarity between the ionic radii of Sr^{++} and La^{+++} (as compared with those of La^{+++} and Ba^{++}) which makes for strong adsorption of La^{+++} by $SrSO_4$. Unfortunately no sufficiently concordant values for the ionic radii concerned are given by various authors.

Some doubt may arise as to whether there is a large proportion of tervalent La^{+++} in solutions of lanthanum nitrate at concentrations smaller than 10^{-3} N. The experimental material, as well as general considerations, suggests that hydrolysis is less than with the corresponding aluminium salts, but the possibility of the existence of more complex ion species of lower valency cannot be ruled out. Nevertheless, the influence of lanthanum nitrate in very dilute solution on the ζ-potential of solids which are not heteropolar in nature, such as cellulose, is *greater* than that of alkaline earth chlorides (11), probably because geometrical considerations mentioned above are important in adsorption on the lattice of an ionic crystal but do not greatly affect adsorption on cellulose. It is probable, therefore, that even very dilute solutions of lanthanum nitrate contain a fair proportion of La^{+++}.

Fig. 4 shows that the potential-increasing effects of $BaCl_2$ on $BaSO_4$, $PbCl_2$ on $PbSO_4$, and $SrCl_2$ on $SrSO_4$, particularly in dilute solution ($1\text{–}2 \times 10^{-4}$ eq./l.), are only little greater than the potential-decreasing effects of alkali sulfates on $BaSO_4$, $PbSO_4$, and $SrSO_4$, respectively. Thus, considering $BaSO_4$, $PbSO_4$, and $SrSO_4$ in their saturated solutions, it is unlikely that preferential adsorption of the metal ion over that of $SO_4^=$ can account fully for the large positive potentials of these 3 sulfates. We therefore conclude that the ζ-potential of these sulfates in their saturated solution in alcohol-water mixtures can be accounted for fully only on consideration of properties of the solids themselves (*cf.* Section IV).

VII. The ζ-Potential of Gypsum

The ζ-potential of gypsum, $CaSO_4 \cdot 2H_2O$, cannot be determined in water because of its high solubility, but only in alcohol-water mixtures. In contradistinction to $BaSO_4$, $SrSO_4$, and $PbSO_4$, which have positive potentials, the potential of natural gypsum is negative, -26 ± 1 mv. It is well reproducible, although less accurately than that of the other sulfates, and shows hardly any change on prolonged streaming. Change of the composition of the solvent mixtures between 24 and 52% (wt.) alcohol produces very little variation of ζ. Exclusion of surface-active impurities cannot be as rigorous in this system[5] as in the previous ones;

---

[5] Gypsum cannot be ignited.

however, the disturbing effect of such impurities is less noticeable with gypsum than with the other sulfates, probably because surface-active substances, which usually render the potential more negative, are adsorbed less on the negative surface of gypsum than on the positive surfaces of $BaSO_4$, $SrSO_4$, and $PbSO_4$.

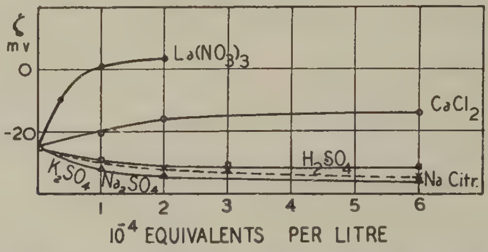

FIG. 6. Plot of the ζ-potential (in mv.) of natural gypsum ($CaSO_4 \cdot 2H_2O$) against the concentration of various electrolytes in alcohol (44.1 wt.-%)—water mixture (20°C.).

Fig. 6 shows the influence of electrolytes on the ζ-potential of gypsum. $CaCl_2$ makes the potential less negative, while alkali sulfates and H_2SO_4 render it more negative, the influence of H_2SO_4 being smaller than that of other sulfates. Nevertheless, the influence of all these electrolytes is comparatively small. Furthermore, there is little difference between the magnitudes of the potential increase due to sulfates and the potential decrease due to calcium salts. Thus the strongly negative potential of gypsum in its saturated solution is not likely to be accounted for by preferential adsorption of $SO_4^=$, but must be explained in terms of properties of the solid similarly to the explanation given previously for $BaSO_4$.

Sodium citrate makes the potential more negative but not quite as much as Na_2SO_4. Thus, the citrate ion, in spite of its tervalency, is less effective than $SO_4^=$, probably because its size and field of force are very different from that of $SO_4^=$. On the other hand, La^{+++} has a stronger influence on the potential than Ca^{++} and makes the potential positive. This, however, may partly be due to adsorption of hydrolysis products, the effect of lanthanum nitrate, as distinct from all other salts, not being quite reversible.[6]

There is a marked difference in electrokinetic properties between natural and precipitated gypsum. Not only is the ζ-potential of precipitated gypsum very small, but it is difficult to reproduce, and the ratio of E/P varies with the pressure, contrary to the Helmholtz-Smoluchowski equation and to our experience with all systesm thus far investigated. Moreover, no reproducible influence of electrolytes on the ζ-potential of precipitated gypsum can be detected.

[6] With thorium nitrate variable positive potentials and formation of gelatinous hydrolysis products were observed.

Photomicrographic and crystallographic examinations have shown that our samples of precipitated gypsum consist chiefly of twinned crystals, the growth of which has been relatively much greater in the direction of the *C*-axis than of the others, thus forming thin monoclinic needles. The crystals are very much thinner than those normally obtained with natural gypsum. According to Wooster (12), the characteristics of gypsum crystals are those of layers of Ca^{++} and $SO_4^{=}$ joined by water molecules, and the coherence of the structure in one direction is due only to water molecules. The linkages between the layers of Ca^{++} and $SO_4^{=}$ are relatively weak, thus accounting for pronounced cleavage planes. Only a small fraction of the surface area of the long and thin precipitated crystals—namely the ends of the needles—has, therefore, strong residual fields. The greater part of the other surfaces consists mainly of structural water molecules, and no Ca^{++} or $SO_4^{=}$ in the actual surface, and is not likely to adsorb $SO_4^{=}$ appreciably. In these circumstances, a double layer of considerable charge density may be formed only at the end of the needles but not at the other planes. This would account for the smallness of the ζ-potential, its lack of reproducibility—since the measured potential is the result of contributions of double layers of high and low charge density, and will depend on the degree of randomness of packing of the crystals—and its insensitivity to addition of electrolytes, since little adsorption will occur on the major fraction of the total surface area.

The well reproducible large potential of the natural gypsum, which is influenced by electrolytes, owing to ion adsorption, in a reproducible fashion, may be explained, according to this hypothesis, by the greater ratio of surfaces with high charge density, and appreciable adsorptive power, to those of low charge density and small adsorptive power.

It is interesting to note that, while natural crystals of $BaSO_4$, $SrSO_4$, and $PbSO_4$ have small (positive) potentials, natural crystals of $CaSO_4 \cdot 2H_2O$ have a high (negative) potential. The small potential of natural $BaSO_4$ (as compared with precipitated and recrystallized $BaSO_4$) has been suggested as being due to the comparative difficulty of releasing $SO_4^{=}$ from the well ordered surface (1). In the case of gypsum, the preferential release of Ca^{++} may be less impeded either by the smallness of Ca^{++} or by the weak forces in a layer lattice crystal in which part of the cohesion is due to water molecules. The weakness of these forces may also be responsible for the smallness of the electrolyte effects.

X. SUMMARY

1. The electrokinetic potentials of natural, precipitated and recrystallized samples of $BaSO_4$, $SrSO_4$, and $PbSO_4$ have been investigated in water and alcohol-water mixtures using the streaming potential method.

The potentials are positive. The natural samples which have very even surfaces always exhibit smaller potentials than precipitated and recrystallized samples having uneven surfaces. The potentials of the three sparingly soluble sulfates in water and alcohol-water mixtures decrease in the order of increasing solubility.

2. The temperature coefficient of the ζ-potential of $BaSO_4$ in its saturated solution is negative. This is not likely to be due to an increase in preferential ion adsorption with the lowering of temperature.

3. The effects of electrolytes have been investigated in water and in alcohol-water mixtures. For the same sparingly soluble sulfate the effects of electrolytes are greater in alcohol-water mixtures than in water. On comparison of various solid sulfates, it is found that the magnitude of the electrolyte effects decreases with increasing solubility of the solid. An explanation of the effect of various electrolytes on the ζ-potential in water and alcohol-water mixtures is attempted.

4. The ζ-potential of natural gypsum investigated in alcohol-water mixtures is negative. Electrolyte influence is smaller than with the other solid sulfates. Precipitated gypsum does not give reproducible values for the ζ-potential.

5. The results of this investigation suggest that the ζ-potential of a heteropolar solid is not solely determined by preferential ion adsorption, but is largely a characteristic of the solid itself. Samples of different origin, or preparation of the same compound, have widely different ζ-potentials. It is shown that this is not due to impurities but to different degrees of surface irregularity. Reference is made to a recent theory by Grimley and Mott relating the ζ-potential to lattice defects in the surface.

References

1. Buchanan, A. S., and Heymann, E., *Nature* **161**, 649 (1948); *Proc. Roy. Soc. London* **195A**, 150 (1948).
2. Grimley, T. B., and Mott, N. F., *Faraday Soc. Discussion* **1**, 3 (1947).
3. Booth, F., *Nature* **161**, 83 (1948).
4. Elton, G. A. H., *Proc. Roy. Soc. London* **194A**, 258 (1948).
5. Guggenheim, E. A., *Trans. Faraday Soc.* **36**, 139 (1940).
6. Bernal, J. D., and Fowler, R. H., *J. Chem. Phys.* **1**, 515 (1933).
7. Rice, O. K., Electronic Structure and Chemical Binding. New York, 1940, p. 408.
8. Literature *vide* Abramson, H. A., Electrokinetic Phenomena, New York, 1940.
9. Ruyssen, R. G., *J. Phys. Chem.* **44**, 271 (1940).
10. Reyerson, L. H., Kolthoff, I. M., and Coad, K., *J. Phys. Colloid Chem.* **51**, 321 (1947).
11. Rabinov, G., and Heymann, E., *J. Phys. Chem.* **47**, 655 (1943).
12. Wooster, W. A., *Z. Krist.* **94**, 375 (1936).

ELECTROKINETIC POTENTIAL AND REVERSIBLE ELECTRODE POTENTIAL OF SPARINGLY SOLUBLE SULFATES. II

A. S. Buchanan and E. Heymann

Department of Chemistry, University of Melbourne, Melbourne, Australia

Received November 19, 1948

Ever since electrokinetic properties have been studied, the question of a possible relationship between the electrokinetic potential and the reversible electrode potential of the same material has been discussed (*cf.* 1, 2). Attempts to measure both potentials with the same material suffered from the fact that, apart from glass, there appears to be no material for which both potentials can be readily determined. As $BaSO_4$ has proved to be a material whose ζ-potential is reproducible for the same sample, an attempt to determine the reversible electrode potential of $BaSO_4$ appears to be justified.

In view of the fact that all electrode potentials are relative to an arbitrarily chosen standard, no comparison of absolute values of electrode and ζ-potential is possible. A comparison must rest on the concentration function of the two potentials.

We have found that, for most electrolytes, the ζ-potential varies linearly with the logarithm of the activity of the potential-determining ion (Table I). Generally, however, this relation holds within certain limits of concentration only, and in some cases it is found that the relation $\Delta \log \zeta = K\Delta \log c$ fits the results better. In no case is $\frac{\Delta\zeta}{\Delta \log c}$ or $\frac{\Delta\zeta}{\Delta \log a}$ equal to the value expected for a reversible electrode.

A close examination of Table I does not reveal any systematic rules for most of these variations, although it is evident that the properties of the solid surface influence ion adsorption appreciably. The results on natural $BaSO_4$, with a well-ordered surface, generally fit the relation $\frac{\Delta\zeta}{\Delta \log c} = K$ up to higher concentrations than do those obtained with recrystallized $BaSO_4$, with a disordered surface. In view of this, it seems probable that, in the absence of other disturbing factors, the change of potential which is presumably due to adsorption of potential-determining ions on a crystal surface is described by the relation $\Delta\zeta = K\Delta \log c$.

TABLE I

Data based on results of the previous paper

Solvent	Solid		Added solute	Relation best fitting change with concentration (c)	Range of concentration in which applicable	$\Delta\zeta$ at this limit	$\frac{\Delta\zeta}{\Delta \log c}$
	Type	Description					
						mv.	*mv.*
H_2O	$BaSO_4$	Natural	$BaCl_2$	$\Delta\zeta = K\Delta \log c$	Up to 0.001 *N*	34	16
H_2O	$BaSO_4$	Recryst. IV	$BaCl_2$	$\Delta\zeta = K\Delta \log c$	Up to 0.00025 *N*	28.5	20
H_2O	$BaSO_4$	Recryst. III	$BaCl_2$	$\Delta\zeta = K\Delta \log c$	Up to 0.00025 *N*	28.5	21
H_2O	$BaSO_4$	Natural	$CaCl_2$	$\Delta\zeta = K\Delta \log c$	Up to 0.001 *N*	8.0	6
H_2O	$BaSO_4$	Recryst. IV	$SrCl_2$	$\Delta\zeta = K\Delta \log c$	Up to 0.0009 *N*	11.0	7
H_2O	$BaSO_4$	Recryst. III	$SrCl_2$	$\Delta\zeta = K\Delta \log c$	Up to 0.0006 *N*	10.5	6.5
H_2O	$BaSO_4$	Natural	Na_2SO_4	$\Delta\zeta = K\Delta \log c$	Up to 0.0004 *N*	24.5	16
H_2O	$BaSO_4$	Recryst. IV	Na_2SO_4	$\Delta \log \zeta = K\Delta \log c$	Up to 0.0002 *N*	16.0	
H_2O	$BaSO_4$	Recryst. III	Na_2SO_4	$\Delta\zeta = K\Delta \log c$	Up to 0.0005 *N*	21.5	14
20.88% EtOH-H_2O	$BaSO_4$	Recryst. IV	$BaCl_2$	$\Delta\zeta = K\Delta \log c$	Up to 0.0002 *N*	50	23
20.88% EtOH-H_2O	$PbSO_4$	Recryst.	$PbCl_2$	Neither of above relations			
20.88% EtOH-H_2O	$SrSO_4$	Recryst.	$SrCl_2$	$\Delta \log \zeta = K\Delta \log c$	Up to 0.0007 *N*	20.5	
20.88% EtOH-H_2O	$BaSO_4$	Recryst.	Na_2SO_4	$\Delta\zeta = K\Delta \log c$	Up to 0.00013 *N*	36.5	18
20.88% EtOH-H_2O	$PbSO_4$	Recryst.	Na_2SO_4	$\Delta \log \zeta = K\Delta \log c$	Up to 0.00025 *N*	28.0	
20.88% EtOH-H_2O	$SrSO_4$	Recryst.	Na_2SO_4	$\Delta\zeta = K\Delta \log c$	Up to 0.0006 *N*	10.0	6.5
20.88% EtOH-H_2O	$PbSO_4$	Recryst.	$La(NO_3)_3$	$\Delta\zeta = K\Delta \log c$	Up to 0.001 *N*	43.0	17
20.88% EtOH-H_2O	$SrSO_4$	Recryst.	$La(NO_3)_3$	$\Delta\zeta = K\Delta \log c$	Up to 0.001 *N*	56.0	23
H_2O	$BaSO_4$	Recryst.	$La(NO_3)_3$	$\Delta\zeta = K\Delta \log c$	Up to 0.0006 *N*	25.0	12
20.88% EtOH-H_2O	$BaSO_4$	Recryst.	$La(NO_3)_3$	Neither of above relations			

This suggestion is reinforced by the fact that a similar relation was obtained by R. G. Ruyssen (3) for precipitated $BaSO_4$, by L. A. Wood (4) for silica with metal chlorides, and by Rutgers and de Smet (5) for glass with solutions of salts of uni- and bivalent cations. Furthermore, the same relation was found by Lange and Berger (6) for the adsorption of potential-determining ions on silver halides, as determined by potentiometric methods. It may be mentioned also that the Volta potentials in electrolyte solutions, which, according to Adam (7) and Chalmers (8), should bear a closer similarity to the ζ-potential than the ordinary electrode e.m.f., vary linearly with the logarithm of the ion activity (9).

We do not possess as yet a satisfactory theory correlating the ζ-potential with the concentration of the electrolyte in solution. A recent attempt in this direction is due to L. B. Robinson (10), who used the methods of statistical mechanics employed by Gurney and Fowler in explaining the metallic electrode potential for an evaluation of the concentration function of the ζ-potential and arrived at an expression very similar to the familiar Nernst equation. Robinson assumed, however, that the amount of adsorption of potential-determining ions is independent of the concentration of these ions in the solution. This assumption is in contradiction to experience, as many investigations on adsorption of electrolytes on heteropolar solids and on glass have shown. Moreover, no distinction is drawn in Robinson's treatment between a ζ-potential and an electrode potential. If this is justified, it is possible that the difference between the experimental value of $\frac{\Delta\zeta}{\Delta \log c}$ and the one expected from the Nernst equation, $\frac{58}{Z}$ mv. (Z: valency), merely reflects the amount of variation of the adsorption of the potential-determining ions with their concentration in the solution.

In view of the absence of a satisfactory theory and, further, considering that there is a variety of processes that may influence the values of $\frac{\Delta\zeta}{\Delta \log c}$, the effects of which cannot be at present disentangled, we have merely listed such values for various systems (Table I) investigated by us, without attempting an explanation. It is noteworthy, however, that, for $BaSO_4$ and aqueous solutions of electrolytes, $\frac{\Delta\zeta}{\Delta \log c}$ is greater for Ba^{++} and $SO_4^{=}$ than for all other ions, irrespective of valency.

The first attempts to measure the electrode potential of $BaSO_4$ are due to Tendeloo (11), who used thin plates of heavy spar and obtained a linear variation of the potential (E) with the log of the barium chloride concentration, $\frac{\Delta E}{\Delta \log c}$ being of the order of 18–26 mv.; no satisfactory results were obtained with K_2SO_4 solutions. Tendeloo's values were subsequently criticized by Anderson (12) as being due to liquid-junction potentials set up in the fine cracks of the plates of heavy spar and not to a true electrode function. Tendeloo did not give any values for the resistance of the plates.

We attempted to prepare $BaSO_4$ electrodes from samples of natural barite of which the ζ-potential was already well known. Flakes of about 1 mm. thickness were chipped off the crystal and ground down, using optical emery, to about 0.3–0.4 mm. thickness. Danger of fracture prevented the preparation of thinner plates. The flake was sealed to the end of a glass tube using a low melting wax with a fatty base (Sira wax). The cell set up was

Ag | AgCl | 0.1 N $BaCl_2$ | $BaSO_4$ plate | electrolyte solution | calomel electrode,

the Ag/AgCl electrode and 0.1 N $BaCl_2$ solution being in the interior of the glass tube. In experiments with $BaSO_4$ plates which had a resistance of only 10–20 megohms, and in which the electrolyte solutions were $BaCl_2$ solutions of various concentrations, the e.m.f. varied linearly with the logarithm of $\alpha_{Ba^{++}}$, $\frac{\Delta E}{\Delta \log a}$ being 17–18 mv. When $SrCl_2$ was the electrolyte, the result was almost exactly the same, and Na_2SO_4 solutions caused changes of e.m.f. in the same direction as $BaCl_2$ but not of the same magnitude. However, if the plate of barite behaved as a $BaSO_4$ electrode, the effect of $SO_4^{=}$ should be opposite to that of Ba^{++}. A few plates were investigated which had much higher resistances ($\simeq$100 megohm) but were not thicker than the first ones; these plates did not give constant e.m.f.s. It was, therefore, suspected at this stage that the electrodes of lower resistance were "crack" electrodes, and that we were measuring liquid-junction potentials. This was confirmed by experiments in which the 0.1 N $BaCl_2$ solution inside the glass tube was replaced by a $AgNO_3$ solution, and the electrolyte solutions outside were $AgNO_3$ solutions of varying concentration. The e.m.f. now varied linearly with the logarithm of the Ag^+ activity, proving that the barite plate having fine cracks merely acted as a membrane permeable for Ag^+.

The only materials of this kind which are amenable to a determination of a true electrode potential are crystals of silver halides. Kolthoff and Sanders (13) obtained electrode plates by fusing the salts into discs which had a resistance of about 10 megohms. The e.m.f.s varied by 57 mv. per tenfold variation of the Ag^+ activity. These authors also attempted to make $BaSO_4$ electrodes but had no success. The success in the case of silver halides is probably due to greater softness of the crystals, as a consequence of which cracks are not formed as easily as with barite, and also to a higher mobility of Ag^+ in the crystal lattice as indicated by a comparatively low resistance. In view of this, it is intended to investigate the ζ-potentials of silver halides and to compare them with the electrode potentials. Preliminary attempts in this direction have been made by Julien (14).

REFERENCES

1. Freundlich, H., Capillary and Colloid Chemistry. London, 1926.
2. Abramson, H. A., Electrokinetic Phenomena. New York, 1940.
3. Ruyssen, R. G., *J. Phys. Chem.* **44**, 271 (1940).
4. Wood, L. A., *J. Am. Chem. Soc.* **68**, 437 (1946).
5. Rutgers, A. J., and de Smet, M., *Trans. Faraday Soc.* **41**, 758 (1945).
6. Lange, E., and Berger, R., *Z. Elektrochem.* **36**, 171 (1930).
7. Adam, N. K., The Physics and Chemistry of Surfaces. Oxford, 1941, p. 303.
8. Chalmers, J. A., *Phil. Mag.* **33**, 399 (1942).
9. Klein, O., and Lange, E., *Z. Elektrochem.* **43**, 570 (1937).
10. Robinson, L. B., *J. Chem. Phys.* **14**, 721 (1946).
11. Tendeloo, H. J. C., *Proc. Koninkl. Nederland. Akad. Wetenschap.* **38**, 434 (1935).
12. Anderson, R. S., *J. Biol. Chem.* **115**, 323 (1936).
13. Kolthoff, I. M., and Sanders, H. L., *J. Am. Chem. Soc.* **59**, 416 (1937).
14. Julien, P. F. J. A., Thesis, Utrecht, 1933.

DETERMINATION OF ELECTROKINETIC POTENTIALS IN CONCENTRATED SOLUTIONS BY THE STREAMING CURRENT METHOD

A. S. Buchanan and E. Heymann

Department of Chemistry, University of Melbourne, Melbourne, Australia

Received November 19, 1948

Introduction

Electrokinetic potentials cannot usually be determined accurately by the streaming potential method in electrolyte solutions more concentrated than about 10^{-3} N. For constant ζ the streaming potential decreases as the conductivity of the system increases, and is usually only of the order of a few mv. for 10 mm. Hg pressure in 10^{-3} N solutions. As a consequence, ζ-potential values in systems of good conductivity are not well known. Some knowledge of such systems would, however, be interesting for theoretical reasons which will be discussed later.

Measurements in comparatively well-conducting systems can be carried out if, instead of the customary procedure of measuring the streaming potential (E) and the resistance (R) between the electrodes, the streaming current $\frac{E}{R} = I$ is measured, as suggested by Neale (1). The modified Helmholtz-Smoluchowski equation[1] then becomes

$$\zeta = \frac{4\pi\eta}{D} \cdot \frac{IC}{P}. \tag{1}$$

It will be shown subsequently that the streaming current remains appreciable, even in well-conducting systems, although E may be too small for accurate determination.

Experimental

The principal requirement is that the galvanometer by which the streaming current is measured must have a resistance which is small compared with the internal resistance of the cell, so that virtually all the charges displaced by the streaming liquid pass through the galvanometer and only a negligible fraction passes back through the cell. It is no disadvantage of the method that current is actually drawn from the cell provided polarization can be avoided.

---

[1] The symbols are the same as those used in the first paper of this series.

For cells containing very dilute electrolyte solutions, the cell resistance may be of the order of 10^5–10^6 ohms, and galvanometers of resistance of the order of 1000 ohms are quite satisfactory. Virtually the whole of the streaming current will pass through the galvanometer in such circumstances. However, even in systems containing $N/10$ solutions which may have resistances as low as 1000 ohms, a galvanometer of 25 ohms resistance will record 97.5% of the total streaming current.

A galvanometer of 630 ohms coil resistance and a sensitivity of 1190 mm./microamp (for a scale distance of 1 m.) was used for very dilute solutions, and a galvanometer of 25 ohms resistance and a sensitivity of 210 mm./microamp for well-conducting systems. The experimental arrangement was the same as in the streaming potential work (*cf.* the first paper of this series), except that the valve potentiometer and Wheatstone bridge were substituted by the galvanometer.

RESULTS AND DISCUSSION

To test the performance of the method, a series of simultaneous measurements of streaming potential and streaming current was carried out using recrystallized $BaSO_4$ and solutions of $BaCl_2$ and K_2SO_4. The results are shown in Table I. I is the streaming current measured in the galvanometer, I_E is the streaming current calculated from the streaming potential E and the resistance R of the cell, ζ_E is the ζ-potential calculated from the streaming potential and ζ_I the ζ-potential calculated from the streaming current determination.

TABLE I

Comparison of Streaming Potential and Streaming Current Determinations
Recrystallized $BaSO_4$, sample IV

Solution	P	E	R	$\frac{I_E}{P} \times 10^6$ $\frac{\text{milliamp}}{\text{cm. Hg}}$	$\frac{I}{P} \times 10^6$ $\frac{\text{milliamp}}{\text{cm. Hg}}$	ζ_E	ζ_I
	cm. Hg	*mv.*	*megohm*			*mv.*	*mv.*
Sat. $BaSO_4$	7.09	455	2.40	28.8	28.8	26.5	26.5
$N/20{,}000$ K_2SO_4	7.85	136	0.835	20.8	20.4	19.2	18.8
$N/10{,}000$ K_2SO_4	8.03	64.0	0.500	15.9	15.1	14.6	13.9
$3/10{,}000$ N K_2SO_4	10.63	15.0	0.195	7.0	5.9	6.4	5.4
Sat. $BaSO_4$	11.34	705	2.29	27.2	27.0	26.2	26.0
$N/50{,}000$ $BaCl_2$	8.17	455	1.72	32.4	33.8	40.4	42.2
$N/20{,}000$ $BaCl_2$	6.89	281	1.06	38.5	40.6	48.2	50.8
$N/2{,}500$ $BaCl_2$	6.02	60.4	0.180	54.8	55.0	68.6	68.8
$N/1{,}000$ $BaCl_2$	5.61	26.5	0.0775	60.4	60.2	75.3	75.1

Cell constant: $C = 9.50$ cm.$^{-1}$.

The agreement between ζ_E and ζ_I is not perfect in all cases, yet no systematic deviation is evident. In a number of experiments, the variation of the streaming current I with the driving pressure (P) was investigated. There was always proportionality as postulated by the Helmholtz-Smoluchowski equation.

Experiments with $BaCl_2$ and $SrCl_2$ solutions were carried out up to a concentration of 0.1 N. There was hardly any evidence of polarization of the Ag-AgCl electrodes even in $N/10$ solutions. However, alkali sulfates could not be investigated at concentrations greater than 10^{-3} N because polarization became appreciable. For the same reason, the ζ-potential of gypsum in its saturated solution in water cannot be investigated; a saturated solution of gypsum is 0.028 N at 20°C.

The results are shown in Fig. 1. The full lines represent ζ-potential values calculated using the dielectric constant of water, while the broken lines refer to ζ-values calculated using the dielectric constants of the respective electrolyte solutions. There is little difference between the two sets of ζ-values up to 10^{-3} N. The dielectric constants of the electrolyte solutions are those determined by Lattey and Davies (2). We have assumed in the calculation that solutions of $SrCl_2$ have the same dielectric constant as those of $BaCl_2$, but this may be only approximately true according to the experimental results of Fradkina (3).

Fig. 1 shows that, for both $BaCl_2$ and $SrCl_2$, the ζ-potential of $BaSO_4$, after the initial increase, begins to decrease at concentrations above

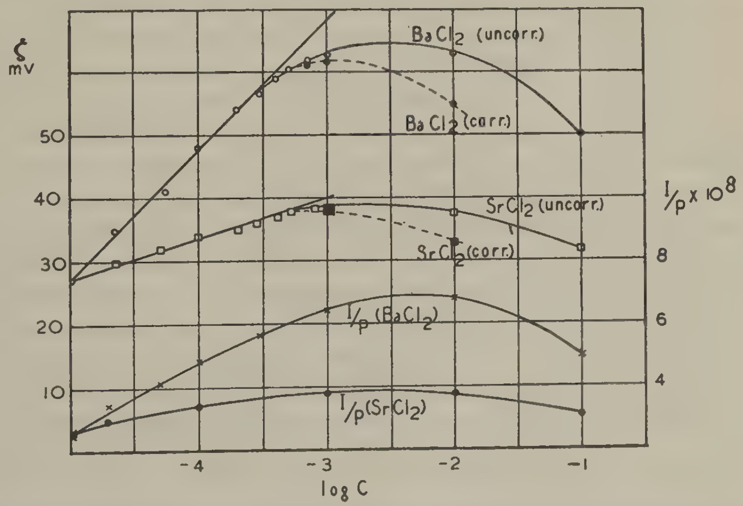

FIG. 1. Plot of the ζ-potential (in mv.) determined by the streaming current method of recrystallized $BaSO_4$ against the logarithm of the concentration of $BaCl_2$ and $SrCl_2$. The two lowest curves show a plot of $I/P \times 10^8$ against the logarithm of the concentration (20°C.).

10^{-3} N, but is still greater than in water at 10^{-2} N. The values in 0.1 N solution are uncertain since the dielectric constant measurements of Lattey and Davies only extend to 10^{-2} N and extrapolation does not appear justified. It may, therefore, be preferable to discuss this result in terms of μ, the electric moment of the double layer. Since

$$\mu = \frac{\zeta D}{4\pi},$$

we obtain by substituting for ζ from Eq. (1)

$$\mu = \frac{I}{P} \cdot \eta C.$$

Fig. 1 shows the variation of $\frac{I}{P}$ with log c, and it is apparent that the electric moment in 10^{-1} N solution is only slightly smaller than in 10^{-3} N solution of $BaCl_2$ or $SrCl_2$.

It has been shown in the previous paper that the relation $\Delta\zeta = K\Delta \log c$ describes the variation of the ζ-potential with concentration up to a limit which varies with the nature and origin of the sample. Above that limit, which, for recrystallized $BaSO_4$ and $BaCl_2$ solution, is at about $10^{-3.5}$ N, ζ begins to deviate irrespective of whether corrected or uncorrected values are considered. In view of our limited knowledge of the factors which determine the above relation, any explanation of the cause of the deviation must be regarded as tentative. Two possibilities suggest themselves: The falling-off of ζ, shown in Fig. 1, may be due either to an abnormal decrease of the charge density as a consequence of an appreciable adsorption of Cl^- (together with Ba^{++}) on the crystal surface at higher concentrations, or to a decrease in the equivalent thickness of the double layer with increasing concentration of electrolyte. The evidence obtained during this investigation does not favor the former alternative, since adsorption of Cl^- on a $BaSO_4$ surface is, in spite of the small energy of hydration of Cl^-, not likely to occur readily for reasons of geometry. We may, therefore, conclude that a compression of the double layer has occurred at higher concentrations of $BaCl_2$, but not to the extent predicted by the theory of Gouy, which suggests an equivalent double layer thickness of the order of 10^{-7} cm. for 0.1 N $BaCl_2$. It may not be easy to reconcile a double layer of nearly molecular dimensions with the high values of ζ and $\frac{I}{P}$ obtained in this investigation. Nevertheless, the measured value of ζ would not be a reliable guide on this point if a simultaneous increase in charge density and decrease in thickness of the double layer had occurred. At present we have not sufficient information to comment further on this point, but would like to refer to a theoretical study by Bikerman (4) on the capacity and the equivalent thickness of the electric double layer on the surface of mercury against electrolyte solutions, in which the theory of Gouy is modified and further developed.

SUMMARY

The streaming current method for measuring ζ-potentials is discussed and its performance compared with that of the streaming potential method. The streaming current method makes it possible to measure the ζ-potential of $BaSO_4$ in solutions of some electrolytes, *e.g.*, $BaCl_2$, $SrCl_2$, up to concentrations of 0.1 N. Even at this comparatively high concentration, the ζ-potential is quite appreciable. The theoretical implications of this result are discussed.

REFERENCES

1. NEALE, S. M., *Trans. Faraday Soc.* **42**, 473 (1946).
2. LATTEY, R. T., AND DAVIES, W. G., *Phil. Mag.* [7] **12**, 1111 (1931); **13**, 444 (1932).
3. FRADKINA, E. M., *J. Phys. U.S.S.R.* **11**, No. 3 (1947).
4. BIKERMAN, J. J., *Phil. Mag.* [7] **33**, 384 (1942).

LIGHT SCATTERING PROPERTIES OF MONODISPERSED SULFUR SOLS. I. MONOCHROMATIC ULTRAVIOLET ANGULAR SCATTERING. II. EFFECT OF THE COMPLEX INDEX OF REFRACTION UPON TRANSMITTANCE [1]

Allen S. Kenyon [2] and Victor K. LaMer

From the Department of Chemistry, Columbia University, New York City

Received February 26, 1948; revised Oct. 13, 1948

INTRODUCTION

When white light is passed through a monodispersed colloid, *e.g.*, an oil aerosol (1) or a sulfur sol (2), in which the radii of the spherical droplets are very uniform and comparable in magnitude to the wavelength of the incident light, brilliant colors appear in the scattering light at well defined angles. These colored bands have been designated as Higher Order Tyndall Scattering Spectra (3).

The angular positions of these colors are a function of the particle radius and the relative (real) index of refraction of the dispersed particles and the medium. They have been used recently for the rapid and precise determination of the particle radius in these systems (1, 2, 3).

In this communication, *monochromatic ultraviolet incident light* will be used. An order in the scattered spectra should appear then as a band of intensity depending upon its position, but narrow in respect to angle, if the system is monodisperse. Since scattering is a function of the ratio of radius to wavelength, the determination of particle size can be extended to smaller radii by substituting ultraviolet for visible light.

The scattering of light by isotropic spherical particles has been treated theoretically by a number of investigators (5–11). The Rayleigh (10) equation is limited to particles whose radii are less than 1/10 the wavelength of light. For larger particle sizes a more general theory utilizing the contribution from many partial electric and magnetic waves is necessary. Mie (6) solved this as a boundary value problem in electromagnetic theory. His treatment and Debye's (7) have been presented in detail by Stratton (13) and briefly in Ref. 3.

---

[1] Presented at the New York meeting of the American Chemical Society, September, 1947, before the Div. of Physical and Inorganic Chemistry.

[2] Present address: Monsanto Chemical Co., Dayton, Ohio.

In extending the earlier work (1) on aerosols to sulfur hydrosols (2), it was found that as many as 9 orders could be demonstrated using natural light when the monodisperse character was improved by controlling the conditions of preparation. LaMer and Johnson (14) confirmed that the number and angular position of the orders depended in a reproducible manner upon the elapsed time after mixing fixed concentrations of the dilute solutions of acid and thiosulfate. The angular positions were then calibrated (3) in terms of radius by comparison with values calculated from the Mie theory and the results verified by direct determination of the radii from the rates of sedimentation. The intensity functions used (3) were computed from the Mie theory for a relative index of refraction of 1.44, since this value of m fitted the experimental data closer than that for the next table, then available for angular dependence, namely, $m = 1.55$. In this research, we find the correct values of m to be employed range from 1.46 to 1.51, depending upon the wavelength.

The scattering coefficient K_S, introduced (15, 16) as a means of estimating the size of polydisperse water fog droplets ($m = 1.33$) from *optical transmission* measurements *as a function of wavelength*, was utilized (1) to determine particle sizes in various monodisperse aerosols ranging from $m = 1.44$ to 2.0. Barnes and LaMer (2) employed this procedure for sulfur sols and found transmission useful for determining not only the radius, but also the number of particles per cc. All of the above studies were conducted for wavelengths at which no absorption occurs and, consequently, functions involving only the real index of refraction were required.

Mie (6) developed his theory in terms of the complex refraction index for application to particles which absorb as well as scatter. The theory has been applied to gold sols (17) and carbon particles (18). Gribnau (19) studied the effects of absorption plus scattering on selenium sols, and reported the results in the form of extinction, scattering and consumptive absorption as a function of wavelength. Her sols, however, were not monodisperse in the sense of the present work and, hence, her curves do not show the detailed structure we have observed.

Sulfur is transparent in the visible, but absorbs (4) appreciably in the ultraviolet below $\lambda = 3000$ Å, in which case m, the real index of refraction, must be replaced in theoretical computations by the complex index of refracion $m^1 = m(1 - ik)$, where k is the coefficient of absorption and $i = \sqrt{-1}$. One of the primary purposes of this investigation was, therefore, to determine the magnitude of this complication in the scattering process, and to compare experimental results with existing theory using simplified expressions for the functions involving m which have become available recently.

THEORY

Scattered Light. When light strikes a particle, periodic oscillations of the electrons are set up. These oscillations produce a field of radiation outside the particle. When the radius of the particles is 1/10 the wavelength of the incident light, a single periodically varying dipole may be substituted for the oscillating electrons. The frequency of oscillation of this dipole will be the same as the incident light, but its amplitude is governed by the optical properties of the particle. If the particle is an isotropic nonabsorbing sphere, the intensities of the scattered light may be written in the form

$$\left.\begin{matrix} J_1 \\ J_2 \end{matrix}\right\} = \frac{\lambda'^2\alpha^6}{8\pi^2R^2}\left(\frac{m^2-1}{m^2+2}\right)\left\{\begin{matrix} 1 \\ \cos^2\theta, \end{matrix}\right. \qquad \begin{matrix} (1) \\ (2) \end{matrix}$$

where J_1 is the intensity of the component whose electric vector is perpendicular to the plane determined by the light source, particle and observer; and J_2 is the component whose electric vector is parallel to the same plane; λ' is the wavelength of the incident and scattered light in the medium and is equal to $\lambda(\text{air})/m_o$ where m_o is the refractive index of the medium; R is the distance from observer to particle and $\alpha = 2\pi r/\lambda'$, r is the radius of the particle, m is the relative refractive index of the particles relative to that of the medium and may be either real or complex, θ is the angle of observation measured from the backward direction of incident light propagation. Eqs. (1) and (2) apply when the incident light has unit intensity and is unpolarized.

When the radius of the particles becomes larger than $\lambda/10$, the scattering no longer depends upon a single electric dipole; instead, many electric and magnetic multipoles must be considered. The scattered field around such a sphere is described mathematically by an infinite series of spherical harmonics. The equations of Mie may be expressed as:

$$\left.\begin{matrix} J_1 \\ J_2 \end{matrix}\right\} = \frac{\lambda'^2}{8\pi^2R^2}\left\{\begin{matrix} |f_1(m, \alpha, \theta|^2 \\ |f_2(m, \alpha, \theta|^2, \end{matrix}\right. \qquad \begin{matrix} (3) \\ (4) \end{matrix}$$

$f_1(m, \alpha, \theta)$ and $f_2(m, \alpha, \theta)$ are complicated functions of index of refraction, radius, wavelength, and scattering angle. Eqs. (3) and (4) reduce to Eqs. (1) and (2) when the radii of the particles are very much smaller than λ. In the case of absorbing materials, some of the radiant energy which penetrates the particle is converted into other forms of energy. This occurs when the conductivity is finite. For such materials, the refractive index is complex. If the particle is nonabsorbing, then m is the ordinary relative refractive index.

The disturbance caused by the particle depends upon the value of α, that is, upon r/λ, and the refractive indices of the medium and particles. As the particles become larger, the coherent radiations from the multipoles will interfere and cause the intensity of the scattered light to have maxima and minima as a function of angle. These variations in intensity depend upon wavelengths and consequently produce the colored bands. The angular positions of orders thus depend upon the wavelength of the incident light and are functions of the particle size and the refractive index of the particle relative to that of the medium. The number of orders in the Tyndall spectra will be set equal to the number of distinct bands of a particular wavelength that are observed from $\theta = 0°$ to 180°. The Tyndall spectrum in the Rayleigh region will be assigned order zero.

The total light energy scattered by one isotropic sphere of any size per second per unit intensity of illumination is

$$S = \frac{\lambda'^2}{2\pi} \sum_{n=1}^{\infty} \frac{|A_n|^2 + |P_n|^2}{2n + 1} \cdot n^2(n + 1)^2. \tag{5}$$

Here A_n and P_n are complex functions of the parameter and the relative index of refraction m. Eq. (5) is the sum J_1 and J_2 (Eqs. (3) and (4)) integrated over all angles (16). When the radius of the particle is small compared to the wavelength, Eq. (5) reduces to the Rayleigh expression

$$S = 24\pi^3 \left(\frac{m^2 - 1}{m^2 + 2}\right)^2 \frac{V^2}{\lambda'^4}, \tag{6}$$

where V is the volume of the particle.

The functions occurring in Eqs. (3) and (4) have been computed and tabulated by Dr. Arnold Lowan and his staff, Mathematical Tables Project, U. S. Bureau of Standards (20); for values of the real index $m = 1.33, 1.44, 1.55$, and 2.0; for angular intervals of 10° from 0° to 180°, and for α values ranging from 0.5 to 6. The α values are given in pairs in which the ratio is 1.2. The ratio of 1.2 was selected by LaMer and Sinclair (1) for the computations because the predominant order colors were red and green when the sol was illuminated with white light.

Order positions for one wavelength can be conveniently determined by comparing for two wavelengths the ratios of their intensities and plotting these ratios as a function of angle. The maxima correspond to the order positions for λ_1'. The light intensities scattered in the forward direction are many times larger than the intensity scattered backwards and a plot of intensity for one wavelength as a function of angle gives a pattern that is not easily interpreted. The ratios of intensities for two properly chosen wavelengths give a more convenient plot.

The theoretical order positions for a particular wavelength can be located from the available tables of intensity functions by calculating the ratios of intensities from $\alpha_1/\alpha_2 = 1.2$ at angular intervals of 10° from 0° to 180°. These calculations are repeated using all available pairs of α values of the same ratio. Curves of order positions as functions of α are obtained from these calculations (Δ's in Fig. 3). Angular order positions for any relative refractive index are determined by graphical interpolation from $m = 1.33$ to 2.0.

Total Scattering and Transmission. When the angular intensity of scattered light is integrated over the surface of a sphere, the result is the total light energy scattered/sec. by one particle. This total energy divided by the energy flux of the incident light gives the scattering cross section of the sphere. If this effective scattering area is divided by the geometrical area, a dimensionless coefficient will result, which will be designated as the scattering coefficient K_s when there is no absorption and the extinction coefficient K_e when there is absorption plus scattering.

These coefficients are related to experimentally determinable quantities as follows:

$$\log I_o/I = K_s \pi r^2 nl/2.3 \qquad \text{(Scattering only)}, \tag{7}$$

$$\log I_o/I = K_e \pi r^2 nl/2.3 \qquad \text{(Scattering plus absorption)}, \tag{8}$$

where I_o/I is the intensity ratio of the incident light to the transmitted light, K_s and K_e are, respectively, the scattering coefficient and the extinction coefficient which describe the total dissipation of incident radiant energy, n is the number of particles per cc. l is the length in cm. of the path traversed by the light, r is the radius of the particle.

Eq. (7) differs from the equation of Stratton and Houghton (15) by a factor of 2. LaMer and Sinclair (1) found (1941–42) that their experimental results did not agree with the theoretical equation of Stratton and Houghton. They questioned the earlier theory and offered Eq. (7) as a substitute. This question has since been treated in detail by Sinclair (21) and Brillouin (22) and independently by Van de Hulst (11), who refers to the independent work of Bricard (12).

K_s and K_e may be expressed in terms of the Mie theory as

$$K_s = \frac{2}{\alpha^2} \sum_{n=1}^{\infty} \frac{n^2(n+1)^2}{2n+1} \{|A_n|^2 + |P_n|^2\}, \tag{9}$$

$$K_e = \frac{2}{\alpha^2} \sum_{n=1}^{\infty} n(n+1)\,(-1)^n R_{\text{eal}}[-iA_n + iP_n]. \tag{10}$$

For detailed definitions of the functions A_n and P_n the reader is referred to the original papers (6, 7), to Van de Hulst (11) and the forthcoming review by Sinclair and LaMer (Aerosol Symposium, *Chem. Rev.* 1949).

Eq. (10) can be written in the form

$$K_e(m, k, \alpha) = R_{\text{eal}}[F(m - imk, \alpha)], \tag{11}$$

where F is a complex function of the complex refractive index $m - imk$. For nonabsorbing particles ($k = 0$) we write

$$F(m, \alpha) = K(m, \alpha) + iL(m, \alpha), \tag{12}$$

where K and L are real functions of the real refractive index m. Then we have:

$$F(m + \Delta m, \alpha) = K(m, \alpha) + \Delta m K'(m, \alpha) + \frac{(\Delta m)^2}{2} K''(m, \alpha) + \cdots$$
$$+ iL(m, \alpha) + i\Delta m L'(m, \alpha) + i\frac{(\Delta m)^2}{2} L''(m, \alpha) \cdots. \quad (13)$$

By substituting $-imk$ for Δm and taking the real part in accordance with Eq. (11), Horenstein and Lowan (23) have set up the following polynomial for the coefficients for either scattering or for scattering plus absorption.

$$K_e(m, -imk; \alpha) = K(m; \alpha) + mkL'(m; \alpha) - \frac{m^2k^2}{2!} K''(m; \alpha)$$
$$- \frac{m^3k^3}{3!} L'''(m; \alpha) + \frac{m^4k^4}{4!} K''''(m; \alpha). \quad (14)$$

The primed quantities denote partial derivatives with respect to m. Van de Hulst (private communication—see Eq. 8.5 of Rev. 11) points out that $F = K + iL$ has the physical significance of giving the amplitude with the correct phase of the forward scattered light. Eq. (14) is a function of m and k only and each α value requires a separate polynomial equation. Equations are presented for α values from 0.5 to 7, and an example for $\alpha = 2$ is given as:

$$K(m, -imk; 2.0) = 138.07672 - 287.92558m + 197.32048m^2$$
$$- 43.95881m^3 + 47.86197mk - 30.96270m^2k$$
$$- 197.32048m^2k^2 + 131.8674m^3k^2. \quad (15)$$

The polynomial form for other α values may be found in the report of Horenstein and Lowan (23).

When the particles are nonabsorbing, the polynomial expressions for all α values reduce to functions of the real refractive index, giving the scattering area coefficient (K_s). The terms in the equation involving k give the contribution of the complex index of refraction. These approximate polynomials are valid only for an absorption index up to 0.1, and for relative refractive indices from 1.33 and 1.65. Considerable error may appear in the extrapolation beyond $m = 1.55$ and below $m = 1.44$ when values larger than 3 are used.

The use of these polynomials permits the computation of $K(m, -mk; \alpha)$ for a range of values of m and k without recourse to Mie's or Stratton's formulae and their complications. It is no longer necessary to refer to an extensive table of Bessel functions $J_{n+\frac{1}{2}}(Z)$ of complex variables for a range of Z and n where Z is equal to $(m - imk)$.

Determination of Particle Size. The size and number of particles are calculated from transmittance measurements using Eqs. (7) and (8). The theoretical log K_s or K_e values are plotted as a function of log α, and the experimental quantities log (log I_o/I) are plotted against log $1/\lambda'$ on the same graph. The displacement along the abscissa necessary to superimpose the theoretical and experimental minima is equal to log $2\pi r$ and the displacement along the ordinate, is equal to

$$(\log K_e \text{ or } K_s) - \log (\log I_o/I) = -\log \pi r^2 nl/2.3. \qquad (16)$$

EXPERIMENTAL

Preparation of the Monodispersed Sols. Monodispersed sulfur sols were prepared by the method of LaMer and Barnes (2) by mixing exactly 1 cc. of 1.0 *M* sodium thiosulfate with 998 cc. of distilled water and adding to this exactly 1 cc. of 1.5 *M* sulfuric acid. All components were maintained at 25°C. ± 0.1° before and after mixing. At desired time intervals, the growth of the particles was stopped by partial decomposition (60–70%) of the stoichiometric amount of thiosulfate by addition of iodine. Complete decomposition of the thiosulfate causes a reversal of the reaction with consequent instability and resolution of the sulfur particles during measurement.

Ultraviolet Angular Scattering. An instrument to measure the ultraviolet "orders" was constructed of the following essential parts: (a) Ultraviolet light source and optical system, (b) an electronic detecting system for measuring the intensity of the scattered light, and (c) a protractor for measuring the angle between the incident light and the point of observation.

The optical system consisted of a quartz lens and parallel slits to collimate into a parallel beam the light from a General Electric AH-4 Mercury Vapor lamp. The scattered light from the sol was passed through a Nicol prism oriented so that only the vertical component of the light reached the detecting system. The 3650 Å line of the mercury spectra was isolated with a Corning glass filter No. 586 and the 4360 Å line was isolated by a combination of Corning filters No. 511 and No. 038. The transmittance of these filters were checked on a calibrated spectrophotometer. The optical system is shown in the sketch of the apparatus in Fig. 1.

The detecting system consisted of an electronic amplifier (24) with an R.C.A. 929 photo tube. The current produced by the light was maintained at zero by means of a back E.M.F. supplied from a potentiometer.

The sulfur sol was placed in an 8 cm. Pyrex crystallizing dish on a circular table which was graduated in degrees. This table turned through an arc of 180° and the angle could be set at intervals of 5° from 30° to 170°.

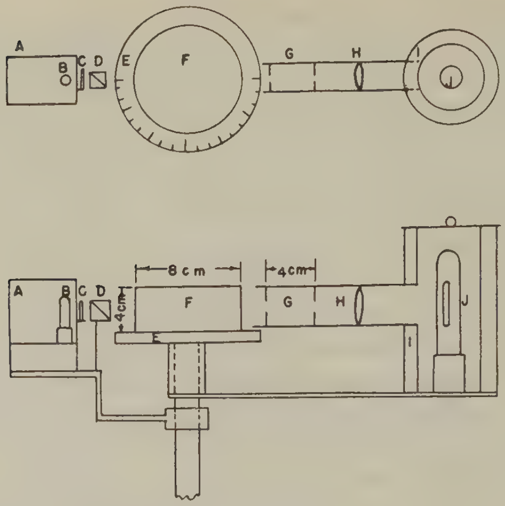

FIG. 1. Angular scattering apparatus.

A = Amplifier
B = Phototube
C = Filter
D = Nicol prisms
E = Protractor stand
F = Crystallizing dish
G = Slits 6 mm × 6 mm
H = Quartz lens 6″ F.L.
I = H_2O cooled jacket
J = AH-4 mercury lamp

Present available tables of intensity functions were constructed on the basis that $\alpha_1/\alpha_2 = 1.2$. Any two wavelengths that are in ratio of 1.2 can be used to determine order positions from the available tables. The 3650 Å and the 4360 Å lines of the mercury spectra are in the ratio 1.195 and therefore meet this requirement. Since there is no absorption for the 4360 Å line, the complex angular scattering functions are not required at this wavelength.

The orders were determined by measuring the intensity of the vertical components (J_1) of the scattered light at 5° intervals from 3° to 170°, at a wavelength of 3650 Å and the measurements repeated for a wavelength of 4360 Å. The ratio of the intensities of these two wavelengths, $J\lambda_{4360}/J\lambda_{3650}$, were then plotted against angle. The angles where this ratio is a maximum correspond to an order of 4360 Å. Likewise, the minima correspond to orders of 3650 Å. The angular scattering in the ultraviolet is plotted for a typical experiment in Fig. 2, where $r = 0.26\ \mu$. Many distinct orders appear even for these small particles. This sol would have exhibited only two indistinct orders if the intensities had been measured in the visible. Johnson and LaMer (14) studied angular scattering using white incident light and measuring the ratio of intensities of the red and green bands as a function of angle θ. They isolated the bands of red and green light by means of Wratten filters having maximum trans-

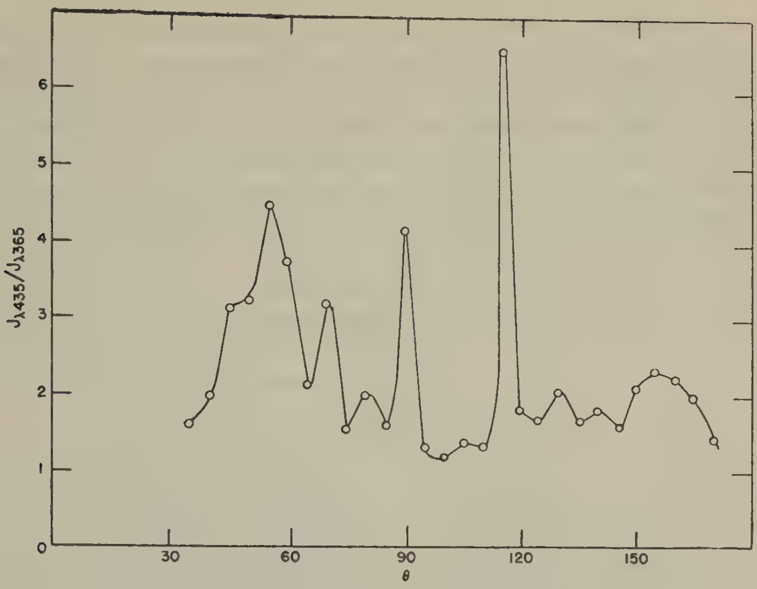

FIG. 2. Ultraviolet angular scattering. $r = 0.26\ \mu$

mittance at 6290 Å and 5240 Å, respectively. With this illumination, the "orders" appear as wide bands, while, with monochromatic illumination, the orders appear as narrower bands.

It is important that the correct relative refractive index m be used to

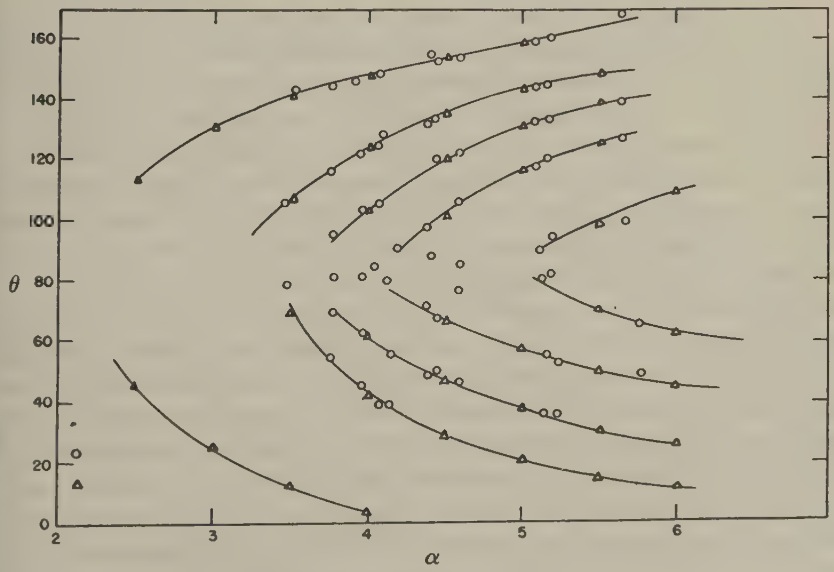

FIG. 3. UV angular scattering for $m = 1.51$. $\lambda' = 326\ m\mu$.

obtain agreement between theory and experiment. For $\lambda = 4360°$ ($\lambda' = 3260$) m is 1.51. Curves for $m = 1.51$ were obtained by graphical interpolation (Fig. 3) from the available tables for $m = 1.33$, 1.44, 1.55, and 2.0. Experimental points are shown in circles. There is remarkably good agreement between theory and experiment.

Table I shows the results of several experiments with the angular order positions. The particle radii are accurate to $\pm 0.005\mu$.

TABLE I

Ultraviolet Angular Scattering

$m = 1.51$

Age in min.	Radius in μ	Order positions $\theta_1, \theta_2, \theta_3, \cdots$ for $\lambda = 4360$
80	.194	53, 70, 81, 95, 115, 145
90	.212	55, 80, 91, 104, 122, 146
90	.205	46, 63, 82, 103, 121, 146
105	.238	—, 45, 65, 85, 105, 121, 153
116	.226	48, 60, 70, 97, —, 131, — (10 cc. of 1 m KCl)
120	.269	36, 52, 85, 95, 120, 132, 143, 160
[a]120	[a].272	[a]56, [a]88, [a]138
120	.264	55, 80, 90, 116, 131, 142, 157
120	.229	50, 66, 88, 121, 132, 152 (10 cc. of 1 M KCl)
150	.294	48, 65, 99, 125, 139, —, 168

[a] Measured in the visible ($\lambda = 6720$).

The radii determined with ultraviolet light agree with those obtained using visible light. Since the experimental values will not fit any other relative index, this agreement shows that 1.51 appears to be the correct relative index of refraction for this system at a wavelength of 4360 Å.

If other wavelengths or other colloidal systems are used, it is necessary to know the relative index and, after knowing this relation, the angle of order appearance as a function of α can be interpolated graphically for any relative index of refraction between 1.33 and 2.0 from the available computations in OSRD Report No. 1857.

Higher orders do not appear in the Tyndall spectra until after the particles have grown to a size corresponding to $\alpha \geq 2$ approximately, *i.e.*, $r \geq \lambda'/3$ or $\lambda/4$. This has been verified theoretically and experimentally. The number of these orders are, therefore, dependent upon the wavelength used. When the wavelength of 6760 Å is used, the smallest particle that will exhibit an order is approximately 0.20 μ.

In the visible, if the sol is relatively polydispersed, the central orders become diffuse and finally disappear. The same phenomenon occurs in the ultraviolet.

Ultraviolet Transmittance and the Use of the Complex Refractive Index. The transmittance of the sols was measured on a Beckman quartz spectrophotometer, Model DU, at intervals of 50 Å from 2850 Å to 4000 Å using 10 cm. quartz absorption cells. The value of I_o was adjusted using a solution of 0.001 M sodium thiosulfate to which was added the same amount of iodine as was used to stop the growth of the sol.

In the case where the particles absorb as well as scatter, the complex refractive index will be required to calculate the extinction area coefficient, K_e. The relative complex refractive index $m = m'(1 - ik)$ where m' is the ordinary relative refractive index and k is the absorption index in the expression

$$I = I_o e^{\frac{-4\pi k x}{\lambda}}, \tag{17}$$

x = the thickness of the layer.

Sulfur exists in colloidal dispersions as S_μ and S_λ (25), the form depending upon the method of preparation. If the sulfur sol is prepared by using concentrated solutions of thiosulfate and acid, S_μ will predominate, but in dilute solutions S_λ is formed. The sols used in these experiments consist chiefly of S_λ since most of the sulfur can be extracted with CS_2. The colloidal sulfur particle consists of sulfur and a film of polythionic acids and thiosulfuric acid (26). Only sulfur absorbs (4) at the wavelengths used in this study so that it was necessary to measure the absorption index of pure sulfur (S_λ). The sulfur was purified according to Bacon and Fanelli (27).

Absorption Index of Sulfur. A cell was fabricated to hold the sulfur at its melting point while transmittance measurements were made. Molten sulfur (S_λ) at a temperature of 119°C. was pressed between two optically flat quartz plates (20 mm. × 20 mm.) by means of four screws on the cell holder. An electric heater was connected to the cell holder and the temperature on this heater was controlled by means of a Variac to maintain the sulfur at its melting point. The transmittance was quickly measured for several wavelengths between 4000 Å and 3200 Å.

The thickness of the sulfur film (approximately 30μ) was measured by means of a microscopic comparator. Several thickness readings were made on the four edges and the average taken as the overall film thickness. The measurements of thickness could be reproduced to within 1μ.

From the thickness and transmittance measurements, the value of the absorption index as a function of wavelength was calculated. Table II shows the averaged results of several determinations and Fig. 4 is a plot of the averaged log k against λ. The decrease in the light transmitted due to reflection has been neglected, because it is small compared to the experimental error in measuring the absorption index.

TABLE II

Absorption Index of Sulfur as Function of Wavelength

λ	k	k(av.)
4000 Å	.0015	.0017
	.0018	
	.0016	
	.0018	
	.0016	
3800	.0030	.0028
	.0025	
	.0030	
3600	.0040	.0044
	.0045	
	.0047	

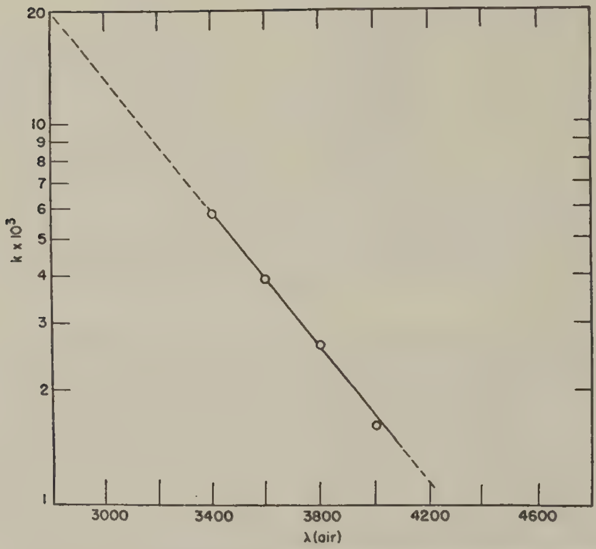

FIG. 4. Absorption index for liquid sulfur (S_λ).

It was found that the following values for the absorption index would be required in the calculation:

λ	k
3000 Å	0.013
3500	0.0045
4000	0.0017

For wavelengths greater than 4000 Å the absorption index can be neglected.

Refractive Index of Sulfur. A linear relationship exists for the logarithm of the absorption index of sulfur as a function of wavelength for normal dispersions over the range involved. The dispersion for sulfur sols in the wavelength regions studied is normal and, therefore, the absorption index can be extrapolated a short distance to wavelengths other than those measured. Lifschitz and Brandt (28) measured the refractive indices of an Odén sulfur sol at several concentrations and at wavelengths from 6563 Å to 4861 Å. They found that the refractive index of the sol was directly proportional to the concentration of the sulfur present. The data are tabulated in Table III, and Fig. 5 shows a plot of the relative refractive indices of sulfur as a function of wavelength. The relative refractive indices used in Fig. 5 were obtained by dividing their averaged index by the refractive index of water at the wavelength in question.

TABLE III

Relative Refractive Index of Sulfur as a Function of λ

Å	m
6563	1.46
5890	1.479
5350	1.495
4922	1.50
4861	1.51

Calculated from averaged data of Lifschitz and Brandt (28).

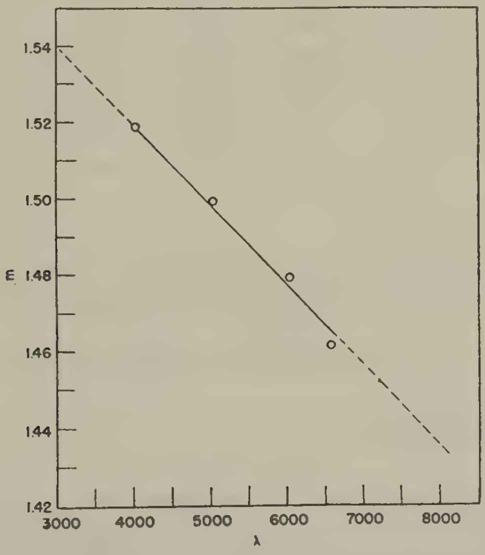

FIG. 5. Relative refractive index for colloidal sulfur.

The curve was extrapolated to the near ultraviolet region. This extrapolation was justified since the refractive index of a sulfur sol was checked by means of a hollow prism on a spectrometer with the mercury spectrum. The relative refractive index to three significant figures as a function of wavelength was verified to be a straight line to $\lambda = 4050$ Å. Further extrapolation to 3000 Å was justified on the basis of experimental checks of particle size as determined by angular scattering and transmittance methods.

The sulfur sol (formed in 0.0010 M $Na_2S_2O_3$ and 0.0015 M H_2SO_4) begins to absorb appreciably at a wavelength of approximately 3800 Å and the absorption maximum is reached at approximately 2800 Å. The studies were extended only to a wavelength of 3000 Å, in order to avoid complications of an anomalous dispersion.

TABLE IV

Theoretical K_s and K_e

α	K_s $m = 1.50$	K_s $m = 1.52$	K_e $m = 1.52$ $k = .0017$	K_s $m = 1.53$	K_e $m = 1.53$ $k = .0045$	K_s $m = 1.54$	K_e $m = 1.54$ $k = .013$
1.0	0.2151	0.2323	0.2394	0.2411	0.2599	0.2501	0.3045
1.5	0.7528	0.8179	0.8289	0.8518	0.8823	0.8867	0.9700
1.8	1.3489	1.4835	1.4921	1.5538	1.5748	1.6259	1.6790
2.0	1.7984	1.9442	1.9463	2.0162	2.0197	2.0874	2.0933
2.5	2.5395	2.7261	2.7273	2.8234	2.9234	2.9234	2.9145
3.0	3.4180	3.5458	3.5324	3.6024	3.5627	3.6544	3.5453
3.6	4.1849	4.2972	4.2740	4.3354	4.2478	4.3612	4.1214
4.5	4.2025	4.0851	4.0067	4.0113	3.9328	3.9293	3.7786
5.0	3.9278	3.8648	3.7813	3.8059	3.7235	3.7241	3.546
5.5	3.1816	2.9480		2.8403	(2.8578)	2.7438	(2.7842)
6.0	2.9039	2.5971		2.4565	[a]2.4807	2.3264	2.4091
6.5	2.3672	2.3260		2.2627	(2.26)	2.1581	(2.2511)
7.0	1.848						
7.2	1.771						
8.0	1.777						

[a] 2.5013 if $k = 0.009$. This corresponds to 100% error in the measurement of the absorption index.

( ) values obtained by an approximation method and are accurate to three significant figures.

K_s = scattering coefficient.

K_e = extinction coefficient.

K_s and K_e as Functions of r/λ. The theoretical values for the extinction coefficients (K_e) calculated using the polynomial formulae for the sulfur sol system which has $m = 1.52$, 1.53, and 1.54 when the absorption index is .0017, .0045, and .013, respectively, are tabulated in Table IV. Similar values for the scattering coefficients (K_s) are also tabulated. The scattering coefficient values (K_s) are the values when the relative refractive index is real or when there is no absorption.

The values of K_e, for α values of 5.5 and 6.5, using the relative index f 1.52, 1.53, and 1.54, and the absorption index of .0017, .0045, and .013, respectively, especially were calculated by Mr. William Horenstein nd staff under the direction of Dr. Arnold Lowan of the Mathematical ables Project, National Bureau of Standards.

The theoretical values for the extinction K_e and scattering K_s coeffi- ients for $m = 1.54$ and K_s for $m = 1.50$ have been plotted logarithmi- ally as a function of α in Fig. 6. In contrast to $m = 1.50$, the plots of the heoretical points for $m = 1.54$ show smooth curves for K_s and K_e with o apparent minima. This is because the theoretical points were calcu- ated for fairly large intervals of α values. To locate a minimum theoreti- ally would require a very large number of intermediate points because t is known that the scattering curve is an oscillating function for large α alues. The minimum in the curve of K_e can be determined experimentally s shown in (29).

Transmittance and angular scattering measurements were accord- ngly made simultaneously on several sols at 90 and 120 min. after mixing he acid and thiosulfate. The radii obtained from angular scattering were

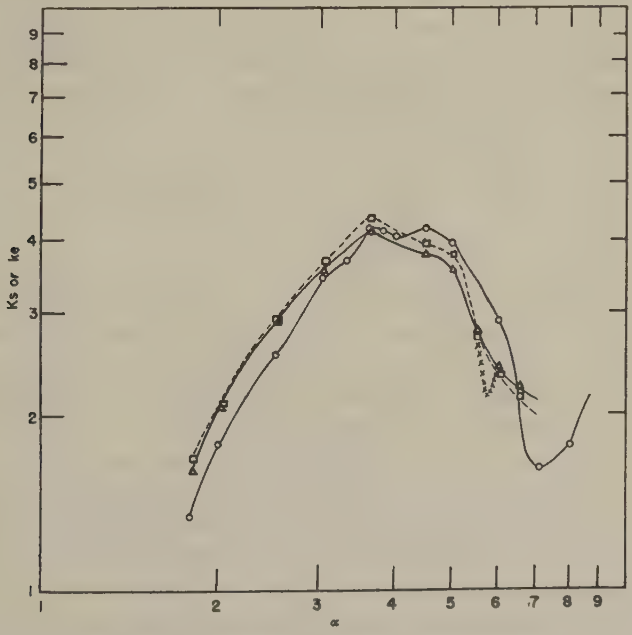

FIG. 6. Theoretical K_s and K_e as a function of α.

○ = K_s for $m = 1.50$
△ = K_e for $m = 1.54$
□ = K_s for $m = 1.54$
x–x–x = Experimental

previously calibrated by a deposition method based upon Stokes' Law. When the log ($\log I_o/I$) was plotted against $\log \alpha$, a minimum was observed at $\alpha = 5.7$. The experimental curve is otherwise superimposed on the theoretical with agreement as shown in Fig. 6.

TABLE V

Determination of α Minima for Transmittance by means of Angular Scattering

Minutes after mixing	Number of particles from transmittance			Radius from angular scattering μ
	λ' (min.) μ	Number $\times 10^{-6}$	α min.	
90	0.250	1.3	5.3	0.21
90	0.255	0.7	5.7	0.23
90	0.254	1.3	5.7	0.23
116	0.256	1.1	5.7	0.23
120	0.280	0.8	6.0	0.27
120	0.276	0.6	6.1	0.27

Table V shows the λ'(min.), the radii obtained by angular scattering, the number of particles per cc., and the calculated α minima. The α minimum depends upon the relative refractive index and the absorption index of the system. The following α minima are applicable for the various minima obtained by transmittance:

λ'min.	α
.250	5.7
.280	6.1
.320	6.8

For larger r values corresponding to $\lambda' > 0.32\mu$, no absorption occurs and the value of $\alpha = 6.8$ determined previously (29) in the visible is constant.

Particle size and number can thus be determined in this system by measuring the transmittance to locate α(min.) and using the appropriate α(min.) when $\lambda' < 0.320$. The $\log I_o/I$ values as a function of λ' for several sols are shown in Fig. 7. The radii and number of particles per cc. have been calculated using $\alpha = 5.7$ and are tabulated in Table VI. The particle size and number can thus be determined without use of the complicated Mie theory and the entire set of measurements can be completed in approximately 10 min.

The theoretical curve of the extinction coefficient as a function of α is given for only one relative refractive index. The experimental curve is obtained by varying the wavelength and, thus, the index of refraction is changed accordingly. Therefore, these two curves can only be compared at one point where the index corresponds. The most characteristic point

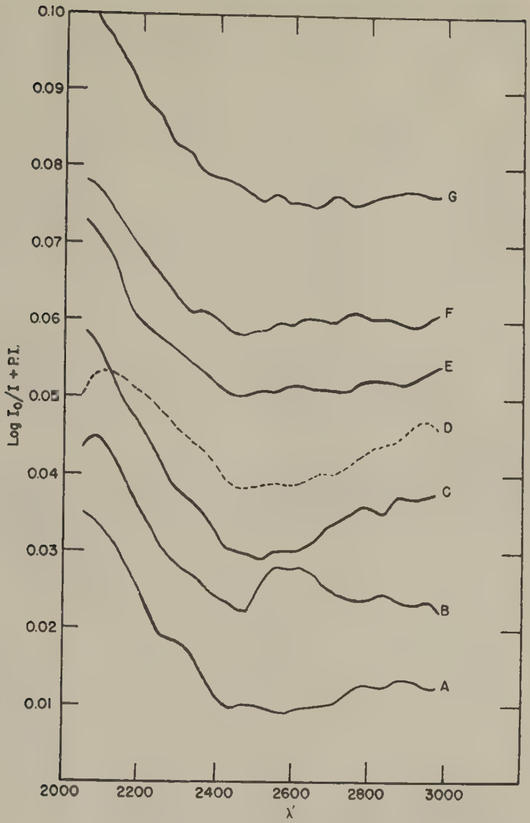

FIG. 7. Ultraviolet transmittance.

Sol	P.I.	Sol	P.I.	Sol	P.I.
A	−0.1	D	.02	F	.04
B	0	E	.03	G	.05
C	+0.01				

P.I. is plotting increment.

TABLE VI

Particle Size and Number Obtained by Transmittance

Sol	Minutes after mixing	λ' (min.)	$n \times 10^{-6}$/cc.	Radius in μ
A	77	0.242	1.4	0.22
B	76½	0.248	1.5	0.23
C	87	0.252	1.3	0.23
D	87	0.245	1.3	0.22
E	80	0.245	1.4	0.23
F	80	0.248	1.2	0.23
G	80	0.252	1.7	0.23

to compare is the minimum. This explains the lack of complete agreement at higher values between experimental and theoretical values obtained previously in the visible (29), where theoretical scattering coefficients, K_s, were used for a fixed relative refraction index of 1.5 in their particle size determinations. Excellent agreement was obtained up to α values of 6, but deviations appeared for values greater than 6.

The absorption index of sulfur is the least accurate of any of the data since the sulfur probably existed as a wedge, and small changes in the temperature would have affected the absorption index. Calculations to test the effect of an error of 100% in absorption index upon the extinction coefficients are shown in the starred value Table IV. Small errors in the absorption index determination do not affect the extinction coefficient appreciably. The calculation is, however, sensitive to small changes in the relative refractive index, and this quantity must be known accurately to three significant figures.

The size distribution of the particles affect the transmittance curves quite noticeably, as shown in Fig. 8. Curve A gives the transmittance of a polydispersed sulfur sol made by adding to water a solution of sulfur in

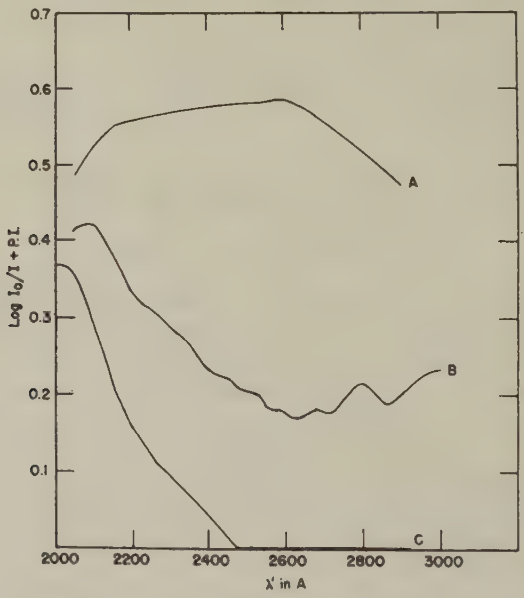

FIG. 8. Effect of size distribution on transmittance.

Sol	Age	P.I.
A		0
B	120 min.	0
C	60 min.	−003

P. I. Plotting Increment

acetone and allowing the resulting larger particles to settle for 2 hrs. No fine structure is evident and no minimum is shown. Curve B shows the transmittance of a monodispersed sol ($r = .27\mu$) 120 min. after mixing the thiosulfate and acid. Considerable fine structure and a minimum exists. Curve C is the transmittance of a thiosulfate-acid solution before any sulfur particles have formed and shows the absorption that exists in the absence of scattering.

The optical scattering methods now available for measuring particle size are:

(a) Angular scattering,
(b) Transmittance,
(c) Depolarization,
(d) Tyndall spectrum of zero order (Rayleigh Equation).

The best procedure to be adopted for a given case depends upon the size of the particles and the optical characteristics of the system, as summarized in Table VII.

TABLE VII

Summary

Optical Methods of Determination of Particle Size

Ratio of r to λ	Equation applied	Method of measurement	Remarks
1/20	Rayleigh	Tyndall spectrum of zero order proportional to r^6/λ^4	The Rayleigh theory is the limiting form of the Mie theory when the radii of the particles are very much smaller than λ.
1/20 to 1/3	Mie	Depolarization	For sizes larger than 1/3 the wavelength of light, α is a multivalued function of depolarization.
1/3 to 1.3	Mie	Angular order positions in the higher order Tyndall spectra	Any two wavelengths can be used, provided that $\lambda_2'/\lambda_1' = 1.2$. (For present available tables.) If absorption is present, then complex index of refraction is required.
1/10 to 1.4	Mie	Transmittance	Real index of refraction in cases where there is no absorption. Complex if absorption is present.
$\gg 1$	Geometrical optics	Diffraction rings Microscope	

SUMMARY

The light scattered by a mondispersed sulfur sol exhibits higher order Tyndall spectra whose wavelengths are dependent upon the composition of the incident light. To study the angular scattering by small particles, an apparatus was constructed, using the ultraviolet spectra and an electronic means of measuring the intensities of the scattered bands.

Monochromatic incident light was furnished by the 3650 Å and 4360 Å lines of the mercury spectra. The intensity of the scattered light of these wavelengths was measured at 5° angular intervals from 30° to 180°. The ratio of $J\lambda 4360/J\lambda 3650$ was plotted against the angle between the point of observation and the backward direction of the incident light propogation. The maxima in such a curve give the location of the 4360 Å "orders." The order positions are a function of the particle size and the relative refractive index of 1.51, and from this the radius was determined directly. The orders are sharp and the error in determining the angular positions has been decreased by replacing natural light by monochromatic incident light.

Transmittance studies have been made on sulfur sols in the region where absorption as well as scattering is present. When absorption exists, the inclusion of complex index of refraction $m' = m(1 - ik)$ is required in all calculations. The complex index of refraction has the effect of reducing the wavelength of the minimum in the curve of the logarithm of the extinction area coefficient as a function of log α. This means that the calculated radius will be smaller than the value obtained if the absorption had been neglected.

In previous investigations it was necessary to use the complex index in extremely complicated and laborious calculations, to determine the value of the extinction area coefficient. With the simplification of the calculation process, which expresses the extinction coefficient as a polynomial involving only the relative index of refraction of the particles and the absorption index, it is possible to make particle size and number determinations in a comparatively easy manner.

A transmittance method has been developed to determine particle size of colloidal sulfur in the region of absorption where the absorption index does not exceed 0.1. The size obtained from transmittance has been calibrated by angular scattering measurements.

CONCLUSIONS

1. The scattering of monochromatic ultraviolet light as a function of angle has been used to determine radius of particles in sulfur sols. It is shown that the observed higher order Tyndall spectra agree with the theoretical positions of the orders when the appropriate complex index of refraction for the wavelength is used.

2. From the available tables, it is now possible to interpolate intensity values for angular scattering positions for any relative index of refraction between 1.33 and 2.00.

3. Transmittance furnishes a simple means of determining size and number of particles in the region where there is absorption as well as scattering, provided that the absorption index k does not exceed 0.1. The Mie theory has been verified, using the complex refractive index $m' = m(1 - ik)$.

4. The extinction area coefficients have been calculated for the sulfur sol system at several indices of refraction.

References

1. LaMer, V. K., and Sinclair, D., OSRD Reports No. 119, Div. b, NDRC No. 57 (July, 1941), No. 1668 (1943), and No. 1857 (1943) available through Office of Technical Services, Department of Commerce as OPB-32200 and OPB 944. See also Sinclair, *J. Optical Soc. Am.* **37**, 475 (1947).
2. LaMer, V. K., and Barnes, M. D., *J. Colloid Sci.* **1**, 71, 79 (1946); **2**, 361 (1947); *ibid.*, **2**, 349 (1947) with Kenyon, A. S., and Zaiser, E. M. See also LaMer, V. K., *J. Phys. Coll. Chem.* **52**, 65 (1948); Sinclair and LaMer, *Chem. Revs.* (1949).
3. Johnson, I., and LaMer, V. K., *J. Am. Chem. Soc.* **69**, 1184 (1947).
4. LaMer, V. K., and Kenyon, A. S., *J. Colloid Sci.* **2**, 257 (1947).
5. Love, A. E. H., *Proc. London Math. Soc.* **30**, 308 (1899); **31**, 489 (1899).
6. Mie, G., *Ann. Physik,* [4] **25**, 377 (1908).
7. Debye, P., *Ann. Physik,* [4] **30**, 57 (1909); *J. Phys. Colloid Chem.* **51**, 18 (1947).
8. Blumer, H., *Z. Physik* **32**, 119 (1925); **38**, 304, 920 (1926); **39**, 195 (1926).
9. Casperson, T., *Kolloid-Z.* **60**, 151 (1932); **65**, 162 (1933).
10. Lord Rayleigh, Scientific Papers **1**, 92–93; **4**, 400 (Cambridge Univ. Press, 1899); *Proc. Roy. Soc. (London)* **84A**, 25 (1911) and **90A**, 219 (1914).
11. Van de Hulst, H. C., Dissertation, Utrecht, 1946.
12. Bricard, J., *J. phys. radium* **4**, 57 (1943); *Ann. geophys.* **2**, 231 (1946).
13. Stratton, J. A., Electromagnetic Theory. McGraw-Hill, New York, 1941.
14. LaMer, V. K., and Johnson, I., *J. Am. Chem. Soc.* **67**, 2055 (1945). Recent unpublished work by James Yates (1948) has shown that the presence of minute traces of oxides of nitrogen, produced by the addition of 10^{-8} M/l. of nitrite is sufficient to delay the production of sulfur and the time of the phase transition. See LaMer, V. K., and Yates, J., *Science* **106**, 508 (1947) and Weissler, A., *J. Colloid Sci.* **3**, 68 (1948).
15. Stratton, J. S., and Houghton, H. G., *Phys. Rev.* **38**, 159 (1931).
16. LaMer, V. K., and Barnes, M. D., *J. Colloid Sci.* **2**, 361 (1947) and Sinclair, D., *J. Optical Soc. Am.* **37**, 475 (1947) for a more precise definition of symbols employed.
17. Steubing, W., *Ann. Physik* [4] **26**, 329 (1908).
18. Reudy, R., *Can. J. Research* **19A**, 117 (1941).
19. Gribnau, F. B., *Kolloid-Z.* **77**, 289 (1936); **82**, 15 (1938).
20. These data are tabulated in OSRD Report No. 1857 (September 1943), Dept. of Commerce, Office of Publication Board, Report No. 944 by LaMer and Sinclair (2), to be republished by the Bureau of Standards. The computations of Blumer (8), while helpful are quite inadequate for the purpose.

21. Sinclair, D., *J. Optical Soc. Am.* **37**, 475 (1947).
22. Brillouin, L., Applied Math. Panel, NDRC Reports No. 87.1 (1943), No. 87.2 (1944).
23. Report of Mr. W. Horenstein to Dr. A. Lowan, Mathematical Tables Project, U. S. Bureau of Standards, entitled "Total Scattering Function for Complex Indices of Refraction."
24. Umberger and LaMer, *J. Am. Chem. Soc.* **67**, 1099 (1945).
25. Freundlich, H., Kapillarchemie. Akademische Verlagsges., Leipzig.
26. Pauli, W., *J. Colloid Sci.* **2**, 333 (1947).
27. Bacon, R. F., and Fanelli, R., *Ind. Eng. Chem.* **34**, 1043 (1942).
28. Lifschitz, V., and Brandt, J., *Kolloid-Z.* **22**, 133 (1918).
29. Barnes, Kenyon, Zaiser and LaMer, *J. Colloid Sci.* **2**, 349 (1947).

THE BINGHAM MEDAL-SOCIETY OF RHEOLOGY, 1948

Twelve excellent and provocative papers were presented at the Annual Meeting, November 5 and 6. Nine are reproduced in detail in this issue. Two of the papers have been submitted for publication in other journals, s indicated with their abstracts which appear herein. Professor Eirich's xcellent review of the recent International Rheological Congress at Scheveningen (The Hague) is presented in condensed form, since the proceedings will be available elsewhere. In addition, a paper by Dr. J. G. Oldroyd, Courtaulds Limited Research Laboratory, England, which the Society would have been pleased to hear, is also included in this issue.

An unusual movie, "High Speed Motion Pictures as a Laboratory Technique" was shown by Drs. E. K. Fischer and J. C. Burnett during he evening's social activities on November 5.

The highlight of the meeting was the presentation of the first annual Bingham Medal to Dr. Melvin Mooney, United States Rubber Co., for utstanding achievements in Rheology. Following are extracts from the eport of the first E. C. Bingham Medal Award Committee to the Executive Committee on the establishment and presentation of the award.

"The death of Eugene Cook Bingham on November 6, 1945, brought o a close a period which might be called the first quarter century of heology as a science. Its history is practically synonomous with the ctivity of that later part of Bingham's life".

—"During this progress (of the Society of Rheology) Professor Bingam was intimately associated with each event and, in most cases, was nstrumental in setting up the course of action. It was fitting, therefore, hat the Society should sponsor the first memorial meeting for its greatest enefactor, namely, the 'Bingham Memorial Symposium on Rheology' which was held November 1 and 2, 1946, at which time Mrs. Bingham was he guest of honor". "—on accepting a gift from Mrs. Bingham in behalf f her husband, the Executive Committee recommended that the gift ould be appropriately used as the initial contribution to a fund to provide suitable award for outstanding achievement in rheology. The Society mmediately authorized—the establishment of the 'E. C. Bingham ward in Rheology' and the solicitation of additional funds to provide or an annual award of a suitably inscribed medal". —"The purpose of he Award—is to recognize outstanding contributions to the science of heology and to foster and encourage such contributions on the part of thers—."

—"The medal may be awarded to any individual who has made outstanding contributions to the science of rheology or to the Society of Rheology within the ten years preceding the date of the award, provided that he has not previously received the award and that he is a resident of North America or a United States Possession. It shall not be necessary that he be a citizen of his country of residence or a member of the Society of Rheology."

Condensations of Dr. Dillon's "citation" of Dr. Mooney and the latter's "acceptance" appear on following pages.

At the 1948 business meeting, the Society voted that the "Rheology Bulletin" be resumed in 1949, and that its form and dates of issue be the responsibility of the editor as prescribed in the Constitution and By-Laws of the Society. In any event, one issue shall appear early in each calendar year and one prior to the Annual Meeting.

W. H. Markwood, Jr.
Editor, Society of Rheology

Introduction of

MELVIN MOONEY

as E. C. Bingham Medalist

J. H. Dillon

Members and guests of the Society of Rheology assembled at its 1948 annual meeting:

It is indeed a pleasant privilege which I hold—that of introducing to you the first recipient of the E. C. Bingham Medal award. The scientist whom we are about to honor thus happens to be an old friend of mine. Hence, I feel that I know him as a man as well as a fellow rheologist.

A native of Kansas City, Missouri, our medalist attended the University of Missouri, receiving the A. B. degree from that institution in 1917. His graduate studies, conducted at the University of Chicago, yielded him the Ph. D. degree in Physics in 1923. In 1928 he accepted a position as physicist with the United States Rubber Company, and his continuous service with that firm since that time has been a story of accomplishment which has established him as one of our leading applied scientists.

He has been an active member of the Society of Rheology since 1930 and served as its president in 1936. He also holds membership in the American Physical Society and was a member of the governing board of the American Institute of Physics from 1936 to 1939.

Even in his earlier papers it was apparent that he possessed that rare gift of competence in both experimental and theoretical science. His studies of the flow of unvulcanized rubber constitute a set of classics, both as regards theoretical soundness and individuality of the laboratory attack. It is not surprising, then, that his fundamental research approach resulted in an instrument used throughout the rubber industry, and known as the Mooney shear viscometer. His efforts have not been confined to the flow of crude and unvulcanized rubbers, however; he has studied the flow of rubber latex profitably—here the Mooney coni-cylindrical viscometer was the practical result. We should hasten to add, of course, that these well-known instruments are only the applied evidence of the excellence of his research attack—the basic work constitutes the major contribution.

In the realm of vulcanized rubbers, our medalist has made further salient contributions. His rather abstract theoretical treatment of rubber elasticity has been verified again and again by subsequent theoretical and experimental work. Some of us who have conversed with him on his current work are awaiting with interest publication of his studies of thixotropy and dynamic properties of rubbers at large strains.

But, in spite of his acknowledged ability and dominance in the field of rubber rheology, our medalist remains a modest, charming individual whose thoughtful comments at our meetings continue to add to, and accelerate, the work of others. On that note, then, ladies and gentlemen, I give you our Bingham Medalist—Dr. Melvin Mooney.

Speech of Acceptance

When I began working 20 years ago with the U. S. Rubber Company, my present employer, my first major assignment was to investigate the problem of controlling the plasticity of raw rubber stocks in the factories. That was obviously a problem in a field which has since then been given the name of rheology. A large fraction of the other problems assigned to me in the intervening years have also been in the field of rheology. To enable me to carry on this work, I was, of course, supplied with laboratory facilities, assistants, and all the usual associated services. Furthermore, it has been my privilege to attend the stimulating meetings of the Society of Rheology every year since its foundation.

With such continuous assignments, support and stimulation for rheological research, I could only be judged grossly incompetent if, over a period of 20 years, I had not made a number of contributions to the growing science of rheology. If these contributions merit the Bingham Medal, surely it will be recognized that those who have been associated with me in any way in my work are entitled to share the honor of the award.

Nevertheless, I will confess that I am sufficiently selfish to be pleased that the Bingham Medal for 1948 is formally awarded to me. One reason that I feel this way is because of my lasting regard for the man in whose honor this medal is awarded, Eugene C. Bingham; and I am glad that one side of the medal carries the likeness of this illustrious leader. Professor Bingham was not only a pioneer and leader in the science of rheology; he was also a man so friendly and generous in all his personal relations that none could know him without loving him. Being one of those fortunate enough to have known and loved him, I am especially grateful for the honor of receiving the first Bingham Award.

M. MOONEY

IMPRESSIONS FROM THE INTERNATIONAL RHEOLOGICAL CONGRESS, SCHEVENINGEN. 1948 *

F. R. Eirich

Polytechnic Institute of Brooklyn, Brooklyn, N. Y.

In view of the scope of the Congress no more than a rather brief and cursory account can be given. The complete record will be found in the proceedings of the Congress which will be available in a few months and which will contain not only all lectures but also most of the discussion remarks.

ORGANIZATION AND EVENTS

The Congress was attended by about 250 registered members from about a dozen countries, including an unusually high percentage of leading names in European rheology. It provided general introductory lectures and short individual lectures grouped into sections such as: theoretical problems, rheological properties of various systems, biological systems, experimental methods, and applied rheology. The number and the standard of the general lectures was unusually high and all but dominated the program. A special attraction was an exhibition of rheological apparatus arranged by R. N. J. Saal. It was remarkable not only for the great number of pieces of apparatus exhibited but in particular for its set up. The leading idea was to achieve a functional classification according to the way by which the deformation of the test piece was achieved, or was changed with time. There were further subdivisions according to the conditions of measurement, range, and accuracy. The section, "Homogeneous shearing stress" contained parallel plates-, ring-, and concentric rotation- and translation viscosimeters, and tensiometers maintaining constant stress. The next heading of "Non-homogeneous stress distribution, with variation of the shearing stress along one coordinate," comprised capillary viscosimeters, plunger-, torsion viscosimeters, *etc.* Then followed instruments where the shearing stress varied along two coordinates, such as compression plastometers and a number of penetration tests, and lastly, stirrer and falling sphere types, viscometers with sloping tube, etc., in which the shearing stress changed along all three coordinates. A further distinction was made as to whether the stress remained constant throughout the time of the measurement, or not, and a special section contained instruments with alternating stresses.

THE LECTURES

Aside from their survey character the general lectures covered a great deal of out of the way subjects, and dealt with new developments.

The "Introductory Remarks on the Problem of Nomenclature" by J. M. Burgers were a condensation of his report in preparation with Scott Blair on the same subject. After emphasizing that there were a number of independent ways for arriving at a self consistent nomenclature, he discussed the merits of the two most obvious possibilities: that of describing materials and material behavior in terms of their physical- or structural qualities, and the phenomenological-mechanical description. The limits of the former arise from our limited knowledge of structures, and as for the latter from frequent experimental difficulties to establish clear cut relations. Preference is given to the phenomenological approach on account of its more direct nature and of its providing mutually independent data.

---

* Presented at the Annual Meeting of the Society of Rheology, November 5 and 6, 1948, New York, N. Y.

H. S. Green's paper dealt with Born's and his attempt to develop a molecular theory of viscosity and other macroscopic quantities on the basis of a knowledge of the force fields and the (statistical) configuration of the constituent molecules. Since any deformation causes a distortion of this configuration, a stress-strain relationship can be arrived at. The formalism had been developed for the viscous case and was now also presented for the elastic response, including a few remarks about relaxation times. Although no numerical values have as yet been calculated, and may not be for some time, it is my impression that Born and Green's attempt represents so far the most significant and satisfactory progress in the *a priori* calculation of mechanical properties. It promises, moreover, to give some information about finite deformations.

In contrast to this structural approach, Weissenberg, and in a subsequent lecture, Reiner, treated the problem of anomalous deformational behavior on a macroscopic-phenomenological basis. Weissenberg reviewed his theoretical and experimental work during and since the war, which is to a large extent already known. His theory deals with a continuity of mass-points with forces arising whenever these mass-points suffer relative displacements. He shows that the 3 superimposed conditions of continuity, equilibrium of forces and the existence of an equation of state are sufficient to determine all possible rheological transformations and respective parameters. The deviations from the simple laws at larger deformations are traced to the coming into play of higher order (non-linear) terms in the stress tensor, and are connected with the behavior of liquids with residual elasticity. He also stresses the fact that what is usually called "normal" behavior is really an exceptional one, representing special cases of the most general behavior.

In a parallel attempt to develop a formalism to cover rheological complexity Reiner gave an important lecture. After reviewing his formulation of rheological equations of state for complex bodies, by building them up from the equations of simpler theoretical bodies, he drew attention to frequently hidden or overlooked forms of behavior such as solid viscosity, volume flow and plasticity, generalized Poisson ratios, bodies which are neither solid nor liquid like that defined by Hohenemser and Prager's linear general rheological equation, and bodies which may differ in their Poisson ratio on extension and compression. In this context it should be mentioned that in a subsequent discussion Reiner asserts that he can give an alternative explanation for Weissenberg's experiments if the assumption is dropped that in simple shear all stresses must vanish where formal resolving into components sets strains equal to zero, and vice versa. Similar comments were also made by Rivlin on the basis of his new theory.

The 4th general lecture was given by Sadron and concerned the viscosity of solutions of macromolecules. It was a brilliant exposition, discussing all the merits as well as shortcomings of the existing theories. In parts he inclines towards the approaches of Burgers, Eisenschitz, Kramers, and criticizes the Kuhn-Huggins theories on account of their relying too much on the applicability of hydrodynamics on a molecular scale.

The three following general lectures dealt with applications of Rheology. *Dr. A. L. Copley* gave a very full account of the problems already touched or waiting for rheological investigations, in Biology. *Dr. Scott Blair* returned to the dispute concerning the Nutting-equation, reiterating its importance for investigations where the sensory qualities of the investigator play a paramount part, and outlined a possible analysis for finding the degree of interdependence between results of a variety of tests. In a most enlightening lecture *Dr. Houwink* illustrated how many industrially important materials have either a high viscosity and no yield value, or an appreciable yield value followed by a low viscosity with low temperature dependence. He showed further how most techincal operations and their power requirements are determined by flow properties, how often operating needs and specifications for the finished product clash, how adverse effects of high concentrations are overcome by the preparation of dispersions, and finally discussed the effects of milling, calendering, of storage, etc., with a wealth of instances where technical solutions of these problems have been found and where they are still wanted.

My own contribution consisted in giving a survey of fundamental experimental methods. After a brief discussion on what might be understood under fundamental methods and what may be learned from them, insisting on the use of instruments with a constant shearing stress throughout the sample, I discussed a few examples from the more recent methods and stressed the merits of vibrational techniques.

Turning briefly to the 40 sectional papers, Goodeve and Weissenberg elaborated further their particular theories of anomalous flow properties. Considerable interest met the papers by Voet, by Gray and by others dealing with investigations of structural properties, or changes, during deformation that help to throw light on the flow mechanism itself, a line of rheological research badly needed. Voet measured dielectric constants, Gray the birefringence, in rotating cylinder instruments, Nitschmann the force necessary to pull threads, and Davies the formation of drops and threads. Burwell dealt with photoelectric effects due to frozen stresses and Gonsalves reported an interesting study of relaxation phenomena in viscose by means of birefringence measurements. The results quoted in these papers are very informative as regards particle interaction and other structural effects on the viscosity. Bearing on a different aspect of the same field is a paper by G. M. Joly on the influence of molecular structure on the activation energy of flow in mono-molecular layers, and a paper by Abadie and Girard on the internal viscosity during dielectric rotation, so important for our understanding of segment behavior in long chain molecules. Lethersich contributed an interesting paper in the related field of creep studies in dielectrics.

As regards the field of molecular hydrodynamics where renewed interest has been aroused by recent work on macromolecular resistance problems, papers were given by Kuhn, Brinkman and Simha, as well as a summary of a discussion of Dutch workers on some of the principles involved. Within the limits of hydrodynamics W. Kuhn's approach seems theoretically vindicated, especially in the light of Kramers' recent paper, but agreement with the experiment could be still improved, and the value of his model experiments remains in doubt. Considerable advance has been achieved by Brinkman and by Simha in the theory of hydrodynamic interaction inside groups of spheres.

Turning to the papers dealing with more practical aspects, there were 3 lectures on the topic of the transition from anomalous to turbulent flow. Of these Oldroyd's mathematical analysis with respect to the presence of a wall effect is of considerable interest. Another group of papers dealt with the behavior of relatively coarse suspensions: H. de Bruijn with the measuring technique, Mardles with surface adsorption and Romanovsky with settling behavior.

On the industrial side there were papers on the rheology of specific tests for rubber, and on the flow of non-vulcanized rubber by Scott, van Rossem, Wren and others. There were further papers on printing inks, on lubricating greases, hardening fats, and building materials. Finally, there was a report by Astbury on the present state of our understanding of muscle contraction, and a very substantial contribution by J. J. Hermans or the theory of swelling which, however, were somewhat outside the scope of the meeting.

Summing up it may be said that the number of front line topics in rheology to which contributions were made was very satisfactory indeed, and that the meeting was most successful in giving a picture of present trends. The most frequently expressed opinion was that the theory had gone well ahead, but that the body of experimental or technical facts to which it could apply was yet rather small. This is, of course, due to the failure of so many rheological instruments to fulfill the requirements for a theoretical interpretation. The difficulties in the way of a radical improvement of this situation, particularly in technical research laboratories, are very considerable. On the other hand, while this state of unintentional cross-purpose exists, the usefulness of rheology in the furtherance of scientific or technical problems must remain below what might otherwise be expected.

Additional Observations

A few topics of private discussions on fundamental questions, at which I happened to be present, may be indicated.

There was, *e.g.*, a certain amount of doubt as regards the legitimacy of applying hydrodynamics in chain molecular problems. This applied especially in cases where particle movements are preponderantly due to Brownian agitation and where inside coiled chain molecules the expanses of solvent are only a few molecules deep. Other difficulties were seen in using the Maxwell Boltzmann distribution in non-equilibrium states such as represented by a flow, in view of the superimposed velocity distribution; similarly the application of Stokes' resistance equation in liquids other than at rest, or for fluctuation phenomena, was questioned. The point was raised whether accepting the increase in viscosity due to rotatory Brownian movement of elongated particles does not necessitate a revision of the prevalent notion that translational Brownian movement does not raise the relative viscosity. Finally Eyring's treatment of flow processes was criticized because of the introduction of h in the absence of quantum effects, and because of the interpretation of the constant in the exponent as an activation energy instead of as a kinetic energy term.

PROPOSED NOMENCLATURE FOR ELASTIC AND INELASTIC BEHAVIOR OF HIGH POLYMERS[1]

Herbert Leaderman

From the National Bureau of Standards, Washington, D. C.

Received February 3, 1949

INTRODUCTION

The purpose of the present paper is to summarize certain general aspects of the mechanical properties of high polymers, and to propose a nomenclature for the description of the observable phenomena. As nearly as possible this nomenclature is consistent with present usage in the high polymer field and in other fields of the study of mechanical behavior.

The study of the mechanical behavior of materials is concerned first with a description of observable phenomena, and secondly with an interpretation of these phenomena in terms of constitution. The present paper is concerned only with the first, or phenomenological aspect, and not with the second, or molecular aspect. In the study of mechanical properties of materials, the procedure is to set up simple models representing to a first approximation the observed behavior of real materials. A system of nomenclature describes observable and related phenomena as manifested by these models. Experiments based on these models may be used to test their validity, and to develop more complicated models which represent more nearly the observed phenomena. The general mechanical behavior of condensed systems has been discussed by Burgers (1), Burgers and Scott-Blair (2), and in reports issued by the British Rheologists' Club (3,4,5). Experience has shown that phenomena which are of importance in some groups of materials are unimportant or absent in other groups. For the further development of such mechanical models it is necessary to consider specific groups of materials.

In recent years, much experimental and theoretical work has been carried out on the mechanical properties of high polymers. Such materials have included raw and vulcanized rubbers; rubberlike plastics; rigid plastics such as polystyrene and cellulose derivatives; and textile fibers such as wool and oriented nylon. These investigations have revealed that high polymers possess certain mechanical properties in common. The similarities in mechanical behavior become even more apparent when polymers are tested under different conditions of temperature and swelling; for example, in experiments of ordinary time-scales, rubber cooled to a sufficiently low temperature possesses the properties usually associated with a rigid plastic, while polymethyl methacrylate heated to a certain temperature range manifests certain of the properties which a raw rubber possesses at room temperature. The following discussion will be restricted to a description of what may be called the *elastic* and *inelastic behavior* of systems comprising or containing long-chain organic molecules, and is concerned mostly with the behavior of amorphous crosslinked and non-crosslinked polymeric systems. The problems of failure and fatigue will not be considered, nor will changes in mechanical properties resulting from chemical change. In general, the elastic and inelastic behavior of high polymers depends upon the *time-scale* of the experiment (under given conditions of temperature and swelling). The description of the stress-strain-time behavior of polymeric systems thus lies within the province of rheology. A survey of the properties of such systems has been made by Simha (6), while a detailed discussion of their behavior under periodic stress has been given by Ferry (7). The proposed standard terms are italicized when first introduced, and are collected together at the end of this paper. The proposed terminology classifies only behavior and not materials; the behavior of a given material depends to a very great extent upon the environmental conditions of the test and the time-scale of the experiment.

---

[1] Presented at the Annual Meeting of the Society of Rheology, New York, N. Y., November 5 and 6, 1948.

The discussion will thus be concerned with the relation between stress, strain and time in a body of a given material under given environmental conditions (such as temperature). If the deformation is homogeneous (such as simple tension, simple shear) the strain at a point can be deduced simply from the deformation of the body as a whole, and, similarly, the stress at a point can be deduced from the applied forces, when inertia effects may be ignored. Except when otherwise stated, it will be assumed that the stress-strain relationships for a given material are obtained by observing load-deformation relationships of a body consisting of the material, when subjected to a homogeneous deformation. Except in the discussion of the propagation of waves in polymer systems, it will be assumed that inertia effects are so small as to be neglected.

I. LINEAR ELASTIC BEHAVIOR OF POLYMER SYSTEMS

A. Hookean Behavior

A material may be said to show *ideal elastic behavior* (under given conditions) when the strain is a unique monotonic function of the stress and is independent of the previous stress history. This implies that instantaneous removal of load from a body at any instant results in instantaneous disappearance of deformation. For example, the relationship between tensile stress and relative length in a specimen of Hevea gum rubber at room temperature, for moderate rates of deformation in the absence of crystallization, corresponds very nearly to ideal elastic behavior.

The application of forces to a body results generally in both a change in volume and a change in shape. In particular, if there is only a change in volume, then the stress at any point is simply a hydrostatic stress. A body may be said to show *Hookean behavior* (or *Hookean elastic behavior*) in dilatation, if the fractional change in volume is proportional to the hydrostatic stress, and, in addition, if it manifests ideal elastic behavior under hydrostatic stress. The ratio of hydrostatic stress to fractional volume change is called the *bulk modulus*, K. *The compressibility* may be defined generally as the rate of decrease of volume per unit volume with hydrostatic pressure. For sufficiently small hydrostatic stresses the behavior of high polymers under hydrostatic stress is Hookean, in which case the compressibility is equal to the reciprocal of the bulk modulus. For high polymers the bulk modulus is of the order of 10^{10} dynes/cm^2. (8).

A simple shear strain γ is an example of change in shape without change in volume. In general, to maintain a simple shear strain in an ideally elastic body a simple shear stress, S, is required, together with other stresses if the shear strain is not small (9). A material may be said to show *Hookean behavior* in shear if the shear stress is proportional to the shear strain. Under these conditions the ratio of shear stress to shear strain is given by:

$$S = G\gamma, \tag{1}$$

where G is called the *shear modulus*. The reciprocal of the shear modulus will be called the *shear compliance*, J. For amorphous isotropic polymers exhibiting approximately Hookean behavior, the shear modulus is either of the order of magnitude of the bulk modulus, namely 10^{10} dynes/cm^2., or of a smaller order of magnitude, approximately 10^6 dynes/cm^2. Such behavior is found, for example, under certain test conditions in ordinary Hevea gum vulcanizates and in slightly crosslinked plastics such as polystyrene crosslinked with divinylbenzene. In experiments of ordinary time-scales the crosslinked polystyrene at room temperature and the rubber at very low temperatures (say below −80°C.), have shear moduli of the order of 10^{10} dynes/cm^2. On the other hand, the rubber at room temperature and the crosslinked polystyrene heated to a certain range of temperature (say about 130°C.) have shear moduli of the order of 10^6 dynes/cm^2. When the shear and bulk moduli are of the same order of magnitude, the body is said to manifest *ordinary elastic behavior* or *ordinary elasticity*. When the shear modulus is of a smaller order of magnitude than the bulk modulus, the material is said to exhibit *rubberlike elastic behavior* or *rubberlike elasticity.* In the case of a crystalline isotropic polymer only part of the material can exhibit rubberlike elasticity, and, hence, such a material may manifest *partial rubberlike elasticity.*

When a body of material manifesting Hookean elastic behavior in dilatation and shear is subjected to a tensile force, the elongation is, in general, proportional to the force only if the fractional increase in length is small. Under these circumstances the ratio of tensile stress to fractional elongation is called *Young's modulus* and is denoted by the symbol E. The ratio of the fractional lateral contraction to the fractional elongation under the same conditions is called *Poisson's ratio.*

B. Viscoelastic Behavior

A material may be said to exhibit *viscoelastic behavior* in shear if, firstly, the relation between shear stress and shear strain at any instant depends upon the previous stress or strain history, when the time-scale of the experiment if of the same order as some characteristic time, and if, secondly, the material exhibits ideal elastic behavior in shear for experiments of very short or very long time-scales. In particular, a material may be said to manifest *linear viscoelastic behavior* in shear if it manifests Hookean behavior in shear for very short or very long values of time scale, when the shear moduli are given by G_2 and G_1, respectively, where $G_2 \gg G_1$. It seems that materials exhibit viscoelastic behavior in dilatation as well as shear (6,10,11); this behavior will not be considered here.

Linear viscoelastic behavior in shear may be represented to a first approximation by the following relationship between shear stress S, shear strain γ, and time t:

$$\left(\frac{G_1 + G_2}{G_2} + \frac{\eta_1 \partial}{G_2 \partial t}\right) S = \left(G_1 + \eta_1 \frac{\partial}{\partial t}\right) \gamma. \tag{2}$$

This behavior is that of a well-known linear mechanical model, consisting of a spring and dashpot connected in parallel with each other and in series with another spring, or of equivalent models (1,12,13). The parameter η_1/G_1 has the dimensions of time and may be called the *retardation time* τ of the body. In general, τ will depend markedly upon the environmental conditions, for example, temperature. Usually, the behavior of a body under stated environmental conditions will be given only qualitatively by Eq. (2), since τ may depend somewhat upon the time-scale and nature of the experiment. An experiment may be made to fit Eq. (2) if, however, τ, and hence η_1, is chosen to fit the particular experiment; for any given experiment the appropriate value of τ may be called the *effective retardation time* for the experiment. If the shear moduli G_1 and G_2 are of the order, respectively, of 10^6 dynes/cm^2. and 10^{10} dynes/cm^2., then the Hookean behavior for the extremes of time-scale corresponds, respectively, to rubberlike elastic behavior and ordinary elastic behavior.

Three special types of history will be considered: constant shear stress applied at zero time, followed by subsequent removal of stress; constant shear strain applied at zero time, followed by subsequent release of the body, and stress varying periodically with time. With the first two types of history, the behavior will be analyzed for a material whose stress-strain-time behavior is given by Eq. (2), and a terminology given for the observable phenomena. In the case of alternating stress history, the treatment will be somewhat more general.

In the first case the shear strain $\gamma(t)$ at a time t after application of a constant shear stress S is given by:

$$\gamma(t) = S/G_2 + (S/G_1)(1 - e^{-t/\tau}). \tag{3}$$

Thus, the deformation consists of two parts. One part corresponds to a high shear modulus; the time required for the attainment of this component of the deformation is not strictly zero, but is the time required for the passage of a stress-wave through the body when the retardation time is long compared to this time. Under these circumstances this component of the deformation is experimentally observable; it may be called the *ordinary elastic deformation*. The quantity G_2 may be called the *ordinary shear modulus*, and its reciprocal, which will be denoted by J_2, the *ordinary shear compliance*. There is, in addition, a second component of deformation on the right hand side of Eq. (3), which increases with time to a limiting value S/G_1. Increase in deformation with time under constant stress or constant load is generally denoted by the term *creep*. In the case of a body, the behavior of which is described by Eq. (2), the deformation eventually completely disappears following removal of load. The deformation given by the second term on the right-hand side of Eq. (3) may thus be thought of as a time-dependent high-elastic deformation; it may be called the *retarded elastic deformation*. The time-dependency is experimentally evident when τ is of the same order as the time-scale of the experiment. Thus, from Eq. (3) the (effective) retardation time of a body under given environmental conditions represents the time for the retarded elastic deformation in a constant-stress test to reach $(1 - 1/e)$ of its final value S/G_1.

In such constant-stress experiments it is a practice to record the ratio of shear strain to shear stress (or of shear stress to shear strain) (14,15), the value of shear strain being that corresponding to some convenient time t, say 10 sec. or 1 min., after application of stress. The value of shear compliance or shear modulus thus obtained may be called the *quasi-static shear compliance* J_t or *quasi-static shear modulus* G_t for the appropriate time-interval t.

When, at any time, the load is removed, the deformation corresponding to the ordinary elastic deformation immediately disappears: this will be called the *ordinary elastic recovery.* The remaining part of the deformation disappears gradually with time; the deformation existing in the body at any given instant following removal of load is called the *residual deformation* at that instant. The gradual disappearance with time of the residual deformation may be called *retarded elastic recovery* or simply *creep recovery.* The quantity G_1 may be called the *high elasticity shear modulus;* the reciprocal quantity J_1 may be called *high elasticity shear compliance.* The quantity η_1 may be called the *internal viscosity.*

Many materials manifest a retarded elastic deformation under constant stress (or load), followed by creep recovery upon removal of stress, the material eventually reattaining its original form. The retarded elastic behavior in materials such as textile filaments and wool is more complicated than the linear behavior of Eq. (2); nevertheless, such behavior should also be considered as viscoelastic behavior.

In the second type of loading history, application of a given shear strain produces a shear stress which gradually decreases with time, eventually to a limiting value. For a body in which stress, strain, and time are related by Eq. (2) the shear stress $S(t)$ at time t after application of a constant shear strain γ is given by:

$$S(t) = G_2\gamma - \frac{G_2{}^2\gamma}{G_1 + G_2}(1 - e^{-t/\tau'}), \tag{4}$$

where τ' may be called the *relaxation time* and is now given by

$$\tau' = \eta_1/(G_1 + G_2). \tag{5}$$

The decay of stress under constant deformation is generally referred to as *stress relaxation.* In the present case, if the body is released at any time, it will eventually return to its original configuration. The stress relaxation is thus a manifestation of viscoelastic behavior, and not of flow or of a chemical reaction. This particular type of relaxation should accordingly be called *viscoelastic relaxation.* In these two types of loading history, changes in stress (or strain) take place after application or removal of a fixed strain (or stress); these changes are due to the existence of a time-dependent elasticity, and not due to flow. The phenomena manifested in these tests may be referred to collectively as *elastic after-effect* or *elastic after-effect phenomena.*

In the third type of loading history, it will be assumed first that the shear stress S in a body varies sinusoidally with time. Now if the relation between shear stress and shear strain can be represented by a linear differential equation with constant coefficients, then, in general, the shear strain will also vary sinusoidally with time, and, moreover, the amplitude of the shear strain will be proportional to the amplitude of the shear stress. A terminology will now be proposed for the general relations between stress and strain under dynamic conditions, and also relating to the behavior of bodies in particular types of experiment. The general characteristics of viscoelastic behavior in these types of experiment will be stated, as well as the specific behavior of materials whose stress-strain-time behavior is given by Eq. (2).

If the shear stress be represented by the real part of

$$S_o e^{j\omega t},$$

then the strain may be represented in general by an equation of the form:

$$\gamma = S_o(A - jB)e^{j\omega t} = S_o\sqrt{A^2 + B^2}e^{j(\omega t - \delta)}, \tag{6}$$

where A and B are usually functions of ω as well as environmental conditions. In particular, for a material exhibiting linear viscoelastic behavior, the solution of Eq. (2) for sinusoidal loading gives:

$$\left.\begin{aligned} A &= \frac{1}{G_2} + \frac{1}{G_1(1 + \omega^2\tau^2)}, \\ B &= \frac{\omega\tau}{G_1(1 + \omega^2\tau^2)}, \end{aligned}\right\} \tag{7}$$

where $\tau = \eta_1/G_1$ as before; τ, the effective retardation time for the experiment, will be dependent upon the time-scale of the experiment as mentioned previously. From Eq. (7) it is seen that when $1/\omega$ is very large compared to τ, then the material exhibits Hookean behavior with a small shear modulus approximately equal to G_1 (since $G_1 \ll G_2$); while, if $1/\omega$ is small compared to τ, the material exhibits Hookean behavior with a large shear modulus G_2. When $1/\omega$ is of the same order as τ, the strain, which is given by the real part of Eq. (6), is seen to be sinusoidal with time, but to lag in phase behind the stress.

For any material in which the shear strain is given by Eq. (6), the ratio of shear stress to shear strain may be called the *complex dynamic shear modulus* G^* and is given by:

$$G^* = 1/(A - jB) = (A + jB)/(A^2 + B^2) = G' + jG''. \tag{8}$$

This is seen to consist of two components, a *real component* of the shear modulus G' given by:

$$G' = A/(A^2 + B^2) \tag{9}$$

which determines the component of the stress in phase with the strain, and an *imaginary component*

$$jG'' = jB/(A^2 + B^2) \tag{10}$$

which determines the component of the stress which is in quadrature with the strain.

The amplitude of the deformation (ignoring phase) is obtained by dividing the stress amplitude by the *absolute value of the dynamic shear modulus* which may be denoted by $|G|$, where

$$|G| = 1/(A^2 + B^2)^{\frac{1}{2}}.$$

Thus,

$$S/\gamma = |G| e^{j\delta}. \tag{11}$$

In a similar way the *complex dynamic shear compliance* J^* is

$$J^* = 1/G^* = A - jB = J' - jJ'' \tag{12}$$

and the *real* and *imaginary components* are given respectively by:

$$J' = A; \qquad jJ'' = jB. \tag{13}$$

The ratio $J''/J' = G''/G'$ is the *loss tangent*, tan δ. The *absolute value of the dynamic shear compliance* $|J|$ is given by

$$|J| = (A^2 + B^2)^{\frac{1}{2}}. \tag{14}$$

When tan δ is different from zero, mechanical energy is converted into heat. This dissipation of mechanical energy under alternating stress due to a viscoelastic or other mechanism is known generally as *internal friction.* Under any such cyclic stress history, the stress-strain behavior of a viscoelastic body is a "loop" when the time-scale is of the same order as the retardation time τ of the body; in particular, the "loop" has the shape of an ellipse for sinusoidal loading (in the steady state). By analogy with magnetic hysteresis, this loop is called the *hysteresis loop;* the phenomenon of internal friction is alternatively known as *hysteresis.* The terms hysteresis loop and hysteresis may also be applied to the behavior of a material exhibiting viscoelastic behavior when the load increases monotonically with time and then decreases again. If the time-scale of the experiment is of the same order as the retardation time, then the stress-strain curve when the load is increasing is not the same as that obtained when the load is decreasing; the resulting stress-strain loop may also be called a hysteresis loop. In particular, for a material exhibiting viscoelastic behavior, the loop becomes closed if sufficient time is allowed for creep recovery, and if the initial and final states are both equilibrium states under the same load. Under these conditions the loop may be referred to as a *viscoelastic hysteresis loop.*

At any given frequency, the energy dissipated per cycle under alternating stress is proportional to the square of the stress (or strain) amplitude. It is convenient to express the mechanical energy dissipated per cycle per unit volume either in terms of the *energy dissipation at unit stress* *amplitude,* which may be denoted by W_s, or the *energy dissipation at unit strain amplitude,* W_γ. Then

$$\begin{aligned} W_s &= |J|\pi \sin \delta, \\ W_\gamma &= |G|\pi \sin \delta. \end{aligned} \tag{15}$$

Thus W_s and W_γ have the dimensions of shear compliance and shear modulus, respectively. It is sometimes convenient to express the energy dissipated under alternating stress as the ratio of the energy dissipated per cycle to the maximum strain energy stored in the cycle (for the same volume of material). This non-dimensional ratio is known as the *specific damping capacity,* ψ. Alternatively, the quantity $(1 - \psi)$ may be called the *resilience.*

From Eq. (6) the rate of shear strain $d\gamma/dt$ is found to be:

$$(d\gamma/dt) = S_o\omega(jA + B)e^{j\omega t}. \tag{16}$$

The ratio of shear stress to rate of shear strain is conventionally defined as the viscosity. In this case the ratio is complex; it may be called the *complex dynamic viscosity* η^* and is given by:

$$\eta^* = \frac{B - jA}{\omega(A^2 + B^2)}. \tag{17}$$

Thus, the complex dynamic viscosity consists of a *real component* η' and an *imaginary component* $-j\eta''$ such that

$$\eta^* = \eta' - j\eta''.$$

The real component η' corresponds to the dissipation of energy, and is thus analogous to resistance in an electrical network, while the imaginary component corresponds to the storage of energy, and is thus analogous to reactance. Thus, by analogy, η^*, η' and η'' may be called, respectively, *specific mechanical impedance, specific mechanical resistance,* and *specific mechanical reactance.* In a similar way, the *specific mechanical admittance* or *complex dynamic fluidity* ρ^* is given by the ratio of rate of shear strain to shear stress. Then

$$\rho^* = \rho' + j\rho'' = \omega(B + jA), \tag{18}$$

where ρ' and $j\rho''$ are, respectively, the *real component* and the *imaginary component of the complex dynamic fluidity;* while ρ' and ρ'' may be termed the *specific mechanical conductance* and *specific mechanical susceptance* respectively.

The dynamic behavior of a body may be studied by making the body under investigation into the elastic member of a vibrating system, so arranged that the period of vibration is long compared to the time for the propagation of a stress-wave through the body. The experiment may be carried out either by displacing, and then releasing, the inertia member of the system, or alternatively by impressing an alternating force on the inertia member. Let it be supposed that the body is in the form of a unit cube, so that unit displacement of the inertia member corresponds to unit shear strain in the body, and let the inertia member be of mass M. In the former case the shear stress in the body is given by:

$$S = -M(d^2\omega/dt^2). \tag{19}$$

If this value for S is substituted in Eq. (2), an equation is obtained for the free oscillation of a mechanical system, the elastic member of which is exhibiting linear viscoelastic behavior. In particular, if the retardation time is very small or very large compared with the period of oscillation, the system will oscillate with a damped harmonic motion; the period will approximately correspond, respectively, to a low shear modulus G_1 or a high shear modulus G_2. In both cases the ratio of the amplitudes of successive oscillations is independent of amplitude. The natural logarithm of this ratio for any given mechanical system is known as the *logarithmic decrement* Δ, and is a measure of the internal friction in the elastic member.

In the second case, let it be supposed that a force $Pe^{j\omega t}$ is acting on the inertia member of the system. The shear stress in the elastic member is then given by:

$$S = Pe^{j\omega t} - M(d^2\gamma/dt^2). \tag{20}$$

If the relation between stress and strain in the elastic member can be represented by a complex shear modulus as before, then the shear stress S in Eq. (20) is equated to $G^*\gamma$, if the elastic member is in the form of a unit cube. The shear strain is then given by (6):

$$\gamma = \frac{Pe^{j(\omega t - \phi)}}{\sqrt{(G' - M\omega^2)^2 + G''^2}}. \tag{21}$$

The angle ϕ may be called the *phase angle*. It is the angle between the vectors representing the applied force and the displacement of the inertia member; it is given by

$$\tan \phi = G''/(G' - M\omega^2). \tag{22}$$

In particular, for a body exhibiting viscoelastic behavior, G'' tends to zero as ω approaches zero and also as ω approaches infinity, while G' approaches G_1 and G_2, respectively. At resonance $\phi = \pi/2$, and, from the corresponding values of M, ω, and $|\gamma|$, the values of G' and G'' can be obtained. Let ω_o be the resonant frequency at which the amplitude of γ is given by $|\gamma|$, and let ω be the frequency at which the amplitude of γ falls to $|\gamma|/\sqrt{2}$. Then the ratio $\omega/2|\omega - \omega_o|$ may be called the *half power width* and is denoted by the symbol Q. It is the reciprocal of the loss tangent of the material at the circular frequency ω when the loss tangent is small. In the case when the general relation between stress and strain is given by Eq. (2), the equation of motion of the inertia member becomes:

$$\left(M \frac{d^2}{dt^2} + \eta_1 \frac{d}{dt} + G_1 \right) \gamma = Pe^{j\omega t} \tag{23}$$

if the period of oscillation is long compared to the retardation time η_1/G_1 and if $G_1 \ll G_2$. The solution of this equation is:

$$\gamma = \frac{Pe^{j(\omega t - \phi)}}{\sqrt{(G_1 - M\omega^2)^2 + \omega^2 \eta_1{}^2}}, \tag{24}$$

where $\tan \phi = \eta_1 \omega/(G_1 - M\omega^2)$.

Finally, there will be considered the case in which the inertia of the body is not negligible so that a wave motion is set up. Consider, for simplicity, a plane shear wave travelling in the x direction; let u be the displacement in the y direction. If ρ is the density and G^* is the complex shear modulus as before, the wave equation is:

$$G^*(\partial^2 u/\partial x^2) = \rho(\partial^2 u/\partial t^2). \tag{25}$$

A solution is:

$$u = Ae^{(j\omega t - kx)} + Be^{(j\omega t + kx)}. \tag{26}$$

The solution represents a wave-motion which is undamped when k is imaginary (that is, when G^* is real), and which is damped when k and G^* are complex. If the real part of k is positive, the first term in the right hand side of Eq. (26) represents a wave travelling in the $+x$ direction, and the second term represents a wave travelling in the $-x$ direction; this may arise, for example, by reflection of the incident wave at a discontinuity. Assuming $B = 0$ and that k is complex, the solution then represents a damped travelling wave. It is customary to call k the *propagation constant;* the *real component of the propagation constant* will be denoted by α, and the *imaginary component of the propagation constant* by $j\beta$. Then

$$k^2 = (\alpha + j\beta)^2 = \frac{-\rho\omega^2(G' - jG'')}{(G'^2 + G''^2)}. \tag{27}$$

Thus G' and G'' can be obtained from the real and imaginary components of k. It is convenient to express k in terms of directly observable quantities. Eq. (26) may be written:

$$u = Ae^{j(\omega t - \beta x)}e^{-\alpha x} = Ae^{j(\omega t - 2\pi x/\lambda)}e^{-x/x_o}. \tag{28}$$

Hence the wavelength λ is given by

$$\lambda = 2\pi/\beta \tag{29}$$

while the *critical damping distance* x_o is given by (17)

$$x_o = 1/\alpha. \tag{30}$$

The critical damping distance is the distance for the amplitude to fall to $1/e$ of its value. A value of the dimensions of shear modulus can be calculated from the observed wavelength λ for a given circular frequency ω, on the assumption that the shear modulus is real (18). This value may be called the *wave shear modulus;* it has been denoted by the symbol $\tilde{G}$. The wave shear modulus is then given by:

$$\tilde{G} = \rho\omega^2/\beta^2 = \rho\omega^2\lambda^2/4\pi^2. \tag{31}$$

II. Inelastic Behavior of Typical Systems

A. Non-Yield Point Behavior

In the systems discussed previously, release of load at any instant would result in a disappearance of the deformation, which would be immediate in the case of ideal elastic behavior and which would take time in the case of viscoelastic behavior. If release of load at any instant does not result in the immediate or eventual disappearance of strain, the material may be said to manifest *inelastic behavior.*

A material may exhibit substantially ideal elastic behavior or viscoelastic behavior in shear provided the shear stress does not exceed a certain value (which may depend upon the time-scale of the experiment as well as on the environmental conditions). However, if this stress is exceeded, the behavior may become markedly inelastic; this behavior may be called *yield-point behavior.* The stress at about which yield-point behavior becomes manifest is called the *yield stress.* There will be considered, first, systems which do not exhibit yield-point behavior; this type of inelastic behavior will be called *non-yield point behavior.* Systems which exhibit non-yield point behavior are, in general, amorphous non-crosslinked polymers above the quasi-second order transition temperature, as well as polymer solutions.

The relation between shear stress S and shear strain for a material exhibiting both non-yield point inelastic behavior and viscoelastic behavior may be represented to a first approximation by an equation of the type (6):

$$\left(G_1\frac{\partial}{\partial t} + \eta_1\frac{\partial^2}{\partial t^2}\right)\gamma = \left[\frac{G_1}{\eta_2} + \left\{\frac{\eta_1}{\eta_2} + \frac{G_1 + G_2}{G_2}\right\}\frac{\partial}{\partial t} + \frac{\eta_1}{G_2}\frac{\partial^2}{\partial t^2}\right]S. \tag{32}$$

Eq. (32) is seen to be related to Eq. (2); the latter can be obtained from Eq. (32) by making η_2 infinite and integrating with respect to time. This equation represents the behavior of a familiar mechanical model consisting of the model mentioned previously in series with a dashpot, or the behavior of equivalent models (1,12,13). The mechanical behavior of a body obeying the above relationship between stress, strain, and time will be examined as before, under conditions of constant stress, constant strain, and periodic stress.

Under a constant shear stress S applied at zero time the shear strain at time t is given by:

$$\gamma(t) = S/G_2 + S/G_1(1 - e^{-t/\tau}) + (S/\eta_2)t, \tag{33}$$

where the retardation time τ is given by η_1/G_1. If, at time t_1, the shear stress is removed, the residual deformation is given by

$$\gamma(t) = S/G_1(e^{-(t-t_1)/\tau} - e^{-t/\tau}) + (S/\eta_2)t_1. \tag{34}$$

Thus, the first term on the right in Eq. (33) represents the ordinary elastic deformation, and the second term represents the retarded elastic deformation. Upon removal of load, the deformation corresponding to the first term disappears immediately, while that corresponding to the second term disappears in the course of time. The deformation corresponding to the third term does not disappear, and represents, thus, an *inelastic deformation*. In particular, this inelastic deformation is proportional to the time t_1 for which the stress had been applied; this type of inelastic deformation is denoted by the term *flow*. The rate of flow in Eq. (33) is thus given by (S/η_2). Where the rate of flow is proportional, as in this case, to the shear stress, the flow is denoted by the term *Newtonian flow* or *viscous flow*. If, for any given experiment, the first two terms are small compared to the third in Eq. (33), the body may be said to exhibit *Newtonian behavior*. The quantity η_2 may be called the *principal viscosity* (in contradistinction to the internal viscosity η_1), the *melt viscosity*, or simply the *viscosity;* $1/\eta_2$ is the ratio of the flow component of the deformation rate $d\gamma/dt$ to the shear stress. Under large shear stresses the third term may become no longer proportional to shear stress; under these conditions the flow is said to be *non-Newtonian*. It may be that the first two terms are unimportant under these conditions. No generally established relationship can be given at the present time for the dependence of flow on shear stress when the flow is non-Newtonian.

It is seen that, in general, for a material manifesting linear non-yield point inelastic behavior, together with linear viscoelastic behavior in shear, the material exhibits Hookean elastic behavior with a shear modulus G_2 for experiments of very short time scales, while the material exhibits Newtonian behavior with a viscosity η_2 for experiments of very long time scales. According to one point of view, the behavior represented by an equation such as Eq. (32) should be termed viscoelastic behavior; the behavior previously considered in connection with Eq. (2), therefore, becomes a special case where flow is absent.

In the second type of history considered previously a constant shear strain γ is applied at zero time. For a body whose behavior is given by

Eq. (32), the stress decays with time according to an equation of the form:

$$S(t) = \gamma[Ae^{-t/\tau_a'} + Be^{-t/\tau_b'}], \tag{35}$$

where A and B are constants and τ_a' and τ_b' are relaxation times. If one of these times is large compared to the time-scale of the experiment, Eq. (35) reduces to Eq. (4), that is, the relaxation is viscoelastic; this is the case when η_2 is large. If one of these times is small compared to the time-scale of the experiment, this corresponds to η_1 being small, and the relaxation of stress is then given by:

$$S(t) = \frac{G_1 G_2 \gamma}{G_1 + G_2} e^{-t/\tau'}, \tag{36}$$

where the relaxation time τ' is equal to $\eta_2/(G_1 + G_2)$. If, at any time t_1, the load be released, there will be an immediate elastic recovery equal to $\gamma e^{-t_1/\tau'}$. There will be no retarded elastic recovery and the body will not reassume its original undeformed configuration. Such a relaxation behavior is known as *Maxwellian relaxation.* It is seen from Eq. (33) that when η_1, and hence τ, is small, a body manifests rubberlike elastic behavior combined with Newtonian flow under a constant shear stress S, if this is small. For the same environmental conditions, and for the same time-scale, the body should show Maxwellian relaxation under constant shear strain.

In the third type of loading history, a periodic shear stress $S_o e^{j\omega t}$ is applied to the body. When ω is very large, the material shows ordinary elastic behavior, with a shear modulus G_2, the shear strain being in phase with the shear stress. When ω is very small, the material shows Newtonian behavior, the rate of shear strain being in phase with the shear stress and the ratio of the latter to the former corresponding to a viscosity η_2.

B. Yield Point Behavior

The following discussion will be concerned chiefly with the behavior of certain polymeric systems in which (a) the length (or tensile stress) increases uniformly with time or (b) in which the tensile stress is constant, In the case of certain crystalline polymers, such as cellulose derivatives. polyethylene and polyamides, the materials behave up to a certain stress in the first type of test approximately as Hookean bodies with Young's moduli of the order of 10^9 dynes/cm^2. to 10^{11} dynes/cm^2., that is, they appear as leathery to rigid plastics. If the stress exceeds a certain value (the yield stress), which depends not only upon the environmental conditions but also upon the time-scale of the experiment, an inelastic deformation appears. If the inelastic deformation resulting from the application of a stress S acting for a time t_1 is proportional to $(S - S_o)t_1$, where S_o is the actual or apparent yield stress, the material is said to exhibit *plastic flow* or *Bingham behavior.*

In general, the inelastic deformation in polymeric systems does not follow Bingham behavior, but occurs in one of two patterns. In the first case, the body in a test at a constant longitudinal strain rate or tensile stress rate manifests a uniform elongation along its length (if it is originally of uniform cross-section); the increase in deformation after the yield-point is exceeded is due mainly to an increase in inelastic deformation. If, on the other hand, the body is subjected to a constant stress for a time t_1 and released, then, after retarded recovery has ceased, an inelastic deformation will remain, if the conditions of test are sufficiently severe. Tests on fresh specimens reveal that the inelastic deformation is, however, not proportional to t_1, but generally tends to a limit as t_1 approaches infinity. In this respect, the behavior differs from that of a material manifesting non-yield point behavior. Such behavior may be called *mechanical conditioning* or *work hardening*. If a body has undergone such a work hardening, it may be found that the elastic (or viscoelastic) behavior is altered, depending upon the amount of inelastic deformation. Here again, the behavior differs from that of a material manifesting non-yield point behavior.

If, under certain conditions, a body which has manifested this type of inelastic deformation be subjected to suitable swelling or thermal treatment when free from load, part or all of the inelastic deformation will be found to have disappeared when the body is restored to its original environmental conditions. Such recovery of inelastic deformation may be called *swelling recovery* or *thermorecovery*, according to the conditions used to effect the recovery. The second pattern of inelastic deformation in polymers is associated with "necking down" when the length of the body or the tensile stress is increased at a uniform rate. The inelastic deformation after the yield-point is exceeded is restricted to a finite portion of the specimen; increase in overall inelastic deformation corresponds to increase n length of the portion of reduced cross-section, at the expense of the material in the unreduced portion, until the specimen is of uniform, reduced cross-section. The material is then no longer capable of further nelastic deformation.

Finally, it may be observed that materials such as polystyrene may exhibit yield-point behavior in compression, while in tension they behave as brittle glasses. It is to be concluded that yield phenomena depend not only on the deviator part of the stress tensor, but also on the hydrostatic stress.

PROPOSED NOMENCLATURE FOR ELASTIC AND INELASTIC BEHAVIOR OF HIGH POLYMERS

(Equivalent terms are bracketed)

Term	*Symbol*
Ideal elastic behavior	
Hookean behavior Hookean elastic behavior	
Bulk modulus	K
Compressibility	
Shear modulus	G
Shear compliance	J
Ordinary elastic behavior Ordinary elasticity	
Rubberlike elastic behavior Rubberlike elasticity	
Partial rubberlike elasticity	
Young's modulus	E
Poisson's ratio	
Viscoelastic behavior	
Linear viscoelastic behavior	
Retardation time	τ
Effective retardation time	τ
Ordinary elastic deformation	
Ordinary shear modulus	G_2
Ordinary shear compliance	J_2
Creep	
Retarded elastic deformation	
Quasi-static shear compliance	J_t
Quasi-static shear modulus	G_t
Ordinary elastic recovery	
Residual deformation	
Retarded elastic recovery Creep recovery	
High elasticity shear modulus	G_1
High elasticity shear compliance	J_1
Internal viscosity	η_1
Relaxation time	τ'
Stress relaxation	
Viscoelastic relaxation	
Elastic after-effect Elastic after-effect phenomena	
Complex dynamic shear modulus	$G^* = G' + jG''$
Real component of the CDSM	G'

Term	*Symbol*
Imaginary component of the CDSM	jG''
Absolute value of the dynamic shear modulus	$\|G\|$
Complex dynamic shear compliance	$J^* = J' - jJ''$
Real component of the CDSC	J'
Imaginary component of the CDSC	$-jJ''$
Loss tangent	$\tan \delta$
Absolute value of the dynamic shear compliance	$\|J\|$
Internal friction	
Hysteresis loop	
Hysteresis	
Viscoelastic hysteresis loop	
Energy dissipation at unit stress amplitude	W_s
Energy dissipation at unit strain amplitude	W_γ
Specific damping capacity	ψ
Resilience	$1 - \psi$
Complex dynamic viscosity	$\eta^* = \eta' - j\eta''$
Specific mechanical impedance	
Real component of the CDV	η'
Specific mechanical resistance	
Imaginary component of the CDV	$-j\eta''$
Specific mechanical reactance	η''
Complex dynamic fluidity	$\rho^* = \rho' + j\rho''$
Specific mechanical admittance	
Real component of the CDF	ρ'
Specific mechanical conductance	
Imaginary component of the CDF	$j\rho''$
Specific mechanical susceptance	ρ''
Logarithmic decrement	Δ
Phase angle	ϕ
Half-power width	Q
Propagation constant	$k = \alpha + j\beta$
Real component of the propagation constant	α
Imaginary component of the propagation constant	$j\beta$
Critical damping distance	x_o
Wave shear modulus	$\tilde{G}$
Inelastic behavior	
Yield-point behavior	
Yield stress	
Non-yield point behavior	
Inelastic deformation	
Flow	

Term	*Symbol*
Newtonian flow Viscous flow	
Newtonian behavior	
Principal viscosity Melt viscosity Viscosity	η_2
Non-Newtonian flow	
Maxwellian relaxation	
Plastic flow Bingham behavior	
Mechanical conditioning Work hardening	
Swelling recovery	
Thermorecovery	

REFERENCES

1. Burgers, J. M., Chapters 1 and 2 in First Report on Viscosity and Plasticity (Committee for the Study of Viscosity of the Academy of Sciences at Amsterdam): *Verhandel. Konink. Akad. Wetenschap. Amsterdam, Afdeel. Natuur k. Sect. I*, **15**, No. 3 (1935).
2. Burgers, J. M., and Scott Blair, G. W., Paper presented at International Rheological Congress, Holland, 1948.
3. Scott Blair, G. W., *Nature* **149**, 197 (1942).
4. Broome, D. C., *ibid.* **149**, 702 (1942).
5. Mardles, E. W. J., *Rheology Bull.* **18**, (2) 8 (1947).
6. Simha, R., *Ann. N. Y. Acad. Sci.* **44**, 297 (1943).
7. Ferry, J. D., Sawyer, W. M., and Ashworth, J. N., *J. Polymer Sci.* **2**, 593 (1947).
8. Scott, A. H., *J. Research Natl. Bur. Standards, U. S.* **14**, 99 (1935).
9. Rivlin, R. S., *Phil. Trans. Roy. Soc. London* **240A**, 57 (1948).
10. Boyer, R. F., and Spencer, R. S., *Advances in Colloid Sci.* **2**, 13 (1946).
11. Nolle, A. W., and Mowry, S. C., *J. Acoust. Soc. Am.* **20**, 432 (1948).
12. Leaderman, H., Elastic and Creep Properties of Filamentous Materials. Textile Foundation, Washington, D. C., 1943.
13. Alfrey, T., Mechanical Behavior of High Polymers. Interscience, New York, 1948.
14. Clash, R. F., and Berg, R. M., *Ind. Eng. Chem.* **34**, 1218 (1942).
15. Liska, J. W., *ibid.* **36**, 40 (1944).
16. Dillon, J. H., Prettyman, I. B., and Hall, G. L., *J. Applied Phys.* **15**, 309 (1944)
17. Ferry, J. D., *J. Am. Chem. Soc.* **64**, 1323 (1942).
18. Ferry, J. D., *J. Research Natl. Bur. Standards U. S.* **41**, 53 (1948).

SOME STUDIES OF PLASTICIZED POLYVINYL CHLORIDE [1]

Turner Alfrey, Jr., and Norman Wiederhorn

Institute of Polymer Research, Polytechnic Institute of Brooklyn, Brooklyn, N. Y.

Richard Stein and Arthur Tobolsky

Frick Chemical Laboratories, Princeton University, Princeton, N. J.

Received February 25, 1949

INTRODUCTION

In a previous publication (1), the creep behavior of plasticized Vinylite YNW was described. At that time, an attempt was made to relate this ehavior to the structure of plasticized polymer compositions. Among the onclusions which were arrived at was that a 3-dimensional gel network of reat permanence must be present. This was necessary to explain the ombination of the *small*, long-time creep, associated with the large hort-time compliance and the essentially complete recovery of films hich had been subjected to stresses for weeks.

The nature of the gel structure has now been studied more thoroughly ith the aid of numerous experimental techniques. The results of this ork not only confirm the existence of a 3-dimensional network system in lasticized polyvinyl chloride and VYNW compositions, but also lead to a airly definite picture of its details. It has been established, on the basis of reep, stress relaxation, dilatometry, birefringence, and X-ray measure- ents, that these materials are partially crystalline in nature. The rela- ive amounts of crystalline and amorphous polymer in any one compo- ition has not been established, but there is no doubt that the crystalline egions comprise but a small fraction of the total composition.

EXPERIMENTAL EVIDENCE FOR MICROCRYSTALLINE STRUCTURE

X-Ray Diffraction Studies

X-ray diffraction studies of plasticized polyvinyl chloride and Vinylite YNW are described in another paper (2). These studies definitely indi- ate these plasticized resins are partially crystalline in nature. Orientation f the films was observed to result in fibre-like diagrams.

Dilatometric Measurements

VYNW films were prepared, containing 15%, 25%, 35%, and 45% ioctyl phosphate (TOP) and tricresyl phosphate (TCP), respectively, as plasticizer. (The method used in the preparation of these and all other films used throughout this work was that described previously by Aiken *et al.*)

---

[1] Presented at the Annual Meeting of the Society of Rheology, New York, N. Y., ovember 5 and 6, 1948.

Weighed quantities of these films were rolled up and charged into calibrated dilatometers. The dilatometers were then filled under vacuum with a 20% solution by weight of KCl. A blank containing only the covering solution was also prepared. In all cases the charge of the individual components was known accurately. The dilatometers were then immersed in a water bath with regulated temperature.

The bath was cooled to 0.0°C. and the levels of the menisci were recorded. The bath was then heated over an 8 hr. period to a final temperature of 90°C. and the changes in level of the menisci were recorded as a function of the temperature. Care was taken to maintain any one temperature for 5–10 min. before taking a reading, so as to be sure that thermal equilibrium was attained.

The expansion of each plasticized sample was then calculated, with corrections for the expansion of the covering liquid and the dilatometer itself. The results were not remarkable. The volume-temperature curves for the samples containing 15% TOP and 15% and 25% TCP showed (small and questionable) changes in slope, at approximately 30°C., 55°C. and 17°C., respectively. The remaining samples gave straight lines when expansion was plotted against the temperature.

The second group of dilatometer measurements were concerned with *time dependence* of the density. Four samples of VYNW, plasticized with 15% and 45% of TOP and TCP, respectively, were charged into calibrated dilatometers and covered with the 20% KCl solution. The dilatometers were heated to 90°C. and held for 30 min. in order to melt out any non-equilibrium structures. They were then plunged into an ice bath and held at 0.0°C. for 20 min.

The samples were then placed in a bath thermostatically controlled at 24.7°C. After the initial expansion of the dilatometer contents due to the attainment of thermal equilibrium, a slow contraction with time was noted. This procedure was repeated at two other final temperatures, namely 53.2°C. and 73.0°C.

In all cases, after the initial expansion due to the attainment of thermal equilibrium, a contraction with time was observed. Thus, even at 73.0°C., samples containing as much as 45% plasticizer exhibit a volume-time relation (see Figs. 1. and 2).

Krevsky (3), who carried out similar work with the systems VYNW-dibutyl phthalate and VYNW-PD16, obtained similar results.

The interpretation of this type of data has generally been associated with second order transition phenomena (4). However, in this instance, in view of the fact that the second order transition points of the samples containing 45% plasticizer are appreciably less than 0.0°C., another explanation is necessary.

The contractions in volume that were observed may be readily understood in terms of a microcrystalline structure for polyvinyl chloride. If plasticized VYNW, at room temperature, is a partially crystalline material, then, as the temperature is increased, the percentage of the segments in crystal micelles must decrease.

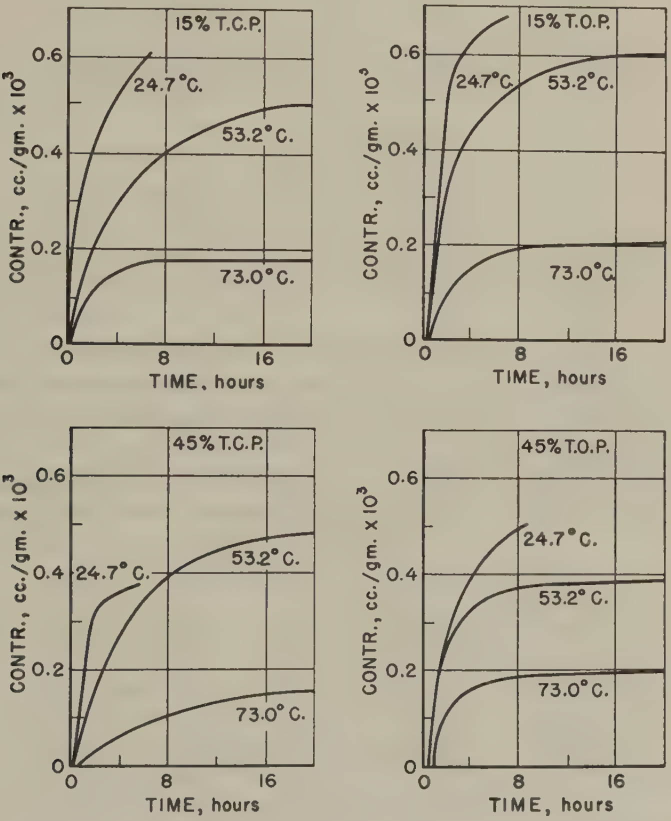

Figs. 1 and 2. Rate of attainment of equilibrium of various plasticized VYNW films.

Consequently at 90.0°C., although the material may not necessarily be amorphous, it is certainly not as highly crystalline as at a lower temperature. Thus, when a sample at 90.0°C. is quenched to 0.0°C. and then heated to an intermediate temperature, it will crystallize at that temperature. However, crystallization of polymeric materials is, in general, a slow process. The contractions which were observed with time can then be interpreted as being the result of an increase in density due to the progressive crystallization of the films.

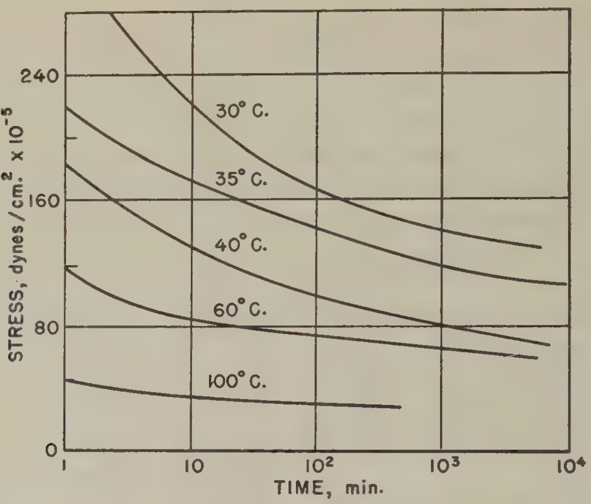

FIG. 3. Stress relaxation of Geon 101 + 30% TCP at various temperatures.

Stress Relaxation and Birefringence Measurments

The birefringence of linear polymeric materials, when they are subjected to a stress, is a phenomenon which is readily understood in its qualitative aspects (5).

An unoriented polymer, when elongated, will exhibit birefringence due to the asymmetry within the bulk sample of the individual elongated chains.

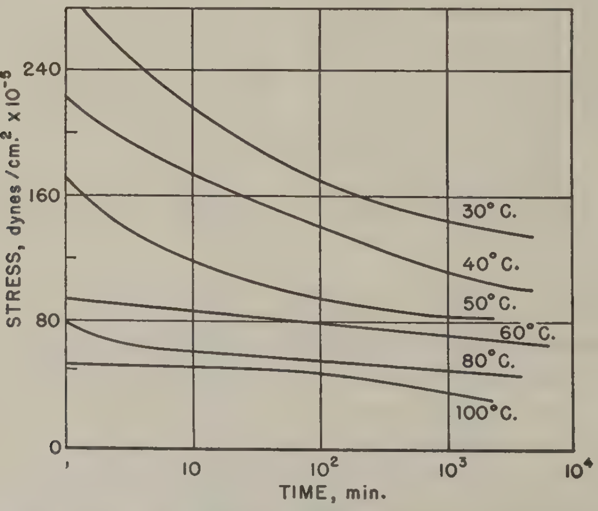

FIG. 4. Stress relaxation of Geon 101 + 35% ditetrahydrofurfuryl sebacate at various temperatures.

If the sample is held at constant length, then a number of different observable phenomena may occur, depending upon the internal changes taking place under the particular set of experimental conditions.

a. The sample may exhibit flow of one chain with respect to another. This will normally manifest itself in a decrease in the tension or the stress required to hold the sample at constant elongation. Also, the flow will result in a more random configuration of the individual chains. This will cause a decrease in the observable birefringence. Thus, a material which exhibits flow will, when held at constant elongation, exhibit a decrease both in tension and in birefringence. Furthermore, it has been established that, for such instances, the stress divided by the birefringence should be a constant.

b. A decay of stress may result from the relaxing of chains by retarded elastic processes. Relaxation by this mechanism is also a consequence of the chains assuming a more highly random configuration. Consequently, the observed birefringence will decrease with the tension. In this instance, as when relaxation is the result of true flow, the stress divided by the birefringence should be constant.

c. A third possible mode of behavior is for the elongated sample to crystallize. Crystallization of a polymeric material under conditions of constant elongation invariably results in a decay of the stress necessary to maintain the elongation. However, this decay of the stress is occasioned by a further orientation of the polymer chains through the formation of crystallites. The birefringence, therefore, will not decay along with the stress, as is true with materials that flow.

The procedure followed in the stress relaxation and birefringence measurements was to stretch a sample of plasticized polyvinyl chloride to a desired elongation, heat to the desired temperature, and measure the stress and birefringence as a function of time in a relaxometer equipped with a continuous recording mechanism for the stress, a source of plane polarized light, and an analyzer for measuring the birefringence.

The results obtained with various samples of plasticized Geon 101 polyvinyl chloride films are presented in Figs. 3 to 6.

Of greater interest and meaning are plots of the stress divided by the birefringence which are shown in Figs. 7 to 9. Here it is seen that, as the temperature is increased, not only does the height of the curve fall, but likewise the curve flattens. A curve with negative slope is indicative of a greater rate of decay of stress at any particular instant of time than rate of decay of birefringence. If the two rates are the same, a horizontal line must result. Such is the case when the stress decay is the result of viscous flow or configurational retarded elasticity within the bulk sample. In these instances, at the lower temperatures where the stress/birefringence ratio exhibits

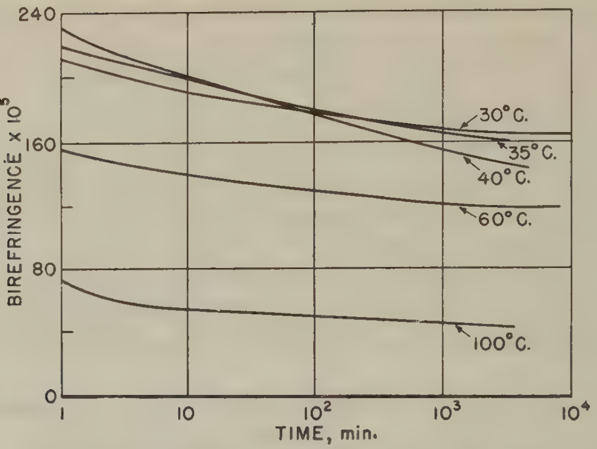

FIG. 5. Birefringence relaxation of Geon 101 + 30% TCP at various temperatures.

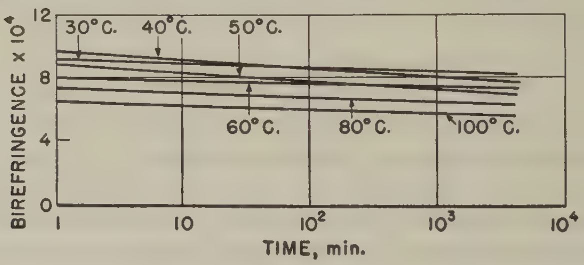

FIG. 6. Birefringence relaxation of Geon 101 + 35% tetrahydrofurfuryl sebacate at various temperatures.

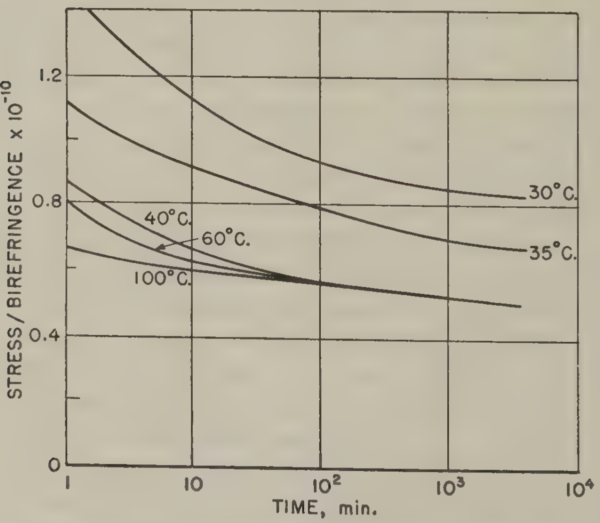

FIG. 7. Ratio of stress to birefringence during relaxation. Geon 101 + 30% TCP

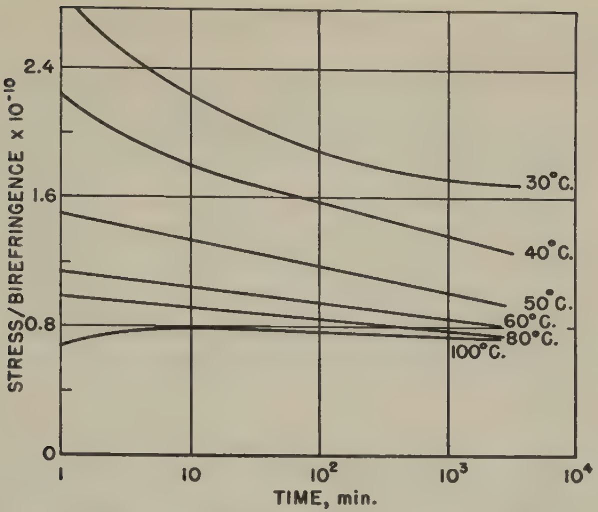

FIG. 8. Ratio of stress to birefringence during relaxation. Geon 101 + 35% ditetrahydrofurfuryl sebacate.

wide deviations from constancy, we must conclude that the structure is not that of a simple linear amorphous polymer.

A second group of experiments concerned with the dependence of stress and birefringence upon temperature were carried out. A Geon 101 film, containing 15% TCP as plasticizer, was elongated 100 % and heated to 100.0°C. It was then held at this temperature until the tension was relatively constant. The sample was then slowly cooled and the stress and

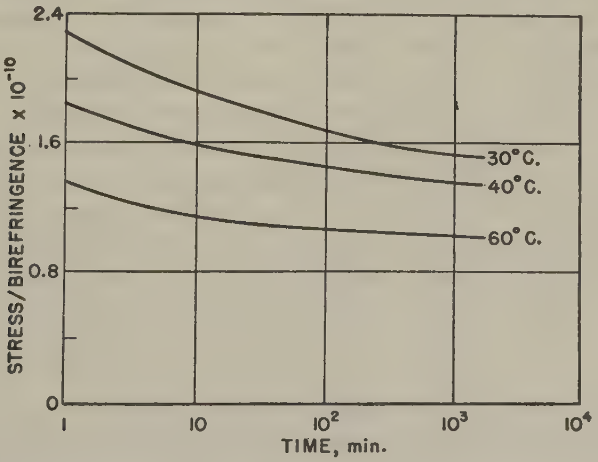

FIG. 9. Ratio of stress to birefringence during relaxation. Geon 101 + 45% ditetrahydrofurfuryl sebacate.

birefringence recorded. The results obtained are illustrated in curves A and A′ of Figs. 10 and 11.

On reheating the sample to 100.0°C., it was determined that these curves are essentially reversible, and repeated heating and cooling cycles invariably give the same curve, provided a maximum temperature of 100.0°C. is not exceeded.

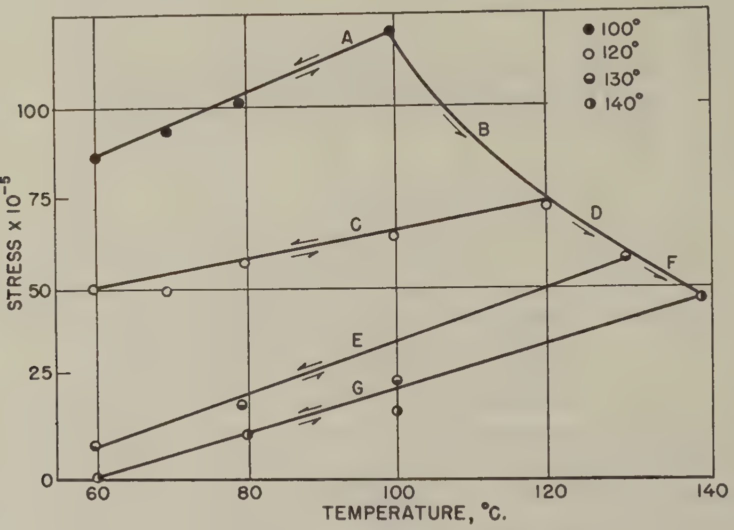

Fig. 10. Stress-temperature relationships. Geon 101 + 15% TCP.

Furthermore, if, during the heating or cooling cycles, the sample is held at a constant temperature for a period of time, there is no change in either the birefringence or stress. If the sample is heated above 100.0°C., for example, to 120.0°C., then curves B and B′ are obtained.

The stress increases during the up-heat until a temperature of 100.0°C. is obtained and then decreases. Similarly, the birefringence remains essentially constant until the temperature at which the cooling cycle was initiated is attained. Then it, too, decreases. If, at 120.0°C. the sample is again cooled, curves C and C′ are obtained. These, likewise, are essentially reversible, provided that the temperature at which the cooling cycle was initiated is not surpassed. If it is, then curves D and D′ result. The processes can then be repeated at higher temperatures as is illustrated in the figures.

The interpretation of these results has been the following: When the sample at 100.0°C. and 100% elongation is cooled, crystalliztaion occurs along the axis of the applied stress. This is observed as a decrease in stress (6) without a corresponding decrease in birefringence.

On heating, the oriented crystallites that were grown during the cooling cycle melt out, and, provided the temperature at which the cycle was initiated is not exceeded, the formation and disappearance of these crystallites is a function only of the temperature.

Furthermore, the presence of the crystallites prevents true flow, consequently permitting the sample to be held at any intermediate temperature for a period of time without any change in either stress or birefringence. This portion of the curve is, therefore, reversible.

If the initial temperature is exceeded, a different internal process takes place. Crystal micelles are melted out, but their removal in this instance does not cause an increase in the stress, as was observed in Curve A, but a decrease. This is occasioned by the fact that the crystallites which are melting are not necessarily oriented and in equilibrium with the stretched structure, but include those which had their genesis during the preparation of the film. Consequently, their removal is equivalent to the removal of points of cross-linking, thereby permitting a decrease in the stress necessary to maintain a given elongation. The corresponding decrease in the birefringence is due to the fact that the absence of certain points of cross-linking permits the further relaxing of individual chains, and consequently the assumption of more random orientations consistent with the elongation and the quantity of crystalline material still remaining. Essentially, there is an increase in the configurational randomness of the sample which is manifested by a decrease in the birefringence.

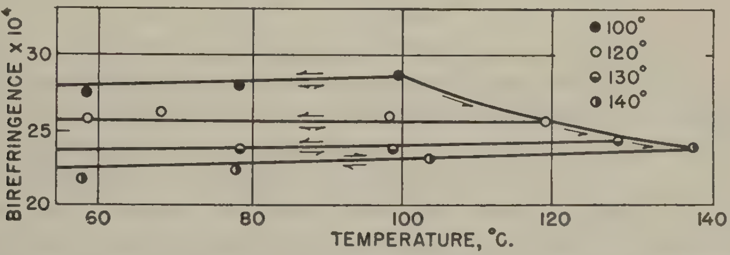

FIG. 11. Stress-birefringence-temperature relationships. Geon 101 – 15% TCP.

If, at the higher temperature, a new cooling cycle is started, then the crystallization that occurs is not the reverse of the melting that had taken place in the attainment of this temperature, but leads to the formation of oriented crystallites, thus decreasing the stress.

The processes which then take place during repeated heating and cooling cycles are basically the same as those occurring during the reversible heating and cooling cycles described previously. The differences found in the height of the curves initiated at 120.0°C., as compared to those initiated at 100.0°C., is due to differences existing in the details of the internal structure. At the higher temperature (120.0°C.), when the cooling cycle is initiated, the sample is less crystalline than at the lower temperature. Furthermore, while cooling from the higher temperature, when the lower (100.0°C.) is reached, although the total quantity of crystalline material may be the same, the details of the crystalline structure are necessarily different. When 100.0°C. is attained, as a result of cooling from 120.0°C., there is present a certain amount of oriented crystallites which were definitely absent when the sample was heated directly to 100.0°C.

The details of the argument used here for the cycles initiated at 100.0°C. and 120.0°C. may be extended in an identical fashion to the cycles initiated at 130.0°C. and 140.0°C.

SPECULATIONS REGARDING DETAILED MECHANISM OF PLASTICIZER ACTION

In a previous publication (1), tensile creep results of vinylite compositions were interpreted on the assumption that the effect of increasing temperature or plasticizer concentration was to rigidly shift the creep curve laterally along the log time axis. Only minor changes in shape and height of the curve were believed to accompany this lateral shift. This particular assumption hardly appears to be tenable in view of the present, more extensive knowledge. It seems nearly certain that the effect of increasing plasticizer concentration or temperature must result in a vertical, as well as a horizontal, displacement of the curve, due to a decrease in the concentration of crystallites. Thus, not only is the retarded elastic response *accelerated*, but, in addition, a more compliant structure is obtained under such circumstances.

Aside from this, any further interpretation of the various tensile creep properties in terms of the work thus far described cannot be considered be more than reasonable assumption. However, with the utilization of the present knowledge of polymeric materials, it is possible to conjecture concerning the mechanism of creep of plasticized vinylite compositions. The proposed theory is based on the following postulates.

1. Polyvinyl chloride and its copolymers with vinyl acteate are characterized by a microcrystalline structure. The crosslinks, which previously had been deemed necessary for explaining many of their properites, may now be considered to be the crystallites.
2. The polycrystalline structure follows the general pattern of crystalline polymers.
3. Different plasticizers affect the microcrystalline structure, the behavior of the plasticized resin being dependent largely upon the resulting microcrystalline structure.

4. Partial melting of the microcrystalline structure may be accomplished by various external factors such as temperature, stress, *etc.*, but upon removal of such a factor recrystallization can be accomplished.

These postulates and their justification may be discussed individually.

Microcrystalline Structure

Although polyvinyl chloride has been shown to exist in a microcrystalline structure, the methods employed do not reveal the size of the crystallites nor the total amount of crystalline material.

The Polycrystalline Structure Follows the General Pattern of Crystalline Polymers

In the discussion presented thus far, it has been tacitly assumed that the behavior of polyvinyl chloride is analogous to that of other crystalline polymers. As a matter of fact, a comparison of its behavior with that of known crystalline materials in certain tensile creep and stress relaxation experiments, has been used as a basis of establishing the fact that it is crystalline. However, for the purpose of continuity, it might be well to discuss the details of the microcrystalline structure.

Firstly, there is no reason to doubt that the chains are bound parallel bundles or micelles, and that each chain passes through one or more such crystalline regions. The portions of the chains which are not in these micelles then constitute the amorphous regions.

Concerning the characteristics of the crystallization of rubber and other polymeric materials, it has been found that the formation of crystallites is a comparatively slow process, the rate being dependent upon temperature. The overall rate of crystallization is the result of two processes, seed formation and crystal growth (7).

A plot of the time necessary for half the total crystallization to take place, *vs.* the temperature, normally exhibits a minimum in a definite temperature range. This minimum corresponds to a maximum rate of crystallization. Thus, for natural rubber, the maximum rate is obtained at about − 25.0°C., whereas above 10.0°C. and below − 50.0°C. the rate of crystallization is, sensibly, zero. The absence of crystallization at temperatures below −50°C. is a clear-cut case of supercooling of an amorphous material to a temperature below which the mobility is insufficient for the formation of crystals (7).

Another characteristic of crystalline polymers is that they melt over a range of temperatures, which is generally quite broad. Furthermore, this melting range varies in position as well as in magnitude, depending upon the temperature at which the crystallization was effected (7).

Although these phenomena have not been studied in detail in plasticized vinylite compositions, the indications are that such materials do behave in an analogous manner.

The fact that crystallization is comparatively a slow process is borne out by various "time dependency" studies which have been made. Firstly, the changes in volume with time observed in the dilatometric measurements, are probably due to the crystallization of the composition.

Furthermore, the work described by Aiken *et al.* (1), in which films of plasticized VYNW were heated to about 130.0°C., cooled to room temperature, and then tested in tensile creep measurements, may now be readily interpreted. These workers found that the height of the creep curve, run at varying intervals of time after the heat treatment, fell as a function of the time. After a number of hours a constant minimum curve was attained. What probably took place in this experiment is that, on heating to 130.0°C., the crystalline character of the film was extensively disrupted. On cooling, recrystallization occurred, but was time-dependent. Since the formation of crystallites results in a tightening of the network structure, and, since a tighter network structure will give rise to a lower creep curve (a less compliant material), recrystallization with time will make itself felt by a falling in the height of the creep curve until the crystallization is complete.

With regard to the wide melting range normally associated with crystalline polymers, although no direct measurements have been made on plasticized vinylite composition, interpretation of other experimental data must lead to the conclusion that, for these materials, a very wide range exists.

Experimentally, it is found that the maximum height of the creep curve for such compositions increases with temperature. From the kinetic theory of rubber elasticity, the height corresponds to the reciprocal of Young's modulus, which, in the case of a cross-linked material is given by (8)

$$1/G = 1/AT\nu(2 - M/M_c),$$

where G is Young's modulus;

T is the absolute temperature;
M is the molecular weight of the chain before cross-linking;
M_c is the average molecular weight of segments between cross-links;
A is a constant;

and ν is the number of cross-links per unit volume.

If ν were to remain constant in the temperature ranges investigated, then $1/G$ (the height of the creep curve) would be inversely proportional to the absolute temperature.

In the proposed structure, ν corresponds to the number of crystallites per unit volume. In the range of temperatures where the quantity of crystalline material decreases with increasing temperature, ν decreases, and the height of the creep curve should increase.

This range, apparently, is very wide, and even at 90.0°C. samples containing up to 50% plasticizer are not completely amorphous. This is evidenced by the fact that, at this high temperature, they do not exhibit irrecoverable flow when subjected to small stresses.

Thus, it is seen that the effect of increasing temperature, throughout the workable range, is to effectively decrease the concentration of crystallites. The effect of increasing plasticizer content is probably the same.

According to Zhurkov (9), and Aiken *et al.* (1), when plasticizer is added to polyvinyl chloride, it serves to solvate or shield points of contact along the chain. The points of contact which they considered may now be thought of as leading to the formation of crystals. Solvation of such points will, therefore, rupture crystallites. The process which takes place may be roughly described by the relation,

$$\text{crystal} + \text{plasticizer} \rightleftharpoons \text{solvated amorphous polymer.}$$

From the law of mass action, an increase in the plasticizer content must result in a decrease in the quantity of crystalline material.

The effect of acetate in chloride-acetate copolymers is probably, also, to decrease the quantity of crystalline material. This is evidenced in the creep curves, where films of resins containing different quantities of acetate, but the same quantity of plasticizer, give different curves. The height of the curve is an increasing function of the acetate content, indicating a looser network structure of the polymeric material. A looser network structure must correspond to less crystalline material. In addition, it has been found that the repeat unit distances in VYNW, a chloride-acetate copolymer, are the same as in Geon 101. Thus, the unit crystal probably consists of only vinyl chloride segments. If this is the case, the random inclusion of acetate segments along the chain must interfere with the formation of crystal micelles. Of course, the greater the quantity of acetate the greater will be this interference, with a consequent decrease in the crystalline character of the polymer.

Effect of Plasticizer upon Microcrystalline Structure

A plasticizer is essentially a non-volatile solvent for the particular polymer with which it is being used. Upon the addition of such a material to polyvinyl chloride-acetate polymers, a microcrystalline structure results. Furthermore, the geometry within the crystallites of the polymer-plasticizer system is independent of the plasticizer and of any vinyl acetate segments which may be present. From these data, the internal structure must consist of two separate disperse regions, namely, the crystalline regions in which there are present only polyvinyl chloride segments and regions containing amorphous polyvinyl chloride-acetate and plasticizer.

As a crude analogy, this system may be considered to be similar to one consisting of a saturated solution in the presence of undissolved solute.

On the basis of this molecular interpretation of the structure of plasticized vinylite films, it is now possible to conjecture concerning the effect of different plasticizers on this structure. This may be done by drawing analogies with systems containing small molecules. This, admittedly, is poor if quantitative results are desired, but for a qualitative discussion it is reasonable.

If solutions of the same volume having the same concentration of a low molecular weight solute are evaporated to a volume such that crystals of the solute are deposited from each, then it is possible to make the following statements:

1. In general, the crystals obtained from the poorer solvent will be smaller than those obtained from the better solvent (10).
2. The total quantity of crystals obtained from the poorer solvent will generally be greater than that obtained from the better.

By analogy, the essential difference in the mode of behavior of various plasticizers lies in their solvent power for polyvinyl chloride, or, conversely their effect on the details of the microcrystalline structure which is obtained in the presence of the plasticizer. When a poor solvent is used as a plasticizer, there will be a larger total quantity of crystalline material than when a better solvent is used. The dimensions of the crystallites will also be affected. One is then tempted to conclude that the differences in the plasticizing action of different materials is principally due to differences in the details of the microcrystalline structure, which they very probably produce.

Continued Creep of Polyvinyl Chloride Compositions

When plasticized polyvinyl chloride films are subjected to a stress at constant temperature, the distortion that takes place is completely recoverable upon removal of the stress. There is no viscous flow, which is readily explained by the 3-dimensional network of the polymer.

However, the creep of polyvinyl chloride differs, in at least one respect, from that of a chemically cross-linked polymer such as a lightly vulcanized rubber. Apparently, the creep of polyvinyl chloride never stops. If the compliance is plotted against log time, then the curve obtained is constantly rising, even after periods of many hundred thousand seconds.

Chemically cross-linked polymers, on the other hand, normally will attain a constant maximum value for the creep curve, unless extraneous factors, such as chemical breakdown, are present.

A satisfactory explanation for this basic difference in the creep behavior is not readily available. That which is now being proposed is purely speculative, and, although it does explain the phenomenon, it must be admitted that the experimental evidence in support of the basic tenet, namely, an external force is capable of rupturing crystallites, is very meager.

The crystalline structure of polyvinyl chloride, although it has been established, has not been described in all its details. One of the principal points of conjecture lies in the distribution in sizes of the crystallites. From the X-ray patterns which were obtained, it is shown that there are many having dimensions greater than 100 Å. In X-ray analysis, crystallites whose dimensions are less than about this figure, normally do not scatter sharply enough to yield crystalline patterns.

In order that a dimension be of this order of magnitude, there must be approximately 25 units in the diffracting plane. It is logical to assume that there is a distribution of sizes, such that some crystallites contain as few as 5 or 10 units and others consist of as many as (or more than) 25 units.

Now, when a stress is applied to a sample, it is possible to consider two individual internal mechanical processes taking place stepwise. Firstly, creep takes place by the elongation of the amorphous regions between crystallites until equilibrium is attained. At this point the stress is distributed among the points of cross-linking, or the crystallites. However, some of the crystallites are very small and their total binding energy consequently is likewise small.

Those crystallites not having sufficient energy to withstand the external force to which they are subjected will be ruptured. When this occurs, the sample is no longer at equilibrium, and there must be a redistribution of the stress among the intact crystallites. Such a redistribution can take place only within a new internal configuration of the chains. Thus, a second creep process results, until a new equilibrium is established. The individual crystallites are now subjected to a greater stress and again those with insufficient binding energy will be ruptured. Such processes are repeated throughout the stressed life of the sample, and will result in a net constantly rising creep curve.

Although the creep process has been considered as taking place in individual steps, this has been merely for the purpose of presentation. In reality, the processes must be continuous, with no clearly defined stages. A much more accurate picture would be one in which the single processes described are superimposed one upon the other.

Evidence in support of this hypothesis has been obtained in the course of the experimental work. Three samples containing 45% TOP as plasticizer were prepared and subjected to tensile creep at 27.5°C. under conditions of equal stress. The creep curves obtained were all essentially identical (less than 2% deviation of any one curve from the mean of all the curves). These films were all stressed for one hour. After stressing, the samples were permitted to recover for one hour, at which time 91% recovery was obtained for all the samples. Immediately after recovery, one of the samples was re-stressed. Two hours later the second sample was stressed again, and 4.5 hr. later, the third sample. The curves obtained are presented in Fig. 12. Here it may be noted that a tensile creep run immediately after recovery of the initial creep is significantly higher than the initial curve, and that, as time progresses, the curves tend to fall toward the initial creep curve. These differences are larger than experimental error.

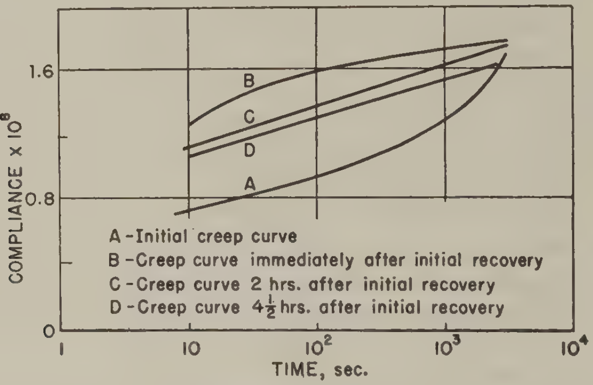

FIG. 12. Effect of previous stress history upon the creep of VYNW films containing 45% TOP.

The interpretation of this experiment has been along the following lines. Slight increases in temperature decrease the quantity of crystalline material as is evidenced by the increased height of the creep curve. Thus, relatively small amounts of energy have a measurable effect upon the quantity of crystalline material, and it is conceivable that the application of an external stress may serve in a similar manner. If this is true, the crystallites when once ruptured take a measurable time to re-form.

Therefore, if a sample is subjected to a stress, two distinct processes take place within the sample. Firstly, the chains are elongated between crystallites, and secondly, the smaller crystallites are ruptured. Every time a crystallite is ruptured, the modulus decreases. Thus, the modulus decreases with time. If, after this initial elongation, the sample is permitted to recover, then, when the recovery is completed, the network will be looser than it was before the sample was stressed.

This is due to the fact that it takes a significant period of time for the ruptured points of cross-linking to re-form. Consequently, if the sample is immediately subjected to a stress a second time, the initial modulus will be less, and consequently the initial portion of the creep curve will be higher.

REFERENCES

1. AIKEN, W., ALFREY, T., JANSSEN, A., AND MARK, H., *J. Polymer Sci.* **2**, 178 (1947).
2. ALFREY, T., STEIN, R., TOBOLSKY, A., AND WEIDERHORN, W., *Ind. Eng. Chem.* in press.
3. KREVSKY, B., Thesis, Polytechnic Inst. of Brooklyn, 1947.
4. ALFREY, T., GOLDFINGER, G., AND MARK, H., *J. Applied Phys.* **14**, 700 (1943).
5. TRELOAR, L. R. G., *Nature* **159**, 231 (1947); SKIN, R., AND TOBOLSKY, A., *J. Textile Research* April–May (1948).
6. MEYER, K. H., AND FERRI, G., *Rubber Chem. and Technol.* **8**, 319 (1935); WOOD, L. A., AND ROTH, F. L., *J. Applied Phys.* **15**, 781 (1944).
7. WOOD, L. A., *Advances in Colloid Sci.* **2**, 58 (1946).
8. FLORY, P. J., *Chem. Phys.* **35**, 51(1944).
9. ZHURKOV, S. N., Compt. rend. acad. sci. U.R.S.S. **47**, 475 (1945).
10. KOLTHOFF, I. M., AND SANDELL, E. B., Quantitative Inorganic Analysis, p. 102. Macmillan, New York, 1947.

VOLUME-TEMPERATURE-TIME RELATIONSHIPS FOR POLYSTYRENE[1]

R. S. Spencer

From the Dow Chemical Company, Midland, Michigan

Received January 6, 1949

INTRODUCTION

The conventional picture of the thermal expansion of a high polymer is as follows: As the temperature is raised the volume increases uniformly according to a certain expansion coefficient. At a particular temperature, or over a short range of temperature, this expansion coefficient changes rather abruptly to a higher value. A similar discontinuity is observable in the specific heat of the polymer, and in various other properties (2,3,4). This characteristic temperature is usually designated the second-order transition temperature, and has been identified with the "softening point," "heat distortion temperature," *etc.*

More detailed observations have revealed that the second-order transition in high polymers is not a true thermodynamical singularity. Jenckel (5) found that a considerable slowing down of the heating process would lower the apparent transition temperature of selenium glass 7°C. A similar 7°C. variation in the apparent transition temperature of polystyrene was reported by Alfrey, Goldfinger and Mark (1) for various heating and cooling rates. Finally, Spencer and Boyer (6) found that, if sufficient time were allowed for the sample to come to volume equilibrium, the volume-temperature curve showed no evidence of a transition between 25°C. and 140°C. The obvious conclusion is that the apparent second-order transition is a rate phenomenon, dependent on both the properties of the material and the conditions of the experiment. A not so obvious corollary is that the values of the expansion coefficients observed are also somewhat dependent upon experimental conditions.

The existence of two mechanisms of thermal expansion was suggested and subsequently confirmed by Alfrey, Goldfinger and Mark (1) and Spencer and Boyer (3,6). One mechanism appears to respond almost instantaneously to temperature changes within the range of interest. The other mechanism produces delayed volume changes at a rate proportional to the difference between the equilibrium volume and the actual volume.

---

[1] Presented at the Annual Meeting of the Society of Rheology, New York, N. Y., November 5 and 6, 1948.

The temperature-dependence of this rate is characterized by an activation energy of 12 kcal./mole. It is apparent, then, that the volume is a function of both time and temperature, and depends also upon the initial state of the polymer, of course. The differential equation describing this relationship was stated by Spencer and Boyer (6), and the result of a graphical solution of the equation for a particular case compared with experiment.

It is the purpose of the present paper to derive a general solution of the fundamental thermal expansion equation and to apply this to certain simple temperature-time relationships. The resulting volume-temperature curves may then be analyzed to determine the dependence of the second-order transition temperature upon such factors as heating or cooling rate, initial condition of the polymer, *etc.* A limited comparison with experiment will be made, and some consideration given to related annealing problems.

GENERAL PROBLEM

Inasmuch as this problem is one essentially mathematical in nature we shall begin by defining certain symbols, as follows:

t = time (min.)
T = absolute temperature
V = specific volume (cm.^{3}-g.$^{-1}$) at t and T
V_e = equilibrium specific volume at T., $= V_o [1 + (\beta_1 + \beta_2)T]$
V_o = equilibrium specific volume at 0°K., by extrapolation
$\Delta V = V - V_e$
ΔV° = the value of ΔV at $t = 0$
β_1 = "instantaneous" volume expansion coefficient (based on V_o)
β_2 = "delayed" volume expansion coefficient (based on V_o)
k = rate constant for delayed isothermal changes. We take this to be of the form $k = Ae^{BT}$, with A and B constants.

Any other special symbols will be defined as needed.

The volume being a function of time and temperature, we may write

$$dV = \left(\frac{\partial V}{\partial T}\right)_t dT + \left(\frac{\partial V}{\partial t}\right)_T dt. \tag{1}$$

In terms of the experimental observations (6) the instantaneous expansion gives

$$\left(\frac{\partial V}{\partial T}\right)_t = V_o \beta_1 \tag{2}$$

and the isothermal delayed expansion gives

$$\left(\frac{\partial V}{\partial t}\right)_T = -k\Delta V = -Ae^{BT} \cdot \Delta V. \tag{3}$$

This last expression brings up an interesting point. It is perhaps more correct to consider k to be of the form $Ae^{-B/T}$, but unfortunately this leads to a rather intractable differential equation. The expression in Eq. (3) gives almost as good a fit to the experimental data and has certain mathematical advantages. As a final check, the more correct but less tractable equation was solved for certain cases by the differential analyzer and fairly good agreement obtained with the solutions given by the form used in this paper.

Substituting (2) and (3) in Eq. (1) we obtain

$$dV = V_o\beta_1 dT - Ae^{BT}\cdot\Delta V dt. \tag{4}$$

Now

$$dV = d(\Delta V) + V_o(\beta_1 + \beta_2)dT,$$

so

$$\frac{d(\Delta V)}{dt} + Ae^{BT}\cdot\Delta V = -V_o\beta_2\frac{dT}{dt}. \tag{5}$$

Considering T as a known function of t, this is simply a linear first-order equation. Defining

$$\phi = A\int e^{BT}dt,$$

the solution of Eq. (5) may be written as

$$\Delta V = \Delta V^\circ e^{\phi_o}\cdot e^{-\phi} - V_o\beta_2 e^{-\phi}\int_{T_o}^{T} e^{\phi}dT, \tag{6}$$

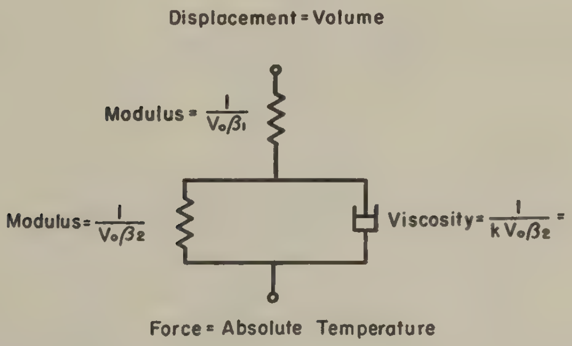
Displacement = Volume
Modulus = $\frac{1}{V_o\beta_1}$
Modulus = $\frac{1}{V_o\beta_2}$
Viscosity = $\frac{1}{kV_o\beta_2}$ =
Force = Absolute Temperature

FIG. 1. Mechanical analogue for the volume-temperature-time relationship for polystyrene.

where ϕ_o and T_o are the values of ϕ and T, respectively, at $t = 0$. This is our general solution, into which may be substituted particular temperature-time relationships of interest. Fortunately, some of the most interesting cases yield solutions in closed form. As a matter of interest, Eq. (6)

leads to the following expression for the expansion coefficient at any point:

$$\frac{dV}{dT} = V_o\beta_1 - \frac{Ae^{BT}\cdot\Delta V}{dT/dt}.$$

The foregoing equations are identical with those governing the behavior of the mechanical system shown in Fig. 1. This diagram will be a familiar one to workers in the high polymer field, inasmuch as it is also a simplified model for the elastic behavior of a polymer. In our case the volume corresponds to displacement and the temperature corresponds to the force applied.

The constants for polystyrene used in all subsequent computations were as given in Table I.

TABLE I

Thermal Expansion Constants for Polystyrene of Molecular Weight 360,000

$A = 1.7531 \times 10^{-11}$ min.$^{-1}$
$B = 0.058363$ °K.$^{-1}$
$\beta_1 = 3.135 \times 10^{-4}$ °C.$^{-1}$
$\beta_2 = 2.054 \times 10^{-4}$ °C.$^{-1}$
$V_o = 0.82871$ cm.^{3}-gm.$^{-1}$

LINEAR CASES

One of the most useful and instructive situations to be able to treat theoretically is that in which the temperature rises or falls linearly with time. Let

$$\frac{dT}{dt} = b,$$

where b is a constant, either positive or negative. In this case

$$\phi = \frac{Ae^{BT}}{bB}$$

and Eq. (6) becomes

$$\Delta V = \Delta V^\circ e^{\phi_o}e^{-\phi} - \frac{V_o\beta_2 e^{-\phi}}{B}[Ei(\phi) - Ei(\phi_o)], \tag{7}$$

where

$$Ei(\phi) = \int_{-\infty}^{\phi} \frac{e^x dx}{x}$$

is the exponential integral, which has been tabulated (7).

In Fig. 2 is shown the volume-temperature curve for the case of heating at 0.82°C./min. from equilibrium at 23°C. The solid line represents Eq. (7) and the circled points are taken from an experimental curve obtained under the above conditions. The agreement between theory and experiment is fairly good. Extrapolation of the two "straight" portions of the

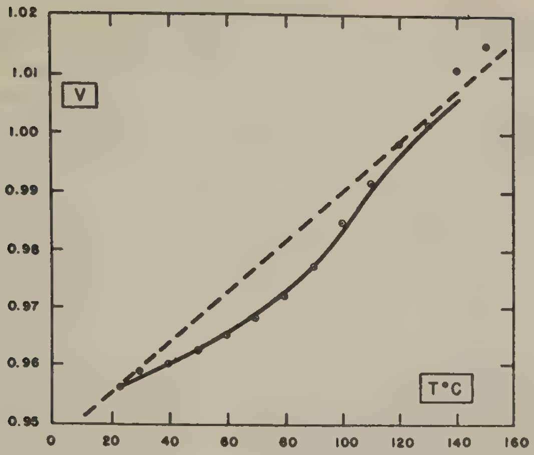

FIG. 2. Volume-temperature curve for $T = 296.2 + 0.82\,t$ and $\Delta V^\circ = 0$. The dotted line gives the equilibrium volume; the points are the results of an experiment carried out under these conditions.

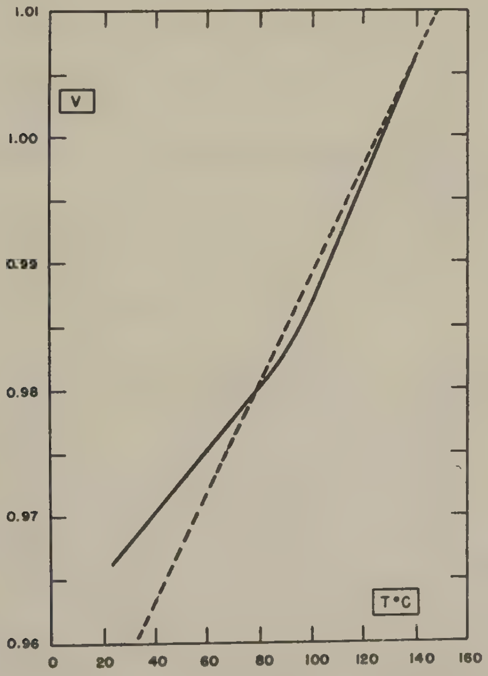

FIG. 3. Volume-temperature curve under same conditions as Fig. 2, except that $\Delta V^\circ = 0.01$ (quenched sample).

curve in the usual fashion would yield an apparent second-order transition temperature of $Tm = 82.5$°C. Fig. 3 shows the volume-temperature curve for the same conditions, except that the polymer was not initially at equilibrium but has $\Delta V^\circ = 0.01$. This might be thought of as representative of a quenched sample. In this case the apparent transition temperature has risen to 93.5°C., as determined graphically by extrapolation.

The effect of heating rate on apparent second-order transition temperature may perhaps best be approached by first formulating a more or less arbitrary definition of Tm. It is not to be expected that this will parallel exactly in all cases the values resulting from the usual handling of experimental data. It should, however, provide a self-consistent way of illustrating the behavior to be expected.

It has been customary to represent the upper and lower portions of the volume-temperature curve by straight lines, and to designate the transition temperature as that corresponding to the point of intersection of these two lines. As an approximation to this graphical procedure, we shall take a tangent through the initial point for the lower straight line, and a tangent through the inflection point for the upper straight line. This inflection point is always present in heating curves, and is particularly noticeable in Fig. 2. If we designate the temperature at which it occurs as T_2, and the corresponding value of ϕ as ϕ_2, it is defined by

$$Ei(\phi_2) + \frac{e^{\phi_2}}{1 - \phi_2} = Ei(\phi_o) + \frac{B\Delta V^\circ e^{\phi_o}}{V_o\beta_2}, \tag{8}$$

which may be solved graphically for ϕ_2. The tangent through this inflection point is given by

$$V = V_o[1 + (\beta_1 + \beta_2)T_2] + \Delta V^\circ e^{\phi_o}e^{-\phi_2} - \frac{V_o\beta_2 e^{-\phi_2}}{B}[Ei(\phi_2) - Ei(\phi_o)] + \left[V_o\beta_1 + V_o\beta_2\frac{\phi_2}{\phi_2 - 1}\right](T - T_2). \tag{9}$$

The tangent through the initial point is given by

$$V = V_o[1 + (\beta_1 + \beta_2)T_o] + \Delta V^\circ + [V_o\beta_1 - \Delta V^\circ B\phi_o](T - T_o). \tag{10}$$

Setting $T = Tm$ at the intersection of these two straight lines, we find

$$BTm = \frac{BT_o + \dfrac{BT_2 + 1}{\phi_2 - 1} + \dfrac{B\Delta V^\circ}{V_o\beta_2}(1 + B\phi_o T_o).}{\dfrac{\phi_2}{\phi_2 - 1} + \dfrac{B\Delta V^\circ\phi_o}{V_o\beta_2}} \tag{11}$$

If we start from equilibrium, so that $\Delta V^\circ = 0$, this may be reduced to

$$BTm = BT_o + \frac{1 + \ln(\phi_2/\phi_o)}{\phi_2}. \tag{12}$$

TABLE II

Dependence of Apparent Second-Order Transition Temperature Upon Rate of Heating from 20°C.

Heating rate (°C.-min.$^{-1}$)	Tm (°C.)
($\Delta V^\circ = 0$)	
0.1	54.0
0.5	74.8
1.0	84.9
($\Delta V^\circ = 0.01$)	
0.1	73.5
0.5	91.9
1.0	99.2

In Table II are listed values of Tm, as defined above, for various rates of heating, and for a sample at equilibrium and a quenched sample. It may be noted that increasing the rate of heating raises the transition temperature, as does also an increase in ΔV°. These conclusions should be generally valid, even with the somewhat arbitrary definition employed for Tm.

Eq. (7) applies equally well to cooling, of course. Fig. 4 shows a volume-temperature curve for cooling from equilibrium at 140°C. at a rate of 0.82°C./min. The low-temperature expansion coefficient is larger than in

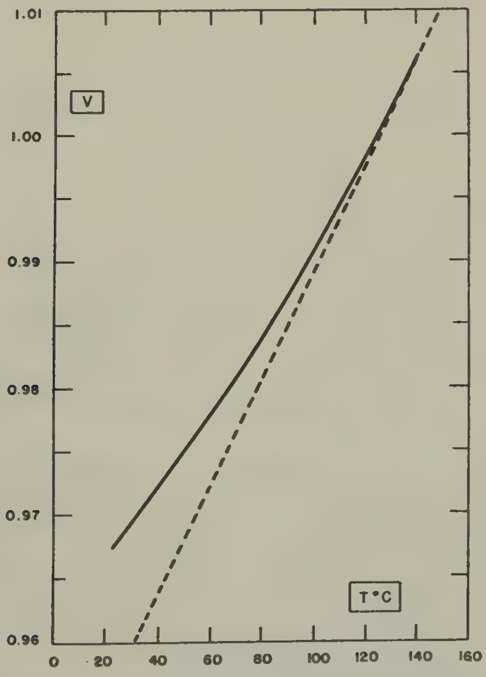

FIG. 4. Volume-temperature curve for cooling from equilibrium at 140°C. $T = 413.2\text{-}0.82\,t$, $\Delta V^\circ = 0$. The dotted line gives the equilibrium volume.

the case of heating, and the apparent second-order transition is in the neighborhood of *Tm* = 85°C. Inasmuch as there is no inflection point in such a cooling curve, the previous definition of *Tm* is no longer useful. Preliminary calculations of the point of intersection of tangents through the initial and final (room temperature) points would seem to indicate that the general observations made in the preceding paragraph still hold good. The rate of cooling does not influence the value of *Tm* quite as much as the heating rate did in Table II, but it is uncertain whether this is attributable to the change over from heating to cooling or to the different way in which *Tm* is defined.

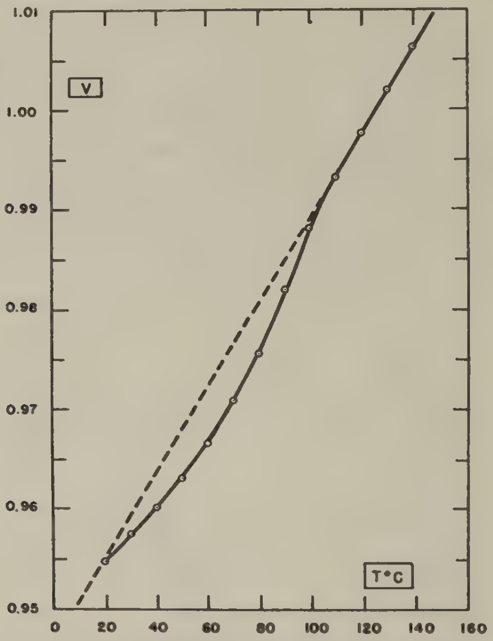

FIG. 5. Volume-temperature curve for multiple step-function heating from equilibrium at 20°C. ΔT = 10°C., Δt = 30 min. The dotted line gives the equilibrium volume.

It is apparent that, when a sample is cooled from equilibrium at some higher temperature to room temperature (say 20°C.) the specific volume will be greater than the equilibrium value. This excess, ΔV, will disappear slowly on standing, *i. e.*, the sample will shrink. The undesirability of this in the case of some molded objects raises the question of the feasibility of minimizing the shrinkage by an annealing process. The annealing cycle would consist of two parts, an initial holding period at a specified temperature to allow the system to come to equilibrium, followed by slow cooling to room temperature. The time-temperature relationships for the holding period were shown in Fig. 5 of Ref. (6) for various percentages of travel over the initial distance from equilibrium. We shall now discuss briefly the remaining question of the excess specific volume at 20°C. after cooling from equilibrium at a higher annéaling temperature.

In the case of linear cooling to a fixed end temperature (20°C.) the two determining factors are the initial temperature, T_o, and the cooling rate, b. Inspection of Eq. (7) shows that, for a considerable range of values of b, the term $Ei(\phi_o)$ becomes negligible as compared to $Ei(\phi)$ as soon as the temperature falls appreciably below T_o. Stated in another way, this means that the volume-temperature curve is determined principally by the cooling rate b, and is almost independent of T_o except at the high temperature end. Thus, the excess specific volume, ΔV, at 20°C. will depend, in first approximation, only upon the cooling rate, in the manner shown in Table III. As the rate becomes increasingly rapid, the ΔV at 20°C. approaches the value corresponding to the expansion coefficient β_2, that is,

TABLE III

Excess Specific Volume Remaining at 20°C. After Cooling from a Higher Annealing Temperature

Cooling Rate (°C.-min.$^{-1}$)	ΔV (20°C.)
0.005	.00123
0.01	.00200
0.05	.00479
0.1	.00637
0.5	.01052

$$\Delta V = \Delta V^\circ + V_o\beta_2\Delta T. \tag{13}$$

This may be shown from Eq. (7) or by straightforward reasoning. Of course, it must be realized that Table III and Eq. (13) refer only to the value of ΔV at the instant the temperature reaches 20°C. If the temperature is subsequently held constant, the value at a later time is obtained by multiplying the initial 20°C. value by e^{-kt}.

In deducing an optimum annealing schedule, it must first be decided how much room temperature shrinkage is permissible. This allowable excess specific volume determines the cooling rate. The optimum holding temperature may then be calculated by balancing the decrease in holding time with rising temperature against the increase in cooling time. These quantities define the annealing schedule, in terms of the holding temperature, holding time and cooling rate. Table IV shows two examples of such schedules, based upon the 90% travel line of Fig. 5, Ref. (6).

NONLINEAR CASES

Volume-temperature curves are sometimes obtained by transferring the sample from bath to bath, each operating at a different temperature, and

TABLE IV

Optimum Annealing Schedules for Volume Stabilization at 20°C.

Allowable shrinkage	Holding temperature	Holding time	Cooling rate	Total time
1%	95.3°C.	68 min.	0.34°C./min.	290 min.
0.5	51.1	461	0.05	1083

allowing enough time in each to permit close approach to thermal equilibrium. We shall idealize this situation by assuming that the temperature is a (discontinuous) multiple step-function of time. That is, at $t = 0$ the temperature jumps from T_o to $(T_o + \Delta T)$, and subsequently jumps up in temperature an amount ΔT at the end of each time interval Δt. The problem is to calculate the excess specific volume $\Delta V^{(n)}$ at the end of the n-th time interval. The solution may be written in the form

$$\Delta V^{(n)} = \Delta V^\circ(\rho_n) - V_o\beta_2\Delta T(\sigma_n), \tag{14}$$

where

$$\rho_n = \exp\left[- Ae^{BT_o}\Delta t \sum_{i=1}^{n} e^{iB\Delta T} \right]$$

and

$$\sigma_n = \sum_{i=1}^{n} \frac{\rho_n}{\rho_{i-1}}.$$

Fig. 5 shows the volume-temperature curve calculated for such a case, in which $T_o = 20$°C., $\Delta T = 10$°C., and $\Delta t = 30$ min. A definitely sigmoid shape is apparent, and the sample is essentially at equilibrium at all temperatures above 105°C.

For some purposes it would be desirable to have a solution at hand for a nonlinear temperature-time relationship which could be used to approximate experimental relationships. For example, one which permits a solution in closed form is the following,

$$T = T_o + a \log(1 + bt), \tag{15}$$

where a and b are constants. This gives

$$\phi = \frac{Ae^{BT_o}(1 + bt)^{aB+1}}{b(aB + 1)}$$

and, on substitution in Eq. (6),

$$\Delta V = \Delta V^\circ e^{\phi_o}e^{-\phi} - \frac{aV_o\beta_2 e^{-\phi}}{aB + 1}[Ei(\phi) - Ei(\phi_o)] \tag{16}$$

as the solution.

An application of this solution was made in the case of a sample brought to equilibrium at 120°C. The bath containing the dilatometer was allowed to come back to room temperature by natural cooling and the temperature and polymer volume were recorded as a function of time. The temperature-time relationship was approximated by Eq. (15) with $a = -66.5$ and $b = 0.02865$ min.$^{-1}$ which gave a fair fit. Fig. 6 shows the volume-temperature curve corresponding to Eq. (16) for this case, and the experimental points for comparison. The agreement is not too bad, except at the very end of the experiment.

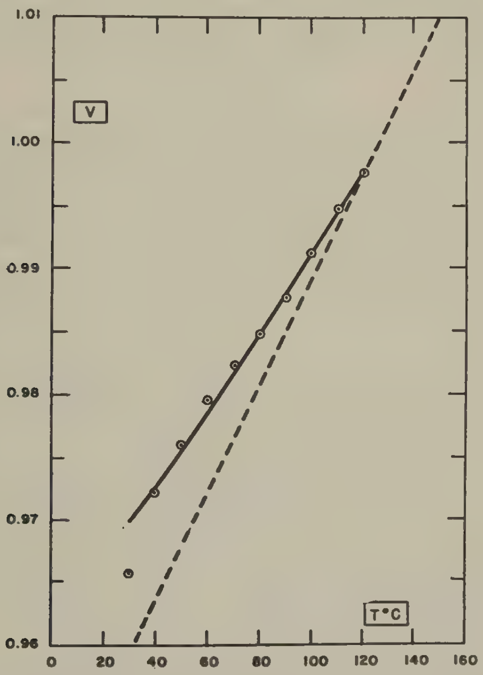

FIG. 6. Volume-temperature curve for natural cooling from equilibrium at 120°C. $T = 393.2 - 66.5 \log_{10} (1 + .02865\,t)$. The dotted line gives the equilibrium volume; the circles are experimental points.

SUMMARY

A differential equation relating the specific volume of polystyrene to time and temperature has been set up and a general solution obtained. This solution may be expressed in terms of known functions for certain temperature-time relationships of interest. Among those discussed in this paper were the cases of linear heating or cooling of both equilibrated and quenched samples, a multiple-step function, and a three-constant logarithmic function. This last case was used to approximate natural cooling, with some success. The effect of heating or cooling rate upon the apparent second-order transition temperature of both equilibrated and quenched samples was discussed. Some applications were made to the problem of annealing for volume stabilization at room temperature.

REFERENCES

1. ALFREY, T., GOLDFINGER, G., AND MARK, H., *J. Applied Phys.* **14**, 700 (1943).
2. BOYER, R. F., AND SPENCER, R. S., *ibid.* **15**, 398 (1944).
3. BOYER, R. F., AND SPENCER, R. S., *ibid.* **16**, 594 (1945).
4. BOYER, R. F., AND SPENCER, R. S., *Advances in Colloid Sci.* **2**, 1 (1946).
5. JENCKEL, E., *Z. Elektrochem.* **43**, 796 (1937).
6. SPENCER, R. S., AND BOYER, R. F., *J. Applied Phys.* **17**, 398 (1946).
7. Tables of Sine, Cosine and Exponential Integrals, New York Mathematical Tables Project, 1940.

THE VISCOUS FLOW OF MOLTEN POLYSTYRENE. II[1]

R. S. Spencer and R. E. Dillon

From the Dow Chemical Company, Midland, Michigan

Received January 24, 1949

INTRODUCTION

The rate of shear of molten polystyrene is determined primarily by 4 factors: shearing stress, temperature, polymer molecular weight, and plasticizer or solvent content. Of these, the first two were discussed in the first paper in this series (9). The present paper considers these same two factors in more detail and also presents data relating to the influence of polymer molecular weight and solvent content. Brief mention is also made of the effect of varying degrees of branching and of thermal breakdown on aging.

The presence of flow orientation during extrusion through a capillary was pointed out previously. At low shearing stresses this results in an increase in diameter of the extruded filament over that of the capillary, by recovery of the orientation. We have found that when the shearing stress exceeds a critical value the extruded filament buckles into a regular spiral. This spiral inception point has been shown to correspond to an isoelongated state with $\bar{\alpha} = 3$. This being the case, the shearing stress at this point should be proportional to the modulus of high elasticity. Confirmation of this view was found in our observations that the capillary wall shearing stress at the spiral point was inversely proportional to the molecular weight, was insensitive to temperature variations, and decreased with addition of solvent.

The present work must be considered as a direct continuation of that reported in our first paper on this subject. The experimental methods and equipment were, by and large, the same as have been described, with modifications and extensions as noted in the next section.

EXPERIMENTAL METHODS

The flow characteristics of molten polystyrene were determined by extruding the material through a capillary, as was described in our previous paper (9). The design of the apparatus was such that the lower end of the capillary was exposed to room temperature. It was found that the exposed end could be as much as 20°C. cooler than the polymer, depending upon capillary dimensions and bath temperature. Under these conditions it is evident that the average temperature of the polymer in the capillary would be slightly dependent upon the extrusion rate, a highly undesirable situation. To correct this the capillary was jacketed and a small heating coil would around the lower end. Thermocouples were placed in the capillary wall at both ends. Two or three trial and error adjustments of the voltage to the heating coil were usually sufficient to bring the temperature to within 0.5°C. of the desired value.

---

[1] Presented at the Annual Meeting of the Society of Rheology, New York, N. Y., November 5 and 6, 1948.

The shearing stress in any given capillary is limited by the capillary dimensions and the gas pressure available. Using nitrogen cylinders, as in our case, this latter factor has a top limit of about 1500 p.s.i. To permit measurements at higher shearing stresses, an adaptor for a small injection molding press was designed, as shown in Fig. 1, by G. D. Gillmore. This attachment uses the same capillaries as the gas-driven viscosimeter, but takes advantage of the much higher pressures possible with the injection molding press, up to 15,000 p.s.i. Inasmuch as the ram pressure is greater than the pressure delivered to the capillary, it is necessary to measure pressure directly at the capillary entrance. This is accomplished by connecting a Bourdon gauge to the adaptor chamber. Both the connecting tube and gauge are filled with a high viscosity silicone fluid. This arrangement does not provide positive separation between the polymer and the

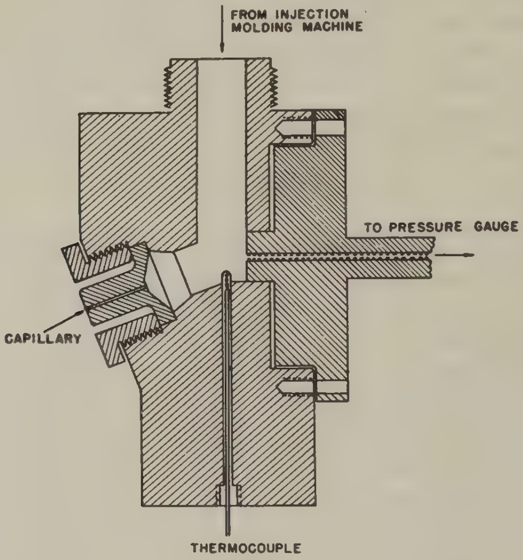

Fig. 1. Adaptor for using an injection molding press as an extrusion viscosimeter.

fluid, and the polymer will eventually plug off the connecting tube. This necessitates regular disassembling and cleaning operations for satisfactory performance. Heat is supplied to the adaptor by two cartridge heaters not shown in Fig. 1, and the polymer temperature is determined with a thermocouple near the capillary entrance.

Certain characteristics of the flow curves of polystyrenes made it seem desirable to be able to work at shearing stresses up to 2×10^6 dynes-cm.$^{-2}$ with a single capillary and a single viscosimeter. This is possible with capillary No. 7 previously described (9), but its dimensions are such that it is more properly termed an orifice. To fill this gap, another capillary, designated as Number 9, was made, having a radius of 0.0519 cm. and a length of 1.242 cm. This provided coverage of the desired range with the gas-driven viscosimeter. For convenience, the dimensions of all capillaries used in this paper follow:

Capillary No.	Radius *cm*	Length *cm.*
1	0.0541	2.062
4	0.1616	5.086
8	0.0529	3.211
9	0.0519	1.242

In attempting to extend the viscosity-temperature relationship to temperatures lower than those feasible with the extrusion viscosimeter, the indentation technique of Pocklington (7) was used. This consisted of placing a weighted steel ball on a disk of hot polystyrene and measuring the radius ρ of the indented circle after a time t. The viscosity was computed from Pocklington's formula

$$\eta = \frac{3RtF}{16\rho^3}, \tag{1}$$

where R is the radius of the ball and F is the force pressing it into the polymer. Since the shearing stresses involved are relatively low, we may consider η as the Newtonian viscosity. At lower temperatures elastic effects become quite troublesome, and it was necessary to allow a recovery period after unloading the sample and before cooling it. In this case the depth of the indentation was measured, rather than its radius. Adhesion of polymer to metal limits the usefulness of the method at higher temperatures.

Discussion

1. *Flow*

The method of obtaining the Newtonian viscosity by extrapolating the flow data to zero shearing stress was described in the first paper of this series (9). It consists of plotting the logarithm of the apparent fluidity as ordinate and the shearing stress at the capillary wall as abscissa. Experience showed that a straight line resulted, in the lower shearing stress region, facilitating the extrapolation. Previous results also indicated, however, that the line became noticeably curved as the shearing stress increased.

It has been found desirable, for a number of reasons, to have at hand a suitable mathematical expression, empirical or otherwise, for the relationship between apparent fluidity and shearing stress. Two suggestions were made in our previous paper, the first a division of the curve into two exponential functions, and the second a two-term power law expression. Neither of these has proven completely satisfactory in representing experimental data. In addition, both have the disadvantage of requiring more than one material constant beyond the Newtonian viscosity.

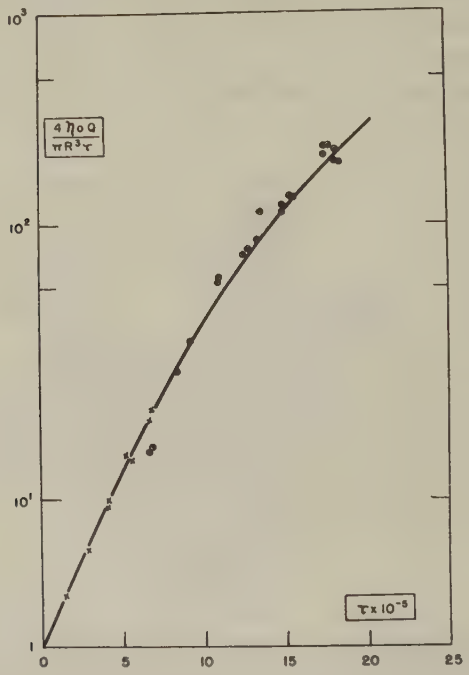

FIG. 2. Apparent fluidity at various capillary wall shearing stresses. Circles are points obtained with the molding press, crosses with the gas-driven viscosimeter. The solid line represents Eq. (2) with $k = 0.3975 \times 10^{-5}$ cm.^{2}-dyne^{-1}.

Let us consider for a moment the mathematical characteristics of the observed function, in the case of capillary flow. We find that, in the region of low shearing stress, the apparent fluidity is roughly exponential in the shearing stress, as mentioned previously. As the shearing stress at the wall increases, the fluidity appears to become proportional to the shearing stress raised to a power between three and four. A function possessing these characteristics is the following polynomial:

$$\phi_A = \frac{1}{\eta_o}\left[1 + k\tau_w + \frac{(k\tau_w)^2}{2!} + \frac{(k\tau_w)^3}{3!} + \frac{(k\tau_w)^4}{4!}\right], \qquad (2)$$

where ϕ_A is the apparent fluidity, η_o is the Newtonian viscosity, k is a material constant, and τ_w is the shearing stress at the capillary wall. The faithfulness with which this function represents experimental data is illustrated in Figs. 2 and 3. Fig. 2 represents data on the flow of a polystyrene sample in two viscosimeters, the Monsanto rheometer used for the bulk of our measurements and the injection molding press adapter described in the preceding section. The solid curve represents the function of Eq. (2) with $k = 0.3975 \times 10^{-5}$ cm.²-dyne⁻¹. In Fig. 3 the same shearing stress region has been covered for a polystyrene of 360,000 molecular weight, using only the Monsanto rheometer with capillary No. 9. The solid line corresponds to a value of $k = 0.353 \times 10^{-5}$ cm.²-dyne⁻¹. These

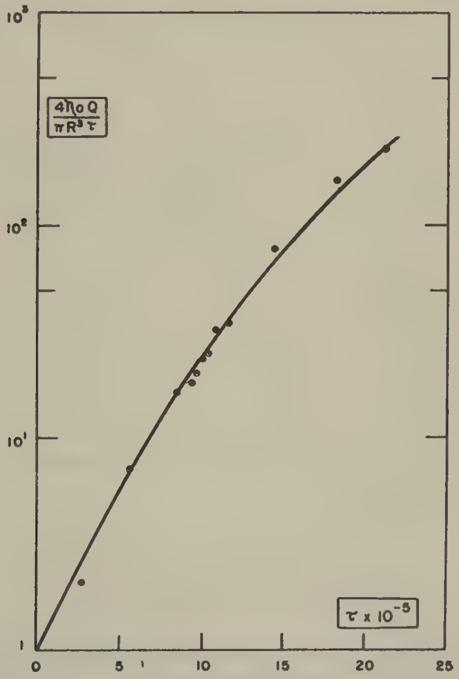

FIG. 3. Apparent fluidity at various capillary wall shearing stresses. All points were obtained using capillary No. 9 with gas pressure. The solid line represents Eq. (2) with $k = 0.353 \times 10^{-5}$ cm.²-dyne⁻¹.

data illustrate our general observation that Eq. (2) gives a good representation of experimental flow curves.

The temperature dependence of the Newtonian viscosity was discussed in our first paper. The uncertainty in temperature in these earlier measurements has been mentioned already, and was thought to be sufficient reason for repeating the experiment with the heated capillary. At the same time the temperature range covered was extended, both with the extrusion viscosimeter and the indentation method. The revised values are listed in Table I and are shown in Fig. 4. The essential features of the temperature-dependence are the same as previously described. Of particular interest is the good agreement between the two methods of measurement, and with the results of Dienes and Dexter (1) on the same material, using a parallel plate plastometer.

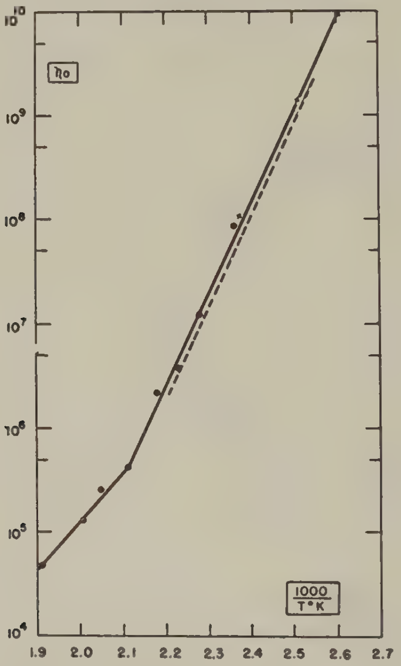

FIG. 4. Temperature-dependence of Newtonian viscosity. Circles are with the extrusion viscosimeter, crosses are by the indentation method, and the dotted line represents data from the parallel-plate plastometer (1).

The influence of molecular weight on the melt viscosity of polystyrene has been reported by Fox and Flory (4), who found that the relationship suggested earlier by Flory (3) was not obeyed. Similar data, extending to somewhat higher molecular weights, are listed in Table II. In Fig. 5 we see that the relationship is closely approximated by a power law, as was

TABLE I

Newtonian Viscosities of Polystyrene
(Mol. Wt. = 360.000)

Temperature	η_o (poises)	Method
250°C.	4.72×10^4	Capillary
225	1.32×10^5	Capillary
215	2.50×10^5	Capillary
200	4.17×10^5	Capillary
185	2.17×10^6	Capillary
175	3.76×10^6	Capillary
165	1.17×10^7	Capillary
150	8.45×10^7	Capillary
148	1.07×10^8	Indentation
125	1.40×10^9	Indentation
110	9.40×10^9	Indentation

TABLE II

Newtonian Viscosities of Polystyrene at 200 C.

Molecular weight by light scattering	η_o (poises)
(Whole polymers)	
86,000	3.50×10^3
162,000	4.00×10^4
196,000	6.25×10^4
360,000	4.81×10^5
508,000	1.00×10^6
560,000	3.33×10^6
(Fractions)	
490,000	1.89×10^6
510,000	1.64×10^6
710,000	6.58×10^6

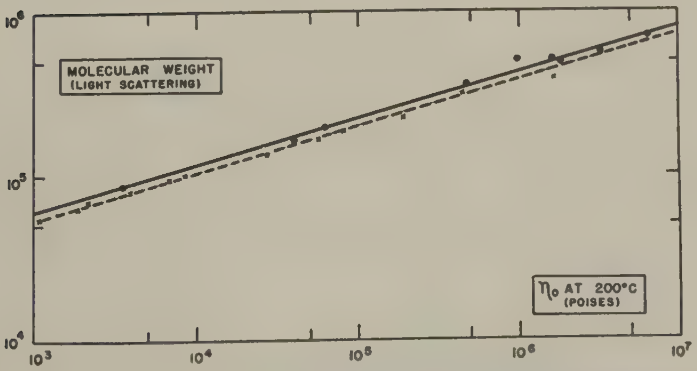

FIG. 5. Effect of polymer molecular weight on the Newtonian viscosity at 200°C. The crosses are data of Fox and Flory (4).

reported by Fox and Flory (4). The data of Fox and Flory on polystyrene fractions within this molecular weight range are also shown in Fig. 5 for comparison. Inasmuch as their values were obtained at a temperature of 217°C., a factor was computed from Fig. 4 and applied to correct their figures to 200 °C. The consistent discrepancy between our viscosities and theirs may be due to the different methods employed in the determination of molecular weights. Our values were based on light scattering measurements, and those of Fox and Flory were computed from intrinsic viscosities. In spite of this, the agreement is not too bad.

We shall now consider briefly the factors influencing the parameter k. The data reported in our first paper would lead one to suspect that k is not very dependent upon temperature, molecular weight, or capillary dimensions. Confirmation for this expectation is found in Table III. No systematic variation of k with the factors tabulated is apparent. These data give $k = 0.356 \times 10^{-5}$ cm.^{2}-dyne^{-1} as an average value for "unplasticized" polystyrene. The addition of a solvent or plasticizer does, however, effect a change in the value of k, as indicated in Fig. 6 for a variety of polymers and solvents. Here we see that k increases with solvent concentration up to 4 or 5% by weight, after which it remains relatively constant to at least 20% solvent.

TABLE III

Constancy of the Parameter k for "Unplasticized" Polystyrenes

Mol. wt.	Temperature	Capillary No.	k(cm.^{2}-dyne^{-1})
162,000	175°C	8	0.365×10^{-5}
196,000	200	9	0.379
242,000	225	8	0.352
280,000	225	8	0.364
360,000	185	8	0.346, 0.366
360,000	200	9	0.353
360,000	225	8	0.375
360,000	250	8	0.335
392,000	250	1	0.320
440,000	250	1	0.330
1,100,000[a]	250	1	0.386

[a] This sample decreased considerably in molecular weight during the measurements. See Table V.

The effect of solvent addition on such other properties as Newtonian viscosity and activation energy of viscous flow is, of course, well known. In the case of polystyrene, work has been reported by Ferry (2), Jenckel and Überreiter (5), Scheele, Alfeis and Friedrich (8), and Spencer and Williams (10). Some further results with the system polystyrene-isopropyl benzene are shown in Table IV. Measurements were carried out at temperatures other than 180°C., but are not listed because of the limitation placed upon concentration range by our equipment. As a matter of interest, the viscosity value of the original polymer computed by extrapolation to 180°C. of the higher temperature region of Fig. 4 is included in the Table. It seems to fit in better with the other data than does the actual value observed at 180°C. In Fig. 7 the activation energies of Table IV, and those reported by Spencer and Williams (10) for the more dilute region, are plotted against concentration of isopropyl benzene, from 0 to 100%. The slight shift in concentrations from those listed in Table IV is occasioned by the fact that our original polymer contained 0.8% of some volatile material.

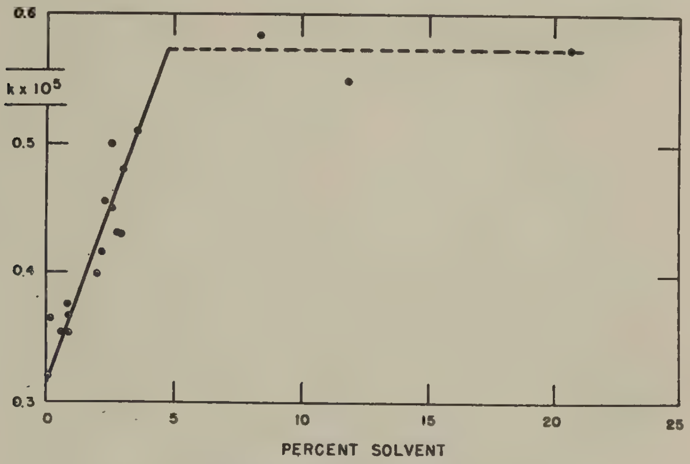

FIG. 6. Influence of solvent concentration on k.

An attempt was made to study the effect of branching on the flow properties of polystyrene by copolymerizing styrene with small amounts

TABLE IV

Effect of Adding Isopropyl Benzene to Polystyrene of 360,000 Mol Wt.

Solvent added	η_0 (180°C.)	k	Activation energy
0 Wt.-%	$2.9\ (1.15^a) \times 10^6$	0.346×10^{-5}	22.2 kcal./mole
5	4.5×10^5	0.455	20.8
10	1.72×10^5	0.586	19.7
15	5.3×10^4	0.562	18.8
20	—	—	16.7

[a] This is the viscosity obtained by extrapolation from the higher temperature region of Figure 4.

of divinylbenzene. The results obtained were so erratic that only very general conclusions can be reached. The addition of divinylbenzene gave polymers of increased molecular weight, and thus of increased Newtonian viscosity. The value of k did not seem to change appreciably, however. These branched polymers appeared to have some kind of loose structure, extending throughout the material, which could be broken down either by prolonged heating or by vigorous shearing. The question of reversibility was not investigated. In Table V are listed typical molecular weight data on these polymers. It is apparent that, as the concentration of divinylbenzene increases, the percentage of breakdown on extrusion through the

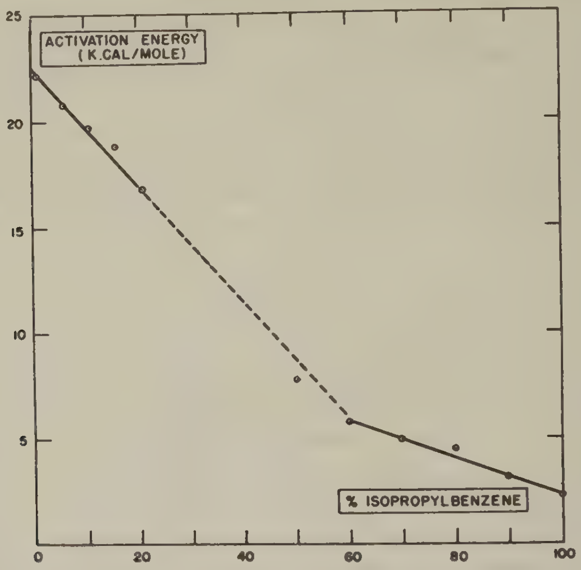

FIG. 7. Activation energy of viscous flow of the system polystyrene-isopropylbenzene.

TABLE V

Polystyrene-Divinylbenzene Copolymers

Divinylbenzene (p.p.m.)	Remarks	Molecular weight
0	As polymerized	366,000
0	Extruded	332,000
10	As polymerized	400,000
25	As polymerized	450,000
25	Extruded	350,000
50	As polymerized	560,000
100	As polymerized	1,100,000
100	Molded	822,000
100	Heated in viscosimeter	639,000
100	Extruded	527,000

viscosimeter also increases. This might be due in part to breakdown of the loose structure just alluded to.

Some breakdown must be expected, of course, due to depolymerization. Our attempts to follow this through viscosity measurements have been unsuccessful except at a temperature of 250°C. These data are shown in Fig. 8 for the polystyrene of 360,000 molecular weight. It will be noted that the viscosities observed during the earlier part of the experiment are somewhat higher than the short-time value reported in Table I. This is fairly typical of all of our results; in fact, at 225°C. we observed a maximum in viscosity. So far, no satisfactory explanation of this effect has presented itself. Only at 250°C. was the continual decrease in viscosity with time observed. At 225°C. and lower, the viscosity appeared to become constant after the initial maximum, within the duration of our experiment.

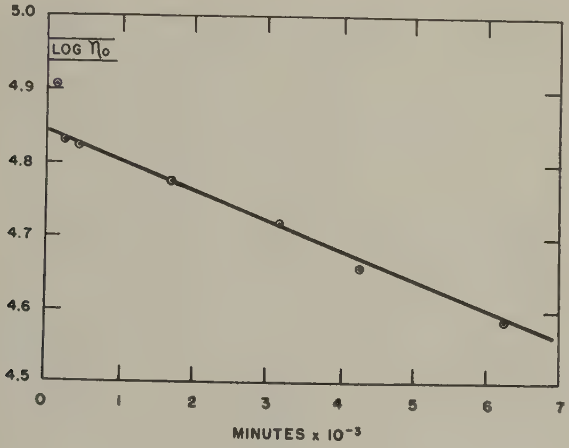

FIG. 8. Aging of polystyrene at 250°C.

2. Flow Orientation

As the shearing stress increases, the appearance of the extruded filament changes, due to flow orientation. The "ballooning" effect, or increase in filament diameter by orientation recovery, was discussed in our first paper. At higher shearing stresses other phenomena become apparent, such as the "turbulence" mentioned by Nason (6).

These effects are illustrated in Fig. 9, and seem to define 3 regions of shearing stress. At lower shearing stresses the filament surface is smooth and the diameter increases with shearing stress in the manner already discussed (9). In an intermediate region, more or less regular spirals are produced, with some roughening of the surface. Finally, at higher shearing stresses the surface becomes relatively smooth again, and the filament takes on the appearance of a series of short segments joined end to end in a somewhat haphazard fashion. The remainder of the present paper will be concerned with the intermediate region and the formation of spirals.

The mechanism of spiral formation is an interesting question in itself, our picture of this process being as follows: The orientation in a filament is a maximum at the capillary wall and drops to zero at the center, along with the shearing stress. As the shearing stress is raised the surface eventually attains the maximum elongation possible for polystyrene, and further raising of the shearing stress only forms a thicker "skin" of polymer at maximum elongation. In this region we have a skin of constant maximum elongation and a core of constant average elongation, all of the

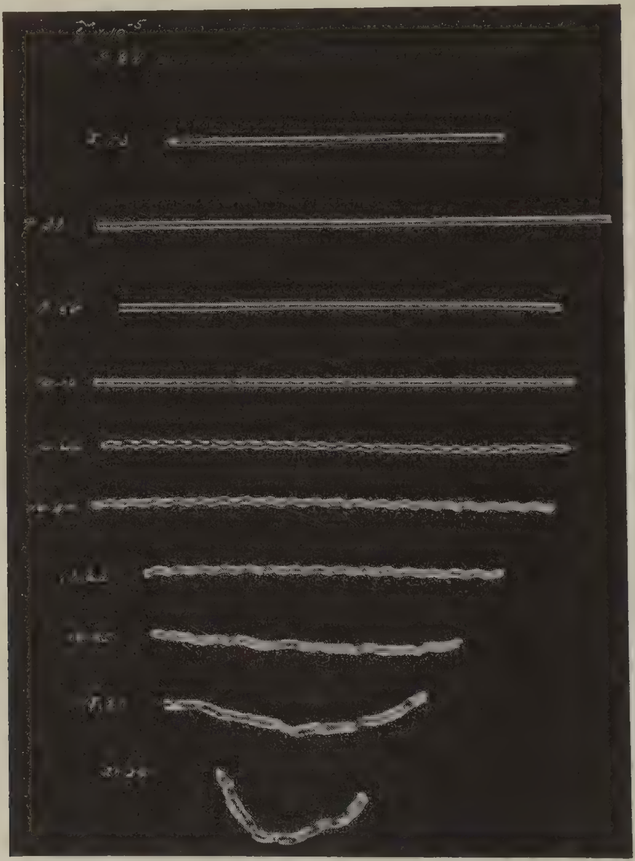

FIG. 9. Effect of shearing stress on surface characteristics of 294,000 mol. wt. polystyrene at 200°C. From top to bottom the corresponding wall shearing stresses are 5.64, 8.53, 9.39, 9.68, 10.12, 10.40, 10.84, 11.63, 14.45, 18.21, and 21.24 × 10^5 dyne-cm.$^{-2}$.

core being oriented less than the skin. The only things that change with shearing stress are the thicknesses of the core and skin. When the filament emerges from the capillary, it cannot cool fast enough to prevent recovery of the orientation, under our experimental conditions. The outside skin would like to contract axially more than the less oriented core and thus compresses it. The system is now unstable and the core buckles into a spiral. This may be domonstrated crudely by analogy, by stretching a thin walled rubber tube over a soft solder core and clamping it in the stretched condition. When the force is removed the system will form spirals, segments, *etc.*, depending on the thickness of the rubber tubing and the amount of initial stretch. The similarity between the configurations exhibited by this model and those found in extruded filaments is rather striking. The explanation outlined above may be satisfactory qualitatively; let us now consider more concrete evidence.

We find experimentally that the point at which spiraling commences is very sharply defined. In one case, for example, an increase of two p.s.i. in total pressure differential was sufficient to produce detectable spirals where there previously were none. This sharp definition seems quite general, but is particularly noticeable with polymers of superior uniformity. By measuring diameters of filaments extruded below the spiral point and extrapolating, it is possible to calculate the average relative length, $\bar{\alpha}$, characteristic of the inception of spiraling. Such figures are shown in Table VI, where we see that the spiral point is defined by $\bar{\alpha} = 3$ for polystyrene, independent of molecular weight, temperature, and capillary dimensions. A single sample containing 15% isopropylbenzene has been run and shows $\bar{\alpha} = 3.28$ at the spiral point, which is probably not significantly different from 3 when the difficulties involved are considered. Thus, we seem to have here a fairly general criterion for the inception of spiraling in extruded polystyrene. From previous observations we would estimate that $\bar{\alpha} = 3$ corresponds to a relative length of $\alpha = 5$, approxi-

TABLE VI

Average Relative Length (Due to Flow Orientation) at the Inception of Spiraling

Mol. wt.	Temperature	Capillary No.	$\bar{\alpha}$ (spiral pt.)
294,000	175°C.	4	2.86
294,000	200	4	3.06
294,000	200	9	2.99
392,000	250	1	3.19
440,000	250	1	3.17
508,000	200	9	2.89
530,000	250	1	2.82
600,000	250	1	2.97

mately, at the surface of the filament. This is in the right neighborhood to be considered as a likely value for the maximum α possible with polystyrene.

Considering the spiral point as an "isoelongated state," it follows that the shearing stress at this point will be proportional to the modulus of rubberlike elasticity. Let us look at the following data with this idea in mind. The influence of molecular weight is shown in Table VII. The modulus, and therefore τ_w at the spiral point, should be inversely proportional to the molecular weight, assuming a constant number of effective secondary "cross-bonds" per molecule. In the last column of table VII is listed the product of τ_w and molecular weight, which is seen to be relatively constant, in agreement with our expectation. The effect of temperature is negligible, as may be seen by referring to Table VIII. The limits listed in this table are not probable errors but represent the uncertainty in interpolation on the pressure gauge. One sample, containing 15% by weight of isopropylbenzene, was run at 150°C. to check the influence of solvent content. As might be expected, the modulus had dropped, giving a shearing stress at the spiral point of 7.04 (± .03) × 10^5 dyne-cm.$^{-2}$, as compared with the values in Table VIII.

TABLE VII

Dependence of Capillary Wall Shearing Stress at Spiral Inception Upon Molecular Weight

Molecular weight	τ_w (dyne-cm.$^{-2}$)	$M \cdot \tau_w$
196,000	14.09×10^5	27.6×10^{10}
294,000	9.90	29.1
378,000	7.24	27.4
508.000	5.85	29.7
527,000	5.27	27.8

TABLE VIII

Temperature-Independence of Capillary Wall Shearing Stress at Spiral Inception

Temperature	τ_w (Spiral)
175°C.	9.93 (±.03)×10^5 dyne-cm.$^{-2}$
200	9.90 (±.07)×10^5
225	10.00 (±.03)×10^5

These data, with other more qualitative observations, suggest that the explanation of spiraling previouly set forth is a fairly plausible one.

SUMMARY

The capillary flow of polystyrene has been studied in some detail. An empirical equation relating apparent fluidity to capillary wall shearing stress has been suggested which fits experimental flow curves well. This equation has the advantage of containing only two material constants:

the Newtonian viscosity, η_o, and a constant, k, characterizing the degree of departure from Newtonian behavior. The influence of temperature, polymer molecular weight, and solvent content on η_o were discussed and suitable data presented. The dependence of the activation energy of viscous flow upon solvent content was illustrated by data on the system polystyrene-isopropylbenzene over the entire concentration range. It was shown that the constant k is relatively independent of temperature and polymer molecular weight. However, as the solvent content increases, k increases, finally assuming a more or less constant value over the range 5–20% solvent.

A critical capillary wall shearing stress was observed, above which the extruded filament buckles into a spiral. This spiral inception point was shown to be an isoelongated state defined by $\bar{\alpha} = 3$. The wall shearing stress at the spiral point was found to vary inversely with the molecular weight. It was relatively independent of temperature and decreased as the solvent content increased. These observations were in accord with the tentative explanation put forth for the phenomenon of spiraling.

REFERENCES

1. DIENES, G. J., AND DEXTER, F. D., *J. Colloid Sci.* **3**, 181 (1948).
2. FERRY, J. D., *J. Am. Chem. Soc.* **64**, 1330 (1942).
3. FLORY, P. J., *ibid.* **62**, 1057 (1940).
4. FOX, T. G., AND FLORY, P. J., *ibid.* **70**, 2384 (1948).
5. JENCKEL, E., AND ÜBERREITER, K., *Z. physik. Chem.* **182A**, 361 (1938).
6. NASON, H. K., *J. Applied Phys.* **16**, 338 (1945).
7. POCKLINGTON, H. C., *Proc. Cambridge Phil. Soc.* **36**, 507 (1940).
8. SCHEELE, W., ALFEIS, M., AND FRIEDRICH, I., *Kolloid-Z.* **108**, 44 (1944).
9. SPENCER, R. S., AND DILLON, R. E., *J. Colloid Sci.* **3**, 163 (1948).
10. SPENCER, R. S., AND WILLIAMS, J. L., *ibid.* **2**, 117 (1947).

FLOW PROPERTIES OF PHENOLIC RESINS[1]

G. J. Dienes

From the Development Laboratories, Bakelite Corporation, Bound Brook, New Jersey

Received January 6, 1949

INTRODUCTION

Parallel plate plastometer measurements have been shown to yield significant rheological data for thermoplastic resins and compounds (1,2,3). The absolute viscosity as well as the viscoelastic properties can be evaluated by this method (2). Parallel plate plastometer measurements should be generally applicable to the measurement of high viscosities. The present paper is concerned with the extension of this method of viscosity determination to thermosetting, in particular to the novolac type phenol-formaldehyde, resins.

PHENOLIC RESINS AS NEWTONIAN LIQUIDS OF HIGH VISCOSITY

Early work by Messrs. Meharg, Welch and Miller (4) with the parallel plate plastometer showed that this instrument should be well adapted to viscosity measurements on novolac type phenol-formaldehyde resins. The instrument, its theory and general techniques of operation have been described previously (1,2). Briefly, a cylindrical test specimen is deformed under a constant load between two parallel plates and the plate separation, h, is measured as a function of time. From these data, a $1/h^4$ *vs.* time curve, which is equivalent to a deformation-time curve, is constructed. The slope of the linear portion of this curve is inversely proportional to the viscosity. The viscosity is calculated by means of the equation (1):

$$\eta = \frac{8.21 \times 10^6 W}{mV^2}, \tag{1}$$

where

η = viscosity in poises
W = load in kg.
V = volume of sample in cm.^{3}
m = slope of the $1/h^4$ *vs.* time curve, cm.$^{-4}$ sec^{-1}.

The volume in Eq. (1) should be the volume of the sample at the test temperature. Since volume expansion data for phenolic resins are not generally available, the volume at room temperature was used in all calculations. This introduces a small error in the absolute viscosity figures.

---

[1] Presented at the Annual Meeting of the Society of Rheology, New York, N. Y., November 5 and 6, 1948.

Sample preparation was found to be quite unimportant. Molded pellets are perhaps the best, but cylinders preformed from powdered resin were found to be very satisfactory. The latter is a very convenient method of sample preparation as it does not require melting the resin prior to testing.

The $1/h^4$ *vs.* time, or deformation-time, curves for novolac type phenolic resins are quite different from those for thermoplastic resins and compounds. These latter are characterized by deformation-time curves initially concave to the time exis. The initial curved portion, which is a measure of recoverable elastic and delayed elastic deformations, is followed by a straight line portion whose slope is a measure of the viscosity. A typical example of such a curve (preheated sample) is shown in Fig. 1 for a vinyl chloride-acetate resin compound (2). A calculable amount of the total deformation is elastically recoverable. The $1/h^4$ *vs.* time curves for novolac type phenol-formaldehyde resins are initially convex to the time axis and become linear, usually in less than 300 sec. A typical curve is shown in Fig. 2. In this case, the initial nonlinear portion is not the result of viscoelastic effects, but is caused by (a) lag in establishing temperature

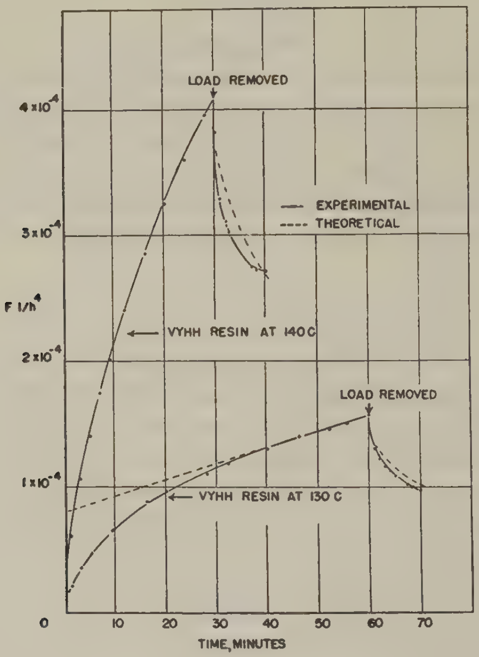

FIG. 1. Typical $1/h^4$ *vs.* time curve for a vinyl chloride-acetate resin compound at 130°C. and 140°C. (2).

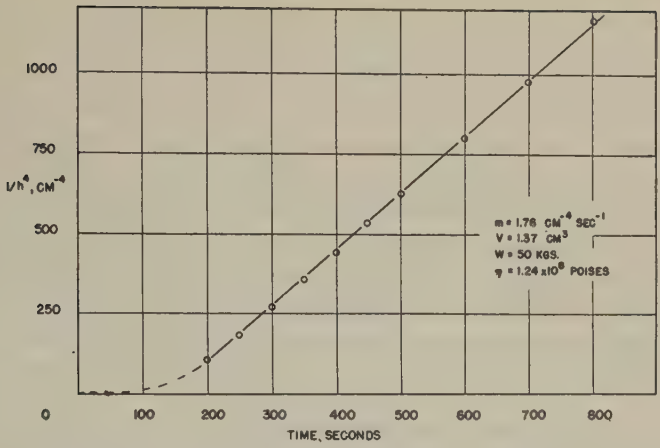

FIG. 2. Typical $1/h^4$ *vs.* time curve for a novolac type phenol-formaldehyde resin at 50°C. (Resin 1).

equilibrium, and (b) inapplicability, at the start of the experiment, of certain assumptions made concerning the boundary conditions in deriving Eq. (1). The deformation is completely irrecoverable.

By preheating the test specimen, or by raising the test temperature, to a point where the viscosity is below 10^6 poises, the $1/h^4$ *vs.* time curves become linear practically from the start. Such a curve is shown in Fig. 3. Evidently, whenever the specimen is quickly deformed to a thin disk, temperature equilibrium, as well as the proper boundary conditions, are rapidly established. Preheating of phenolic resins is not recommended,

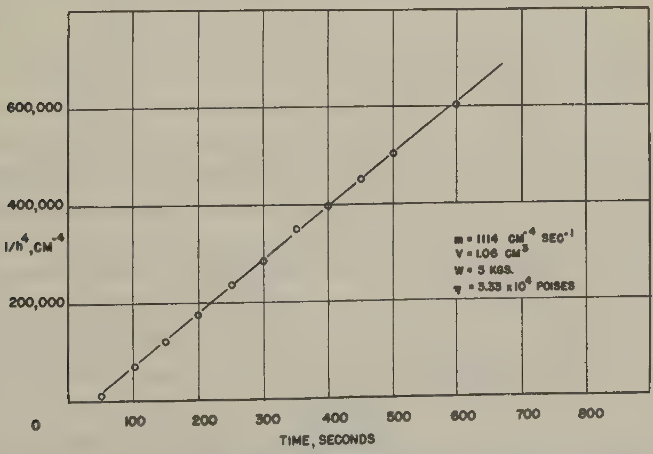

FIG. 3. Typical $1/h^4$ *vs.* time curve for a novolac type phenol-formaldehyde resin at 85°C. (Resin 1).

nor is it necessary since no rheological significance is attached to the initial portion of the curve, as moisture or uncombined phenol may be lost, thereby altering the flow properties.

The linearity of the $1/h^4$ *vs.* time curves (except for initial temperature effects) and the absence of viscoelastic effects indicates that novolac resins are simple Newtonian liquids of high viscosity. Indeed, Eq. (1), derived on the basis of Newtonian behavior, is accurately obeyed. No dependence of the viscosity on specimen volume or applied load has been observed. Thus, simple Newtonian behavior is established at the low rates of shear available in the parallel plate plastometer.

To investigate the behavior of these resins at high rates of shear, volume rate of discharge-pressure curves were obtained using a simple extrusion plastometer. At different driving pressures, the resin was allowed to flow through dies of various diameters and the volume rate of discharge was measured. Volume rate of discharge-pressure curves were found to be linear and the viscosities claculated by Poiseuille's formula were found to be independent of the diameter of the extrusion dies. Typical data are shown in Fig. 4 with the die dimensions and the calculated viscosities indicated on the graph. Furthermore, viscosities measured by this method agreed very well with parallel plate viscosity measurements as shown in Table I. It is felt that the above experiments prove quite conclusively the simple Newtonina nature of novolac type phenol-formaldehyde resins.

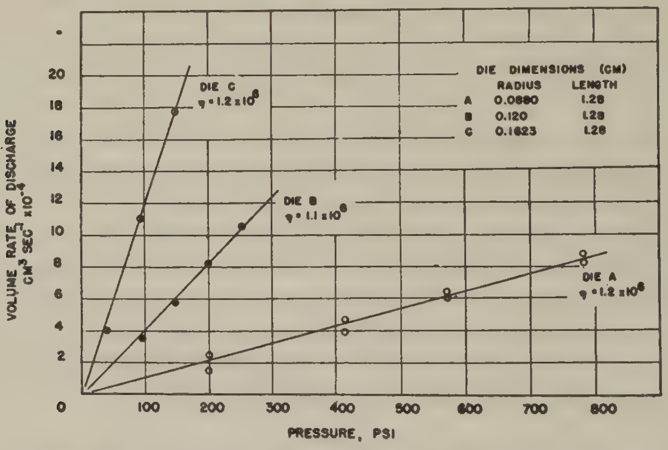

FIG. 4. Volume rate of discharge *vs.* pressure curves for a novolac type phenol-formaldehyde resin. Die dimensions as indicated. Viscosities calculated by Poiseuille's formula (Resin 2).

It is well known that the moisture content of a phenolic resin influences strongly the flow properties. This point was investigated in a preliminary

TABLE I

Viscosity of a Novolac Type Phenol-Formaldehyde Resin

Temperature	Viscosity, poises			
	Parallel plate plastometer	Extrusion plastometer		
		Die A	Die B	Die C
°C				
70	1.3×10^6	1.2×10^6	1.1×10^6	1.2×10^6
80	1.3×10^5	1.3×10^5	—	—

manner. Powdered samples of a resin were allowed to dry over $CaCl_2$ as well as to pick up moisture while conditioned at 100% humidity. In this way the moisture content was made to vary from about 0.2% to 5.0%. Viscosities were measured at convenient intervals. The results are shown in Fig. 5. The viscosity is seen to fall approximately exponentially with increasing moisture content. It is recommended, therefore, that measurements on different resins be carried out at comparable moisture contents.

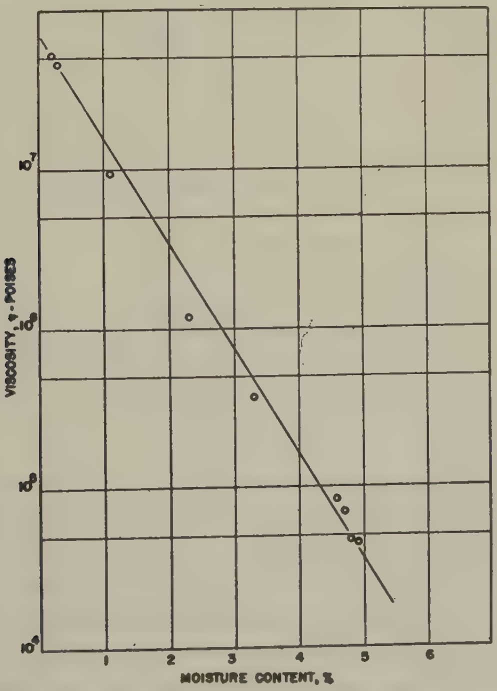

Fig. 5. Log viscosity *vs.* moisture content curve for a novolac type phenol-formaldehyde resin (Resin 1). Viscosities measured at 60°C.

Viscosity-Temperature Characteristics

The viscosity of phenolic resins was found to be highly temperature sensitive. Over the range covered by the plastometer, the viscosity-temperature characteristics follow the well known exponential relation

$$\eta = Ae^{E/RT}, \tag{2}$$

as illustrated by typical examples in Figs. 6 and 7. The values of E, the so called activation energy for viscous flow, are in the range of 50–70 Kcal./mole for novolac type phenol-formaldehyde resins. This temperature sensitivity is high in comparison with most thermoplastic materials.

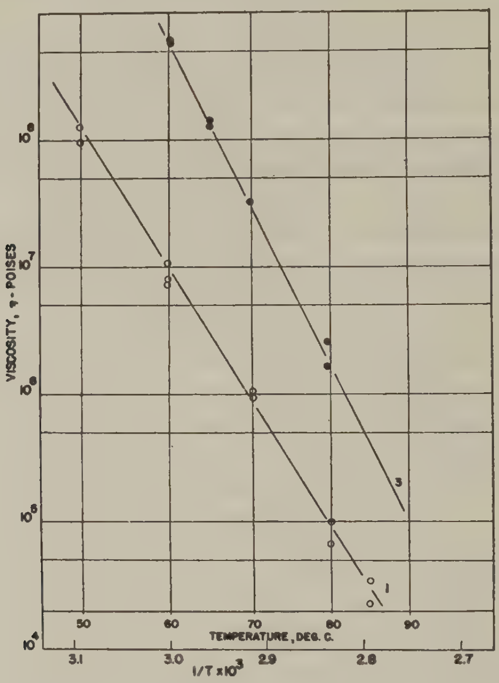

Fig. 6. Typical log viscosity *vs.* $1/T$ curves for novolac type phenol-formaldehyde resins (Resins 1 and 3).

Measurements on a set of carefully dried resins indicated that a close relation exists, for these Newtonina liquids of high viscosity, between the softening point, as measured by the ball and ring test, and the visocity-temperature characteristics. The viscosity-temperature data are shown in Fig. 7. Table II lists the results of the ring and ball tests as well as the viscosities at the ring and ball temperature as read off Fig. 7. It is shown

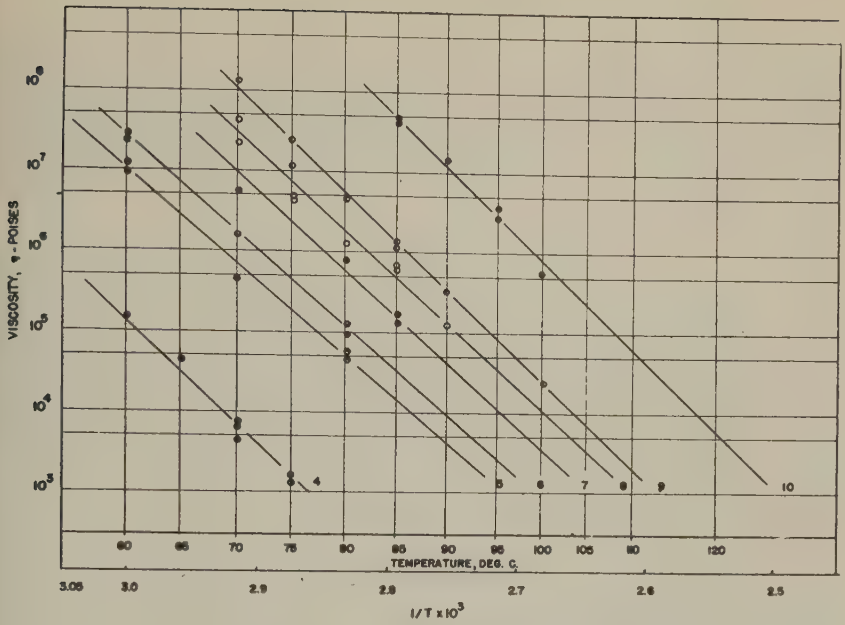

FIG. 7. Log viscosity *vs.* $1/T$ curves for a series of carefully dried phenolic resins (Resins 4–10).

quite clearly that, for these resins, the ball and ring softening point corresponds to a fixed viscosity (about 8600 poises) and represents, therefore, a single point on the viscosity-temperature curve.

TABLE II

Resin no.	Ring and ball softening point °C	Viscosity, poises, at ring and ball softening temperature (from η *vs.* $1/T$ curves of Fig. 7)
4	70	7,000
5	87.2	8,000
6	91.7	7,000
7	95	10,000
8	99.4	10,000
9	104	8,000
10	117	10,000
		Average 8,600

The relation proposed between ring and ball softening point and viscosity properties may be limited to materials of about the same temperature sensitivity. Similar results have been noted by Eaton (5) on asphalts of known viscosity.

ACKNOWLEDGMENTS

The writer is indebted to Mr. F. D. Dexter for carrying out the high rate of shear experiments. Grateful acknowledgment is also made to associates at the Bakelite Development Laboratories for many helpful discussions. It is also a pleasure to acknowledge the helpful assistance drived from the earlier unpublished work on the parallel plate plastometer by Messrs. V. E. Meharg, L. E. Welch and W. A. Miller of the Bakelite Research Laboratories.

SUMMARY

The parallel plate plastometer method of determining high viscosities has been extended to novolac type phenol-formaldehyde resins. The deformation-time behavior of these materials is contrasted with that of thermoplastic vicoelastic substances. The phenolic resins are shown to be simple Newtonian liquids of high viscosity even at high rates of shear. No complicating elastic effects have been observed. The viscosities of these resins are highly temperature sensitive with an activation energy of viscous flow in the 50–70 Kcal./mole range.

REFERENCES

1. DIENES, G. J., AND KLEMM, H. F., *J. Applied Phys.* **17**, 458 (1946).
2. DIENES, G. J., *J. Colloid Sci.* **2**, 131 (1947).
3. DIENES, G. J., AND DEXTER, F. D., American Chemical Society Meeting, New York, September, 1947.
4. MEHARG, V. E., WELCH, L. E., AND MILLER, W. A., unpublished data.
5. EATON, F. C., *J. Rheol.* **2**, 392 (1931).

THE MEASUREMENT OF STARCH PASTE VISCOSITY [1]

Welker G. Bechtel [2]

Penick and Ford, Ltd., Cedar Rapids, Iowa

and

Earl K. Fischer

Institute of Textile Technology, Charlottesville, Virginia

Received February 3, 1949

INTRODUCTION

Methods for measurement of the flow properties of starch pastes are numerous. Testing instruments range from extremely simple funnel-type "viscometers" to specially constructed devices designed to form the starch paste and measure the flow properties simultaneously. There is considerable need for a sound method of testing and specifying the physical properties of starches by both the starch-producing and -consuming industries. The problems associated with this measurement are not only those of instrumentation, however, for the process by which starch is brought from a dry powder to a usable paste involves a complicated series of colloidal changes.

This article is concerned with a study of the controlled pasting of starch and an examination of the flow properties of the starch pastes by means of several instruments. The objectives of the experiments were (a) determination of differences in the flow properties of pastes made with corn starches from different manufacturers, (b) correlation of the data obtained, using different instruments, with the fluidity ratings of the manufacturers, and (c) analysis of the rheological properties of the starch pastes.

For these purposes, commercial starches of the types supplied to industry were obtained. Measurements were made on the Corn Industries viscometer (23) and the modified Stormer viscometer (13,24) described in previous papers. The results show that the differences between starches can be determined systematically, and are satisfactorily reproducible, and that the data can be computed and expressed in rational units. It is not suggested that data of the type obtainable by these methods do more than indicate the physical properties of the pastes, however, because different starch-modification procedures presumably could lead to comparable rheological properties.

---

[1] Presented at the Annual Meeting of the Society of Rheology, New York, N. Y., November 5 and 6, 1948.

[2] Fellow of the Corn Industries Research Foundation.

Before proceeding to the experimental work, descriptions of the commercial forms of starch and a brief review of prior work on starch-paste measurements will be given.

Commercial Forms of Starch

Pearl, powdered, lump, and crystal are the forms in which starch is marketed (17). The pearl form is starch in the form of small grits or pellets; it is starch which has been dried but not ground. There is widespread misuse of the term "pearl" starch to indicate an unmodified or native starch. Since not only unmodified but also modified starches are marketed in all forms, the term "pearl" should not be used to designate only an unmodified starch. The powdered form is starch which has been ground and then bolted through a cloth of about 100-mesh. Crystal starch is prepared by filtering the starch with suction in porous boxes lined with filter cloth, after which it is dried in kilns, while lump starch is made by pressing starch into a cylinder after which it is dried slowly and broken into pieces.

Much of the starch used by the textile, paper, adhesives, and laundering industries has been modified to provide a series of grades which vary in time of pasting, viscosity of the cooked paste, and film-forming properties. The common methods of modifying starch are the following: acid modification, in which the starch suspended in water is treated at a moderate temperature with a mineral acid; oxidation, in which an aqueous suspension of starch is treated with an oxidizing agent such as sodium hypochlorite; dextrinization, in which normally dry starch is heated with acid; the British gum process, in which dry starch is treated with heat alone or with the addition of a small amount of mineral acid. Descriptions of these processes are given by Kerr (21,22) and by Radley (29).

Some confusion apparently arises from the term "gum" which is assumed generally to designate a British gum and to be a highly modified product. Actually, British gums are made in many degrees of modification, and in their paste properties some of them resemble acid-modified starches of low degree of modification. On the other hand, certain highly oxidized starches used in the paper industry are also termed gums, although the process of manufacture is entierly different from that of British gums. These trade designations emphasize the need for specification in terms of the physical properties of the pastes.

Ratings usually refer to some property associated with viscosity, such as "thin-" or "thick-boiling," or are expressed as "fluidity," in numerical terms ranging usually from 10 to 90. Fluidity ratings often refer to the alkaline fluidity test (8,28), but various manufacturers have so altered the test procedures that, while fluidity values are consistent for a given manufacturer's products, they will vary from one manufacturer to another. Sometimes fluidity ratings refer to the volume of cooked starch paste which flows from an efflux viscometer in a standard time. As a consequence, the numerical values merely indicate differences within a series; they cannot be considered to have any absolute significance.

Viscometric Measurements of Starch Pastes

The purposes of routine tests of consistency in the starch-producing industry are (a) control of the reaction during chemical modification so that uniform products may be obtained, and (b) a final test of quality of the finsihed product. Since the changes occurring during processing take place continuously, it is necessary to stop the reaction quickly by neutralization of the slurry when the desired degree of modification has been obtained. It is necessary, therefore, that the test method be rapid, and the time from sampling to completion of the test should be less than 30 minutes.

The starch-consuming industries require a method of grading which provides a reliable index to the physical properties of the starch pastes. This is necessary to establish suitable limits for formulation and application, not only for control of a given operation, but also to assist in selection of alternative products.

For industrial testing, it is necessary to prepare the starch pastes in a uniform manner. The factors which must be controlled in preparing a starch paste are as follows: (a) the initial temperature of the water used to form the slurries should not vary greatly; (b) the rate of increase of temperature of the starch suspension should be the same in all tests; (c) the highest temperature at which the paste is cooked should not vary more than a few tenths of a degree Centigrade from one test to the next; (d) the rate of stirring should be duplicated; (e) the entire volume of paste should be heated uniformly; (f) the total elapsed time from the start of cooking to sampling for a rheological measurement should be duplicated; (g) evaporation of water should be prevented or compensated by replacement.

Interest in the pasting properties of starches and their rheological properties has been shown for many years. An extended series of measurements on 3% pastes has been reported by Richardson and Waite (31) using capillary viscometers at a constant shearing stress of 100 dynes/cm.^{2} The rate of shear was, accordingly, variable. Despite this limitation the rise in viscosity with gelatinization and the subsequent decrease in viscosity as the paste was agitated were clearly shown. Farrow, Lowe and Neale (11) recognized the importance of studying starch pastes at known rates of shear so that apparent viscosity could be expressed at given rates of shear in terms of the constants of a simple equation, independent of the kind of viscometer and its dimensions. They were able to obtain approximate correlation, over a limited range of shear rates, of viscosity measurements made in capillary viscometers of various dimensions and in a Couette type viscometer.

Caesar and Moore (9) devised an instrument which provided a graphical record of the changes occurring during a pasting process. In this instrument, the torque variation during stirring was measured by means of a recording wattmeter, and the curves so obtained indicated the change in viscosity with gelatinization, continued cooking, and cooling. These investigators concluded that modification of the starch was clearly evident from the shape of the curve, because each starch exhibited characteristic pasting properties. Tapioca, corn, potato, and wheat starches were studied in these tests, and a concentration of 20% was found most suitable for the instrument. This method is of considerable interest, but the concentration limit is somewhat high, and it is insufficiently sensitive at lower viscosities.

A rotating cylinder viscometer has been described by Barham, Wagoner and Reed (3). This instrument also provides readings during the cooking process. Measurements were made on potato, tapioca, corn, and kafir starches, and the shape of the curves was found characteristic for the different starches. Additional work by the same investigators (4), on potato and sweet potato starch, showed that varietal and environmental influences affected the viscosity, gelatinization temperature, and granule size.

A recent paper, by Higginbotham (18), contains a description of an instrument for recording the consistency of starch pastes by means of a mechanical dynamometer. Data are obtained during the cooking process. Sago, tapioca, farina, and corn starches of both unmodified and treated types were studied. The experimental results quite clearly distinguish between the pasting characteristics of the different products. Higginbotham preferred a pasting temperature of 99°C. for the reason that some starches, particularly unmodified corn and wheat, are said to gelatinize slowly and incompletely at 90°C., although the higher temperature is not comparable with mill conditions.

Anker and Geddes (1) and Meiss, Treadway and Smith (26) have used the Brabender "Amylograph" to study the effect of a number of variables on the pasting process.

The more commonly used industrial viscometers cannot be used in starch paste studies without considerable uncertainty in the validity of the measurements. For many years orifice or efflux viscometers have been used; of these the Scott (25) and the fluidity funnel (8,28) are typical. For rapid determinations on pastes of low viscosity, pipettes such as the Dudley (2) are sometimes used. Capillary viscometers are frequently employed in research (but not industrial) methods. By applying pressure to the capillary, as in the methods of Richardson and Waite (31), and Brimhall and Hixon (7), the range of the capillary viscometer is extended to practical starch concentrations. The falling-ball viscometer is inconvenient and time consuming to use, and the results are not reproducible with sufficient precision (28). These instruments are inadequate, however, because a single flow time on a sample does not adequately characterize the rheological properties of a given starch paste.

Commercial rotational viscometers of the MacMichael and Stormer types need modification before they become suitable for starch paste measurements. Lack of proper temperature control is one of the more serious deficiencies of these instruments. Moreover, as they are usually operated, the great advantages of the rotating cylinder viscometer are not realized. Suitable modification of the Stormer viscometer has been described by Fischer and Lindsley (13,24).

The instrument developed by Kesler and Bechtel (23) overcomes the limitations of previous instruments in providing a continuous record of the change in consistency of the paste during the cooking process. This instrument, designated the Corn Industries viscometer, is described in detail below.

Viscometric Units

Starch pastes generally exhibit pseudoplastic flow properties, *i.e.*, the rate of flow increases faster than the shearing stress (12). For comparison of different materials, it is necessary to specify the rate of shear, and the viscometric designation then becomes "apparent viscosity" (η_a). There has been little attempt in either the starch or textile industries to specify starch viscosities in absolute units for the reason that the instruments usually employed measure flow under extremely complex conditions. Thus, it is necessary to maintain agitation during pasting which is sufficient to keep the starch in suspension but not so vigorous as to promote mechanical disintegration of the starch granules. Instruments designed for the purpose of measuring changes in viscosity during pasting have been noted above; some investigators prefer to specify the change in flow properties in terms of torque (g.-cm.) for the instrument used. Calibration to provide data in poises is given by Barham *et al.* (3) and Kesler and Bechtel (23).

Some objection may be raised to the specification of apparent viscosities in absolute units, since this term has become associated with unknown rates of shear and is, accordingly, useful only with a given instrument. When apparent viscosities are given in terms of known rates of shear, then this objection presumably would be overruled. Apparent viscosity is essentially a shear dependent viscosity and is established by the ratio of shearing stress to rate of shear. The use of data for η_a has the advantage that a comparison of starches under comparable conditions, independent of the instrument, may be made. This point has been discussed by Fischer and Lindsley (12,13).

The term *viscosity* is used in this paper for convenience, but it should be understood that the meaning is qualified. Alternatively, the term *consistency* appears to be acceptable.

EXPERIMENTAL PROCEDURES

Since the purpose of these experiments was a comparison of different types of starches and a study of the flow properties of the pastes made from them, measurements were made by means of the Corn Industries viscometer and the modified Stormer viscometer. The former instrument provided a controlled and reproducible method for pasting as well as a record of the change in consistency as cooking progressed. The Stormer viscometer supplemented the Corn Industries viscometer by allowing measurements at higher rates of shear and by providing a complete flow

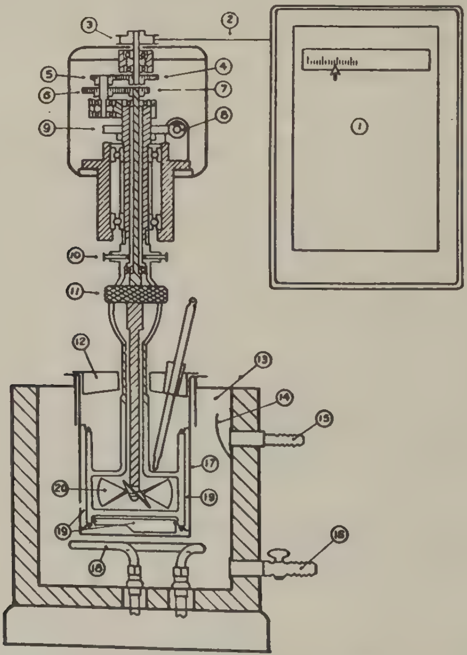

FIG. 1. Sectional drawing of Corn Industries viscometer. Legend: *1.* recorder and dynamometer (dynamometer not shown); *2.* cable from viscometer to recorder; *3.* cable drum; *4, 5, 6, 7,* gears of sun and planet differential; *8.* worm, turned by synchronous motor (not shown); *9.* worm gear; *10.* spring pins for holding center shaft; *11.* coupling to attach stirrer; *12.* condenser cover; *13.* water bath; *14.* baffle to maintain water level; *15.* overflow; *16.* drain cock; *17.* starch beaker; *18.* electric heater (1000 watts, thermostatically controlled); *19.* scraper blades; *20.* propeller.

curve of rate of shear *vs.* shearing stress. Procedures adopted for the tests are given below.

Corn Industries Viscometer

The characteristic features of this instrument have been noted above (23). A diagram of the construction is given in Fig. 1. The instrument consists of a vessel *17* immersed in a water bath *13*. The starch paste is stirred by an agitator which consists of two parts: a scraper *19* and a propeller *20*. The propeller is driven at a constant speed of 60 r.p.m. by a synchronous motor through a sun and planet differential. The torque on the propeller is transmitted through the differential to drum *3* which is attached by the cable *2* to a dynamometer (not shown) built into the recorder *1*. A record of the torque on the propeller is obtained continuously from the start of the test.

The starch pastes were prepared by stirring the starch into water at room temperature to give a total of 1000 g. The stirrer was started, the slurry was then poured quickly into the metal beaker immersed in the heating jacket at 90–92°C. and the recording mechanism started. The process of pasting then continued without further attention. The instrument had previously been calibrated and the viscosity calculated from the data for torque by means of the empirical relation: η_a (poises) = torque (g.–cm.)/35. Measurements can be duplicated with a precision of ± 2%.

Modified Stormer Viscometer

The procedure for using the Stormer viscometer, modified to operate with concentric cylinders, has been described (12,13). For the purposes of these tests, the bob was made of a laminated plastic material to reduce the conduction of heat from the hot starch pastes to the bearing assembly on the viscometer to a negligible amount. The dimensions of the cylindrical units used are as follows:

Cup radius	1.746 cm.
Bob radius	1.565 cm.

Most of the measurements were made at 90°C. ± 1°, close to the pasting temperature of 90–92°C. For comparison with the Corn Industries viscometer, 8–10 readings were made at low rates of shear (to 50 r.p.m. or 45 sec.$^{-1}$). Other measurements were made to 400 r.p.m. (360 sec^{-1}). The pastes prepared in the Corn Industries viscometer were used directly. A second method of pasting was based on the use of a double boiler of 1 l. paste capacity, equipped with a high-speed impeller agitator. The cooking temperature was 90–92°C., and was timed from the onset of gelatinization.

Computation of apparent viscosities (η_a) from these data was made from the curve of torque *vs.* rate of shear, by the tangent method (12). The viscometer constant for the conversion of instrument data to poises was corrected for end-effect, as described in a previous paper (24). Below 1 poise, it was necessary to use a series of constants for unit changes in viscosity. This was done by computing a separate constant for each 0.1 poise difference. The data for η_a are estimated to be accurate within ± 10%.

Alkaline Fluidity Test (8)

Five g. of starch are stirred to a slurry with 10.00 ml. of distilled water in a 250 ml. Erlenmeyer flask. Then 90 ml. of 1.0% NaOH solution at 75°F. are added, with stirring. Stirring is continued for 3 min., after which the flask is placed in a water bath maintained at 75°F. for 30 min. The fluidity funnel is also kept in the water bath. It is removed and allowed to drain for 3 min. before the test, but is not otherwise dried.

At the end of this time, the contents of the flask are poured into the fluidity funnel so that the stem is completely filled and free from air bubbles. A graduated cylinder of 100 ml. capacity is placed under the

TABLE I

General Data on Starch Samples

Sample no.[a]	Description	Moisture	pH
		per cent	
F-3	Corn, 80 fluidity	12.5	4.4
H-9E	Corn, 70 fluidity	13.4	6.1
G-2	Corn, 60 fluidity	12.3	5.9
C-6	Corn, 60 fluidity	12.5	5.1
D-4	Corn, 55 fluidity	12.4	5.2
H-9B	Corn, 50 fluidity	14.0	5.6
I-10B	Corn, 50 fluidity	13.1	5.7
C-5	Corn, 40 fluidity	12.2	6.1
A-8	Corn, 40 fluidity	12.2	5.0
H-9D	Corn, 20 fluidity	12.7	6.2
I-10A	Corn, 20 fluidity	13.0	7.0
C-11	Corn, low modification British gum	10.5	5.3
E-1	Wheat, thin-boiling	12.4	5.9
E-20	Wheat, unmodified	11.8	5.0
D-21	Milo sorghum	11.9	4.6
K-23	Potato, white, Dutch	13.2	5.4
J-18	Potato, unmodified, Idaho	16.4	5.3
L-24	Sweet potato	11.7	6.3
C-22	Tapioca, high-grade Sando	11.1	6.1
F-19	Rice, unmodified	11.6	3.5

[a] Letters refer to code identifying different manufacturers.

stem of the funnel and the starch paste allowed to flow. The volume of paste which flows in 70 seconds is the alkaline fluidity (also called "alkali fluidity" or "tip" test).

Two forms of funnel are in use. These are described by Morgan and Vaughn (28) and Buel (8). The original type of funnel is an ordinary 60° glass funnel of 4 in. top diameter. The stem is shortened to a few cm. Attached to it by a piece of rubber tubing is a special tip, made by heating a glass tube to make a narrow orifice. Total length of funnel stem and tip is about 3 in. One hundred ten ml. of water are poured into the funnel, and when 100 ml. of water flow from the orifice in 70 seconds, the funnel is considered satisfactory.

Starch Samples

The starches were commercial samples. They were used without treatment of any kind.

Moisture determinations were made by heating in a vacuum oven at 110°C. for 16–20 hr. The pH values were made on slurries containing 2 g. of starch in 18 ml. of distilled water by means of a glass-electrode potentiometer. Pertinent data are assembled in Table I.

Experimental Results and Discussion

Pasting Characteristics

In Fig. 2, torque *vs.* time curves for a series of starches during pasting are given. These curves were plotted directly from data obtained on the Corn Industries viscometer. In the first part of the pasting cycle, as the temperature rises, the starch slurry approaches gelatinization; a maximum in the curve is reached, and, as pasting continues, there is first a rapid fall in torque (resistance to stirring) followed by a leveling off of the curve. At 60 minutes, the spacing of the curves is fairly characteristic for the different types of modified starches, except for curve I-10A, which will be discussed later. From the entire curve it is possible to infer the following: (a) extent of modification of starches during or after chemical treatment; (b) quality of a production batch of starch of any grade; (c) information about the nature of an unknown starch, since different starches produce viscosity curves of characteristic form. From the time required for the initial viscosity rise, and the time taken to reach the maximum viscosity, information is obtained regarding the ease and extent of granule swelling. The extent of lowering of viscosity on continued cooking for an arbitrary time indicates the resistance of the starch to the effects of heat and agitation.

Computed values for apparent viscosity are presented in Tables II and III. For the series of acid-modified corn starches the range was 1.1 to 28

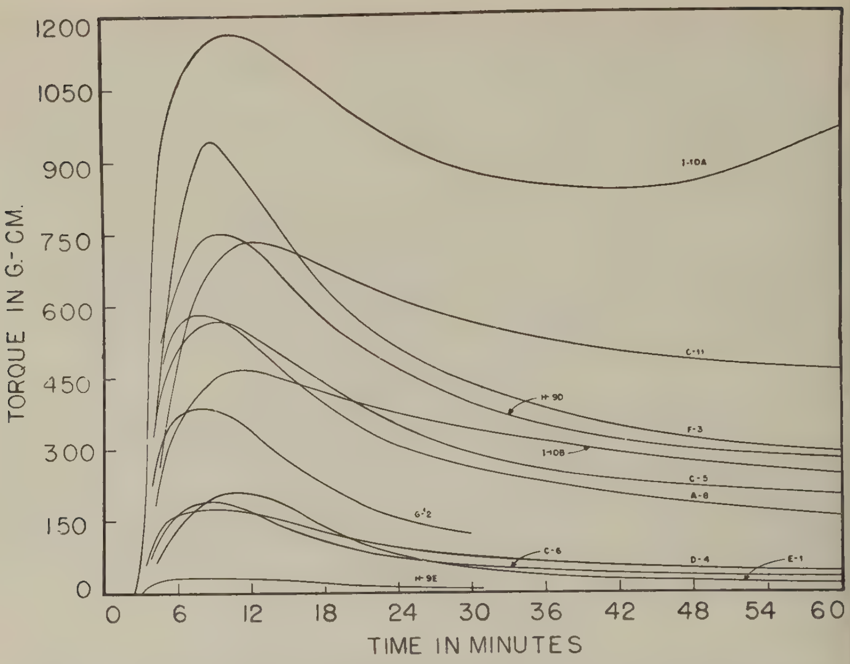

FIG. 2. Change in consistency of starch pastes during cooking. (Corn Industries viscometer; 10% paste concentration. See Table I for identification of starch samples.)

TABLE II

Comparison of Apparent Viscosities of Starch Pastes Measured on Corn Industries and Modified Stormer Viscometers

(All pastes 10% dry basis; 90–92°C. cooking temperature; 1 hr.)

Starch no.	η_a Corn industries viscometer	η_a Modified stormer viscometer (poises)		Manufacturer's fluidity rating
		Rate of shear		
		3.6 (*sec.*$^{-1}$)	18 (*sec.*$^{-1}$)	
	poises			
10A	28.	24.	9.7	20
11	13.	11.	5.1	—
10B	9.7	13.	—	50
9D	8.1	9.7	4.2	20
3	8.0	6.2	4.1	80
5	5.7	7.0	2.9	40
8	4.4	5.2	2.8	40
4	1.2	2.8	1.6	55
9B	1.1	—	1.4	50

TABLE III

Apparent Viscosities of Different Starches

(Corn Industries viscometer; 5% concentration; cooking time 1 hr.)

Starch no.	Type	Apparent viscosity
		poises
20	Wheat	0.45
19	Rice	1.9
17	Corn	3.3
21	Milo sorghum	4.0
22	Tapioca	5.7
24	Sweet potato	8.1
23	Potato	9.1
18	Potato	15.0

poises for 10% pastes cooked for 1 hr. The commercial range of corn starches includes more highly modified types which have a viscosity as low as 0.2 poise after 0.5 hr. of cooking. Measurements on the modified Stormer viscometer on the same pastes are also presented in Table II; comparison of the two sets of data is discussed later. Under certain conditions of cooking, some starches exhibit a secondary rise in the viscosity-cooking time curve, yielding a second maximum, after which the viscosity falls in the normal manner. Such a curve is shown in Fig. 2, Curve 1-10A. The full significance of this observation has not been established.

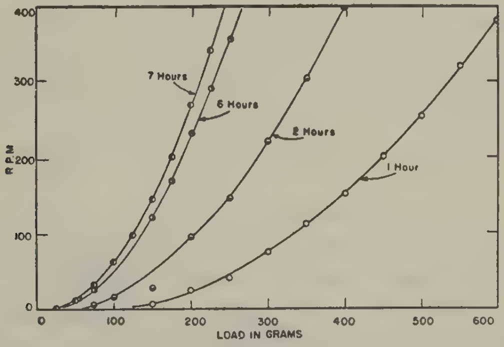

FIG. 3. Flow curves obtained after different periods of cooking. (Low acid modification starch; pasted in double boiler; 9% paste concentration.)

The flow curves obtained with the modified Stormer viscometer on a corn starch after different periods of cooking are shown in Fig. 3.

The significance of these rheological changes can be correlated with colloidal changes in the starch granule. When a water suspension of starch is heated, no changes are observed in the appearance of the granules until certain critical temperatures are reached. At temperatures which are characteristic of individual starch varieties and chemical modifications, the granules begin to swell, the birefringent crosses which are observable under a polarizing microscope disappear (14,33), the suspension becomes translucent (27,32), and the viscosity begins to increase rapidly. These changes are caused by rapid hydration of the starch; the process, called gelatinization, is irreversible. Since the temperature range within which gelatinization occurs is characteristic of each kind of starch if conditions of cooking are uniformly controlled, it is frequently used as a means of identifying starches (14).

Katz (19,20) and others have observed that the granules continue to swell during the period of viscosity increase and that, at the maximum viscosity, swelling has likewise reached a maximum. The lowering of viscosity on continued cooking is attributed to the gradual leaching of soluble matter from the granules, with consequent granule shrinkage, to increased ease of deformation of the tender, swollen granules, and to granule disintegration. The relative importance of these processes in any particular case depends on the source of the starch and the process of manufacture, as well as on a number of other factors. Potato starch granules and those of highly modified starches of all kinds are easily ruptured, while native or unmodified corn starch granules are strongly resistant, even at high temperature and with vigorous agitation. Important among the factors which affect the rate of viscosity drop are the rate at which the starch suspension was heated, the final paste temperature, pH, and concentration. These factors have recently been studied by Bechtel (5).

Although a paste may show no detail under a microscope, it is certain that it is not completely dispersed into units of molecular dimensions, for it can be shown that, when such a paste is subjected to violent agitation, the viscosity is further lowered. Starch paste viscosity is, therefore, due to the presence of swollen granules, granule fragments, and colloidal particles.

A study of starch pastes, made by Gallay (15), and by Gallay and Bell (16), shows that acid-modified starches have lower viscosity than unmodified starch of the same natural variety because the granules are so altered during the chemical modifying process that they have greatly lessened swelling power and are brittle and much less resistant to disintegration. Sjostrom (35) has made an extensive study of the pasting process with similar findings.

A question of importance is whether the pasting process is accompanied by chemical degradation of the starch, especially on long cooking. Several methods have been developed for determining the extent of chemical degradation of starches caused by any chemical or physical treatment. Among these are the alkali number of Schoch and Jensen (34), the copper reduction number of Richardson, Higginbotham and Farrow (30), the modification of this procedure by Farley and Hixon (10), and the determination of viscosity. All of these methods have been employed frequently. As shown by Schoch and Jensen, the alkali number of commercial unmodified corn starch samples varies between 9.8 and 12.1. When such a starch was autoclaved for 4 hr. at 19 lb. steam pressure (125°C.), it was found that, between pH 5.9 and 6.3, no increase in alkali number occurred, indicating that inappreciable chemical degradation had taken place. From pH 5.0 to 5.9, the increase in alkali number was small. Below 5.0 and above 6.3, the rate of degradation increased. From these results, it seems that corn starch can be cooked at the boiling point for a considerably longer period than 4 hr. in the normal pH range for this starch, without chemical degradation.

Agitation

There is interest in whether or not variation in agitation rate during pasting results in different flow properties. The evidence from the experiments performed thus far is that the rate of pasting is the variable chiefly affected, provided that starch concentration and temperature are held constant for a given starch. The rate of pasting in the double boiler was approximately double that of the Corn Industries viscometer. By chance, in one experiment, samples were taken from the two pasting vessels at the same point of breakdown; the curves are reproduced in Fig. 4. A cooking period of 0.5 hr. in the double boiler (closed circles) corresponded with

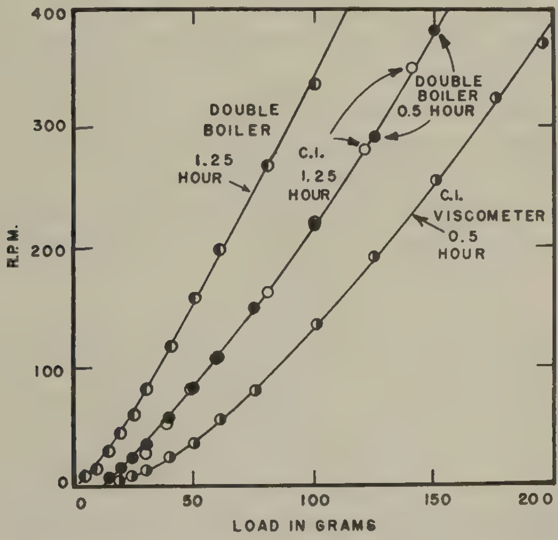

FIG. 4. Flow curves obtained with different cooking procedures, illustrating effect of agitation on rate of pasting. (Starch 1; 10% concentration.)

1.25 hr. in the Corn Industries viscometer (open circles). No difference is distinguishable.

Rate of Shear

Although the effect of rate of shear on the flow properties of pseudoplastic materials is fairly well known, measurements are frequently made in which no attempt is made either to obtain data at a constant rate of shear or to ascertain the magnitude of the rate of shear. Consequently, many measurements are of virtually no significance.

In a coaxial cylindrical viscometer the rate of shear may be readily computed from the dimensions of the cup and bob, the clearance, and the rate of rotation. Convenient methods for this computation have been discussed by Fischer and Lindsley (12,13). In the Corn Industries viscometer the rate of shear cannot be computed, but that it was reasonably constant appeared, at the start of this work, to be an acceptable assumption. An effective rate of shear for this instrument was estimated by comparing values for apparent viscosity with those computed at different rates of shear from the Stormer viscometer data on the same starch pastes. In the data of Table II it will be seen that a rate of shear of 3.6 sec.$^{-1}$ brings the Stormer data into fair alignment with the values from the Corn Industries viscometer. Considering the difference in the two types of instruments and the methods of operation, it is remarkable that the data are as close as observed. The construction of the stirrer and scraping blades appears to be such that effective turnover of the paste is accomplished along with good heat transfer and avoidance of turbulence.

The effect of rate of shear on computed values of apparent viscosity is shown in Table IV. In the range of 18 to 300 sec.$^{-1}$ a considerable de-

TABLE IV

Effect of Rate of Shear on Apparent Viscosities of Starch Pastes

(Stormer viscometer measurements; η_a values in poises; temperature 90–92°C.)

Starch	No.	Conc. 5% rate of shear (*sec.*$^{-1}$)				Conc. 10% rate of shear (*sec.*$^{-1}$)			
		18	50	100	300	18	50	100	300
Corn (unmodified)	17	0.40	0.38	0.35	0.29	—	—	—	—
Corn (acid modified)	9D	—	—	—	—	4.2	2.3	1.6	1.2
Corn (acid modified)	5	—	—	—	—	1.3	0.90	0.78	0.52
Potato (Idaho)	18	1.1	0.79	0.67	0.44	—	—	—	—
Rice	19	0.45	0.32	0.26	0.26	3.9	2.9	2.3	0.72
Sweet potato	24	0.83	0.63	0.46	0.34	6.7	4.2	3.7	2.1
Potato (Dutch)	23	0.57	0.42	0.26	0.25	3.8	2.8	2.4	1.5
Tapioca	22	0.93	0.63	0.45	0.29	7.8	6.5	5.5	4.1
Milo sorghum	21	0.90	0.49	0.36	0.22	7.7	3.5	3.6	2.4
Wheat	20	0.31	0.31	0.28	0.28	4.6	3.3	2.5	2.2

crease in the apparent viscosities of most of the samples will be observed. Corn and wheat unmodified starches exhibit a somewhat smaller change than potato and acid-modified corn starches. This observation accords with other criteria for the resistance of the granules to pasting. From the comparisons which have been made thus far in this work, the change of apparent viscosity with rate of shear would appear to be a useful supplementary means for characterizing starch properties.

Change in Apparent Viscosity with Concentration

When the concentration of starch is increased, certain changes become evident from the curves of apparent viscosity *vs.* time of cooking. Each increment in concentration results in a greater increase in apparent viscosity than its preceding. As the starch concentration is increased the following changes have been noted: (a) the initial rise, associated with gelatinization, occurs at successively lower temperatures; (b) the rate of rise of the curve is more rapid; (c) the maximum in the curve occurs at lower temperatures; (d) the decrease in apparent viscosity on continued cooking is more rapid. Although the magnitude of the change depends on the starch variety and the treatment to which it has been subjected, data typical of acid-modified starches are given in Table V. These results can be ascribed to the increased number of granules which are present to absorb water and swell, presenting internal resistance to shear.

TABLE V

Change in Apparent Viscosity of Starch Pastes with Concentration

(Acid modified corn starch; Corn Industries viscometer.)

Concentration	Temp. initial rise	Temp. at maximum η_a	Maximum η_a	η_a at 30 min.
per cent	°C.	°C.	*poises*	*poises*
7	73.3	86.0	2.8	1.7
8	70.8	84.0	5.9	3.3
9	69.0	80.7	10.	5.1
10	68.0	78.3	17.	7.9
11	67.6	76.0	27.	11
12	67.3	74.5	39	14
13	67.0	73.0	52	17

Alkaline Fluidity Tests

It has been mentioned that fluidity ratings given by different manufacturers may be based on different test procedures. The values given by each manufacturer are consistent for his own products, but may not agree with those of other starch producers. This lack of agreement is evident in Table II, where the manufacturers' fluidity ratings are given with the results of tests of cooked paste made in the two instruments. When the alkaline fluidity test is used it is found that there is good agreement between the results of this test and the consistency of the cooked starch paste, provided the starches compared are of the same natural variety and modified by the same process.

To determine the relationship between alkaline fluidity values, obtained by a standardized procedure, and the consistency of cooked pastes of acid-modified corn starches, alkaline fluidity tests were made by the method of Buel (8). These values were compared with the consistnecy of the starches after 1 hr. cooking under uniform conditions in the Corn Industries viscometer. It is shown in Table VI that as the alkaline fluidity of these starches increases the consistency decreases. Similar relationships have been found between alkali fluidity and consistency of hot starch pastes after other times of cooking as well. Alkaline fluidity values for other starches do not accord with the data in Table VI. For example, for a British gum (sample 11) the alkaline fluidity is 21 and the apparent viscosity 13.1 poises; for a wheat starch, the comparable figures are 55 and 0.51 poise.

TABLE VI

Comparison of Alkaline Fluidity Values and Apparent Viscosity of Starch Pastes

(Acid modified corn starches 10% dry basis; fluidity values by method of Buel (8); rheological data with Corn Industries viscometer.)

Alkaline fluidity value	Apparent viscosity
	poises
8	28.
16	8.0
20	7.6
23	5.8
31	4.4
51	0.94
53	0.94
53	0.77
54	1.2

It is recognized in the industry that the alkaline fluidity test is of limited rheological significance. Nevertheless, acid-modified corn starches give volumes of flow that are roughly proportional to the volumes obtained when these starches are cooked with water and tested. Although this test is also used sometimes for oxidized corn starches and for starches of varieties other than corn, there is in these cases no proportionality between alkaline fluidity and hot-paste fluidity. Here the test is made an arbitrary standard.

Plasticity of Starch Pastes

In a previous paper (12) the possibility for plastic flow (6) and thixotropy in methyl cellulose solutions and starch pastes was discussed. The most commonly observed flow curve for starch pastes is of the pseudoplastic type, in which the resistance to shear decreases continuously as the rate of shear increases. No clear evidence has been obtained from these experiments that starch pastes are plastic when maintained at pasting temperatures, and pastes which can be cooled to room temperature without gelling continue to show pseudoplastic flow. If other factors are introduced (*e.g.*, greatly increased starch concentration, gelation, or compounding with other ingredients), then plastic flow and thixotropy may become evident.

SUMMARY

1. Measurement of the flow properties of starch pastes with the precision and accuracy required for industrial purposes is feasible. The methods described utilize the Corn Industries viscometer and a modified Stormer viscometer. The former provides a continuous record of the change in flow properties during pasting at a controlled cooking temperature; the latter supplements the data obtained during pasting with a rate of shear-shearing stress curve from which the apparent viscosity, expressed in poises, can be computed at any given rate of shear.

2. Rheological data on a variety of commercial starches were obtained. The effect of rate of shear, concentration of the starch, and other factors are discussed. In all cases a curve typical of pseudoplastic flow was obtained.

3. Continuous decrease in apparent viscosity occurs during the pasting process with the greatest change in the first hour; for many starches a fairly level viscosity is obtained after one hour cooking at 90–92°C. Vigorous agitation, in contrast to that obtained with low-speed sweep agitators, produces a more rapid decrease in viscosity, but differences in agitation apparently do not alter the nature of the pasting process.

4. The effect of rate of shear on the computed values for apparent viscosity is great. Satisfactory measurements can be made only when the rate of shear is constant or when the magnitude can be determined and specified. The measuring methods described are reproducible and characterize the starches with respect both to rate of pasting and the flow properties of a given paste at different rates of shear. Industrial measurements can be made more precise by these means, and discrepancies in standardization and grading can be largely eliminated.

REFERENCES

1. ANKER, C. A., AND GEDDES, W. F., *Cereal Chem.* **21**, 335–60 (1944).
2. BALDERSTON, L., *J. Am. Leather Chemists' Assoc.* **8**, 47–49 (1913).
3 BARHAM, H. N., WAGONER, J. A., AND REED, G. N., *Ind. Eng. Chem.* **34**, 1490–95 (1942).

4. Barham, H. N., Wagoner, J. A., Williams, B. M., and Reed, G. N., *J. Agr. Research* **68**, 331–45 (1944).
5. Bechtel, W. G., *Cereal Chem.* **24**, 200–214 (1947).
6. Bingham, E. C., Fluidity and Plasticity. McGraw-Hill Book Co., New York, 1922.
7. Brimhall, B., and Hixon, R. M., *Cereal Chem.* **19**, 425–441 (1942).
8. Buel, H., *8th Intern. Congress Applied Chem., Washington and New York, Orig. Comm.* **13**, 63–76 (1912).
9. Caesar, G. V., and Moore, E. E., *Ind. Eng. Chem.* **27**, 1447–51 (1935).
10. Farley, F. F., and Hixon, R. M., *Ind. Eng. Chem., Anal. Ed.* **13**, 616–617 (1941).
11. Farrow, F. D., Lowe, G. M., and Neale, S. M., *J. Textile Inst.* **19**, T18–T31 (1928).
12. Fischer, E. K., and Lindsley, C. H., *J. Colloid Sci.* **3**, 111–28 (1948).
13. Fischer, E. K., and Lindsley, C. H., *Textile Research J.* **18**, 325–37 (1948).
14. Francis, C. K., and Smith, O. C., *Ind. Eng. Chem.* **8**, 509–11 (1916).
15. Gallay, W., *Can. J. Research* **14B**, 409–14 (1936).
16. Gallay, W., and Bell, A. C., *ibid.* **14B**, 360–72, 381–90 (1936).
17. Gill, L. O., TAPPI Monograph No. 3, Starch for Paper Coating, Chapter IV, pp. 19–20, 1947.
18. Higginbotham, R. S., *J. Textile Inst.* **38**, T131–T150 (1947).
19. Katz, J. R., *Textile Research* **9**, 69–78 (1938).
20. Katz, J. R., Desai, M. C., and Seiberlich, J., *Trans. Faraday Soc.* **34**, 1258–68 (1938).
21. Kerr, R. W., *J. Am. Chem. Soc.* **65**, 188–93 (1943).
22. Kerr, R. W., Chemistry and Industry of Starch. Academic Press, New York, 1944.
23. Kesler, C. C., and Bechtel, W. G., *Anal. Chem.* **19**, 16–21 (1947).
24. Lindsley, C. H., and Fischer, E. K., *J. Applied Phys.* **18**, 988–96 (1947).
25. MacNider, G. M., *Ind. Eng. Chem.* **4**, 417–22 (1912).
26. Meiss, P. E., Treadway, R. H., and Smith, L. T., *Ind. Eng. Chem.* **36**, 159–63 (1944).
27. Morgan, W. L., *Ind. Eng. Chem., Anal. Ed.* **12**, 313–17 (1940).
28. Morgan, W. L., and Vaughn, N. L., *Ind. Eng. Chem.* **35**, 233–38 (1943).
29. Radley, J. A., Starch and Its Derivatives. Chapman and Hall, Ltd., London, 1943.
30. Richardson, W. A., Higginbotham, R. S., and Farrow, F. D., *J. Textile Inst.* **27**, T131–57 (1936).
31. Richardson, W. A., and Waite, R., *ibid.* **24**, T383–416 (1933).
32. Samec, M., Kolloidchemie der Starke. Steinkopf, Dresden, 1941.
33. Schoch, T. J., *Cereal Chem.* **18**, 121–128 (1941).
34. Schoch, T. J., and Jensen, C. C., *Ind. Eng. Chem., Anal. Ed.* **12**, 531–32 (1940).
35. Sjostrom, O., *Ind. Eng. Chem.* **28**, 63–74 (1936).

AN EXPERIMENTAL STUDY OF THIXOTROPY IN BENTONITE SUSPENSIONS [1,2]

Turner Alfrey, Jr.,[3] and Charles W. Rodewald[4]

Received February 25, 1949

INTRODUCTION

The experimental evaluation of the rheological properties of thixotropic systems has never been carried out in a completely satisfactory manner. The reasons for this become apparent if the fundamental nature of the problem is considered.

Thixotropic suspensions are, in general, non-Newtonian. At a given stage in the sol-gel transformation, the flow properties are not describable by a single number such as the coefficient of viscosity. The whole flow curve must be specified—*i.e.*, the function $D(S)$ where D is the velocity gradient (or rate of shear) and S is the shearing stress. A complete specification of the rheological properties of a thixotropic system should start with the specification of $D(S)$ for every stage in the sol-gel transformation. If we assume (as the simplest case) that the degree of gel structure can be adequately represented by the value of a single parameter σ[5] which goes from a minimum value in the completely agitated sol to a maximum value in the completely set gel, then the problem is to specify the flow curve $D(S)$ for every value of σ.

This, however, is only a beginning. A *complete* specification of the rheological properties must also entail knowledge of how the structure

---

[1] Submitted by Turner Alfrey, Jr., in partial fulfillment for the degree of Master of Science at Washington University, 1940.

[2] Presented at the Annual Meeting of the Society of Rheology, New York, N. Y., November 5–6, 1948.

[3] Polymer Research Institute, Polytechnic Institute of Brooklyn, Broolkyn, N. Y.

[4] Washington University, St. Louis, Mo.

[5] This assumption is a definite oversimplification of the structural variability in a thixotropic suspension, as proven by data presented later in this paper. The structure of a bentonite suspension of given composition *cannot* be specified by one single parameter. *At least* two parameters would be necessary, since the structural changes spoken of in this paper as "aging" can be distinguished from those referred to as "setting." Furthermore, when a rheopectic sol is gently agitated, it is quite reasonable to expect not only that setting is *accelerated*, but that the sequence of structures formed will be different from any which are formed during the slower gelation without agitation. However, for a suspension of definite age, studied by the methods described in this paper, the assumption seems justified.

(or σ) changes with time under various conditions—first of all, while standing quietly, and also while undergoing various degrees of agitation.

The difficulties as encountered in such an investigation are of two main types:

1. Those associated with the non-Newtonian character of the suspension at any given stage of gelation, and
2. Those associated with the fact that the structure changes with time; in particular, that the *act of measurement* may affect the structure being measured.

The first type of difficulty is common to all non-Newtonian fluids, whether they exhibit thixotropy or not, and sharply restricts the latitude in the geometry of the measuring instrument. For simple interpretation of data, the shearing stress should be as uniform as possible throughout the instrument. In practice, this indicates the use of concentric cylinders rotating relative to each other. While, in principle, it is possible to determine $D(S)$ relationships for non-Newtonian fluids using instruments in which this requirement is not met (*e.g.*, capillary tubes), in the case of thixotropic suspensions this leads to an impracticable compounding of difficulties. While useful qualitative information concerning thixotropic gelation has been obtained by such methods as the inverted tube technique, capillary tubes, *etc.*, they can hardly be considered as quantitative and fundamental from the rheological standpoint.

The various experimental methods which will be considered here differ primarily in the approach to the second type of "difficulty" above—*i.e.*, to the fundamental problem of thixotropic gelation and breakdown. The method chosen for this investigation is closely modeled after that of Pryce-Jones (10), who developed an instrument which he called a "torsional pendulum thixotrometer." This apparatus consists of a stationary container and an inner bob suspended from a torsion-head marked off in degrees. A sample of the thixotropic material is agitated "thoroughly" outside the instrument, then poured into the chamber. After standing for a known length of time, the torsion head is quickly turned through a definite angle. The progress of the suspended cylinder is observed by means of a light beam reflected from a mirror at the bottom of the wire. Both cylinders and paddles have been used as bobs. Pryce-Jones also used a modification which he called an electromagnetic thixotrometer. In it, the torsion was introduced by a magnet suspended on the wire, in a controllable magnetic field, instead of by rotation of a torsion head. The data obtained from torsion pendulum thixotrometers are, in practice, plotted as scale reading *vs.* time; a series of curves are plotted on the same sheet to show the effect of setting time. Gamble used such curves to correlate the thixotropy of paint with other properties, such as leveling, brushability, settling, *etc.* He points out that, to predict the properties of a paint, the whole series of curves must be known. Neither the viscosity immediately after agitation nor the consistency after long standing will alone define the rheological properties of the system, or even allow empirical predictions to be made. This general method is very well suited to the study of the *undisturbed gelation process;* it tells nothing about the rate of breakdown under agitation. The validity of the method is based upon two assumptions:

(1) By "thorough" agitation, it is possible to "iron out" effects of recent mechanical history and return the system to a reproducible starting point.

(2) At any stage in the gelation process it is possible to carry out measurements of the rheological properties of the suspension at that degree of structure; *i.e.*, the act of measurement does not disturb the structure appreciably in the interval of time required to determine the properties. As will be shown, both assumptions are valid in case of a bentonite suspension *of a given age.*

Two other approaches should be mentioned here. The first is that of Ambrose and Loomis (1), who report that reproducible viscosity measurements for thixotropic suspensions are possible if "equilibrium" is established between gel formation and destruction. They state that such an equilibrium can be reached in a rotary viscosimeter which is allowed to run until a constant stress is observed at a constant rate of shear. They considered the material in the instrument when equilibrium has been established to be in an intermediate state between sol and gel, where the rate of gelation is just counterbalanced by the breakdown caused by flow. This conception is correct only in the case where the shear gradient and shearing stress are quite uniform throughout the instrument. In cases where large variations in flow gradient exist throughout the insturment these variations are accentuated by the process of gelation. In the parts of the instrument where the shear stress is small, the suspension is relatively protected and gel formation proceeds readily; this, in turn, reduces the rate of flow in this portion still further so that the gel is protected and further gel formation proceeds to an even greater extent. On the other hand, in those parts of the instrument where the flow gradient is large, the gel is broken down to a particularly large extent; the resulting high fluidity tends to concentrate the flow still further in this region, leading to still further breakdown. This can be demonstrated very spectacularly in the MacMichael viscosimeter.[6] A stationary gel builds outward from the suspended bob; another gel builds inward from the rotating cup, and turns with it. All the flow is restricted to a narrowing channel between the two gels. The final "equilibrium" between gelation and breakdown exists only at the interfaces between the channel and the two gels. In the channel itself, flow is vigorous, and the material is quite fluid. In the gels there is no observable flow at all, and the process of gelation presumably continues there in much the same way as in a stationary container.

---

[6] It should be pointed out that the MacMichael viscosimeter referred to here is not a concentric cylinder instrument. The bob consists of a horizontal, flat, circular disc, from the center of which arises a cylindrical shaft; this bob is suspended from the torsion wire in a rotating cylindrical cup.

A very interesting method of studying the rheological properties of thixotropic suspension has been developed by Green and Weltmann, and involves the hystereses in D-S curves as D is increased and then decreased. As the rate of shear, D, is being increased, the gel structure is greater than the "equilibrium" structure for that value of D; therefore, the stress is higher than the "equilibrium" value. As the rate of shear is being decreased, the structure is always less developed than the "equilibrium" structure. Thus, if the rate of shear is increased from zero to some maximum value and then decreased to zero again, the observed D-S curve will exhibit a hysteresis loop—and the size of this loop will depend upon the *rate* of changing D. The existence of 3 distinct features of the curves—shape, loop size, and sensitivity to the rate of change of D—permit a 3-fold differentiation of thixotropic systems. The experimental details of this method have been very beautifully worked out and extremely interesting results have been obtained. It is probably the most rapid method giving quantitative results which allows multiple differentiation among materials, and, as a result, it is admirably suited for the empirical differentiation among different commercial products of a thixotropic nature. However, from a physicochemical standpoint, the process of *undisturbed gelation* plays a very important and central role—and here the general method of Pryce-Jones appears to be preferable.

METHOD AND APPARATUS

The instrument used in the major part of this investigation was a modification of the torsional pendulum thixotrometer of Pryce-Jones (10). The instrument consisted of a cylindrical brass shell suspended, by a torsion wire, within the annular space between two concentric, stationary, brass cylindrical shells (see Fig. 1). The suspended shell had an inner diameter of 7.96 cm. and an outer diameter of 8.27 cm. The annular space within which it was hung had an inner diameter of 6.92 cm. and an outer diameter of 9.59 cm. The stationary base was mounted upon a tripod provided with leveling screws. The moving cylinder was suspended, by means of the torsion wire, from a stationary arm which extended from a vertical rod rising from the tripod. The moving cylinder was equipped with a horizontal pointer, and the stationary base supported a circular scale, graduated in 100 equal parts. When in operation, the suspended cylinder was turned through some definite angle, away from the equilibrium position, and then released. The torsion wire tended to return it to its original position, and the material within the instrument opposed the motion. The rate of progress was observed; in general, readings of angular displacement from the equilibrium position were taken every 5 seconds.

The stationary annular cup of the instrument was constructed in such a way that it could be taken apart and cleaned after each investigation. It was made up of 2 concentric brass tubes, which screwed on to a staggered base. The suspended cylinder was fitted with a brass center shaft which made contact with a bearing at the center of the base. The torsion wires used were standard MacMichael torsion wires, manufactured for use in the MacMichael viscosimeter. A brake, with spring, was provided so that the suspended cylinder could be held motionless in any position for any desired length of time.

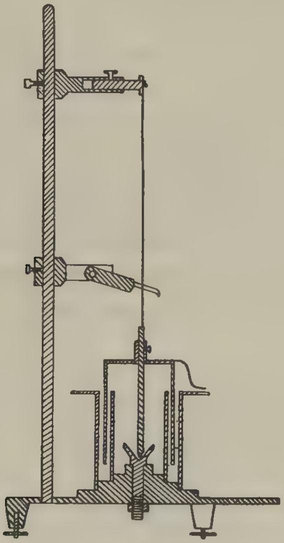

FIG. 1. Diagram of the instrument.

The investigation of the properties of a given suspension was carried out as follows. A sample of the suspension was agitated thoroughly in a mechanical shaking machine. It was then introduced into the thixotrometer, and the movable cylinder was rotated through a definite angle and then released. The progress of the cylinder through the suspension was observed and recorded. The instrument was then dismantled and cleaned, and a new sample introduced. This procedure did not yield reproducible results, because of an inevitable lapse of time between cessation of agitation and beginning of measurement. Before the measurement could begin, it was necessary to pour the material into the instrument, clamp the scale in the proper position, suspend the movable cylinder from the cross arm, and turn it through an angle. The procedure was modified, therefore, to allow agitation of the sample after it had been introduced into the instrument, and after the scale and the movable cylinder had been put into place. The movable cylinder was used to agitate the material within the instrument by hand, attaining a reproducible degree of destruction of the bentonite gel structure. This method led to reproducible results. Before being introduced into the instrument, the material was shaken for 10 min. in the mechanical shaker to insure uniformity of composition.

All measurements using this instrument were taken at 22–23°C.

The thixotropic materials studied were aqueous suspensions of bentonite. Bentonite is a volcanic ash of very fine particle size. Chemically, it is a hydrous aluminum silicate, with appreciable amounts of alkali oxides. The bentonite used was a commercial product, Volclay Micron Bentonite, sold by the American Colloid Co. The suspensions were prepared by sprinkling bentonite on the surface of a known volume of water. Agitation was avoided until all the bentonite had been added and dispersed.

The effects of ethyl alcohol and dioxane as addition agents were studied. The ethyl alcohol used was 95% alcohol. The dioxane was purified by distillation over sodium. A test run was made with U. S. P. castor oil.

TABLE I

Concentrations and Ages of Bentonite Suspensions

Suspension	Concentration *per cent*	Age
A-1	5.66	Fresh
A-2	5.66	1 Day
B-1	5.95	Fresh
B-2	5.95	1 Day
C-1	6.19	Fresh
C-2	6.19	Fresh
C-3	6.19	1 Day
C-4	6.19	3 Days
D-1	6.28	Fresh
E-1	6.37	Fresh
E-2	6.37	1 Day
E-3	6.37	3 Days
E-4	6.37	3 Days
E-5	6.37	6 Days
E-6	6.37	6 Days (0°C.)
E-7	6.37	14 Days
E-8	6.37	14 Days (0°C).
F-1	6.54	Fresh
F-2	6.54	Fresh
F-3	6.54	1 Day

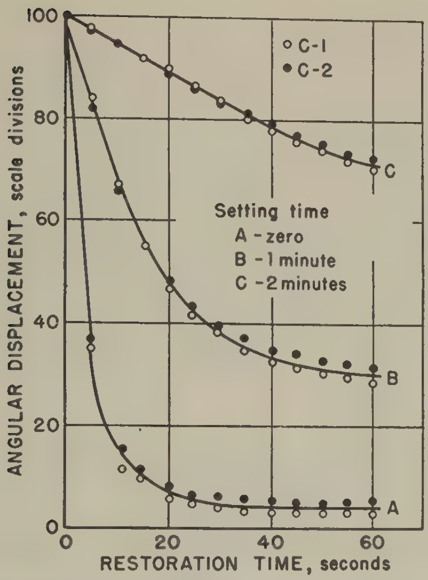

FIG. 2. Restoration curves for two identical suspensions, C-1 and C-2, after different "setting times."

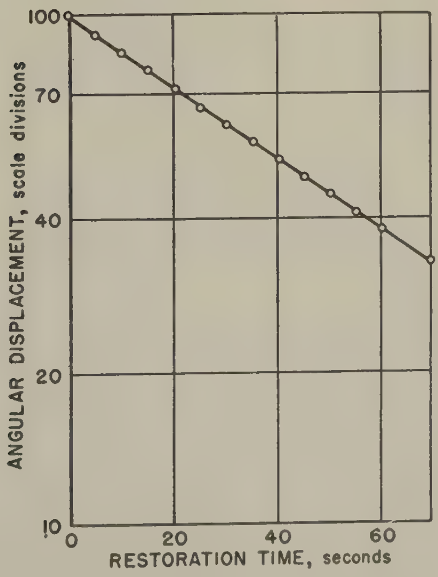

FIG. 3. Restoration curve for castor oil.

Experimental Results and Discussion

Bentonite suspensions of various concentrations and ages were investigated. Table I lists the different suspensions according to age and concentration, and designates each by a symbol by which it will be represented in the subsequent discussion. Each separate suspension was investigated using different initial displacements and different setting times.

The reproducibility of the results is indicated in Fig. 2. This figure shows restoration curves from an initial angular displacement of 100 units of 2 different fresh suspensions containing 6.19% bentonite, after setting the times of zero, 1 min., and 2 min. The general form of these restoration curves is typical of the results obtained throughout the investigation.

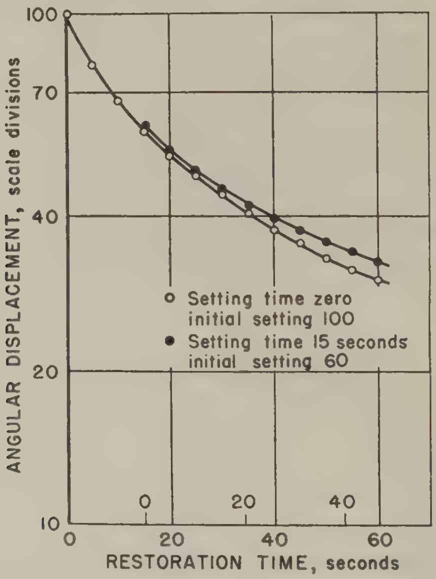

Fig. 4. Indication of gel formation during measurement (see text).

If the material under investigation was a simple Newtonian liquid, the plot of log R *vs.* time should be a straight line. This was found to be true for castor oil, as shown in Fig. 3. The upward curvature exhibited by the restoration curves of bentonite suspensions might arise from either of two causes: a building up of structure during the course of the experiment, or simply a non-Newtonian flow curve. In the case of thoroughly agitated sols, the chief cause is the process of gelation which begins to take place when agitation is ceased, even in the presence of the (relatively mild) stirring action of the cylinder. This fact is illustrated by the data presented graphically in Fig. 4. These data were obtained in the following way: A bentonite suspension was introduced into the instrument and agitated. The cylinder was released from an angle of 100 scale units, and the restoration curve was recorded and plotted. It was observed that, after 15 sec., the pointer was at about 60, and after 30 sec., at about 45. The gel was then agitated, and the cylinder set at a scale reading of 60. After a quiet setting time of 15 sec., the cylinder was released, and its restoration curve recorded and plotted. As shown in Fig. 4, the restoration curve from an angle of 60, after 15 sec. quiet standing, is very nearly the same as that part of the original restoration curve from 100 which lies below 60. The same procedure was followed from a scale reading of 45 after 30 sec. setting time, and a similar check was obtained. The implication is that immediately after thorough agitation, the process of gel formation is not greatly hindered by a mild stirring action such as that introduced by the rotating cylinder.

Newtonian Behavior of Thoroughly Agitated Suspensions

When restoration experiments were carried out from different initial angular displacements immediately after thorough agitation, the initial slopes of the restoration curves were found to be practically identical, indicating that immediately after agitation the bentonite suspensions were essentially Newtonian fluids. Fig. 5 shows the results of such an experiment using bentonite suspension F-3. If the initial slope of the logarithmic curve is multiplied by 2.303 times the initial scale reading, the

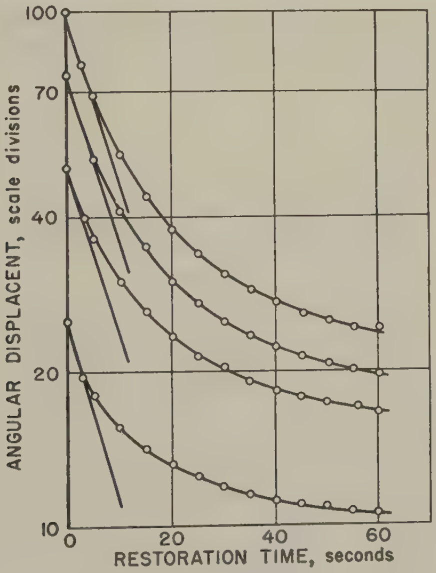

Fig. 5. Restoration curves of suspension F-3 from different initial angles, immediately after agitation.

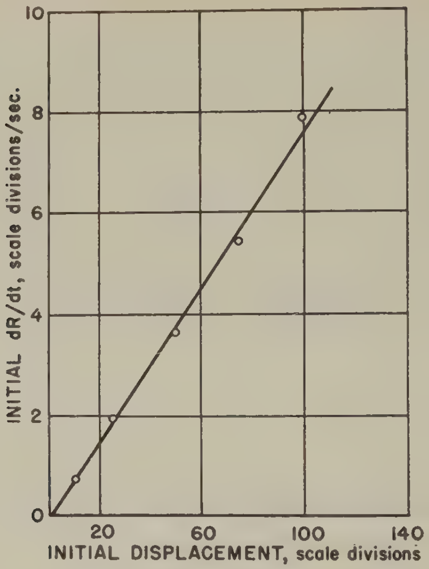

FIG. 6. Initial rates of restoration in Fig. 5, plotted against initial displacement. (Essentially a plot of rate of shear *vs.* shearing stress.)

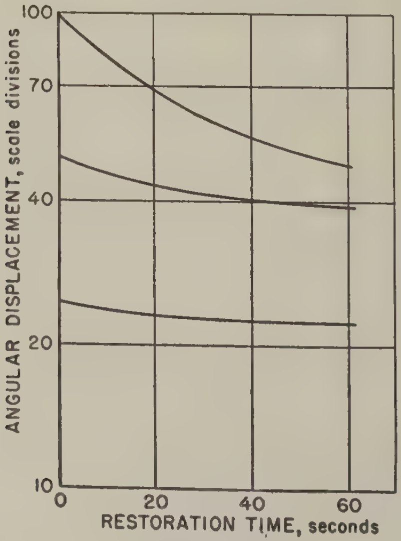

FIG. 7. Restoration curves of suspension F-3 from different initial angles, after 1 min. setting time.

result obtained is the initial value of dR/dt. Fig. 6 shows that for sample F-3, immediately after agitation, dR/dt is directly proportional to R.

Similar sets of runs from different initial angular displacements were carried out on sample F-3 after it had set for 1 min. and 2 min., respectively, after agitation. The logarithmic restoration curves are shown in Figs. 7. and 8. Fig. 9 shows a relation between the initial rate of restoration and the initial deformation, for the case of the 2 min. setting time. In this case, an apparent yield point has developed, and the slope of the curve has been diminished. (Note the difference in ordinate scale between Figs. 6 and 9.) Similar results were obtained on a number of other suspensions, although good straight lines, such as that of Fig. 9, were not always obtained. For example, see Fig. 10, which refers to a bentonite suspension of concentration 5.95%, which had been aged one day after preparation. The following generalization seems warranted: immediately after agitation, bentonite suspensions of this concentration range are very nearly ideal Newtonian fluids, but, upon standing undisturbed, develop apparent yield points.

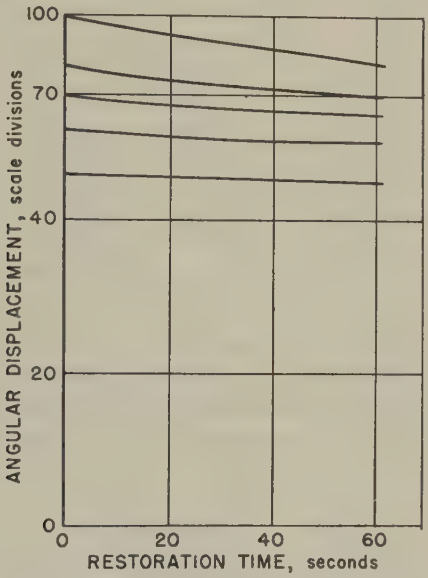

Fig. 8. Restoration curves of suspension F-3 from different initial angles, after 2 min. setting time.

Double Variability of Thixotropic Suspensions

One fact which was brought out very clearly in this investigation was the impossibility of adequately characterizing a thixotropic suspension by one number, such as a "setting time." It is possible for one suspension to be extremely fluid immediately after agitation but to exhibit a rapid gelation process, in contrast to another suspension which is much less fluid after agitation, but gels more slowly. The rheological characteristics of two such suspensions would be entirely different, and yet they might exhibit the same "setting time," based on the time required to reach some arbitrary degree of consistency. This is shown dramatically in Figs. 11 and 12. Note that sample C-1 immediately after agitation is extremely fluid, but that, within 2.5 min. it can set up to an extremely high degree of consistency. On the other hand, sample E-3 immediately after agitation still exhibits a relatively low fluidity, but requires a considerably longer time to develop a marked increase in consistency.

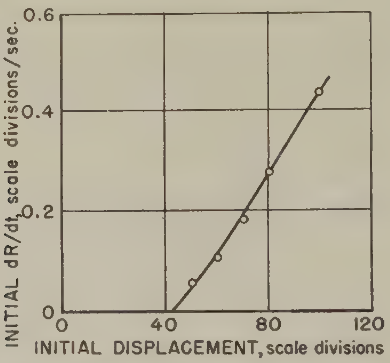

FIG. 9. Initial rate *vs.* initial angle for suspension F-3, after 2 min. setting time.

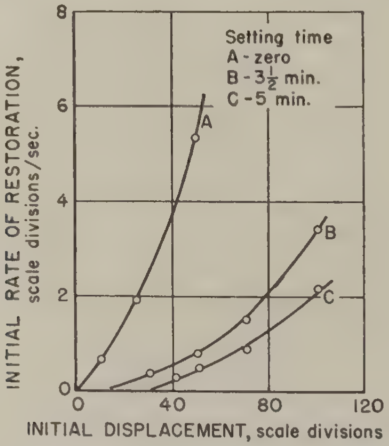

FIG. 10. Initial rate *vs.* initial angle for suspension B-2, after different setting times.

Age of Gel: Effect Upon Thixotropic Properties

The marked difference between the rates of gelation of the two samples shown in Figs. 10 and 11 is due to the fact that sample C-1 was studied immediately after preparation of the suspension, whereas sample E-3 had been allowed to age for 3 days before being studied. In every case investigated, the effect of aging was found to be the same. Fresh suspensions were always found to be more fluid than aged suspensions immediately after agitation. The process of gelation, however, took place much more rapidly in fresh suspensions than in those which had been allowed to age.

Note that the *gelation* process for a suspension of a definite age is semi-reversible, in the sense that thorough agitation will destroy the structure, returning the suspension to a reproducible sol state. Upon quiet standing, the gelation process occurs at the same rate time after time. The slow aging process is superimposed on this gelation. Aging is not mechanically reversible, at least under the conditions of agitation used in our experiments.

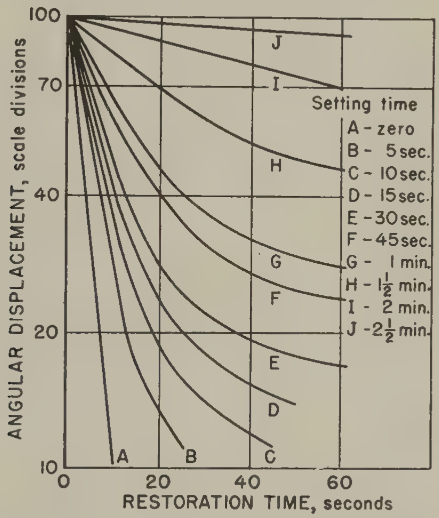

FIG. 11. Effect of setting time on restoration curves of a fresh suspension, C-1.

One possible explanation of the above observations is that the potential energy curve for two bentonite particles possesses two minima—a shallow minimum at fairly large distance of separation, and a deeper minimum for small separation—these two minima being separated by a potential barrier (6,7). If this is true, the processes of gelation and aging could be interpreted as follows. Gelation consists of the establishment of a loose structure as bentonite particles arrange themselves at the larger equilibrium separation. This type of structure development can occur fairly rapidly, since all that is required is for the bentonite particles to diffuse into the proper positions. Such structure can also be broken up by mechanical agitation, because of the shallowness of the potential minimum involved. Aging would be interpreted as the formation of more closely bound clusters of bentonite particles held together at the smaller equilibrium distance. Because of the intervening potential barrier, the aging process is relatively slow. Because of the depth of the inner potential minimum, these dense aggregates, once formed, would be difficult to break up by mechanical agitation of the sort employed in our experiments. Finally, a bentonite suspension in which considerable "aging" had occurred could be expected to exhibit different gelation properties than a fresh gel, because of the larger effective particle size of the suspension. In fact, the results actually observed seem very reasonable; aged suspensions are less fluid immediately after agitation, but are slower to gel. However, much independent evidence from other methods would have to be obtained before one could establish such a detailed mechanism for gelation and aging.

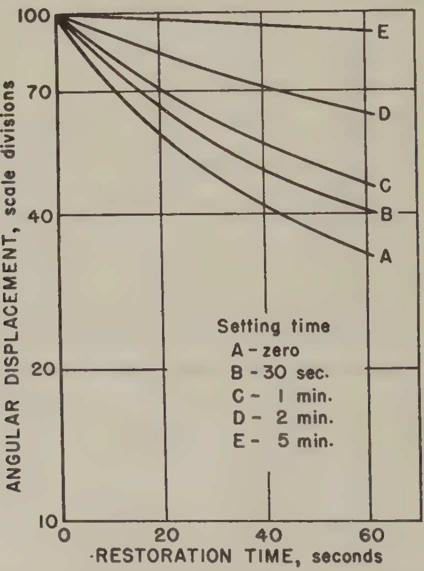

FIG. 12. Effect of setting time on restoration curves of an "aged" suspension, E-3.

A number of studies were made comparing the rate of aging of bentonite suspensions at room temperature and at 2°C. (the actual rheological measurements were all carried out at 22–23° C.) It was observed that the samples which had been aged at the lower temperature exhibited a greater fluidity immediately after agitation than the samples which had been aged at the higher temperature. The rate of gelation, however, was greater for the samples which had been aged at 2°C. These facts would indicate that the aging process takes place at slower rates at low temperatures than at high.

Effect of Addition Agents upon Thixotropic Properties of Bentonite Suspensions

One of the theoretical explanations of thixotropy depends upon the formation of complexes in water (9). These complexes result from hydrogen bonds among water molecules. On the basis of this theory, it would be expected that an addition agent which reduced hydrogen bonding in water would also have a large effect upon the thixotropic nature of an aqueous suspension. To test this possibility, suspensions of bentonite were prepared which contained either dioxane or ethyl alcohol as addition agents. Dioxane is known to reduce hydrogen bonding in water by a great deal, even in small quantities; alcohol is known to have only a small effect upon the extent of hydrogen bonding in water (5). It would be expected, therefore, on the basis of the cybotactic theory of thixotropy, that dioxane would have a greater effect than alcohol upon the thixotropic character of aqueous suspensions. In the few cases which were investigated, this was found to be true. When a suspension was prepared containing 6.37% bentonite and 1% dioxane, the properties were found to be greatly different from those of a 6.37% suspension in pure water. In fact, when the movable cylinder was released, the damping factor was so small that the cylinder actually passed the equilibrium position, in 4.6 sec., and oscillated about it. This indicates a fluidity much greater than any observed in the case of bentonite suspensions in pure water. Even in this extremely fluid suspension, however, there was a tendency toward weak gelation. If the cylinder was held for a "setting time" of 2 min. before being released, the time of passing the equilibrium position was increased to 6.2 sec. After a setting time of 10 sec., the time was increased to 7.0 sec. After a setting time of 25 min., it required 20 sec. for the cylinder to return to an angular displacement of 5 scale divisions. In other cases, aqueous suspensions of bentonite were prepared and allowed to age for one day. At the end of that time, dioxane was added in various amounts. The effect of dioxane thus added to an aged aqueous suspension of bentonite was less than the effect in the case of the suspensions where bentonite was added to a dioxane-water mixture.

In contrast with these results, the thixotropic properties of a suspension of bentonite in a 99:1 water-alcohol mixture were found to be practically identical with those of an aqueous suspension of the same bentonite concentration.

SUMMARY OF RESULTS AND EVALUATION OF THE METHOD

The experimental method utilized in this investigation possesses several major flaws, the chief of which are the poor temperature control and the awkward manual method of agitating the suspension. (The use of ultrasonic waves suggests itself as an alternative in the latter case.) The *general* approach described here does, however, offer some significant advantages in the study of thixotropic suspensions.

(1) By focusing attention on the *initial* rates of restoration, it is possible to determine the *D-S* curve (flow curve) of a suspension *at a given stage of gelation*. This practically eliminates uncertainties arising from an alteration of the structure by the act of measurement.

(2) Bentonite suspensions are found to be essentially Newtonian *immediately following thorough agitation*. The gelation process introduces an apparent yield point, and also reduces the *slope* of the flow curve.

(3) The gelation process is reversible, in the sense that thorough agitation returns the system to a reproducible sol state, which subsequently undergoes reproducible gelation.

(4) Superimposed upon the mechanically reversible gelation process is a slower, mechanically irreversible process of consolidation, referred to here as aging. At any stage in the aging process, a mechanically reversible gelation phenomenon exists; but the gelation properties are different for gels of different age.

(5) The rate of aging is dependent upon temperature.

(6) Traces of dioxane very markedly reduce the tendency toward gelation.

REFERENCES

1. AMBROSE, H. A., AND LOOMIS, A. G., *Physics* **4**, 265–73 (1933).
2. BROUGHTON, G., AND SQUIRES, L., *J. Phys. Chem.* **40**, 1041–53 (1936).
3. FREUNDLICH, H., Thixotropy, Herman et cie., Paris, 1935.
4. GAMBLE, G., *Ind. Eng. Chem.* **28**, 1205–10 (1936).
5. GORDY, W., *J. Chem. Phys.* **4**, 769–71 (1936).
6. HAMAKER, H. C., *Rec. trav. chim.* **55**, 1015–26 (1936).
7. HAMAKER, H. C., *ibid.* **56**, 3–25 (1937).
8. HAUSER, E. A., AND REED, C. E., *J. Phys. Chem.* **41**, 911–934 (1937).
9. KISTLER, S. S., *ibid.* **36**, 2948–66 (1932).
10. PRYCE-JONES, J., *J. Oil and Colour Chemists' Assoc.* **17**, 305–75 (1936).

THE SIGNIFICANCE OF THE CRITERION FOR ADDITIONAL PLASTIC DEFORMATION OF METALS[1,2]

By D. C. Drucker

Brown University, Providence, Rhode Island

Received January 6, 1949

INTRODUCTION

In all of the following discussion it is supposed that the deformation is isothermal and time or viscosity effects are absent. The reasonable and commonly accepted assumption is made throughout that a yield or loading surface exists which depends upon the state of stress and strain and history of loading. In other words, at each stage of a plastic deformation or unloading, there is some function of stress $f(\sigma_{ij})$, such that no additional plastic deformation takes place when f is smaller than some number k. Plastic flow occurs when $f = k$ for materials which do not work-harden (ideal plasticity), when f exceeds k for work-hardening materials. Two simple examples of f are the maximum shear stress (Tresca) and the second invariant of the stress deviation (Mises), $J_2 = \frac{1}{2}s_{ij}s_{ji}$, or, equivalently, the octahedral shearing stress (Nadai), Fig. 1a. In general, both f and k depend upon the state and history of the material.

A mathematical theory of plasticity for work-hardening metals in which the loading function depends upon stress alone will be termed stress hardening. A theory in which the material when unloaded exhibits no directional properties will be called isotropic, although strong anisotropy may be introduced by the state of stress. The most general form of f for an isotropic stress hardening theory is

$$f = f(\sigma_1, \sigma_2, \sigma_3), \tag{1}$$

where σ_1, σ_2, σ_3 are the principal stresses. When the stress components with respect to an arbitrary set of rectangular axis are given instead, f is more conveniently written as

$$f = f(J_1, J_2, J_3), \tag{2}$$

where $J_1 = \sigma_{ii}$, the sum of the principal stresses, is not very important

---

[1] The conclusions presented here were obtained in the course of research conducted under Contract N7onr-358 sponsored jointly by the Office of Naval Research and the Bureau of Ships.

[2] Presented at the Annual Meeting of the Society of Rheology, New York, N. Y., November 5 and 6, 1948.

and is usually dropped [1,2,3][3]; $J_2 = \frac{1}{2}s_{ij}s_{ji}$ is proportional to the square of the octahedral shearing stress, and $J_3 = \frac{1}{3}s_{ij}s_{jk}s_{ki}$. Anisotropic stress hardening theories can also be devised. Direction is important, so that

$$f = f(\sigma_{ij}) \tag{3}$$

contains the stress components for fixed axes and not the invariants or the principal stresses.

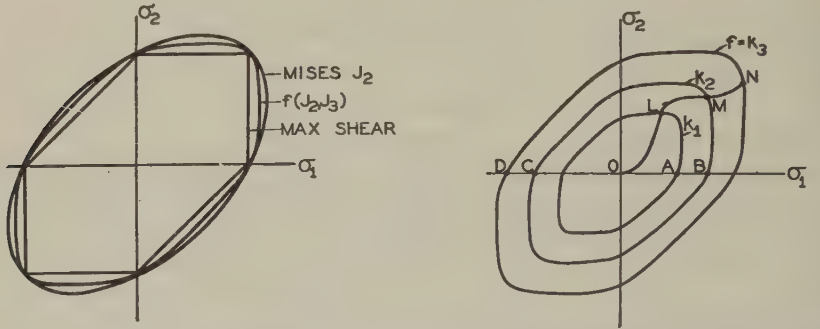

a. Several yield conditions.

b. Sections of a family of loading surfaces for a stress hardening material $k_3 > k_2 > k_1 > 0$.

Fig. 1. Yield or loading surfaces.

The value of f remains constant for an ideally plastic material as there is just one yield surface, but f increases for a stress hardening one, Fig. 1b, where a definite family of loading surfaces exists.

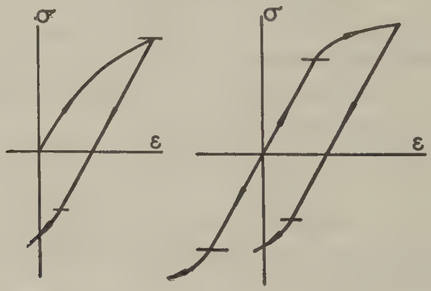

Fig. 2. Bauschinger effect. An unequal raising of the flow limit or actual lowering when the flow stress is reversed.

Stress-hardening theories are at best but a first approximation to the physical behavior of metals [4]. They cannot exhibit a true Bauschinger effect, the unequal raising of the flow limit or often a lowering when the flow stress is reversed, Fig. 2, which means that the loading function depends upon strain as well as stress, $f = f(\sigma_{ij}, \epsilon_{ij})$. The elastic or recoverable strains ϵ_{ij}^e will be assumed given by a generalized Hooke's law which may be anisotropic. In abbreviated form

---

[3] Numbers in brackets refer to the bibliography at the end of the paper.

$$\epsilon_{ij}^e = C_{ijkl}\sigma_{kl}. \tag{4}$$

Therefore, for clarity the more general form of f should be written as

$$f = f(\sigma_{ij}, \epsilon_{ij}^p), \tag{5}$$

where ϵ_{ij}^p represents the components of plastic strain. Form (5) contains (2) as a special case. As for the simpler theories, f may remain constant or it may vary as the deformation proceeds. In the latter case, f really involves history of loading as well as existing stress and strain. Some path of loading terms may be included explicitly (history) and f written directly as f (stress, strain, history). Again f may remain constant or may change.

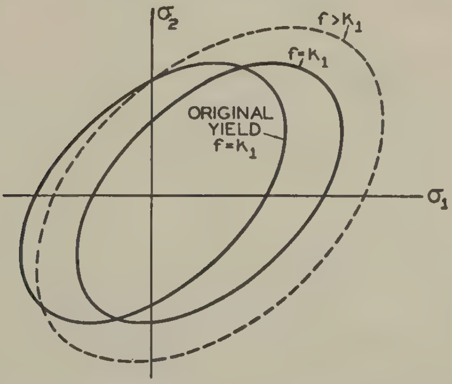

FIG. 3. Sections of loading surfaces for $f = f(\sigma, \epsilon)$ as in Eq. 15. Solid curve on right for f unchanged dashed curve for f increasing (simple tension).

So far, the loading criterion alone has been considered, no mention has been made of the plastic stress-strain relations. It is not obvious that there is a necessary connection between f and the stress-strain relation, although Mises has long used the idea of a plastic potential in several cases

$$d\epsilon_{ij}^p \approx \partial f/\partial\sigma_{ij},$$

or

$$d\epsilon_{ij}^p = \lambda\partial f/\partial\sigma_{ij}. \tag{6}$$

In the next sections it is shown that this relation is valid for materials obeying $f(\sigma_{ij}) = k$ (fixed constant) and also for those which work-harden, provided the strain increments are linear in the stress increments when loading occurs;

$$d\epsilon_{ij}^p = F_{ijkl}d\sigma_{kl}, \tag{7}$$

where the F_{ijkl} generally are functions of stress, plastic strain, and plastic strain history. To do so, it is necessary to be explicit about the meaning of work-hardening (Fig. 4) or stability of plastic flow. For simple tension or compression, the stress must be a monotonically increasing function of the strain; and constancy of stress as strain varies defines ideal plasticity, $f = k$. A direct extension to more general loading is clear if all stress components increase in ratio as the strain components do. When the stress-strain state from which the plastic flow process starts is arbitrary, as is the direction in which the flow proceeds, work-hardening may be defined as meaning that an increase in the *plastic* as well as the total work per unit volume is required for each unit increase of c in $\Delta\epsilon_{ij} = c\epsilon_{ij}{}^o$ or $\Delta\epsilon_{ij}{}^p = c\epsilon_{ij}{}^o$. That is, as the plastic or total strain increments from the starting point get larger in ratio, more and more work is dissipated per unit volume for any given change in any one of the components of strain. In an ideally plastic material, this rate of dissipation is constant. For the preceding statements to have meaning, $\Delta\epsilon_{ij}$ must be a plastic deformation initially and not an elastic unloading.

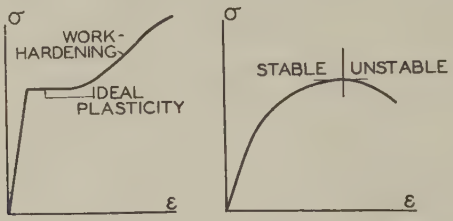

FIG. 4. Work-hardening *vs.* instability of plastic flow.

STRESS-STRAIN RELATIONS AND GEOMETRY [4]

The significance of the loading function is clearer when f is interpreted geometrically as a surface in stress space, in plastic or total strain space, and in combined stress and plastic strain space. The well-known yield surfaces for isotropic stress theories are especially simple cases. Isotropy means that it is permissible to consider principal stresses σ_1, σ_2, σ_3 only so that a 3-dimensional space can be employed in which there is the cube for the maximum normal stress theory, the hexagonal cylinder for maximum shear stress, and the circular cylinder for shear strain energy. Fig. 1a is a plot of some sections for $\sigma_3 = 0$. If ideal plasticity is assumed, one surface gives a complete description. Each point inside the surface represents an elastic state of stress, each point on it a plastic state.

If stress hardening occurs, the surface moves outward with the stress point as the stresses go beyond the original and subsequent yield limits but remains fixed as the stress point moves around inside. When $\sigma_1 + \sigma_2 + \sigma_3$ is assumed without influence, the family of loading surfaces is a fixed nested set of cylinders, the common axis being equally inclined to the coordinate axes. The magnitudes of the plastic strain components do not enter into the shape of the surfaces nor, in general, do they determine which surface governs at any stage of the deformation. This, of course, does not mean that the loading surface and changes in strain are unrelated. On the contrary, the relation is explicit as will be proved later.

---

[4] The derivations and concepts which follow can, of course, be rephrased in purely algebraic language.

If, for example, the Mises $f_1 = J_2$ is used, the stress-strain relation will be of the Prandtl-Reuss type

$$d\epsilon_{ij} = d\epsilon_{ij}{}^e + d\epsilon_{ij}{}^p, \tag{8}$$

in which

$$d\epsilon_{ij}{}^e = C_{ijkl}d\sigma_{kl} = \frac{1+\nu}{E}d\sigma_{ij} - \frac{\nu}{E}\delta_{ij}d\sigma_{kk}, \tag{9}$$

and

$$d\epsilon_{ij}{}^p = \lambda\frac{\partial f_1}{\partial \sigma_{ij}} = \lambda s_{ij}, \tag{10}$$

where ν is Poisson's ratio, E is Young's modulus, s_{ij} is the stress deviation $\sigma_{ij} - \frac{1}{3}\sigma_{kk}\delta_{ij}$, σ_{kk} is the sum of the principal stresses, and δ_{ij} is the Kronecker delta. The coefficient λ has different forms depending upon the assumption as to the material. With the hypothesis of ideal plasticity, when the stress point lies on the yield surface, the plastic strain is not limited by the stress-strain relation. If the material stress hardens, λ becomes

$$\lambda_1 = F(J_2)dJ_2, \tag{11}$$

so that

$$d\epsilon_{ij}{}^p = F(J_2)s_{ij}dJ_2. \tag{12}$$

Squaring each of the terms represented by Eq. (12) and adding, $d\epsilon_{ij}{}^p d\epsilon_{ij}{}^p = F^2(J_2)s_{ij}s_{ij}(dJ_2)^2 = F^2(J_2)2J_2(dJ_2)^2$. It is seen by taking the square root of both sides and integrating, that $\int\sqrt{d\epsilon_{ij}{}^p d\epsilon_{ij}{}^p}$ must be a function of J_2. There will be a unique inverse for a work hardening material so that J_2 or f_1 is a function of $\int\sqrt{d\epsilon_{ij}{}^p d\epsilon_{ij}{}^p}$ a relation found by Cunningham, Thomsen, and Dorn [5].

The loading function f_1 is thus uniquely related to an integrated function of the strain increments but, as previously stated, not the strain itself. If, as an example, a bar is pulled beyond its original yield point and then compressed back to its original size so that the final strain is zero, f_1 will have increased both in the stretching and the compressing process. Referring to Fig. 1b, this type of theory states that as σ_1 goes from O to A elastic action only takes place ($f = k_1$ is supposed to be the original yield surface); as σ_1 increases further, plastic flow occurs and the loading surface moves outward. If, at B, the stress is removed (B to A to O) and then reversed, no yielding occurs until point C on $f = k_2$ is passed. Then further compression to D produces more plastic deformation and the loading surface continues to move outward as the stress point does. During the loading phases, f and $\int \sqrt{d\epsilon_{ij}{}^p d\epsilon_{ij}{}^p}$ increase. The same action holds for all stress paths as for this special one. Path OLMN establishes the same successive loading surfaces, M corresponding to B, N to D.

When f is of more general form, $f_2 = f(J_2, J_3)$, Prager and his coworkers have shown the sufficiency of Eq. (6) and given

$$\begin{aligned} \lambda_2 &= F(J_2, J_3) df_2, \\ d\epsilon_{ij}{}^p &= F(J_2, J_3) \frac{\partial f_2}{\partial \sigma_{ij}} df_2, \end{aligned} \tag{13}$$

for the stress hardening case. Again, f_2 is not related to the state of strain but instead to an integrated form of the strain increment invariants.

It is interesting to note that the increment of plastic work

$$dW = \sigma_{ij} d\epsilon_{ij}{}^p = \lambda \sigma_{ij} \frac{\partial f}{\partial \sigma_{ij}} = \lambda n f, \tag{14}$$

when f is homogeneous of degree n in the stresses as it is for these theories.

When fixed cartesian components of stress are employed instead of principal stresses, the surfaces cannot be constructed or drawn easily except in special sections. For anisotropic theories and for theories involving strain, although the language and concepts of geometry are always very helpful, the reduction to three dimensions is possible in particular cases only. Consider, for illustration, fixed axes x, y, z in an originally isotropic material and a loading process in which the principal stresses and strains are at all times in the x, y, z directions. A permissible form of f which gives a Bauschinger effect is

$$\begin{aligned} f_3 = (\sigma_x - \tfrac{1}{3}\sigma_{kk} - m\epsilon_x{}^p)^2 + (\sigma_y - \tfrac{1}{3}\sigma_{kk} - m\epsilon_y{}^p)^2 \\ + (\sigma_z - \tfrac{1}{3}\sigma_{kk} - m\epsilon_z{}^p)^2, \end{aligned} \tag{15}$$

where m is a constant. Eq. (15) is the Mises yield condition when the plastic strains are zero.

As for the stress theories, it can be assumed that f remains constant [6] or that it changes in value as the deformation proceeds. In the first case, the surface of constant f remains fixed in combined stress-strain space, in the second it moves about. In both cases the surface alters in stress space alone but does not simply expand outward as in Fig. 1b. Subsequent surfaces now do not form a one parameter family but intersect the previous ones as shown in section by Fig. 3. It is these surfaces in stress space that determine whether or not additional plastic deformation occurs. A change of stress in the interior is purely elastic, plastic deformation takes place when the stress point moves outside of the surface; loading occurs when

$$\frac{\partial f}{\partial \sigma_{ij}} d\sigma_{ij} > 0. \tag{16}$$

Ideal plasticity requires $f = f(\sigma_{ij})$ and therefore is ruled out, but a surface fixed in stress-strain space has some similarity to one fixed in stress space alone. The history of loading does not enter in either case. All that counts is the final result—the state of stress and strain. History does matter when the surfaces move, and they must move as the strain increment is known to depend upon stress, strain, and history in real metals.

The preceding discussion has given the general picture and stated a few results and limitations. Two important features of the loading surface and the stress-strain relations will now be proved for any function f (stress, strain, history).

1. The loading surface in stress space must be convex with respect to the origin [6].

This follows directly from the concept that unloading or removing all stresses at a material point in ratio cannot produce plastic deformation at that point. Such unloading in ratio is represented by a straight line in stress space from the stress point on the loading surface to the origin of coordinates. All such radial lines must, therefore, not intersect the loading surface at an intermediate point.

2. The vector whose components are proportional to the increments in plastic strain must be normal to the loading surface in stress space, *i.e.*, $d\epsilon_{ij}{}^p = \lambda \partial f/\partial \sigma_{ij}$ where λ is a scalar. For a work-hardening material, obeying Eq. (7),

$$d\epsilon_{ij}{}^p = G \frac{\partial f}{\partial \sigma_{ij}} \frac{\partial f}{\partial \sigma_{kl}} d\sigma_{kl}, \tag{17}$$

where G is a scalar which may depend upon stress, strain and history.

Consider a work-hardening metal, a state of stress, σ_{ij}, on the loading surface, and a neighboring state $\sigma_{ij} + d\sigma_{ij}$ outside. The stress increments $d\sigma_{ij}$ represent loading, Eq. (16); that is, they produce further plastic deformation $d\epsilon_{ij}{}^p$ as well as elastic strains $d\epsilon_{ij}{}^e$. For very small $d\sigma_{ij}$ and $d\epsilon_{ij}$, the total work done per unit volume is $(\sigma_{ij} + \frac{1}{2}d\sigma_{ij})d\epsilon_{ij}$ or

$$dW_{t1} = (\sigma_{ij} + \tfrac{1}{2}d\sigma_{ij})(d\epsilon_{ij}{}^e + d\epsilon_{ij}{}^p). \tag{18}$$

Now suppose the stress increments to be $2d\sigma_{ij}$ instead of $d\sigma_{ij}$ or, if the idea of work-hardening given in the introduction is to be used directly, imagine the procedure reversed to make the $d\epsilon_{ij}$ the independent quantities. They produce the $d\sigma_{ij}$ and the work done is, of course, the same. Doubling the $d\epsilon_{ij}$ will double the $d\sigma_{ij}$ and *vice versa*, as the relation (7) between the infinitesimals is linear. The total work in this second case is

$$dW_{t2} = (\sigma_{ij} + d\sigma_{ij})2(d\epsilon_{ij}^e + d\epsilon_{ij}^p). \tag{19}$$

From the definition of a work-hardening material (see Introduction), it follows that $dW_{t2} - dW_{t1}$ must be greater than dW_{t1} or

$$d\sigma_{ij}(d\epsilon_{ij}^e + d\epsilon_{ij}^p) > 0. \tag{20}$$

Condition (20) can be derived directly by writing

$$\frac{\partial}{\partial \sigma_{kl}}[\sigma_{ij}(d\epsilon_{ij}^e + d\epsilon_{ij}^p)]d\sigma_{kl} > 0.$$

This condition was found by Prager to be sufficient for uniqueness in the sense that, given the state of stress and strain throughout a body, definite increments in the surface tractions should produce unique stress increments in the interior. The above means of establishing the necessity of (20) shows directly what the uniqueness requirement represents. The plastic flow is unstable at any interior point where (20) is not satisfied. This does not occur in a work-hardening material, by definition, and does not take place in metals without upper and lower yield points. The necking point and beyond in a tensile specimen is such a case of instability but is in terms of force not stress; the true stress-strain curve does not reach a maximum and then drop off, but continues to climb, Fig. 4.

In condition (20), the elastic term $d\sigma_{ij}d\epsilon_{ij}^e$ is always positive so that it cannot be concluded definitely from (20) that $d\sigma_{ij}d\epsilon_{ij}^p$ must be. However, work hardening means more than $dW_{t2} - dW_{t1} > dW_{t1}$, it means that the *plastic* work increment (assuming plastic deformation takes place) increases as well as the total; or

$$dW_2 = (\sigma_{ij} + d\sigma_{ij})2d\epsilon_{ij}^p \tag{21}$$

must exceed twice

$$dW_1 = (\sigma_{ij} + \tfrac{1}{2}d\sigma_{ij})d\epsilon_{ij}^p. \tag{22}$$

This proves the necessity for

$$d\sigma_{ij}d\epsilon_{ij}^p > 0, \qquad (23)^5$$

when $d\epsilon_{ij}^p$ exists and the material work hardens. As for (20), condition (23) follows directly from $\frac{\partial}{\partial \sigma_{kl}}(\sigma_{ij}d\epsilon_{ij}^p)d\sigma_{kl} > 0$.

Interpreting the preceding geometrically, as Prager has done [6], σ_{ij}, the coordinates of a stress point on the loading surface, can be considered

---

[5] This result can be shown to follow directly from a criterion of stability of equilibrium.

as a vector in stress space from the origin to the point; $d\sigma_{ij}$ is a vector in this same space. Plastic deformation occurs when $d\sigma_{ij}$ points outward from the loading surface. If the axes are now taken as representing strain instead of stress, $d\epsilon_{ij}$, $d\epsilon_{ij}{}^e$, $d\epsilon_{ij}{}^p$ also may be taken as vectors.

Linearity between the infinitesimal changes of stress and of strain, Eq. (7), means that the strain increments produced by a $d\sigma_{ij}$ can be computed by breaking $d\sigma_{ij}$ up into components none of which, however, may by themselves cause unloading. In particular, $d\sigma_{ij}$ may be decomposed into a component in the tangent plane and a component normal to the loading surface. All loading vectors may be so decomposed into one which produces elastic strain increments only and the normal component which accounts for all the plastic changes in addition to the elastic which must always occur. As $d\epsilon_{ij}{}^p$ depends upon the normal component only, its direction must be the same for all $d\sigma_{ij}$ constituting loading.

Eq. (23) states in geometric language that the scalar product of vectors $d\epsilon_{ij}{}^p$ and $d\sigma_{ij}$ must be positive, or that the angle between their directions must not exceed 90°. The only direction which makes an angle of 90° or less with all possible $d\sigma_{ij}$ constituting loading is the normal to the loading surface. Therefore, $d\epsilon_{ij}{}^p$ is proportional to $\partial f/\partial\sigma_{ij}$, a normal vector. As the magnitude of $d\epsilon_{ij}{}^p$ is proportional to the magnitude of the normal component of $d\sigma_{ij}$, the constant of proportionality will be the scalar product of $d\sigma_{ij}$ and the normal vector $\partial f/\partial\sigma_{ij}$ multiplied by a scalar function of stress, strain and history; $d\epsilon_{ij}{}^p = (G)\left(\frac{\partial f}{\partial\sigma_{ij}}\right)\left(\frac{\partial f}{\partial\sigma_{kl}}\, d\sigma_{kl}\right)$, Eq. (17).

When the material does not work-harden, by definition $d\sigma_{ij}d\epsilon_{ij}{}^p = 0$ and the angle between the stress increment vector and the plastic strain increment vector must be 90°. For plastic flow to continue, the stress increment vector which now cannot point outside must lie in the loading surface and therefore again $d\epsilon_{ij}{}^p$ is normal to the surface although Eq. (7) does not apply.

The combination of the convexity of the loading surface with respect to the origin and the normality of the strain increment vector insures the positiveness of the plastic work increment $\sigma_{ij}d\epsilon_{ij}{}^p$. This sum is the scalar product of the stress vector which is radial outward and the strain increment vector which is normal, and for positiveness the angle between them cannot exceed 90°. Convexity means that the radius and the outward normal make an acute angle with each other.

$$f = f\ (\text{stress, strain, history}).$$

If the proper expression for the loading surfaces can be written down, it has been shown that the stress strain relation for loading, $\frac{\partial f}{\partial\sigma_{ij}}\, d\sigma_{ij} > 0$, will be

$$d\epsilon_{ij}{}^p = G \frac{\partial f}{\partial \sigma_{ij}} \left(\frac{\partial f}{\partial \sigma_{kl}} d\sigma_{kl} \right), \tag{17}$$

$$d\epsilon_{ij}{}^e = C_{ijkl} d\sigma_{kl}, \tag{24}$$

$$d\epsilon_{ij} = d\epsilon_{ij}{}^e + d\epsilon_{ij}{}^p, \tag{8}$$

which should hold for all work-hardening materials obeying Eq. (7) whether isotropic or anisotropic elastically or at first yielding. For unloading, or neutral changes in stress, $\frac{\partial f}{\partial \sigma_{ij}} d\sigma_{ij} \leq 0$, Eq. (24) alone is used, and alone continues to be valid until the stress point moves outside the last established loading surface (*e.g.*, at point C in Fig. 1b).

Prager [6] has considered the special case, $f(\sigma_{ij}, \epsilon_{ij}{}^p)$ a fixed constant, in detail. The restriction on f is very severe

$$\frac{\partial f}{\partial \sigma_{ij}} \frac{\partial f}{\partial \epsilon_{ij}{}^p} < 0 \tag{25}$$

Forms such as $f(\sigma_{ij} - m\epsilon_{ij})$ are, therefore, permissible. Eq. (15), of the form $f(s_{ij} - m\epsilon_{ij})$, is exactly the same kind of function when $\epsilon_{kk}{}^p$, the sum of the principal plastic strains, is zero. In all cases, setting $df = 0$ yields

$$G = - \frac{1}{\frac{\partial f}{\partial \sigma_{kl}} \frac{\partial f}{\partial \epsilon_{kl}{}^p}},$$

and

$$d\epsilon_{ij}{}^p = \frac{\partial f / \partial \sigma_{ij}}{- \frac{\partial f}{\partial \sigma_{kl}} \frac{\partial f}{\partial \epsilon_{kl}{}^p}} \left(\frac{\partial f}{\partial \sigma_{mn}} d\sigma_{mn} \right) \cdot \tag{26}$$

However, such restriction is not necessary and, in fact, prevents the fitting of some experimental data, for, as is well known, straining a metal into the plastic range and reversing the loading to bring back the original configuration changes the original yield point. Analogously to the Prager incremental stress hardening theory, f may change in value. The function G may then be chosen as a function of stress, strain, and history to fit actual data, while for expression (15) set equal to zero it turns out that G is a constant.

$$f = f\,(\text{strain}).$$

In the plastic bending or buckling of beams, plates, and shells, total displacements or strains are usually treated as the independent variables. It would be very convenient, and it might seem quite reasonable, instead of a stress hardening theory to postulate an isotropic strain hardening theory of plasticity in which infinitesimal changes in stress are given by the existing state of strain, ϵ_{ij}, and the infinitesimal changes in strain [7]

$$d\sigma_{ij} = H_{ijkl} d\epsilon_{kl}. \tag{27}$$

This form is the inverse of Eq. (7). Isotropy even in the extended sense here, drastically restricts (27). It means that the loading surface exists in a principal strain space ϵ_1, ϵ_2, ϵ_3 (no ordering in accordance with magnitude) and is not altered by an interchange of subscripts 1, 2, 3. Strain hardening, as used here, means that the family of surfaces distinguishing loading from unloading remains fixed in strain space; successive surfaces do not intersect. Each of these surfaces is one of unchanged plastic strain and so corresponds to isolated points in a plastic strain space.

One physical difficulty with such an isotropic theory is in the shape of the loading surface it calls for. Suppose, for example, that a medium carbon steel body is subjected to simple tension, σ_1, which produces a total strain in the 1-direction of

$$\epsilon_a = \epsilon_1{}^e \text{ (say 0.002)} + \epsilon_1{}^p \text{ (say 0.02)}$$

and a strain in the cross directions $\epsilon_2 = \epsilon_3 = -\epsilon_c$ where ϵ_c is approximately half as large as ϵ_2. Isotropy then requires that $\epsilon_1 = -\epsilon_c$, $\epsilon_2 = -\epsilon_c$, $\epsilon_3 = \epsilon_a$ also be a point on the loading surface. Elastic changes in *shear* strains of over 2% are thus possible in such a theory, despite the physical incorrectness of so large a value for medium carbon steel.

Anisotropic strain hardening theories containing history could avoid this difficulty. In fact, the isotropic stress hardening type, Eqs. (1) or (2), is such a theory as it gives anisotropic surfaces in strain space which move about as the deformation proceeds.

CONCLUSION

The work of Mises and Prager is extended within the framework of present mathematical theories of plasticity. Consideration is given to the simplest theories and to general types without time effects in which the loading criterion involves strain as well as stress and the path of loading has influence. It is demonstrated that loading surfaces in stress space must be convex with respect to the origin and that the plastic strain increment considered as a vector must be normal to the surface or $d\epsilon_{ij}^p = \lambda \partial f / \partial \sigma_{ij}$ where λ is a scalar. For work hardening material $\lambda = G \left(\frac{\partial f}{\partial \sigma_{kl}} d\sigma_{kl} \right)$, where G may be a function of stress, strain and history of loading.

It is also shown that the mathematically very useful type of theory which might be termed isotropic strain hardening is unfortunately not physically permissible.

Notation. The tensor notation is used partly to save space but mainly to simplify the development and description of the ideas presented. Conversion to the usual engineering symbolism is made in the following manner:

σ_{ij} represents all or any of the components of stress, σ_x when i and j are each 1, σ_y when each are 2, τ_{xy} when $i = 1$, $j = 2$, τ_{yz} when $i = 2$, $j = 3$, *etc.*

ϵ_{ij} represents all or any of the components of strain, *e.g.*, the normal strain ϵ_x when $i = j = 1$ and *one-half* the shearing strain γ_{xy} when $i = 1$, $j = 2$.

$d\sigma_{ij}$ and $d\epsilon_{ij}$ denote infinitesimal increments in stress and strain respectively

e and p used as superscripts indicate elastic and plastic strain components as distinguished from their sum which has no superscript

s_{ij} the stress deviation is $\sigma_{ij} - \frac{1}{3}\sigma_{kk}\delta_{ij}$ where

δ_{ij} the Kronecker delta is unity for $i = j$ and zero for $i \neq j$

J_2 the second invariant, $\frac{1}{2}s_{ij}s_{ji}$, is proportional to the shear strain energy or to the square of the octahedral shearing stress

J_3 the third invariant, $\frac{1}{3}s_{ij}s_{jk}s_{ki}$, is necessary in stress hardening theories to obtain the best agreement with experimental data [4].

Repeated subscripts in a single term or product denote summation, *e.g.*,

$$\sigma_{kk} \equiv \sigma_{ii} = \sigma_x + \sigma_y + \sigma_z$$

$$\begin{aligned}\sigma_{ij}d\epsilon_{ij} &= \sigma_x d\epsilon_x + \sigma_y d\epsilon_y + \sigma_z d\epsilon_z + \sigma_{xy}d\epsilon_{xy} + \sigma_{yx}d\epsilon_{yx} + \cdots \\ &= \sigma_x d\epsilon_x + \sigma_y d\epsilon_y + \sigma_z d\epsilon_z + \tau_{xy}d\gamma_{xy} + \tau_{yz}d\gamma_{yz} + \tau_{zx}d\gamma_{zx}\end{aligned}$$

$$\begin{aligned}\frac{\partial f}{\partial \sigma_{kl}}d\sigma_{kl} = {} & \frac{\partial f}{\partial \sigma_x}d\sigma_x + \frac{\partial f}{\partial \sigma_y}d\sigma_y + \frac{\partial f}{\partial \sigma_z}d\sigma_z \\ & + \frac{\partial f}{\partial \tau_{xy}}d\tau_{xy} + \frac{\partial f}{\partial \tau_{yz}}d\tau_{yz} + \frac{\partial f}{\partial \tau_{zx}}d\tau_{zx} + \cdots\end{aligned}$$

A system of equations is abbreviated similarly, *e.g.*,

$$d\epsilon_{ij}{}^p = \lambda \frac{\partial f}{\partial \sigma_{ij}} \text{ means } d\epsilon_x{}^p = \lambda \frac{\partial f}{\partial \sigma_x}, \cdots, d\epsilon_{xy}{}^p = \lambda \frac{\partial f}{\partial \tau_{xy}},$$

while

$$\begin{aligned}\epsilon_{ij}{}^e &= C_{ijkl}\sigma_{kl} \text{ represents all equations} \\ \epsilon_x{}^e &= C_{xxxx}\sigma_x + C_{xxyy}\sigma_y + C_{xxzz}\sigma_z + C_{xxxy}\tau_{xy} + \cdots + C_{xxzx}\tau_{zx}, \textit{ etc.}\end{aligned}$$

and

$$\epsilon_{xy} = \tfrac{1}{2}\gamma_{xy} = C_{xyxx}\sigma_x + C_{xyyy}\sigma_y + C_{xyzz}\sigma_z + C_{xyxy}\tau_{xy} + \cdots + C_{xyzx}\tau_{zx}, \textit{ etc.}$$

REFERENCES

1. PRAGER, W., *J. Applied Phys.* **16**, 837–840 (1945).
2. HANDELMAN, G. H., LIN, C. C., AND PRAGER, W., *Quart. Applied Math.* **4**, 397–407 (1947).
3. HODGE, P., AND PRAGER, W., *J. Math. Phys.* **27**, 1–10 (1948).
4. DRUCKER, D. C., The Relation of Experiments to Mathematical Theories of Plasticity, *J. Applied Mech.*, to appear.
5. CUNNINGHAM, D. M., THOMSEN, E. G., AND DORN, J. E., *Am. Soc. Testing Materials Proc.* **47**, 546–553 (1947).
6. PRAGER, W., Recent Developments in the Mathematical Theory of Plasticity presented to the 7th Intern. Cong. Applied Mech., London, 1948.
7. TRIFAN, D., *Quart. Applied Math.* **6**, 417–427 (1949).

PRESENT STATUS OF THE INTRINSIC VISCOSITY DETERMINATION[1]

W. E. Davis and J. H. Elliott

From the Hercules Experiment Station, Hercules Powder Co., Wilmington 99, Delaware

Received January 24, 1949

INTRODUCTION

The intrinsic viscosity is probably the most frequently measured property of polymers, since it offers the simplest means of characterizing molecular size. For example, this determination is a useful research tool when studying polymerization, since, even if intrinsic viscosity has not been calibrated in terms of molecular weight for the particular polymer under investigation, it still may be used to give a relative measure of the extent of polymerization. In view of the widespread use of this determination, it was considered desirable to present some observations on the solution of some problems involved in such determinations and to indicate how the test has been put on a standardized basis, which makes it useful in the hands of nontechnical personnel.

EXPERIMENTAL TECHNIQUES AND EQUIPMENT

In any discussion of the elimination of errors and difficulties peculiar to viscosity determination, the kinetic energy correction must be given first consideration. With the usual type of capillary viscometers, such as the Ostwald, Cannon-Fenske, or Ubbelohde, theory does not permit the rigorous calculation of the kinetic energy correction from viscometer dimensions. The usual method of determining the magnitude of this correction is to calibrate the viscometer with two different liquids of known viscostiy according to A. S. T. M. Method D445-42T. This correction can be quite appreciable, for example, when measuring an acetone solution in a viscometer which gives approximately 100 sec. for water. Here, the correction applied to the solvent viscosity amounts to about 20%. An error of 10% in the value of the kinetic energy correction in such a case would introduce an error of approximately 2% in the specific viscosity. There are several ways in which such errors may be minimized. The length of the capillary can be greatly increased, for example, by bending it in the form of a spiral. The flow time may be increased, either by decreasing the radius or by using a more viscous solvent. A practical limit is soon reached, however, beyond which a decrease in the radius of the capillary is unsatisfactory, due to the fact that the slightest contamination of the solutions by dust or by tiny gel particles will make viscosity determinations impossible. In our laboratories we have an Ubbelohde viscometer which gives for water a flow time of about 300 sec. at 25°C. In about half of the determinations made with this viscometer, difficulty is encountered due to contamination of the solutions, and we feel that its diameter (approximately 0.5 mm.) represents about the lower limit beyond which it is undesirable to decrease capillary size. When it is practical, the use of a more viscous solvent is a satisfactory way of avoiding the necessity of using small capillaries with their resultant difficulties, while still obtaining adequate flow times. In all cases, the kinetic energy correction, determined by calibrating the viscometer with two known liquids should be applied as long as it is as great as, or greater than, the stop watch error (approximately 0.2 sec.).

---

[1] Presented at the Annual Meeting of the Society of Rheology, New York, N. Y., November 5 and 6, 1948.

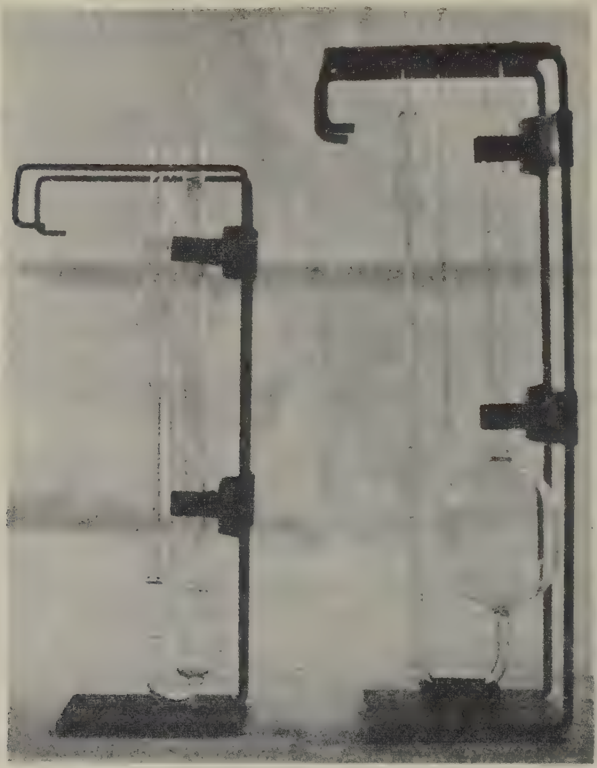

FIG. 1. Comparison of conventional (left) and modified (right) Ubbelohde viscometers.

The second difficulty we wish to discuss is one which may be encountered in accurate viscosity determinations, and which has already been mentioned, namely, erroneous flow times caused by partial plugging of the capillary by either dust or small gel particles, which are sometimes present in the solution being measured. In some cases this error may be overcome by filtering the solutions through a medium porosity sintered glass filter, or even by straining through a 100-mesh stainless steel screen. This procedure, however, suffers from the inherent disadvantage that dust from the air can get back into the solutions during ordinary manipulation, and there is always the danger of the concentration changing during the filtering operation, particularly if volatile solvents are used. These difficulties due to dust and gel may be eliminated by using a viscometer with a larger capillary radius. This procedure, however, in turn leads to lower flow times and higher kinetic energy corrections with their attendant uncertainties, unless this can be offset by using a higher viscosity solvent.

Fig. 1 shows, together with the conventional model, a modified Ubbelohde viscometer which has been evolved in our laboratory. This improved viscometer is similar to the usual commercial model in all respects except that the sample reservoir has been modified so as to have a capacity of about 120 ml. Since only 12 ml. of solution is required to determine a viscosity, using this instrument, it can be seen that such a sample, after it has been put into the viscometer, may be diluted by suitable solvent additions to as much as one-tenth of its original concentration. It has been found that, for standardized intrinsic viscosity measurements, this procedure of diluting in the viscometer markedly improves the precision of the results. In addition, when such dilutions are made, the sample is subjected to less handling and exposure to the air than when a stock solution is diluted in a separate vessel; consequently, the danger of dust contamination is minimized. The time necessary for adequate mixing of the diluted solutions averages about 5 min.

The effect of varying velocity gradients has been found to be negligible when low values (up to 5) of specific viscosity are being determined. The usual range of shear rates encountered in such measurements is about 200 to 500 reciprocal seconds.

Volume errors introduced in loading the viscometer may lead to considerable errors in viscosity in the case of the Ostwald viscometer. This source of error is minimized in the case of the Cannon-Fenske viscometer and is absent in the case of the Ubbelohde.

The observed viscosities are a very sensitive function of the concentration, and errors here lead to considerable uncertainty in the intrinsic viscosity. It has been found in this laboratory that dilution of a stock solution by volume in an Ubbelohde viscometer minimizes concentration errors, particularly when these measurements are being carried out by nontechnical personnel. Weight dilution is more accurate than volume dilution in the viscometer itself, but is not justified because of the other errors inherent in the viscosity determinations. Weight dilution, however, makes it possible to assume that the concentration of the various solutions is exact, thereby permitting a least-square determination of intrinsic viscosity. Concentration errors are generally caused by evaporation of the solvent during handling and diluting of the various solutions. This error may be minimized by diluting in the viscometer, preferably employing a solvent of low volatility.

TREATMENT OF DATA

The above observations on technique cover only part of the problem of determining intrinsic viscosity. Having obtained a good set of data, it is essential that it be treated so as to yield the maximum of useful information with the least expenditure of time and effort. In handling viscosity data obtained in the form of a series of flow times in a given viscometer on a routine basis, several extremely advantageous short cuts have been found. For example, in calibrating the viscometers, the kinetic energy correction is calculated by substituting two sets of values of η, d, and t in the equation

$$\eta = k\,d\left(t - \frac{c}{t}\right)$$

so that thereafter it is possible to calculate very rapidly the value of $\left(t - \frac{c}{t}\right)$, *i.e.*, the flow time corrected for the kinetic energy effect. It may be noted here that this correction seldom exceeds 0.5% of the flow time and is usually well below 0.3% when the methods discussed above for obtaining flow times are followed.

For the purpose of calculating intrinsic viscosity, it is not necessary actually to calculate the solution viscosities. Our usual practice is to determine intrinsic flow time; the error involved in so doing is negligible, as is shown in a later portion of this discussion. However, when reporting the results of routine determinations of intrinsic viscosity, the person who requested the work is given the actual viscosity figures. This serves two purposes: (1) the person who requested the work may wish to calculate the intrinsic viscosity himself, and may not be familiar with the fact that flow times can be used just as well as viscosities; (2) calculation of the viscosity of the solvent serves as a check on the absence of systematic errors.

The next step in the determination is to convert the data to specific viscosities (η_{sp}) or flow times and these to reduced viscosities (η_{sp}/c) or reduced flow times. In this latter calculation the actual values of concentration are not essential; we assume that the original solution turned in for determination of intrinsic viscosity is of 1% concentration and make all the calculations on that basis. Then, the reported intrinsic viscosity need only be divided by the true concentration of the original solution to obtain the true intrinsic viscosity. Since the usual dilution ratios used in the volume dilution are $\frac{2}{3}$, $\frac{1}{2}$, $\frac{2}{5}$, $\frac{1}{3}$, $\frac{1}{4}$, and $\frac{1}{5}$, this simplifies to a considerable extent the calculation of reduced flow times.

Since intrinsic viscosity is defined as the limit of reduced viscosity as the concentration approaches zero, some sort of extrapolation is necessary. This is usually a graphical extrapolation, but whether graphical or by some more elaborate statistical method, it is essential that the function plotted be a linear function of concentration. Also, this linearity should hold and the data should be taken over a range of concentrations several times (in our work 5–15 times) the range of the extrapolation. These requirements are best filled by the Martin (1) and Baker (2) equations:

$$\log \eta_{\text{sp}}/c = \log [\eta] + k[\eta]c, \tag{1}$$

$$\eta_r = \left(1 + \frac{[\eta]c}{a}\right)^a, \tag{2}$$

Both of these equations are used in our work. The Baker equation is particularly useful in that it affords an accurate representation of viscosity data up to higher concentrations than the Martin equation. However, in order to plot the Baker equation, the exponent a must be known, and this involves a series of trials of different values of a to see which one gives the best straight line. When the viscosity data are for low concentrations this decision is not easy because in plotting $\eta_r^{1/a}$ against c the low power of η_r makes the linearity relatively insensitive to variations in a at low values of η_r. Fortunately, the value of $[\eta]$ obtained is also relatively insensitive to variations in a when the concentrations are low, so that the practice, recently become fairly common in the literature, of using $a = 8$ for all systems can yield good values of $[\eta]$.

When Eqs. (1) and (2) are solved for η_{sp} and the resulting expressions expanded as power series in $[\eta]c$, it becomes apparent that, at low concentration, k and a are connected by the relation

$$\frac{a-1}{2a} = 2.303\ k. \tag{3}$$

Any variation in k must be accompanied by a corresponding change in a, and, as the data in Table I show, k quite commonly varies from 0.15 to 0.20 for a single system, which corresponds to a change in a from 3.2 to 13, approximately. Since, as discussed below, it is frequently desirable to know something about the comparative concentration behavior of viscosity for several samples, and the Baker equation is quite unadapted to show up such variations, the Martin equation is usually employed in handling data at low concentrations. It gives, in a single plot, values of both $[\eta]$ and the slope constant k. The latter may, to a first approximation, be considered as a constant for a given solute-solvent system; that it varies with both solute and solvent is shown in Table II. Examination of numerous values of k for a single solute-solvent system shows, however, that variations in k occur which are greater than experimental error and, moreover, are susceptible of explanation on the basis of known variations in the structure of the solute. This is the case with the data for nitrocellulose in Table I. It is apparent that a given cellulose nitrated with a mixture containing phosphoric acid has a higher k than the same cellulose nitrated with a mixture in which the diluent is acetic acid. Also, of a series of samples all nitrated with the phosphoric mixture, those with higher $[\eta]$ tend to have higher values of k and, on fractionation, the material with high k tends to concentrate in the first fractions. These phenomena are all consistent with the idea that variations in k can be due to presence in the polymer of a group, such as $-OPO_3H_2$, capable of creating a strong attraction between

TABLE I

Slope Constants of Various Nitrocelluloses

Nature of sample	k in Martin Eq.
Head fraction of cellulose nitrate	0.17
Tail fraction of cellulose nitrate	0.15
Low-viscosity cellulose nitrate	0.16
High-viscosity cellulose nitrate	0.20
Cellulose nitrated with H_3PO_4 mixture	0.20
Cellulose nitrated with acetic acid mixture	0.18

TABLE II

Slope Constants for Various Solutes and Solvents

Solute	Solvent	Average k
Cellulose	Cuprammonium	0.12
Cellulose	Cupriethylenediamine	0.18
Cellulose nitrate	Acetone	0.16
Cellulose acetate	Acetone	0.19

TABLE III

Variations in Slope Constant for Ethyl Cellulose

Nature of sample	k in Martin Eq.
No bound metal	0.148
0.02 meq. COOH/g., neutralized with Ba	0.240
0.03 meq. COOH/g., neutralized with Ba	0.285
0.03 meq. COOH/g., neutralized with Na	0.163

chains. This is shown even more clearly by the data for ethylcellulose in Table III, where the slope constant depends on the carboxyl content of the polymer and on the amount of divalent metal ion present. Such variations, which are frequently of significance in connection with other properties of cellulose derivatives, are most easily detected by use of the Martin equation.

TABLE IV

Fit of Data for Cellulose Nitrate with Martin Equation

Concentration g./100 g.	Log reduced viscosity (log η_{sp}/c)	
	Observed	For least-squares line
0.0998	1.348	1.348
0.0596	1.242	1.242
0.0445	1.203	1.203
0.0291	1.162	1.162
0.0086	1.109	1.109
0.1010	1.387	1.382
0.0602	1.282	1.284
0.0450	1.241	1.247
0.0294	1.202	1.209
0.0087	1.169	1.159
0.0980	1.061	1.063
0.0568	1.002	1.001
0.0416	0.979	0.979
0.0263	0.958	0.956
0.0066	0.925	0.927
0.0980	0.672	0.669
0.0586	0.644	0.645
0.0438	0.635	0.637
0.0288	0.623	0.628
0.0088	0.622	0.616
0.0613	1.451	1.450
0.0366	1.356	1.359
0.0274	1.325	1.325
0.0181	1.292	1.290
0.0055	1.243	1.245

In applying the Martin equation to a given set of data, the question sometimes arises whether the concentrations should be in g./100 ml. or g./100 g. It is apparent from an examination of Eq. (1) that the straight line relation cannot hold in both cases. However, the deviation depends only on the rate of increase of density with concentration and, as this is usually small, the difference is within experimental error. The values of k obtained when concentrations in g./100 g. are used will be slightly higher than that obtained with concentrations in g./100 ml., while if $[\eta]_w$ is the intrinsic viscosity based on g./100 g., $[\eta]_v$ that based on g./100 ml.,

$$[\eta]_w = [\eta]_v d_o,$$

where d_o is the density of the solvent. It might also be pointed out here that the use of flow times in place of actual viscosities has no effect on $[\eta]$, and gives a slightly lower value of k, thus helping to compensate for the use of concentrations in g./100 g.

Finally, by way of illustration, the data in Table IV are presented to show the goodness of fit for viscosity data with the Martin equation. It can be seen that this is very good, and, in fact, taking into account the standard deviations in calibrating the viscometer and determining the flow times on the unknown, it can be shown that the standard deviation in $[\eta]$ is almost always less than 2% and frequently less than 1%.

Using the dilution viscometer on a routine basis, duplicate determinations of intrinsic viscosity generally give results showing a maximum spread of 2% of the average.

SUMMARY

To summarize, the points which appear to us of importance in making rapid, accurate determinations of $[\eta]$ and at the same time obtaining as much accessory information as possible are as follows:

(1) Filtration of all solutions (including solvent) and exclusion of dust from all apparatus to as great an extent as possible;

(2) Use of a viscometer with a large enough capillary to reduce difficulties due to residual dust, together with a high-viscosity solvent to give higher flow times;

(3) For rapid work, dilution by volume in the viscometer; for most accurate work, dilution by weight using a solvent of low volatility to reduce concentration errors;

(4) Application of the kinetic energy correction whenever it equals or exceeds stop watch error;

(5) Use of flow times rather than actual viscositites for calculation of η_{sp}/c;

(6) Optionally, use of artificial concentrations based on assumption that stock solution is 1%, followed by correction of intrinsic viscosity to basis of true concentration;

(7) Extrapolation of η_{sp}/c to infinite dilution by means of the Martin equation, whereby both $[\eta]$ and the slope constant are obtained.

APPLICATION OF THE RISING-COLUMN CAPILLARY VISCOMETER TO THE HIGH-VISCOSITY RANGE[1]

F. S. Stow, Jr., K. H. Horowitz and J. H. Elliott

Hercules Experiment Station, Hercules Powder Co., Wilmington 99, Delaware

Received February 15, 1949

ABSTRACT

The rising-column capillary viscometer has been adapted to the determination of the viscosity of liquids having viscosities of 10^3–10^5 poises or higher. The operation of this instrument has been analyzed, taking into account apparatus constants and sources of error such as kinetic energy, surface tension, annular pressure drop, and possible end effects. Several forms for the equation for the viscosity in terms of apparatus constants and applied pressure are presented and their range of applicability analyzed. Based on this analysis, a set of instruments has been constructed and tested with hydroabietyl alcohol (50,000–75,000 poises) at room temperature. The results were checked by determination of the viscosity by the falling-ball method at comparable maximum shear rates, 0.001–0.015 sec.$^{-1}$. The results by these independent methods are in good agreement.

INTRODUCTION

The rising-column capillary viscometer has been in use for a number of years. Pochettino (1) in 1914 used it to determine the viscosity of bituminous materials. Rhodes, Volkmann and Barker (2) have extended the mathematical foundation, and Flory (3) has used the method to determine the viscosity of molten linear polyesters.

This method has been in use in our laboratories for about 10 years for the determination of the viscosity of a molten dark-colored resin. An extension of this method was, therefore, considered when it recently became necessary to determine the viscosity of polymer solutions having viscosities of 10^3–10^5 poises or above. It was also desired to examine these solutions at very low maximum shear rates and to investigate the effect of different maximum shear rates.

The rising-column capillary viscometer is shown schematically in Fig. 1. It offers a number of advantages for this type of investigation. A wide range of viscosities may be measured by this type of instrument, since, by a judicious selection of tube radius, length of flow, and applied pressure, determinations may be made in a reasonable time. In addition, by suitable changes in applied pressure, measurements at a number of shear rates can be made consecutively with only one charging of the viscometer. This is particularly true if the length of flow per determination is kept small, which was done in this work. Use of a cathetometer to measure this length permits a length of 2 mm. to be used with no loss in accuracy. This type of viscometer has the further advantages that only a small sample is required, the entire apparatus may be immersed in a liquid thermostat, it is easy to clean, and bubbles in the liquid under investigation, which are particularly troublesome in measurements on high-viscosity materials, may be removed before the capillary is immersed.

---

[1] Presented at the Annual Meeting of the Society of Rheology, New York, N. Y., November 5 and 6, 1948.

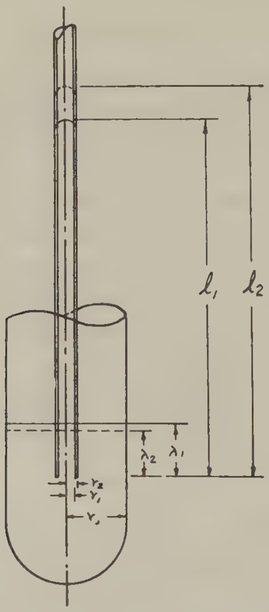

FIG. 1. Schematic diagram of rising-column capillary viscometer.

After preliminary experimentation, it was found that the viscosities calculated from instrument constants, using the equation given by Rhodes, Volkmann and Barker (2), were not in good agreement with simultaneous measurements made on the same liquid by the falling-ball method. This is undoubtedly due to the markedly different conditions of operation used in the present work, namely, low pressures, short length of capillary filled by the liquid, larger capillary radii, relatively small annulus, and small lengths of flow. It was also suspected that errors due to surface tension, annular pressure drop, and possible end effects might be present. Therefore, an analysis of the instrument was carried out so that apparatus constants and operating conditions could be selected to eliminate or minimize errors.

Fig. 1 shows the essential dimensions of the viscometer, together with their symbols. Pochettino calculated viscosity in poises (η) using the equation:

$$\eta = \frac{gH\gamma_1^2\Delta t}{4(l_2^2 - l_1^2)} \tag{1}$$

where H is the applied pressure in cm. of water. This is simply Poiseuille's Law and does not take into account the effect of the column height on the applied pressure. H. Rhodes, Volkmann and Barker (2) took this static head of the column into account, and derived the following equation:

$$\eta = \frac{g\gamma_1^2\rho\Delta t}{8\left[\left(\frac{H}{\rho} + \lambda\right)\ln\frac{\left(\frac{H}{\rho} + \lambda\right) - l_1}{\left(\frac{H}{\rho} + \lambda\right) - l_2} - (l_2 - l_1)\right]}, \tag{2}$$

where ρ is the density of the liquid and λ is the length of capillary submerged in the sample. In our preliminary experiments the change in λ amounted to 2–4% of the change in l during the course of a measurement. An attempt to correct for this by modifying Eq. 2 by inserting the true final effective pressure in the logarithmic term gave:

$$\eta = \frac{g\gamma_1^2\rho\Delta t}{8\left[\left(\frac{H}{\rho} + \lambda\right)\ln\frac{\left(\frac{H}{\rho} + \lambda\right) - l_1}{\left(\frac{H}{\rho} + \lambda\right) - l_2 - \Delta\lambda} - (l_2 - l_1)\right]}. \tag{3}$$

As will be shown later, this equation was unsatisfactory. Therefore, an analysis of the instrument was carried out considering λ as a variable.

Referring to Fig. 1, H is the external pressure in g./cm.^{2} under which, in time Δt, the liquid of density ρ(g./cm.^{3}) flows from l_1 to l_2 in the capillary and λ_1 to λ_2 in the annulus. At any instant Poiseuille's Law will be obeyed (kinetic energy correction negligible)

$$\eta = \frac{\pi g r_1^4 P\Delta t}{8l\Delta V}, \tag{4}$$

where P is the effective pressure, and $\Delta V/\Delta t$ is the volume rate of flow. This reduces to:

$$\eta = \frac{g r_1^2 P\Delta t}{8l\Delta l}. \tag{5}$$

The instantaneous pressure is given by:

$$P = H + \rho\lambda - \rho l. \tag{6}$$

It is obvious that l and λ are related since:

$$-\pi(r_3^2 - r_2^2)\Delta\lambda = \pi r_1^2 \Delta l, \tag{7}$$

where r_3 is the radius of the container and r_2 is the outer radius of the capillary.

$$-\Delta\lambda = A\Delta l, \qquad \text{where} \qquad A = \frac{r_1^2}{r_3^2 - r_2^2},$$

λ at any instant is given by:

$$\lambda = \lambda_1 + A(l_1 - l) \tag{8}$$

Substituting this value in Eq. 6

$$P = H + \rho\lambda_1 + A\rho(l_1 - l) - \rho l, \tag{9}$$

or

$$P = H + \rho\lambda_1 + A\rho l_1 - \rho l(A + 1).$$

This value of P is now substituted into Eq. 5, the differences changed to differentials, and the resulting equation integrated between the limits l_1 at t_1 and l_2 at t_2. This leads to the following expression for η:

$$\eta = \frac{\rho g r_1^2 \Delta t (A+1)^2}{8\left[\left(\frac{H}{\rho} + \lambda_1 + A l_1\right) \ln\left[\frac{\frac{H}{\rho} + \lambda_1 - l_1}{\frac{H}{\rho} + \lambda_1 - A(l_2 - l_1) - l_2}\right] - (A+1)(l_2 - l_1)\right]} \tag{10}$$

As has been pointed out by earlier workers (2), this type of equation is arithmetically weak when the two terms in the denominator become nearly equal, which is the case when the viscosity is very high ($>10^5$ poises). The term $(l_2 - l_1)$ is determined experimentally and amounts to a fraction of a centimeter, estimated to 4 decimal places. The difference between the terms in the denominator is then known to only two significant figures. To overcome this difficulty, Eq. 10 was expanded in series form to give:

$$\eta = \frac{g r_1^2 \Delta t}{8\left(\frac{1/2(l_2^2 - l_1^2)}{H + \rho\lambda_1 + \rho A l_1} + \frac{1/3(l_2^3 - l_1^3)(A + 1)}{(H + \rho\lambda_1 + \rho A l_1)^2} + \cdots + \frac{[1/(n + 1)](A + 1)^{n-1}(l_2^{n+1} - l_1^{n+1})}{(H + \rho\lambda_1 + \rho A l_1)^n}\right)}. \tag{11}$$

This equation (11) is equally useful in both the high- and low-viscosity ranges. When H is less than 3 times the magnitude of l, however, the series converges quite slowly and the solution becomes quite burdensome.

Since solutions of all the above equations for viscosity in terms of instrument constants involve laborious calculations, an equation

$$\eta = \frac{gr_1^2[H - \rho(l_a - \lambda)]\Delta t}{8l_a\Delta l}, \tag{12}$$

was derived from Poiseuille's Law. Here $l_a = \frac{l_1 + l_2}{2}$ and λ is an assumed constant depth of immersion.

Before the final viscometers were constructed it was considered desirable to establish the range of operating conditions under which each of these equations (2, 3, 10, 11, 12) would be valid. An instrument could then be designed for which the simplified Eq. (12) could be used for most of the expected experimental work.

The ranges of synthetic data used for testing these equations are as follows:

$$\frac{g\gamma_1^2\rho\Delta t}{8} = 5000 \text{ g./sec.}$$

$\rho = 1.0000$ g./cm.^{3}
$r_1 = 0.2000$ cm.
$\lambda_1 = 1.0000$ cm.
$t = 1000$ sec.
$A = 0.0500$
$l_1 = 1.0000$ to 10.0000 cm.
$l_2 = 1.2000$ to 10.2000 cm.
$\Delta l = 0.2000$ to 6.0000 cm.
$H = 4.000$ to 109.000 g./cm.^{2}

These data are similar to those met under experimental conditions. Various combinations of these conditions were chosen and viscosities calculated by each of these 5 equations. Eqs. 10 and 11 are theoretically correct and identical, and were used as a reference. Under certain conditions Eq. 10 lacks precision, and under others the series expansion in Eq. 11 converges very slowly. In cases where the results calculated by these equations did not agree, the obviously appropriate equation was used.

These calculations led to the following general conclusions: Eq. 2 falls down under conditions where the logarithmic term is nearly equal to unity, which occurs when the applied pressure is high (about 50 cm. of H_2O) and the measured length of flow is small. In addition, if the experimental conditions are such that the depth of immersion changes appreciably, this equation is inadequate. Eq. 3, which contains an approximate correction for change in depth of immersion, is unsatisfactory in all cases tested, giving low values consistently and sometimes leading to grossly incorrect results.

Eq. 10, like Eq. 2, becomes arithmetically weak when the logarithmic term approaches unity. Eq. 11, which is mathematically equivalent to Eq. 10, converges very slowly when the net pressure is below 2 cm. of H_2O, thus requiring the computation of an unreasonable number of terms.

Since it was desired to utilize the arithmetically simple Eq. 12 with the final viscometers, the conditions under which its use is possible were carefully investigated. As would be expected, it is inapplicable when there is any appreciable change in the depth of immersion. In addition, the change in length of filled capillary must be kept small, since, when this changes by a factor of two or more, the time average length differs appreciably from the simple average length used in this equation. With sufficiently small lengths of flow, where the simple average may be safely used, any kinetic energy correction vanishes, since we have essentially uniform flow through a portion of a long tube (4).

It was thought that the pressure drop in the annulus might be appreciable. This was calculated using the equation given by Page (5).

$$\frac{V}{t} = \frac{\pi(r_3^2 - r_2^2)\Delta P}{8\eta l}\left[(r_3^2 + r_2^2) - \frac{(r_3^2 - r_2^2)}{\ln\frac{r_3}{r_2}}\right], \qquad (13)$$

where V is the volume of liquid discharged. It was found that, under any reasonable operating conditions, this annular pressure drop necessitated an insignificant correction to the applied pressure. The surface tensions of typical liquids to be investigated were measured, and a maximum pressure effect of 0.2 g./cm.^{2} calculated. For conditions of low pressure and short length of filled capillary this effect may amount to 5–6%, but, with higher pressures and greater lengths of filled capillary, this effect is reduced to 0.2%. The final correction considered was the so-called end effect which consists of a hypothetical addition of the length of the capillary to account for the resistance in the sample caused by converging stream lines. The literature is by no means clear on the exact magnitude of this effect or even on its existence (6,7). A reasonable maximum correction for this effect, assuming its existence, is an addition to the length of the tube equal to one tube radius. Such an addition introduces a considerable correction when the height of liquid column is short, but becomes a maximum of 2% when the height is 10 cm. or greater.

Based on the above analysis, rising-column capillary viscometers were designed and constructed to incorporate the following operating features which permit the use of the simplified Eq. 12:

1. Change in depth of immersion negligible.
2. Change in height of filled capillary during measurement less than 5% of the average height.

3. Height of liquid in the capillary in the range of 8–12 cm.
4. Flow measured over intervals of less than 1 cm., using a cathetometer.

EXPERIMENTAL

The viscometer used in this work is shown in Fig. 2. In this particular instrument, r_1 is 0.3846 cm., r_2 0.6406 cm., and r_3 1.0948 cm. (See Fig. 1 for definition of terms.) r_1 was measured directly with a cathetometer and r_2 with micrometer calipers, while r_3 was calculated from weight measurements when loaded with mercury to 2 different levels. All are average values. A series of height and weight measurements on a mercury column in the capillary showed a maximum variation of 2% in r_1 over the length of the capillary.

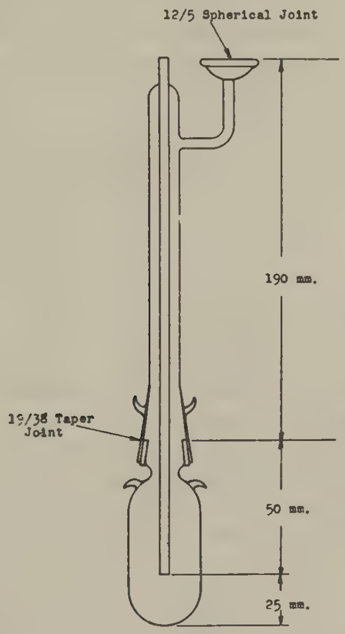

FIG. 2. Rising-column capillary viscometer.

The experimental procedure was as follows: The viscometer vessel was loaded with hydroabietyl alcohol (Abitol [2]) to a height 1 cm. above the bottom of the capillary. After allowing sufficient time for the bubbles to reach the surface of the sample, the capillary was inserted, and the assembled viscometer placed in the constant temperature bath. Nitrogen, applied under pressure to the side arm of the viscometer, forced the liquid up the clean capillary. After a height of 10 cm. was reached, a series of rate measurements was made under varying pressures. The meniscus was timed over a rise of not less than 2 mm. and over a time interval of not less than 2 min. All height measurements (λ, l_1, l_2, and the manometer column) were made with a cathetometer.[3] In each series, 5 or more determinations were made before removing and cleaning the capillary.

---

[2] Registered trademark U.S. Pat. Off.

For comparison, the viscosity was determined by the falling-ball method, using a 2.5 × 35 cm. Pyrex tube and steel balls of diameters 0.0620 in. and 0.2556 in. The tubes were loaded with a portion of the same sample used for the capillary viscometer. The two instruments were placed in the same constant-temperature water bath, and measurements carried out simultaneously. These precautions were necessary, owing to the great temperature coefficient of viscosity of hydroabietyl alcohol in this range. The balls were timed for falls of 1 to 4 mm., with the balls at least 50 mm. apart and 50 mm. from the top or bottom of the tube. The time interval was always greater than 3 min.

Viscosities by the capillary method were calculated using Eq. 12, which is accurate to about ±1% for these conditions. For the falling-ball method the Faxen modification of Stokes' Law was used (8):

$$\eta = \frac{2}{9}\frac{gr^2(D-d)t}{S}\left(1 - 2.104\left(\frac{r}{R}\right) + 2.09\left(\frac{r}{R}\right)^3 - 0.95\left(\frac{r}{R}\right)^5\right), \qquad (14)$$

where g is the acceleration of gravity;
D is the density of the sphere;
d is the density of the liquid;
S is the distance fallen in time t;
r is the radius of the sphere;
R is the radius of the cylinder containing the liquid.

The maximum shear rate for capillary viscometers is given by $\frac{4\Delta l}{\Delta t r_1}$ (9), while that for the falling-ball method is given by $\frac{3S}{2rt}$ (10).

The compressed gas for operation of the viscometer is supplied by a reservoir, whose pressure was maintained by a suitable bubble tube. A mercury manometer, connected to the reservoir and read with the cathetometer, indicates the pressure applied to the side arm of the viscometer.

The water bath, in which the viscometers were immersed, was equipped with cooling coils for use below room temperature. The temperature was controlled to approximately ±0.02°C. In the high-viscosity range for hydroabietyl alcohol, this temperature variation will cause a viscosity variation of about ±2%.

---

[3] For pressures above 5 cm. of water, a mercury manometer was used and the readings converted to pressures in cm. of water. A Gaertner cathetometer with a range of 10 cm., which could be read to 0.0001 cm. was used for all length measurements.

TABLE I

Viscosity Determinations on Hydroabietyl Alcohol

Vertical capillary viscometer

Temp.	ρ	Time	λ_1	l_1	l_2	Δl	H	Viscosity	Max. shear rate
(°*C.*)	(*g./cm.*^{3})	(*sec.*)	(*cm.*)	(*cm.*)	(*cm.*)	(*cm.*)	(*cm.* H_2O)	(*poises*)	(*sec.*$^{-1}$)
18.0	1.004	658.0	2.1608	10.2291	10.4517	.2226	61.1949	70,420	.00704
18.0	1.004	3463.2	2.1276	11.2648	11.4674	.2026	19.2294	69,580	.00122
18.0	1.004	1539.6	2.0856	11.8823	12.1037	.2214	36.4059	71,400	.00299
19.0	1.003	591.0	1.9948	11.5940	11.7914	.1974	54.3200	53,080	.00695
19.0	1.003	677.2	1.9967	11.9054	12.1238	.2184	54.3200	53,080	.00671
19.0	1.003	462.0	1.9682	12.4334	12.6427	.2093	76.2519	56,060	.00903
19.0	1.003	481.2	1.9570	12.7375	12.9486	.2111	76.2519	53,910	.00913
19.0	1.003	339.6	1.9483	13.3082	13.5462	.2380	118.7666	52,990	.01458
19.0	1.003	343.6	1.9168	13.7166	13.9476	.2310	118.7666	53,400	.01398

Falling-ball method

Temp.	ρ	Diam. of ball (density =7.80)	Reading 1	Reading 2	Drop	Time	Viscosity	Max. shear rate
(°*C.*)	(*g./cm.*^{3})	(*cm.*)	(*cm.*)	(*cm.*)	(*cm.*)	(*sec.*)	(*poises*)	(*sec.*$^{-1}$)
18.0	1.004	0.1575	2.8054	2.5937	.2117	1919.6	72,920	.00210
18.0	1.004	0.1575	2.5845	2.3719	.2126	1924.2	72,780	.00211
18.0	1.004	0.6492	3.3169	3.0834	.2335	218.0	71,100	.00506
18.0	1.004	0.6492	3.0508	2.8130	.2378	229.2	73,400	.00490
19.0	1.003	0.1575	6.1466	6.0164	.1302	860.4	53,146	.00288
19.0	1.003	0.6492	5.0583	4.7108	.3475	233.4	51,130	.00703
19.0	1.003	0.6492	4.6007	4.2866	.3147	213.0	51,550	.00698
19.0	1.003	0.6492	4.1754	3.9006	.2748	184.4	51,100	.00704
19.0	1.003	0.1575	6.0020	5.7993	.2027	1365.8	54,190	.00283

DISCUSSION

Table I and Figs. 3 and 4 show the results obtained where this rising-column capillary viscometer was used to determine the viscosity of hydroabietyl alcohol at 18.0 and 19.0°C. These results are compared with simultaneous measurements made using the falling-ball method. The viscosity was plotted against maximum shear rate, because it was suspected that hydroabietyl alcohol might exhibit non-Newtonian behavior. No evidence of such behavior was found. It will be noted that viscosities determined by these two methods are in good agreement, the deviations being random and of the order of ±2%. Part of this deviation is undoubtedly due to inadequate temperature control, as previously mentioned.

This work demonstrated the correctness of the design and selection of operating conditions of the rising-column capillary viscometer. It has

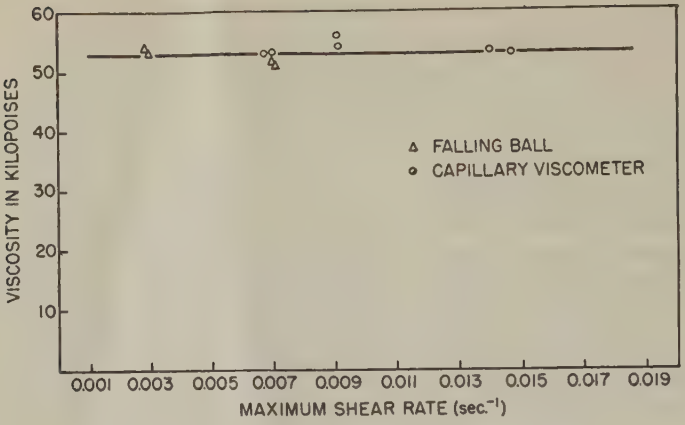

Fig. 3. Viscosity of hydroabietyl alcohol at 19.0°C.

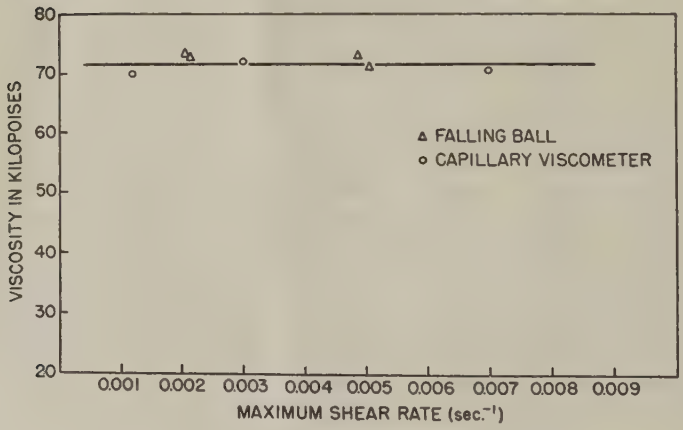

Fig. 4. Viscosity of hydroabietyl alcohol at 18.0°C.

been used in our laboratories to investigate the rheological properties of polymer solutions over the range of viscosities 5,000–130,000 poises.

For this type of investigation, the particular advantages of this viscometer—namely, small sample required, ease of removing bubbles, and very low but continuously variable maximum shear rates—enabled measurements to be made under conditions where other common viscometric methods are impractical.

References

1. Pochettino, A., *Nuovo Cimento* **8**, 77 (1914).
2. Rhodes, E. O., Volkmann, E. W., and Barker, C. T., *Eng. News-Record* Nov. 21, 1935.

3. Flory, P. J., *J. Am. Chem. Soc.* **62**, 1057 (1940).
4. Hatschek, E., Viscosity of Liquids, p. 20. D. Van Nostrand, New York, 1928.
5. Page, L., Introduction to Theoretical Physics, 2d Ed., p. 260. D. Van Nostrand, New York, 1935.
6. Bingham, E. C., Fluidity and Plasticity, p. 21 ff. McGraw-Hill, New York, 1922.
7. Barr, G., A Monograph of Viscometry, p. 20 ff. Oxford Univ. Press, London, 1931.
8. Faxen, H., *Ann Physik* **68**, 8 (1922).
9. Ref. 7, p. 275.
10. Ref. 7, p. 280.

THE INTERPRETATION OF OBSERVED PRESSURE GRADIENTS IN LAMINAR FLOW OF NON-NEWTONIAN LIQUIDS THROUGH TUBES

J. G. Oldroyd

From Courtaulds, Limited, Research Laboratory, Maidenhead, England

Received November 4, 1948

INTRODUCTION

The interpretation of observations on laminar flow of non-Newtonian liquids and plastic solids in straight tubes, in particular the detection of anomalous behavior near the tube wall, has received considerable attention in the literature [*cf.* Scott Blair (1)]. Recent experiments in this laboratory on flow of high-polymer solutions through tubes are described by Toms (2,3). The observation of some unexpectedly high rates of flow when the mainstream is turbulent may, it is thought, indicate a persistence of anomalous behavior near the tube wall, even when the mainstream has ceased to be laminar. A method has been suggested elsewhere (4) for detecting a wall effect when the main stream is fully turbulent; in the present paper, we consider the methods that are available for interpreting observations on laminar flow through straight tubes of uniform circular cross-section. We are not concerned here with end corrections, but shall assume that a sufficient number of readings with different tube lengths are available, so that the pressure gradient in the region of steady flow is known as a function of the volume rate of flow. We may then assume that we are dealing with smoothed data rather than discrete observations.

The following notation is used:

a	internal radius of tube.
e_{rz}	rate-of-strain tensor component in shear ($\frac{1}{2}\partial w/\partial r$ in axially symmetric rectilinear flow).
p	isotropic pressure, assumed a linear function of z only.
p_{rz}	stress tensor component in shear.
Q	volume rate of flow.
r	radial distance from axis of tube.
w	velocity component in z-direction, assumed a function of r only.
z	distance measured along tube axis in direction of flow.
ϵ	thickness of anisotropic layer near tube wall.
ζ	effective slip coefficient at tube wall.
ζ_0, ζ_1	limiting values at low and at high stresses, respectively.

η	viscosity.
η_0, η_1	limiting viscosities at low and at high rates of shear.
ϑ	Bingham yield value, defined as the intercept on the stress axis of the asymptote to the stress/rate-of-strain curve.
ρ	density (constant).
σ, σ_0	variables of the "sigma phenomenon" (5).
τ	$-\frac{1}{2}a\,dp/dz$, the shear stress at the tube wall.
ϕ	$-8Q/(\pi a^4 dp/dz)$, the apparent fluidity as defined by Poiseuille's formula.

Several authors (5,6,7,8) have pointed out that, on the assumptions of

(i) rectilinear flow with axial symmetry (w, a function of r only, as the only velocity component),

(ii) the absence of slip at the wall ($w = 0$ on $r = a$),

(iii) a functional relationship in simple shear connecting rate of strain and shear stress

$$e_{rz} = f(p_{rz}), \tag{1}$$

the odd function f being completely defined by physical constants of the material,

the functional relationship connecting $Q/(\pi a^3)$ and τ (or ϕ and τ) is independent of tube diameter. The relationship is given by Schofield and Scott Blair (5) as

$$\frac{Q}{\pi a^3} = \frac{4}{\tau^3}\int_0^\tau \xi d\xi \int_\xi^\tau f(x)dx.$$

After an integration by parts, it may be written in the form

$$\phi = \frac{8}{\tau^4}\int_0^\tau \xi^2 f(\xi)d\xi = F(1/\tau), \tag{2}$$

where

$$F(\xi) \equiv 8\xi^4 \int_0^{1/\xi} x^2 f(x)dx. \tag{3}$$

It is suggested that from the observed dp/dz and Q, ϕ be plotted against $1/\tau$ for different tube diameters on the same diagram. When (ϕ, $1/\tau$) curves for different diameters coincide, this method appears to have advantages over others. If the curves show a spread, we conclude—as with (ϕ, τ) or $[Q/(\phi a^3), \tau]$ curves (5,9)—that the assumption (iii) needs modification near the tube wall. The two possibilities are considered separately below. In all cases, the relationship (Eq. 1) is assumed to hold in steady flow in the bulk of the material *remote from boundaries*. The viscosity η, a function of shear stress (or of rate of strain) is defined by $1/(2\eta) = f(p_{rz})/p_{rz}$; in particular $1/(2\eta_0) = f'(0)$, and $1/(2\eta_1) = f'(\infty)$.

Isotropic Materials

If the (ϕ, $1/\tau$) curve is unique, there is justification for assuming that the liquid (or plastic solid) is behaving isotropically everywhere, including the immediate neighborhood of the wall. Then the even function F is known (graphically) and the stress/rate-of-strain relationship (Eq. 1) can in theory be deduced by noting that

$$f(\xi) \equiv \frac{1}{8\xi^2}\frac{d[\xi^4F(1/\xi)]}{d\xi}. \tag{4}$$

(*Cf.* Rabinowitch (6) and Mooney (8), who give a formula for rate of shear at the wall as a function of τ involving differentiation of a known functional relationship.) In practice, a very sharply defined smooth curve is needed before the differentiation involved in Eq. (4) can be carried out numerically. But a good deal of qualitative, and some quantitative, information about the function f can be deduced simply by inspection of the $(\phi, 1/\tau)$ graph. This is best achieved by recording for comparison the $\phi = F(1/\tau)$ curves which correspond to some of the simple idealized forms of $e_{rz} = f(p_{rz})$ curves as follows. Since f is defined to be an odd function, it suffices to restrict attention to positive arguments.

a. Newtonian Liquid. For a liquid of constant viscosity η_1, $f(\xi) \equiv \xi/(2\eta_1)$, and it is easily verified by substituting in Eq. (3) and integrating that $F(\xi) \equiv 1/\eta_1$. The apparent fluidity $F(1/\tau)$ is a constant, as it must be. More generally, if the experimental values of ϕ and $1/\tau$ are plotted to give a graphical representation of $\phi = F(1/\tau)$, the departure from the form $\phi =$ constant is a measure of the extent to which the liquid is not Newtonian.

b. Bingham Solid. A plastic material with yield value ϑ and constant mobility η_1 gives

$$\begin{aligned}
f(\xi) &= 0 && (\xi \leqslant \vartheta),\\
f(\xi) &= \tfrac{1}{2}(\xi - \vartheta)/\eta_1 && (\xi \geqslant \vartheta),\\
F(\xi) &= (1 - \tfrac{4}{3}\vartheta\xi + \tfrac{1}{3}\vartheta^4\xi^4)/\eta_1 && (\xi \leqslant 1/\vartheta),\\
F(\xi) &= 0 && (\xi \geqslant 1/\vartheta).
\end{aligned}$$

c. Liquid with Viscosity Decreasing as Rate of Shear Increases. A liquid with $\eta_0 > \eta_1$ and Bingham yield value ϑ is represented by an idealization in which the stress/rate-of-strain curve consists of two straight lines, thus:

$$\begin{aligned}
f(\xi) &= \tfrac{1}{2}\xi/\eta_0 && [\xi \leqslant \eta_0\vartheta/(\eta_0 - \eta_1)],\\
f(\xi) &= \tfrac{1}{2}(\xi - \vartheta)/\eta_1 && [\xi \geqslant \eta_0\vartheta/(\eta_0 - \eta_1)],\\
F(\xi) &= [1 - \tfrac{4}{3}\vartheta\xi + \tfrac{1}{3}\eta_0^3\vartheta^4\xi^4/(\eta_0 - \eta_1)^3]/\eta_1 && [\xi \leqslant (\eta_0 - \eta_1)/(\eta_0\vartheta)],\\
F(\xi) &= 1/\eta_0 && [\xi \geqslant (\eta_0 - \eta_1)/(\eta_0\vartheta)].
\end{aligned}$$

d. Liquid with Viscosity Increasing as Rate of Shear Increases. The idealization of this case is formally the same as (*c*) with $\eta_0 < \eta_1$ and a negative value of ϑ.

Graphical representations of $f(\xi)$ and $F(\xi)$ are given in Figs. 1 and 2 for the cases (*a*), (*b*), (*c*) with $\eta_0 = 5\eta_1/3$, and (*d*) with $\eta_0 = 3\eta_1/5$ and

$-\vartheta$ as Bingham yield value. It is seen that distinct forms of $(\phi, 1/\tau)$ curves result from distinct forms of stress/rate-of-strain curves. It should, therefore, be possible, with this method of plotting, to see at a glance the manner in which any particular liquid under consideration departs from Newtonian behavior. The general character of the stress/rate-of-strain relationship can be inferred by comparing an observed $\phi = F(1/\tau)$ graph with the special forms (*a*), (*b*), (*c*), (*d*), without detailed analysis of particular deviations from these types. It is also possible to obtain quantitative information about the function f by inspection of $F(1/\tau)$ in the limiting cases of τ small and τ large in the following way.

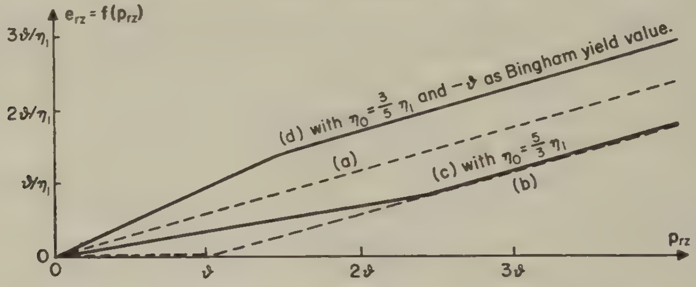

FIG. 1. Some idealized stress/rate-of-strain relationships.

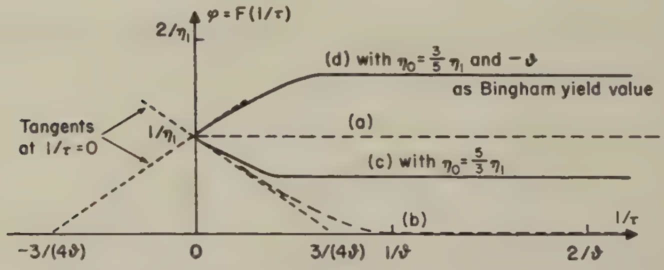

FIG. 2. The corresponding $(\phi, 1/\tau)$ curves.

A Brief Analysis of the General $(\phi, 1/\tau)$ *Curve.* For small rates of strain, we may write

$$f(\xi) = \frac{\xi}{2\eta_0} + \frac{f''(0)\xi^2}{2!} + \frac{f'''(0)\xi^3}{3!} + \cdots,$$

and hence, for small τ, Eq. (3) gives

$$F(1/\tau) = 1/\eta_0 + \tfrac{4}{5}f''(0)\tau + \tfrac{2}{9}f'''(0)\tau^2 + \cdots. \tag{5}$$

The limiting value of $F(1/\tau)$ as $1/\tau$ tends to infinity is $1/\eta_0$.

For sufficiently large rates of strain, we assume the viscosity tends to a finite value and the stress/rate-of-strain curve has an asymptote

$e_{rz} = \frac{1}{2}(p_{rz} - \vartheta)/\eta_1$. Then, for large τ, Eq. (3) gives

$$F(1/\tau) = \frac{4}{\eta_1\tau^4}\left\{\int^{\tau} x^2[x - \vartheta + O(1/x)]dx + \text{constant}\right\}$$
$$= \frac{1}{\eta_1}\left\{1 - \frac{4\vartheta}{3\tau} + O\left(\frac{1}{\tau^2}\right)\right\}. \qquad (6)$$

If the curve $\phi = F(1/\tau)$ is well defined[1] near $1/\tau = 0$, values of η_1 and ϑ are given by the ordinate and slope of tangent at $1/\tau = 0$; more precisely, this tangent has intercepts $1/\eta_1$ and $3/(4\vartheta)$ on the ϕ and $1/\tau$ axes, as in Fig. 3.

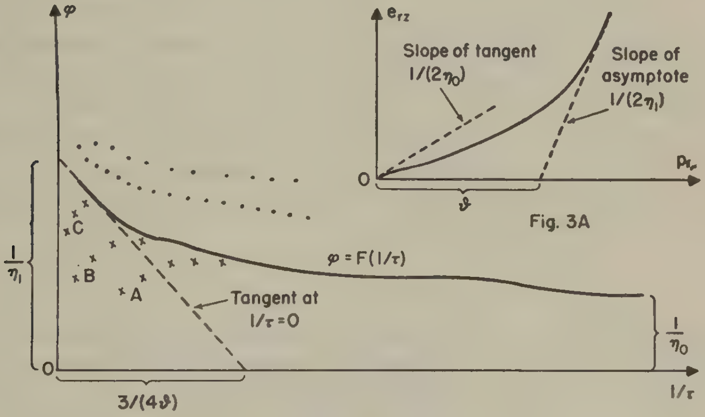

FIG. 3. The general case.

By these simple constructions, the tangent at the origin and the asymptote of the stress/rate-of-strain curve are defined (*cf.* Fig. 3A). It is claimed as an advantage of the present method of plotting over others that it is not necessary to estimate the slope and intercept of the asymptote of a drawn curve, sometimes a hazardous operation.

In the above special cases (*b*) and (*c*), $F(\xi)$ appears as a decreasing function of ξ. If $F(1/\tau)$ is observed to increase with $1/\tau$ at any value of $1/\tau$, it is easily proved that the viscosity must increase with increasing shear stress in some range of stress. For, from Eq. (3),

$$\frac{1}{8}F'(1/\tau) = \frac{4}{\tau^3}\int_0^{\tau} x^2 f(x)dx - f(\tau) = \frac{4}{\tau^3}\int_0^{\tau}\left\{\frac{f(x)}{x} - \frac{f(\tau)}{\tau}\right\} x^3 dx. \qquad (7)$$

If $F'(1/\tau)$ can be positive, $f(x)/x > f(\tau)/\tau$ for a range of values of x less than τ and, from continuity, $f(x)/x$ must decrease in part of that range

---

[1] Care must be taken to exclude points corresponding to non-laminar flow at high pressure gradients, *e.g.*, points at A, B, C, for different tube diameters in Fig. 3. The points at A arise from turbulent flow in a wider tube and the points C in a narrower tube than B. Laminar flow will persist up to larger values of τ in narrower tubes.

In other words, η increases with p_{rz} in a certain range of values of p_{rz}. The point is clearly illustrated by case (*d*) above. The converse theorem is not true.

WALL EFFECTS

Near the wall of the tube the shear strain may not be a function of shear stress alone. The wall introduces a preferred direction; and at the wall an otherwise isotropic material may behave anisotropically—for example, if there are polymer molecules in solution and a constraint is imposed by the wall on the rotational freedom of the molecules near the wall. The assumptions of rectilinear flow and of zero slip at the boundary are retained, but assumption (iii) is not valid everywhere and Eq. (2) cannot be deduced: ϕ will depend on a as well as on τ. Several $(\phi, 1/\tau)$ curves will be observed, one for each value of a. It is usually found in such cases that the apparent fluidity increases as a decreases.

A good description of the expected velocity profile is given by Schofield (10). His treatment suggests that, as a mathematical device to obtain a first approximation, we may replace a thin abnormal layer near the wall by a modified boundary condition

$$w = w_a \quad \text{on} \quad r = a$$

in investigating the new $(Q, dp/dz)$ relationship; w_a represents an *effective* velocity of slip at the wall. Reiner (9) has shown that the effect of such a boundary condition is to replace Eq. (2) by the relation

$$\phi = F(1/\tau) + 4w_a/(a\tau). \tag{8}$$

In general, w_a may be supposed a function of τ, the shear stress at the wall, and, for small stresses, proportional to τ. For larger τ, it is possible that w_a does not increase indefinitely but remains bounded; in any case, it is plausible to assume that w_a/τ remains bounded. Then $\phi - F(1/\tau)$ may be, say, roughly proportional to $1/\tau$ for large τ and roughly constant for smaller τ, being also inversely proportional to a. Instead of the continuous line representing $\phi = F(1/\tau)$ in Fig. 3, it is possible that a series of curves indicated by dotted lines could be observed for different a. If one of these curves were used uncorrected as a representation of $\phi = F(1/\tau)$, a completely false picture of the stress/rate-of-strain relationship would be obtained. In particular, a single observed curve showing an increase of ϕ with $1/\tau$ at large τ may be a manifestation of a wall effect rather than an indication either that viscosity increases with the rate of shear at large rates of shear or that the flow is non-laminar.

The connection between the stress/rate-of-strain relationship and the $(\phi, 1/\tau)$ curves can be obtained, without introducing the existence of an effective velocity of slip as a separate postulate at the outset, in the following way. We suppose Eq. (1) to hold in the main body of liquid flowing in a pipe, the coefficients of f involving only (scalar) physical constants of the material. In a layer of thickness ϵ (independent of a) next to the wall, we suppose the rate of strain is a function, depending on ϵ, of the stress $r\tau/a$ *and of the distance from the wall* $a - r$, so that we may write

$$-\frac{1}{2}\frac{dw}{dr} = f\left(\frac{r\tau}{a}\right) \qquad (0 \leqslant r \leqslant a - \epsilon),$$

$$-\frac{1}{2}\frac{dw}{dr} = f\left(\frac{r\tau}{a}\right) + g\left(\epsilon, \frac{r\tau}{a}, a - r\right) \qquad (a - \epsilon \leqslant r \leqslant a),$$

where the coefficients in g involve only physical constants of the material. From the assumption of no slip at the wall, it follows that

$$Q = 2\pi \int_0^a r^2 f\left(\frac{r\tau}{a}\right) dr + 2\pi \int_{a-\epsilon}^a r^2 g\left(\epsilon, \frac{r\tau}{a}, a - r\right) dr$$

and the equation replacing Eq. (2) is, therefore,

$$\phi = F(1/\tau) + \frac{8}{\tau^4}\int_{\tau(1-\epsilon/a)}^{\tau} \xi^2 g(\epsilon, \xi, a - a\xi/\tau)d\xi,$$

or

$$\phi = F(1/\tau) + G(\epsilon, a, \tau). \tag{9}$$

If ϵ is very small compared with a, it may be supposed a function of the stress at the wall τ alone, so that

$$\phi = F(1/\tau) + G(a, \tau). \tag{10}$$

We have, approximately,

$$\phi = F(1/\tau) + \frac{8}{\tau^4}\int_{\tau(1-\epsilon/a)}^{\tau} \tau^2 g(\epsilon, \tau, a - a\xi/\tau)d\xi = F(1/\tau) + \frac{8h(\epsilon, \tau, \epsilon)}{a\tau},$$

where

$$h(\epsilon, \tau, \xi) \equiv \int_0^{\xi} g(\epsilon, \tau, x)dx.$$

The coefficients of h involve only physical constants of the material. Also $\epsilon = \epsilon(\tau)$, so that we have the relation

$$\phi = F(1/\tau) + 4\zeta(\tau)/a, \tag{11}$$

where F is defined by Eq. (3) and neither F nor ζ depends on a. Eq. (8) is merely another way of writing Eq. (11), defining the *effective velocity of slip* by

$$w_a = \tau\zeta(\tau). \tag{12}$$

The function ζ may be called the *effective slip coefficient*, being the effective velocity of slip per unit shear stress at the wall. Its definition is in terms of the function g, namely,

$$\zeta(\tau) = \frac{2}{\tau}\int_0^{\epsilon(\tau)} g[\epsilon(\tau), \tau, x]dx. \tag{13}$$

A function of τ only, it is in some ways analogous to a variable fluidity, but has the dimensions of $M^{-1}L^2T$, *i.e.*, of fluidity × length. The limiting value ζ_1 at large τ may be supposed finite, and is zero if w_a is bounded when τ increases indefinitely. Mooney (8) uses a slip coefficient, equivalent to $\zeta(\tau)$, obtained by *postulating* an (effective) velocity of slip at a wall; the effect on Couette viscometer readings is also discussed by him.

It is interesting to recall the method of analyzing results, designed to give a measure of wall effects, put forward by Schofield and Scott Blair (5,11). This method consists in plotting $Q/(\pi a^2)$ against τ and observing a straight line of slope σ at large values of τ. Now, using Eq. (11),

$$Q/(\pi a^2) = \tfrac{1}{4}a\tau\phi = \tfrac{1}{4}a\tau F(1/\tau) + \tau\zeta(\tau),$$

and at large τ we have, from Eq. (6), the approximate result

$$\frac{Q}{\pi a^2} = \frac{a\tau}{4\eta_1}\left\{1 - \frac{4\vartheta}{3\tau} + O\left(\frac{1}{\tau^2}\right)\right\} + \tau\left\{\zeta_1 + O\left(\frac{1}{\tau}\right)\right\}.$$

Therefore

$$\sigma = \zeta_1 + \tfrac{1}{4}a/\eta_1. \tag{14}$$

Schofield and Scott Blair next plot σ against a and note the intercept σ_0 of the resulting straight line on the σ axis. From Eq. (14), the predicted slope of the (σ, a) line is $1/(4\eta_1)$ and σ_0 is to be identified with our ζ_1. This method of plotting will detect a wall effect, provided that ζ_1 is not zero, but would fail to do so if w_a were bounded at high stresses.

More generally, the value of ζ at a given finite τ can be obtained by plotting ϕ at fixed τ against the reciprocal of tube radius. According to Eq. (11), the curve should be a straight line with an intercept $F(1/\tau)$ on the ϕ axis and slope $4\zeta(\tau)$. By drawing such graphs, the curve $\phi = F(1/\tau)$ can be constructed and used, as for an isotropic material, to give information about the stress/rate-of-strain relationship. Also the effective slip coefficient ζ can be studied as a function of τ. By plotting ζ against τ, the limiting value ζ_1 at large τ can be found. If sufficient data are available, there are reasons for preferring this method of finding ζ_1 to the identification of ζ_1 with σ_0, as usually constructed, namely:

(i) It is immediately obvious whether the experimental data for laminar flow refer to sufficiently high values of τ to justify assuming that $\zeta(\tau)$ has reached a constant value. If not, the method still gives precise information about the effective slip coefficient at finite stresses.

(ii) The construction of σ_0 is usually carried out without a check that sufficiently high stresses at the wall have been reached in laminar flow. In fact a "best straight line" is often drawn through observed $[Q/(\pi a^2), \tau]$ points when the position of the asymptote is in doubt. Then σ_0 is not necessarily a good approximation to ζ_1, and has no obvious fundamental significance.[2] As an illustration, we suppose that only two radii of tube have been used (a' and a''), so that there are just two points to define a (σ, a) line. They are given, not by Eq. (14), but by

$$\sigma' = \zeta_1' + a'/(4\eta_1), \qquad \sigma'' = \zeta_1'' + a''/(4\eta_1), \tag{15}$$

where one or both of ζ_1', ζ_1'' may differ from the limiting value ζ_1 of ζ. The intercept of the straight line joining the two points is easily shown to be

$$\sigma_0 = \frac{a'\sigma'' - a''\sigma'}{a' - a''} = \frac{a'\zeta_1'' - a''\zeta_1'}{a' - a''}, \tag{16}$$

which may differ considerably from ζ_1.

CONCLUSIONS

Data from at least two diameters of tube should always be obtained, and the results expressed graphically by plotting ϕ against $1/\tau$. Only if all such data referring to laminar flow lie on the same curve, within experimental error, is it possible to derive η_0, η_1, ϑ directly by assuming a unique relation $\phi = F(1/\tau)$. If observed $(\phi, 1/\tau)$ curves for different tube diameters differ, and if the relative displacements of the curves are consistent with a general relationship of type (Eq. 11), there is reason to suppose a thin layer with anisotropic rheological properties exists near the tube wall. If the curves are sufficiently well defined by large numbers of consistent readings from different tubes, the relation (Eq. 11) can be used to obtain $F(1/\tau)$ and $\zeta(\tau)$. The curve $\phi = F(1/\tau)$ can be constructed and used, as for a liquid not showing wall effects, to define the stress/rate-of-strain relationship for the material in an isotropic condition (*i.e.*, remote from boundaries).

Two functions, dependent only on physical properties of the material, are to be associated with a non-Newtonian liquid (or plastic solid) which shows a wall effect, in order to specify its macroscopic flow properties completely. They are:

(i) the viscosity, η, a function of stress (or of rate of strain), with the dimensions of $ML^{-1}T^{-1}$.

(ii) an effective slip coefficient at a boundary, ζ, a function of shear stress at the boundary, with the dimensions of $M^{-1}L^2T$.

---

[2] *Cf.* Ref. (11).

These functions can be constructed, by the methods outlined in this paper, from measurements on steady laminar flow through tubes. The viscosity alone specifies the properties of an isotropic material completely; in the absence of wall effects, ζ vanishes.

SUMMARY

It is possible to detect anomalous flow of a non-Newtonian liquid near a rigid boundary, by plotting the apparent fluidity (as given by Poiseuille's formula) against the reciprocal of the shear stress at the wall in laminar flow through tubes of various diameters. This method of plotting has some advantages over others. If the properties of the liquid in shear are everywhere specified by a unique stress/rate-of-strain relationship, all the plotted points should lie on a single curve, and a wall effect is indicated if distinct curves arise from different diameters of tube. It is shown that a wall effect can be measured by an effective slip coefficient, which is a function of the stress at the wall. The mathematical argument is based on the assumptions (i) that the flow is rectilinear, (ii) that there is no actual slip at the wall, and (iii) that the functional relationship between stress and rate-of-strain is dependent on the normal distance from a solid boundary, in a thin layer of liquid near the boundary only.

REFERENCES

1. SCOTT BLAIR, G. W., An Introduction to Industrial Rheology, Churchill, London, 1938.
2. TOMS, B. A., *J. Colloid Sci.*, in press.
3. TOMS, B. A., Paper read to the First International Congress on Rheology, Scheveningen, 1948.
4. OLDROYD, J. G., Paper read to the First International Congress on Rheology, Scheveningen, 1948.
5. SCHOFIELD, R. K., AND SCOTT BLAIR, G. W., *J. Phys. Chem.* **34**, 248 (1930).
6. RABINOWITCH, B., *Z. phys. Chem.* **145A**, 1 (1929).
7. REINER, M., *J. Rheology* **1**, 250 (1930).
8. MOONEY, M., *ibid.* **2**, 210 (1931).
9. REINER, M., *ibid.* **2**, 337 (1931).
10. SCHOFIELD, R. K., *Physics* **4**, 122 (1933).
11. SCHOFIELD, R. K., AND SCOTT BLAIR, G. W., *J. Phys. Chem.* **35**, 1212 (1931).

A THEORY OF ANOMALOUS VISCOSITY AND ELASTICITY[1]

Charles Mack

Technical and Research Department, Imperial Oil, Ltd., Sarnia, Ontario, Canada

Received January 24, 1949

Anomalous viscosity and elasticity are observed with what may be termed "plastic systems." The relationship between shearing stress and rate of shear for anomalous systems at constant temperature can often be expressed by

$$v = \text{const. } \sigma^{1/b}, \tag{1}$$

or

$$v = \text{const. } \exp. (\sigma/b), \tag{2}$$

where v = shear-rate, σ = shearing stress, b = constant. Similar expressions are obtained for anomalous elasticity by replacing v by the shear-strain γ. In neither case has the coefficient of viscosity, $\eta = \partial\sigma/\partial v$, or the modulus of rigidity, $G = \partial\sigma/\partial\gamma$, the proper dimensions. Further, if an experiment is carried out in one direction and the direction of stress is reversed, then the material must deform with the same shear-rate in the opposite direction. With σ negative, v should be also negative, a condition which is not satisfied at all by Eq. (2) and is satisfied in the case of Eq. (1) only when $1/b$ is 1,3,5, *etc.* but not for other values. A theory of anomalous viscosity and elasticity must explain these discrepancies and must express the mechanical properties in terms of exact quantities.

Plastic systems are disperse systems and can be divided into systems containing rigid molecules and systems containing flexible molecules. Disperse systems resemble solutions. In dilute solutions, the solute molecules are distributed at random and move freely in the solvent. At high concentrations each solute molecule occupies a definite volume of the system and prevents its neighboring molecules from occupying certain positions as a result of steric hindrance. Such systems, therefore, are not completely isotropic and exhibit orientation effects of the dissolved molecules. The degree of anisotropic distribution of orientation increases with increasing concentration and with increasing deviation from spherical shape of the solute molecule. If, at higher concentrations, certain positions are forbidden to a solute molecule at rest, it follows that many more positions resulting from the rotation are forbidden to a molecule in motion. The end effect would then be a restriction of motion, and, to bring about flow, more positions would have to be made available to the molecule in motion. Such an effect can be obtained only by an increase in the volume of the system, which is indicated in all cases where Poisson's ratio, compressive strain/tensile strain, is smaller than 0.5.

---

[1] Abstract of a paper presented before the Annual Meeting of the Society of Rheology, New York, N. Y., November 5 and 6, 1948, based on the following publications by the author: Plastic Flow, Creep and Stress Relazation, Parts I, II, III, and IV., *J. Applied Phys.* **17**, 1086, 1093, 1101 (1946); **19**, 1082 (1948).

Plastic systems at rest consist of a number of molecules, the larger part of which are confined to their positions under the influence of steric hindrance and cannot move to other positions, whereas the remainder is free to do so. This consideration explains the existence of yield values. Under stresses up to the yield value, the deformation is mainly elastic, *i.e.*, a deformation during which the individual molecules retain their neighbors, and part of the energy introduced into the system is used to increase the volume of the intermolecular space or holes. At stresses in excess of the yield value, some of the molecules have accumulated enough energy and can move into the holes formed. As a plastic system contains molecules of various sizes and a hole can accommodate only a part of a large molecule, a molecule or unit of flow will be referred to this part.

The distribution of the molecules over localized and non-localized positions is comparable to an order-disorder arrangement. Denoting the fraction of molecules on the ordered or α-sites by n_α the fraction of molecules on the disordered or β-sites by n_β, and the ratio of the number of holes to the number of molecules by α, the coefficient of viscosity for a plastic system consisting of rigid molecules is expressed by:

$$\eta = (n_\beta - n_\alpha)(1 - \alpha)\sigma/v, \tag{3}$$

where σ = shearing stress and v = rate of shear. This equation can be applied to any system, the plastic deformation of which is not recoverable, and expresses the mechanical properties in terms of a coefficient of viscosity with proper dimensions. With the appropriate choice of the distribution of the molecules over the α- and β-sites of the lattice, any kind of relationship between shearing stress and shear-rate can be established.

With $n_\beta - n_\alpha$ increasing with increasing shearing stress, the number of holes also increases and the viscosity decreases; this is the condition for simple plastic flow. A similar behavior is experienced with thixotropy. However, here $n_\beta - n_\alpha$ increases not only with increasing stress but also with time at constant stress. With $n_\alpha = 0$ and $1 - \alpha$ replaced by $1 + \alpha$, the number of holes decreases with increasing stress and the viscosity increases. This condition is connected with stress-hardening, *i.e.*, a hardening of the system under the influence of stress. For the condition of hardening as a function of time or strain, n_α is also zero, and n_β decreases at constant shearing stress with increasing time or shear-strain. The term

α can be constant and independent of the shearing stress or can vary with the stress. With α = constant, the shear-rate becomes a power function of the shearing stress, and with α being variable in such a way, that at two different stresses, σ and σ_0, $(1 - \alpha)\sigma$ is equal to $(1 - \alpha_0)\sigma_0$ the shear-rate becomes an exponential function of the shearing stress. The term $1 \pm \alpha$ corresponds to constant b in Eqs. (1) and (2).

A change in the order-disorder arrangement of the molecules under the influence of a shearing force is accompanied by a change in the field of force around a molecule and by a change in entropy. If the number of molecules on the β-sites increases, the entropy change is comparable to the entropy of fusion; conversely, the entropy change is comparable to the entropy of crystallization if the number of molecules on the α-sites increases.

The concept of a change in the order-disorder arrangement of the molecules in a plastic system under stress also explains the strength of such systems. Systems whose shear-rate increases proportionally more than the shearing stress, undergo a change from a state of lesser disorder to a state of greater disorder, and their strength is, therefore, determined by their yield values. Plastic systems, which are subject to hardening under the influence of stress, time or strain, on the other hand, shift to a state of greater order with increasing stresses and reach maximum orientation effects when the number of molecules on the β-sites become a minimum. At this point the system behaves like a rigid body, at least in the direction of the deformation and the yield value has increased. Any further increase in stress will increase the number of holes and thus allow the molecules to shift from the α-sites to the β-sites. The system reverts, therefore, from a state of order to a state of disorder, resulting finally in its failure. The maximum strength for such systems is obtained at the point where the number of molecules on the β-sites are at a minimum.

In the case of flexible molecules, the system usually contains large flexible chain molecules, and the mechanical properties are referred to as rubber-elasticity. The segments of these large molecules are assumed to be distributed at random over the α- and β-sites. At shearing stresses of small magnitude, the deformation is connected with the elastic deformation of the segments on the α-sites and obeys Hooke's law. At greater stresses the segments on the β-sites perform rotational and translatory motions and are shifted into the α-sites. The deformation connected with this transition from one site to another consists of two parts. One part, being translatory, is a function of time and is a viscous deformation; the other part consists of an elastic deformation, which the segment undergoes after its arrival at the α-site. The viscous deformation is accompanied by an increase in the volume of the holes, which are closed again after the segments have occupied the α-sites. The net result is a constancy of the volume which has been observed for such systems under stress. The mechanical behavior of such systems under shear is experssed by

$$G\gamma + \eta v = n_\beta(1 + \alpha)\sigma - 2\, n_\beta \alpha \sigma_\beta, \tag{4}$$

where G = modulus of rigidity, γ = shear-strain, σ_β = shearing stress connected with the viscous deformation; the other terms have the same meaning as before. The elastic shear strain γ and the shear-rate v can be power functions or exponential functions of the corresponding stresses as in the case of plastic flow, and the experiments have to be properly chosen for the evaluation of these functions. If the applied stress is kept constant until equilibrium is reached, then v and σ_β become zero and

$$G\gamma = n_\beta(1 + \alpha)\sigma. \tag{5}$$

With the segments on the β-sites shifting into the α-sites, n_β decreases with increasing shearing stress and reaches a minimum as a result of the orientation in the same way as in the case of anomalous vicosity connected with stress-hardening. The orientation of the segments in such systems understress has been demonstrated by X-ray diagrams and is an accepted fact. On unloading, the system returns to an unstrained state and original state of disorder, and for this condition Eq. (4) also holds with the sign reversed.

The mechanical properties of plastic systems are determined by the distribution of the molecules over the α- and β-sites of the lattice and are, therefore, a function of the volume or of the coordinates of space. It can, therefore, be expected that the mechanical properties of such systems vary with the dimensions of the test-specimen under stress.

PLASTICIZING LINEAR POLYMERS[1]

C. B. Havens

From the Saran Development Laboratory, The Dow Chemical Company, Midland, Michigan

Received January 24, 1949

A solvent power theory of plasticizer action based on the Arrhenius and Flory equations is presented. The melt viscosity of plasticized polymers deviates from the Arrhenius equation. The deviation is attributed to coiling or uncoiling of the polymer chain due to solvent effect. An equation is derived which expresses the degree of uncoiling, R-value, as the ratio of the hypothetical to the actual molecular weight:

$$R = \frac{\log N_f - (V_s \log N_s)}{V_o \log N_o},$$

where N_f = viscosity of plasticized polymer, V_o = volume fraction of unplasticized polymer, and N_o its viscosity, V_s = volume fraction of solvent or plasticizer, and N_s its viscosity.

On the basis of this theory, it is concluded that two important criteria in evaluating plasticizer effectiveness are plasticizer viscosity and plasticizer solvent power. Low-viscosity plasticizers are considered to be more effective than high-viscosity plasticizers. Poor solvent plasticizers are more effective in reducing melt viscosity, and less effective in reducing Young's modulus than are good solvent plasticizers.

Experimental data on vinylidene chloride—vinyl chloride copolymers are presented. The good solvent plasticizers are found to improve elongation and impact strength, whereas poor solvent plasticizers do not.

---

[1] Abstract of paper presented at the Annual Meeting of the Society of Rheology. New York, N. Y., November 5 and 6, 1948. To be published in an early issue of *Ind. Eng. Chem.*

SCATTERING OF LIGHT DURING THE PROCESS OF GEL FORMATION

Mata Prasad and K. D. Venkatesha Doss

From the Chemical Laboratories, Royal Institute of Science, Bombay, India

Received September 1, 1948; revised February 23, 1949

In recent years the method of light scattering has been widely used in colloidal chemistry to obtain information regarding the structure, shape and size of the colloidal particles. A theory of light scattering was developed by Love (1). Mie (2) developed another theory of scattering and obtained an expression for the intensity of the scattered light. Lord Rayleigh (3) applied a correction to Love's theory and obtained an expression different from that of Mie, for the intensity of the light scattered by spherical particles of any size.

The study of light scattering by gels both during and after setting, has contributed a good deal toward the solution of the problems of the mechanism of their formation and their structure. The variations in the intensity of the light scattered by gel-forming systems on changing various factors, such as the temperature, concentration, mechanical treatment, pH, aging, and others, have been quantitatively determined by Mardles (4), Kraemer and coworkers (5), Holweda (6), and Krishnamurthi (7). Krishnamurthi (7) measured the depolarization of the light scattered by agar sols and gels, using nonpolarized incident light, at different temperatures, and deduced that the particles in the gel state are larger in size or greater in number, or both, than those in the sol state. Subbaramiah (8) and Krishnan (9) have shown that, in order to elucidate the size and shape of the particles in the colloidal state, it is necessary to determine the values of the depolarization factors, ρu, ρv and ρh of the scattered light obtained on using incident light unpolarized, vertically and horizontally polarized, respectively. Subbaramiah (10) has determined the changes in the intensity of the scattered light and in the values of ρu, ρv and ρh during the setting of gels of silicic acid, stearic acid and sodium stearate. Recently, a systematic study of the depolarization factors and the intensity of scattered light by gels of silicic acid, thorium arsenate and thorium molybdate has been made by Prasad and Guruswamy (11). They have obtained by calculation the intensity of anisotropic scattering and separated the density scattering from the total scattering, and from their results, they have attempted to explain the mechanism of the formation of these gels. They conclude that the micelles of the gels grow bigger during the formation of gels and that their linear dimensions are smaller than the wavelength of light.

In a recent paper (12), Hoover, Putnam and Wittenberg pointed out that "in order to arrive at the true depolarization values it is essential that the scattered light be viewed against its *natural background* rather than against a *limited background*. The Cornu method, in which the scattered light is viewed against its natural background, gives true values just so long as the multiple scattering is not too intense." Lotmar (13) and Krishnan (14) have studied the influence of secondary scattering on depolarization measurements, and have concluded that the limited background method (also called diaphragm method) gives abnormally high values of depolarization factors. However, Subbramania, Gururaja Doss and Sanjiva Rao (15), who have recently studied the effects of background and slit width on the depolarization values of stearic acid and benzopurpurine sols, find that the difference between the values of the depolarization factors obtained by the natural and limited background methods is not very prominent. The method of observation adopted by Prasad and Guruswamy (11) was not the natural background method.

Prasad and Modak (16), and Prasad and Guruswamy (17), have shown, by using the arrangement designed by Prasad and Gogate (18), that there are 3 types of gels with reference to the opacity changes they exhibit during setting: (a) those that *increase* in opacity (gels of stannic phosphate and stannic arsenate), (b) those which neither increase nor decrease in opacity (thorium phosphate gels), and (c) those that *decrease* in opacity (ceric phosphate gels). Prasad and coworkers have pointed out that the changes in opacity are due to the change in size and shape and the state of aggregation of the gel particles during the formation of gels.

The present investigation deals with the measurement of the intensity and the depolarization factors (ρu, ρv, ρh) of the light scattered by the 3 types of gels mentioned above. Since the course of gelation is greatly modified by the presence of electrolytes and nonelectrolytes [*cf.* Prasad, Desai and Mehta (19), Prasad, Mehta and Parmar (20)], the effects of the addition of these agents to the gel-forming mixtures on the depolarization factors and the intensity of the scattered light during the formation of the aforesaid gels were also determined. The electrolyte and nonelectrolyte used were HCl and ethyl alcohol, respectively.

EXPERIMENTAL

1. Description of the Method of Measuring the Depolarization Factors

The description of the natural background method for the measurement of the depolarization factors is given in some detail in this paper, particularly because these details are not available at any one place in the literature, and often mistakes have occurred for want of them.

The arrangement used for the measurement of the depolarization factors by this method is shown in Fig. 1.

A rectangular glass cell C (4″ × 2.5″ × 0.9″) was used to contain the gel-forming mixture. It was painted dull black entirely except for the three openings or slits marked as x, y, and z (x and z being for the entrance and exit of the incident beam, and y for the passage of the scattered light). The opening y was rectangular (20 mm. × 5 mm.) and was situated 3 mm. from the face of the cell at which the light was incident. The thickness of the incident beam was so adjusted by means of a slit that it was less than 2.5 mm. × 2.5 mm. The glass cell was placed in a groove in a suitably cut hollow wooden box, painted black, and was in turn fixed permanently in another large wooden box, also painted black inside, having a slit to admit the incident light, and provided with a suitable glass door, for taking the glass cell out of the groove or placing it back.

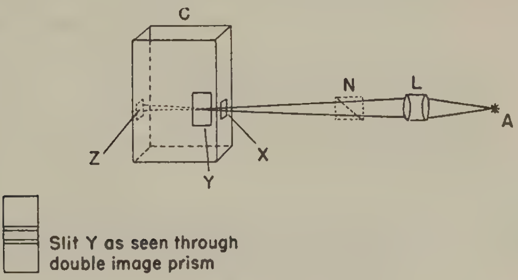

FIG. 1.

Sunlight, when available, and light from a 100 c.p. Pointolite A when sunlight was not available, was condensed on the gel-forming mixture contained in the glass cell by means of a long focal length high quality lens L (f = 30 cm.). It was so arranged that the glass cell was at the focal plane and the most intense part of the parallel track of the incident beam was exactly opposite to the center of the slit y.

The double image prism was first set in front of the slit y so that it could split up the horizontal and vertical components one below the other. It was then moved forward or backward until the two images were just separated, one below the other. Thus, the two images of the beam were viewed against the same background (uniform bright layer of the medium behind the beam).

A nicol D was placed in front of the prism and was set at such positions where the two images of the bright slit appeared to be of equal intensity. If 2 θ is the angle between two positions of the nicol symmetrical with respect to the horizontal vibration direction, the depolarization factor ρ is given by $\tan^2\theta$, and the percentage depolarization by $\tan^2\theta \times 100$.

2. The Measurement of the Intensity of Scattering

The intensity of the scattered light was measured by the photoelectric method adopted by Ananthakrishnan (21) and Prasad and Guruswamy (11).

3. Preparation of Gels

a. (*i*) *Stannic Phosphate Gels.* These were prepared by the method of Prasad and Desai (22), using 15% solution of $SnCl_4$ (A) and 2 *N* H_3PO_4 (B). (A) was prepared by dissolving 150 g. of $SnCl_4$ in distilled water to which 2 cc. of conc. HNO_3 were added. It was then boiled for some time, and after cooling, was made up to 1 l.

TABLE I

Stannic Phosphate Gels

Time in min.	1	3	5	10	15	20	30	40	50	60	70
(a) A = 25; B = 6; *t* = 20											
ρu	—	1.1	0.76	1.97	5.7	—	14.0	17.1	18.9	—	—
ρv	—	0.76	0.275	0.275	2.2	—	4.1	5.3	—	—	—
ρh	—	42	—	61	57	—	—	—	—	—	—
I	0.5	0.7	1.6	7.9	16.1	23	29.5	35.7	35.7	—	—
(b) A = 25; B = 5; *t* = 26											
ρu	1.7	—	87	87	90	90	86	—	—	—	—
ρv	1.1	—	1.5	1.5	2.8	8.7	14.1	16.3	18.02	—	—
ρh	—	—	0.77	0.49	0.77	2.8	4.1	7.2	7.2	—	—
I	0.6	0.9	—	4.7	13.6	21.1	29.8	—	—	—	—
(c) A = 25; B = 4; *t* = 40											
ρu	—	2.2	—	2.2	—	2.8	—	12.0	—	15.5	16.3
ρv	—	0.9	—	0.9	—	—	1.5	2.2	4.3	5.7	—
ρh	—	—	—	—	—	47	36	—	48	43	—
I	0.6	0.5	—	1.9	5.0	9.3	16.8	21.8	—	29	30
(d) A = 25; B = 5; C = 1; *t* = 25											
ρu	1.3	1.1	—	1.97	4.5	7.6	13.3	14.7	14.7	—	—
ρv	0.49	0.27	—	0.48	0.9	1.7	3.8	7.7	8.2	—	—
ρh	—	—	—	—	—	—	—	—	—	—	—
I	0.5	0.7	1.2	4.3	11.2	16.5	18.8	19	—	—	—

TABLE I—*Continued*

Time in min.	1	3	5	10	15	20	30	40	50	60	70
(e) A = 25; B = 5; C = 3; t = 40											
pu	3.0	—	1.4	—	1.5	3.4	7.2	—	—	—	—
pv	0.7	—	—	—	0.382	—	1.51	3.78	—	—	—
ph	—	35	—	—	—	—	—	—	—	—	—
I	0.5	0.6	0.8	2.6	6.1	—	24.5	28.6	—	—	—
(f) A = 25; B = 5; D = 1; t = 28											
pu	1.1	—	0.77	1.3	2.5	5.3	5.7	16.3	18	—	—
pv	0.37	—	—	0.28	1.11	—	2.5	4.9	7.2	—	—
ph	33.49	—	—	—	—	—	22.30	—	—	—	—
I	0.4	—	0.6	3.3	9.6	15.8	22.7	—	—	—	—
(g) A = 25; B = 5; D = 10; t = 58											
pu	5.3	—	4.9	3.1	3.1	1.5	1.7	1.97	2.5	5.7	7.2
pv	1.1	—	—	0.77	0.77	0.38	0.38	0.77	0.77	0.77	1.97
ph	—	—	—	4.0	—	—	33	—	—	—	40
I	0.4	—	0.45	—	0.5	—	—	9.6	—	—	20

(*ii*) *Stannic Arsenate Gels.* These were prepared by the method adopted by Prasad and Desai (22), using 15% solution of $SnCl_4$ (A) prepared as described above and 10% solution of pyroarsenic acid (B).

b. Thorium Phosphate Gels. These were prepared by the method of Prasad, Parmar and Mehta (20), using 6% solution of thorium nitrate (A) and 2 N H_3PO_4 (B). The gels obtained had the unique property of being very highly transparent throughout the process of gelation. They were quite stable.

c. Ceric Phosphate Gels. These were prepared by the method of Prasad and Desai (22), using 6% solution of cerium nitrate (A) and 10% solution of secondary potassium phosphate (K_2HPO_4) (B). On mixing the components of the gel-forming mixture, a milky, thick, turbid solution was formed, the turbidity disappearing after a few minutes. The gels on setting were highly translucent or transparent and were also thixotropic.

All substances used for the preparation of the several solutions were B.D.H. chemicals.

For the preparation of gels various volumes of (A) and (B) were taken in two different test tubes, the volume in each made up to 25 cc. by addition of distilled water. The two solutions were then mixed, the total volume of the gel-forming mixture being almost 50 cc. in all cases.

The mixture was transferred to the glass cell and the depolarization factors measured at different intervals during and after gelation. The results obtained for the stannic phosphate, stannic arsenate, thorium phosphate, and ceric phosphate gels are given in Tables I to IV. In these tables, A and B represent the volumes in cc. of the solutions of the components of the gel-forming mixtures (*cf.* preparation of gels), C and D represent cc. of the HCl and ethyl alcohol, respectively, added to the gel-forming mixtures and *t*, the time of setting in minutes, unless otherwise stated.

Discussion of Results

1. Stannic Phosphate Gels

It will be seen from Table I that the values of *ρv* are low (almost equal to zero) in the beginning of gelation. In many cases they then slightly but

TABLE II

Stannic Arsenate Gels

Time in min.	1	5	10	15	20	30	35	45
(a) A = 25; B = 5; *t* = 20								
ρu	1.3	—	13.3	17.2	29.5	32.0	—	36.1
ρv	0.28	—	1.97	—	8.7	—	—	13.3
ρh	33	—	—	—	—	—	—	—
I	0.2	1.3	5.1	12	15.7	15.6	—	—
(b) A = 25; B = 4; *t* = 39								
ρu	2.2	2.5	5.3	18	—	28	—	—
ρv	0.76	0.76	2.2	5.3	—	13.3	—	—
ρh	—	43	—	38	—	—	—	—
I	0.2	0.4	1.8	4.5	—	11.6	—	15.4
(c) A = 25; B = 3; *t* = 95								
ρu	—	1.5	1.5	3.1	—	—	—	21.8
ρv	—	0.275	0.275	0.489	—	—	—	8.22
ρh	—	—	—	—	—	—	—	—
I	—	—	0.5	0.75	1.0	3.1	—	5.3
(d) A = 25; B = 5; C = 1; *t* = 20								
ρu	1.97	4.5	17.1	27.1	45.5	—	—	—
ρv	0.27	1.11	9.3	9.9	18.9	—	—	—
ρh	—	—	—	—	—	—	—	—
I	0.4	1.5	5.5	12.7	15.5	—	—	—

TABLE II *Continued*

Time in min.	1	5	10	15	20	30	35	45
(e) A = 25; B = 5; C = 3; t = 30								
ρu	—	1.3	4.5	14.0	24.9	—	—	—
ρv	0.038	0.489	2.8	7.2	9.4	12.0	—	—
ρh	—	—	—	—	—	—	—	—
I	0.3	0.8	4.3	—	11.5	14.5	22.5	—
(f) A = 25; B = 5; D = 1; t = 19								
ρu	2.5	3.4	9.3	29.5	30.7	34.7	—	37.6
ρv	0.9	1.2	3.1	11.9	—	14.7	—	19.8
ρh	55	53	48	56	—	58	—	—
I	0.4	2.3	11	18	17	—	—	—
(g) A = 25; B = 5; D = 10; t = 60								
ρu	—	1.97	—	3.1	6.2	18.02	18.02	—
ρv	—	0.49	—	0.62	3.1	—	5.3	—
ρh	—	—	—	—	—	—	—	—
I	0.3	0.4	—	—	3.8	—	11.0	—

TABLE III

Thorium Phosphate Gels

A	B	Added substance	ρu	ρv	ρh	I
25	2	Nil	6.7	2.2	42	0.2
25	2	C = 3	7.2	2.5	49	0.2
25	2	D = 10	5.3	1.5	40.5	0.2

definitely decrease for some time and then increase steadily and continue to increase even after the gel has set, until a certain maximum is reached. Any deviation from the zero value of ρv is indicative of the anisotropic condition of the particles. Therefore, it appears that the particles are not anisotropic in shape and/or structure in the early stages of gelation, but they become anisotropic and the anisotropy increases as the gelation progresses.

Similarly, in many cases, the values of ρu decrease slightly at first, then increase during the gel-formation and continue to increase, even after the gel has set, until a maximum value is attained. However, the intensity of the scattered light increases continuously. This shows that the particles continually increase in size during and after the setting of the gel. The observed initial slight fall in ρu is, therefore, due to the particles becoming more symmetric in shape and/or structure in the early stages of gelation.

The values of ρh are not reliable, since it is very difficult to measure them accurately. However, they are far lower than 100, indicating that the size of the particles in the gel-forming system is comparable to the wavelength of light in their linear dimension. It has not been possible to calculate the values of ρh from Krishnan's relation, because, the gel-forming systems being dynamic, the values of ρv and ρu undergo change even for a slight difference in the time required to take the readings.

It will be observed that, on increasing the amount of phosphoric acid in the gel-forming mixture, (1) no definite regular changes in ρv take

TABLE IV

Ceric Phosphate Gels

Time in min.	1	5	10	20	25	40	50	60	70	hr.
(a) A = 25; B = 6; t = 14 hr.										(20)
ρu	—	—	—	21.8	—	17.1	15.5	12.6	8.8	3.5
ρv	—	—	7.2	6.7	—	4.5	4.5	3.1	3.1	1.1
ρh	—	—	—	—	—	—	—	—	—	49
I	28.5	—	—	—	25	—	—	—	—	—
(b) A = 25; B = 5; t = 14 hr.										(17)
ρu	28.3	23.8	22.75	18.0	14.7	—	—	8.2	—	1.97
ρv	11.2	8.2	7.2	3.8	3.1	—	—	2.5	—	1.5
ρh	—	—	—	—	22.0	—	—	36	—	93
I	25.5	25.5	—	—	17.3	—	—	5.8	—	—
(c) A = 25; B = 4; t = 24 hr.										(21)
ρu	17.1	15.5	—	—	13.3	12.6	—	—	—	3.1
ρv	3.8	—	3.8	—	3.1	2.2	—	—	—	1.3
ρh	—	—	—	—	—	—	—	—	—	—
I	24.3	24.2	19.5	10	7.5	—	—	—	—	—
(d) A = 25; B = 5; C = 1; t = 24 hr.										(25)
ρu	30.7	24.8	19.8	—	10.0	—	6.2	—	—	2.5
ρv	11.2	8.2	4.9	—	3.1	—	2.2	—	—	1.11
ρh	—	—	—	—	—	—	42	—	—	76
I	26	26	—	—	15.5	—	—	—	—	—

TABLE IV *Continued*

Time in min.	1	5	10	20	25	40	50	60	70	hr.
(e) A = 25; B = 5; C = 3; *t* = 24 hr.										(24)
ρu	36.1	26.0	—	21.8	11.2	—	—	—	4.5	2.8
ρv	14.0	11.9	—	4.1	3.1	—	—	—	1.5	1.3
ρh	—	—	—	—	—	—	—	—	44	78
I	—	23.8	—	—	22	—	—	—	—	—
(f) A = 25; B = 5; D = 1; *t* = 24 hr.										(22)
ρu	33.3	—	21.8	15.5	—	—	—	—	7.6	2.2
ρv	8.7	—	4.5	—	—	—	—	—	—	1.1
ρh	—	—	—	—	—	—	—	—	46	93
I	23.5	—	23	22.7	—	—	—	5.7	5.4	—
(g) A = 25; B = 5; D = 10; *t* = 24 hr.										(19)
ρu	36.1	21.8	17.3	17.3	—	—	—	—	—	3.8
ρv	7.7	—	3.8	3.4	—	—	—	—	—	1.3
ρh	—	—	—	—	—	—	—	—	—	49
I	26	22.5	—	17	—	—	—	—	—	—

place, but probably the particles become less anisotropic, (2) the rate of increase in intensity of the scattered light, that is, the rate of growth of the gel particles, increases (*cf. I-t* curves, Fig. 2) and (3) the time of setting decreases. It was noted that the transparency of these systems also decreases on such an addition.

It will be seen from I (d), (e), (f), and (g) that the changes in *ρv*, *ρu* and *I* during gelation of a gel-forming mixture take place in the same manner in the presence of HCl and alcohol as without their addition. Hence, it appears that, even in the presence of HCl and alcohol, the particles in many of these gel-forming mixtures continuously increase in size and at first are more symmetric and isotropic and gradually develop the anisotropy of shape and/or structure. The addition of HCl and alcohol casuses a decrease in (1) *ρv*, that is, the particles become less anisotropic in shape and/or structure and (2) the rate of increase in *I*, that is, the rate of growth of the particles of the gels. This effect is most marked in the presence of 10 cc. of alcohol, in which case the gel becomes opaque after 16 hr., probably due to the evaporation of most of the alcohol, and the particles become highly anisotropic.

Krishnan classifies particles for which the values of *ρu*, *ρv* and *ρh* are less than one as "ellipsoidal particles of finite size" and those for which

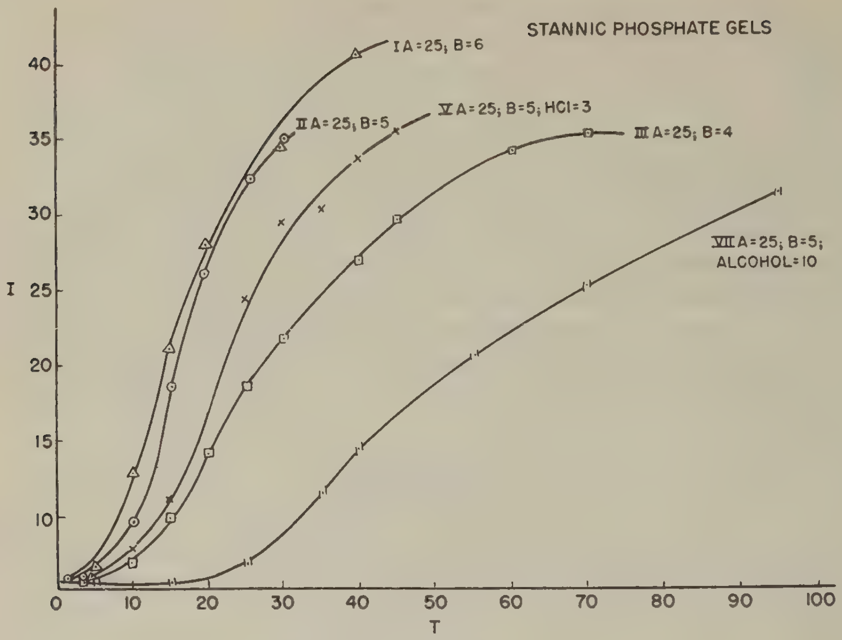

FIG. 2.

$\rho u = 0$, $\rho v = 0$, $\rho h \sim 1$ as "small spherical particles." Accordingly, the values of ρu and ρv indicate that, in all stannic phosphate gel-forming mixtures, the particles are small and nearly spherical in the early stages of gelation and they become more and more ellipsoidal and tend to attain a finite size as the gelation progresses.

2. Stannic Arsenate Gels

The behavior of these gel-forming mixtures, as revealed from the data given in table II, is similar to that of the mixtures giving rise to the stannic phosphate gels. This means that (1) the particles in these mixtures are small, nearly spherical and not anisotropic in shape and/or structure at the early stages of gelation, (2) they increase in size and become more and more anisotropic as the gelation progresses, and these changes continue even after the gel has set, (3) their linear dimensions are comparable to the wavelength of light, (4) the rate of their growth (*cf.* *I*-*t* curves, Fig. 3) increases, and their anisotropy decreases, as the amount of pyroarsenic acid in the gel-forming mixture is increased. Such an addition also decreases the time of setting and the transparency of gels, and (5) the addition of HCl and ethyl alcohol (1) increases the time of setting of the gels and makes them more transparent, (2) retard the rate of growth of the particles, and (3), although no regular changes have been noticed in the anisotropy of the particles on the addition of HCl, ethyl alcohol definitely causes the particles to become less anisotropic in shape and/or structure.

Separation of Density and Anisotropy Scattering

Prasad and Guruswamy (11) have deduced that density scattering I_D, is given by the relation:

$$I_D = \frac{KCV}{\sigma} = \frac{KC^2}{N\sigma^2},$$

where σ = the density of the medium,
C = amount of colloidal matter,
K = a constant,
V = the volume of the scattering particles and
N = number of particles in unit volume.

Hence, the values of I_D at different intervals of time for a system undergoing gelation would be directly proportional to the volume and inversely proportional to the number of the particles formed in the system during gelation.

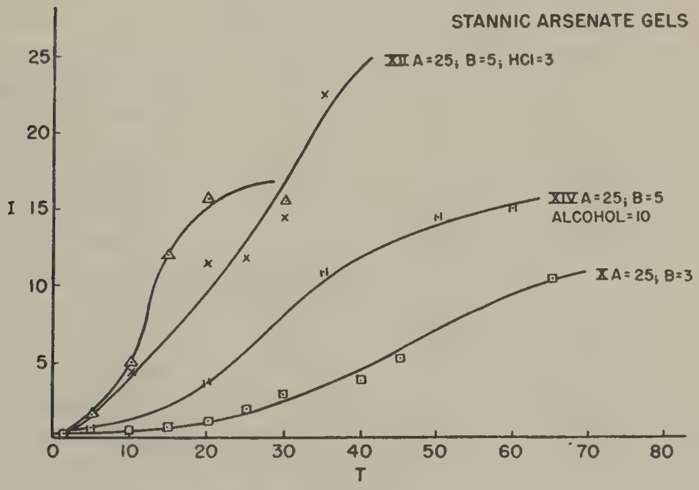

FIG. 3.

Further, since the total intensity of the scattered light is the sum of the intensities due to density (I_D) and anisotropy (I_A) scattering, $I_A = I - I_D$. The values of I_D and I_A have been calculated in the case of one typical gel of both stannic phosphate and stannic arsenate, and are given in Table V. The volumes of the particles (V) have been expressed in relation to the final volume of the particles when the gelation is complete.

It is seen from the above table that the anisotropy scattering increases rapidly during gelation and, in the case of stannic arsenate, appraoches closer to the value of I_D toward the later stages of gelation. This shows that, during these stages especially, the intensity of the scattered light is appreciably affected by the anisotropic nature of the particles in both gels, although the predominant contributing factor throughout the process is the density scattering. The increase in I_D indicates that the number of particles in the gel diminish during gelation, that is, the process of coagulation is operative during the formation of the gel. This conclusion is supported by the fact that the volume of the individual particles increases in size during gelation (*cf.* last column of the table) and attains a practically constant value after some time, which may be greater or less than the time of setting of the gel. The final volumes of particles in the gels of stannic phosphate and stannic arsenate are, respectively, 5 and 7 times their initial volumes.

TABLE V

Time	$\frac{6+6\rho}{6-7\rho}$	I	I_D	I_A	$V=I_D/IF$
min.			(a) Stannic Phosphate Calculated from Table I (b)		
10	1.034	4.7	4.54	0.16	0.208
15	1.060	13.6	12.8	0.80	5.587
20	1.160	21.1	18.2	2.90	0.835
25	1.275	26.8	21.0	5.80	0.964
30	1.368	29.8	21.8	8.00	1.000
			(b) Stannic arsenate Calculated from Table II (c)		
10	1.034	0.50	0.482	0.018	0.149
15	1.070	0.75	0.70	0.05	0.217
25	1.320	2.00	1.51	.49	0.467
45	1.640	5.30	3.23	2.07	1.000

It follows from the above observations, that, when stannic chloride and phosphoric or pyroarsenic acid are mixed, a colloidal solution of stannic phosphate or stannic arsenate is immediately formed. The particles in these sols are very nearly spherical (very low values of ρv) and their size is comparable to the wavelength of light (very low values of ρu, and ρh less than 100). With the lapse of time, the sol is gradually coagulated (as evidenced by an increase in the volume and a decrease in the number of particles) but the linear dimensions of the coagulated particles are never larger than the wavelength of light. Also, during gelation the particles become more and more anisotropic in shape and/or structure. The slow changes in the values of $\phi\ I$ (*cf.* last part of *I-t* curves) probably correspond to that stage of gelation during which the particles in the gel-forming system take up plenty of the dispersion medium and become heavily hydrated, whereby the viscosity of the system increases enormously and brings about its setting to the gel state. Further, in some cases, the particles of the gel continue to grow in size and become more and more anisotrpoic in shape and/or structure for some time, even after the gels have set.

3. Thorium Phosphate Gels

Since the values of I, ρu, ρv and ρh remain constant throughout (*cf.* Table III), it follows that the particles continue to remain in their initial state with respect to size, shape and structure, during the process of gel-formation. The values of ρu and ρv are very low—not much greater than zero. The values of ρh lie between 40–50. Hence, it may be safely concluded that the particles in the gels are spherical or isotropic, or very slightly ellipsoidal or anisotropic in shape and/or structure.

While the addition of HCl brings about little alteration in the anisotropic nature or size of the particles (*cf.* values of ρu and ρv, Table III), the presence of alcohol in the gel-forming mixtures appears to make the gel particles very slightly more isotropic and spherical. It was also observed that the addition of HCl and alcohol increases the time of setting of the gels.

The values of I_D and I_A have been calculated as before for the mixture formed from A = 25 cc., B = 2 cc., and are found to be 0.173 and 0.027, respectively. Since these values do not change during gelation, it can be inferred that no changes take place in the anisotropy, the number and the volume of the gel particles during setting.

It was observed that, when thorium nitrate and phosphoric acid are mixed, thorium phosphate, which is immediately precipitated, redissolves completely on shaking. The data given in Table III show that the particles in the system have a finite size, less than the wavelength of light, and are very slightly anisotropic in shape and/or structure. Since there is no indication of any appreciable decrease in the number of particles, it can be presumed that, unlike the cases of stannic phosphate or stannic arsenate gel-forming mixtures, coagulation, as determined by the agglomeration of the individual particles, does not take place in this case. Since the shape, size and structure of the particles continue to be the same, the setting of the gel can only be explained by assuming that the particles become highly hydrated and these highly hydrated entities form the ultimate structure of the gel. The transparent nature of the resulting gel and of the gel-forming mixture throughout the process of gelation is due to the fact that very nearly the original size of the particles in the sol state is maintained during gelation. It must, however, be stated that, since no special precautions were taken to render the gel-forming solutions dust-free, the dust particles present may have played some part in influencing the values of the depolarization factors. Also, the values of depolarization factors may be changing during gelation to a small extent imperceivable by the experimental arrangement employed in this investigation.

4. Ceric Phosphate Gels

It will be seen from Table IV that the values of ρu, ρv and I are finite and above zero (ρu being fairly high) when the constituents of the gel-forming mixture are mixed, and that they fall off gradually as the process of gelation commences, until they become very low, nearly equal to zero. This shows that the particles in this gel-forming mixture are anisotropic in shape and/or structure in the beginning and lose their anisotropism gradually and decrease in size enormously during gelation, until they become almost isotropic and spherical. These changes take place almost within one hour while the gel is still far from the stage of setting (t varying from 14 to 24 hr.).

The values of ρh range approximately between 22 and 93, showing thereby that, initially, the linear dimension of the particles are comparable to the wavelength of light, while subsequently their size decreases appreciably.

Since this gel is thixotropic, the values of the depolarization factors were obtained after shaking the set gel. It was found that the values of these factors did not alter, showing thereby that the particles did not undergo any change in shape, size or structure on shaking.

The addition of increasing amounts of potassium phosphate increases the rate of fall of the intensity of the scattered light, that is, the rate of decrease of the particles in the gel-forming system during the process of setting (*cf.* I-t curves, Fig. 4). Further, although such an addition causes no definite regular changes in the values of ρv, it appears that the particles become more anisotropic in shape and/or structure.

The addition of HCl to the gel-forming mixtures appears to have no definite effect on the nature of the particles of the gel, but (except during the first 20 min., when the gel-forming mixture is opaque) the rate of fall in intensity of the scattered light, that is, the rate of decrease in the size of the particles in the gels, is increased. The addition of alcohol to the gel-forming mixture produces the same effect as the addition of HCl in the changes in the size of the particles during gel-formation, with the difference that the particles become less anisotropic in shape and/or structure.

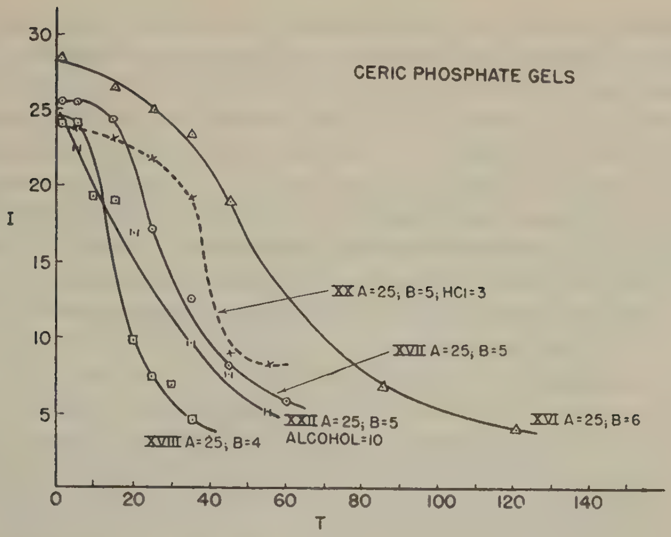

FIG. 4.

The values of I_D and I_A have been claculated for the gel-forming mixture formed from A = 25 cc. and B = 5 cc., and are given in Table VI.

It will be evident from the table that the anisotropy scattering is far less than the density scattering throughout, that is, the total intensity of the scattered light is predominantly due to the density and not to the anisotropy scattering. Since I_D and I_A decrease steadily during the first hour after the components of the gel-forming mixtures are mxied, it follows that the number of particles increases and that the particles lose their anisotropism of shape and/or structure during this period. This shows that the particles of the gel-forming substance are peptized from the clusters that they may have formed at the time of mixing A and B. This is also evidenced from the fact that the volume of the individual particles is reduced during this process; the size of the particles at the end of 1 hr. is about $\frac{1}{3}$ of the initial size.

TABLE VI

Time	$\frac{6+6\rho}{6-7\rho}$	I	I_D	I_A	$V=I_D/IF$
min.					
15	1.6	24.5	15.3	9.2	3.16
25	1.385	17.3	12.5	4.8	2.58
35	1.26	12.7	10.1	2.6	2.08
60	1.198	5.8	4.85	0.95	1.00

It follows from the above discussion that, when cerium nitrate and potassium phosphate are mixed, an immediate precipitation of ceric phosphate takes place. The particles of this precipitate are (1) fairly large (perhaps in clusters) and are comparable in their linear dimensions to the wavelength of light (*cf.* low values of ρh and high values of ρu and I), and (2) slightly anisotropic (ρv nearly 8). Because of the large dimensions of the particles of the gel the gel-forming mixture is opaque. After about 1 hr., the particles of the precipitate (1) split off from their clusters and thus become reduced in volume as indicated by low values of I and ρu and high values of ρh and, increase in number, and (2) gradually lose their anisotropy (ρv tends to zero) and become very small in size (ρh becomes nearly 90). After 1 hr. or so, when (1) the number of particles becomes maximum, and (2) their size becomes minimum, (3) their shape becomes very nearly spherical, and (4) their nature becomes almost isotropic, the particles slowly become heavily hydrated and thereby the gel-forming system becomes very viscous and sets to a gel in quite a long time. The set gels are transparent because the particles contained in them are very small in size.

The fact that shaking the gel introduces no alteration in the nature or size of its constituent particles shows that it only overcomes the forces binding the particles and does not break them into finer entities.

ACKNOWLEDGMENTS

Our best thanks are due to Dewan Bahadur Dr. K. R. Ramanathan M.A., D.Sc., Superintendent Meteorologist, Poona, for a loan of a double image prism and nicol used in this investigation. Our thanks are also due to Dr. S. S. Dharmatti, Ph.D., F. Inst. P., for his assistance.

SUMMARY AND CONCLUSIONS

A systematic study of 3 types of gels with regard to their opacity has been made using the scattering technique. The depolarization factors of the scattered light have been measured by the natural background method of observation, and the intensity determined by the photoelectric method. The results obtained have been used to follow the process of formation of the gels and the changes in the nature of the particles during the process of setting. A very interesting feature of the paper is the explanation offered for the process of formation of the 3 types of gels on the basis of the data obtained in this investigation.

(i) In gel-forming systems which increase in opacity during setting, the particles grow in size, become more and more anisotropic, coagulate by a process of aggregation (as indicated by decrease in number and increase in size), and finally set to an opaque gel, the opacity being due to the increased size of the particles in the same volume of the gel.

(ii) In systems which neither increase nor decrease in opacity during setting, there is no increase in the number and volume and anisotropy of the particles during the gel formation. In such cases, the gelation is brought about by the process of hydration. The set gels are transparent since their particles are of the same small size as at the commencement of the process of gelation.

(iii) In systems which decrease in opacity during setting, the particles are at first in large aggregates and highly anisotropic; subsequently they split up into smaller particles and become very small and isotropic. It takes a long time for such gel-forming systems to set.[1]

REFERENCES

1. LOVE, *Proc. London Math. Soc.* **30**, 308 (1899).
2. MIE, G., *Ann. Physik* **25**, 377, 428 (1908).
3. LORD RAYLEIGH, *Phil. Mag.* **47**, 375 (1899); **84**, 25 (1911).
4. MARDLES, *Trans. Faraday Soc.* **18**, 318 (1923).
5. KRAEMER AND COWORKERS, *J. Phys. Chem.* **29**, 1169 (1925); **31**, 764 (1927).
6. HOLWEDA, *Rec. trav. chim.* **50**, 601 (1931).
7. KRISHNAMURTHI, *Proc. Roy. Soc. London* **122A**, 76 (1929); **129A**, 490 (1930).
8. SUBBARAMIAH, D. S., *Proc. Indian Acad. Sci.* **1**, 709 (1935).
9. KRISHNAN, R. S., *ibid.* **1**, 717, 782 (1935).
10. SUBBARAMIAH, K., *ibid.* **5–6**, 128, 138, 499 (1937).
11. PRASAD AND GURUSWAMY, *ibid.* **19A**, 47 (1944).
12. HOOVER, PUTHAM AND WITTENBERG, *J. Phys. Chem.* **46**, 81 (1942).
13. LOTMAR, *Helv. Chim. Acta* **21**, 792 (1938).
14. KRISHNAN, R. S., *Proc. Indian Acad. Sci.* **9**, 303 (1939).
15. SUBBRAMANIA, DOSS, G., AND RAO, S., private communication to the authors.
16. PRASAD AND MODAK, *Proc. Indian Acad. Sci.* **12**, 235 (1940).
17. PRASAD AND GURUSWAMY, S., *ibid.* **19**, 47 (1944).
18. PRASAD AND GOGATE, *ibid.* **17**, 161 (1943).
19. PRASAD, DESAI AND MEHTA, *J. Phys. Chem.* **36**, 1324 (1932).
20. PRASAD, PARMAR AND MEHTA, *J. Indian Chem. Soc.* **13**, 69, 128, (1936).
21. ANANTHAKRISHNAN, *ibid.* **1**, 201 (1934).
22. PRASAD AND DESAI, *J. Univ. Bombay* **7**, 132 (1938).

---

[1] The set gels are transparent because the size of the particles decreases considerably during the early stages of gelation and then remains practically constant.

There is a striking parallelism between the changes in the values of the intensities of scattered light and the depolarization factors.

Since heavy hydration of the constituent particles in a gel is the essential requirement of gel-formation, the aforesaid observations indicate that there is some definite relation between the density of charge of the colloidal particle and its hydration tendency. In the first type of gels, the colloidal particles formed must undergo decrease of charge (as revealed by their undergoing coagulation), in the second type, the particles formed have such density of charge that it needs no reduction (by coagulation), and, in the third type, the particles carry very low density of charge which must be increased (as revealed by the process of peptization), before they can be in a state for becoming heavily hydrated.

X–RAY INVESTIGATIONS OF THE STRUCTURE OF COLLOIDAL ELECTROLYTES. IV. A NEW TYPE OF MICELLE FORMED BY FILM PENETRATION [1]

William D. Harkins and Rose Mittelmann

George Herbert Jones Chemical Laboratory, University of Chicago, Chicago 37, Illinois

Received September 24, 1948; revised December 30, 1948

I. Introduction

Penetration of Monolayers of Long Chain Polar-Nonpolar Molecules by Molecules of Detergents and the Structure of the Micelle

In 1935 Schulman and Hughes (1) showed that if a solution of sodium hexadecyl sulfate is injected under a condensed monolayer of hexadecyl alcohol, the molecules of the detergent penetrate the monolayer and thereby increase the film pressure. From sharp kinks in the film pressure-molecular area curve Schulman considered that compounds with the ratios of sulfate to alcohol of 1:1 and 1:3 are formed. Harkins and Florence changed this technique (2, 3, 4). They first put the dilute solution of the detergent into the trough, allowed time for adsorption to occur, then swept off the monolayer and immediately, before adsorption reoccurred, spread a monolayer of the alcohol over the surface. The results of work by Harkins, Copeland and Gordon (5) are exhibited in Fig. 1. A period of 12 hr. or more, during which the film pressure was obtained every five minutes by a recording film balance, insured the attainment of equilibrium.

The curves exhibit no kinks and thus no evidence for compound formation. It was found that at equilibrium, 3×10^{-6} molar detergent increased the film pressure at 25°C. from 1 dyne per cm. to 45 dynes per cm. at a molecular area of 26 sq. Å. for the alcohol.

The existence of this phenomenon gives a suggestion that its reverse should be investigated. Since long chain alcohols are insoluble in water the most favorable situation would be that in which they be given an opportunity to penetrate between the soap ions in a micelle.

Preliminary Work on the Diameter of the Micelle

However, what led to the present investigation was the discovery of a new long-spacing X-ray band (6, 7, 8). The Bragg spacing obtained

---

[1] This investigation was carried out under the sponsorship of the Reconstruction Finance Corporation, Office of Rubber Reserve, in connection with the Government's synthetic rubber program.

from the apparent maximum of this band was found to give a value close to, but very slightly less, than twice the length of the soap molecule. For example the Bragg spacing found was 30 Å for the potassium soap of the 8 C atom *n*-acid and 47 Å for 16 C atoms. This suggested that upon the development of the proper theory this band would give a measure of the thickness of the micelle. On this account it was designated as the micelle thickness or *M*-band. Various calculations made upon an uncertain basis indicated that if the micelle is considered as a cylinder its diameter is very nearly the same as its thickness. Since the edges of the cylinder would have to be rounded off, the shape would be very close to that of a sphere.

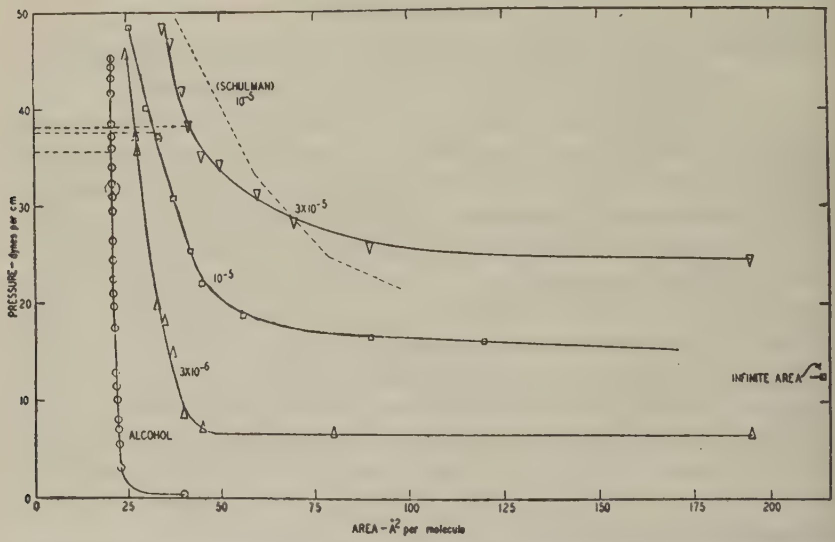

FIG.1. Film pressure-molecular area curves of hexadecyl alcohol over 0.3×10^{-6}, 1×10^{-5}, and 3×10^{-5} molal solution of sodium hexadecyl sulfate. (From work by Harkins, Copeland and Gordon (5).)

A remarkable feature of the preliminary results was that although the apparent diameter could be varied greatly by the use of a different soap and the resultant change in the length of the soap molecule, it remained constant between concentrations of 4.8 and 20% potassium dodecanoate and between 2.3 and 16.5% of the tetradecanoate, and with these and all other soaps through the total range of concentrations in which the band was shown plainly in the tracings.

II. NUMBER OF SOAP IONS IN A MICELLE

A few values which have been determined are as follows.

1. Cetyl pyridinium chloride (salt present) 70 chains (9).

2. Duponol (sodium salts of sulfated aliphatic alcohols). Micelle molecular weight = 12,500 (10).

3a. Sodium dodecyl sulfate (plus salt). 87 chains (11). b. Sodium dodecyl sulfate (0.7 moles per kg. solution). 57 chains (8).

4. Sulfonated di-2-hexyl succinate (salt present) = Aerosol MA. 24 chains (12).

5a. Dodecyl ammonium chloride. 67 chains (13). b. *n*-dodecyltrimethyl ammonium bromide. 64 chains (14).

6. Calculations now in progress in this laboratory by the use of the corrected *M*-band spacings and apparent densities indicate that for soaps of from 6 to 16 C atoms the variation in number (in the absence of salt) lies between limits of about 30 and 100 chains.

III. Solubilization and Models for the Micelle

If a hydrocarbon oil is dissolved in the micelle the spacing is increased by $\Delta(2r)$ which, when calculated on the basis of what appears to be a correct theory, gives values in a 0.33 molal (8.65%) solution of sodium dodecyl sulfate of 11.2 Å and 11.4 Å respectively for ethyl benzene and *n*-heptane. These values, since the hydrocarbon dissolves in the interior hydrocarbon region of the micelle, and avoids the polar outer region, may be considered as the mean diameter of the solubilized oil, although so few molecules are solubilized that they cannot well take on the shape of a sphere.

It is not the purpose of this paper to consider the relative value of the various models which have been suggested for the micelle. However, since the X-ray work presented here was incited by a simple model (15), it may be considered here. Stack up a pile of dollars until it becomes approximately as high or higher than the diameter of the dollar. Let this represent a highly magnified model of the cylindrical micelle, which obviously does not exist. Assume now that the top and bottom of the cylinder are covered by the ionic groups and that the hydrocarbon groups are oriented vertically inside with their ends in contact. This would be a crystalline micelle. However, the short spacing X-ray band, except for the larger spacing it indicates (4.5 Å) is almost the same as the water band (3.1 Å). Thus the micelle appears to be a liquid structure and will therefore, on account of the free interfacial energy involved, take on as nearly a spherical shape as is possible. However it is possible that it cannot do this and also preserve its essential characteristic as a double layer of oriented ions. Water and hydrocarbon, even on a molecular scale, exhibit a high free energy when in contact, so the truly cylindrical form with flat ends is an improbable one, since at the edge of the cylinder water and hydrocarbon would be in contact. The solution of the problem is found in the flexibility of molecules which are made up largely of flexible hydrocarbon chains. This allows a part of the ionic groups which would be present in the crystal cylindrical model to cover to some extent the hydrocarbon chains at the ends of the micelle, which otherwise would be in contact with the water.

Consider a very minute island of condensed film of a detergent supposed to exist as a monolayer on water. Actually this would have to be a patch surrounded by an identical monolayer. Assume that the island contains 70 molecules. Its area is ca. 2100 sq. Å, which corresponds to a patch 42 Å by 50 Å, with the molecules oriented with their chains perpendicular to the water and with the ionic ends toward the water. This monolayer is now to be picked up and folded back upon itself in such a way that the orientation toward the now external water is preserved as much as possible and the ends of the hydrocarbon chains come into contact. This gives a double layer "biscuit" whose top, bottom and edge are covered as completely as possible by the ionic groups. Such a model may be considered as a cross between a cylinder and an oblate spheroid, or by penetration of water between the polar groups the form attained may be that of a sphere. With a definite soap the thickness of the "biscuit" is constant, *i.e.*, independent of concentration and equal to about twice the length of the soap molecules, but its diameter may vary, although seemingly not with concentration.

The ends of the cylinder do not contain 35 ionic groups each, since some of these groups are utilized in rounding off the edge of the cylinder.

In general the thickness and diameter of the cylinder (or biscuit) are nearly the same.

The interfacial tension between the micelle and the water with ionic atmosphere is very small, but the small size of the micelle gives a relatively high internal pressure, so the micelle takes on as nearly a spherical shape as possible, when the other constraints are involved. The question which now arises is as follows: may not a spherical micelle, as proposed by Hartley, meet all of the conditions imposed upon it by the results of experiment? The ions in the micelle exhibit a repulsion which increases the outer area of the micelle. This should allow penetration of water between the polar ionic heads, thereby increasing the area per ion much above that found from the short X-ray spacing which is about 27 Å^2. This value may be assumed to be related to the spacing of the hydrocarbon chains in the inner hydrocarbon portion of the micelle, since it has the value of the similar spacing in a liquid hydrocarbon.

If the spherical model is to be demonstrated as the better, then it is essential to show that what may be explained in the quasi-cylindrical model by a second dimension (diameter in addition to thickness), is due to differences in density of the micelle under different conditions.

At the present time no phenomenon or quantitative relationship is known which indicates the spherical model to be inapplicable. There is a possible exception to this. Debye and Anacker (13) by light scattering measurements find that the mass of the micelle of dodecylamine hydrochloride is increased by a very large factor (3.25) by a small concentration ($m = 0.046$) of sodium chloride. This would indicate an increase in diameter of a sphere of nearly 50% if the density were to remain constant. Such an increase does not accord with a spherical model. On the basis of the quasi-cylindrical model the diameter would be increased by about 80%.

The quasi-cylindrical model has been discussed here because it was on this basis that it was considered:

1. That n-long chain alcohols would solubilize in the micelle by penetration between the long chain soap ions and thus would not increase its thickness.
2. That with alcohols of about half the chain length of the soap the more probable change would be a *decrease* in diameter.

IV. DETERMINATION OF THE POSITION OF THE MAXIMUM OF THE *M*–BAND AND THE RELATED DIAMETER OF THE MICELLE

In the work already published (6, 7, 8) the position of the maximum of the M-band and the value of the related diameter of the micelle, were calculated by empirical methods.

In connection with this project Dr. M. L. Corrin developed recently, on the basis of a theory of scattering by spherical particles, a much more accurate method of determining the spacing, and on the basis of this theory the diameters of micelles which contain alcohols have been calculated.

It is evident that several different radii for the micelle could be considered and that each radius should be defined specifically. For example the mean radius of the hydrocarbon core is less than that of the micelle as a whole. The radii presented in this paper are presumably closer to the latter. The presentation of the details involved will be discussed in a forthcoming paper by Corrin. What is presented here is sufficient to exhibit the effect of alcohols on the radii of soap micelles. For each soap (or detergent) the radius of the micelle as determined is nearly the same as the length of the soap molecule, as calculated from atomic constants.

Thus the solubilization of 3.1% of alcohol in 22.75% of the soap, which contains 12 C atoms per molecule, gave the greatest decrease in micellar radius when the alcohol molecule contained 6 C atoms, or half as many as the molecule of soap. However the decrease is almost as high as this between 3 and 8 C atoms for the alcohol.

However there is a complication, in that the 3 lowest alcohols are miscible with water, so not nearly all of these alcohols are present in the micelle. The 4, 5, 6, and 7 C atom alcohols have solubilities at 20°C. of 7.9%, 2.5%, 0.59%, 0.1%, so the relative amount present in the micelle increases with chain length.

The interpretation of the decrease in diameter of the micelle by alcohols may be that the alcohol chain is shorter than that of the soap and does not penetrate so far into the central portion. This would leave a hole, but the hydrocarbon chains of the soap fold to fill it. This shortens the effective length of the soap chain. Other work in this laboratory (16, 17) shows that whereas hydrocarbons which solubilize in the inner part of the micelle, have little effect on the critical micelle concentration, *n*-alcohols produce a very great lowering (the lowering increases rapidly with the number of C atoms in the alcohol), which is evidence that they play a part similar to that of the soap molecules themselves.

V. Materials and Apparatus

Most of the work was done on aqueous solutions of sodium dodecyl sulfate, partly because this detergent is much more stable in solution than the corresponding pure soap (potassium dodecanoate), partly because it gives very smooth, clear X-ray diffraction bands. It has the advantage that the *I*-band does not appear until a very large concentration is attained.

Relatively pure sodium dodecyl sulfate (NaDS) kindly supplied by the Procter and Gamble Company was used for the determinations after purification by recrystallizing three times from absolute ethanol. It was then dried to constant weight over potassium hydroxide in a good vacuum.

The alcohols were distilled and the middle constant boiling fraction used.

The apparatus and experimental procedure was the same as described in an earlier paper (18).

VI. Effect of n–Alcohols on the Diameter of the Sodium Dodecyl Sulfate Micelle

The effect of *n*-alcohols on the diameter of the sodium dodecyl sulfate micelle is shown in Table I.

It can be seen that with a 0.33 *M* solution of sodium dodecyl sulfate the addition of *n*-heptanol, *n*-octanol and *n*-decanol in amounts to make the solutions 0.281 *M*, 0.186 *M* and 0.164 *M* respectively, decreased the diameter by 1.4 Å, 1.3 Å, and 1.8 Å, or by essentially the same small value. The decrease in diameter is more pronounced in solutions of higher detergent concentration. The changes in the diameter due to the same amount (3.0–3.2 g.) of *n*-alcohols per 100 g. of 1,02 *M* sodium dodecyl sulfate solution are also shown in Fig. 3.

TABLE I

The Effect of "Penetration" on the Micelle Diameter ($2r_M$) of Sodium Dodecyl Sulfate (NaDS)

% NaDS by wgt.	Moles of NaDS per 1000 g. solution	Moles of NaDS per 1000 g. water	Additive	G. additive per 100 g. NaDS soln. only	Moles additive per 1000 g. NaDS soln. only	Moles additive per 1000 g. water only	$2r_M$	$\Delta(r_M)$
8.65	0.30	0.33	—	—	—	—	43.7	—
8.65	0.30	0.33	Heptanol	2.98	0.257	0.281	42.3	−1.4
8.65	0.30	0.33	Octanol	2.21	0.170	0.186	42.4	−1.3
8.65	0.30	0.33	Decanol	2.16	0.150	0.164	41.9	−1.8
8.65	0.30	0.33	Decyl	1.85	0.116	0.127	44.0	+0.3
8.65	0.30	0.33	amine	1.74	0.109	0.119	43.8	+0.1
15.7	0.54	0.65	Butanol	2.68	0.362	0.430	41.9	−1.8
15.7	0.54	0.65	Butanol	4.71	0.636	0.755	41.6	−2.1
15.7	0.54	0.65	Butanol	6.85	0.925	1.098	41.1	−2.6
22.75	0.79	1.02	—	—	—	—	43.6	—
22.75	0.79	1.02	Methanol	3.12	0.975	1.262	39.7	−3.9
22.75	0.79	1.02	Ethanol	3.10	0.674	0.872	42.1	−1.5
22.75	0.79	1.02	Propanol	3.10	0.518	0.669	38.3	−5.3
22.75	0.79	1.02	Butanol	3.10	0.419	0.542	37.8	−5.8
22.75	0.79	1.02	Pentanol	3.13	0.356	0.460	37.8	−5.8
22.75	0.79	1.02	Hexanol	3.04	0.298	0.386	37.4	−6.2
22.75	0.79	1.02	Heptanol	3.15	0.271	0.352	38.0	−5.6
22.75	0.79	1.02	Octanol	3.04	0.234	0.303	38.0	−5.6
22.75	0.79	1.02	Nonanol	3.05	0.212	0.274	39.4	−4.2
22.75	0.79	1.02	Decanol	3.10	0.196	0.251	40.3	−3.3
24.8	0.93	1.14	—	—	—	—	43.7	—
24.8	0.93	1.14	Methanol	1.28	0.400	0.532	39.9	−3.8
24.8	0.93	1.14	Ethanol	1.84	0.400	0.532	39.2	−4.5
24.8	0.93	1.14	Propanol	2.40	0.400	0.532	38.7	−5.0
24.8	0.93	1.14	Butanol	2.96	0.400	0.532	37.6	−6.1
24.8	0.93	1.14	Pentanol	3.59	0.408	0.543	37.5	−6.2
24.8	0.93	1.14	Hexanol[a]	4.08	0.400	0.532	?	

[a] This "solution" was a clear but stiff gel.

(The presence of alcohols, except for the low members of the homologous series, usually increases the viscosity of the detergent solution. Addition of 4.08 g. of hexanol to 100 g. of 24.8% sodium dodecyl sulfate solution gave a clear but stiff gel at room temperature. It is interesting to note in this case that instead of the usual broad and diffuse appearance of the M-band—especially at higher detergent concentrations—now it becomes a broad but distinct band, with about the same spacings as when a gel is not formed.) (Fig. 2.).

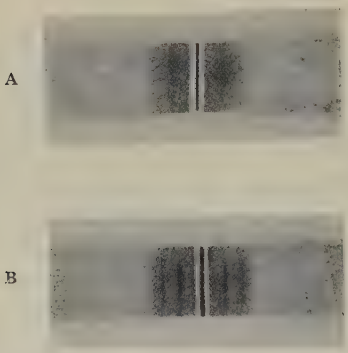

FIG. 2A. The effect of gel-formation on the X-ray diffraction bands of 24.8% sodiu dodecyl sulfate solution. Film of 24.8% NaDS with A. 3.59 g. pentanol added to 100 g detergent solution (viscous liquid). B. 4.08 g. hexanol added to 100 g. detergent solution (clear gel).

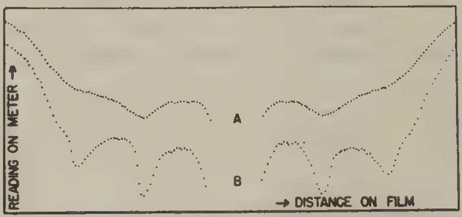

FIG. 2B. Photometer tracings of the films shown in Fig. 2A.

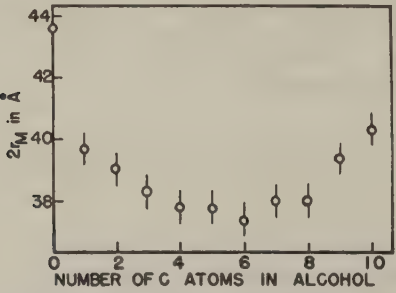

FIG. 3. The effect of n-alcohols on the diameter of micelles in 22.75% sodium dodecyl sulfate solution.

Table II gives values for hydrocarbons which are *solubilized* in the micelles. These are presented for comparison.

VII. LONG I-BAND SPACINGS

The long X-ray spacings used by all other investigators are somewha longer than the *M*-band spacings. They decrease with increasing soa concentration, and are evidently related to the intermicellar distance

TABLE II

The Effect of "Solubilization" on the Micelle Diameter of Sodium Dodecyl Sulfate

% NaDS by wgt.	Moles of NaDS per 1000 g. solution	Moles of NaDS per 1000 g. water	Additive	G. additive per 100 g. NaDS soln. only	Moles additive per 1000 g. det. soln. only	Moles additive per 1000 g. water only	$2r_M$	$\Delta(2r_M)$
8.65	0.30	0.33	Ethyl benzene	2.81	0.265	0.290	54.9	11.2
8.65	0.30	0.33	Heptane	1.46	0.146	0.160	55.1	11.4

However, whether there is any simple relationship between the Bragg value of the *I*-spacing and any useful mean distance between micelles in a soap solution, is unknown. The *I*-spacings deserve consideration as giving a qualitative idea of the distance between micelles. The values given below are simple Bragg spacings of the maximum of the *I*-band, which has a much sharper peak than the *M*-band.

Addition of normal alcohols to a soap or detergent solution always causes an increase in the intensity of the *I*-band. The spacing of the *I*-band however is decreased by the lower, water-soluble, and increased by the higher insoluble alcohols. From Fig. 4 it can be seen that if the same weight of different alcohols (3.0–3.2 g. alcohol per 100 g. detergent solution) is added to a 22.75% sodium dodecyl sulfate solution, the *I*-spacing as a function of the number of C atoms in the alcohol shows a minimum with propanol (the highest infinitely water soluble member of the homologous series); butanol (its solubility in water is about 7.9%) still lowers the original *I*-spacing. Beginning with pentanol, however

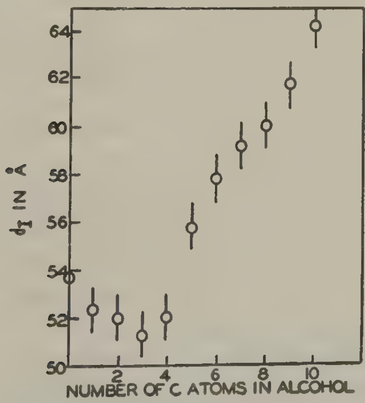

FIG. 4. The effect of n-alcohols on the long spacing (d_I) of 22.75% sodium dodecyl sulfate solution.

(this is only to about 2.7% soluble in water, *i.e.*, below the amount added) the increase in the *I*-spacing is almost a linear function of the number of C atoms in the alcohol. With enough alcohol the *I*-band commonly appears at a soap concentration far below the minimum at which it appears with the pure soap.

Table III shows the change in the *I*-spacing of sodium dodecyl sulfate which accompanies the addition of alcohols.

Addition of methanol or ethanol to sodium dodecyl sulfate solution makes the X-ray pattern more diffuse so that measurement of the *M*-band is not possible with larger amounts of methanol or ethanol. The *I*-spacing decreases with increasing amounts of alcohol. However it is interesting that even as much as 38.9 g. methanol per 100 g. aqueous sodium dodecyl sulfate solution shows a diffraction pattern, thus indicating the presence of micelles in this highly alcoholic solution. However, the pattern is so diffuse that the resolution of it would be meaningless. Table IV and Fig. 5 show the changes in the *I*-spacing of sodium dodecyl sulfate with methanol and ethanol added.

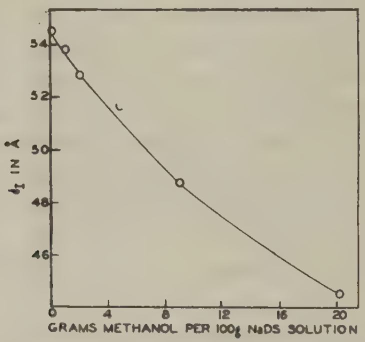

FIG. 5. The effect of methanol on the long spacing (d_I) of 20.0% sodium dodecyl sulfate solution.

As mentioned before, addition of alcohols increases the intensity of the *I*-band. Butanol was chosen to study this effect in detail, partly because the working range of this alcohol is larger than that of the higher alcohols, where the penetration is limited more quickly by saturation, and where even before saturation gel-formation causes very difficult working conditions, and partly because this alcohol has quite a striking effect on the intensity of the *I*-band.

Fig. 6 and Table V show the increased range of the *I*-band. The lines for the NaDS solution only and for 6.7 g. butanol per 100 g. NaDS solution, though they consist of three points only (the lines are the calculated best lines through these three points) are included to show the

TABLE III

A. The Effect of "Penetration" of Alcohols on the I-Spacing of Sodium Dodecyl Sulfate

% NaDS by wgt.	Moles NaDS per 1000 g. soln.	Moles NaDS per 1000 g. water	Additive	G. additive per 100 g. NaDS sol. only	Moles add. per 1000 g. deter. sol. only	Moles add. per 1000 g. water only	d_I ±1Å	Δd_I ±2Å
7.65	0.27	0.29	Butanol	6.85	0.925	1.002	59.2	[a]
9.0	0.31	0.34	Butanol	4.70	0.636	0.698	57.9	[a]
10.1	0.35	0.38	Butanol	4.71	0.636	0.708	56.9	[a]
12.5	0.43	0.50	Butanol	6.89	0.931	1.064	54.0	[a]
13.1	0.45	0.52	Butanol	4.71	0.636	0.732	54.7	[a]
15.7	0.54	0.65	Butanol	4.71	0.636	0.755	53.5	[a]
15.7	0.54	0.65	Heptanol	2.09	0.180	0.214	63.6	[a]
15.7	0.54	0.65	Heptanol	3.45	0.300	0.353	64.9	[a]
17.5	0.61	0.74	Heptanol	2.00	0.172	0.209	58.9	[a]
17.5	0.61	0.74	Heptanol	3.34	0.286	0.349	63.3	[a]
17.5	0.61	0.74	Pentanol	5.70	0.647	0.785	57.1	[a]
22.75	0.79	1.021	None	—	—	—	53.7	—
22.75	0.79	1.021	Methanol	3.12	0.975	1.262	52.3	−1.4
22.75	0.79	1.021	Ethanol	3.10	0.674	0.812	52.0	−1.7
22.75	0.79	1.021	Propanol	3.10	0.518	0.669	51.2	−2.5
22.75	0.79	1.021	Butanol	3.10	0.419	0.542	53.0	−0.7
22.75	0.79	1.021	Pentanol	3.13	0.356	0.460	55.8	+2.1
22.75	0.79	1.021	Hexanol	3.04	0.298	0.386	57.8	+4.1
22.75	0.79	1.021	Heptanol	3.15	0.271	0.352	59.2	+5.5
22.75	0.79	1 021	Octanol	3.04	0.234	0.303	60.1	+6.4
22.75	0.79	1.021	Nonanol	3.05	0.212	0.274	61.7	+8.0
22.75	0.79	1.021	Decanol	3.10	0.196	0.251	64.2	+10.5
24.8	0.93	1.144	None	—	—	—	53.2	—
24.8	0.93	1.144	Methanol	1.28	0.400	0.532	52.4	−0.8
24.8	0.93	1.144	Ethanol	1.84	0.400	0.532	52.7	−0.5
24.8	0.93	1.144	Propanol	2.40	0.400	0.532	52.1	−1.1
24.8	0.93	1.144	Butanol	2.96	0.400	0.532	52.4	−0.8
24.8	0.93	1.144	Pentanol	3.59	0.403	0.543	55.8	+2.6
24.8	0.93	1.144	Hexanol[b]	4.08	0.400	0 532	56.0	+2.8

B. The Effect of "Solubilization" on the I-Spacing of Sodium Dodecyl Sulfate

% NaDS by wgt.	Moles NaDS per 1000 g. soln.	Moles NaDS per 1000 g. water	Additive	G. additive per 100 g. NaDS sol. only	Moles add. per 1000 g. deter. sol. only	Moles add. per 1000 g. water only	d_I ±1Å	Δd_I ±2Å
24.8	0.93	1.144	Benzene	3.17	0.406	0.537	59.8	+6.6
24.8	0.93	1.144	Benzene	4.08	0.523	0.696	60.5	+7.3

---

[a] There is no I-band noticeable in the X-ray diffraction of pure aqueous sodium dodecyl sulfate at this detergent concentration.

[b] This "solution" was a clear but stiff gel.

TABLE IV

The Effect of Methanol and Ethanol on the I-Spacing of Sodium Dodecyl Sulfate

% NaDS by wgt.	Moles NaDS per 1000 g. soln.	Moles NaDS per 1000 g. water	Additive	G. add. per 100 g. NaDS sol. only	Moles add. per 1000 g. NaDS sol. only	Moles add. per 1000 g. water only	d_I ±1Å	Δd_I ±2Å
20.0	0.69	0.867	—	—	—	—	54.6	—
20.0	0.69	0.867	Methanol	1.10	0.343	0.430	53.9	−0.7
20.0	0.69	0.867	Methanol	2.10	0.656	0.820	52.9	−1.7
20.0	0.69	0.867	Methanol	4.82	1.506	1.883	51.7	−2.9
20.0	0.69	0.867	Methanol	8.95	2.797	3.496	48.8	−5.8
20.0	0.69	0.867	Methanol	20.06	6.269	7.836	44.6	−10.0
20.0	0.69	0.867	Methanol	38.90	12.156	1.519	?	
20.0	0.69	0.867	Ethanol	2.13	0.463	0.579	54.7	+0.1
20.0	0.69	0.867	Ethanol	4.85	1.054	1.318	50.6	−4.0
20.0	0.69	0.867	Ethanol	8.22	1.787	2.234	48.8	−5-8
22.75	0.79	1.022	—	—	—	—	53.7	—
22.75	0.79	1.022	Methanol	3.12	0.975	1.262	52.3	−0.4
22.75	0.79	1.022	Methanol	4.82	1.506	1.949	48.8	−4.9
22.75	0.79	1.022	Methanol	6.40	2.000	2.590	50.0	−3.7
22.75	0.79	1.022	Methanol	38.90	12.156	15.736	?	
22.75	0.79	1.022	Ethanol	3.10	0.674	0.872	52.6	−1.1
22.75	0.79	1.022	Ethanol	4.81	1.046	1.354	50.5	−3.2

TABLE V

The Effect of Butanol on the I-Spacing of NaDS Solution

% NaDS by wgt.	Moles NaDS per 1000 g. solution	Moles NaDS per 1000 g. water	G. butanol per 100 g. NaDS sol. only	Moles butanol per 1000 g. NaDS sol. only	Moles butanol per 1000 g. water only	d_I ±1Å	d_I[a] ±2Å
9.0	0.31	0.34	4.71	0.636	0.699	57.9	[a]
10.1	0.35	0.38	4.71	0.636	0.708	56.9	[a]
13.1	0.45	0.52	4.71	0.636	0.732	54.7	[a]
15.7	0.54	0.65	4.71	0.636	0.738	53.5	[a]
17.9	0.62	0.76	4.75	0.642	0.782	52.9	[a]
21.4	0.74	0.94	4.73	0.639	0.813	52.0	−2.0
7.7	0.26	0.36	6.85	0.925	1.003	59.2	[a]
12.5	0.43	0.50	6.89	0.931	1.064	54.0	[a]
15.7	0.54	0.65	6.85	0.925	1.098	53.0	[a]

[a] There is no I-band noticeable in the X-ray diffraction of pure aqueous sodium dodecyl sulfate at this detergent concentration.

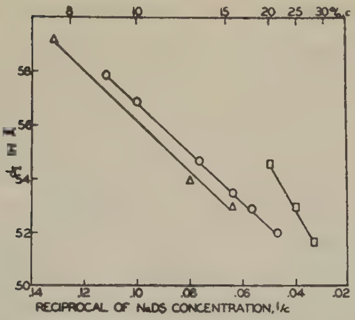

FIG. 6. The effect of butanol on the long spacing (d_I) of aqueous sodium dodecyl sulfate. (The squares represent aqueous NaDS only; the circles represent NaDS solution with 4.7 g. butanol added to 100 g. detergent solution and the triangles represent NaDS solution with 6.9 g. butanol added to 100 g. detergent solution.)

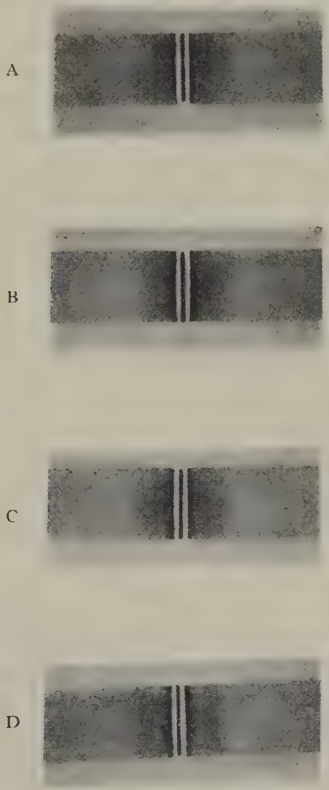

FIG. 7a. The effect of butanol on the X-ray diffraction bands of sodium dodecyl sulfate solution. Film of A. 15.7% aqueous NaDS solution. B. 2.7 g. butanol added to 100 g. of the same solution. C. 4.7 g. butanol added. D. 6.9 g. butanol added.

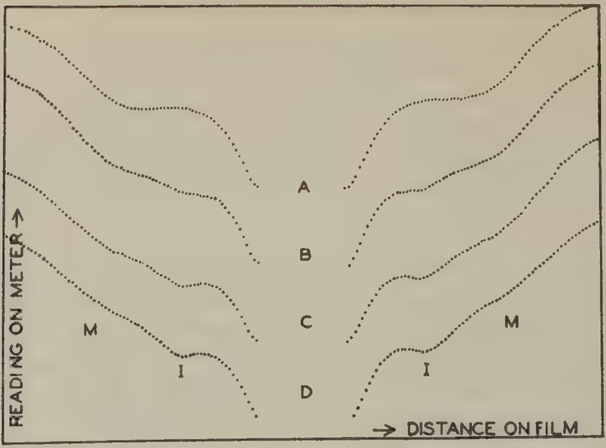

FIG. 7b. Photometer tracings of the films shown in Fig. 7a.

difference in the range of the *I*-band with and without butanol. It should be noted that with 6.9 g. butanol per 100 g. NaDS solution the *I*-band appears even at as low a concentration as 7.65%, whereas in a pure aqueous NaDS solution it does not begin to appear until about 16%.

The effect of butanol on the X-ray diffraction bands of sodium dodecyl sulfate can be seen best in the photometer tracings of films which were taken with increasing amounts of butanol added to a 15.7% sodium dodecyl sulfate solution. As Fig. 7 shows, 2.7 g. butanol per 100 g. sodium dodecyl sulfate solution already causes a distinct *I*-band, and in the case of 6.9 g. butanol the *I*-band becomes so prominent that it overshadows the *M*-band. (In the figures the readings on the photometer in arbitrary units are plotted against distance on the film. Readings were taken every 0.005 of an inch.)

ACKNOWLEDGMENT

We wish to thank Dr. M. L. Corrin, whose theory has been used as a basis for the calculations of the M-spacings given in this paper.

SUMMARY

1. X-ray evidence is presented which shows micelles which contain from a third to half as many molecules of a moderately long chain (6 to 10 C atoms) alcohol as soap are not increased in diameter above that of the micelle of soap alone. On the contrary the diameter is decreased by as much in some instances as 6 Å (Table I). This is just the opposite of the effect produced by the solubilization of a hydrocarbon which may increase the diameter by as much as 11 Å (Table II) or even more.

2. Other work in this laboratory shows that whereas hydrocarbons which solubilize in the inner nonpolar part of the micelle have little effect

on the critical concentration, long chain n-alcohols produce a very great lowering, which is evidence that they play a part similar to that of soap molecules themselves.

3. These relations indicate that the alcohols (amines and other polar nonpolar molecules also) form a new type of micelle in which the amphipathic molecules take a position which is essentially the same as that of the soap molecules, with their polar groups toward the water and their hydrocarbon chains between those of the soap, in which position the diameter is not increased. A possible explanation of the decrease is as follows. Consider a normal 6 C atom alcohol between molecules of a 12 C atom soap. The chain of the alcohol cannot extend as far into the interior of the micelle as those of the soap. This would result in a hole at the inner end of the alcohol chain. However if the hydrocarbon chains of the soap fold into these holes, they would be partly filled and the effective length of the hydrocarbon chains of the soap thereby reduced, which would decrease the diameter of the micelle.

4. The diameters of micelles were calculated on the basis of a theory of X-ray scattering from a system of spherical particles. The values obtained indicate a spacing of 43.6 Å for sodium dodecyl sulfate, independent of soap concentration.

5. Bragg spacings are listed for the long spacing or I-band used by all other investigators, but since no theory by which they can be utilized has been developed, they serve only as a qualitative indication of a change of distance between the micelles.

References

1. Schulman, J. H., and Hughes, A. H., *Biochem. J.* **29**, 1242 (1935).
2. Unpublished work done in connection with investigations of mixed monolayers.
3. Harkins, W. D., and Florence, R. T., *J. Chem. Phys.* **6**, 847 (1938).
4. Florence, R. T., and Harkins, W. D., *ibid.* **6**, 856 (1938).
5. Harkins, W. D., Copeland, L. E., and Gordon, B., Surface Chemistry, *Am. Assoc. Advancement Sci., Publ.* **21**, 79 (1943).
6. Stearns, R. S., private communication, July, 1946.
7. Mattoon, R. W., Stearns, R. S., and Harkins, W. D., *J. Chem. Phys.* **15**, 209 (1947).
8. Mattoon, R. W., Stearns, R. S., and Harkins, W. D., *ibid.* **16**, 644 (1948).
9. Hartley, G. S., and Runnicles, D. F., *Proc. Roy. Soc. London* **168A**, 420 (1938).
10. Miller, G. L., and Anderson, K. J. I., *J. Biol. Chem.* **144**, 475 (1942).
11. Hakala, N. V., Dissertation, Univ. of Wisconsin, 1943.
12. Vetter, R. J., *J. Phys. Colloid Chem.* **51**, 262 (1947).
13. Debye, P., and Anacker, E. W., private communication.
14. Debye, P., Bueche, A. M., Cashin, W. M., and Anacker, E. W., private communication.
15. Harkins, W. D., *J. Chem. Phys.* **16**, 156 (1948).
16. Corrin, M. L., and Harkins, W. D., *J. Chem. Phys.* **14**, 640 (1946).
17. To be published.
18. Harkins, W. D., Mattoon, R. W., and Corrin, M. L., *J. Am. Chem. Soc.* **68**, 220 (1946).

CHANGES IN SOLUBILIZING POWER WITH CONCENTRATION FOR VARIOUS DETERGENTS

J. W. McBain and Harriette M. Huff[1]

Stanford University, Stanford, California

Received November 12, 1948; revised March 18, 1949

Introduction

It has long been known that substances otherwise insoluble may be brought into solution in dilute solutions of soaps or colloidal electrolytes. It was found (1) that thermodynamically stable, reversible equilibria, and therefore a definite solubility, are involved if proper precautions were taken. Many investigations have since shown that this phenomenon occurs only to a minor degree until colloidal particles have appeared in the soap solution itself. The term solubilization was introduced (2,3,4) to distinguish this from the related but different processes of hydrotropy, ordinary colloidal solution, colloidal suspension, emulsification, blending, and cosolvency; and "solubilization" was there defined as consisting in the incorporation of the substance in or upon the colliodal particles of the colloidal electrolyte. This, then, could depend upon the kind of colloidal particle or micelle that is present in a given solution. Results obtained in this and previous papers (5,6,7,8) show that, even for a given solubilized material, the solubilizing power of the micelles often differs in different concentrations of the same detergent, although this is not true of some fatty acid soaps. Hence, the micelles present in one concentration are not the same as those present at other concentrations of that same colloidal electrolyte. It is, therefore, necessary to assume different kinds of micelles or different proportions of different micelles for a given colloidal electrolyte, depending upon such factors as concentration, temperature, added salts, and other added materials.

Materials

Where not otherwise stated, experiments were carried out with Orange OT, FD and C Orange No. 2, 1-*o*-tolylazo-2-naphthol, M.W., 262.3. It was recrystallized from boiling ethyl alcohol to produce large, dark red crystals free from powder.

For some experiments, Brilliant Oil Blue, M.W. 308, was supplied by the National Aniline Division of the Allied Chemical and Dye Corporation It was similarly recrystallized.

---

[1] nee McHan.

In a very few experiments, carotene ($C_{40}H_{56}$, M.W. 536.9) was used as supplied by the Eastman Kodak Company. It contained 90% β- and 10% α-carotene.

Sodium linolenate, with 3 double bonds, was prepared by neutralizing Kalhbaum linolenic acid with NaOH obtained from metallic sodium.

Triton-B laurate was made from Röhm and Haas Triton-B (benzyltrimethylammonium hydroxide, containing no unquaternized material), by neutralizing with the equivalent amount of Kahlbaum lauric acid.

Sodium dihexyl sulfophthalate (M.W. 436.2) was supplied by the Monsanto Chemical Company.

Aresklene "400" (M.W. 486), Aresket "300" (M.W. 311), and Areskap "100" (M.W. 328)were each supplied by the Monsanto Chemical Company and stated to be 99% pure. The formulas are given in the legend of Fig. 2b.

Zephiran (M.W. determined by titration, 342.2) was supplied by the Sterling-Winthrop Research Institute as 97% pure. It is alkyl (coconut)) benzyldimethylammonium chloride.

Cetylbenzyldimethylammonium chloride (M.W. 385.5) was supplied by the William S. Merrell Company as 93.3% pure.

The sodium lauryl oxyethaneamidosulfoacetate ($C_{11}H_{23}COOC_2H_4$-$NHOCCH_2SO_3Na$), M. W. 384, was supplied by Lever Bros. as 87.6% active ingredient, the remainder being Na_2SO_4.

Neutronyx 228, "a fatty acid polyethylene oxide condensation product" (M.W. assumed 600) was used as supplied by the Onyx Oil and Chemical Company.

Carbowax 4000 (M.W. approximately 2900) (a polyethylene oxide) was used as obtained from the Carbide and Carbon Chemical Corporation.

EXPERIMENTAL PROCEDURE

The precautions taken in measuring solubilization of dye are described in previous communications (3,7,8,9).

Ten ml. of each detergent solution was placed in glass vials which had caps lined with pure gold or platinum. A small excess of the recrystallized dye was added to each vial and the vials inclined at a 45° angle on a rotating shaker in a water thermostat at 25° ± 0.2°C. After an agitation of 24 hr., the vials were examined to ascertain whether any of the dye remained on the bottom of the vial. If additional amounts were required, the vials were allowed to shake for another 24 hr. At the end of this time, the vials were allowed to stand vertically in the thermostat for 2 days to complete the sedimentation of any suspended dye. A large excess of dye was avoided in order that sorption of the soap or detergent on the dye particles would not be appreciable. The clear supernatant liquid was examined in the light of a strong electric bulb. If visually clear, a 1 ml.

portion was removed with a calibrated pipette and diluted with 50% aqueous acetone. Further determinations at intervals of 2 days were made with repeated agitation of the samples if results agreeing within 0.2% transmission were not obtained within a week.

A Lumetron colorimeter, Model 402E with a B420 blue filter was used for the transmission measurements of Orange OT and carotene, and a B590 Orange filter for the Oil Blue.

Modifications of the method are necessary when the original detergent solutions are colored. For these, the percent transmission of the detergent solution without dye was first determined after diluting to the same concentration as the diluted dye-detergent solution. The observed value, which was very small, was then expressed in mg. of dye/100 ml. and subtracted to give the final result for the dye solution.

It is well known that sometimes in very dilute solution, a spurious semblance of solubilization occurs through suspension of minute particles of dye. The result is magnified in the subsequent calculation of the ratio of dye to detergent. This was avoided in a number of cases by using the device of McBain and Green (8) which avoid solid dye altogether. An almost, but not quite, saturated solution of dye is made in an indifferent hydrocarbon of fairly high molecular weight such as mesitylene. This is equilibrated with the aqueous layer.

Experimental Results

The data are given in graphical form. Just as it is usual when examining gas laws at constant temperature to plot not only P *vs.* V, but also to plot PV *vs.* P; so, here, the data are plotted both in the form of mg. dye dissolved in 100 ml. of solution *vs.* concentration of detergent, and also in g. dye per mole of detergent *vs.* concentration of detergent. Each method has its use.

It is customary to subtract the solubility of dye in water alone before plotting the data. This cannot be done here because the solubility of dye in water is below the level of measurement (7). Any correction to the graphs would therefore be wholly negligible.

Sodium Linolenate, Triton-B Laurate, and Sodium Dihexylsulfophthalate

The data are assembled and compared in Figs. 1a and b. Ordinary soaps usually show no solubilization until approaching the critical concentration for the initiation of micelles, thereupon gradually building up to an approximately constant ratio between moles of dye solubilized and moles of soap present (8). A closer examination showed that, in more concentrated solutions, they become more efficient solubilizers and the mol ratio rises again, particularly with sodium soaps (5). Many other detergents show a similar behavior. Sodium linolenate here belongs to such a type.

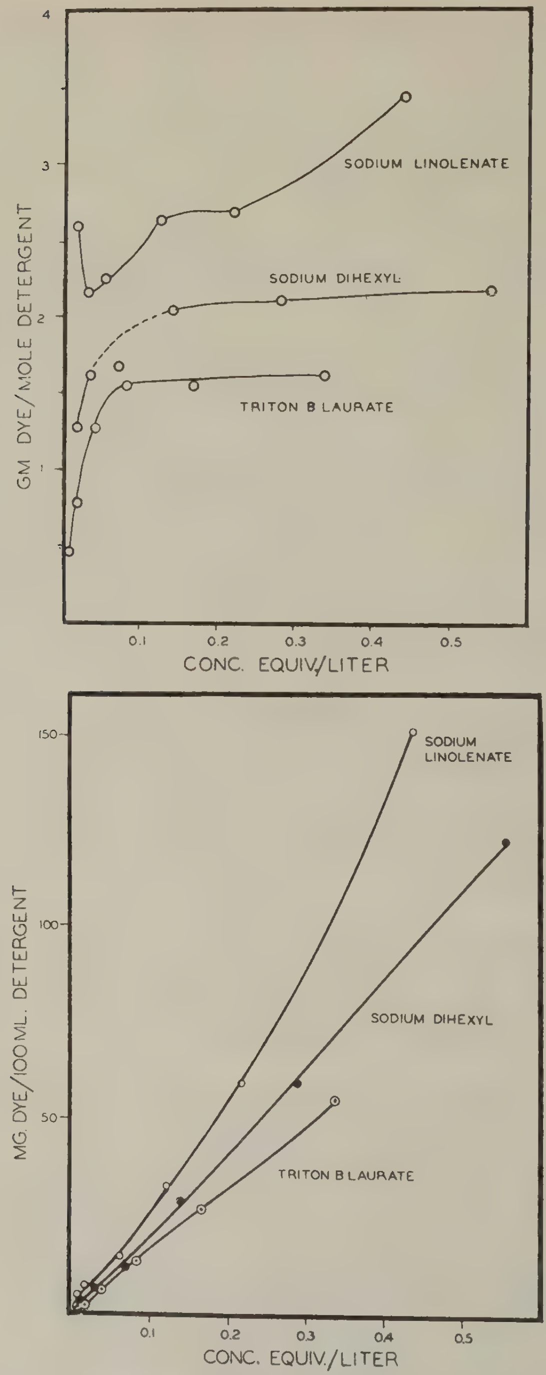

FIG. 1a and b. Solubilization of Orange OT by different concentrations of sodium linolenate, sodium dihexylsulfophthalate, and Triton B laurate saturated with solid dye.

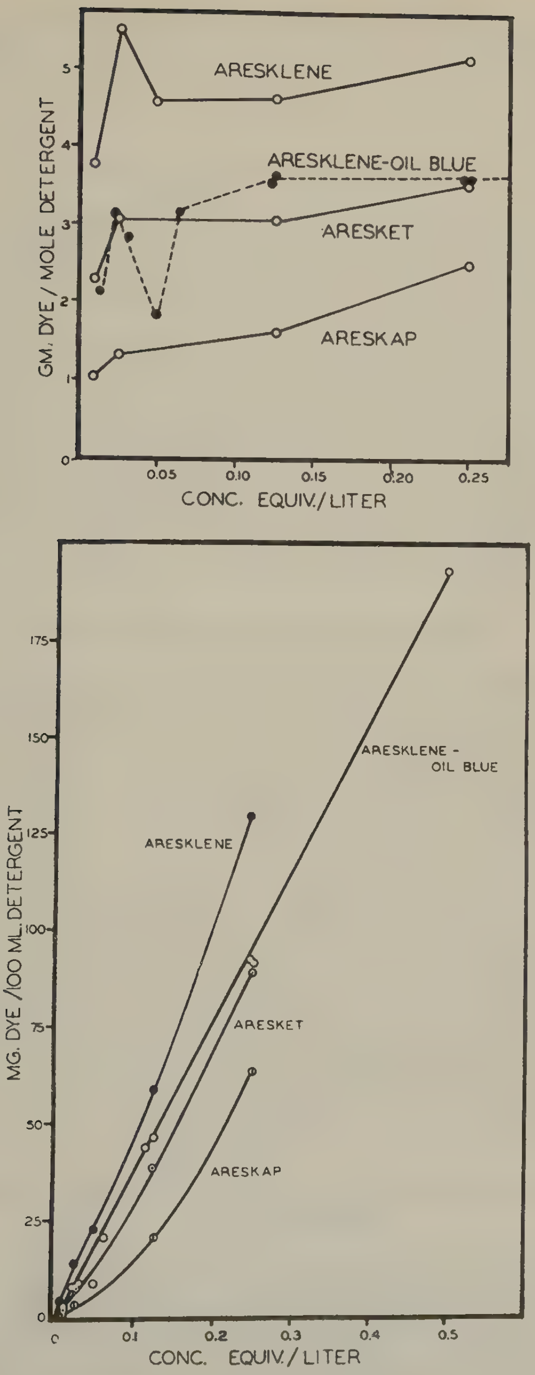

FIG. 2a and b. Solubilization by various concentrations of three related detergents in equilibrium with crystalline Orange OT, and, where indicated, with Brilliant Oil Blue.

Its solubilizing power is only a little less than that of sodium oleate, more like potassium oleate, and double that of the laurates. The high point at 0.015 *N* solution was not checked for suspension with mesitylene solution, but the liquid was visually clear.

Aresklene, Aresket, and Areskap

The data for these 3 interesting related detergents are given in Figs. 2a and b, where formulas are given in the title of the figure. The optimum solubilization point observed for Aresklene in 0.025 *N* solutions was found to be real and not due to suspended material.

Of the 3 detergents, Aresklene, with its high molecular weight, is the most effective. It is very interesting in having two polar dissociated SO_3Na groups—one of the very few polyvalent detergents hitherto tested. The single hydroxyl group on the second ring of Areskap is shown to be a handicap, in spite of the fact that the dye being solubilized is itself a polar substituted naphthol, and also in spite of the fact that the osmotic coefficients of Aresket and Areskap, as well as their conductivities, are practically identical (9).

Alkyldimethylbenzylammonium Chlorides

The alkyldimethylbenzylammonium chlorides are cationic detergents, which as a class, are better solubilizers than anionic or nonionic,(10), and that proved to be the case here. The data are collected in Fig. 3a and b and 5b. Several series of measurements were made with Zephiran, and the results given are the mean for each concentration. One thing was always characteristic: there was a smooth curve of g. dye/mole of detergent from 0.7 down to 0.3 *N*; there was a sudden rise to 0.03 *N* and just as sharp a decline on further dilution. In studying dilute solutions more closely, there appeared to be a slight maximum at 0.16 *N* and a slight minimum at 0.13 *N*, but these may be within experimental error.

The very pronounced maximum at 0.03 *N* is not due to suspension, because this point was confirmed by eliminating solid dye altogether, and instead using a solution of Orange OT in mesitylene at a concentration 10% less than saturation. The results with Brilliant Oil Blue also show a pronounced maximum at this same concentration.

Neutronyx and the Lauric Acid Ester of N-β-Hydroxyethylacetamide Sodium Sulfonate

The data for these two detergents of the same order of magnitude as the sodium linolenate are graphed in Figs. 4a and b. It is interesting again to see that a given weight of either detergent is more effective in rather dilute solution, although the highest point was not tested for suspension. How-

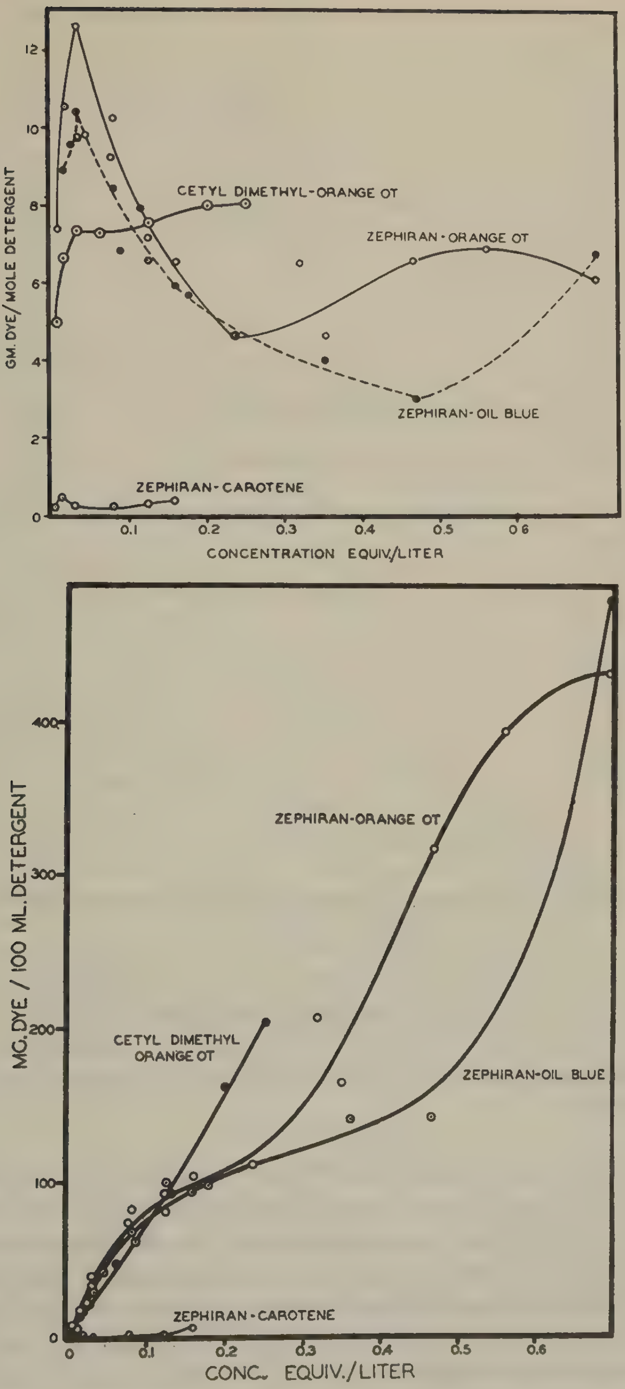

FIG. 3a and b. Solubilization by Zephiran and cetyldimethylbenzylammonium chloride showing great differences in solubilizing power of the same weight of detergent in different concentrations.

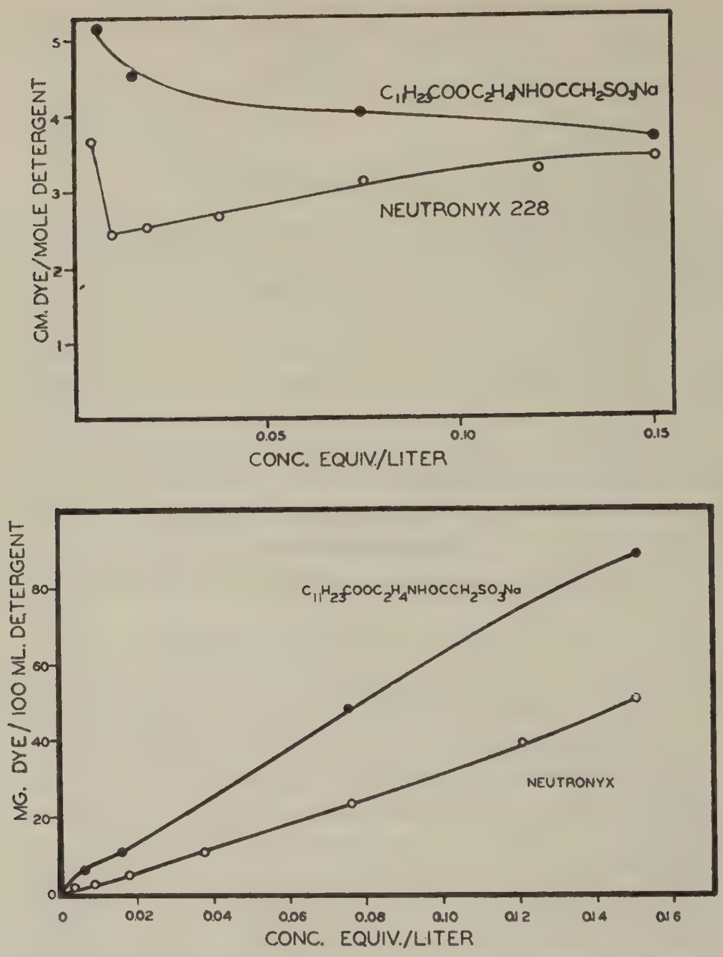

FIG. 4a and b. Solubilization of Orange OT by the nonionic detergent Neutronyx and the anionic sodium lauryloxyethaneamidosulfoacetate.

ever, the Neutronyx, after its minimum in 0.01 N solution, rises again with concentration.

Carbowax

The data for the Carbowax are given in Figs. 5a and b. Conductivity indicated that the Carbowax contained slight electrolytic impurities. The apparent solubilizing power of the Carbowax is magnified by over 10-fold in the calculation because of the very high molecular weight of the Carbowax as compared with the soaps. Carbowax is an extremely feeble solubilizer on a weight for weight basis.

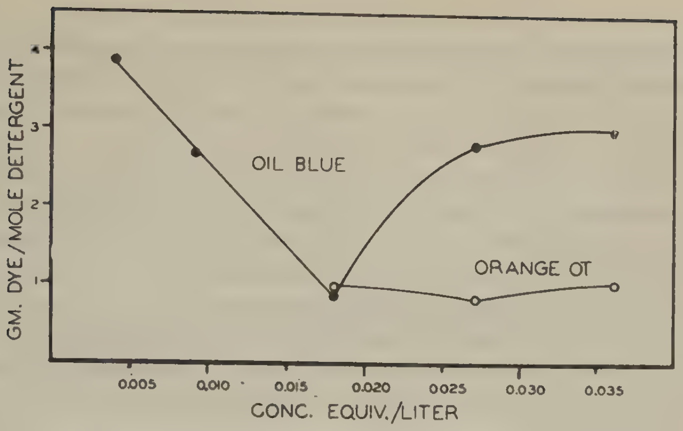

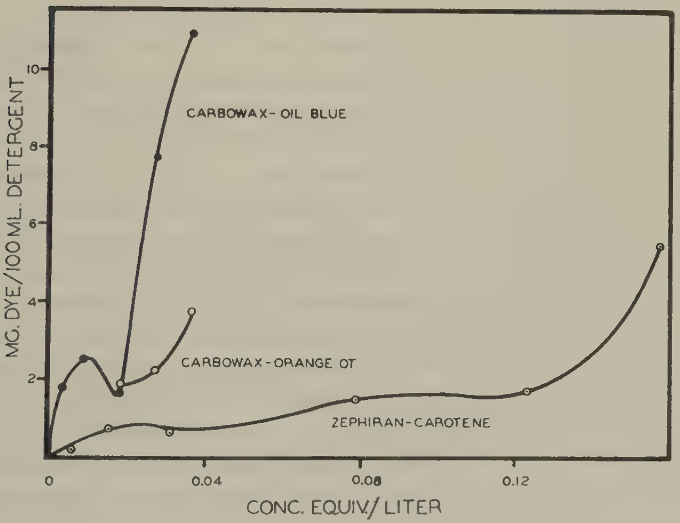

Fig. 5a. Grams Orange OT and, over a wider concentration, of Brilliant Oil Blue, solubilized by Carbowax. Weight for weight this lies far below any detergent.

Fig. 5b. Solubilization of Orange OT and Brilliant Oil Blue by Carbowax. Also carotene by Zephiran; note the greatly enlarged vertical scale. (Compare Fig. 3b.)

Discussion

In agreement with all previous evidence, solubilizing power has been shown to differ greatly for different detergents. In general, it is greatly enhanced by high molecular weight, even after taking into account the extra weight of a mole of detergent. Further, cationic detergents are excellent solubilizers. A molecule like polyethylene oxide, with no distinctive groups at the ends, is a very feeble solubilizer, though it becomes very good as soon as a fatty acid radical or a substituted benzene ring is attached at one end. The example of Aresklene here shows that two ionizable groups on the same molecule can give an excellent solubilizer.

Biochemists refer to the "choleic acid principle" for bringing substances into solution. One might with equal lack of justification refer to a "fatty acid principle" when discussing soaps. Neither fatty acid nor choleic acid can solubilize anything in water, nor do free alkalies such as potassium or sodium hydroxide or Triton-B solubilize anything in water. It is the compound, soap, or bile salt, that solubilizes by virtue of its being itself soluble in addition to forming colloidal particles which can incorporate in or upon themselves otherwise insoluble material.

A highly significant aspect of our results is the variation in solubilizing power with change in concentration of the same detergent. This is shown especially in Fig. 3b by the cationic detergents, but it is also clearly evident in other graphs.

Whereas, in the simplest cases, such as with some ordinary soaps, a detergent may show a solubilizing power per mole that is almost independent of concentration once colloid is fully formed, the behavior in other cases is by no means so simple (5,6,7,8). In some, by far the maximum effectiveness is attained in dilute solution, as with Zephiran for Orange OT, for Brilliant Oil Blue, and for carotene; or, as with Aresklene or $RCOOCH_4NHOCCH_2SO_3Na$, with Orange OT. The sodium soaps (5) of ordinary fatty acids show a marked increase with concentration, after a period of uniform effectiveness, as in Fig. 1. Potassium laurate with dimethyl phthalate shows an optimum power in 0.1 *N* solution (6). Minima are observed in several of the curves in Figs. 2b, 3b, 4b, and 5b. Richards and McBain (11) found that the solubilizing power per mole of cetylpyridinium chloride for benzene, octane, and octyl alcohol was markedly different with different concentrations of the detergent.

It clearly follows that the colloidal particles in a given concentration of a given detergent differ in solubilizing power from those in other concentrations of the same detergent. Hence, the colloidal particles in different concentrations must themselves be different.

It seems evident that no one formulation of a micelle is valid over a whole range of concentration. The average composition and size of micelles have been shown by conductivity and freezing point to vary over the whole range (12,13). We believe that a number of different kinds, shapes and sizes of colloidal particles of micelles must exist in a given detergent solution, and that the equilibria between them shift with changes of concentration, temperature, and added substances.

Winsor (14), in discussing certain hydrotropic phenomena, concludes "that energy differences between the different micellar forms are small and that probably all three exist in equilibrium in the solution, their relative proportions depending upon the ratio of *R* and the relative proportions of the components of the system." Kolthoff and Stricks (7) state, "thus it seems that with dodecylamine hydrochloride and detergents behaving similarly, there may be at least two different types of micelles with different solubilizing power, and that, with increasing concentration, relatively more of the micelles are formed with the greater solubilizing power."

Many investigators at the present time do not recognize the existence of any but micelles of fixed size and composition, some assuming that the only micelle is a constant sphere. Others go to the opposite extreme of assuming that *all* of the colloidal electrolyte is in the form of *lamellar* micelles, either the double leaflet originally suggested by McBain, or the parallel arrangement of such micelles introduced by Hess and other German investigators in their long series of papers between 1937 and 1942. We consider both of these extremes untenable if all the evidence is taken into account.

The density of solutions shows two critical concentrations (15,16) —one at the rather high concentration of about 10% which is about where the X-ray long spacing d_1 begins to appear. In lauryl sulfonic acid solutions the migration number rises above the first critical concentration but falls again abruptly at 0.06 m (17,18).

Some colloidal electrolytes of sufficiently high molecular weight show, at the first critical concentration, an increase of conductivity even *above* that at infinite dilution (19,20,21), followed by the usual great decrease at higher concentration; that is, some micelles are better conductors than the fully dissociated ions and others of the same detergent are much less effective. An earlier example of a detergent giving at first an increased conductivity in the neighborhood of the critical concentration after formation of micelles was published by Haffner, Piccione and Rosenblum (22) and confirmed by ourselves.

The following aspects of X-ray observations, which have been the subject of study by many investigators, may be interpreted as supporting the point of view that different proportions of various micelles may exist in different concentrations (23), even in the same detergent. Some detergents give no X-ray diagrams; whereas, in others, such as soaps, they are highly developed, although all are fully colloidal (24). In some, the X-ray spacing is developed only after a small amount of organic liquid has been added. In soaps and closely related detergents, as first reported in the papers by Hess and other German workers, there is a dilute range above the first critical concentration at which the colloid present is not evident to X-ray examination. The X-ray long spacing, d_1, does not appear until a concentration of 5 or 10% or higher, the "second critical concentration." This long spacing steadily increases in intensity with concentration. Somewhere between the first and second critical concentration appears the d_M band discovered by Harkins (25) and collaborators in their own and in one of Kiessig's photographs. This, for some reason, in contrast to d_1, passes through a maximum intensity and falls off again with increasing concentration.

It is difficult to reconcile all these phenomena with any concept of a single micelle of constant size and kind in all solutions of detergents.

SUMMARY

1. The solubilization of dyes by a series of very different detergents has been studied over a range of concentration for each detergent.

2. The change in solubilizing power with change in concentration is very different for different detergents. Some show a pronounced maximum at a concentration at which they have just become colloidal. Some show maxima and minima or other changes with concentration.

3. It follows, in agreement with other evidence, that the micelles or colloidal particles in any one concentration of a detergent differ from those in other concentrations of the same detergent. There must be an equilibrium between different kinds of micelles present in the same solution, changing with concentration and other factors.

REFERENCES

1. McBain, J. W., and McBain, M. E. L., *J. Am. Chem. Soc.* **58**, 2610 (1936).
2. McBain, J. W., *Advances in Colloid Chem.* **1**, 99 (1942).
3. McBain, J. W., and Merrill, R. C., *J. Phys. Chem.* **46**, 10 (1942).
4. McBain, J. W., and Merrill, R. C., *Ind. Eng. Chem.* **34**, 915 (1942).
5. Green, A. A., and McBain, J. W., *J. Phys. & Colloid Chem.* **51**, 290 (1947).
6. McBain, J. W., and McHan, H., *J. Am. Chem. Soc.* **70**, 3838 (1948).
7. Kolthoff, I. M., and Stricks, W., *J. Phys. & Colloid Chem.* **52**, 915 (1948).
8. McBain, J. W., and Green, A. A., *J. Am. Chem. Soc.* **68**, 1731 (1946).
9. Cushman, A., Brady, A. P., and McBain, J. W., *J. Colloid Sci.* **3**, 425 (1948).
10. McBain, J. W., and Richards, P. H., *Ind. Eng. Chem.* **38**, 642 (1946).
11. Richards, P. H., and McBain, J. W., *J. Am. Chem. Soc.* **70**, 1338 (1948).
12. van Rysselberghe, P., *J. Phys. Chem.* **43**, 1049 (1939).
13. van Rysselberghe, P., *ibid.* **48**, 62 (1944).
14. Winsor, P. A., *Trans. Faraday Soc.* **44**, 381 (1948).
15. Hess, P., Philippoff, W., and Kiessig, H., *Kolloid-Z.* **88**, 40 (1939).
16. Vetter, R. J., *J. Phys. & Colloid Chem.* **51**, 262 (1947).
17. McBain, M. E. L., *J. Phys. Chem.* **47**, 196 (1943).
18. Neff, L. L., Wheeler, V. L., Tartar, H. V., and Lingafelter, E. C., *J. Am. Chem. Soc.* **70**, 1989 (1948).
19. Ralston, A. W., Eggenberger, D. N., and duBrow, P. L., *ibid.* **70**, 977 (1948).
20. Moillet, J. L., Collie, B., Robinson, C., and Hartley, G. S., *Trans. Faraday Soc.* **31**, 120 (1935).
21. Brown, G. L., Grieger, P. F., and Kraus, C. A., *J. Am. Chem. Soc.* **71**, 97 (1949) (Fig. 4).
22. Haffner, F. D., Piccione, G. A., and Rosenblum, C., *J. Phys. Chem.* **46**, 662 (1942).
23. McBain, J. W., and Hoffman, O. A., *J. Phys. & Colloid Chem.* **53**, (1949).
24. McBain, J. W., and Marsden, S. S., Jr., *Acta Crystallographica* **1**, 270 (1948).
25. Mattoon, R. W., Stearns, R. S., and Harkins, W. D., *J. Chem. Phys.* **15**, 209 (1947).

PHYSICOCHEMICAL INVESTIGATION OF A CATION EXCHANGE RESIN (AMBERLITE IR100)

I. RESIN EQUILIBRIA

E. Heymann and I. J. O'Donnell

From the Department of Chemistry, University of Melbourne, Melbourne, Australia

Received December 27, 1948

INTRODUCTION

Exchange resins have found many practical uses, particularly in the separation of rare earths, transuranial elements, and fission products. However, the fundamental side of the field is still in a comparatively preliminary state of investigation. Two important papers by Boyd, Schubert and Adamson (1) and by Bauman and Eichhorn (2) have been published recently dealing with the thermodynamics of ion exchange equilibria. We have attempted to obtain information about the strength of binding of various cations in the resin by an investigation of equilibria between the resin and electrolytes in solution and of the electrical conductivity of the swollen resin containing various cations.

EXPERIMENTAL

The commercial product [1] Amberlite IR100, on treatment with water, yielded a yellow liquid which was acid in reaction and probably contained part of the resin that had been oversulfonated. To remove all soluble material, the resin was left with water at 80°C. for several weeks, the water being renewed frequently. The hydrogen form of the resin was obtained by prolonged washing with N/10 HCl until the ash content was reduced to 0.00%, indicating that all metal ions had been removed. This product was then washed with conductivity water until, on standing with water for 2 days, no change in conductivity or pH was recorded. Afterwards, the resin was air-dried. The moisture content was between 21.8 and 22.0%.

For the exchange experiments, 0.400 g. of resin (in some series of experiments larger quantities were employed) was allowed to stand with 100.0 ml. of salt solution of varying concentrations for 24 hr., the mixture being shaken occasionally, after which time 20.00 ml. aliquots were withdrawn, and the acid liberated (A_L) titrated against N/50 $Ba(OH)_2$, using phenolphthalein. The pH of the equilibrium solutions was determined using a glass electrode. Preliminary experiments had shown that the exchange reaction with salts of strong acids was complete after 4–5 hr., and that the temperature coefficient between 0 and 40°C. was practically zero for the sodium-hydrogen exchange.

---

[1] We are indebted to the Resinous Products and Chemical Co., Philadelphia, and to the Fletcher Chemical Co., Melbourne, Australia, for the supply of resin.

Equilibrium curves for LiCl, NaCl, Na_2SO_4, $CaCl_2$, and $BaCl_2$ were determined in the concentration range of 1 *N* to 0.002 *N*, reagents of "Analar" purity being used.

Equilibria with salts of weak acids, such as sodium benzoate, sodium acetate, sodium monochloroacetate, sodium trichloroacetate, and calcium acetate were also investigated. With many of these salts it was found necessary to allow the resin-salt mixture to stand for much longer periods to obtain equilibrium (up to 48 hr.). Calcium acetate (A. R. Merck) was employed, and the solutions of the other salts made up by bringing the solutions of the acids concerned, of standard purity, to the pH of the salt solution calculated by the hydrolysis equation for a dilute solution. As in many cases, particularly in concentrated solutions, this pH differs from the phenolphthalein change over point; we always determined the amount of acid required to bring the salt solution to that point, and corrected our titration values of the equilibrium solutions (containing salt plus acid liberated) accordingly. Moreover, in order to assess accurately the amount of weak acid liberated by reaction of the salt with the resin, the experimental values were corrected by taking into consideration the amount of acid bound by molecular adsorption to the resin. For this purpose, the molecular adsorption of the acids concerned on the resin was determined.

Potentiometric titrations were carried out by suspending the ground-up resin in *N* KCl solution and titrating with $Ba(OH)_2$, using a glass electrode and a Cambridge potentiometer. The suspension was stirred continuously and CO_2 was excluded. HCl was used for back titration.

The sulfur determinations on a micro scale were performed by oxidizing the resin with Na_2O_2 in a nickel bomb (3). We are indebted to N. L. Lottkowitz in this Department for carrying out the sulfur determinations.

RESULTS AND DISCUSSION

The essentially strong acid nature of the resin is suggested by our curves of potentiometric titration (Fig. 1). The interpretation of such curves is rendered difficult by drifting of pH during titration and by hysteresis on back titration, the amount of hysteresis increasing when the resin is allowed to stand with alkali for 3 hours before back titration (Fig. 2). Gregor and Bregman (4) have shown recently, in a careful study of various resinous exchangers, that curves of potentiometric titration may not reveal the presence of weakly acid groups unless about 24 hr. are allowed to establish equilibrium for each addition of alkali. They were

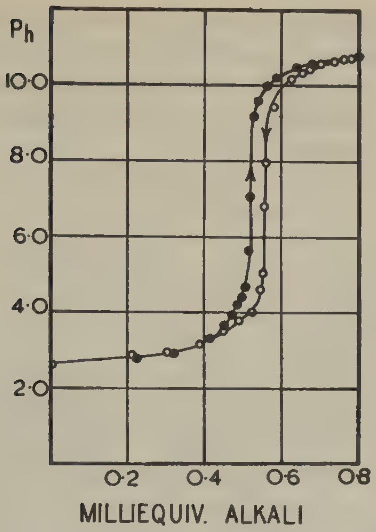

FIG. 1. Potentiometric titration of 0.40 g. Amberlite IR100 in 150 ml. *N* KCl. Quick forward titration with baryta and immediate back titration with HCl.

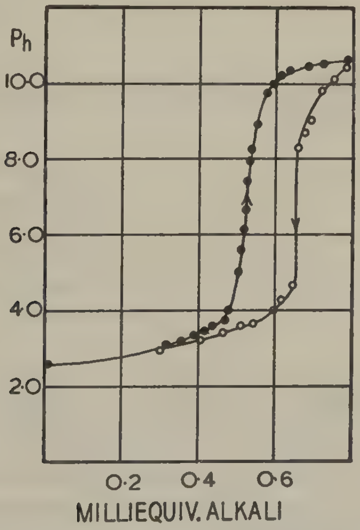

FIG. 2. Potentiometric titration of 0.40 g. Amberlite IR100 in 150 ml. *N* KCl. Interval of 3 hr. between quick forward titration with baryta and quick back titration with HCl.

able to show that the reactions involving weakly acid groups are much slower than those involving strongly acid groups, which they attribute to better accessibility of the latter in the resin structure. In view of these results, it would appear that drifting and hysteresis in our experiments are the result of slow (diffusion controlled) reactions involving weakly acid groups. If the quick forward titration curve can be taken as characteristic for the strong acid groups, Figs. 2 and 3 would indicate 1.25–1.30 × 10^{-3} g.-eq. of hydrogen/1 g. of air-dried resin (0.78 g. of anhydrous resin) originating from such groups.

The sulfonic acid groups[2] of Amberlite IR100 react with neutral salts in solution according to the equation

$$\underset{\text{resin phase}}{\boxed{RSO_3^-H^+}} + Na^+ \rightleftarrows \underset{\text{resin phase}}{\boxed{RSO_3^-Na^+}} + H^+.$$

The equilibrium exchange curves (Fig. 3) for NaCl, Na_2SO_4, LiCl, $CaCl_2$, and $BaCl_2$, show that, in all these cases, nearly the same value for the limiting exchange (at high salt concentration) is obtained. The amount of exchange is expressed as mg.-eq. of acid liberated/1 g. of air-dried resin (A_L). The pH of the equilibrium solutions under the conditions of the limiting exchange is 2.0–2.5. Fig. 3 shows that 1 g. of air-dried resin contains 1.20 × 10^{-3} g.-eq. of hydrogen exchangeable in this pH range.

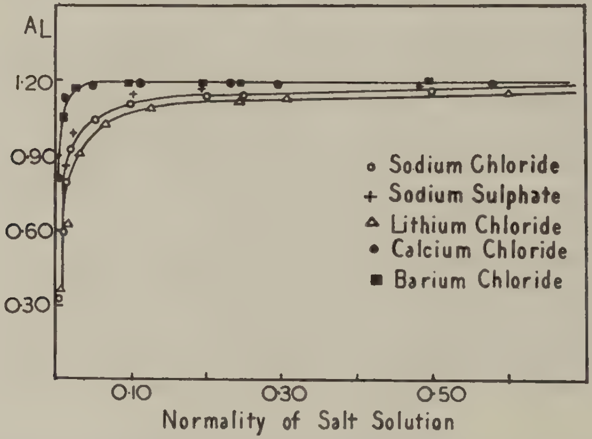

FIG. 3. Equilibria between 0.40 g. Amberlite IR100 and 100 ml. of solutions of various salts of strong acids. Plot of acid liberated (A_L) in mg.-eq./1 g. of air-dried resin against the normality of the salt solution.

The sulfur content of the air-dried resin is 4.19 ± 0.04%. If we assume all the sulfur to be present in sulfonic acid groups, this corresponds to 1.30 × 10^{-3} g.-eq. of sulfonic acid hydrogen/1 g. of air-dried resin. This is in excellent agreement with the strong acid equivalent indicated by potentiometric titration and lends support to the assumption that all the sulfur is present in sulfonic acid groups.[3] However, this acid value is about 8% higher than that indicated by the limiting exchange at $pH = 2.0–2.5$, suggesting that not all sulfonic acid groups react in this range, even in presence of great excess of salt. Experiments on the resin conductance (*cf.* the following paper) also suggest that sulfonic acid hydrogen is not completely exchanged at $pH < 3.5$.

---

[2] The strong acid groups in Amberlite resins are —CH_2—SO_3H (8).

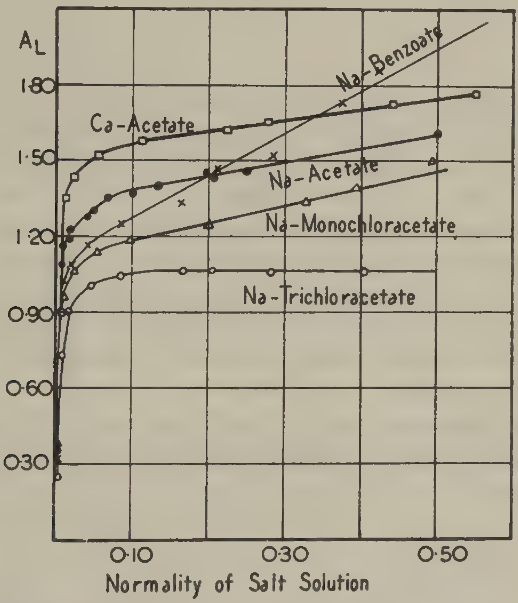

FIG. 4. Equilibria between 0.40 g. Amberlite IR100 and 100 ml. of solutions of various salts of weak acids. Plot of acid liberated (A_L) in mg.-eq./1 g. of air-dried resin against the normality of the salt solution.

When an approximately neutral ($pH \simeq 6$) solution of $BaCl_2$ is streamed through a resin plug until all the acid formed during exchange is washed out and finally excess $BaCl_2$ is removed by water, the resin contains after this treatment $1.37(\pm 0.02) \times 10^{-3}$ g.-eq. of Ba/1 g. of air-dried resin. This is about 5% more than the sulfonic acid equivalent calculated from the sulfur content and from potentiometric titrations, suggesting that acid groups weaker than $-SO_3H$ are able to exchange hydrogen for metal ions at a pH near neutrality.

[3] The possibility of part of the sulfur in another sulfonic acid resin (Dowex 50) being present in sulfone cross-links has been suggested by Bauman and Eichhorn (2).

The values for the sulfur content and the exchange equivalent are lower than those quoted by Tompkins (8). This is probably the result of the loss of soluble sulfonic acid during the treatment of the resin with water at 80°C.

Further evidence for the action of such groups emerges from equilibrium experiments with salts of weak acids, shown in Fig. 4. With such salts, except sodium trichloroacetate, the exchange value is appreciably greater than the content of sulfonic acid groups of the resin, and increases roughly in the order of decreasing acid dissociation constants, as would be expected. The pH in these equilibrium solutions is very much higher (4–8) than in the equilibrium solutions with salts of strong acids (2–3), and the greater exchange values are the result of acid groups in the resin which are weaker than $-SO_3H$, presumably $-COOH$, and phenolic $-OH$ coming into action at high pH. It is surprising, however, that sodium trichloroacetate has a lower limiting exchange value than NaCl.[4]

Reference to Fig. 3 shows further that the limiting exchange value is reached at lower concentrations of the equilibrium solution for alkaline earth chlorides than for alkali chlorides. This may be due partly to the different shape of an ideal mass action isotherm involving square terms (*cf.* 2), but mainly to a stronger binding of bivalent cations. The stronger binding of Ca^{++} as compared with Na^+ is also shown on comparison of the equilibrium curves for calcium acetate and sodium acetate.

The equilibria between the resin and salts of strong acids were analyzed by the law of mass action.

Bauman and Eichhorn have derived a mass action expression for the exchange reaction by an application of the Donnan equilibrium principle. For the reaction

$$\boxed{RSO_3^-H^+} + Na^+ = \boxed{RSO_3^-Na^+} + H^+,$$

they obtain

$$\frac{a_{NaR}a_{HS}}{a_{HR}a_{NaS}} = 1, \tag{1}$$

where a_{NaR} is the activity of the sodium ions and a_{HR} that of the hydrogen ions in the resin phase, and a_{NaS} and a_{HS} the corresponding activities in the solution phase. As the above expression is equal to the thermodynamic equilibrium constant, K_a, of the resin reaction, it follows that, for equilibria between a strong acid resin and a strong electrolyte salt, K_a is unity. It may be objected that the Donnan equilibrium approach is somewhat artificial[5] in this case, because the behavior of ions, and of multivalent ions in particular (*cf.* the next paper), in the resin phase is different from that in solution. However, Eq. 1 may be postulated as an equation defining the exchange equilibrium, *viz.*:

---

[4] The same was found by Heymann and Rabinov (5) for the reaction between sodium trichloroacetate and the carboxyl groups contained in cellulose and oxycellulose.

[5] The experiments of Bauman and Eichhorn have shown that the penetration of HCl into the resin is not quantitatively described by the Donnan equations.

$$\frac{a_{\text{NaR}}a_{\text{HS}}}{a_{\text{HR}}a_{\text{NaS}}} = \frac{\gamma_{\text{NaR}}[\text{Na}^+]_{\text{R}}\gamma_{\text{HS}}[\text{H}^+]_{\text{S}}}{\gamma_{\text{HR}}[\text{H}^+]_{\text{R}}\gamma_{\text{NaS}}[\text{Na}^+]_{\text{S}}} = K_a = 1, \tag{2}$$

because the resin would not be expected to show preference for any univalent cation, if the ionic constituents of both resin and solution phase behaved as ideal mixtures. Any deviation from this state may be expressed either in terms of an equilibrium constant or in terms of ratios of activity coefficients, *viz.* $\frac{\gamma_{\text{HR}}}{\gamma_{\text{NaR}}}$ and $\frac{\gamma_{\text{HS}}}{\gamma_{\text{NaS}}}$.

We cannot evaluate K_a from experimental data because the activity coefficients in the resin cannot be determined by independent methods.[6] However, we can calculate

$$\frac{[\text{Na}^+]_{\text{R}}\gamma_{\text{HS}}[\text{H}^+]_{\text{S}}}{[\text{H}^+]_{\text{R}}\gamma_{\text{NaS}}[\text{Na}^+]_{\text{S}}} = K'. \tag{3}$$

Comparison of Eqs. (2) and (3) gives

$$K' = \frac{\gamma_{\text{HR}}}{\gamma_{\text{NaR}}}. \tag{4}$$

The ratio of activity coefficients of hydrogen and metal ion in the resin may thus be estimated from equilibrium data, but the values obtained will only be approximate for reasons explained later.

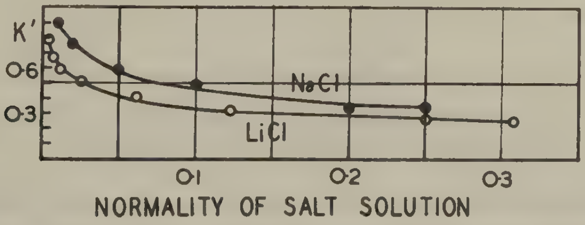

Fig. 5. Plot of K' against the normality of the salt solution.

Fig. 5 shows values of K' in exchange experiments with a hydrogen resin and solutions of NaCl and LiCl. The activity coefficients in the solution phase were taken from Landolt-Börnstein, and it was assumed that the mean activity coefficient of a salt in a mixture was the same as that of the pure salt at the ionic strength of the mixture.

---

[6] We are in doubt as to whether one suggested method of calculating activity coefficients (1), employing an empirical treatment due to Kielland (6) and based on the van der Waals' equation, is sound. The suitability of the latter equation for a system in which the deviation from ideality is partly due to Coulomb forces, is questionable.

K' is the ratio of activity coefficient of hydrogen to that of the respective univalent cation in the resin phase. It is seen that $\frac{\gamma_{HR}}{\gamma_{LiR}} < \frac{\gamma_{HR}}{\gamma_{NaR}} < 1$, but both ratios do not seem to be very different from unity for very dilute solutions of electrolyte. Boyd, Schubert and Adamson (1) have suggested that, for univalent ions which are not widely different in size, the activity coefficient ratio in the resin phase should be approximately equal to unity.

The fact that the activity coefficients of H^+ and of alkali metal ions for small concentrations of the latter) in the resin are of the same orders of magnitude is good evidence in favor of the strong acid nature of the resin. For weakly acid groups, we would except $\gamma_{HR} \ll \gamma_{NaR}$.

The equilibrium curves (Fig. 3) for the chlorides of the bivalent cations reach the limiting exchange at very low concentrations of these salt) in the solution and are, therefore, not suitable for the calculation of equilibrium constants. The experiments indicate, however, that K' is greater than for uni-univalent electrolytes in qualitative agreement with Boyd, Schubert and Adamson. The bivalent cations are bound more strongly by the resin than the univalent ones.

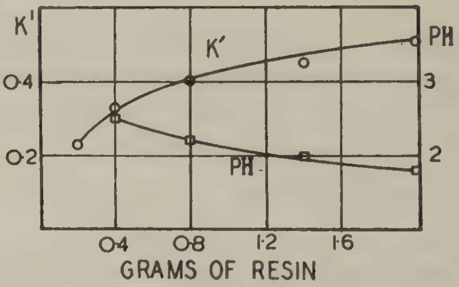

FIG. 6. Plot of K' and of the pH against the weight of the resin at constant initial normality (0.1 N) of the salt solution.

Fig. 5 shows that K' varies appreciably with the concentration of the salt solution in experiments in which the ratio of weight of resin to volume of solution is kept constant. For reactions between hydrogen resin and alkali chlorides in solution, K' decreases with increasing concentration of the latter, corresponding with increasing concentration of bound alkali metal ion in the resin phase.[7] Similarly, in experiments in which the ratio of resin to salt solution is varied (Fig. 6), but the initial salt (LiCl) concentration in the solution is kept constant, K' increases with increasing ratio of resin to salt solution, which corresponds with decreasing pH in the solution and a decreasing concentration of bound alkali metal ion in the resin phase.

[7] The limiting concentration of bound alkali metal ion in the resin phase is about $1 - N$.

A moderate variation of $K' = \frac{\gamma_{HR}}{\gamma_{NaR}}$ in the experimental concentration range would be expected as a result of the same causes which are responsible for the well-known variations of activity coefficients of HCl and of alkali metal salts with concentration in aqueous solution. In that case, however, $\frac{\gamma_{HCl}}{\gamma_{NaCl}}$, for instance, *increases* with increasing concentration. The *decrease* of $K' = \frac{\gamma_{HR}}{\gamma_{NaR}}$ with increasing concentration would, therefore, appear to be due to additional effects peculiar to the system under investigation, some of which are listed below:

(a) Eq. 4 is only approximate, due to the neglect of varying degrees of swelling with different cations and different salt concentrations (Gregor, 7).

(b) The assumption that the activity coefficient of a salt solution containing a mixture of two salts is the same as that of the pure salt at the ionic strength of the mixture is correct only for solutions of low ionic strength. At higher ionic strengths, K' may, therefore, depend also on the activity coefficient ratio in the solution.

(c) Apart from the exchange reaction, there will be a penetration of salt into the swollen resin phase, the extent increasing with increasing concentration of salt in the solution. Hence, the total ion concentration in the swollen resin phase will be greater in equilibrium with a concentrated salt solution than with a dilute one. As a consequence, the activity coefficients of H^+ and of the metal ions in the resin phase will be influenced with increasing concentration in the solution, but not necessarily to the same extent.

Furthermore, a decrease of K' with increasing concentration of the salt solution, and with decreasing ratio of resin to salt solution at constant initial concentration of the latter, could be visualized if there were either $-SO_3H$ groups of varying acid strength in the resin, or if some of the more weakly acid groups could take part in the exchange reaction under the conditions of the equilibrium experiments at low pH. The latter alternative is improbable in view of the results discussed previously, and also in view of some experiments on resin conductance which will be discussed in the next paper. Nevertheless, it is noteworthy that Bauman and Eichhorn, working with Dowex 50, which is reported to contain little or no $-COOH$, have obtained good constancy for their equilibrium constants up to concentrations in the solution of 1 *N*.

SUMMARY

1. Equilibria between a sulfonic acid resin (Amberlite IR100) and salts of strong and weak acids are investigated. The limiting exchange (at

high concentrations) is nearly the same for all alkali and alkaline earth chlorides and sulfates at low pH. It is greater for salts of weak acids, at higher pH, and increases in the order of decreasing acid dissociation constant. This suggests that the resin contains groups which are more weakly acid than $-SO_3H$, probably $-COOH$ and phenolic $-OH$. The limiting exchange at pH = 2.0–2.5 is a few per cent below the strong acid equivalent as characterized by the sulfur content and the potentiometric titration curves.

2. The law of mass action is applied to resin equilibria with salts of strong acids. The ratio of activity coefficients of the hydrogen ion to that of metal ion in the resin phase shows a marked variation with the experimental conditions. A number of possible causes for this is discussed.

REFERENCES

1. Boyd, G. E., Schubert, J., and Adamson, A. W., *J. Am. Chem. Soc.* **69**, 2818 (1947).
2. Bauman, W. C., and Eichhorn, J., *ibid.* **69**, 2830 (1947).
3. Alicino, J. F., *Ind. Eng. Chem., Anal. Ed.* **13**, 506 (1941).
4. Gregor, H. P., and Bregman, J. I., *J. Am. Chem. Soc.* **70**, 2370 (1948).
5. Heymann, E., and Rabinov, G., *J. Phys. Chem.* **45**, 1152 (1941).
6. Kielland, J., *J. Soc. Chem. Ind.* **54**, 232T (1935).
7. Gregor, H. P., *J. Am. Chem. Soc.* **70**, 1293 (1948).
8. Tompkins, E. R., *Isotopes Division Circular* **C–10**, U. S. Atomic Energy Commission, Oak Ridge, Tenn. (1948).

PHYSICOCHEMICAL INVESTIGATION OF A CATION EXCHANGE RESIN (AMBERLITE IR100)

II. RESIN CONDUCTANCE

E. Heymann and I. J. O'Donnell

From the Department of Chemistry, University of Melbourne, Melbourne, Australia

Received December 27, 1948

INTRODUCTION

As pointed out in the preceding paper, there is no possibility of an experimental determination of ionic activities in the resin phase, but a calculation from the activities in the solution in equilibrium with the resin may be possible by a treatment similar to that suggested by Hartley and Roe (1) for the calculation of activities at interfaces. This treatment, however, involves the ζ-potential between the resin and the solution.

We attempted to measure the ζ-potential using the streaming potential method. Purified granular resin was packed in a cylindrical tube between two perforated platinum electrodes, coated with a layer of silver and silver chloride to avoid polarization, and water streamed through this plug. It was soon found that a determination of the ζ-potential of a cation exchange resin is not possible in this way, because the swollen resin phase, although free from foreign electrolyte, has a conductivity more than 1000 times greater than that of ordinary distilled water. Thus, the electrodes between which the streaming potential is to be measured are virtually short-circuited by the well-conducting resin phase, and, as a consequence, the streaming potential is very small, although the ζ-potential may be appreciable. We thus have conditions in which the Helmholtz-Smoluchowski equation cannot be applied.

The high conductivity of the swollen resin phase of a cation exchange resin of the sulfonic acid type is due to a large number and an appreciable mobility of hydrogen or alkali metal ions in the resin phase as a result of the strong acid nature of the $-SO_3H$ groups. Conductivity measurements may, therefore, be expected to give an estimate of the degree of freedom of various cations in the resin.

EXPERIMENTAL

It was desired to measure the electrical conductivity of a plug of swollen resin under circumstances in which one ionic species could be replaced by another without removing the resin from the conductivity cell. A cylindrical cell, shown in Fig. 1, was used. The two electrodes were perforated platinum discs, 1.35 cm. in diameter and coated with platinum black. The distance between the electrodes varied between 2.0 and 4.0 cm. in different experiments, and quantities of resin from 2.5 to 4.0 g. (grain size: 0.2–1.0 mm.) were packed between them. The cell was connected to a container holding the salt solution under investigation. The resistance of the resin plug was determined by a Wheatstone net, using induction-free shielded resistances and a ratio arm, a variable condenser parallel to the cell and a telephone, the source of current being a 1000 cycle valve oscillator. The cell constant (C) was calculated from the dimensions of the cell.

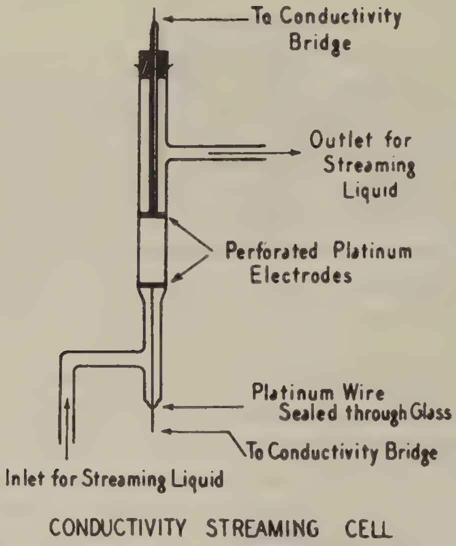
To Conductivity Bridge
Outlet for Streaming Liquid
Perforated Platinum Electrodes
Platinum Wire Sealed through Glass
To Conductivity Bridge
Inlet for Streaming Liquid
CONDUCTIVITY STREAMING CELL

FIG. 1. Conductivity streaming cell.

The resistance of the hydrogen resin was determined first, and a solution of a salt streamed through the plug afterwards. To free the plug from excess salt when the exchange reaction was complete, conductivity water was streamed through until the resistance became constant. This is the resistance of the resin salt. The course of the exchange reaction and the removal of acid and excess salt was followed by measuring the resistance of plug and effluent, and also the pH of the effluent. It is noteworthy that the resistance of the plug of resin salt (*e.g.*, Na resin) remains constant while water is streamed through, and the conductivity of the effluent water is not appreciably higher than that of the influent. The salt of a strong base and the strong resin acid is thus not decomposed by hydrolysis (*cf.*, however, the succeeding section).

After treatment with one salt solution, $N/10$ HCl, or $N/10$ HNO_3 in some cases, was streamed through the plug to remove the bound metal cations, and conductivity water afterwards to remove the acid, a check being maintained on the conductivity of the plug and effluent water to show when the removal of acid was complete. Then another salt solution was streamed through and the procedure repeated.

All experiments were carried out with salts of A.R. purity. Resistance values were recorded at 18.0°C. Variation of the A.C. between 1000 and 3000 cycles caused no variation of the resistance. In most experiments, the salt solutions were $N/10$, but higher concentration gave the same conductivity of the resin salt after excess electrolyte was washed out. It made no difference whether chlorides, nitrates or sulfates were used.

After the cell had first been packed, the resin plug was left in contact with water for a few days before the experiment was started in order to allow swelling to take place. Moreover, it was necessary to carry out several exchange experiments before reproducible results could be obtained.

An alternative method for the removal of alkali metal ions is that of electrolysis of the resin plug between perforated platinum electrodes with simultaneous streaming of water to remove the electrolysis products. This method may be convenient generally in order to regenerate an alkali metal resin to the hydrogen form, particularly if only 75–80% regeneration is required. Complete regeneration by electrolysis is uneconomical because the current yield decreases rapidly as the regeneration proceeds, since the mobile hydrogen ions in the swollen resin phase carry an increasing fraction of the total current in place of the alkali metal ions, which are virtually the sole current carriers at the beginning of the electrolysis. Electrolysis is, however, not suitable for the regeneration of alkaline earth and heavy metal resins because of their low conductivity (*cf.* succeeding section).

RESULTS AND DISCUSSION

I

From the cell resistances (R) obtained and the cell constant (C) were derived the following conductivities:

(*1*) The specific conductivity (κ) of the plug. This is an average conductivity of swollen resin plus free water contained between the electrodes.

(*2*) The equivalent conductivity, $\Lambda = \frac{\kappa}{n}$, n representing the number of equivalents of exchangeable hydrogen/cc. of cell space. The value of Λ is characteristic for the swollen resin phase since the conductivity of the water is negligibly small compared with that of the resin phase.

Several series of experiments were carried out, with varying distance between the electrodes and varying tightness of packing. One series is reported in detail (Table I) to give an idea of the degree of reproducibility achieved; l_c is the equivalent ionic conductivity at infinite dilution for an aqueous solution at 18°C.

Table II shows average values for each ionic species bound in the resin for two plugs of different length.

Plugs 6 and 7 differ with respect to the distance between the electrodes and the tightness of packing as shown by the values of n. The values of Λ and l_c/Λ vary somewhat with the tightness of packing owing to a varia-

TABLE I

Amberlite IR100

Plug 6: 1.35 cm. diam.; 4.0 cm. length. Weight of resin: 3.53 g.
$C = 2.79$ cm.$^{-1}$; $n = 7.64 \times 10^{-4}$ equiv./cm.^{3}

Ion	R in ohms	$\kappa \times 10^3$	Λ	l_c	l_c/Λ
Na^+	1820	1.54	2.01	43.4	21.6
H^+	204	13.6	17.9	313.9	17.5
Na^+	1835	1.52	1.99	43.4	21.8
H^+	204	13.6	17.9	313.9	17.5
Na^+	1845	1.51	1.98	43.4	21.9
H^+	201	13.9	18.2	313.9	17.3
K^+	1345	2.07	2.72	64.6	23.8
H^+	203	13.8	18.0	313.9	17.5
NH_4^+	1150	2.43	3.18	64.7	20.4
H^+	202	13.8	18.1	313.9	17.4
Li^+	2515	1.11	1.45	33.3	22.9
H^+	203	13.7	18.0	313.9	17.5
K^+	1375	2.03	2.66	64.6	24.3
H^+	201	13.9	18.2	313.9	17.3
Na^+	1855	1.50	1.97	43.4	22.1
H^+	201	13.9	18.2	313.9	17.3
NH_4^+	1155	2.42	3.16	64.7	20.4
H^+	201	13.9	18.2	313.9	17.3
Li^+	2495	1.12	1.46	33.3	22.8
H^+	202	13.8	18.1	313.9	17.3
Li^+	2515	1.11	1.45	33.3	22.9
H^+	197	14.2	18.6	313.9	16.9
Mg^{++}	7000	0.40	0.52	45.9	88
H^+	196	14.2	18.6	313.9	16.8
Ca^{++}	7320	0.38	0.50	51.9	104
H^+	195	14.3	18.7	313.9	16.8
Ba^{++}	12700	0.22	0.29	55.4	190
H^+	202	13.8	18.1	313.9	17.4
Na^+	1850	1.51	1.98	43.4	22.0
K^+	1380	2.02	2.65	64.6	24.4
H^+	197	14.2	18.6	313.9	16.9
Ag^+	8620	0.32	0.42	54.0	127
H^+	201	13.9	18.2	313.9	17.3

TABLE II

Amberlite IR100

Plug 6: 1.35 cm. diam.; 4.0 cm. length. Weight of resin: 3.53 g.
$C = 2.79$; $n = 7.64 \times 10^{-4}$ equiv./cm.^{3} [a]

Ion	R in ohms	Λ	l_c	l_c/Λ
H^+	200 ± 5	18.3	313.9	17.2
Li^+	2505 ± 10	1.46	33.3	22.8
Na^+	1849 ± 5	1.98	43.4	22.0
K^+	1375 ± 5	2.66	64.6	24.3
NH_4^+	1153 ± 5	3.17	64.7	20.4
Ag^+	8600 ± 100	0.42	54.0	130
Mg^{++}	7000 ± 100	0.52	45.9	90
Ca^{++}	7300 ± 100	0.50	51.9	100
Ba^{++}	12700 ± 200	0.29	55.4	190
La^{3+}	45000	0.07	61.0	~ 900
Th^{4+}	74000	0.05	23.5	~1000

Plug 7: 1.35 cm. diam.; 2.64 cm. length. Weight of resin: 2.49 g.
$C = 1.84$; $n = 8.18 \times 10^{-4}$ equiv./cm.^{3}

Ion	R in ohms	Λ	l_c	l_c/Λ
H^+	133	17.0	313.9	18.6
Li^+	1620	1.39	33.3	24.0
Na^+	1203	1.87	43.4	23.2
K^+	870	2.59	64.6	24.9
NH_4^+	753	2.99	64.7	21.6

[a] In all experiments on resin conductance, the value of n is calculated from the limiting exchange (1.20×10^{-3} g.-eq. of exchangeable hydrogen/1 g. of air-dry resin). If n is calculated from the sulfur content or the potentiometric titration curves (1.30×10^{-3} g.-eq.), the values of Λ become 8% smaller and those of l_c/Λ 8% greater.

tion of the effective cross-section of the plug. However, the order of the Λ and l_c/Λ values for the various ions bound in the resin is the same for all plugs investigated irrespective of the experimental conditions.

The reproducibility in one plug is of the order of ±2% for the hydrogen resin, ±0.5% for the alkali metal resins, but much less for resins in which the hydrogen is substituted by multivalent ions. As the accuracy of the resistance measurement is greater than the above figures, the experimental limits of accuracy are determined by the degree of completeness of the exchange reaction and perhaps by variations in the degree of swelling of the resin plug.

II

The resistances listed in Table II can be classed in 4 groups: the hydrogen resin, having a low resistance; the alkali metal resins possessing somewhat higher resistances; next come the silver and alkaline earth resins, and finally the lanthanum and thorium resins, which are very poor conductors. These resistances are determined by the degree of tightness of binding and the mobility of the respective ion. Hydrogen ion is weakly bound in the anion sponge of the sulfonic acid resin, $-SO_3^-H^+$ being strongly acidic, and has a high mobility. The alkali metal ions are also weakly bound, alkali metal salts of sulfonic acids being strongly dissociated, but alkali metal ions possess a lower mobility than H^+. Silver and the multivalent ions are obviously bound fairly firmly, as shown by the high resistances and small Λ values.

The differences in tightness of binding are shown more clearly on considering the l_c/Λ values. A small value indicates comparatively free migration, whereas a large value indicates strong restriction of migration. The values of l_c/Λ are of the same order of magnitude (17–24) for the alkali metal resins (incl. NH_4^+) and the hydrogen resin. In other words, for these ions the conductance in the swollen resin phase is roughly proportional to the mobility at infinite dilution of the ion in water. Thus, the restriction to ionic migration imposed on these ions "bound" in the resin is of the same order of magnitude for all ions of this group. The equivalent ionic conductivity is about 20 times smaller than in aqueous solution at infinite dilution. This reduction is largely due to the porous labyrinth structure of the resin, which lengthens the effective path and reduces the effective cross-section available for migration. It is interesting to note that for NaCl the diffusion rate also is very much smaller in a resin than in aqueous solution (2). Interionic attraction is likely to make only a comparatively small contribution to this restriction of ionic migration; this is suggested by a comparison of the equivalent conductivity of the respective salt in water, at a concentration corresponding to that in the resin phase, with the Λ_∞ value of the salt.

The next group includes Ag^+, Mg^{++}, Ca^{++}, and Ba^{++}. In this group there is no proportionality between resin conductance and ionic mobility in aqueous solution, suggesting that the energy barriers involved in ionic migration of these ions in the resin are very different from those of the first group. The stronger binding is suggested by the higher l_c/Λ values. The resin salts of this, as well as of the following group, show little dissociation, as evidenced by the low conductivity.

The rate of the exchange reactions in this group is much smaller than with alkali metal salts (*cf.* also 3).

Lanthanum and thorium, having l_c/Λ values of the order of 1000, and very small resin conductances, are still more strongly bound than bivalent cations. The exchange reactions are very slow in this group, and the reproducibility of the resistance measurements is much less satisfactory than in the previous cases. This is probably accounted for by varying degrees of completeness of the exchange reactions, as small amounts of unexchanged H^+ will have a large influence on the plug resistance. In addition, exchange involving complex or partly hydrolyzed ionic species may cause complications in this group.

The values shown in Table II suggest the following series for the strength of binding:

$Th^{4+} > La^{3+} \gg Ba^{++} > Ag^{+} > Ca^{++} > Mg^{++} \gg$ alkali metal ions $> H^+$.

The quantity which has been described somewhat loosely as "strength of binding" on the evidence of the l_c/Λ values may in future be expressed in terms of potential energy barriers involved in ionic migration. The order of the height of these barriers is similar to that suggested by the equilibrium studies of Boyd, Schubert and Adamson (4), except in the case of the alkali metal resins (*cf.* later).

The behavior of the various resin salts bears some resemblance to that of salts of different solubilities. The alkali metal resins showing large rates of reaction and comparatively high conductivity, which is proportional to the ionic mobility in dilute solution, must have a diffuse arrangement of the cations in the swollen resin. On the other hand, the resin salts of multivalent ions, and of silver, showing small rates of reaction, large values of K' (*cf.* the preceding paper) and low conductivities are likely to have their cations more closely associated with the negative groups of the resin and resemble sparingly soluble salts. The tightness of binding of cations in the resin salts may be expected to depend on:

(*1*) the attraction between the negative groups of the resin and the respective cation which increases with increasing charge (valency) of the latter; and

(*2*) the hydration of the cation. With bivalent cations l_c/Λ decreases with increasing energy of hydration.

The l_c/Λ value of the silver resins is much higher than that of resin salts with other univalent cations; moreover, the exchange reactions involving silver are slower. The behavior of this metal is, thus, irregular. This has a parallel in the small solubility of silver salts of many organic acids.

The l_c/Λ value of hydrogen is of the same order of magnitude as that of the alkali metal ions. This illustrates well the strong acid nature of the sulfonic acid resins. If they were weakly acidic, hydrogen would be mainly covalently bound, and, as a consequence, the resin conductivity would be low and l_c/Λ high.

III

We investigated another Amberlite resin of a sulfonic acid type (IR100-H.A.G.). This resin was completely freed from soluble material and had undergone several exchange cycles before it was supplied to us.

The rate of exchange is smaller than with Amberlite IR100, and the limiting exchange at pH = 2.0–2.5 slightly greater, namely 1.38×10^{-3} g.-eq. of exchangeable hydrogen/1 g. of air-dried resin (moisture content: 19.0%).

Table III shows the results obtained.

TABLE III

Amberlite IR100-H.A.G.

Plug 8: 1.35 cm. diam.; 3.65 cm. length. Weight of resin: 3.54 g.
$C = 2.55$; $n = 9.34 \times 10^{-4}$ equiv./cm.^{3}

Ion	R in ohms	Λ	l_c	l_c/Λ
H^+	905	3.02	313.9	104
Li^+	14,400	0.189	33.3	176
Na^+	10,200	0.268	43.4	162
K^+	8,200	0.333	64.6	194
NH_4^+	6,900	0.396	64.7	164
Mg^{++}	62,000	0.044	45.9	1040
Ca^{++}	48,000	0.057	51.9	910
Ba^{++}	73,000	0.037	55.4	1480

This resin shows the same gradation of values of R, Λ, and l_c/Λ as the previous one, but the absolute values of R and l_c/Λ are 6–10 times greater than for Amberlite IR100. This is most probably due to smaller porosity, which is also indicated by the comparative slowness of the exchange reactions. As a consequence, the migration of all ions is more strongly impeded in this resin than in Amberlite IR100.

IV

The question arises as to whether the comparatively small differences in l_c/Λ between the alkali metal ions can be regarded as significant for the tightness of binding or whether there are other effects which may modify the value of l_c/Λ. If the results could be interpreted solely in terms of strength of binding, the order would be

$$K^+ > Li^+ > Na^+ > NH_4^+ > H^+$$

for Amberlite IR100, and

$$K^+ > Li^+ > Na^+ = NH_4^+ > H^+$$

for Amberlite IR100-H.A.G. These series are not in agreement with that obtained by Boyd, Schubert and Adamson (4) from their equilibrium studies with Amberlite IR1, which is

$$K^+ > NH_4^+ > Na^+ > H^+ > Li^+.$$

Nevertheless, it must be borne in mind that equilibrium constants and activity coefficient ratios vary with the experimental conditions, as shown in the preceding paper. On the other hand, the discrepancy may be the result of second order effects which may modify the resin conductivity.

Firstly, there is the effective pore diameter of the resin in relation to the diameter of the hydrated ions to be considered. The hydrogen ion, notably possessing an anomalous (Grotthuss-like) mechanism of migration, may be less impeded in the labyrinth structure of the resin than the strongly hydrated Li^+. This may account for the discrepancy of the position of H^+ and Li^+ in the l_c/Λ series as compared with the equilibrium series. This argument receives a measure of support from the fact that the finely porous Amberlite IR100-H.A.G. shows a greater difference between the l_c/Λ values of hydrogen and of the alkali metals than Amberlite IR100, which has a more open structure. In fact, the possibility of the migration of H^+ involving partly a proton transfer between H_3O^+ and $-COOH$ or $-OH$ groups of the resin, in addition to the proton transfer between H_3O^+ and H_2O which characterizes the migration in water, may be taken into consideration.

Secondly, varying degrees of swelling of the resin due to the different cations may affect the values of R and l_c/Λ. Our experience does not suggest thus far that the swelling is responsible for more than second order effects in the case of Amberlite IR100 and IR100-H.A.G. Preliminary experiments with Dowex 50 have shown, however, that the differences in swelling between the various resin salts are much greater with Dowex than with the Amberlites, rendering the interpretation of conductivity data with Dowex 50 more difficult.

V

Up till now we have assumed in this discussion that the exchangeable hydrogen originates from the sulfonic acid groups. However, as the solutions streamed through the plug are nearly neutral, there is a possibility that a small amount of more weakly acid groups, such as $-COOH$, may take part in the reaction (*cf.* the preceding paper). Evidence in favor of this suggestion emerges from several experiments in which KCl and NaCl solutions of various pHs were streamed through the resin plugs, and the resistances were determined *after the salt solution was replaced by water.* Fig. 2 shows the plug resistances (R) in water in relation to the pH of the salt solution streamed through the plug; the desired pH was obtained by adding appropriate amounts of HCl to the salt solution. At low pH, R is low because only part of the hydrogen of the $-SO_3^-H^+$ groups is replaced by K^+ or Na^+. R increases with increasing pH, because replacement becomes more complete, and reaches a maximum at pH $\simeq 3.5$, but falls slightly at higher pH. This falling off is probably due to a (partial) re-

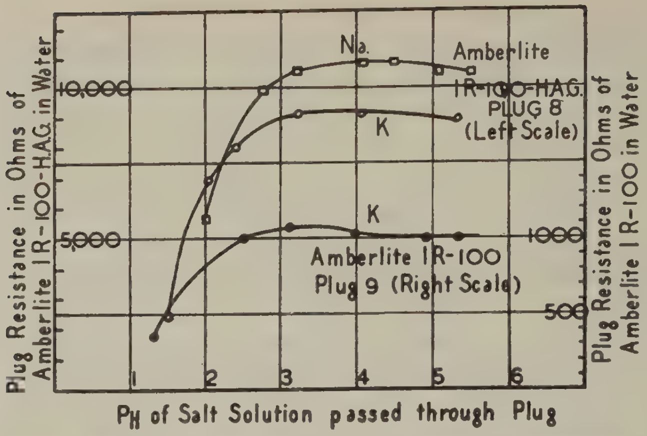

FIG. 2. Resistance of plug of resin salt (Na, K) in water plotted against the pH of the salt solution (NaCl, KCl) that was streamed through the plug.

placement of hydrogen belonging to a more weakly acid group (*e.g.*, $-COOH$) by K^+ or Na^+ at pH > 3.5, since the alkali salts of such acids are more strongly dissociated than the acids themselves. The effect is only small—*R* at pH = 5 is about 3% smaller than at pH = 3.5—either because there is only a small number of weak acid groups capable of reacting in this pH range, or because of partial hydrolysis of the K or Na salts of weakly acid groups on streaming water through the plug (*cf.* later). The experiments suggest that the replacement of sulfonic acid hydrogen by alkali cations is complete at pH = 3.5.

There is experimental evidence for the occurrence of a hydrolytic change involving the salts of weakly acid groups. Fig. 3 shows the change of resistance of a plug of resin, originally in the hydrogen form, with time,

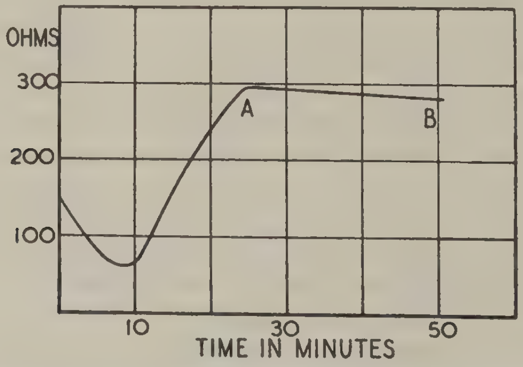

FIG. 3. Resistance of a plug of resin, originally in the hydrogen form, while an $N/10$ KCl solution is streamed through, plotted against time.

while $N/10$ KCl solution (pH $\simeq$ 6) is streamed through. At first there is a fall of resistance owing to the liberation of HCl, but the resistance soon rises as the more mobile H^+ in the resin phase is replaced by the less mobile K^+. On further streaming (beyond point A) of the KCl solution, the resistance decreases slowly. We interpret this as being due to reaction of a weakly acid group with KCl with the formation of a strongly dissociated salt, but the possibility of a change of the amount of swelling being partly responsible cannot be excluded with certainty. At this stage (point B), the pH of the effluent is slightly lower, and its conductivity slightly higher, than that of the influent, due to the formation of a small amount of HCl on reaction of a weakly acid group of the resin with KCl. If, subsequently, water is streamed through the plug, the pH of the effluent water is slightly higher than that of the influent, owing to hydrolysis of the K salt of a weakly acid group. The resistance of the plug after this procedure is the same as that obtained when streaming of KCl was interrupted at point A and water streamed subsequently. It is likely, therefore, that, on reaching point A, all $-SO_3H$ groups, and perhaps also some more weakly acid groups, have reacted, and that, on further streaming of KCl solution, reaction occurs with groups which are more weakly acid than the previous ones and whose potassium salts are easily hydrolyzed. These experiments, together with those shown in Fig. 2, constitute additional evidence for the facts established in the previous paper, namely, that the resin contains, besides $-SO_3H$, groups of various acid strengths whose salts are hydrolyzed to different extents.

Summary

1. The electric conductivity of swollen resin plugs packed between perforated platinum electrodes, and containing various bound cations, is investigated in a special streaming cell, which allows of replacement of one ionic species by another in the same plug. This method proves to be a useful tool in the investigation of the strength of binding of cations in the resin.

2. The hydrogen resin is a fairly good conductor; the conductance of alkali metal resins is about 6–12 times smaller, while resins in which hydrogen is replaced by ions of higher valency, or silver, are poor conductors. For hydrogen and alkali metal resins, the resin conductance is roughly proportional to the mobility of the respective cations in water, but no such proportionality exists for resins containing silver or ions of higher valency. It is concluded that the latter are much more tightly bound than the former, the order being

$Th^{4+} > La^{3+} \gg Ba^{++} > Ag^{+} > Ca^{++} > Mg^{++} \gg$ alkali metal ions $> H^{+}$.

3. The variation of the resistance of plugs of alkali metal resins with the pH of the salt solution used in the exchange reaction is studied. The resistance has a maximum at pH $\simeq 3.5$ but falls when the pH of the salt solution is higher. It is suggested that up to pH $\simeq 3.5$ the $-SO_3H$ groups are involved, but that groups of a more weakly acid nature come into action at higher pH. There is evidence of hydrolysis of alkali metal salts of the latter groups on streaming water through the resin plug.

REFERENCES

1. Hartley, G. S., and Roe, J. W., *Trans. Faraday Soc.* **36**, 101 (1940).
2. Bauman, W. C., and Eichhorn, J., *J. Am. Chem. Soc.* **69**, 2830 (1947).
3. Nachod, F. C., and Wood, W., *ibid.* **67**, 629 (1945).
4. Boyd, G. E., Schubert, J., and Adamson, A. W., *ibid.* **69**, 2818 (1947).

SURFACE FILMS OF SOLUBLE DETERGENTS[1]

A. P. Brady

From the Stanford Research Institute, Stanford, Calif.

Received December 30, 1948

INTRODUCTION

The force-area diagram for films of soluble surface-active agents on water cannot be studied by the ordinary film balance techniques because of the tendency of the film to leave the surface and enter the bulk of the liquid when the film is compressed.

A previous approach to eliminate this difficulty was to study higher, insoluble homologues of the compound of interest. For this reason the C_{22} sodium alkyl sulfate (1) and alkyl pyridinium halides (2) have been studied. However, the quite different type of curves obtained (two-dimensional solid in the first case, vapor in the second) cannot with any assurance be extrapolated to the lower soluble homologues now under examination. The present approach is directly to study the compounds of interest, but to vary the substrate and to use rapid compression of the films. By using a sufficiently high concentration of salt in the substrate, all the detergents reported on here can be made nearly insoluble, and a force-area diagram can therefore be obtained if compression is sufficiently rapid.

MATERIALS

Aerosol OT (sodium di-2-ethylhexylsulfosuccinate) was the 100% grade of the American Cyanamid Co. Dodecyl sodium sulfonate was a preparation from the Laboratory of Professor H. V. Tartar, University of Washington. Alkyl sodium sulfates were special preparations furnished by the duPont Co. The E-607 derivatives [(N-acylethanolaminoformylmethyl) pyridinium chlorides] were especially purified samples furnished by the Emulsol Corporation.

APPARATUS

Because compression must be rapid, some type of recording film balance must be used. In the present work, this device was a simplified version of the Wilhelmy-Dervichian balance (3). The compression barrier was automatically driven by arms riding on a helical screw driven by an adjustable speed D.C. shunt motor (which gives a constant, but only approximately known, speed). These arms also operated switches near the start and end of the compression that made reference marks on the kymograph sheet running during the experiment. The position of the balance arm was read through a telescope and scale. Marks can be made on the kymograph sheet by a hand key at any desired scale interval. Fig. 1 gives a schematic diagram of the balance's electrical circuit. From the kymograph record, and from the known speed of the kymograph and the known position of the barrier at the start and end reference marks, both the speed of compression and the scale reading at any position of the barrier can be computed. Then (from the calibration obtained before each run) this scale reading can, in turn, be converted to surface pressure.

---

[1] This work was carried out under a contract between the Office of Naval Research and Stanford University, under the direction of Professor J. W. McBain.

Most of the films were spread from a solution of a mixture of 67% isopropanol and 33% water, since this mixture dissolved all the surface active agents used in these investigations. Experiments with Aerosol OT spread from water, isopropanol, and from benzene, showed, within experimental error, no effect from the solvent used. The volume of solution spread (*ca.* 0.1 cc.) was measured from a syringe pipette with a micrometer head to an accuracy of about 1%. The temperature was 20 ± 1°C.

Since all the films studied are appreciably soluble in water, a spurious curve, due to the rate of dissolution being comparable to the rate of compression, must be guarded against. The relation of dissolution to com-

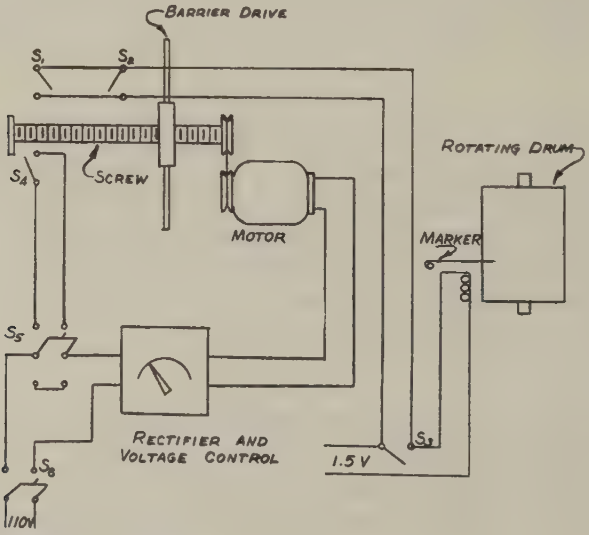

FIG. 1. Diagram of barrier drive and kymograph circuit. S_1, S_2, Time marking switches to give barrier speed and position. S_3, Hand key. S_4, Switch to stop motor at end of sweep. S_5, Shorting switch to allow reversal of motor. S_6, Main switch.

pression was checked by comparing curves obtained at various barrier speeds. The limiting factor in the allowable compression speed is the inertia of the balance arm, in the present case the inertia was such as to limit the speed to about 0.7 cm./sec.

RESULTS AND DISCUSSION

Force-area curves for E-607 derivatives spread on 16.6% NaCl are given in Fig. 2. The dodecyl derivative is too water-soluble to obtain a significant compression curve with the present apparatus. The E-607 compounds gave films of the expanded type. Adam (2) has reported that C_{22} straight chain pyridinium salts give the same type of film. Fig. 3 gives data for some sulfonates and sulfates on the same substrate (dodecyl sulfonate was used here rather than the sulfate because of the high solubility of the latter). It can be seen that Aerosol OT, dodecyl sulfonate and tetradecyl sulfate give curves of the same form as the E-607 derivatives, except that the first is a less compressible film. The higher sulfates, however, give a break in the compression curve reminiscent of the phase change in films of myristic acid. It does not, however, appear to be as simple as this, as will be brought out later.

Figs. 4 and 5 give compression curves on successively weaker salt solutions. The dotted curves are for substances obviously dissolving sufficiently rapidly in the particular salt solution to affect the compression curve at higher pressures. Only the octadecyl sulfate was sufficiently insoluble to give a reproducible compression curve on pure water. From these data it can be seen that reducing the salt concentration moves the curves to the right (a larger area per molecule at a given surface pressure), and that in the C_{16} and C_{18} derivatives, the break in the curve moves to slightly higher pressures. As the salt concentration is decreased to the point where the film becomes appreciably soluble at higher pressures, the movement of the curve to the right ceases at low pressures. Under such circumstances, the curve actually moves to the left at high pressures, but this is obviously due simply to dissolution of the film.

For two reasons the interpretation of the break in the C_{16} and C_{18} curves as a phase change seems to be an over-simplification. The first is that, except at lower salt concentrations, the molecular areas involved are much too small (the limiting area of the hydrocarbon group is 18.5 Å^2; the presence of the polar group should increase this appreciably). Although if, as Stenhagen did for the C_{22} sulfate (1), one corrects all limiting areas to 18.4 Å^2 and presumes that the smaller areas are due to dissolution before compression, the curves at all salt concentrations will nearly coincide. However, one is then forced into the untenable position that dissolution is the more rapid the higher the salt concentration. The second difficulty lies in the effect of aging of the surface. All the surfaces

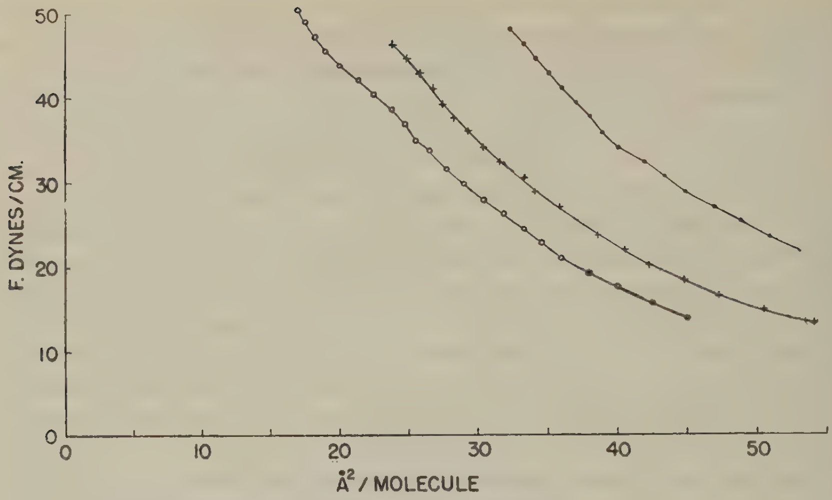

FIG. 2. Force-area curves for E-607 derivatives. ○ C_{18}, + C_{16}, ● C_{14}.

in Figs. 4–7 were aged 1–10 minutes; within these limits the aging time has no observable effect. Experiments on C_{16} and C_{18} sulfates, in which the surface was allowed to age for 2 hours, however, showed a change in character of the compression curve, in that the film is more expanded and the apparent phase change has completely disappeared (Fig. 6). It

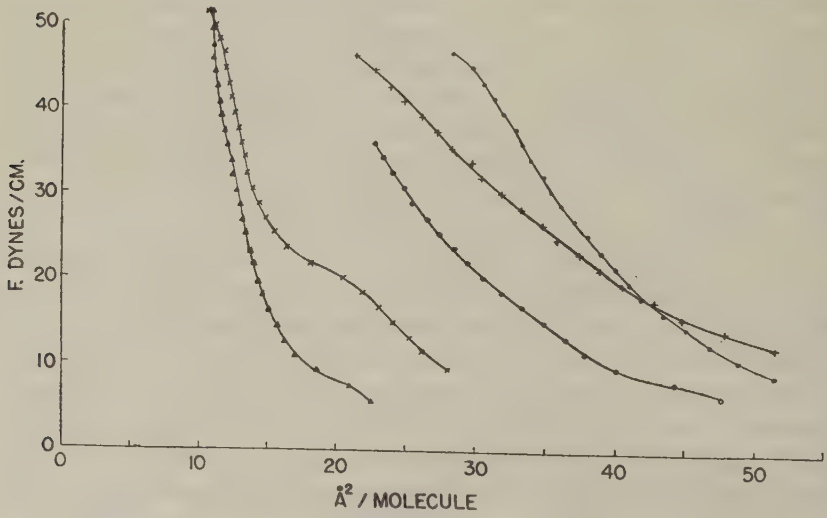

FIG. 3. Force-area curves for sulfates and sulfonates. Substrate 16.6% NaCl. △ C_{18} sodium sulfate, × C_{16} sodium sulfate, ○ C_{14} sodium sulfate, + C_{12} sodium sulfonate, ● Aerosol OT (mult. area scale by two).

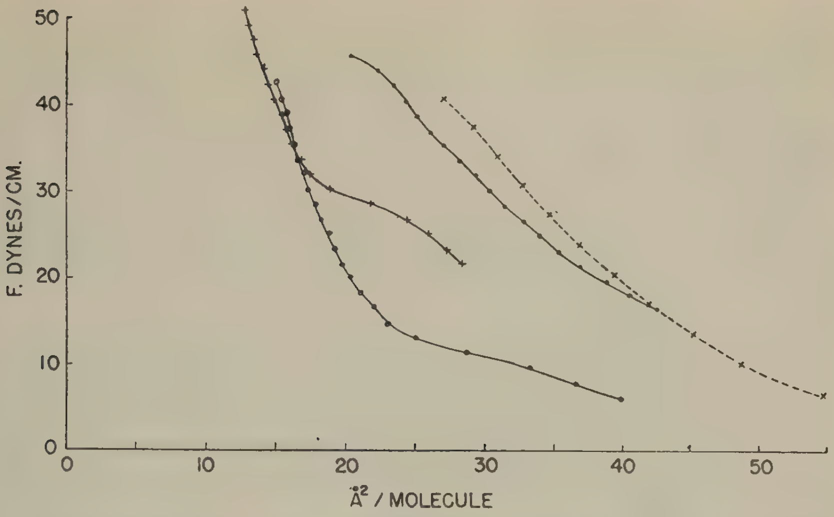

FIG. 4. Force-area curves for sulfates and sulfonates. Substrate 9.1% NaCl. × Aerosol OT (dissolving), ● C_{14} sulfate, + C_{16} sulfate, ○ C_{18} sulfate.

therefore appears that the observed flat in the force-area curve is caused only by imperfect orientation, and probably results from a sliding of one layer of molecules over another. Such a phenomenon would have to be considered in problems connected with foam formations where relatively fresh surfaces are subjected to rapid expansion and compression.

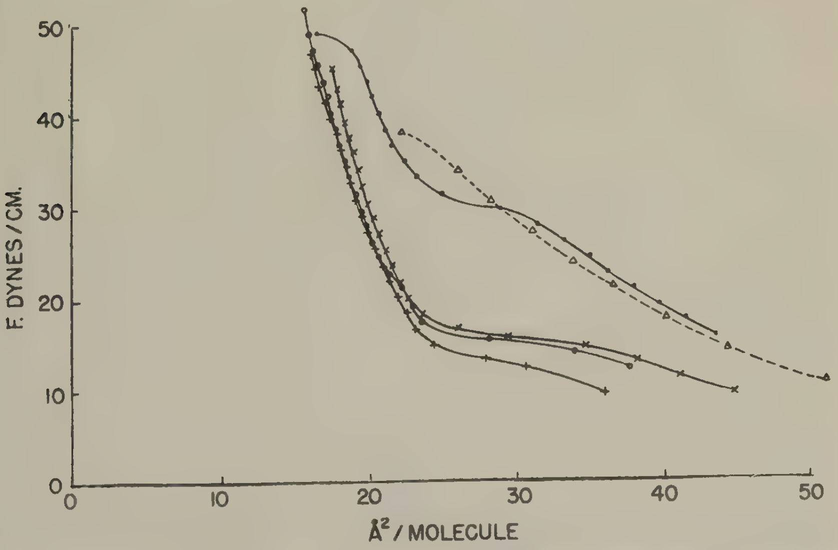

FIG. 5. Force-area curves for sulfates. ● C_{14} on 4.8% NaCl (dissolving), ● C_{16} on 4.8% NaCl, + C_{18} on 4.8% NaCl, ○ C_{18} on 2.4% NaCl, × C_{18} on 0.5% NaCl.

The substitution of $CaCl_2$ for NaCl in the substrate is also of interest in this connection. Such a substitution has only a minor influence on the compression curves for Aerosol OT and the lower alkyl sulfates, but it can be seen from Fig. 7 that the higher calcium alkyl sulfates show no apparent phase changes; indeed, the curves are quite similar to those obtained for the aged sodium films. This is in accord with the view that the break in the compression curves for fresh films over NaCl is an oversliding of layers rather than a phase change to close packed heads and tails. Films on a $BaCl_2$ substrate were found to be too fragile to give a significant compression curve.

If the curves for each of the alkyl sulfates are examined at the lowest NaCl concentration at which a compression curve can be obtained without appreciable dissolution, it is found that the C_{12}, C_{14}, and the lower branch of the C_{16} curves nearly all coincide. The composite curve can be expressed with fair accuracy over the surface pressure range 10–40 dynes/cm. by the equation:

$$\pi = \frac{1400}{A} - 16,$$

where π denotes the surface pressure in dynes/cm., and A is the area in Å^2/molecule. If this curve is compared with the adsorption calculated by the Gibbs adsoprtion equation from the surface tension data on solutions of foam-fractionated detergents (4), it is found that the adsorption at a given surface pressure, as calculated from the present force-area curves, is almost precisely twice that calculated from surface tension data on solutions. A similar comparison of a derived surface tension curve for hypothetical "neutral" potassium laurate (4) with force-area curves obtained with carboxylic acids on NaOH (5), again leads to an approximate factor of 2. If the surface tension data are to be believed, it must then be concluded that the condition of the film on a salt substrate differs appreciably from a film of the same material in equilibrium with bulk solution. On the other hand, at a surface pressure of 33 dynes, the microtome (6) gave an area of 29–32 Å^2/molecule as compared to 29 Å^2 predicted from Eq. (1). At lower concentrations and surface pressures, the microtome and interferometer methods gave considerably larger areas than predicted from Eq. (1). The only other attempt, insofar as the writer is aware, to so compare results from force-area curves in a film balance with surface tension results with solutions, is that of Schofield and Rideal (7), using lauric acid. These authors found good agreement. However, there is one important difference between their comparison and the present one—the surface tension measurements did not deal with a dissociated solute, since HCl was added to suppress ionization of the lauric acid.

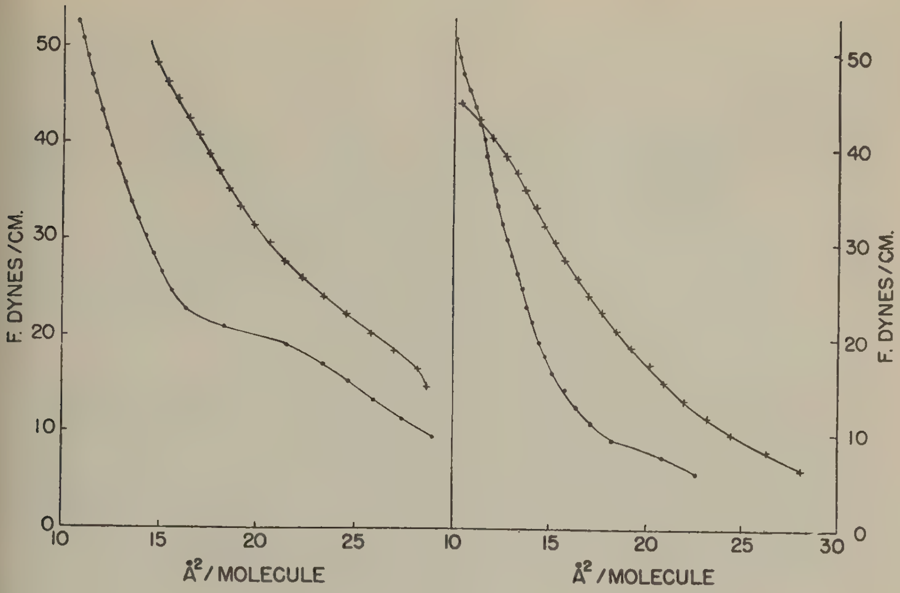

(a) (b)

FIG. 6 (a). Effect of age on $C_{16}OSO_3Na$. Substrate: 16.6% NaCl. ● Surface aged 1–10 min. + Surface aged 2 hr. (b) Effect of age on $C_{18}OSO_3Na$. Substrate: 16.6% NaCl. ● Surface aged 1–10 min. + Surface aged 2 hr.

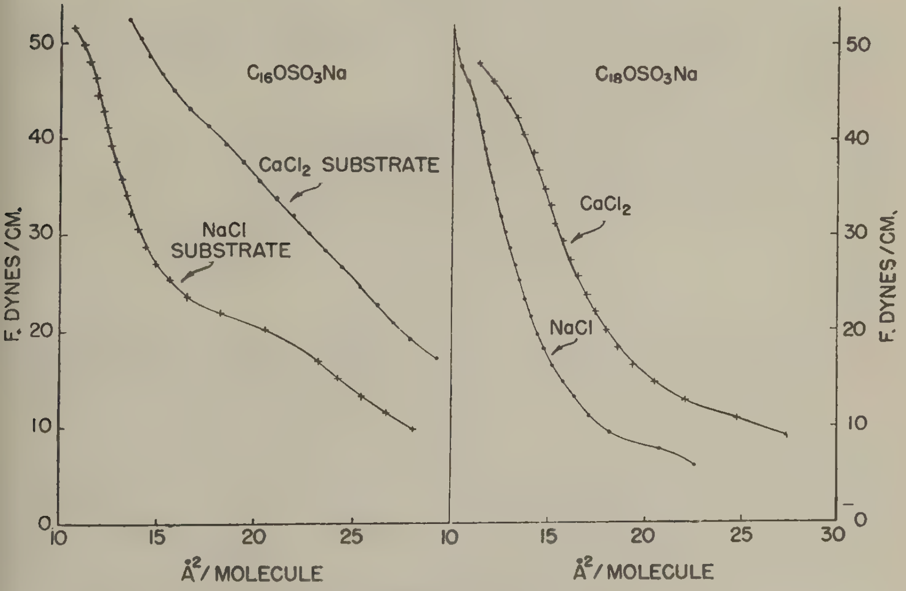

FIG. 7. Effect of calcium ion.

SUMMARY

The force-area diagrams for films of a number of water-soluble detergents were determined by using salts in the substrate to reduce solubility, and by employing rapid compression. Curves were obtained with films of some pyridinium salts, Aerosol OT, sodium lauryl sulfonate, and the C_{14} to C_{18} derivatives of sodium alkyl sulfates. The latter were used with varying amounts of salt in the substrate. All films, with the exception of the C_{16} and C_{18} sulfates, were of the expanded type. The exceptions showed an apparent phase change, but the break in the curve, since it disappeared on allowing the film to age for an hour, was shown to arise from a non-equilibrium arrangement of the film.

Substitution of $CaCl_2$ for NaCl in the substrate was without appreciable effect, except that the break in the curve for the higher homologues was eliminated without the necessity for aging.

A comparison of the results of this investigation on undissolved films with results below the critical concentration on solutions of detergents and soaps indicates that the films are not the same under the two conditions. Surface tension and microtome measurements show that, at a given "surface pressure," films on solutions occupy about twice the area of films on a salt substrate. Above the critical concentration, present measurements agree well with microtome results on solutions, but again not with surface tension results.

REFERENCES

1. STENHAGEN, E., *Trans. Faraday Soc.* **36**, 496 (1940).
2. ADAM, N. K., Physics and Chemistry of Surfaces, Oxford University Press, 1939, p. 129.
3. DERVICHIAN, D. G., *J. phys. radium* **6**, 427 (1935).
4. BRADY, A. P., *J. Phys. Colloid Chem.* **53**, 56 (1949).
5. ADAM, N. K., AND MILLER, J., *Proc. Roy. Soc. London* **142A**, 401 (1933).
6. MCBAIN, J. W., AND WOOD, L. A., *ibid.* **174A**, 286 (1940).
7. SCHOFIELD, R. K., AND RIDEAL, E. K., *ibid.* **109A**, 57 (1925); **110A**, 167 (1926).

DIFFUSION-CONTROLLED REACTION RATES

Frank C. Collins* and George E. Kimball

From the Department of Chemistry, Columbia University, New York, N. Y.

Received March 3, 1949

INTRODUCTION

The theory of the kinetics of colloid coagulation as a diffusion-controlled process was originally developed by Smoluchowski (1) using Fick's law of diffusion. As ordinarily applied, the theory is based on the assumptions that around one of the reactant particles a concentration gradient for the other species is set up, and that the rate of flow of particles in this concentration gradient is governed by Fick's law of diffusion. The fundamental differential equation

$$\frac{\partial c}{\partial t} = D\nabla^2 c \tag{1}$$

is solved with the boundary condition $c = 0$ on the surface of a sphere of radius R, this sphere representing the distance of closest approach of two particles. The simultaneous diffusion of both species of particles is taken care of by taking D to be the sum of the diffusion coefficients of the two species.

The solution to Eq. (1) with this boundary condition is

$$c(r, t) = c_o\left[1 - \frac{R}{r}\, erfc\, \frac{r - R}{\sqrt{4Dt}}\right], \tag{2}$$

where

$$erfc\; x = \frac{2}{\sqrt{\pi}}\int_x^\infty e^{-z^2}dz \tag{3}$$

and c_o is the initial concentration of the diffusing species, supposed uniform at $t = 0$. The flux across the boundary sphere at $r = R$ is

$$\Phi = 4\pi R^2 D\left(\frac{\partial c}{\partial r}\right)_{r=R} \tag{4}$$

$$= 4\pi DRc_o\left(1 + \frac{R}{\sqrt{\pi Dt}}\right). \tag{5}$$

---

* Present address: Polytechnic Institute of Brooklyn.

In the colloid coagulation process, the time-dependent term is small and may be neglected.

The Smoluchowski theory was extended to ordinary bimolecular chemical reactions by Sveshnikoff (2) in connection with the quenching of fluorescence in liquid solution. Here there is competition between a first and a second order reaction. After photo-excitation of a fluorescent molecule, fluorescence may ensue or the molecule may be deactivated by collision with a quencher. The normal half-life of the excited state is of the order of 10^{-8} sec. and the quenching process is presumably diffusion-controlled. A further modification of the original Smoluchowski theory by Sveshnikoff (2) was to assume that if only a fraction α of the collisions is effective, the only modification needed is to multiply the flux given by Eq. (5) by the factor α.

The Smoluchowski theory was further developed by Umberger and LaMer (3) to include diffusion in a potential field as in the case of ions, following Debye (4). Use was made of the transient term in Eq. (5) because of the extremely short half life of the excited species. Following a suggestion from one of us (G. E. K.), Williamson and LaMer (5) abandoned the use of the transient term in the Smoluchowski equation, pointing out that there is but little difference between the Smoluchowski limiting flux and the encounter frequency using a quasi crystalline liquid model.

On closer examination of this theory, a number of disturbing points may be raised. First, what is the nature of the postulated concentration gradient? Suppose that our two species of particle are A and B, and that we consider the neighborhood of a certain A particle. Initially, this is surrounded by a uniform concentration of B. A gradient in this concentration can only be set up by the reaction of B particles with the A particle. But this reaction can only take place once. After such a reaction there is no longer an A particle at the center, and the concentration gradient so formed seems to have lost its interest.

Second, the flux given by Eq. (5) becomes infinite at $t = 0$. In most cases the flux falls to a reasonable value in an extremely small time, and the total amount of reaction predicted is finite, but nevertheless the singular rate at $t = 0$ is a blemish on the theory, and, in the case of the quenching of fluorescence, where the important time interval is the first 10^{-8} sec. after excitation, the initial rate may be very significant.

Third, when not every collision between particles is effective, the Sveshnikoff procedure of multiplying the flux by α is not self-consistent. From Eq. (2) we find that decrease of the total amount of the diffusing species from the amount present at $t = 0$ is

$$M = c_o \int_R^\infty 4\pi r R \, erfc \, \frac{r - R}{\sqrt{4Dt}} \, dr. \tag{6}$$

The time derivative of this is

$$\frac{dM}{dt} = 4\pi DRc_o\left(1 + \frac{R}{\sqrt{\pi Dt}}\right). \tag{7}$$

This is exactly equivalent to Eq. (5). But if the flux is modified by a factor α, not equal to unity, the flux is no longer equal to the rate of decrease of the total amount of the diffusing species. It follows that Eq. (2) cannot correctly describe the concentration when $\alpha \neq 1$.

We attempt in this paper to remove these difficulties.

THE NATURE OF THE CONCENTRATION GRADIENT

Let us first consider a system containing only a single A particle and a single B particle in a volume V, which may or may not be filled with solvent. By a well-known theorem (1) we may consider the A particle stationary and let the B do all the moving. In such a system the concentration of B is $1/V$, in the sense that probability of finding the B particle in the volume element dv is $(1/V)dv$.

To study the behavior of this system, let us consider a large number N of replicas, with the initial position of the B molecule distributed at random in the various replicas.

To any of these replica systems, Fick's law should apply, provided that c is interpreted as the probability density of the position of the B particle. But in the course of its motion, the B particle may approach the A particle to the distance R, the reaction distance. At such a point, the reaction may or may not take place. If it does not, the B particle will diffuse away. If it does, both the A and B particles are destroyed. However, instead of removing such systems from our assembly, it makes no difference if we assume instead that the A and B molecules are marked as "reacted," and allow the diffusion to continue. By this device we can keep the total number of replica systems constant.

Now suppose that we divide our volume V into a large number of equal volume elements Δv_k. The state of any replica system can be specified by stating the volume element containing the B particle, and whether or not reaction has taken place. The state of the whole assembly can be specified by giving a set of numbers N_k and M_k, where N_k is the number of systems in which the B particle is in Δv_k and has not reacted, and M_k is the number of systems in which the B particle is in Δv_k and has reacted. By letting Δv_k approach zero, we are led to two functions $n(x, y, z)$ and $m(x, y, z)$ such that $n(x, y, z)dxdydz$ is the number of unreacted systems in which the B particle lies in the volume element $dxdydz$ located at x, y, z, and $m(x, y, z)$ is the number of reacted systems in which the B particle is in $dxdydz$.

Except at the reaction surface, we may assume for the present that the values of n and m change according to the diffusion equations

$$\frac{\partial n}{\partial t} = D\nabla^2 n, \tag{8}$$

$$\frac{\partial m}{\partial t} = D\nabla^2 m. \tag{9}$$

Further, since no systems leave the assembly, the sum $n + m$ must remain constant both in time and space. It follows, therefore, that whatever law we assume to govern the conversion of unreacted to reacted particles at the reaction surface, the gradients at this surface must satisfy

$$\left(\frac{\partial n}{\partial r}\right)_R = -\left(\frac{\partial m}{\partial r}\right)_R \tag{10}$$

A suitable boundary condition at $r = R$, together with a zero normal derivative of both n and m on the surface of the volume V, therefore, should enable both the functions n and m to be found as functions of time.

At any time, the function n will be smaller near the A particle than elsewhere, while the function m will be larger near the A particle than elsewhere. The integral of n over the entire volume must steadily decrease, while that of m must increase with time.

Now the fundamental question is: If we know that at time t the A particle has not reacted, what is the probability of finding the B particle in the volume element $dxdydz$? Note that this asks for an *a posteriori* probability, which must be distinguished carefully from the probability of finding the B particle in the volume element $dxdydz$ if we do not know whether or not the A particle has reacted. The fallacy of the argument that no concentration can be set up until the A molecule has reacted lies in the fact that the knowledge that an A molecule has existed for a length of time without reacting *does* affect the *a posteriori* probability.

By Bayes' theorem, the *a posteriori* probability of finding the B particle in the volume element $dxdydz$, if we know that the A particle has not reacted is

$$\frac{n(x, y, z)dxdydz}{\int\int\int_V n(x, y, z)dxdydz}. \tag{11}$$

This is correct whether the reaction with A destroys the B molecule (as in the case of an ordinary chemical reaction) or does not (as in the case of the quenching of fluorescence). On the other hand, if we do not know whether or not A has reacted, the probability of finding the B particle in $dxdydz$ is

$$\frac{1}{N}n(x, y, z)dxdydz \tag{12}$$

if the reaction destroys the B particle, and

$$\frac{1}{N}[n(x, y, z) + m(x, y, z)]dxdydz \tag{13}$$

if the reaction does not destroy the B particle. This last expression reduces to $\frac{dxdydz}{V}$, a constant, but is not ordinarily the probability we wish.

If we turn our attention to the A particle, the probability that it has not reacted at a given time is

$$\frac{1}{N}\int\int\int_V n(x, y, z)dxdydz. \tag{14}$$

We must distinguish between two reaction rates. The *a priori* probability at $t = 0$ that the A particle will react between t and $t + dt$ is the simple derivative of Eq. (14)

$$-\frac{1}{N}\left[\int\int\int_V \frac{\partial}{\partial t} n(x, y, z)dxdydz\right] dt. \tag{15}$$

But if, at time t, we *know* that A has not yet reacted, the *a posteriori* probability that A will react in dt is

$$-\frac{\int\int\int_V \frac{\partial}{\partial t} n(x, y, z)dxdydz}{\int\int\int_V n(x, y, z)dxdydz} dt. \tag{16}$$

Replacing $\frac{\partial n}{\partial t}$ by $D\nabla^2 n$ (Eq. 8), and application of the divergence theorem, the probabilities (15) and (16) can be expressed as surface integrals. Eq. (15) becomes

$$-\frac{D}{N} dt \int\int_{\text{Surface}} (\nabla n)\cdot \mathbf{n} dS \tag{17}$$

and (16) becomes

$$-Ddt\frac{\int\int_{\text{Surface}} (\nabla n)\cdot \mathbf{n} dS}{\int\int\int_V ndxdydz}, \tag{18}$$

where, in these equations, $\mathbf{n}$ is the outward normal. But on the outer surface of V, $\nabla n = 0$, so that these reduce to

$$-\frac{4\pi R^2 Ddt}{N}\left(\frac{\partial n}{\partial r}\right)_R \tag{19}$$

and

$$-\frac{4\pi R^2 Ddt\left(\frac{\partial n}{\partial r}\right)_R}{\iiint_V ndxdydz} \tag{20}$$

Obviously Eq. (19) is exactly the same as the result which would have been obtained if we had considered the rate of destruction of B particles in a single system consisting of one A particle at the origin surrounded by N B particles diffusing and being destroyed at the surface of the A particle.

We must now generalize these results by considering an A particle in a volume V containing M B particles. If we assume the B particles to be independent, the *a priori* probability that the A particle has not reacted with any particular B particle is still given by Eq. (14). Putting

$$\frac{1}{N}\iiint_V ndxdydz = 1 - \delta, \tag{21}$$

the probability that the A particle has not reacted with any B molecule is

$$Q = (1 - \delta)^M,$$

which, if M is large and δ is small but $M\delta$ is of the order of unity, then by a well-known theorem (6)

$$Q = e^{-M\delta}. \tag{22}$$

The reaction rate Φ_M is now

$$\begin{aligned}\Phi_M &= -\frac{\partial}{\partial t}e^{-M\delta}\\ &= Me^{-M\delta}\frac{\partial\delta}{\partial t}\\ &= Me^{-M\delta}4\pi R^2\frac{D}{N}\left(\frac{\partial n}{\partial r}\right)_R.\end{aligned} \tag{23}$$

If $M\delta$ is small this is simply M times the result of Eq. (19)

$$\Phi_M = 4\pi R^2\frac{DM}{N}\left(\frac{\partial n}{\partial r}\right)_R. \tag{24}$$

If we define a concentration c and c_o by

$$c = \frac{M}{N}n, \qquad c_o = \frac{M}{V},$$

then c obeys Fick's law, and the rate of reaction becomes

$$\Phi_M = 4\pi R^2 D\left(\frac{\partial c}{\partial r}\right)_R. \tag{25}$$

This is exactly the result used by Smoluchowski and Sveshnikoff as far as its mathematical interpretation is concerned, but its physical significance is different.

If $M\delta$ is not small, Eq. (25) cannot be regarded as correct but should be replaced by Eq. (23). In this case we may still write

$$\frac{\partial \ln Q}{\partial t} = -4\pi R^2 D \left(\frac{\partial c}{\partial r}\right)_R. \tag{26}$$

BOUNDARY CONDITIONS

In the above treatment, the boundary conditions at $r = R$ have been left unformulated. As pointed out in the introduction, the usual boundary condition, $c = 0$ at $r = R$, cannot be correct if not every B particle which reaches the reaction radius reacts. An obvious modification is to assume that the probability that a B particle reacts with an A particle is proportional to the probability that the B particle lies between $r = R$ and $r = R + \Delta R$, where ΔR is a small distance. This is equivalent to the assumption

$$\Phi_M = k 4\pi R^2 c(R), \tag{27}$$

where k is of the nature of a specific reaction rate. Combining this with Eq. (25), we find the boundary condition

$$c(R) = \gamma \left(\frac{\partial c}{\partial r}\right)_R \tag{28}$$

with $\gamma = \dfrac{D}{k}$.

The solution of Eq. (1) with the boundary condition (28) is well known (7). The solution is

$$c/c_o = 1 - \frac{R-\beta}{r}\left\{ erfc\,\frac{r-R}{\sqrt{4Dt}} + e^{(Dt/\beta^2)+(r-R)/\beta} erfc\left(\frac{\sqrt{Dt}}{\beta} + \frac{r-R}{\sqrt{4Dt}}\right)\right\}, \tag{29}$$

where β is related to γ by

$$\frac{1}{\beta} = \frac{1}{\gamma} + \frac{1}{R}. \tag{30}$$

The expression for Φ_M becomes

$$\Phi_M = 4\pi D c_o \left[R - \beta + \frac{(R-\beta)^2}{\beta} e^{Dt/\beta^2} erfc\,\frac{\sqrt{Dt}}{\beta} \right]. \tag{31}$$

There are a number of interesting points concerning this solution. At large values of t we may use the asymptotic expression (8)

$$erfc\,x = \frac{1}{\sqrt{\pi}} e^{-x^2}\left(\frac{1}{x} - \frac{1}{2x^3} + \frac{3}{4x^5} - \cdots\right)$$

to obtain

$$\Phi_M = 4\pi D c_o (R - \beta)\left[1 + \frac{R - \beta}{\sqrt{\pi D t}}\left(1 - \frac{\beta^2}{2Dt} - \cdots\right)\right]. \tag{32}$$

We see that even at large times this never reduces to Eq. (5), but differs from it by the replacement of R by $R - \beta$.

At small times, we find

$$\Phi_M = 4\pi D c_o (R - \beta)\left[1 + \frac{R - \beta}{\beta}\left(1 - \frac{2}{\beta}\sqrt{\frac{Dt}{\pi}} - \cdots\right)\right]. \tag{33}$$

This remains finite even at $t = 0$, the limiting value at $t = 0$ being in fact $4\pi R^2 k c_o$.

There are two other important limiting cases, those for large and small values of the specific rate k. For small k, γ is large and β is nearly equal to R. In fact, we may put

$$\beta = R - \frac{R^2}{D} k. \tag{34}$$

Correct to terms of order k^2 we then have

$$\Phi_M = 4\pi R^2 c_o k\left[1 + \frac{Rk}{D} e^{Dt/R^2} \operatorname{erfc} \frac{\sqrt{Dt}}{R}\right] \tag{35}$$

As k approaches 0, we have a smooth transition to ordinary reaction kinetics.

For large k, on the other hand, γ and β both become small, and are given by

$$\beta = \gamma = \frac{D}{k};$$

under these conditions, Eq. (32) again applies. Rearranging as a power series in β gives

$$\Phi_M = 4\pi D c_o R\left(1 + \frac{R}{\sqrt{\pi D t}}\right)\left(1 - \frac{\beta}{R}\right)\cdots. \tag{36}$$

This goes smoothly into the Smoluchowski form as β approaches zero.

Diffusion as a "Jump" Process

With the modification of the boundary condition given by Eq. (28), and the reinterpretation in terms of *a posteriori* probability, the objections stated at the beginning of this paper have been removed. However, it has long been realized that Fick's law is not an exact description of the diffusion process, but rather the limiting form approached by the equations describing the Brownian motion of the particles. This Brownian motion may be approximated by the assumption that the particles move by jumps of mean square length $\langle l^2 \rangle$ with a jumping frequency ν. The diffusion constant is then

$$D = \tfrac{1}{6}\nu\langle l^2 \rangle \tag{37}$$

and Fick's law is obtained by letting $\langle l^2 \rangle$ approach 0 and ν approach infinity in such a way that D remains constant. The earlier work in this field is admirably summarized by Chandrasekhar (9).

In particular, it has been shown that, if the jumping particles are destroyed on reaching a surface, the distribution of the particles approaches the solution of the diffusion equation with its boundary condition $c = 0$ on the surface in question. We must now consider the question: If diffusion is represented by the "jump" picture, but with only a probability p of being destroyed if they strike a boundary surface, is the boundary condition of Eq. (28) its proper limiting boundary condition?

To this end we shall consider only the case of a plane boundary, and a distribution of particles uniform in the directions parallel to this plane, so that the problem can be considered as one-dimensional. Taking x as the coordinate perpendicular to the boundary plane, we shall suppose that the jump lengths are governed by a distribution function $\varphi(s)$, such that the probability that a given component of any jump lies between s and $s + ds$ is $\varphi(s)ds$. The function $\varphi(s)$ must satisfy the equations:

$$\int_{-\infty}^{\infty} \varphi(s)ds = 1, \tag{38}$$

$$\int_{-\infty}^{\infty} s\varphi(s)ds = 0, \tag{39}$$

$$\int_{-\infty}^{\infty} s^2\varphi(s)ds = \tfrac{1}{3}\langle l^2 \rangle. \tag{40}$$

If the concentration of particles is given by $c(x, t)$, and the jumps take place at random times, then $c(x, t)$ must satisfy the equation

$$\frac{\partial c(x, t)}{\partial t} = -\nu c(x, t) + \nu \int_{-\infty}^{\infty} c(x - s, t)\varphi(s)ds \tag{41}$$

at least in regions far from the boundary.

If the boundary is taken to be at $x = 0$ (with the particles on the positive side) the rate at which particles strike the boundary is

$$\Phi_0 = \nu \int_{-\infty}^{0} \varphi(s) \int_{0}^{s} c(x, t)dxds. \tag{42}$$

In order to be able to go to the limit of infinitesimal jumps at infinite frequency, let us introduce a parameter λ in the following way. We keep the function $\varphi(s)$ unchanged, but reinterpret it by the assumption that

$\varphi(s)ds$ is the probability of a jump component lying between λs and $\lambda(s + ds)$. We also reinterpret ν, by taking the jump frequency to be ν/λ^2. This makes the mean square jump length $\lambda^2\langle l^2\rangle$, but keeps D the same. Eq. (41) now must be modified to

$$\frac{\partial c(x, t)}{\partial t} = -\frac{\nu}{\lambda^2} c(x, t) + \frac{\nu}{\lambda^2}\int_{-\infty}^{\infty} c(x - \lambda s, t)\varphi(s)ds \tag{43}$$

and Eq. (42) to

$$\Phi_0 = \frac{\nu}{\lambda^2}\int_{-\infty}^{0} \varphi(s)\int_{0}^{\lambda s} c(x, t)dxds. \tag{44}$$

The actual situation is given by $\lambda = 1$, and by going to the limit $\lambda = \infty$ we should approach Fick's law.

By taking λ small enough, we can make Eq. (43) apply at any $x > 0$. If we expand $c(x - \lambda s, t)$ in a power series in λ

$$c(x - \lambda s, t) = c(x, t) - \lambda s\left(\frac{\partial c}{\partial x}\right)_{x, t} + \tfrac{1}{2}\lambda^2 s^2\left(\frac{\partial^2 c}{\partial x^2}\right)_{x, t} - \cdots \tag{45}$$

and substitute in Eq. (43), we obtain

$$\begin{aligned}\frac{\partial c(x, t)}{\partial t} = &-\frac{\nu}{\lambda^2} c(x, t) + \frac{\nu}{\lambda^2} c(x, t)\int_{-\infty}^{\infty}\varphi(s)ds\\ &-\frac{\nu}{\lambda}\left(\frac{\partial c}{\partial x}\right)_{x, t}\int_{-\infty}^{\infty} s\varphi(s)ds\\ &+\tfrac{1}{2}\nu\left(\frac{\partial^2 c}{\partial x^2}\right)_{x, t}\int_{-\infty}^{\infty} s^2\varphi(s)ds\\ &-\tfrac{1}{6}\nu\lambda\left(\frac{\partial^3 c}{\partial x^3}\right)_{x, t}\int_{-\infty}^{\infty} s^3\varphi(s)ds + \cdots\\ &+\frac{(-1)^m}{m!}\nu\lambda^{m-2}\left(\frac{\partial^m c}{\partial x^m}\right)_{x, t}\int_{-\infty}^{\infty} s^m\varphi(s)ds\\ &= D\left(\frac{\partial^2 c}{\partial x^2}\right)_{x, t} + \sum_{m=1}^{\infty}\frac{(-\lambda)^m}{(m + 2)!}\nu\mu_{m+2}\left(\frac{\partial^{m+2}c}{\partial x^{m+2}}\right)\lambda^m,\end{aligned} \tag{46}$$

where we have put

$$\mu_m = \int_{-\infty}^{\infty} s^m\varphi(s)ds. \tag{47}$$

As $\lambda \to 0$ the series term approaches 0, and Eq. (46) approaches Eq. (1).

In Eq. (44), expanding $c(x, t)$ about $x = 0$

$$\int_0^{\lambda s} c(x, t)dx = \lambda s c(0, t) + \tfrac{1}{2}\lambda^2 s^2\left(\frac{\partial c}{\partial x}\right)_{0, t} - \cdots \tag{48}$$

and

$$\Phi_o = \frac{\nu}{\lambda} c(0, t) \int_{-\infty}^{0} \varphi(s)ds + \tfrac{1}{2}\nu \left(\frac{\partial c}{\partial x}\right)_{0,\,t} \int_{-\infty}^{0} s\varphi(s)ds + \tfrac{1}{6}\nu\lambda \left(\frac{\partial^2 c}{\partial x^2}\right)_{0,\,t} \int_{-\infty}^{0} \varphi(s)ds + \cdots. \tag{49}$$

Now

$$\int_{-\infty}^{0} \varphi(s)ds = \tfrac{1}{2} \tag{50}$$

and we can define

$$\mu_m' = 2 \int_{-\infty}^{0} s^m \varphi(s)ds. \tag{51}$$

Hence

$$\Phi_o = \frac{\nu}{2\lambda} c(0, t) + \tfrac{1}{4}\nu\mu_1' \left(\frac{\partial c}{\partial x}\right)_{0,\,t} + \tfrac{1}{12}\nu\lambda\mu_2' \left(\frac{\partial^2 c}{\partial x^2}\right)_{0,\,t} + \cdots. \tag{52}$$

As λ → 0, Φ_o therefore becomes infinite. We are, however, interested in the reaction rate $p\Phi_o$, and we must give attention to the behavior of p as λ is varied. The increase in the jumping frequency as λ → 0 is one of our own making. If we assume p to be independent of λ, then a particle situated near the reaction surface will have a rate of reaction which increases without limit if λ is made to approach 0. In order to obtain a reaction rate which approaches neither 0 nor ∞ as λ → 0, we may take p proportional to λ. We therefore assume

$$p = p_o\lambda. \tag{53}$$

Then

$$p\Phi_o = \frac{\nu p_o}{2} c(0, t) + \frac{p_o}{4} \nu\lambda\mu_1' \left(\frac{\partial c}{\partial x}\right)_{0,\,t} + \cdots \tag{54}$$

and now in the limit λ → 0

$$p\Phi_o \rightarrow \frac{\nu p_o}{2} c(0, t). \tag{55}$$

Now for any positive x, however small, the fact that, in the limit λ → 0, Eq. (1) applies, implies in turn that the leftward flux across the surface at x is

$$\Phi_x = D \left(\frac{\partial c}{\partial x}\right)_{x,\,t} \tag{56}$$

If we let x approach 0, this approaches

$$\Phi_o' = D \left(\frac{\partial c}{\partial x}\right)_{0,\,t}. \tag{57}$$

But, since the particles are conserved, this requires $p\Phi_o = \Phi_o'$ and

$$\frac{\nu p_o}{2} c(0, t) = D \left(\frac{\partial c}{\partial x} \right)_{0, t} \tag{58}$$

This is essentially equivalent to the assumption of Eq. (28), and we have established the fact that the limiting form of the equations for "jump" diffusion lead to the modified boundary condition.

INITIAL REACTION RATE

The above formulated boundary condition has been shown to be valid at large values of the time but involves a "reaction rate" constant k which has not been definitely evaluated. In this section a power series solution will be developed for use at small times which enables evaluation of the constant k. The method, while perfectly general, will be discussed in the one-dimensional case for the sake of brevity. The concentration as a power series in t is

$$c = \sum_{k=0}^{\infty} c_k t^k, \tag{59}$$

which, substituted in Eq. (41) and equating the coefficients of corresponding powers of t, leads to the following recursion formula:

$$(k + 1)c_{k+1}(x) = - \nu c_k(x) + \nu \int_{-\infty}^{\infty} c_k(x - s)\varphi(s)ds. \tag{60}$$

Using the given initial condition and any specific function $\varphi(s)$, the coefficients in Eq. (59) may be calculated using Eq. (60).

Assuming that every particle entering the origin reacts, we have the rate equation

$$\Phi = \frac{\partial}{\partial t} \int_0^{\infty} c dx$$
$$= \sum_{k=1}^{\infty} (k + 1)t^k \int_0^{\infty} c_{k+1} dx. \tag{61}$$

The initial rate involves only the first term of the series and is readily found to be

$$\Phi(O) = \frac{\nu c_o \mu_1'}{z}, \tag{62}$$

where μ_1' is defined as in Eq. (51). The constant k may then be evaluated using the one-dimensional analog of Eq. (27) and is

$$k = \frac{\nu}{2} \mu_1'. \tag{63}$$

For the case of incomplete reaction, the rate constant k may be adjusted by multiplication by a suitable probability factor.

CONCLUSION

The fundamental concepts of the Smoluchowski theory have been shown to be valid and to enter into all bimolecular reaction processes. A modified solution to the diffusion equation has been obtained which avoids the singularity of the original Smoluchowski solution at the starting point of time. The modified solution is extended to the case where only a fraction of the encounters of the reactants brings about reaction and leads to limiting forms corresponding to diffusion control and activation energy control.

A detailed investigation of the applications of the above conclusion to a number of reactions which are wholly or partially diffusion-controlled is being started. These include quenching of fluorescence and free radical polymerizations.

REFERENCES

1. SMOLUCHOWSKI, M. v., *Ann. Physik* **48**, 1103 (1915); *Z. physik. Chem.* **92**, 129 (1917).
2. SVESHNIKOFF, B., *Acta Physicochim. U.R.S.S.* **3**, 257 (1935).
3. UMBERGER, J. Q., AND LAMER, V. K., *J. Am. Chem. Soc.* **67**, 1099 (1945).
4. DEBYE, P., *Trans. Electrochem. Soc.* **82**, 265 (1942).
5. WILLIAMSON, B., AND LAMER, V. K., *J. Am. Chem. Soc.* **70**, 717 (1948).
6. FRY, T. C., Probability and Its Engineering Uses, p. 107. Van Nostrand, New York, 1928.
7. CARSLAW, H. S., Mathematical Theory of the Conduction of Heat in Solids, p. 50. MacMillan, London, 1921.
8. DWIGHT, H. B., Tables of Integrals and Other Mathematical Data, p. 115. Macmillan, New York, 1934.
9. CHANDRASEKHAR, S., *Rev. Mod. Phys.* **15**, 1 (1943).

Letter to the Editor

MOLECULAR WEIGHT OF β-LACTOGLOBULIN AS DETERMINED BY LIGHT-SCATTERING MEASUREMENTS

The light-scattering method of Debye (1) has been used to determine the molecular weight of β-lactoglobulin. An absolute turbidimeter (2) was used. The lactoglobulin was prepared from milk by the method of Sorensen and Sorensen (3). It was recrystallized immediately before use. Isoelectric solutions in 0.1 *M* phosphate buffer of pH 5.2 were filtered by pressure through an ultrafine sintered-glass filter. Turbidities were determined for a series of protein concentrations, at wavelengths 436 and 546 mμ. The turbidity of the buffer was subtracted from that of each solution. Protein concentrations were determined by drying aliquots to constant weight and subtracting the corresponding weight of buffer solids. The function Hc/τ was plotted against c (Fig. 1). $H = 32\pi^3 n_o^2\,[(n-n_o)/c]^2/3N\lambda^4$; c = protein concentration, g./ml.; τ = turbidity, cm.$^{-1}$; n_o = refractive index of buffer; n = refractive index of protein solution; λ = wavelength of light, cm.; N = Avogadro's number. The specific refractive increment, $(n-n_o)/c$, was determined with a differential refractometer (4). The values obtained at 25°C. were 0.189 at 436 mμ and 0.183 at 546 mμ. These were obtained in 0.1 *M* NaCl at pH 5.2, but there is no reason to expect that the values in 0.1 *M* phosphate buffer of the same pH would be significantly different. The values agree well with those of 0.1892 and 0.1818, respectively, found by Pedersen (5) in 0.5 *M* NaCl. Values of 0.193 and 0.186 were calculated from data of Perlmann and Longsworth (6). The cause of the difference between these and the values used in this

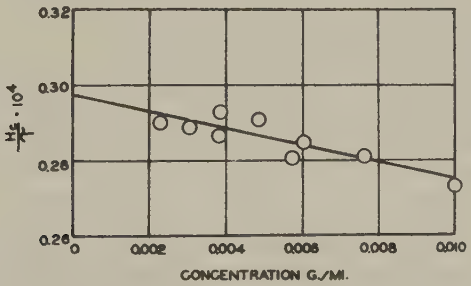

FIG. 1. Light scattering of lactoglobulin solutions as a function of concentration. Each point is an average of one determination at 436 mμ and one at 546 mμ.

paper is not clear at present, but probably lies either in the method of determining protein concentration or in the purity of the sample.

Values of Hc/τ at the two wavelengths differed by about 8%, the 546 mμ values being higher. Average values are plotted in Fig. 1. Extrapolation to zero concentration of the best straight line through these points, determined by the method of least squares, gives the reciprocal of the molecular weight, which, thus determined, was 33,700. This figure has been corrected for the depolarization of the scattered light, which was found to be $\rho_v = 0.015$.

Bull and Currie (7) have summarized previous determinations of molecular weight of β-lactoglobulin. The values obtained most frequently were roughly 42,000 and 35,000. The present value lends weight to the 35,000 group. Recently Senti and Warner (8) have redetermined the molecular weight by the X-ray diffraction method, obtaining 35,400 on wet crystals and 35,600 on air-dried crystals.

1. Debye, *J. Applied Phys.* **15**, 338 (1944).
2. Brice, *Bull. Am. Phys. Soc.* **24**, 37 (1949). (Abstract N1.) See also Speiser and Brice, *J. Optical Soc. Am.* **36**, 364 (1946). (Abstr.) To be published in detail.
3. Sorensen and Sorensen, *Compt. rend. trav. lab. Carlsberg, Sér. chim.* **23**, 55 (1939).
4. Brice and Speiser, *J. Optical Soc. Am.* **36**, 363 (1946). (Abstr.)
5. Pedersen, *Biochem. J.* **30**, 961 (1936).
6. Perlmann and Longsworth, *J. Am. Chem. Soc.* **70**, 2719 (1948).
7. Bull and Currie, *ibid.* **68**, 742 (1946).
8. Senti and Warner, *ibid.* **70**, 3318 (1948).

Eastern Regional Research Laboratory,
U. S. Department of Agriculture,
Philadelphia 18, Penna.

M. Halwer
B. A. Brice

Received February 18, 1949

BOOK REVIEWS

Submicroscopic Morphology of Protoplasm and Its Derivatives. By A. FREY-WYSSLING, trans. by J. J. HERMANS and M. HOLLANDER. Elsevier Pub. Co., New York, Amsterdam, London, Brussels, 1948. 255 pp., 160 figs. Price $6.00.

A monograph written by a recognized world authority, reviewed by one who regards himself as something of an authority on the same subject, is certain to result in a well catalyzed article. This is good, in a way, but there is the likelihood of a somewhat prejudiced report. However, it is better to run that risk than attempt to digest an article without a ferment. After all, the reader has the advantage of both the author's and the critic's views, and may, therefore, judge for himself. Herein lies the only justification of criticism; no review is wholly and intelligently impartial. The present situation is all the more difficult because Frey-Wyssling has given us an excellent book. I find myself in agreement with him on nearly all major conclusions. How, then, to criticize it with force?

The book itself presents a most favorable impression. It is an excellent example of the printer's art, good in format, and abundantly illustrated. The contents are not wholly new but rather a glorification of the first edition. The text does, however, contain new material; it is rounded out better than the first presentation.

Frey-Wyssling lays emphasis, in his title, on the *submicroscopic* morphology of protoplasm. It is true that protoplasmologists, if I may coin a word, have ceased to regard the visible structure of protoplasm as significant. They have turned to the structure which lies beyond that which one can see. Physicists and chemists have long since done this, and dealt almost wholly with the submicroscopic world. Biologists were slow in following, failing to realize that the visible structure need have nothing whatever to do with the basic structure of living matter. This failure was particularly noticeable in the false emphasis laid on the visible protoplasmic emulsion. An emulsion has no more to do with the fundamental structure of living matter than the emulsion of butterfat in milk has to do with the clotting of milk. Frey-Wyssling knows this well from his own research. But he now leans too far, albeit in the right direction, by giving over-enthusiastic support to the electron microscope. I do not share his enthusiasm in this respect. The electron microscope is without question a remarkable invention, but as yet it has given us mostly silhouettes; we want to see, not contours, but inner structure. I thoroughly believe in the future of the electron microscope, for I have myself taken up each new optical method with avidity, the polarizing microscope, dark-field condenser, Spierer lens, ultraviolet illumination, X-rays, phase microscope, ever hoping to see further into the structure of living matter. The electron microscope is at its best in revealing the submicroscopic fibers of cellulosic material; it is probably these pictures which arouse Frey-Wyssling's admiration, as they do mine.

I also find myself in philosophical disagreement with Frey-Wyssling when he tells us that submicroscopic morphology was formerly "an exciting and inspiring field of trial and error"; but now, he says, our science has lost one of its most attractive features; we no longer have the satisfaction of arriving at results by indirect methods. "This romance of discovery has given place to the technical problem of obtaining objects thin enough to get the best possible image in the electron microscope." To this, I reply that I find research just as full of trial and error as it ever was, and nowhere is this more evident than in the use of the electron microscope; Frey-Wyssling's Fig. 102 is proof of this. As for the romance, Frey-Wyssling disproves his own statement, for his book is fascinating reading from beginning to end, exceedingly stimulating, with ample controversy; not a page is dull.

The order of presentation of subjects in Frey-Wyssling's monograph is as follows: (1) a little of colloid chemistry, (2) the principles of crystal, polymer, and gel structure, (3) the fine structure of cytoplasm, nucleus, chloroplasts, and erythrocytes, and (4) the fine structure of protoplasmic derivatives (cellulose, chitin, silk, keratin, collagen, and myosin). The discussion of these subjects covers 230 pages.

The above titles indicate how highly specialized certain branches of science have become. There are not many men of science whose interests cover such varied subjects. The chemist who can understand, "The monomer of pectic acid is α-galacturonic acid," is not likely to have the slightest idea what mitochondria, chondriosomes, chondriomes, chromidia, and biosomes are; indeed, how many biologists can define them all with accuracy? I do not view this diversity with alarm, but, on the contrary, delight in the knowledge that biology is becoming an exact science through chemical interpretations of what were once mystical concepts; hypothetical biosomes, pangens, genes *et al.*, will soon become micellae, molecular aggregates, and polymers.

The selection of subjects to be discussed, the authors to be quoted, and the arrangement of material is every author's prerogative. Sometimes the selection is purely emotional, based on what and whom we like. Omitting those whom we do not like is a thoroughly understandable human trait. In Frey-Wyssling's case the war undoubtedly had a great deal to do with his selection of authors and material. Among the omission of authors, I shall mention only Szent-Györgyi whose work in biophysics, biochemistry, and experimental medicine is of such great value to students of living matter.

Among the omissions of subject matter, I should like to have seen some mention of those problems which are so much to the fore today, such as narcosis, anesthesia, and toxicity, which are not referred to in Frey-Wyssling's monograph. More attention could have been given to protoplasmic streaming and forms of cellular movement. Frey-Wyssling devotes much attention to molecular fibers, having long been a firm believer in their value to the biologist in the interpretation of the mechanism of protoplasmic properties, of reversible gelation, elasticity, contractility, and tensile strength. He could now apply them to protoplasmic locomotion. This property of protoplasm is soon to receive a thorough treatment from a younger member of my laboratory; the theory is based on the fibrous molecule.

Frey-Wyssling gives support to the view, long held by some protoplasmologists, that, when nature wants strength or a structural mechanism with which to do work, she chooses the linear molecule. The spherical proteins are now usually relegated to the important, but passive, role of food supply. Living protoplasm is a dynamic system, a functioning mechanism. It must, therefore, hold together, and it cannot do this without continuity in structure; fibrous, not globular, units make this possible.

The foregoing problem played a role in the early chemistry of jellies, the structure of which was said by Wo. Ostwald to be that of an emulsion. Just how an emulsion can be elastic, establish an imhibition pressure, and exhibit contractility is beyond comprehension. So thought Donnan, Hatschek, Freundlich, Staudinger, and Kraemer. Frey-Wyssling is well aware of this; throughout the book the word "emulsoid" does not once appear. It is this feature of Frey-Wyssling's monograph which will give the greatest satisfaction to chemists. He lays emphasis on the universality of the fibrous structure of matter, from the coarse fascicular skeleton of vegetable sponges to the microscopic fibrils of wood, the network of collagen fibers in skin and fibrin, the polypeptide framework of protoplasm, and the structure of elastic jellies.

In the discussion of this subject Frey-Wyssling calls me mildly to account for postulating the classical brush-heap. But this is now history; besides, I got it from Carothers, who got it from Freundlich, Staudinger, Mark and Meyer. Furthermore,, a brush-heap is wonderfully elastic, and so is protoplasm. Since these early brush-heap days, we have all, including Frey-Wyssling, organized, oriented, and aligned our unordered pile of fibers into crystallites, fibrillae, and grids. But at that, I am not so sure we can discard the brush-heap; it still has its uses. It explains, what Frey-Wyssling understands so well, the extraordinary swelling of protoplasm. Some non-living gels hold as much as 99.8% water in 0.2% of solid matter. Of cells, which swell to 10 or more times their original volume, Frey-Wyssling rightly asks: "What system other than a molecular frame could be inflated to a 10-fold volume without losing its inner structure?" I should like to select the foregoing remark, as indicative, not only of the excellence of Frey-Wyssling's thinking, but of that for which the modern structural biophysicist stands.

To this basic concept we need add but one feature to complete the picture. Frey-Wyssling did this some years ago with his *Haftpunkte*, for which the chemists have other expressions. What we call these binding points, whether lateral bonds, hydrogen bonds, or fluid unions, is of no matter; the important fact is that these lateral ties are not rigid but capable of easy adjustments which make it possible to have shifting micelles, fluid brush-heaps, flexible lattices, and labile protein grids. The living fabric is ever changing, but it must hold together. To accomplish this, fibers are necessary. We cannot weave cloth of sand.

Frey-Wyssling indulges in an interesting speculation; he states that one distinction between dead and living matter "lies in the fact that in cytoplasm the junctions are continuously reconstructed." Actually, junctions are repeatedly reformed in any good thixotropic gel. However, it is true that the distinction between the living and the non-living may, in large measure, rest on molecular organization. But Frey-Wyssling, knowing that there is more to life than this, adds that the reconversion of junctions "proceeds according to some definite plan about which we remain completely in the dark." He concludes with: "Bio-colloids have no structure in the ordinary physical sense, but are organized in an exceedingly complicated way." He is absolutely right, but what we want to know is, what *is* this organization? As philosophers, we may indulge in such speculations, but as biochemists we had better keep to the known physical properties of gels, living as well as non-living.

Having laid much emphasis on the role of continuity in structure, and molecular fiber in living matter, it is necessary to point out that not all protoplasmic molecules are, or need be, linear in form. The chlorophyll molecule is regarded as globular. This is not alone Frey-Wyssling's view, for this molecule has long been so regarded. There is no difficulty here, because chlorophyll is not a structural protein; it has none of the mechanical properties of protoplasm, of muscle, nerve, and tendon; but it is a remarkable catalyst and one would expect some complexity.

The chloroplast and red blood cell may be regarded as sacs holding their respective pigments in true solution, or as colloidal sponges soaked in their respective pigments. If the chlorophyll molecule is globular, then I see no escape from the fact that the chloroplast is a sac. Frey-Wyssling views the matter somewhat differently. He supports the idea, for which he is primarily responsible, that the chloroplast is a layered structure. Fluorescent studies indicate that chlorophyll, in nature, is in true solution, and adsorption spectra indicate that it is in colloidal dispersion. The two conditions are said to be satisfied by the assumption that the heme portion of chlorophyll is adsorbed to a protein film which is layered between films of oriented lipoids.

The low molecular weight of chlorophyll, 1,000 compared to 1,000,000 for many proteins, suggests a globular rather than a linear form of the molecule, but we should bear in mind that both chlorophyll and hemoglobin are not simple molecular dispersions. The heme constituents of chlorophyll and hemoglobin function in close association with other molecules, probably adsorbed to a protein complex, a concept which Frey-Wyssling advances in conection with hemoglobin, and is familiar to biochemists in enzymes where an active prosthetic group rides on a protein carrier.

In fairness to the view which opposes the fibrous concept of protoplasmic structure, it should be stated that some biochemists regard all molecules within cells as globular. This does not mean, however, that nature cannot elaborate endlessly long molecular chains where such are needed for extracellular mechanical purposes. Fibroin and long cellulose fibers are too well known to question their existence. But the qualities of fibroin and cellulose are the properties of protoplasm. The elasticity, tensile strength, and flow birefringence of protoplasm point very strongly to a linear form of its basic structural protein. The most recent, and by far the most satisfactory, theory of protoplasmic streaming (by Mr. Ariel Loewy, and now in press) is based on such a concept.

It is unlikely that one can as yet arrive at any final conclusion in regard to the structure of the chloroplast and the erythrocyte. Cytologists speak of grana, platelets, stroma, and reticula, while chemists talk of micelles, monomolecular films, grids and lattices. At least, all agree on some type of continuity in structure, and this is the chief and essential quality of living matter. Protoplasm is not a solution.

It would seem that we have had trouble enough without now turning to the gene. The geneticists' gene reminds me of Dr. Swann's definition of the ether, "an imaginary substance postulated to carry our misconceptions from one place to another." I grant that geneticists must have mechanisms to account for hereditary traits and the gene is one of them, and perhaps this is sufficient justification for Frey-Wyssling's speculation on the physics and chemistry of the gene.

The chief value of Frey-Wyssling's monograph lies in its intrinsic worth to the student of protoplasm; but it will serve another purpose. It will show the chemist that the study of living matter has become his problem, whether he likes it or not. Unfortunately, he does not always like it. It will show the medical man that the complexity of man's body obscures many a correlation which is revealed in a study of protoplasm. That which the medical worker chooses to regard as a very special case, and he chooses to regard most medical problems as very special cases beyond interpretation by the chemist, often nicely falls under a good chemical hypothesis. And, lastly, Frey-Wyssling's book will convince the young student of the significance of structural chemistry, of mechanisms in the analysis of living processes.

William Seifriz, Philadelphia, Pa.

Plasticity as a Factor in the Design of Dense Bituminous Road Carpets. By L. W. Nijboer, Senior Research Engineer, Amsterdam Laboratory of the N. V. De Bataafsche Petroleum Maatschappij (Royal Dutch Shell Group). 184 pp. Elsevier Pub. Co., Inc. Price $5.25.

Roads and airport landing fields are important factors in our present day economy, and bitumen, a colloidal material, is the binding agent used in a large percentage of the "paved" surfaces laid down throughout the world. Much must be known about the flow and adhesive properties of this binder and about the bitumen-aggregate mixture which constitutes the load-carrying surface. The author has raised so many questions concerning the plastic properties of dense bituminous road carpets that persons interested in road building will do well to study this book. The word *study* should be emphasized because a cursory reading will result in more mental confusion than understanding.

The introductory chapter is so limited that much of the available literature is omitted or given scant discussion; certain comments are so brief as to give little of the original investigators' concepts, ideas or points of view. The reference to the well-known Clifford Richardson as Clive Richardson is an example of the small errors that mar portions of the book.

A rather complete and detailed discussion is given of the Triaxial Shear Test Method for evaluating the properties of bitumen-aggregate mixtures; the apparatus used is described and the preparation of samples is outlined. Validity of the theory and reproducibility and accuracy of this method of test are discussed and illustrated by experimental data. The author concludes that "the resistance of a bituminous-aggregate mixture to plastic flow is described by three clear physical constants: a coefficient of friction, a viscosity and an initial resistance."

The effect of bitumen, filler and coarse aggregate on the plastic properties of the mixture is discussed on the basis of data obtained by the Triaxial Shear method. Venezuelan, Mexican and Californian asphalts are used as representative sources of bitumen. The arresting statement is made (p. 63) that "a harder bitumen has a greater lubricating effect than a softer one." The author advances the concept that the initial resistance of the pavement must be ascribed to the presence of a layer of bound bitumen on the aggregate surface, and that the properties of the bound bitumen more nearly approach those of a solid than a liquid. On p. 73 it is argued that differences between the strengths of the layers of bound bitumen are related to differences in asphaltene content.

Computation of absolute viscosities of the bitumen from penetration values (p. 72) is not sound and the use of such calculated values will lead to errors. Apparatus and methods have been available for some time for determining directly the absolute viscosities of paving grade bitumens.

Prandtl's theory of bearing capacity is discussed and experimental data obtained by die and cone tests are used to check the theory. An expression is developed for the design of carpets of a predetermined "Prandtl bearing capacity." A relationship also is formulated between weight, dimensions, speed and number of passes of the road roller, and the mechanical properties of the bituminous carpet. A laboratory roller used in conjunction with a 30 ton hydraulic press was employed to obtain data to check the relationship established.

The complexities encountered in grading of aggregate, bitumen content, voids and filler/bitumen ratio are satisfactorily reviewed and some experimental results are given. Chapter VII on "Structural Design of Mixtures for Dense Carpets" gives equations for calculating the bearing capacity (stability) of a road mixture under stationary load and under moving traffic. Also, the relationships involved in compaction by rolling are condensed and summarized.

This book should serve as a stimulus for research and a source of discussion and debate among serious investigators in the field of bituminous paving technology.

R. N. TRAXLER, Port Neches, Texas

THE CROSS-SECTIONAL AREAS OF MOLECULES ADSORBED ON SOLID SURFACES

H. K. Livingston

E. I. du Pont de Nemours and Company, Wilmington, Delaware

Received March 24, 1949; revised May 23, 1949

INTRODUCTION

The quantitative investigation of physical adsorption on solids of known areas was made possible by the Brunauer-Emmett-Teller theory of multilayer adsorption (1). This theory characterizes adsorption isotherms in terms of the amount of gas adsorbed when a monomolecular layer forms on the solid. At this point the solid surface of known area is in a condition roughly comparable to that of a water surface of known area on which there is a monomloecular layer of an insoluble substance such as myristic acid. The cross-sectional areas of molecules in insoluble condensed monolayers on water have been investigated in detail and the data for 29 different homologous series have been summarized by Adam (2). It is proposed to develop a similar summary of cross-sectional area data for molecules adsorbed on solid surfaces, based on the Brunauer-Emmett-Teller theory.

The Brunauer-Emmett-Teller theory of adsorption (1) leads to the equation

$$v_m = \frac{v(p_o - p)\,(p_o - p + cp)}{cpp_o}, \tag{1}$$

v_m = volume of vapor required to form a monomolecular layer.
v = volume of vapor adsorbed at pressure p.
p = pressure of vapor.
p_o = saturation pressure of the vapor.
c = constant.

This equation has been widely used to determine specific surfaces of solid adsorbents, by combining it with the equation for a monomolecular layer

$$\Sigma = N v_m \sigma / V, \tag{2}$$

Σ = specific surface of the adsorbent.
N = Avogadro number.

σ = cross-sectional area of a single molecule, measured in the plane of the solid surface (for convenience the shorter term *section area* will be generally used to designate this quantity).

V = volume of one mol of vapor.

SUMMARY OF CROSS-SECTIONAL AREA DATA

Nitrogen is most frequently chosen as the adsorbate when the Brunauer-Emmett-Teller method is used to determine the specific surface of a solid adsorbent. For this reason, it is logical to refer the section area of adsorbed molecules to the section area of nitrogen. An extensive compilation of section area ratios is given in Table 1. The data are expressed as the section area ratio (σ_x/σ_n), which is the ratio of the indicated section area

TABLE I

Section Area Ratios (from Eqs. (1), (2), *and* (3))

Vapor	Temperature	Section area ratio (σ_x/σ_n)	Solid	Ref.
	°C.			
H_2	−253	0.54	Ni foil	3
D_2	−253	0.48	Ni foil	3
CH_4	−183	1.04	Ni foil	3
C_2H_2	−78	1.37	Porous glass	4
C_2H_6	−183	1.49	TiO_2-I[b]	5
		1.42	KCl and NaCl	5
C_4H_8 (1-butene)	0	2.64	2 oxides[a]	6
n-C_4H_{10}	0	2.83	2 zinc dusts[a]	7
		2.87	Silica gel	1
		2.89	6 metals and oxides[a]	6
		3.04	4 porous glasses[a]	4
		3.21	Porous glass	8
		3.43	Glass beads	9
C_6H_6	25	1.68	TiO_2-II[b]	10
		2.13	TiO_2-I[b]	10
n-C_7H_{16}	24	3.00	Graphite	11
		3.60	SiO_2	11
		3.76	$BaSO_4$	11
		3.99	TiO_2-I[b]	11
NH_3	−32	0.95	Porous glass	4
O_2	−183	0.88	Porous glass	8
		1.02	Silica gel	12
H_2O	24 or 25	0.60	TIO_2-II[b]	10
		0.69	TiO_2-I[b]	11
		0.69	SiO_2	11
		0.71	TiO_2-I[b]	10
		0.77	$BaSO_4$	11
		1.20	Porous glass	4

TABLE I—*Continued*

Vapor	Temperature	Section area ratio (σ_x/σ_n)	Solid	Ref.
	°C.			
C_3H_7OH	24 or 25	1.15	TiO_2-II[b]	10
		1.28	TiO_2-I[b]	10
		1.30	TiO_2-I[b]	11
		1.33	SiO_2	11
CO	−183	1.06	Silica gel	1
CO_2	−78	1.24	Porous glass	4
		1.29	Silica gel	1
N_2O	−78	1.14	2 charcoals[a]	13
		1.69	C black	13
Ne	−253	0.65	Ni foil	3
CS_2	0	2.46	2 Zn dusts[a]	7
$CHFCl_2$	0	2.48	6 metals and oxides[a]	6
C_2H_5Cl	0	1.61	Graphite	14
A	−195	0.88	Porous glass	8
		0.95	4 porous glasses[a]	4
		1.01	Fe catalyst	15
	−183	0.96	Porous glass	8
		1.01	Fe catalyst	15
		1.07	Silica gel	1
Kr	−195	1.09	$CaCO_3$-VI[b]	16
		1.19	$CaCO_3$-III[b]	16
		1.20	$CaCO_3$-IV[b]	16
		1.20	TiO_2-I[b]	16
		1.28	6 metals and oxides[a]	6
		1.33	Porous glass	16

[a] This ratio represents the average obtained with all the solids studied.

[b] The Roman numerals designate specific samples of adsorbents that have been widely used in adsorption studies.

with the adsorbed vapor under consideration to the section area of nitrogen. This ratio can be obtained from the equation

$$\frac{v_n \sigma_n}{V_n} = \frac{v_x \sigma_x}{V_x}, \tag{3}$$

where v_n and v_x are the volumes of vapor required to form a monomolecular layer of nitrogen (n) or any other vapor (x) and V_n and V_x are the corresponding molar volumes. The data were obtained by reviewing the published adsorption data in which nitrogen and one or more other vapors have been used with the same solid and the resluting isotherms have been fitted to Eq. (1).

The area occupied by an adsorbed molecule must depend on the nature of the solid surface. It is possible for the ratio (σ_x/σ_n) for any given vapor to vary from one solid surface to another for either of two reasons: (1) the solid may contain pores of variable diameter; or (2) the packing of the adsorbed molecules may change. For the purposes of this paper, it is desirable to minimize these variations. This will be done by placing the greatest weight, in determining the "best value" from Table I, on values for non-porous oxides. Porous adsorbents and metals will be used only to supply confirmatory data, unless no other data are available.

The "best value" for the ratio (σ_x/σ_n) has been multiplied by what is believed to be the "best value" for σ_n to obtain the cross-sectional area values given in Table II.

TABLE II

Cross-Sectional Areas of Adsorbed Molecules

Vapor	Temperature	Area	Two-dimensional van der Waals' constant	Volume factor[a] ($W^{2/3}$)	Indicated packing factor
	°C.	*Å²/mol.*	*Å²/mol.*	*Å²/mol.*	
H_2	−253	8.3	11.9	13.0	0.64
D_2	−253	7.2	—	11.5	0.63
CH_4	−183	16.0	16.4	15.1	1.06
C_2H_2	−78	21.1	18.6	17.2	1.23
C_2H_6	−183	22.5	21.6	21.3	1.06
C_4H_8 (1-butene)	0	40.6	—	(28.2)	—
n-C_4H_{10}	0	44.6	33.0	(29.4)	—
C_6H_6	25	32.3	33.0	27.9	1.16
n-C_7H_{16}	24	59.4	47.0	(39.0)	—
N_2	−196	15.4	15.4	14.8	1.04
NH_3	−32	14.6	15.0	11.9	1.23
O_2	−183	14.6	13.5	12.9	1.13
H_2O	24 or 25	10.8	13.1	9.7	1.11
C_3H_7OH	24 or 25	19.8	31.0	(24.8)	—
CO	−183	16.3	15.6	15.4	1.06
CO_2	−78	19.5	16.5	(15.6)	—
N_2O	−78	20.4	16.9	(15.5)	—
Ne	−253	10.0	9.1	9.1	1.10
CS_2	0	37.9	23.5	(21.6)	—
$CHFCl_2$	0	38.2	27.2	(24.2)	—
C_2H_5Cl	0	24.8	27.3	(23.8)	—
A	−195	14.6	13.6	13.0	1.12
	−183	15.5	13.6	13.2	1.17
Kr	−195	18.5	15.7	14.0	1.32

[a] ($W^{2/3}$)-values for the more unsymmetrical molecules have been placed in parentheses.

The two-dimensional van der Waals' constant was shown by Hill (17) to give section areas of the correct order of magnitude for use in adsorption calculations. This constant (symbol: b) represents the minimum area to which the molecules can be compressed. Hill has proposed that it be evaluated by the equation

$$b = (6.354 \times 10^{-16})\ (T_c/P_c)^{2/3}, \tag{4}$$

where T_c and P_c are the critical temperature and pressure. This equation was used to obtain the values given in Table II.

Emmett and Brunauer (18) proposed that the area of adsorbed molecules was related to the volume factor $W^{2/3}$, where $W = (M/N\rho)$, M is the molecular weight, N is the Avogadro number, and ρ is the liquid or solid density. They assumed that

$$\sigma = 1.091\ (M/N\rho)^{2/3}. \tag{5}$$

The author has shown (11) that the more general equation

$$\sigma = F\ (M/N\rho)^{2/3}, \tag{6}$$

can be used. F is the "packing factor," which, for the common types of two- and three-dimensional packing, can be calculated form a consideration of the relation of molecular radius (R) to the volume factor (W) and the relation of the effective section area (σ) to the molecular radius. The packing factors for 6 different types of packing are summarized in Table III.

TABLE III

Packing Factors

Number of nearest neighbors		
Two-dimensional packing	Three-dimensional packing	Packing factor
4	6	1.000
4	8	1.192
4	12	1.262
6	6	0.866
6	8	1.032
6	12	1.091

(These results represent revisions of those given in Table III of Ref. 11.)

In Table II, values for ($W^{2/3}$) are based on the liquid density (extrapolated, in some cases) of the adsorbate at the temperature of adsorption. The "indicated" packing factors were calculated from eq. (6). It will be noted that all the values except three (those for H_2, D_2, and Kr) are within the range indicated by Table III.

DISCUSSION OF RESULTS

A. The Section Area of Nitrogen

The "best value" for σ_n has been taken to be 15.4 Å^2/molecule. Emmett and Brunauer (18) originally assumed that σ_n was either 16.2, based on the liquid density of nitrogen, or 13.8 Å^2/mol., based on the solid density of nitrogen. The comparison of the specific surfaces of adsorbents calculated by the Braunauer-Emmett-Teller method with those obtained by non-adsorption methods of determining specific surface has indicated (19,20) that 16.2 is a better value than 13.8, but there is some evidence to suggest that 16.2 is somewhat too high. Arnell and Henneberry (21) report specific surface data obtained by electron microscopy, permeability, and nitrogen adsorption for 9 different carbon blacks. The section area of 16.2 was used for the nitrogen molecule. The surfaces calculated by the adsorption method averaged 12% higher than those calculated by other methods.

The data in Table II show that if σ_n is given the value indicated by the two-dimensional van der Waals' constant for nitrogen, the agreement between the section areas of the other molecules and the areas indicated by the liquid density or van der Waals' constant is quite good, provided that the molecules are of approximately spherical shape. If σ_n had been taken to be 16.2, the section areas for these molecules would have been uniformly high. Referring to the "Indicated Packing Factors" in Table II, and omitting H_2 and D_2 as anomalous, the average F is 1.13 for 12 different molecules, when F for N_2 is taken to be 1.04. If $F = 1.09$ had been assumed for N_2, as indicated by Eq. (5), the average for all molecules would have been 1.18. That is, if $F = 1.09$ is the most common value for spherical molecules, as proposed by Emmett and Brunauer (18), it is necessary to take a lower value of F for nitrogen in order that other molecules may approach $F = 1.09$ more closely.

The use of $\sigma_n = 16.2$ has become more common since Harkins and Jura (22) reported that this value checked the results of an area determination made by their absolute calorimetric method. This method, which is so difficult to carry out experimentally that it has been applied to only two solids, consists in determining the heat evolved when a solid in equilibrium with the saturated vapor of a liquid is immersed in the bulk liquid. The ratio of the heat of immersion/g. to the surface enthalpy of the liquid in equilibrium with its saturated vapor (expressed in heat units/cm.^{2}) gives the surface of the vapor-coated solid in cm.^{2}/g. This surface (designated Σ') differs from the surface of the solid without adsorbate (designated Σ) by a factor that is proportional to the extent to which the solid deviates from the ideal case of a single continuous plane surface.

Harkins and Jura found Σ' for the anatase sample known as "TiO_2-I" to be 14.4 m.^{2}/g. From a consideration of the particle size, it was estimated that the true value of Σ was between 13.5 and 14.1 m.^{2}/g. It does not appear impossible that the true value would lie outside this range, however. A second determination on another TiO_2 sample gave $\Sigma' = 9.1$ and Σ = approx. 8.9 m.^{2}/g. The nitrogen adsorption data on these samples were used to determine v_n by Eq. (1). Solution of Eq. (2) for σ, using the Σ estimates of Harkins and Jura, gives, in the case of TiO_2-I, $\sigma = 15.7$–16.4 and for the other sample, σ = approx. 15.2.

These results do not give any particular preference to 16.2 as a unique value for the section area of nitrogen. It would appear that, if the Harkins-Jura estimate of the $\Sigma:\Sigma'$ ratio of TiO_2-I is correct, σ_n is slightly greater than 15.4 for this particular adsorbent. The data in Table II suggest that 15.4 is approximately correct for most oxides and is an excellent value to use—at least until it is possible to apply the Harkins-Jura calorimetric method more widely (that is, when the required calorimetric measurements for determining Σ' and sufficient information to fix the Σ/Σ' ratios are available for a large number of solids).

B. *Monatomic Molecules*

Suitable adsorption data are available (Table I) for the noble gases neon, argon, and krypton. The preferred section areas (Table II) indicate a packing factor of 1.1 for neon and argon near their boiling points. For these gases, the section areas are similar to, but slightly larger than, the two-dimensional van der Waals' constant. Krypton apparently has an unusually large packing factor.

C. *Diatomic Molecules*

The section areas of hydrogen and deuterium (Table II) are unusually low, when compared with either the liquid density or van der Waals' values, but the adsorption data were obtained on a metal surface (3) and may be anomalous because of chemisorption or unusual packing. The section areas of nitrogen, oxygen, and carbon monoxide as given in Table II are all within one Å²/molecule of the van der Waals' value and the indicated packing factors are 1.09 ± 0.05, which is a reasonable result.

D. *Triatomic and Tetratomic Molecules*

The relatively complex triatomic and tetratomic molecules are less likely to pack in a simple manner and give conventional packing factors. Thus, though the section area of ammonia checks quite well with the van der Waals' value, acetylene, carbon dioxide, and nitrous oxide have areas higher than the van der Waals' value by 2.7, 3.0, and 3.5 Å²/molecule, respectively. The water section area is lower than the van der Waals' value, but is equal to the liquid density value if $F = 1.1$. The area for carbon disulfide obtained from the one available set of adsorption data (7) is much higher than would be predicted from the liquid density or van der Waals' constant. This abnormal result may be due to the fact that the data for CS_2 were determined from adsorption on a metal surface.

E. *Polyatomic Molecules*

Like other symmetrical substances, methane has a section area within 10% of the volume factor or van der Waals' values. Ethane has a section area that is also in excellent agreement with the calculated values, in marked contrast to acetylene (see above). The linear paraffinic molecules of *n*-butane, 1-butene, and *n*-heptane have section areas higher by 30% or more than the liquid density value. This is to be expected, since these molecules could not fit into the simple type of packing required by Eqs. (5) or (6). The minimum area for linear heptane molecules packed as closely as possible has been shown (11) to be 42.3 Å². The corresponding minimum area for butane and butene molecules is 25 Å². There are now sufficient adsorption data to show quite conclusively that the true areas are much higher.

Benzene has a section area quite close to that predicted from the van der Waals' constant. The low section area of *n*-propanol relative to the volume factor or van der Waals' constant is probably due to the high degree of two-dimensional order that this molecule would possess in the adsorbed state. As shown in Table III, when two-dimensional packing is closer than three-dimensional packing the packing factor is particularly small. The value 19.8 given in Table II for the *n*-propanol area is equal to the area calculated from the X-ray dimensions of the molecule, assuming closest packing (11). The area found for ethyl chloride is consistent with a packing factor of $F = 1.04$. The section area of dichlorofluoromethane, on the other hand, is higher than would be predicted from the van der Waals' constant or volume factor, corresponding to a packing factor $F = 1.58$. The difference between the results with these two halogenated compounds may be due to the difference in the nature of the adsorbents with which they were used.

THE JURA-HARKINS ADSORPTION ISOTHERM

Jura and Harkins (23) proposed a new adsorption isotherm in which a linear plot of (log p) *vs.* v^{-2} is used to determine the slope A, from which the specific surface can be determined by the equation

$$A = \Sigma^2/k^2, \tag{7}$$

where k is a constant for any given adsorbate. Harkins and Jura (24) have given recommended values for k for several different gases.

It has generally been found that specific surfaces calculated by the Harkins-Jura method agree very well with those calculated by the Brunauer-Emmett-Teller method (9,21,24,25,26,27). This is to be expected, since, when the constant c (see Eq. (1)) is in the range 25–250, the two equations both give a satisfactory fit to the same adsorption data (28,29,30), and Harkins and Jura have chosen their k values (24) to be consistent with Brunauer-Emmett-Teller adsorption results obtained with the adsorbent "TiO_2-I." As discussed in the preceding section, Harkins and Jura (22), on the basis of their absolute calorimetric determination of surface area, chose 16.2 Å²/mol. as the cross-sectional area of the nitrogen molecule.

Agreement is not always observed, however, between the Jura-Harkins and Brunauer-Emmett-Teller calculations. Porous adsorbents that form multilayers only a few molecules thick do not give adsorption data that agree with Eq. (1) but do agree with the Brunauer-Emmett-Teller "n" equation, which is comparable to Eq. (1) but contains exponential n terms, in which n = the maximum number of molecules in the multilayer at $p = p_o$. Joyner, Weinberger and Montgomery (31) found that, when n was small, the Jura-Harkins equation could not be used. T. D. Smith and Bell (32) have shown that this result would be predicted from a mathematical treatment of the "n" equation. At present, it appears that the Jura-Harkins theory frequently gives a more accurate fit of experimental adsorption data at low and moderately high pressures than the Bruanuer-Emmett-Teller equation, but is more restricted in its utility as a means of determining the specific surface of solid adsorbents.

One difficulty with the Jura-Harkins equation is that the recommended values for the constant k, used in determining specific surfaces, are based on results obtained with one adsorbent only (TiO_2-I). It is true that this has led to better results than were obtained by other methods in some cases. The surface areas calculated from butane adsorption data using the Harkins-Jura equation have been found by Davis and DeWitt (9) to give better agreement with nitrogen areas than could be obtained from Brunauer-Emmett-Teller calculations on the same data. As these authors pointed out, this results from the use of a section area of 32 Å^2/mol., calculated from Eq. (5), for the Brunauer-Emmett-Teller calculations while the Harkins-Jura k value used corresponded to $\sigma = 56.6$ Å^2/molecule. If the section area for butane given in Table II had been used, however, the results of the Brunauer-Emmett-Teller calculation would have been as satisfactory as the Jura-Harkins result.

Harkins and Jura (24) have considered in detail the manner in which the section area of nitrogen varies for different adsorbents. In this treatment they have assumed that k always has the value obtained for TiO_2-I. For 90 different adsorbents, the constants of the Jura-Harkins and Brunauer-Emmett-Teller isotherms were determined. The specific surface Σ was evaluated from Eq. (7) with a constant value for k, and Eq. (2) was used to calculate σ. Actually, as has been pointed out by Emmett (29) and the author (30), there is no reason to assume that k is a constant and σ a variable when comparing adsorption data for different surfaces. If this assumption were valid the section area of nitrogen would vary from 13 to 17 Å^2/molecule as c varies from 25 to 250. While such a variation in section area is not impossible, a variation in k of equal magnitude is at least as plausible.

OTHER ADSORPTION ISOTHERMS

Several modifications of the Brunauer-Emmett-Teller have been proposed recently. McMillan (33) proposed an equation to be applied to adsorption on composite surfaces. The monolayer adsorption gave a better agreement with experimental data at pressures below that for monolayer formation. The same v_m value would be used with McMillan's equation as with Eq. (1).

Anderson (34) developed a modified Brunauer-Emmett-Teller equation containing a new constant in addition to v_m and c. For several nitrogen, acetylene, and ammonia isotherms, the specific surface values calculated by the new equation were 10–20% higher than those obtained using Eq. (1). Anderson and Hall (35) later proposed a 4-constant equation that incorporates the concepts used in Anderson's original equation. The new equation gave specific surfaces within ±10% of those obtained from Eq. (1). R. N. Smith and Pierce (14) derived a 4-constant equation by a modified Brunauer-Emmett-Teller treatment assuming the presence of active centers. The specific surfaces indicated by their equation were within 20% of the conventional Brunauer-Emmett-Teller value in many cases, but they also cite examples where their method gives values that are higher or lower by a factor of 5–10. The isotherms for which the difference was greatest were generally those for solids of low adsorptive capacity for which experimental accuracy is poor.

As mentioned in the preceding section, the so-called "n" equations of Brunauer, Emmett and Teller (1) must be applied to adsorption on porous solids. Joyner, Weinberger and Montgomery (31) found the difference between specific surfaces obtained from Eq. (1) and those obtained from the related "n" equation to be of the order of 1% for nonporous oxides, but the difference was about 20% for porous carbon blacks. The present tabulation places little reliance on data for carbon blacks. None of these new adsorption equations seems to offer any basis for altering the previous conclusions regarding the best value for cross-sectional areas.

The effect of temperature on the section area of adsorbed molecules has not been dealt with in any detail in any of the various theoretical treatments of adsorption. Brunauer (15) suggests that σ should vary as $\rho^{2/3}$, but gives examples where this is not so. Certainly it is to be expected that the packing factor F in Eq. (6) will vary with temperature, just as ρ does. For the purposes of this summary, it must be concluded that, at present, reliable values can be assigned to the section areas at only one temperature for each adsorbate. More work must be done before a study of temperature variations can be undertaken.

CONCLUSIONS

The cross-sectional area of adsorbed molecules on solid surfaces can be assigned definite values for those molecules for which sufficient adsorption data are available. The areas assigned are accurate for physically adsorbed molecules only. DeBoer (36) has shown recently that iodine adsorption under conditions that may involve chemisorption fits the Brunauer-Emmett-Teller equation, but the value for monolayer adsorption given by the equation is in error by a factor of 3. Similar results might be expected in any case where chemisorption occurs.

The values for the cross-sectional areas given in this paper have, in general, been obtained from data for molecules adsorbed on oxide adsorbents, since more data are available for solids of this type. There is no reason for limiting the application of these section area data to non-porous solids. Porous solids, however, cannot be used for comparing different adsorbates if the pore dimensions are such as to "screen" the molecules being adsorbed and offer a noticeably greater adsorbing surface to small molecules than to large ones.

Summary

Values have been assigned to the cross-sectional area of adsorbed molecules on solid surfaces for 23 different molecules. In calculating the areas, a value of 15.4 Å^2/molecule has been taken as standard for nitrogen adsorbed at −196°C. The results are consistent with the areas predicted for the molecules on the basis of their liquid densities and two-dimensional van der Waals' constants. The values are based on adsorption isotherms that are in agreement with the Brunauer-Emmett-Teller theory of physical adsorption. None of the more recently-published theories of physical adsorption has been applied to a sufficient number of experimental isotherms to justify its use in cross-sectional area calculations.

References

1. Brunauer, S., Emmett, P. H., and Teller, E., *J. Am. Chem. Soc.* **60**, 309 (1938).
2. Adam, N. K., The Physics and Chemistry of Surfaces, p. 50, Oxford, 1941.
3. van Itterbeek, A., and Borghs, J., *Z. physik. Chem.* **50B**, 128 (1942).
4. Emmett, P. H., and Cines, M., *J. Phys. & Colloid Chem.* **51**, 1248 (1947).
5. Ross, S., *J. Am. Chem. Soc.* **70**, 3830 (1948).
6. Davis, R. T., DeWitt, T. W., and Emmett, P. H., *J. Phys. & Colloid Chem.* **51**, 1232 (1947).
7. Emmett, P. H., and Cines, M., *ibid.* **51**, 1329 (1947).
8. Emmett, P. H., and DeWitt, T. W., *J. Am. Chem. Soc.* **65**, 1253 (1943).
9. Davis, R. T., and DeWitt, T. W., *ibid.* **70**, 1135 (1948).
10. Gans, D., Brooks, U. S., and Boyd, G. E., *Ind. Eng. Chem., Anal. Ed.* **14**, 396 (1942).
11. Livingston, H. K., *J. Am. Chem. Soc.* **66**, 569 (1944).
12. Emmett, P. H., *Advances in Colloid Sci.* **1**, 1 (1942).
13. Reyerson, L. H., and Wertz, J., unpublished data from a Naval Research Report.
14. Smith, R. N., and Pierce, C., *J. Phys. & Colloid Chem.* **52**, 1115 (1948).
15. Brunauer, S., The Adsorption of Gases and Vapors, Princeton, 1943.
16. Beebe, R. A., Beckwith, J. B., and Honig, J. M., *J. Am. Chem. Soc.* **67**, 1554 (1945).
17. Hill, T. L., *J. Chem. Phys.* **16**, 181 (1948).
18. Emmett, P. H., and Brunauer, S., *J. Am. Chem. Soc.* **59**, 1553 (1937).
19. Bugge, P. E., and Kerlogue, R. H., *J. Soc. Chem. Ind.* **66**, 377 (1947).
20. Anderson, R. B., and Emmett, P. H., *J. Applied Phys.* **19**, 367 (1948).

21. Arnell, J. C., and Henneberry, G. O., *Can. J. Research* **26A**, 29 (1948).
22. Harkins, W. D., and Jura, G., *J. Am. Chem. Soc.* **66**, 1362 (1944).
23. Jura, G., and Harkins, W. D., *J. Chem. Phys.* **11**, 430 (1943).
24. Harkins, W. D., and Jura, G., *J. Am. Chem. Soc.* **66**, 1366 (1944).
25. Jura, G., and Harkins, W. D., *ibid.* **68**, 1941 (1946).
26. Joyner, L. G., and Emmett, P. H., *ibid.* **70**, 2353 (1948).
27. Joyner, L. G., and Emmett, P. H., *ibid.* **70**, 2359 (1948).
28. Livingston, H. K., *J. Chem. Phys.* **12**, 466 (1944).
29. Emmett, P. H., *J. Am. Chem. Soc.* **68**, 1784 (1946).
30. Livingston, H. K., *J. Chem. Phys.* **15**, 617 (1947).
31. Joyner, L. G., Weinberger, E. B., and Montgomery, C. W., *J. Am. Chem. Soc.* **67**, 2182 (1945).
32. Smith, T. D., and Bell, R., *Nature* **162**, 109 (1948).
33. McMillan, W. G., *J. Chem. Phys.* **15**, 390 (1947).
34. Anderson, R. B., *J. Am. Chem. Soc.* **68**, 686 (1946).
35. Anderson, R. B., and Hall, W. K., *J. Am. Chem. Soc.* **70**, 1727 (1948).
36. de Boer, J. H., *Rec. trav. chim.* **65**, 576 (1946).

THEORETICAL CONSIDERATIONS OF DETERGENCY

Ernst K. Goette

From the Department of Applied Science in Tanning Research, Institute of Scientific Research, University of Cincinnati, Ohio

Received January 6, 1949; revised April 13, 1949

I. General Considerations of Detergency

A. *Introduction*

This review is an attempt to offer a coherent presentation of experimental facts and theoretical considerations which have been published chiefly since 1939. The work done prior to 1939 has been dealt with extensively (13, 89). In the following discourse the term "soap" will be used in its broadest sense to include soap-like materials as well as true soaps.

TABLE I

Classification of Soaps

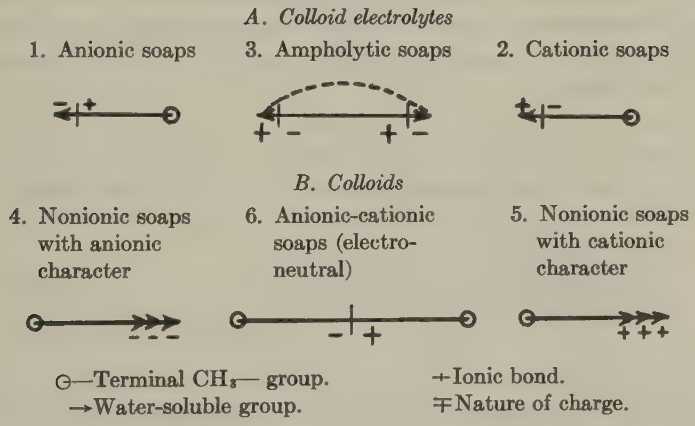

The author (26) has suggested a classification of soaps into 6 groups as shown in Table I. Three groups are colloid electrolytes which show both the characteristics of single electrolytes and of colloids, depending on their concentrations, and the other 3 groups have only colloidal properties at higher concentrations. Among the colloidal electrolytes, the **anionic soaps** which form surface active anions are the most important group for cleaning applications. Examples are the single soaps with a carboxyl group, alkyl sulfates, alkansulfonates, alkylarylsulfonates, and fatty acid condensation products like Igepon T. The **cationic soaps** which form surface active cations cannot be used for cleaning action except at relatively high concentrations. Among this group are alkylpyridinium chloride and many other substances which are valuable in many industrial applications. The **ampholytic soaps** are surface-active products with betaine structure, for example, soaps with the general formula

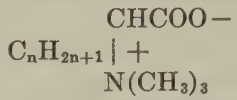

$$C_nH_{2n+1}\overset{\displaystyle CHCOO^-}{\underset{\displaystyle N(CH_3)_3}{|^{+}}}$$

Among the colloids, the **nonionic soaps** with **anionic character** are surface-active substances which contain, besides the paraffinic chain, a number of hydrophilic points like ether or hydroxyl groups. Solution in water takes place through the formation of hydrogen bonds between the oxygen atoms and water. Condensation products of fatty acids, fatty alcohols, alkylphenols with ethylene oxide and alkyl glucosides are examples of this group. **Nonionic soaps** with **cationic character** are scarcely known. Condensation products of polyalkylene polyamines with alkyl halides which are described in the German patent 668,744 belong to this group. It is not to be expected that they have any value for cleaning action. The **anionic-cationic soaps** which are formed from equivalent amounts of anionic and cationic soaps are only colloidally soluble in the absence of electrolytes, and cannot be used for cleaning. Many important and useful substances belong mutually to two classes, *e.g.*, fatty acid-albumin condensation products or alkyl polyglycol ethers with a terminal sulfonic acid group.

TABLE II

Average Composition of the Oily Compound in Naturally Domestic Dirt

Free fatty acids (Mean C_{38}, I.V. 46)	31.4%
Triglycerides of fatty acids (Mean C_{38}, I.V. 46)	29.2%
Saturated and unsaturated fatty alcohols, cholesterol (Mol. wt. 275, I.V. 63)	15.3%
Hydrocarbons, saturated and unsaturated (Mean C_{20}, I.V. 50)	21.0%

The aim of a washing process is to transport the dirt as completely as possible from the substratum into the aqueous washing liquor during the washing operation and to completely remove the dirt in the rinsing process. The basis of all considerations in a washing process must be the dynamic equilibrium of the dirt on the substratum with the dirt in the washing liquor. All other factors being constant, the equilibrium ratio is dependent on the character of the dirt and the kind of substratum, *e.g.*, rayon and wool are easier to clean than cotton if the dirt is the same. The oily constituent in natural domestic dirt was studied by Brown (9).

Cotton shirts, linen pillow cases, tea-towels and woolen socks contain, after ordinary use, a mean value of 0.75% oil. The average composition of the oil is given in Table II.

Recent work of general interest regarding detergency and practical detergency tests has been presented in numerous papers (5, 15, 40, 43, 76, 78, 84, 90, 91, 93). Chwala and Martina (14), Sisley (80), and Aickin (3) published summaries concerning cleaning action.

B. Removal of Solid Soil, Particle Size

Practical experience and laboratory experiments have shown that the less dispersed the dirt is, the easier it is to remove (29). Experience with different model dirts has clearly demonstrated the influence of particle size on the removability. It is well known that large soot particles are easily and completely removable, but the ultramicroscopically fine carbon particles from India ink are not. A suspension of indigo in water was proposed by Heermann (36) as a standard dirt and it is relatively easy to remove. But the removability is very much reduced if an indigo sol is used for soiling the fabric. This sol is produced by oxidation of leucoindigo solution with air in the presence of protective colloid. In this connection, it is of interest that fast dying can be done without vatting (4) by using a very fine dispersion of vat dye, *i.e.*, by the Abbot-Cox process.

Ferric oxide is also easy to remove if it is used according to the directions of Bosshard and Sturm (6), *i.e.*, precipitated on the wool fiber with ammonia from any ferric salt. The ferric oxide formed on drying is large grained, but, if very fine airborne siliceous dirt is used to soil the fabric, the ferric oxide contained in the dirt remains on the fiber after several washings with the best detergent. The preceding examples may be sufficient to show the importance of particle size. The following Figures, 1 and 2, show schematically the dependence of cleaning action on the particle size of the dirt. It is very difficult to remove the dirty rings

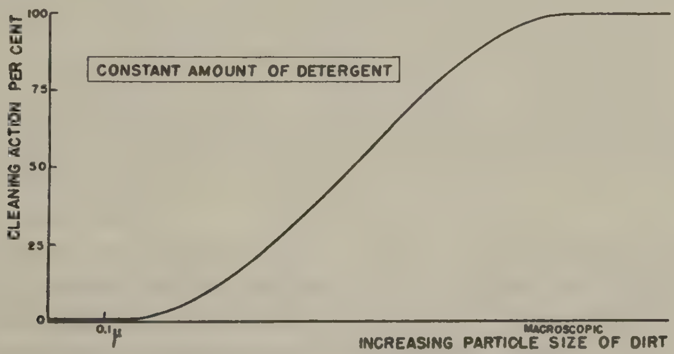

FIG. 1.

from collars and cuffs. Dirt of this kind is so finely dispersed that the particles cannot be distinguished by the ordinary optical microscope. Special kinds of dirt, such as coarse particles, skin shreds, water-soluble substances, and special albuminic dirts will not be considered in this review, since the most important types of dirt, and the most difficult to remove, are the very fine soot and mineral particles which are attached to the fabric.

The energy necessary for washing increases with decrease in particle size. As the particle size becomes smaller and smaller, a dimension is reached beyond which it is impossible to remove the particles with the best detergent. It must be appreciated that the dirt particles which are not removable have a size of about 0.1 μ and smaller. Perhaps, the smaller dirt particles can enter inside the substratum and, therefore, it is not possible at all to remove them by common means without disturbing the substratum, which is suggested by Kling (47). Bacon and Smith (5) established the existence of a quantitative relationship between the concentration of a soap and the mechanical work required in removing solid soil in a detergent process. The experimental data show that the concentration of detergent (C), mechanical force (F), and time (T) are quantitatively related to each other in bringing about the removal of soil (S). For intermediate ranges of soil removal, the following equation is valid:

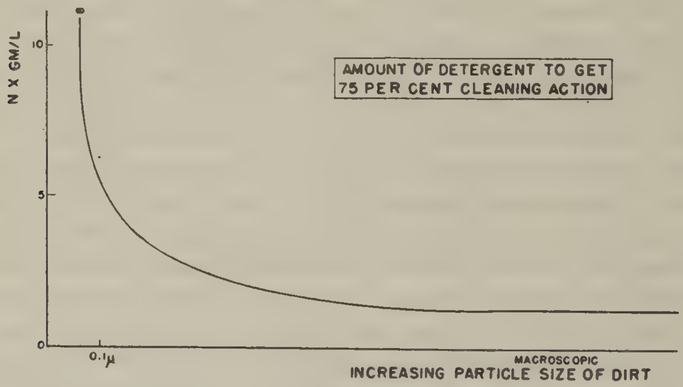

FIG. 2.

$$S = K(CFT)^n. \tag{1}$$

The mechanical force was varied by using stainless steel balls of various different sizes and numbers in a launderometer using various rotational speeds. The per cent of soil removal was calculated from reflectivity relative to that of MgO. The change of reflectivity, although not a linear function of colored soil removed, was related to soil removal by means of a graph. The actual values of K and n for various detergents is the subject of current investigation by Bacon and Smith (5)

C. Removal of Fatty Soil

The removal of soil caused by fatty materials is more dependent upon their chemical character than upon the distribution of the soil on the fabric, because the fatty soil is liquid at the normal washing temperatures. The removal of oily dirt was studied by Kling, Langer and Haussner (49). In agreement with Adam (1), they found that the oil film on the fiber surface in the presence of the detergent solution contracts to droplets which then float away.

On this basis, Kling (46) and Kling and Koppe (48) derived a formula for the work done in washing. This formula concerns the removal of oils and fatty dirt only.

Before washing, the greasy and oily dirt is uniformly distributed on the fiber with a contact angle, $\Phi \approx 0$ if measured in the oil phase. Later, during washing, Φ approaches 180° as the oil forms droplets, and the substratum surface is then covered with the aqueous solution. The work to substitute the oil by the aqueous solution is identical with the work for washing:

$$-W \simeq F\,(\Delta j + \sigma AB), \tag{2}$$

W = work of washing (dynes cm.),
F = area of contact with the substratum surface (cm.^{2}),
Δj = difference between the wetting tensions of the substratum for the washing liquor and for the oil (dynes cm^{-1}),
σAB = interfacial tension between both liquid phases (dynes cm^{-1}).

Aickin (3) very carefully examined the influence of neutral and alkaline salts on the detergent action of a secondary alkyl sulfate with a molecular weight of 304, which corresponds to about a 13-carbon chain paraffin. The branched product shows faster wetting action and is, therefore, more hydrophilic than the normal alkyl sulfate with the same molecular weight (26). Aickin worked with solutions of 1 g. of alkyl sulfate/l. (accordingly with the critical micelle concentration of $3.1 \times 10^{-3}\ M$). The substratum was wool, soiled with olive oil. The detergent action of adding several salts followed, without exception, the course of the interfacial tension.

Experiments by Palmer (64), on the removal of olive oil from wool with alkyl sulfate solutions containing salts, are in agreement with the above relationship because better cleaning action was observed for those solutions showing greater interfacial tension-lowering. It is considerably more difficult to develop a formula which will give quantitative results in the case of removing solid particles of colloidal dimensions during the washing process.

The amount of detergent adsorbed by the substratum must also be considered. The amount of sodium alkyl sulfate adsorbed by wool increases as the salt concentration increases, as is also shown by Aickin (3). The detergent power of the different types of detergents varies. In general, the removability of the dirt decreases with increasing melting point of fatty substances present in the soil. Therefore, the cleaning of raw wool, and the cleaning of textile fibers lubricated with fats and waxes in general, is done at a temperature above the melting point of the fats or waxes. Fatty soils which contain hydrophilic groups are more easily removed than are fatty soils which have been oxidized or resinified.

Utermohlen and Wallace (88) studied the influence of aging on the removal of solid and oily dirt from fabric. A generally recognized method for studying the removal of standard dirt does not exist, although many different kinds of recipes and evaluations of results can be found. However, it is possible to arrive at some general conclusions from the results of the different authors.

D. Wetting Action and Cleaning Action

Each washing process begins with the wetting of the more or less hydrophobic material. The best detergents are, at the same time, not the best wetting agents and *vice versa*. Several general rules have been derived from a study of the relationship between the chemical constitution and activity of wetting agents by Goette (26). These rules are also applicable to detergents. Systematic research with homologous series, such as the sodium soaps of fatty acids, sodium alkyl sulfates and sodium alkansulfonates, has indicated there is an optimum cleaning action depending on the number of carbons in the paraffin chain. This is true for both detergent action and wetting action. In all cases, the best wetting agent has a shorter paraffin chain than the best detergent in the same homologous series as shown in Fig. 3. In Fig. 3, N is about 1 in the case of sodium alkyl sulfates. In a scheme given by Rehbinder (74), the relation between the degree of dispersion, detergency and interfacial tension was first suggested. The position of the 2 optima for wetting action and for cleaning action varies with the kind of hydrophobic part of the molecules in the homologous series. For good cleaning action, a soap must be more hydrophobic or less hydrophilic, whereas, for good wetting action, the soap must be less hydrophobic and more hydrophilic, as shown in Fig. 3.

Branches in the paraffin chain change the optimum number of carbon atoms in the chain effective for wetting action and for cleaning action to higher numbers, and many experiments have shown that the absolute value for the best wetting action increases with the number of CH_3— end-groups within a given homologous series (26).

By the addition of a second hydrophilic group in the molecule, the wetting action and the detergent action depend mostly upon the position of the second hydrophilic group with respect to the first, and both actions will be reduced by the second hydrophilic group. Pure sodium oleylsulfonate is an excellent detergent, whereas the same soap, in which the double bond has been sulfated, is a poor detergent (85).

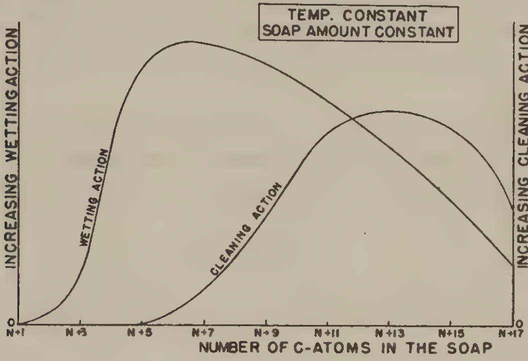

FIG. 3.

The wetting activity, and also the detergency, of a soap can be influenced by adding neutral salts. A very impressive example is the measuring of the wetting time of cotton yarn using solutions of sodium alkoxy acetate and $(NH_4)_2SO_4$ at different concentrations (26). On the other hand, the cleaning action of a pure solution of sodium dodecyl sulfate can be increased by adding a certain amount of any neutral salt but, if an optimal amount is exceeded, the cleaning action is retarded (29). This effect is dependent on the number of carbons in the paraffinic chain and also on the general construction of the molecule.

II. THE IMPORTANCE OF THE CRITICAL MICELLE CONCENTRATION (C.M.C.)

A. Values for C.M.C. Influence of C-Number, Hydrophilic Groups, and Temperature

A typical property of soaps is the formation of micelles above a characteristic concentration which is called the critical micelle concentration. The C.M.C. decreases with the number of carbon atoms for each member in each homologous series. Hess, Philippoff and Kiessig (38), and later Klevens (45), have published reviews on the dependence of C.M.C. on the length of the paraffin chain with the sodium salts of fatty acids, sodium alkyl sulfates and sodium alkansulfonates. The critical concentration of micelle formation can be determined by many physical methods. Numerous soap properties undergo radical change at the C.M.C. (71). Insofar as cleaning action is concerned, concentrations below the C.M.C. are most important because cleaning is maximal at the C.M.C. Ekwall and Lindblad (21) have found by careful pH measurements of sodium laurate solutions in the absence of carbon dioxide that below 0.006 N sodium laurate, a 1–1 electrolyte is formed. With increasing concentration, several changes occur with the formation of anions with charges ranging from 2 to 6, at the concentrations given in Table III. Only at 0.028 N concentrations of sodium laurate (20) do the anions with multiple charges form micelles. The micelle structures themselves are not considered in this paper.

In Table IV we review the C.M.C. of many anionic soaps and of one nonionic soap. This does not include some data where the C.M.C. is only indicated by graphs without specific values having been established.

TABLE III

Sodium laurate concentration $M \times 10^{-3}$	Charges of laurate anion
0–6[a]	1
6–21	2
21–28[b]	4
28–37	6

[a] Known as the "limit concentration," the concentration below which the soap is a 1–1 electrolyte (12).

[b] C.M.C.

The older determinations (31, 55, 70) of the surface activity of alkyl sulfates show that at the C.M.C. there is not only a break in the concentration *vs.* surface tension curve, but there is also a minimum. Miles and Shedlovsky (61) were able to show that the minimum is caused by the presence of a small amount of free fatty alcohols in the soap samples. Pure sodium dodecyl sulfate, from which the fatty alcohol had been extracted with ethyl ether for 36 hr., shows only a break at the C.M.C. but not a minimum. Reichenberg (72) gave a theoretical explanation for the effect of impurities at the C.M.C. of the soaps.

Cushmann, Brady and McBain (18) and Gonick and McBain (30a) were able to show that organic cations in anionic soaps have a remarkable influence on the C.M.C. Potassium laurate has a C.M.C. of 24×10^{-3} and the benzyltrimethylammonium salt has a C.M.C. of 10×10^{-3}.

Results from different laboratories show that there are some important variations between the values for the C.M.C. and the influence of the temperature on the C.M.C. (see Table IV). This may be understandable,

A.1. Sodium soaps

Methods and references	Conductivity		Diffusion		pH		Surface activity[a]		Viscosimetry	
	Ekwall (20)		Lamm, Högberg (50)		Ekwall, Lindblad (21)		Powney, Addison (68)		Hess and coworkers (37–39)	
No. of carbon atoms	C.M.C.	°C.	C.M.C.	°C.	C.M.C.	°C.	C.M.C.	°C.	C.M.C.	°C.
8	—	—	—	—	—	—	—	—	360	20
10	95–100	20	—	—	—	—	—	—	124	20
12	28	17–70	10–35	20	27	60	21	70	29–36	26–75
14	7	17–80	—	—	—	—	2.9	70	—	—
16	3.2	52	—	—	—	—	0.65	70	3	70
18	—	—	—	—	—	—	0.075	70	—	—
Oleate	?	—	—	—	—	—	—	—	0.1;0.23	20

A.2. Potassium soaps

Methods and references	Conductivity				Density		Refractive index				Solubility of org. liquids	
	Cushmann, Brady, McBain (18)		Brady, Huff (8)		Bury, Parry (12)		Klevens (45)		Harkins (33)		Stearns, Oppenheimer, Simon, Harkins (82)	
No. of carbon atoms	C.M.C.	°C.	C.M.C.	°C.	C.M.C.	°C.	C.M.C.	°C.	C.M.C.	°C.	C.M.C.	°C.
8	—	—	—	—	470	25	390	25	450	45	600	?
10	—	—	—	—	—	—	98	25	118	45	—	—
12	24	25	35;24;20; 22;31	0;25;50; 70;90	49–44	25–35	25.5	25	30.5	45	22.6	?
14	—	—	—	—	—	—	6.6	25	7.4	45	—	—
16	—	—	—	—	—	—	1.8	35	1.9	45	—	—
18	—	—	—	—	—	—	—	—	—	—	—	—
Oleate	<50	25	—	—	—	—	—	—	—	—	—	—

TABLE IV—*Continued.*

B. Sodium alkyl sulfates

Methods and references / No. of carbon atoms	Conductivity										Freezing point	
	Haffner, Piccione, Rosenblum (31)		Lottermoser, Püschel (55)		Powney, Wood (70)		Schmidt, Larsen (77)		Ward (92)		Johnston, McBain (41)	
	C.M.C.	°C.	C.M.C.	°C.	C.M.C.	°C.	C.M.C.	°C.	C.M.C.	°C.	C.M.C.	°C.
8	130	25	—	—	—	—	—	—	—	—	—	—
10	31	25	—	—	—	—	—	—	—	—	—	—
12	8.1	25	3–6.3	25–60	9.3	60	8.3	25	7.2	20	26	0
14	—	—	1.6–2.5	40–60	2.6	60	—	—	—	—	—	—
16	—	—	0.4–0.6	40–60	1.0	60	—	—	—	—	—	—
18	—	—	0.3	60	0.41	60	—	—	—	—	—	—

B. Sodium alkyl sulfates

Methods and references / No. of carbon atoms	Osmotic pressure		Refractive index		Spectrum of dyestuffs		Surface activity						Viscosimetry	
	Hess, Suranyi (39)		Klevens (45)		Harkins, coworkers (16, 17, 33)		Brady (7)		Lottermoser, Stoll (56)		Powney, Addison (67)		Hess and co-workers (37, 38)	
	C.M.C.	°C.	C.M.C.	°C.	C.M.C.	°C.	C.M.C.	°C.	C.M.C.	°C.	C.M.C.	°C.	C.M.C.	°C.
8	—	—	155	25	—	—	—	—	—	—	—	—	—	—
10	—	—	41	25	38.7–40	?	—	—	—	—	—	—	—	—
12	6.95	21	10	35	60.2–61.2	?	8		6.9	20	7.7–8.0	60	9	20
14	—	—	2.9	45	6.1;6.5	?	—	—	2.2	40	2.0–2.1	60	3	75
16	—	—	0.9	52	0.4	35.8	—	—	0.87(1.7)	60	0.34–0.47	60	—	—
18	—	—	—	—	—	—	—	—	1.0(2.1)	60	0.17–0.22	60	—	—

C. Sodium alkanesulfonates

Methods and references / No. of carbon atoms	Conductivity		Osmotic pressure		Refractive index		Solubility		Spectrum of dyestuffs		Surface and interfacial tension	
	Wright, Abbott, Sivertz, Tartar (94)		Johnston, McBain (41)		Harkins (33) Klevens (44)		Tartar, Wright (74)		Klevens (44)		Lingafelter, Wheeler, Tartar (53)	
	C.M.C.	°C.	C.M.C.	°C.	C.M.C.	°C.	C.M.C.	°C.	C.M.C.	°C.	C.M.C.	°C.
8	—	—	—	—	150–155	25	—	—	140–150	25	—	—
10	40;43;58	40;60;80	—	—	41–43	25	40	22.5	37–39	25	37;31.7	40
12	11;12;15	40;60;80	17	0	10–11	35	9.8	31.5	8.8–9.5	33.5	10; 7.3	40
14	2.5;3.3;4.6	40;60;80	—	—	2.9–3.2	45	2.7	39.5	2.35–2.6	42.5	2.7;1.7	40
16	—	—	—	—	0.9–1.2	52	1.05	47.5	0.75–0.85	50	—	—
18	—	—	—	—	—	—	0.75	57	—	—	—	—

D. Different soaps

Soaps	Methods	References	C.M.C.	°C.
Benzyltrimethylammonium laurate	Conductivity	Cushman, Brady, McBain (18)	10	25
Hexanolamine oleate	Freezing point	Gonick, McBain (30a)	0.6	0
Calcium dodecyl sulfate	Surface activity	Lottermoser, Stoll (56)	1	60
Magnesium dodecansulfonate	Surface activity	Lingafelter, Wheeler, Tartar (53)	5.5	40
Sodium octyl benzenesulfonate	Conductivity	Paquette, Lingafelter, Tartar (65)	11;12;15	25;40;60
Sodium dodecyl benzenesulfonate	Conductivity		1.2	60
Diisobutyl sulfosuccinate	Conductivity	Haffner, Piccione, Rosenblum (31)	(1.4)	25
Di(methylamyl) sulfosuccinate	Conductivity	Haffner, Piccione, Rosenblum (31)	30^b	25
Di(2-ethylhexyl) sulfosuccinate	Cond., osmotic pr.	Haffner . . .(31), McBain, Brady (58)	5.5;^{b}4	25
Di-*n*-octylsulfosuccinate	Conductivity	Haffner, Piccione, Rosenblum (31)	0.9^b	25
Nonaethyleneglycol monolaurate	Freezing point, osmotic pressure	Gonick, McBain (30)	0.63	0

---

[a] In the presence of 0.1% NaOH.

[b] Values are corresponding to the C.M.C. of straight chain sulfates adding the numbers of C-atoms in both alkyl groups.

considering that the soap solutions are very sensitive systems and each external force acting during the measurement would be able to change the balance of aggregation. Time has an influence on the surface tension which is shown by Nutting, Long and Harkins (63). The safest procedure for determining C.M.C. would be the refractometric method on which Klevens (45, 46) especially relies. This method does not involve the addition of an extraneous substance or the application of some external force.

TABLE V

C.M.C. $M \times 10^{-3}$

Temp. °C.	$C_{10}H_{21}SO_4Na$	$C_{12}H_{25}SO_4Na$	$C_{11}H_{23}COOK$[a]	$C_{13}H_{27}COOK$
25	41	—	25.5	6.6
30	—	—	26.0	—
35	42	10	27.0	7.0
45	45	11	30.5	7.4
55	49	12	35.0	7.9
65	55	14	42.0	8.6

[a] Not in agreement with the values given by Brady and Huff (8).

Using the refractometric method, it was possible to make clear the influence of temperature on the C.M.C. (45). These results indicate that the C.M.C. increases with increasing temperature (Table V). It is possible to calculate the C.M.C. for each member of a homologous series at a constant temperature, if the C.M.C. is known for any member then:

$$\log(\text{C.M.C.}) = A + BN, \tag{3}$$

where N = number of carbon atoms in chain,
B = an empirical constant (may be taken to be log 2 with sufficient accuracy),
A = a constant for the particular temperature and homologous series, which may be determined from a known value of the C.M.C. for one member of the series.

B. Changing of C.M.C. in the Presence of Salts

Corrin and Harkins (16) and Klevens (45) have demonstrated the changes in the C.M.C. of soap, applying change in spectral absorption of pinacyanol chloride (33) in the presence of added salts, using sodium decylsulfonate and potassium laurate. These authors stated the general rule that the log of the C.M.C. of anionic soaps is linearly dependent upon the log of the cation concentration of the added salt. The different salt anions have no influence upon the aggregation of anionic soaps (16, 45). This result is in agreement with the experiment by Powney and Addison (67) who studied, by surface and interfacial tension measurements, the changing of C.M.C. of dodecyl sulfate solutions containing various concentrations of added NaCl and $CaCl_2$. Corrin and Harkins (16) used sodium dodecyl sulfate with increasing amounts of NaCl, Na_2SO_4 and $Na_4P_2O_7$. Fig. 4 gives the C.M.C. values (16, 67) with pure sodium dodecyl sulfate and also in the presence of NaCl, Na_2SO_4 and $Na_4P_2O_7$. Powney and Addison (67) report that $CaCl_2$ causes the alkyl sulfate to aggregate 40 times more than NaCl, and that this relation is the same for the coagulation of colloids which follow the Schulze rule (79).

C. C.M.C. and Detergent Action

Preston (71) presents the idea that a "critical washing concentration" exists, beyond which further addition of detergent does not increase the washing power, and that this critical washing concentration is about the same as the C.M.C. Palmer (64) gives a discussion of the importance of the micelles in detergency, and he emphasizes that detergency does not depend on the presence or absence of micelles. On the other hand, McBain and Woo (59) suggest that one of the factors in detergency is the dissolution of oil in the micelles of the detergents. Preston did not try to establish a correlation between C.M.C. and the critical washing concentration in the case of sodium oleate, because the C.M.C. for sodium oleate cannot be stated exactly. Turning now to di-*n*-octyl sulfosuccinate which is a good wetting agent but not a good detergent agent, Haffner concluded that its C.M.C. is about the same as that of hexadecyl sodium sulfate (31). However, there is no doubt that the optimum washing concentration of this sulfosuccinate is much higher than that of hexadecyl sodium sulfate. There would, therefore, appear to be no agreement in this case between C.M.C. and optimum washing concentration. However, the C.M.C. for this sulfosuccinate is based upon meager experimental data.

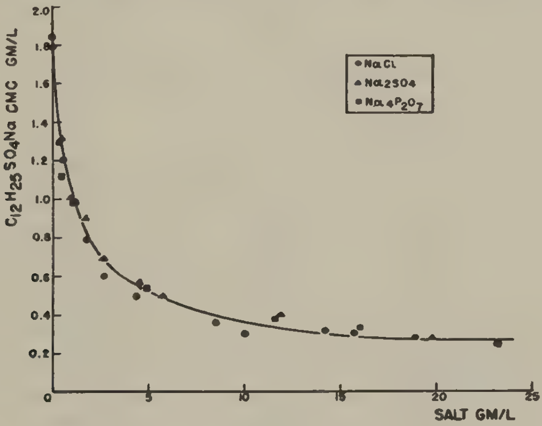

FIG. 4.

McBain and Bolduan (57) found, by the freezing point lowering method, an agreement with the values given by Haffner and coworkers (31), but it is not possible to establish from their paper exact values for C.M.C.

If maximum washing power is reached at the C.M.C. in the case of a simple detergent system, it does not follow that the break in the detergency curve necessarily coincides with the C.M.C., even in this case. As reported in Fig. 2, the ability of a detergent to remove dirt varies with the size of the dirt particles, and, if these are very large, they may be washed away before the full detergent power of the solution is utilized. Only in case the full detergent power is utilized could we expect agreement between C.M.C. and the break in the detergency curve. Furthermore, with dirt of extremely small particle size, cleaning becomes so poor that breaks in the detergency curve can scarcely be detected.

Preston (71) shows that detergent action, colloid formation, and surface activity are different manifestations of the same characteristic of the detergent for pure soaps alone. But it still must be proven that Preston's hypothesis is correct if alkali or neutral salts are present, as in the case under practical washing conditions.

It has been stated (3, 64) that the addition of neutral salts has an important influence on the cleaning power, this is much more the case with the addition of alkali, *e.g.*, $Na_4P_2O_7$. If a pure solution of dodecyl sulfate is used, at a concentration below the C.M.C., and Na_2SO_4 and NaCl or, even better, $Na_4P_2O_7$ is added, the detergent power will be increased. The optimum cleaning action of the liquid, that is, Preston's critical washing concentration, will be reached at a lower concentration by adding $Na_4P_2O_7$ than by adding Na_2SO_4, because $Na_4P_2O_7$ has more washing action than Na_2SO_4 (35). However, Fig. 2 shows that both salts affect C.M.C. about equally, indicating that the critical washing concentration and C.M.C. in the presence of electrolytes are not necessarily the same. Although the sodium ion shifts the detergency curve to the left, and may be predominant in reducing C.M.C., alkalinity and the nature of the individual salt anions also influence detergency.

D. Foam Properties and C.M.C.

There is a relation between foam properties and C.M.C. The maximum half-life time attained by foam volumes as determined by Goette (28) occurs at approximately the same concentration as the C.M.C. This correlation is shown in Figs. 5–7 for the alkyl sulfates, alkyl sulfonates, and fatty acid soaps. Older experiments by Goette (25) with the foam number bulb of Stiepel (83) show that the amount of liquid which is converted into foam at the end of the agitation period reaches a maximum value at concentrations which are above the C.M.C. in the case of sodium alkyl sulfates (Table VI).

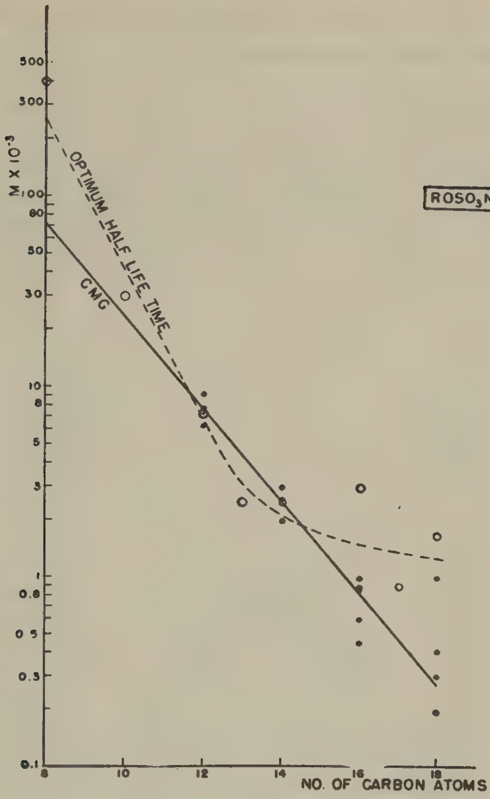

FIG. 5.

Lederer (52) found that the amount of liquid which becomes foam increases inversely as the square root of time. This relationship makes it possible to determine, at the end of the agitation period, the exact amount of liquid in the foam for zero time by extrapolation. This cannot be found by direct observation. Furthermore, it was found (25) that the amount of liquid which is converted into foam depends on the length of the paraffin chain and on the temperature. Therefore, it may be possible that the best

TABLE VI

Concentrations $M \times 10^{-3}$ for Maximum Amount of Liquid Converted into Foam in Relation to the C.M.C. of Sodium Alkyl Sulfates

C-atoms	Maximum liquid into foam (25)	C.M.C. (70)
12	50	9.3
14	60	2.6
16	25	1.0
18	5	0.41

agreement between optimum half-life time of the foam volume and C.M.C. would be dependent on the temperature.

III. The Importance of the Interfacial Potentials

A very important factor in the detergency process is the interfacial potential or ζ-potentials between the surface and the detergent solution and between the soil and the solution. For like ζ-potentials between the soil and the solution and between the substratum and the solution, the higher these ζ-potentials the greater will be the detergent effect. The differences between anionic soaps and cationic soaps and the different salt effects can be understood very well on the basis of changing interfacial potential.

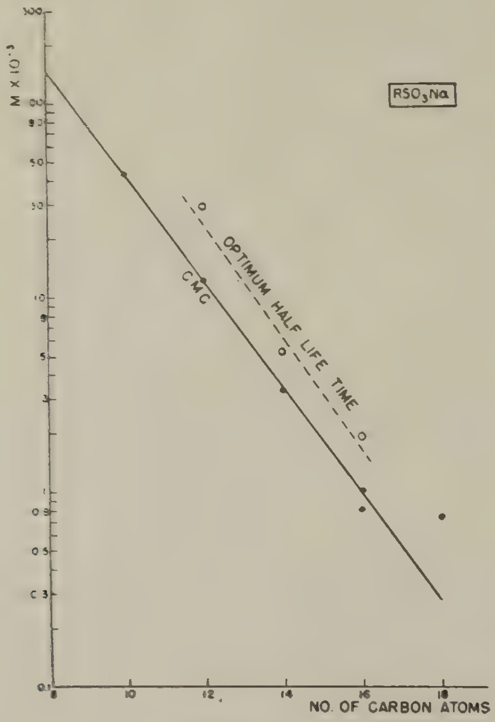

Fig. 6.

A. *The Effect of Anionic Soaps and of Cationic Soaps*

In the case of both cationic and anionic soaps, the paraffin chain of the surface-active ion is adsorbed preferentially by fatty dirt and fat-free insoluble surfaces (60, 32, 49a). An adsorption by fatty dirt takes place because the paraffin chain is soluble only in the fatty dirt and not in the aqueous solution, whereas the fatty ion, because of its water insolubility and surface activity, is adsorbed by the solid surfaces. The result is a net decrease in free energy of the fatty ion when it is adsorbed on the solid surface. The preferentially adsorbed ion determines the kind and magnitude of the ζ-potential of the dirt and substratum. In the case of anionic soaps, a higher negative potential results on both the fiber (87) and the dirt, and, in the case of cationic soaps, the substratum and the dirt will become more positively charged. It is possible to show experimentally that in each case the paraffinic ions are preferentially adsorbed rather than their counter ions. Inorganic pigments, *e.g.*, $BaSO_4$, ZnS, ZnO, TiO_2, can be used to impart dullness to otherwise shiny rayon surfaces. All these pigments are negatively charged. Either anionic or cationic soaps can be used to obtain stable suspensions. There is one process to combine the use

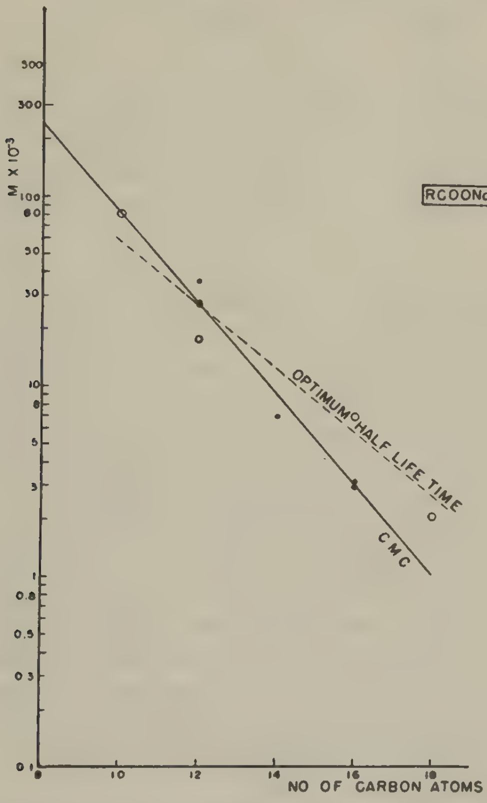

FIG. 7.

of anionic and cationic soaps (27) in which the pigment is at first suspended in a solution of anionic soap and then precipitated with a stoichiometric amount of cationic soap. If a surplus of cationic soap is used, then a stable positively charged suspension of the pigment results.

The adsorption of positively charged particles by rayon is so rapid that a single immersion in a bath will completely exhaust it. If too high a surplus of cationic soap is used to produce the positively charged suspension, the pigment will not go completely onto the fiber surface, because the fiber surface will be also positively charged by adsorbed fatty cations.

The impossibility of cleaning with cationic soaps below a soap concentration of about 10 g./l. is only to be understood if we assume that the dirt preferentially adsorbs the cationic fatty ions and that only with higher amounts of cationic soaps can the substratum also be positively charged. It is necessary to clarify this assumption by further experimental work.

In practical concentrations of about 0.05–2% soap, without exception, only the anionic soaps and the non-ionic soaps with anionic character are real detergents. It is claimed by other authors that the action of the soaps of polar construction can be explained by the good contact obtained between the hydrophobic dirt and the paraffinic chain during the washing process, while at the same time the hydrophilic parts of the soap remain dissolved in water. The detergent builds a bridge between water and dirt. This working hypothesis was established by Goette (25). Similar considerations have also been proposed (2, 19, 23, 34, 51, 60, 73, 81).

The details of the soap orientation on the substratum are not clear. A glass surface covered with paraffinic cations, after treatment with a solution of any cationic soap, is persistently hydrophobic (26, 62); but a glass surface covered with paraffinic anions, after treatment with anionic soap solution, remains hydrophilic. In this connection it may be of interest to mention that dry anionic soaps are difficult to wet with water but dry cationic soaps are wettable without difficulty (29). At present, these phenomena have not been explained.

Brill and Rieder (10) used X-ray diffraction methods for investigating soap films on the surface of thin nitrocellulose films and found that the soap films made with 0.1% soap solutions probably contain several molecular layers. If more dilute solutions are used, it should be possible to obtain monomolecular films. The newly formed films can be rinsed off very easily, but if they are aged several days, or if the films are formed at higher temperature (85°C.), they are more difficult to rinse off.

Taking up the surface-active anions, the dirt and the substratum will acquire an increased negative charge, and electrostatic repulsion takes place between the dirt and the substratum (see Table VII). In general,

TABLE VII

Detergent Action and Zeta-Potentials

Solution	Molarity	Detergency value $10 \times Q^a$ Goette (25)	Zeta-potentials (volt) against aqueous phase				
			Mineral oil droplets		Solid particles		
					Carbon	Ferric oxide	Cellulose
			Powis (66)	Urbain & Jensen (87)	Urbain & Jensen (87)	Urbain & Jensen (87)	Bull & Gortner (11)
Water	—	±0.0	−0.046	0.086	−0.052	−0.028	−0.010
KCl	0.01	±0.0	−0.046	—	—	—	−0.0124
Na_2SO_4	0.0035	—	—	—	−0.057	—	—
$K_4Fe(CN)_6$	0.01	+0.7	−0.070	—	—	—	—
$K_4Fe(CN)_6$	0.0036	—	—	—	−0.060	—	—
Na_3PO_4	0.0036	—	—	—	−0.063	—	—
$BaCl_2$	0.01	−0.5	−0.018	—	—	—	−0.0060
$AlCl_3$	0.01	−1.6	+0.0025	—	—	—	−0.0034
Sodium palmitate	0.0036	—	—	—	−0.069	—	—
Sodium oleate	0.0036	—	—	−0.151	−0.083	—	—
Dilute soap solution	?	—	—	—	—	−0.078	—

^{a} $Q = \log \frac{W_s}{W_0}$; W_s = whiteness after washing with detergent solution.
W_0 = comparison value with buffer solution at the same pH.

all dirts and substrata have, in aqueous solutions, a negative charge because the dielectric constant of water is extremely high. Actual measurements of the ζ-potentials of various fibers in water are reported by Karrer and Schubert (42) as given in Table VIII.

The increase in cleaning action with increasing soap concentration up to the C.M.C. (71) can be deduced from the values of the electrostatic

TABLE VIII

Fiber	Zeta-potential against water
Cotton mercerized	−0.015
Cotton not mercerized	−0.038
Wool	−0.048
Viscose rayons	−0.0017 to −0.008
Cuprammonium rayon	−0.005
Acetate rayon	−0.036
Pyridinized cotton	+0.019
Pyridinized rayon	+0.0086

Except for the aminated yarns, the textiles show a negative ζ-potential against water.

forces. Ekwall and Lindblad (21) found that soaps form anions with increasing valences before micelles are formed. These highly charged anions cause an increasing interfacial potential with increasing soap concentration (see Table III).

Urban and Jensen (87) investigated the influence of soaps on the interfacial potential of emulsified oil droplets and suspended small carbon particles. If soap is present, the value of the negative interfacial potential of solid and oily particles increases, details are given in Table VI. The longer the paraffin chain of a soap, the higher is the interfacial potential. For a given soap, the interfacial potential depends but little on the soap concentration. It is also to be noted that, near the C.M.C., no break in the value of the interfacial potential takes place. In addition, the alkalinity of the soap solution is not sufficient to account for the interfacial potential of the carbon particles suspended in the solution.

The optimum protective action against the sedimentation of Ilmenite Black on clean cotton fabrics is reached with the soaps at the following concentrations (69) (see Table IX).

TABLE IX

Soap	Optimum for protective action $M \times 10^{-3}$	C.M.C. $\times 10^{-3}$
Sodium laurate	5	About 30
Sodium stearate	0.13	About 0.6
Sodium oleate	0.5	About 0.1

The cationic soaps are not able to clean in customary laundry concentrations, about 0.05–2% soap. In "washing" textiles soiled with artificial standard dirt, made from India ink without oil, cationic soaps cause a redistribution of the carbon of the soil over the cotton without any of the carbon getting into the liquor. It is possible to obtain two completely homogeneously soiled cotton fabric pieces by using one soiled piece and one clean piece in the same solution of cationic soap during the "washing" process (29). This simple experiment shows that the dirt is also movable but a definite removal does not take place, because an electrostatic attraction, and not a repulsion, occurs. With concentrated solutions of cationic soaps, it is possible to get cleaning action (29), but it is necessary to use many times the highest usual amount of anionic soap (∼10% and more). This fact is in support of the importance of the interfacial potential, because, with high concentrations of cationic soaps, the substratum is also positively charged. Kling, Langer and Haussner (49) showed the same mechanism in the case of oily dirt. They used wool soiled with peanut oil. A solution of 0.4% dodecylpyridinium bromide, like the anionic soaps, causes the oil to form into droplets because the hydrophobic part of the molecule is going into the oily dirt phase and the hydrophilic group remains soluble in the aqueous phase. Kling, Langer and Haussner (49) were able to observe microscopically that the oil is moveable but it remains on the substratum surface like the solid dirt in a solution of cationic soap. The distribution of the displaced oil on the fibers appears different (49). Oily dirt can be removed if the concentration of the cationic soap is high.

The mechanism is thus the same with solid and oily dirt, and the cleaning phenomena with both anionic and cationic soaps can be explained in terms of interfacial potentials.

B. Electrolyte Effects

The various changes of cleaning power of the soaps on addition of neutral salts and/or alkalies cannot be explained solely in terms of the C.M.C. In agreement with Corrin, Harkins and Klevens (16, 44), Powney and Addison (67) were able to show that, in the case of alkali salts, concentration and valence of the cations have an influence on the changing of the C.M.C. of anionic soaps. On the other hand, the different anions have an individual, very important influence on the cleaning action. The experiments by Powney and Wood (70), who studied the movement of oil drops in an electrical field, show that the mobility is increased with increasing anion valence and with increasing pH of the alkaline salts. These experiments are in good agreement with the detergent action of these substances. Fig. 8 shows the comparison of the cleaning action

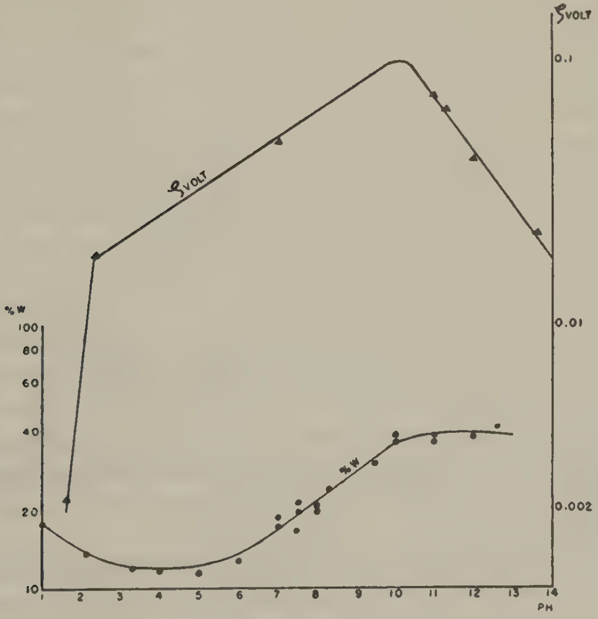

FIG. 8.

(per cent whiteness "*W*") of soapless buffer solutions given by Goette (24) with an oiled India ink dirt model on fabric and the ζ-potentials (volt) given by Ellis (22) with unbuffered solutions of HCl and NaOH at the same pH. Between pH 5 and pH 10.2, the cleaning action increases with increasing negative ζ-potential of the oil drops. Above pH 10.2, the cleaning action remains constant, but the ζ-potentials decrease with increasing pH. However, the cleaning action is also dependent on the ζ-potential of the substratum against the aqueous phase and not only on the ζ-potential of the oil drops. A complete agreement between whiteness and ζ-potential is not to be expected, because the experimental evidence is still too incomplete. Experiments by Goette (25) compared the detergent action of 0.01 M $K_4Fe(CN)_6$, KCl, $BaCl_2$, and $AlCl_3$ solutions with the cleaning action given in Fig. 8 of dilute buffer solutions at the same pH. The $K_4Fe(CN)_6$ solution cleans better than a buffer solution at the same pH because the $Fe(CN)_6^{-4}$ is preferentially adsorbed. No difference is noted with KCl. $BaCl_2$ solutions do not clean as well as the corresponding buffer solution (25) because the Ba^{++} ion is adsorbed; a still greater decrease in cleaning action is noted with the $AlCl_3$ solution because of cation adsorption. The fact that the alkyl sulfates clean in acid solutions can be understood, because the positively charged H ions are displaced by surface-active anions (25). These effects are in agreement with the valences and charges of the ions which are adsorbed by substratum and dirt, and with the generalization given (25). The results are also in full agreement with the effect of salts on the electric mobility and ζ-potential of paraffin oil droplets about 1μ in radius. This latter study was made by Powis (66), and the data are given in Table VI. The experimental method of Goette (25) is not completely correct, because buffer solutions also have a definite influence, as was shown by Lottermoser and Flammer (54), whose experiments were conducted in the presence of Igepon T. Rhodes and Wynn (75) studied the influence of sodium salts and obtained the same results, namely, that the salts increase the cleaning action of soaps. The effect of the salt increases with increasing valence of the salt anions.

Powney and Noad (69) have demonstrated the suspending power of detergents and salts with cotton fabrics when shaken in a suspension of Ilmenite Black, an inert model dirt. Na_2CO_3 and NaOH cause an increase in deposition which can be attributed to the sodium ion effect rather than to any pH effect. In contrast to this behavior, sodium hexametaphosphate and sodium pyrophosphate have a protective action still appreciable at a concentration as low as 5–10 p.p.m.

All these experiments show that the interfacial potential and not the formation of micelles is to be considered in explaining the detergency process.

IV. Complex Phenomena with Salts

In the presence of sodium alkyl sulfates, the influence of Ca^{++} in the washing liquor is very complicated, and more so in the case with fatty acid salts. Above the C.M.C. of the sodium salt in a homologous series of alkyl sulfates, the Ca salts which are formed by using hard water are very highly soluble in the excess of sodium salt, and below the C.M.C. they are less soluble (67). This fact must be kept in mind when proving the Ca^{++} resistance of soaps. Goette (25) established that the detergent action of sodium alkyl sulfate in water of 10 German degrees of water hardness is better than in water of 0° hardness to a 14-carbon chain paraffin. With a longer paraffin chain, increasing hardness decreases detergent action because the higher molecular weight calcium salts are not soluble enough. Solubility factors thus complicate attempted correlation of washing and of C.M.C. influence in the presence of $CaCl_2$, which decreases C.M.C. irrespective of the length of the carbon chain of the detergent. The solubility of ethylbenzene in a 10% solution of potassium laurate increases if KCl is added, it increases less when adding an equivalent amount of K_2SO_4, and still less with an equivalent amount of $K_4Fe(CN)_6$. Stearns et al. (82) state that this remarkable effect depends on the sizes of the Cl^-, SO_4^{-2} and $Fe(CN)_6^{-4}$ ions.

V. Summary

1. Solid particles are more difficult to remove than oily and fatty dirts. In the case of solid dirts, the smaller the particle size the more difficult is the removal of the dirt, whereas, in the case of oily soils, the surface-active products cause droplet formation followed by soil removal.

2. Looking at a homologous series of any soap, with increasing C-number the optimum wetting action will be reached earlier than the optimum washing action. Branches in the paraffin chain shift both optima to a higher C-number. In this case the absolute value for the wetting action will be increased. A second hydrophilic group in the detergent reduces both wetting action and cleaning action.

3. The C.M.C. of anionic soaps and electroneutral soaps are reviewed because numerous soap properties show a break at or near the C.M.C. There is a break in the detergency curve which is in agreement with the C.M.C. in those cases where the full detergent power is utilized and where the dirt is not of an extremely small particle size. Furthermore, of practical interest is the break in the curves of surface activity, foam characteristics and solubility of oils and Ca-soaps at the C.M.C.

4. In the presence of electrolytes, C.M.C. and critical washing concentration are not necessarily the same. Of basic importance in understanding the detergent action of soap and washing alkalies are the inter-

facial potentials between the soiled surface, the dirt and the aqueous solution. The kind and the degree of these potentials are dependent on the ions of soap aggregates which are adsorbed preferentially by dirt and substratum. The loosening of the dirt from the substratum takes place because the detergent, due to its polar construction, goes between the dirt and the substratum. Electrostatic forces are the influencing factors which cause the loosening of the dirt; this process will be supported by mechanical movement. In general, the dirt cannot be removed if cationic soaps are used in low concentrations because the surface-active ions produce a positive charge on the dirt. But a cleaning effect with cationic soaps is possible if their concentration is high enough to give the substratum surface a positive charge.

5. The cleaning activity of neutral or alkaline salts is dependent on the charge of their anions. Salts with multivalent cations decrease the cleaning action, because the preferentially adsorbed cations give a positive charge to the dirt as with cationic soaps. At high salt concentrations, agglomeration of the dirt takes place and the pH value also has a very important influence on the cleaning action. Therefore, cleaning action with salts present is dependent on the amount of salt and the kind and degree of charged ion preferentially adsorbed by the dirt and substratum.

6. The increase in cleaning action with concentration of pure soap solutions below the C.M.C. can be explained by the increase in valence of the aggregating soap ions before the C.M.C. is reached and the formation of micelles takes place.

REFERENCES

1. ADAM, N. K., *J. Soc. Dyers Colourists* **53**, 121 (1937); ADAM, N. K., AND JESSOP, G., *J. Chem. Soc.* **127**, 1863 (1925).
2. ADAM, N. K., *J. Phys. Chem.* **29**, 87 (1925).
3. AICKIN, R. G., *J. Soc. Dyers Colourists* **60**, 36, 41, 60, 170 (1944).
4. ANON., *Silk and Rayon* **20**, 555 (1946).
5. BACON, O. C., AND SMITH, J. E., *Ind. Eng. Chem.* **40**, 2361 (1948).
6. BOSSHARD, E., AND STURM, H., *Chem. Ztg.* **54**, 762 (1931).
7. BRADY, A. P., *J. Phys. & Colloid Chem.* **53**, 56 (1949).
8. BRADY, A. P., AND HUFF, H., *J. Colloid Sci.* **3**, 511 (1949).
9. BROWN, C. B., *Research* **1**, 46 (1947).
10. BRILL, R., AND RIEDER, F., *Z. angew. Chem.* **53**, 100 (1940).
11. BULL, H. B., AND GORTNER, R. A., *J. Phys. Chem.* **35**, 309 (1931).
12. BURY, C. H., AND PARRY, G. A., *J. Chem. Soc.* **1935**, 626.
13. CHWALA, A., Textilhilfsmittel: Chemie, Kolloidchemie, Anwendung. Vienna, 1938.
14. CHWALA, A., AND MARTINA, A., *Melliand Textilber.* **18**, 725, 998 (1937).
15. CLARK, R., AND HOLLAND, V. B., *Am. Dyestuff Reptr.* **36**, 734 (1947).
16. CORRIN, M. L., AND HARKINS, W. D., *J. Am. Chem. Soc.* **69**, 679 (1947).
17. CORRIN, M. L., KLEVENS, H. B., AND HARKINS, W. D., *J. Chem. Phys.* **14**, 480 (1946); KLEVENS, H. B., *ibid.* **14**, 742 (1946).
18. CUSHMANN, A., BRADY, A. P., AND MCBAIN, J. W., *J. Colloid Sci.* **3**, 425 (1948).
19. DONNAN, F. P., AND POTTS, H. E., *Kolloid-Z.* **7**, 208 (1910).

20. Ekwall, P., *Kolloid-Z.* **101**, 135 (1942); *Z. physik. Chem.* **161A**, 195 (1932).
21. Ekwall, P., and Lindbald, L. G., *Kolloid-Z.* **94**, 42 (1941); see also Stauff, J., *Z. physik. Chem.* **138A**, 55 (1938); **185**, 45 (1939); *Kolloid-Z.* **96**, 244 (1941).
22. Ellis, R., *Z. physik. Chem.* **78**, 32 (1912).
23. Freundlich, H., Kapillarchemie II, 507. Leipzig, 1932.
24. Goette, E., *Kolloid-Z.* **64**, 222 (1933).
25. Goette, E., *ibid.* **64**, 327, 331, (1933).
26. Goette, E., *Chemie, Die* **57**, 67 (1944).
27. Goette, E., *Melliand Textilber.* **17**, No. 3 (1936).
28. Goette, E., *ibid.* **29**, 65, 105 (1948).
29. Goette, E., unpublished data.
30. Gonick, E., and McBain, J. W., *J. Am. Chem. Soc.* **69**, 334 (1947).
30a. Gonick, E., and McBain, J. W., *J. Colloid Sci.* **1**, 127 (1946).
31. Haffner, F. D., Piccione, S. A., and Rosenblum, C., *J. Phys. Chem.* **46**. 662(1942).
32. Harkins, W. D., *Colloid Symposium Monograph* **II**, 141 (1925).
33. Harkins, W. D., *J. Am. Chem. Soc.* **69**, 1428 (1947).
34. Harkins, W. D., Davies, and Clark, *ibid.* **39**, 354, 541 (1917).
35. Harris, J. C., Eck, J. R., and Cobbs, W. W., *Oil & Soap* **19**, 3 (1942).
36. Heermann, P., *Öl-u. Fettind.* **44**, 361 (1924).
37. Hess, K., *Fette u. Seifen* **49**, 81 (1942).
38. Hess, K., Philippoff, W., and Kiessig, H., *Kolloid-Z.* **88**, 40 (1939).
39. Hess, K., and Suranyi, L. A., *Z. physik. Chem.* **184A**, 321 (1939).
40. Holland, V. B., and Petra, A., *Am. Dyestuff Reptr.* **32**, 534 (1943).
41. Johnston, S. A., and McBain, J. W., *Proc. Roy. Soc. (London)* **181A**, 119 (1942).
42. Karrer, P., and Schubert, H., *Helv. Chim. Acta* **11**, 221 (1928).
43. Kind, W., and Oldenroth, O., *Fette u. Seifen* **46**, 292 (1939).
44. Klevens, H. B., *J. Phys. & Colloid Chem.* **51**, 1143 (1947).
45. Klevens, H. B., *ibid.* **52**, 130 (1948).
46. Kling, W., *Melliand Textilber.* **28**, 197 (1947).
47. Kling, W., *ibid.* **28**, 428 (1947).
48. Kling, W., and Koppe, H., *ibid.* **30**, 23 (1949).
49. Kling, W., Langer, E., and Hauser, I., *ibid.* **25**, 198 (1944); **26**, 12, 56 (1945).
49a. Kruyt, H. R., and Troelstra, S. A., *Kolloidchem. Beih.* **54**, 262 (1943).
50. Lamm, O., *Kolloid-Z.* **91**, 275 (1940); Lamm, O., and Hogberg, H., *ibid.* **91**, 10 (1940).
51. Langmuir, I., *J. Am. Chem. Soc.* **39**, 1848 (1917).
52. Lederer, E. L., *Fettchem. Umschau* **40**, 69 (1933).
53. Lingafelter, Wheeler, Tartar, *J. Am. Chem. Soc.* **68**, 1490 (1946).
54. Lottermoser, A., and Flammer, H., *Kolloidchem. Beih.* **45**, 359 (1937).
55. Lottermoser, A., and Püschel, F., *Kolloid-Z.* **63**, 175 (1933).
56. Lottermoser, A., and Stoll, F., *ibid.* **63**, 49 (1933).
57. McBain, J. W., and Bolduan, *J. Phys. Chem.* **47**, 95 (1943).
58. McBain, J. W., and Brady, *J. Am. Chem. Soc.* **65**, 2072 (1943).
59. McBain, J. W., and Woo, *J. Phys. Chem.* **42**, 1099 (1942).
60. Meyer, K. H., and Mark, H., Der Aufbau der hochpolymeren organischen Naturstoffe, pp. 29, 185. Leipzig, 1930.
61. Miles, G. D., and Shedlovsky, L., *J. Phys. Chem.* **48**, 57 (1944).
62. Neville, H. A., and Jeanson, C. A., *ibid.* **37**, 1001 (1937).
63. Nutting, S. C., Long and Harkins, *J. Am. Chem. Soc.* **62**, 1496 (1940).
64. Palmer, E. C., *J. Soc. Chem. Ind. London (Trans.)* **60**, 56, 60 (1941).
65. Paquette, Lingafelter and Tartar, *J. Am. Chem. Soc.* **65**, 686 (1943).

66. Powis, F., *Z. physik. Chem.* **89**, 98, 179, 186 (1914).
67. Powney, J., and Addison, C. C., *Trans. Faraday Soc.* **33**, 1243 (1937).
68. Powney, J., and Addison, C. C., *ibid.* **34**, 372 (1938).
69. Powney, J., and Noad, R. W., *Textile Mfr.* **66**, 32 (1940).
70. Powney, J., and Wood, L. J., *Trans. Faraday Soc.* **36**, 57 (1940).
71. Preston, W. C., *J. Phys. & Colloid Chem.* **52**, 84 (1948).
72. Reichenberg, D., *Trans. Faraday Soc.* **43**, 467 (1947).
73. Reychler, A., *Kolloid-Z.* **12**, 277; **13**, 252 (1913).
74. Rehbinder, P., Physicochemical Work on Cleaning Action. Leningrad, 1935. Chapter 1, Graph 1.
75. Rhodes, F. H., and Wynn, C. S., *Ind. Eng. Chem.* **29**, 55 (1937).
76. Rideal, E. K., *Chemistry & Industry* **1948**, 403, 409.
77. Schmidt, G., and Larsen, E. C., *Z. Elektrochem.* **44**, 651 (1938).
78. Schnyder, A., *Tech.-Ind. u. Schweiz. Chem.-Ztg.* **25**, 66 (1942).
79. Schulze, H., *J. prakt. Chem.* **25**, 431 (1882); **27**, 320 (1883).
80. Sisley, J. P., *Corps. gras, savons* **1**, 66 (1943); **2**, 13, 77 (1944).
81. Spring, W., *Kolloid-Z.* **4**, 161 (1909); **6**, 11, 109, 164 (1910).
82. Stearns, R. S., Oppenheimer, H., Simon, E., and Harkins, W. D., *J. Chem. Phys.* **15**, 496 (1947).
83. Stiepel, C., *Seifensieder-Ztg.* **41**, 347 (1913).
84. Sylvester, S. F., *Am. Dyestuff Reptr.* **36**, 91 (1947).
85. Szegö, L., and Malatesta, L., *Atti. congr. naz. chim. pura applicata* **5**, I. 569 (1936); *Chimica e industria (Milan)* **17**, 339 (1935).
86. Tartar, H. V., and Wright, K., *J. Am. Chem. Soc.* **61**, 539 (1939).
87. Urban, W. M., and Jensen, L. B., *J. Phys. Chem.* **40**, 821 (1936).
88. Utermohlen, W. D., and Wallace, E. L., *Textile Research J.* **17**, 670 (1947).
89. Valkó, E., Kolloidchemische Grundlagen der Textilveredlung. Berlin, 1937.
90. Van Zeile, B. S., *Oil & Soap* **20**, 55 (1943).
91. Vaughn, T. A., and Vittone, A., *Ind. Eng. Chem.* **33**, 1011 (1941); **35**, 1094 (1943).
92. Ward, H. F. H., *Proc. Roy. Soc. London* **176A**, 412 (1940).
93. Whitehead, R. B., *Ciba Rev.* **1945**, 1789.
94. Wright, K. A., Abbott, A. D., Sivertz, V., and Tartar, H. V., *J. Am. Chem. Soc* **61**, 549, 553 (1939).

ADSORPTION OF LONG-CHAIN ELECTROLYTES FROM AQUEOUS SOLUTION ON GRAPHITE OF KNOWN AREA AND ON POLYSTYRENE[1]

M. L. Corrin, E. L. Lind,[2] Adelle Roginsky and William D. Harkins

From the Department of Chemistry, University of Chicago, Chicago, Illinois

Received January 10, 1949; revised February 23, 1949

Introduction

The adsorption of long-chain electrolytes from aqueous solution onto solids of known area has been the subject of but little experimental investigation. Held and Samochwalov (1) measured the adsorption isotherm of sodium laurate on barium sulfate; the adsorption of sodium oleate and of sodium nonylate upon cinnabar was studied by Held and Khainsky (2). Equilibrium concentrations of the long-chain electrolytes for which adsorption values were determined by these workers extended over a small range; the surface areas of the solids were measured microscopically. Adsorption at the interface between aqueous solutions of sodium oleate and hydrocarbon emulsion droplets of known area was studied by Fischer and Harkins (3); the surface area of the droplets was determined microscopically. The adsorption of long-chain electrolytes upon proteins or upon animal or vegetable fibers involves specific chemical interaction (4) and, hence, does not come within the scope of this discussion.

It is the purpose of this paper to present primarily the adsorption isotherms of two long-chain electrolytes upon ash-free graphite of known surface area. The surface of this adsorbent is hydrophobic. Some data for adsorption of one long-chain electrolyte upon polystyrene are included, although the surface area of this solid is by no means accurately known. The areas occupied per adsorbed molecule on the surface of the solids have been calculated as a function of the equilibrium electrolyte concentration. These areas are of value with respect to the soap titration technic for the estimation of particle size in polymer latices (5); data for polystyrene are included primarily for this reason.

---

[1] This investigation was carried out under the sponsorship of the Reconstruction Finance Corporation, Office of Rubber Reserve, in connection with the Government's synthetic rubber program.

[2] Present address: Central Washington College of Education, Ellensburg, Washington.

EXPERIMENTAL

Materials

Graphite. The graphite used in this investigation was supplied by Dr. Lester L. Winter of the National Carbon Company. According to Dr. Winter, the surface of the graphite is free of carbon-oxygen complexes. The ash content is less than 0.009%.

Polystyrene. This material was supplied by Professor G. S. Whitby of the University of Akron. It was prepared by emulsion polymerization and had been subjected to careful purification.

Sodium Dodecyl Sulfate. This was part of a lot obtained from the research laboratories of Procter and Gamble Company. This material was extracted with diethyl ether, recrystallized twice from ethanol and dried *in vacuo.* The critical concentration of this substance, as determined by the dye spectral method (6), was identical with that of a highly purified sample of the salt supplied by Professor H. V. Tartar.

Potassium Myristate. Eastman myristic acid was recrystallized several times from ethanol, subjected to low pressure hydrogenation over platinum oxide and neutralized with a slight excess of KOH in hot ethanol. The soap was recrystallized 3 times from ethanol and dried *in vacuo.*

Water. Conductivity water was used throughout this investigation.

Determination of the Areas of the Solids

The areas of both graphite and polystyrene were determined by means of nitrogen adsorption at liquid nitrogen temperatures; these measurements were made by P. R. Basford. The specific area of the graphite as calculated by the equation of Brunauer, Emmett and Teller (BET) (7) on the assumption that the area per adsorbed nitrogen molecule is 16.2 A^2 ($\sigma_N = 16.2$ A^2) is 3.47 m.^{2}/g. The area calculated by the method of Harkins and Jura (HJ) (8) is 3.45 m.^{2}/g. The BET and HJ plots for graphite are given in Figs. 1 and 2.

The adsorption isotherm of nitrogen at 77.8°K on polystyrene is plotted in Fig. 3. The specific area calculated by the BET method from this isotherm is 107.7 m.^{2}/g. ($\sigma_N = 16.2$ A^2), while that calculated by the HJ method is 94.1 m.^{2}/g. These plots are shown in Figs. 4 and 5. This sample of polystyrene is undoubtedly porous. It has also been pointed out by Dr. George Jura (9) that some nitrogen may dissolve in the polystyrene at liquid nitrogen temperature. The high values of the area per adsorbed molecule on polystyrene obtained in the adsorption measurements from aqueous solution, as discussed below, may be due to porosity alone or to both porosity and errors in the area determination arising from solution

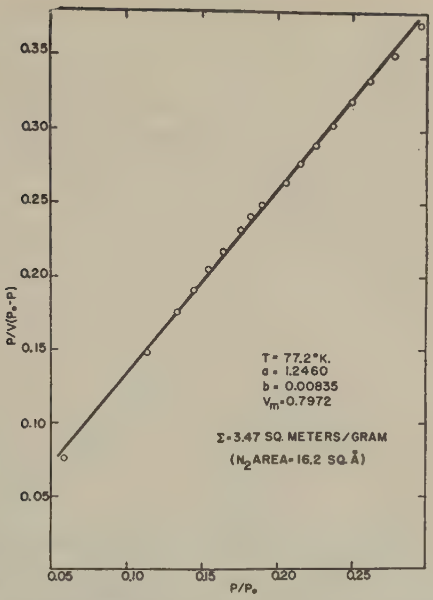

FIG. 1. Brunauer, Emmett and Teller plot of nitrogen adsorption at 77.2°K on graphite.

of nitrogen in the solid. It is thus likely that the area value assigned to the polystyrene is of little significance. We are thus forced to consider the form of the adsorption isotherm obtained on this material rather than absolute values of specific adsorption.

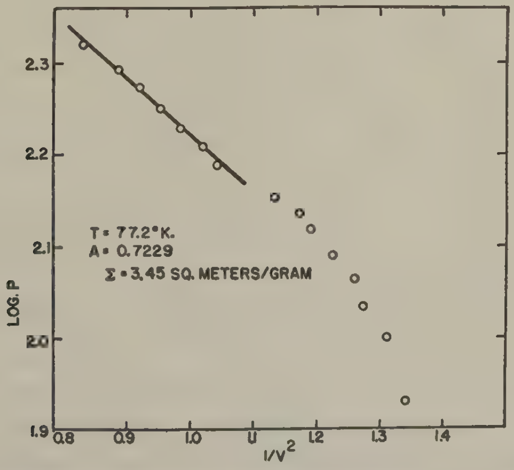

FIG. 2. Harkins and Jura plot of nitrogen adsorption at 77.2°K on graphite.

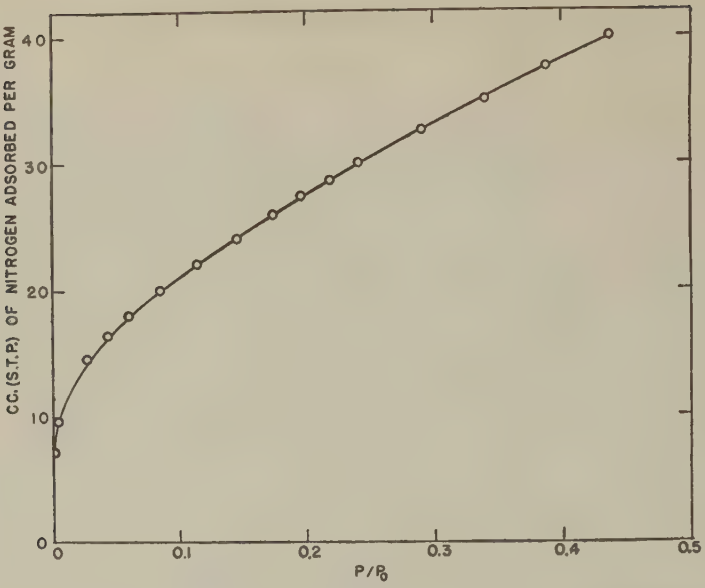

FIG. 3. The adsorption isotherm of nitrogen at 77.8°K on polystyrene.

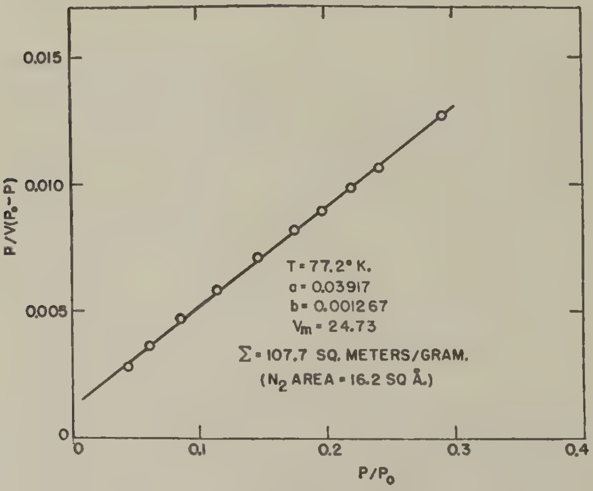

FIG. 4. Brunauer, Emmett and Teller plot of nitrogen adsorption at 77.8°K on polystyrene.

Determination of the Adsorption Isotherms from Solution

Solutions employed in this investigation, both for the preparation of electrolyte-adsorbent systems and for interferometric reference standards, were made up by weight. Both salt and solvent were known to 0.1 mg.

The weights used had been calibrated and the proper buoyancy corrections were applied.

From 10 to 15 g. of graphite (or 0.5 g. of polystyrene) known to 0.1 mg. was placed in 100 ml. bottles, the screw caps of which were provided with metal foil liners. Approximately 40 g. of the proper electrolyte solution was weighed into each of these bottles; the weight of the solution was known to 0.1 mg.

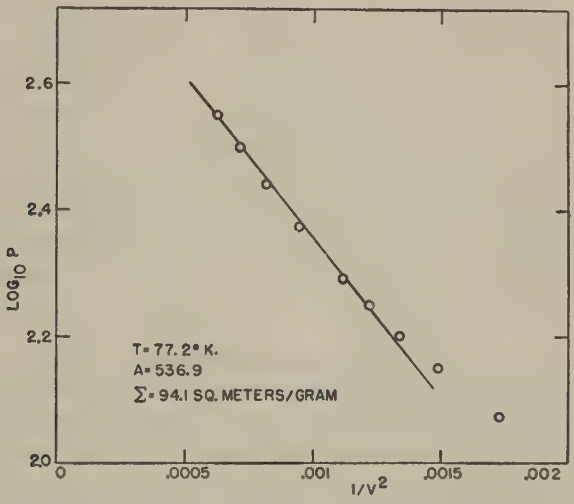

Fig. 5. Harkins and Jura plot of nitrogen adsorption at 77.8°K on polystyrene.

The sample bottles were shaken vigorously by hand and then rotated end-over-end in a bath held to ±0.01°C. for 18 hr. An increase in time of agitation to 170 hr. was found to have no effect on the results. The sample bottles were placed upright in the bath for 2 hr. and much of the solid allowed to settle to the bottom. The adsorbent was then removed by centrifugation and the solution returned to the bath for 15 min. With graphite, a centrifugation time of 5 min. at 5000 *g* was sufficient; with polystyrene 10 min. at 25,000 *g* failed to remove the last traces of adsorbent from suspension. In all cases reported, and on the basis of visual evidence, the graphite was thoroughly dispersed in the electrolyte solution. At several low concentrations of electrolyte, the dispersion was obviously incomplete; these experiments were rejected.

The solutions obtained after removal of the solid were analyzed by means of a Haber-Rayleigh-Zeiss interferometer with a light path of 20 cm. through the solution; these analyses were made at room temperature. Each unknown solution was measured against a reference solution of approximately the same concentration. The unknown solution was then replaced in turn by at least 3 solutions of known composition in the same concentration range as the unknown. The composition of the unknown was then read off the calibration plot thus obtained; the reading was always one of interpolation and in no instance of extrapolation.

With sodium dodecyl sulfate the analyses were carried out directly on the residual solutions. Due to the marked turbidity of potassium myristate solutions in the neighborhood of the critical concentration it was necessary to dilute quantitatively the residual solutions of this salt until clear solutions were obtained. The precision of the myristate measurements is, therefore, somewhat less than that of the sulfate.

Calculations

It is obvious that, in adsorption from solution, both solvent and solute are present in the interfacial region. It is possible, however, in the case of solutions, to calculate the adsorption of one component only if some assumption is made concerning the concentration of the other component in the surface. In the case of the graphite systems let us consider the two possible extremes.

(A) The concentration of water at the interface is zero.

(B) The concentration of water at the interface is equal to the concentration of water on the surface when adsorption takes place from the saturated vapor in the absence of other materials; *i.e.*, the mole fraction of the solvent is unity.

Assumption (A) represents a lower limit that approaches validity as the bulk concentration of water approaches zero; assumption (B) represents an upper limit as the bulk concentration of electrolyte approaches zero.

On the basis of assumption (A) the specific adsorption of the long-chain electrolyte, x, expressed in g. of salt adsorbed/g. of adsorbent, may be calculated from the equation

$$x = \frac{W\,M_s}{Z(1000 + C_1 M_s)}\,(C_1 - C_2), \tag{1}$$

in which W is the weight of solution initially added to the solid; M_s, the molecular weight of the long-chain electrolyte; Z, the weight of the solid adsorbent; and C_1 and C_2, respectively, the molal concentration of electrolyte in solution before and after adsorption.

On the basis of assumption (B) the specific adsorption is given by the equation

$$x = \frac{W\,M_s}{Z(1000 + C_1 M_s)}\left\{C_1 - \left[1 - \frac{S_w Z \Sigma_G M_w \cdot 10}{N_o\,W}\,(1000 + C_1 M_s)\right]{}_2\right\},$$

in which S_w is equal to the number of molecules adsorbed/cm.^{2} from the saturated vapor; Σ_g, the specific surface area of the graphite in m.^{2}/g.; M_w, the molecular weight of water; and N_o, Avogadro's number. The value of S_w may be obtained by crude extrapolation of the data of Harkins, Jura and Loeser (10) as 5×10^{15} molecules/cm.^{2}

Some values of x, the specific adsorption, for sodium dodecyl sulfate on graphite calculated from the experimental observations on the basis of assumption (A) and of assumption (B) are given in Table I.

TABLE I

The Specific Adsorption of Sodium Dodecyl Sulfate on Graphite as Calculated on the Basis of Two Extreme Assumptions Concerning the Concentration of Solvent at the Interface

Equilibrium concentration of salt (molal)	x, Specific adsorption g./g. adsorbent		Deviation of x between assumption (A) and assumption (B)
	Assumption (A)	Assumption (B)	
1.944×10^{-3}	.002022	.002024	0.1%
1.224×10^{-2}	.003206	.003224	0.6%
4.097×10^{-2}	.002472	.002553	2.5%

Actually assumption (B) should depart increasingly from validity as the electrolyte concentration increases. Therefore, since these two assumptions represent extremes, and since the experimental error of the measurements is on the order of 1–2%, any error introduced into the calculation of the adsorption isotherms through lack of information concerning the solvent concentration at the interface is within the experimental error of the measurements herein reported. This may not be true in the case of more concentrated solutions.

Precision and Reproducibility of Results

It is possible that the dispersion of the adsorbent may be incomplete and variable if the experimental technic described above is employed. If such an effect occurs, it should show up in a lack of reproducibility. Although it is difficult and not especially desirable to prepare two identical samples, two such attempts were made. In one instance, values of x were .002434 and .002420 at equilibrium concentrations of 6.175 and 6.177×10^{-3} molal; the deviation in x was 0.7%. In the other instance, the values of x were .003068 and .003051 at equilibrium concentrations of 8.603 and 8.598×10^{-3} molal; the deviation in x was 0.6%. These two results tend to rule out the possibility of error introduced by incomplete dispersion of the solid.

The maximum error introduced in the analyses of the residual solutions should be constant in absolute magnitude with respect to concentration. This maximum error in the interferometric measurements is on the order of $\pm 2 \times 10^{-5}$ in molality. This leads to a maximum error in x of 0.7% in the most concentrated and of 0.8% in the least concentrated solutions investigated. Thus, the maximum possible error in the determination of specific adsorption values is on the order of 1–2%.

Results and Discussion

The isotherms of sodium dodecyl sulfate at 30°C. and of potassium myristate at 35°C. on graphite are plotted in Fig. 6. These isotherms are

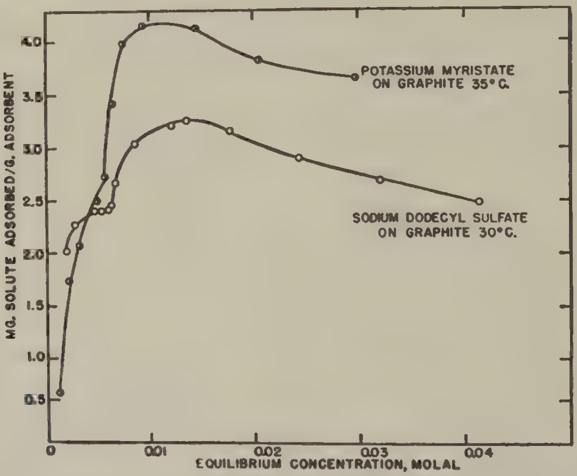

FIG. 6. Adsorption isotherms of sodium dodecyl sulfate at 30°C. and of potassium myristate at 35°C. on graphite.

similar in overall form. With the sulfate a definite discontinuity in the isotherm occurs at the critical concentration for micelle formation (determined by the dye method as 6.1×10^{-3} molal). It is possible that a much less marked discontinuity appears in the myristate isotherm at the critical concentration (5.9×10^{-3} molal). A maximum in the specific adsorption is also apparent in both plots. This maximum occurs at a concentration of approximately 1.3×10^{-2} molal for the sulfate and of 1.0×10^{-2} molal for the myristate. The isotherms of both the sulfate and myristate at concentrations less than the critical concentration are not of the Langmuir or Freundlich types and cannot be represented by the equations characteristic of gaseous or condensed surface films.

Some measurements were made of the adsorption of dodecylammonium chloride, potassium oleate and potassium laurate upon graphite.

No complete isotherms are available, since the supply of graphite was exhausted before this experimental work could be completed. With these three electrolytes, however, it has been definitely established that the adsorption isotherm passes through a maximum.

The areas per adsorbed molecule (or ion), σ, for sodium dodecyl sulfate and potassium myristate are plotted as a function of the equilibrium concentration in Fig. 7; σ is defined as the total surface area of the solid divided by the number of adsorbed molecules. Values of σ for sodium dodecyl sulfate on polystyrene are included in this plot, although they are of little absolute significance. In the relative sense, however, the graphite and polystyrene results are similar in that, in both instances, σ goes through a minimum.

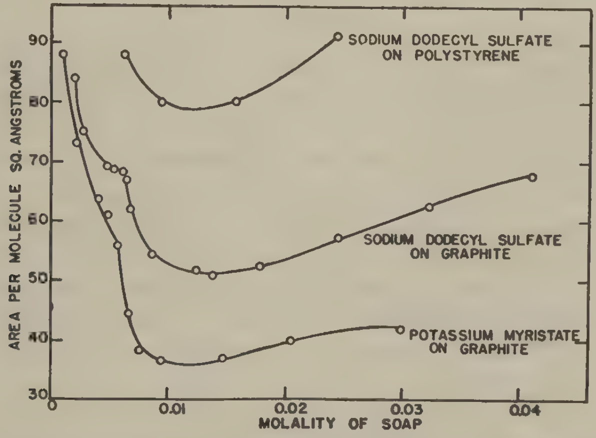

FIG. 7. Areas occupied per adsorbed molecule (or ion) for sodium dodecyl sulfate and potassium myristate on graphite, and of sodium dodecyl sulfate on polystyrene.

With graphite and sodium dodecyl sulfate, σ is 68.3 A^2 at the critical concentration and 51.0 A^2 at the minimum; with potassium myristate σ is 56.0 A^2 at the critical concentration and 36.6 A^2 at the minimum. For potassium laurate the value of σ at the critical concentration is on the order of 45 A^2; this is somewhat higher than that of the myristate.

The values of σ for adsorption from aqueous solution on the graphite surface are considerably greater than those observed for compressed films of fatty acids on an aqueous subphase. This increase in area per adsorbed molecule can possibly be attributed to the existence of repulsive forces between the ionic head-groups of the adsorbed long-chain ions.

It has been shown, on theoretical grounds (11), that the activity of long-chain ions should go through a maximum with respect to overall concentration of the electrolyte if the equilibrium between the single ions, counterions and aggregate is governed by a simple form of the mass action principle. It is impossible to determine experimentally the activity of a single ion. Measurements of the mean ion activity in solutions of dodecyl sulfonic acid (12), however, lend some support to the theoretical arguments. If it be assumed that only single ions are adsorbed at the solid-solution interface, the maximum in the isotherm can be attributed to a maximum in the activity of the adsorbed ion.

The reason for the discontinuity in the sodium dodecyl sulfate isotherm at the critical concentration for micelle formation is unknown. This discontinuity may be in some way related to the discontinuity in the rate of change of surface tension with time at the critical concentration (13). This may indicate that the nature of the adsorption process is altered in the presence of micelles.

SUMMARY

The adsorption isotherms of sodium dodecyl sulfate and potassium myristate on ash-free graphite of known area have been determined at 30°C. and 35°C., respectively. The experimental methods are discussed in some detail. Calculations, based on two extreme assumptions concerning the concentration of solvent in the surface region, yield values of the specific adsorption which differ by less than the experimental errors of the observations. The isotherm of sodium dodecyl sulfate exhibits a discontinuity at the critical concentration for micelle formation; it is possible that a similar discontinuity occurs in the myristate isotherm. Both isotherms pass through a maximum at equilibrium concentrations above the critical concentration.

The adsorption of sodium dodecyl sulfate on polystyrene has been measured over a short concentration range; the specific area of this solid is not known with any degree of precision. This isotherm also exhibits a maximum at approximately the same equilibrium concentration at which a maximum in the isotherm of the same salt on graphite occurs.

The areas per adsorbed molecule have been calculated for sodium dodecyl sulfate and potassium myristate on graphite as a function of the equilibrium concentration of electrolyte. The minimum area per molecule is 51.0 A^2 for the sulfate and 36.6 A^2 for the myristate.

REFERENCES

1. HELD, N. A., AND SAMOCHWALOV, K. N., *Koll.-Z.* **72**, 13 (1935).
2. HELD, N. A., AND KHAINSKY, I. A., *ibid.* **76**, 26 (1936).
3. FISCHER, E. K., AND HARKINS, W. D., *J. Phys. Chem.* **36**, 98 (1932).
4. See VALKO, E. I., *Ann. N. Y. Acad. Sci.* **46** (6), 451 (1946).
5. HOROVITZ, K., *Phys. Rev.* **29**, 617 (1927); JORDAN, H. F., private communication, 1931; EWART, R. H., AND WHITE, L. M., private communication, 1941; HARKINS, W. D., AND ADINOFF, B., private communication, 1943; MARON, S. H., ELDER, M. E., AND ULEVITCH, I. N., private communications, beginning 1945.

6. Corrin, M. L., and Harkins, W. D., *J. Am. Chem. Soc.* **69**, 679 (1947).
7. Brunauer, S., Emmett, P. H., and Teller, E., *ibid.* **60**, 309 (1938).
8. Harkins, W. D., and Jura, G., *ibid.* **66**, 1366 (1944).
9. Jura, G., personal communication.
10. Harkins, W. D., Jura, G., and Loeser, E. H., *J. Am. Chem. Soc.* **68**, 554 (1946).
11. Hartley, G. S., and Murray, R. C., *Trans. Faraday Soc.* **31**, 183 (1935); Wright, K. A., and Tartar, H. V., *J. Am. Chem. Soc.* **61**, 544 (1939); Scott, A. B., Tartar, H. V., and Lingafelter, E. C., *ibid.* **65**, 698 (1943); Wohl, K., *Ann. N. Y. Acad. Sci.* **46** (6), 402 (1946).
12. Neff, L. L., Wheeler, O. L., Tartar, H. V., and Lingafelter, E. C., *J. Am. Chem. Soc.* **70**, 1989 (1948).
13. Powney, J., and Addison, C. C., *Trans. Faraday Soc.* **33**, 1252 (1937); Adam, N. K., and Shute, H. L., *ibid.* **34**, 758 (1938); Nutting, G. C., Long, F. A., and Harkins, W. D., *J. Am. Chem. Soc.* **62**, 1496 (1940); Tartar, H. V., Sivertz, V., and Reitmeier, R. E., *ibid.* **62**, 2375 (1940).

LIGHT SCATTERING INVESTIGATION OF THE STRUCTURE OF TRANSPARENT OIL-WATER DISPERSE SYSTEMS. II

J. H. Schulman and J. A. Friend

From the Department of Colloid Science, University of Cambridge, England

Received February 3, 1949

INTRODUCTION

Following up work by Schulman and McRoberts (1), Schulman and Riley (2) carried out an X-ray investigation of the transparent homogeneous liquid systems which can be obtained by mixing a nonpolar oil and an aqueous solution of a soap, in the presence of a long chain alcohol. By changing the components, either conducting (water-continuous) or nonconducting (oil-continuous) systems could be prepared. It was postulated that the dispersed phase was present in spherical water or oil droplets stabilized by an interfacial mixed monolayer of the soap and alcohol molecules. The droplets were supposed to be arranged in uniform close-packing, as the oil-water ratio was about unity in the cases investigated. On the basis of this model, the diameters and intermicellar distances could be calculated. X-ray long-spacing bands were, in fact, observed in all cases, corresponding to repeat distances which, on the whole, agreed well with the predicted values. X-ray diffraction bands were investigated over the range 90–600 Å.

In an attempt to obtain an independent confirmation of the model suggested, the systems were studied using a light-scattering technique based upon those recently developed for the study of high-polymer solutions. It was, however, more convenient to treat the experimental data from the standpoint of the equations developed by Rayleigh (3) rather than those due to Debye (4) based on Einstein's fluctuation theory and commonly used for the determination of molecular weights. Rayleigh's equation is, for the case of *unpolarized* incident light (see Stiles (5) and La Mer and Sinclair (6)):

$$\frac{i_\theta}{I_o} = \frac{9\pi^2}{2r^2\lambda^4}\left(\frac{m^2-1}{m^2+2}\right)^2(1+\cos^2\theta)NV^2, \qquad (1)$$

where i_θ = intensity of light scattered at angle θ to primary beam.
I_o = intensity of incident light of wavelength (in the solution) λ.
r = distance of the observer from the source of scattered light.
θ = angle between the incident and scattered beams (measured backwards).

m = refractive index of scattering unit w.r.t. solvent.
N = no. of scattering units/cc.
V = volume of scattering unit.

Since NV was known (being the volume of the dispersed phase) it was possible to find V directly. The volume of the interfacial monolayer was included in calculating NV, and hence the volume V will be that of the whole micelle including this monolayer, which is about 25 Å thick.

It is obvious that, in systems such as those described by Schulman and Riley, in which the intermicellar distances were generally of the order of 20 Å, or one-tenth of the micelle diameter, the conditions necessary for the validity of the Rayleigh equation are not satisfied. This equation was derived for gases, in which the scattering by one molecule is independent of any other molecules. The case of dilute solutions is similar, but clearly, at high concentrations, there will be considerable interference between adjacent molecules resulting in a diminished intensity of scattered light; an effect which will be much more noticeable in the present case. Alternatively, if we adopt the terminology of the Einstein-Smoluchowski fluctuation theory (7, 8), in which scattering is regarded as due to local discontinuities in the solvent medium due to the presence of solute molecules, we can say that, because of the high degree of ordering in the liquid lattice, there can only be very small fluctuations. Hence, the scattering will be less than would be expected if the micelles could move independently of each other. In other words, if the Rayleigh equation is used to calculate the micelle diameters, the calculated values will all be too small. Further, if the systems are diluted by increasing the ratio of continuous to dispersed phase, we shall expect that the calculated diameter will increase, and finally the theoretical diameter should be obtained when the micelles are able to move freely. These expectations were, in fact, realized, and the limiting values for the micelle diameters in all the cases investigated agreed very well with those calculated from theory.

It is shown, therefore, that the X-ray diffraction bands give the mean distance between the centers of neighboring micelles and that the light scattering intensities give the diameter of the micelle.

EXPERIMENTAL

The light-scattering apparatus used was of the simplest. A beam of light from a Mazda "Mercra" 80 watt mercury lamp controlled to constant voltage, was rendered parallel by a suitable lens system, and passed through a Wratten No. 50 filter to isolate the 4358 Å line. The solution under examination was contained in a glass cell, 1.3 cm. × 1.3 cm. × 10 cm., and the intensity of the scattered light was measured by means of an R.C.A. 931-A photomultiplier, specially chosen for sensitivity from a large selection, fixed to an arm which could be rotated to take readings at any desired angle of observation. In this work only light scattered at 90° to the incident beam was measured. The cell and photomultiplier were enclosed in a light-tight box to eliminate stray light. The power source for the dynodes consisted of 90 v. dry batteries, which proved quite satisfactory for the purpose. Fatigue of the photo-cell was not troublesome, as it was not operated for more than a few minutes at a time, and the photo-currents encountered were usually below 20μa.

Since the intensity of the direct beam of light from the lamp was 10^4–10^5 times that of the scattered light, it was necessary to reduce it in order to measure it without damaging the photo-cell. This was done by inserting a filter combination consisting of two dark blue and two neutral filters (Hilger glass filters H.508). The transmission of these filters was measured by two methods, as follows:

(a) the transmission was determined using a Spekker absorptiometer, and added: mean value *0.0066*,

(b) the intensity of the transmitted light with the filters in position was compared with that of the incident beam without filters but reflected at 90° to its direction by means of a prism. From the optical constants of the prism and Fresnel's equations, it was found that the reflexion coefficient at 45° incidence was 0.051. Using this figure, the transmission coefficient of the filter combination was found to be *0.0063*. A mean value of *0.00645* was used.

As a check on the direct method of determining i_θ/I_o, a solution of polystyrene of known turbidity was used as a standard of comparison. This enabled the turbidity (τ) of any other solution to be determined, and hence i_θ/I_o could be found from the relation, implicit in Rayleigh's formulae for τ and i_θ/I_o,

$$\tau = \frac{16}{3}\pi r^2 \left(\frac{i}{I_o}\right),$$

where i is now the value of i_θ at $\theta = 90°$. Results obtained by the two methods agreed satisfactorily within the limits of experimental uncertainty, namely ±5%.

Experiments were also carried out using light polarized with its electric vector perpendicular to the plane of the primary and secondary beams. Using the formula valid for this case,

$$\frac{i_\theta}{I_o} = \frac{9\pi^2}{r^2\lambda^4}\left(\frac{m^2-1}{m^2+2}\right)^2 \sin^2\theta\cdot NV^2, \tag{2}$$

results were obtained which agreed very well with those obtained using unpolarized light, *e.g.*,

	Specimen	A 18	A 13	9	A 22
Polarized light	i/I_o	1.83×10^{-5}	2.14×10^{-4}	2.50×10^{-5}	1.20×10^{-5}
Unpolarized light	i/I_o	0.93×10^{-5}	1.16×10^{-4}	1.22×10^{-5}	0.62×10^{-5}

Some depolarization of the light scattered at 90° was observed, but no correction for this was applied in the present work.

The liquids used in the preparation of the mixtures examined were all purified by distillation. Foreign particles, usually such a trouble in light-scattering measurements, were not present in any noticeable quantities, and their effect was, in any case, minimized, as all measurements of the intensity of scattered light were made at 90° to the primary beam.

The refractive indices of the liquids concerned were measured on an Abbé refractometer, which gave results sufficiently accurate for the present purpose. It was assumed that the refractive index of a micelle was the same as that of a mixture of all its components in the proportions in which they were present in the micelle. It was found experimentally that this was almost exactly that calculated, assuming that the refractive indices of the components could be added to give the refractive index of the mixture; and this was used to calculate the refractive index of a mixture which was too opaque for accurate measurement in the refractometer. The results tabulated below are typical.

System	*n*(calc.)	*n* (obs.)
1.0 cc. oleic acid 5.0 cc. 0.316 *N* KOH 0.4 cc. *p*-methylcyclohexanol	1.3657	1.3660
1.5 cc. oleic acid 5.0 cc. 0.474 *N* KOH 0.6 cc. *p*-methylcyclohexanol	1.3774	1.3780

The mixtures were prepared as previously described (1, 2) by adding an alcohol *slowly* (it is essential to add the alcohol very slowly in the initial stages), to a mixture of oil and aqueous soap solution, stirring vigorously all the time. A complete study was made of the system water-potassium oleate-benzene-*p*-methylcyclohexanol, and the results obtained are described in this paper.

To study the effect of dilution upon the apparent diameter of the micelles, the volume of benzene added was varied, all other quantities being kept constant, thus keeping the size of the micelles constant in a given series. Systems containing 0.75, 1.00, 1.50, 2.00, and 3.16 cc. oleic acid neutralized with the correct quantity of KOH dissolved in 5.0 cc. water, were studied. The volume of benzene was varied from 5.0 cc. to 30.0 cc. where possible. The total volume of the micellar phase was calculated from the known quantities taken. There was always some excess *p*-methylcyclohexanol present, which dissolved in the benzene and increased the volume of the continuous phase. In most cases, several times the theoretical volume of alcohol was necessary to obtain a fluid transparent solution, and the quantity required was usually not the same for any two systems containing the same volume of oleic acid and other ingredients, a phenomenon which appears in the earlier work (see, for example, Schulman and Riley's (2) Table I, specimens 9, 10, 17, 18, and 20, 21). Our experimental results are tabulated below:

TABLE I

Vol. of oleic acid	Specimen no.	NV	g	d (Å)	Log d	d_o (Å) from graph
0.75 cc.	A 48	0.442	1.53	80	1.90	330
	A 50	0.301	2.82	108	2.04	(Calc., 363)
	A 49	0.202	4.80	143	2.16	
	A 51	0.183	5.41	168	2.23	
1.00 cc.	A 33	0.420	1.77	62	1.79	283
	A 39	0.246	3.92	115	2.06	(Calc., 280)
	A 32	0.142	7.77	173	2.24	
1.50 cc.	A 35	0.520	1.31	32	1.51	210
	A 36	0.358	2.55	58	1.76	(Calc., 201)
	A 37	0.232	4.71	90	1.95	
	A 31	0.192	5.97	112	2.05	
	A 38	0.167	7.10	114	2.06	
2.00 cc.	A 40	0.569	1.18	31	1.49	165
	A 41	0.409	2.25	44	1.65	(Calc., 164)
	A 42	0.259	4.46	72	1.86	
	A 43	0.190	6.65	93	1.97	
3.16 cc.	A 45	0.564	1.48	29	1.46	107
	A 46	0.433	2.47	31	1.49	(Calc., 120)
	A 47	0.291	4.60	47	1.67	
	A 44	0.214	6.92	57	1.76	

NV represents the total volume of micellar phase per cc. of solution, *i.e.*, it is the volume concentration of micelles in the solution. However, the densities of all the micelles can be taken as 1.00, so that NV is equal to the concentration of micellas in g./cc. of solution. d is the diameter calculated from the Rayleigh formula. d_o is the limiting diameter as determined from Fig. 1.

It should be noted that the phase ratio g of Schulman and Riley was calculated neglecting the volume of the interfacial monolayer which forms the surface of a micelle. When allowance is made for this, it is easy to construct curves similar to those of their Fig. 5, showing the gap between spheres of a given diameter at different phase ratios. From such a diagram it can be seen that for diameters of 100, 200 and 400 Å, the gaps at $g = 5.0$ are 10, 64 and 185 Å, respectively. Hence, there will still be interference in the light scattered from these solutions, and much higher phase ratios would be necessary to eliminate this effect. It has not proved possible to achieve this. The highest value of g used (from Table I) was 7.77 in specimen A 32. From Schulman and Riley's formula (10) it is calculated that the intermicellar gap for a diameter of 280 Å would be 160 Å, so that, even under the best conditions obtained, the spheres are still quite closely packed. Systems more dilute than those described have not been prepared for this system.

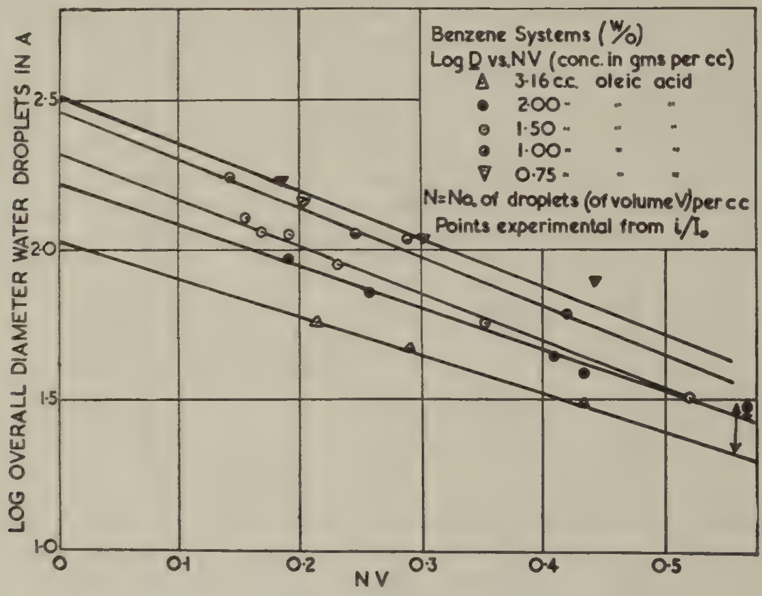

FIG. 1.

It was clear from the experimental results that some form of extrapolation to infinite dilution was necessary to obtain the true diameter of the micelles. That the data should be represented by a graph of log d against concentration (*i.e.*, NV) was suggested by the following consideration:

We have from Rayleigh's formula, for micelles of a given size

$$\frac{i}{I_o} = K \cdot NV^2; \qquad \text{and} \qquad \frac{i_o}{I_o} = K \cdot NV_o^2,$$

where i, i_o are the apparent and true values of the scattered intensity at 90°, and V, V_o are the apparent and real micellar volumes. Now it is reasonable to assume that i and i_o are related by an exponential formula; *i.e.*, we write, following Rayleigh (9),

$$i = i_o \cdot e^{-\mu N V_o^2},$$

since the loss in intensity of i may be regarded as due to secondary scattering effects; in the case of independent particles we should, of course, have $\mu = \frac{24\pi^3}{\lambda^4}\left(\frac{m^2 - 1}{m^2 + 2}\right)^2 \cdot l$ where l is the distance travelled by the scattered light through the solution. (However, in this case there would, of course, be no secondary scattering.) We then have

$$KNV^2 = KNV_o^2 \cdot e^{-\mu N V_o^2},$$

or

$$\log (KNV^2) = \log (KNV_o^2) - 2.30\mu\, NV_o^2,$$

which may be written

$$\begin{aligned} \log d &= \log d_o - A \cdot V_o(NV_o), \\ &= \log d_o - B(NV_o), \end{aligned}$$

where A and B are constants and d_o is the true diameter of the spheres.

The graphs in Fig. 1 were plotted assuming this relationship, and it is clear that it represents the experimental facts well. The values of d_o in Table I were obtained from this graph, and with the values of the slope B, similarly obtained, were used to construct the curves in Fig. 2, which show how the original experimental data fit an exponential formula. The irregularities in the region of high concentration (0.4–0.6 g./cc.) are only to be expected, as there the systems are "squashed," *i.e.*, display negative spacings [see Table II of ref. (2)]. However, the values of d_o agree extremely well with the calculated diameters, and it seems clear that the model suggested for these systems is the correct one. Absorption of the 4358 Å light was significant in the most concentrated systems, and spectrophotometric measurements indicated that the values of d for the spheres should be increased by about 3%. This has not been done in the Table, as little meaning can be attached to exact values under these conditions.

A measurement was made on specimen A 51, using a yellow filter isolating the lines of λ 5770 Å and λ 5790 Å; and an apparent diameter of 212 Å was found, compared with 168 Å when light λ 4358 Å was used. It is probable that this is due to the large size of the spheres, which are approaching the limit of λ/15, above which intramicellar effects would be expected to cause a diminution in the observed intensity of the scattered light. (See Rayleigh's law.)

Two specimens were examined which contained caesium iodide in the aqueous phase. One (A 52) contained 2.00 cc. oleic acid and 20.0 cc.

benzene with the intramicellar phase, 0.45 *M* with respect to CsI. The other (A 53) contained 1.50 cc. oleic acid and 30.0 cc. benzene, and the micelles were 0.81 *M* with respect to CsI. The experimental diameters were 80 Å and 148 Å, respectively, whereas those for specimens of the same composition, but having no CsI in the aqueous phase are, from Fig. 2, 70 Å and 110 Å, approximately. It seems, therefore, that the presence of salts causes an increase in the area occupied by the potassium oleate molecules in the interfacial layer.

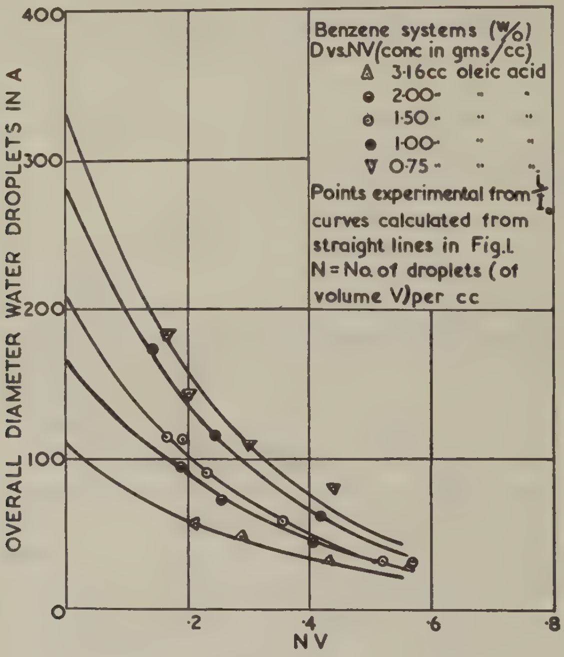

FIG. 2.

A corresponding study of the nujol-in-water systems described by Schulman and Riley is made difficult by the two following considerations:

(1) Any excess *p*-methylcyclohexanol will remain in the interior of the micelles, and will, therefore, swell them by different amounts for each member of a series having the same volume of intramicellar phase.

(2) Since there is an equilibrium between potassium oleate in the micelles and in the aqueous phase, dilution of the systems by simply increasing the volume of water taken will cause soap molecules to leave the interfaces. This will mean a change in the size of the droplets, which will become progressively larger for a given quantity of soap, as the phase ratio is increased.

Both these factors mean that the dispersed micelles change their character in a manner which does not occur with the oil-continuous systems on dilution.

An attempt was made to prepare a water-continuous series containing 2.00 cc. oleic acid in the micelles, using a dilute solution of potassium oleate as continuous phase. The concentration adopted for this solution was 1%, the amount of oleic acid assumed by Schulman and Riley to be present in the bulk aqueous phase. The first homogeneous phase to be obtained with specimens containing 5 cc. and 10 cc. aqueous phase was a transparent, birefringent gel. On adding more *p*-methylcyclohexanol, the gel broke into two liquid layers, and, with still more alcohol, redispersed giving a clear conducting liquid system, non-birefringent and resembling, except for a somewhat higher viscosity, those obtained in the first part of this work. The phase ratios, however (calculated from the formula given by Schulman and Riley) were 0.67 and 1.03, and it is clear that the systems were too tightly packed for the light-scattering to be of any significance.

On the other hand, when the aqueous phase had a volume of 20 cc., a homogeneous liquid system formed first with about 3 cc. *p*-methylcyclohexanol (intermediate between the 3.0 and 5.5 cc. required in the cases mentioned above). However, the system was a good deal more viscous than the liquid systems prepared with much less water present. This, coupled with the small amount of *p*-methylcyclohexanol required, seemed to indicate that what had been obtained was really analogous to the gel phase of the 5 cc. and 10 cc. systems, rather than to their liquid phases. However, it proved impossible to obtain this second stage by adding more *p*-methylcyclohexanol, as the only result was to cause a turbidity in the viscous system, which finally broke up.

Incidentally, it seems, from experiments carried out, that the volume of alcohol necessary to form a gel does not vary from member to member of a series to the same extent as the volume required for a liquid system.

Discussion of Results

It can be seen from the investigation of the structure of the oil-water disperse system, by (1) surface physicochemical methods, giving information as to the extent of the interfacial area, the structure of the interface, and phase continuity, by (2) the X-ray method, giving the dimension of the distance between the centers of neighboring aggregates, and by the light scattering method, giving the diameter of the aggregate, that these systems are composed of spherical micelles of either water droplets in oil-continuous media or oil droplets in water-continuous media, which are surrounded by a mixed monolayer of the soap molecule and amphipathic dispersing molecule. The overlapping results from these investigations give one not only information on the structure of these systems, but confirmation of the validity of the various laws that one is applying.

a. Rayleigh's Law

It can be seen from the light-scattering data in Table I that the sizes of the aggregates at infinite dilution agree with Rayleigh's formula, except when the ratio of the dimension of the aggregate to the wave length is greater than 1/15, when the law no longer holds. It is known further that, for large particles, if the aggregates are not spherical, the relationship between the intensity of the scattered light at 90° is no longer dependent on the fourth power of the wavelength, but on the second power. A correction factor for the dissymmetry of scattering of the large aggregate as described by Debye (4) enables the fourth power law to be applied.

b. Smoluchowski-Einstein Theory

In a dilution series, as seen in Fig. 3, of the droplets of constant diameter, it is evident that there is very little light-scattering from the concentrated aggregate systems, which upon dilution give strong light-scattering. The intensity of this scattering in the dilute systems is, of course, related to the size of the aggregate in relation to the wavelength of the incident light. Fig. 3 gives the dilution effect on the light scattering, the intensity of which increases on dilution. The tubes refer to points on the 1 cc. oleic acid curve in Fig. 2. It is assumed that, in the concentrated systems, no concentration fluctuations can occur sufficient to produce much light scattering (11).

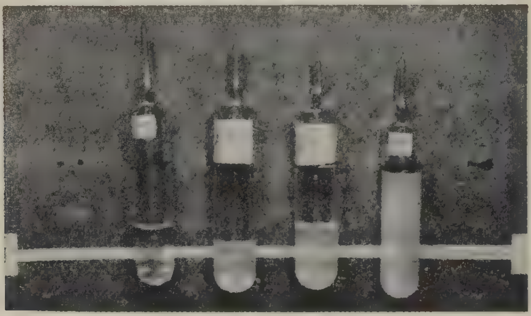

FIG. 3. Concentration series diameter size 280 Å, showing diminution of light-scattering on increasing concentration of water droplets in benzene.

(c) *Effect of Increasing the Wavelength of the Incident Light*

In Fig. 4 is shown the increase in light-scattering due to the increasing diameter of the spherical droplets at approximately the same concentration throughout (see Table I). It is interesting that the light-scattering is radically reduced if the tubes are viewed with a red lamp, no pronounced light-scattering being visible in the above series under these conditions, as expected from Rayleigh's law with the long wavelengths.

d. Comparisons between Light Scattering and X-Ray Diffraction Measurements

It can be seen in comparing the X-ray with the light-scattering results for the diameters of the aggregates with decreasing quantity of soap-alcohol complex, that the corrected Bragg X-ray figures for large diameters are greater than those calculated from surface chemical data, whereas the light scattering results follow very closely the calculated values. All three values are in close agreement for diameters less than 300 Å.

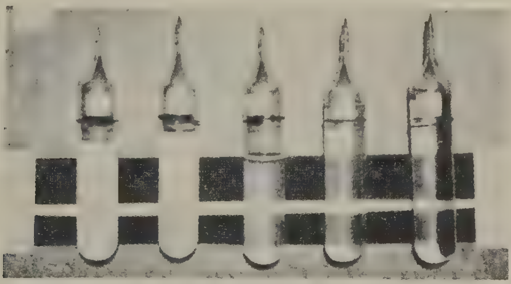

FIG. 4. Shows increase of light-scattering as diameter of water droplets increase. All tubes contain a dilute concentration of water droplets in benzene. (Left to right A51 A32 A31 A43 A44)

The uncorrected Bragg X-ray figures for the large diameters seem to fit the surface chemical and light-scattering results much better. It was suggested by Schulman and Riley that the 1.23 liquid correction factor need not remain constant for varying particle diameter. There seems to be evidence in comparing the values for the diameters of the micelles by the three different methods, that the 1.23 factor might be approaching unity with increasing diameter of particle.

e. Viscosity Changes in the Water-Continuous Systems

Recently, Winsor (10) has described the preparation of various oil-water disperse systems, but does not seem to be in agreement that the systems are composed of spherical oil or water droplets surrounded by a mixed monolayer of the soap and alcohol molecules for the water- or oil-continuous systems. The structures of those systems giving anomalous electrical conductivity, with a streaming birefringence and high viscosity, has still to be worked out, and are almost certainly composed of lamellar or cylindrical shaped aggregates. In the preparation of the water-continuous systems as described here, a transparent birefringent highly viscous phase could be detected as already described by Winsor. This reverts to a thin non-birefringent system on further titration with the alcohol, and it is interesting that, if these systems are made dilute with water, which is the continuous phase, they become very viscous again.

It could be supposed that, since these preparations contain a high concentration of soap, the location of the soap molecules is important for the overall viscosity. If the soap molecules are in the interface of the spherical aggregates, the system will be of low viscosity, but, if some of the soap passed into the bulk phase, which would occur on dilution for the water-continuous systems, the overall viscosity would markedly increase. This, of course, would not take place on dilution of the water droplets in an oil-continuous medium, and this is confirmed experimentally.

f. Comparison with the Light-Scattering Work on Polymer Solutions

Previous work on the determination of size and shape of polymers by the light-scattering method has given good agreement between the molecular weights determined by this method and other standard methods (osmotic pressure, ultracentrifuge, and X-ray), using the Debye formulation of the Smoluchowski-Einstein concept. Schulz's work (3c), using the Rayleigh formula for polystyrene solutions, gives very poor agreement between the determined and osmotic pressure molecular weights. Polymers of molecular weights up to 600,000 were tried. In this work with spherical water droplets, good agreement was obtained with X-ray determinations and surface chemistry up to an apparent molecular weight for the 360 Å diameter droplets of nearly 30,000,000. Schulz's paper only became available after this work was completed. Staudinger's work (3b) on this subject, which is not yet available, found good agreement in the case of glycogen solutions using the Rayleigh formula, as compared with osmotic measurements.

ACKNOWLEDGMENTS

We are greatly indebted to Dr. P. Doty, Harvard University, for originally building the light scattering apparatus, and for much help in improvements.

One of us (J. A. F.) is indebted to the Australian Council for Scientific and Industrial Research for the award of a Senior Studentship during the tenure of which this work was carried out.

SUMMARY

A light-scattering investigation was carried out on the oil-water disperse systems to augment the information on their structure as found by X-ray and surface chemical methods.

It was found that the concept that the transparent non-birefringent oil-continuous oil-water disperse system consisted of water droplets of uniform size and packing surrounded by a mixed monolayer of soap and long chain alcohol molecules, was in agreement with the light-scattering results.

Using Rayleigh's formula, dimensions were obtained for the diameters of the droplets over the range 100–400 Å agreeing with those calculated by surface chemical methods.

REFERENCES

1. SCHULMAN, J. H., AND MCROBERTS, T. S., *Trans. Fadaday Soc.* **42B**, 165 (1946).
2. SCHULMAN, J. H., AND RILEY, D. P., *J. Colloid Sci.* **3**, 383 (1948).
3. (a) RAYLEIGH, LORD (Hon. J. W. STRUTT), *Phil. Mag.* [4] **41**, 107 (1871).
    (b) STAUDINGER, H., *J. makromol. Chem.* **1**, 185 (1943).
    (c) SCHULZ, G. V., *Z. physik. Chem.* **194**, 1 (1944).
4. DEBYE, P., *J. Phys. Colloid Chem.* **51**, 18 (1947).
5. STILES, W. S., *Phil. Mag.* [7] **7**, 204 (1929).
6. (a) LA MER, V. K., AND SINCLAIR, D., *O.S.R.D. Rept. No.* **1857** (1943).
    (b) SINCLAIR, D., *J. Optical Soc. Am.* **37**, 475 (1947).
7. EINSTEIN, A., *Ann. Physik* **33**, 1275 (1910).
8. SMOLUCHOWSKI, M., *ibid.* **25**, 205 (1908).
9. RAYLEIGH, LORD, *Phil. Mag.* [5] **47**, 375 (1899).
10. WINSOR, P. A., *Trans. Faraday Soc.* **44**, 376 (1948).
11. OSTER, G., DOTY, P. M., AND ZIMM, B. H., *J. Am. Chem. Soc.* **69**, 1193 (1947).

DETECTION OF A WALL EFFECT IN LAMINAR FLOW OF SOLUTIONS OF A LINEAR POLYMER

B. A. Toms

Courtaulds, Limited, Research Laboratory, Maidenhead, Berks., England

Received February 9, 1949

INTRODUCTION

In a recent discussion (1) of experimental observations on the flow of solutions of polymethyl methacrylate through straight tubes at large Reynolds numbers, I adduced evidence of anomalous behavior near the tube wall when the mainstream had ceased to be laminar. The present paper is concerned with results which were obtained at the same time, and with the same liquids, but which refer mainly to laminar flow. These data are interesting for two reasons: they indicate that there is a "wall effect" in laminar flow of linear polymer solutions, and they serve also to establish concordance between two methods (one of them new) of detecting a flow anomaly of this kind (2,3). In addition, a critical Reynolds number for the breakdown of laminar flow in linear polymer solutions has been determined.

Notation

a = radius of bore of flow tube (cm.).
C = polymer concentration (g./l., of solution).
l = length of flow tube (cm.).
p = measured pressure head (dynes/cm.^{2}).
$-dp/dz$ = pressure gradient along axis of flow tube (dynes/cm.^{3}).
Q = Volume rate of flow (cm.^{3}/sec.).
R = Reynolds Number = $2a\rho U_m\phi$ (dimensionless).
R_0, R_1 = Values of R corresponding with ϕ_0 and ϕ_1 respectively.
U_m = $Q/\pi a^2$ = mean linear rate of flow along axis of tube (cm./sec.).
w_a = $\tau\zeta(\tau)$ = effective velocity of slip (cm./sec.).
η = coefficient of viscosity, defined as the ratio of shear stress to velocity gradient in material remote from boundaries (poise).
η_0, η_1 = limiting values of η at very small and very large rates of strain, respectively.

η_{sp} = $(\eta_{\text{solution}}/\eta_{\text{solvent}} - 1)$.

$[\eta]$ = intrinsic viscosity of polymer, defined as $\underset{c \to 0}{\text{Limit}} (\eta_{sp}/c)$, where c is expressed as grams of polymer per 100 ml. of solution.

ζ = an effective slip coefficient at the tube wall, a function of τ.

ζ_0, ζ_1 = limiting values of ζ at low and high stresses, respectively.

ρ = density (g./cm.^{3}).

σ = slope of asymptote to (U_m, τ) curve.

σ_0 = intercept on σ-axis of (σ, a) curve.

$\tau = \frac{1}{2}a\left(-\frac{dp}{dz}\right)$ = shear stress at tube wall (dynes/cm.^{2}).

$\phi = \frac{1}{\eta} = \frac{8Q}{\pi a^4}\bigg/\left(-\frac{dp}{dz}\right)$ = apparent fluidity as defined by Poiseuille's formula.

ϕ_0, ϕ_1 = limiting values of ϕ corresponding with η_0, η_1.

EXPERIMENTAL

Materials

The polymethyl methacrylate was a commercial specimen which had been ground to a powder. The intrinsic viscosity $[\eta]$, determined in monochlorobenzene solution at 25°C., was found to be 3.90. The chain-length distribution of the polymer was unknown.

The solvent used throughout was redistilled monochlorobenzene having $\rho_{25} = 1.09950$ g./cm.^{3} and $\eta_{25} = 7.56 \times 10^{-3}$ poise.

Polymer solutions were gently mixed at room temperature, solutions of smaller concentration being obtained by progressive dilution of a stock containing 30 g. polymer/l.

Apparatus and Methods

Flow Tubes. Four straight metal tubes of uniform bore and circular cross-section were used. Their ends had been cut off square by means of a lathe.

TABLE I

Dimensions of Metal Flow Tubes

Tube no.		Composition	a	l	Wall thickness
					cm.
"A"	A1	Brass	0.202 ± 0.0016	12.5	0.053
	A2	Brass	0.202 ± 0.0016	25.0	0.053
	A3	Brass	0.202 ± 0.0016	50.0	0.053
B		Duralumin	0.064_5	50.0	0.094

Experiments on Flow at Large Reynolds Numbers. The flow tube (A1, A2, A3, or B) was fitted with 2 rubber bungs (one being pushed on from each end) and these were inserted into the base-holes of two straight-sided aspirator bottles of conventional pattern (capacity 2000 ml.). In this way, there was assembled an apparatus comprising two upright cylindrical glass jars connected, near their bases, by a horizontal straight tube, one end of which projected a short distance into the body of each reservoir. It was arranged that this apparatus could be immersed in water kept at 25°C. (±0.1°).

Two horizontal lines were scratched on the outside of one reservoir: these indicated a difference in level corresponding to 1000 ml. of water at 25°C. The positions of these marks were such that the liquid surface stood midway between them when the assembled apparatus contained 2000 ml. of liquid and the air pressure was the same in both reservoirs.

This apparatus was joined in a pneumatic circuit designed so that the air pressure above the liquid surface in one reservoir of the flow apparatus could be varied independently of that in the other. Thus, with one reservoir open to the atmosphere and the other connected with a partially evacuated vessel of 200 l. capacity, liquid could be made to pass at constant speed, through the flow tube, from one bottle to the other; and the flow could quickly be stopped, or its direction reversed, by appropriate manipulation of two 3-way taps. The pressure head causing flow was shown on a mercury manometer; the rate of flow Q was found by measuring the time required for the liquid level to fall from the upper to the lower scratch-mark on the graduated reservoir.

By this method the rates of flow corresponding to a number (usually about 35) of pressure heads between 10 and 500 mm. Hg could rapidly be determined. The scatter amongst measurements was satisfactorily small, and smooth curves were drawn through the plotted points giving the relation between Q and pressure head for the passage of each liquid through the 4 tubes. Average values of p, corresponding to selected values of Q, were read off from these curves and were the data from which proper pressure gradient/rate of flow relations were subsequently derived.

Experiments on Flow at Small Reynolds Numbers. In the case of tube B, which was comparatively long and of narrow bore, the volume rate of flow did not exceed 5 cm.^{3}/sec., even when the greatest possible pressure head (500 mm. Hg) was used. It was, therefore, practicable to make reliable experiments with tube B at quite small rates of flow using the apparatus described above. This could not be done with tube A, or at any rate with the shorter lengths of it (A1, A2) and so another flow apparatus was made: this was modeled on the pattern first described by Erk (4), and contained the flow tubes A1 (l = 12.5) and A3 (l = 50). These tubes were connected together in series, and the form of the apparatus made it possible to measure the fall in (hydrostatic) pressure between the ends of each tube when liquid passed through the assembly with a range of small, constant speeds. Rates of flow were determined by measuring the time required to discharge a known volume from an exit tube. The apparatus was immersed in water kept at 25°C. (±0.1°), and yielded reproducible results which were consistent with those obtained for tube A with the other flow apparatus.

Experimental Determination of the Nature of the Flow Régime. For a Newtonian liquid, the familiar Reynolds number serves to define conditions favorable to the persistence of either laminar or turbulent flow during passage of the liquid through a tube. In the case of a non-Newtonian liquid, however, for which the viscosity is a function of the rate of shear, it is not immediately obvious how a Reynolds number should be computed. It is, however, reasonable to assume that only those limiting values of the viscosity which are defined as η_0 and η_1 could be considered in this connection. To determine which of these 2 parameters was the more suitable, it was decided to use an adaptation of that elegant method for determining the nature of the flow régime in a pipe which was first used by Osborne Reynolds (5).

RESULTS AND DISCUSSION

Determination of the Pressure Gradient/Rate of Flow Relations

From Observations Made with Tube A. As explained, the experimental results were reduced, for each of the liquids examined, to a set of smoothed values of p and Q. There were thus available, for each liquid, 3 values representing the pressure heads required to maintain a specified rate of flow in each of the 3 pieces of tube A. When it had been confirmed (by combining the results obtained from the 3 lengths of tube) that uniform flow conditions had been reached, corresponding values of Q and $-dp/dz$ were readily derived. That is to say, appropriate correction was made for the reduction, or loss, of pressure head effective in causing flow which arises from the acquisition of kinetic energy by the flowing liquid and through that local dissipation of energy which occurs where a liquid enters a tube from a reservoir ("Couette effect"). It is of interest that, for all the liquids examined and over the whole range of observed values of Q, the total loss of head attributable to the causes mentioned was found to be very nearly equal to ρU_m^2.

It may be noted here that all the measurements made with tube A2 were repeated in each of 3 straight tubes having the same linear dimensions as A2 but differing from it in regard to the shape of the entrance end. Apart from the expected observation that a bellmouth reduced the total pressure head required to maintain a given rate of flow, the results obtained differed in no essential feature from those secured with Tube A2.

From Observations Made with Tube B. Since only one length of tube B had been used in the experiments, it was necessary, in making the analysis of the smoothed data (p, Q values), to adopt a slightly different procedure. It seemed reasonable to suppose that the magnitude of the overall allowance to be made for end effects and the kinetic energy correction should be the same as that which had been found for tube A. Each observed value of p, the pressure head, was, therefore, reduced by an amount equal to ρU_m^2 and the remainder was regarded as the pressure head effective in causing the observed flow through tube B.

Treatment of the Pressure Gradient/Rate of Flow Data

By the Method of Schofield and Blair (2). For each liquid, $Q/\pi a^2$ was plotted against τ and the slope σ of this curve was estimated in the region just before the breakdown of laminar flow. Two values of σ, corresponding to tubes A and B, were, of course, obtained for each liquid. These were plotted against a and joined by a straight line. In the cases of monochlorobenzene and those solutions in which the concentration of polymer did not exceed 2.5 g./l., this straight line, when produced, passed through the origin. By definition, its slope was equal to $\phi_1/4$ where ϕ_1 represents the fluidity at large rates of shear. With the more concentrated polymer solutions, however, the straight line joining the (two) plotted points made an intercept on the σ-axis. It was assumed, following Schofield and Blair, that the slope of this line represented $\phi_1/4$ and that the positive values of σ_0 were indicative of anomalous behavior in a layer of liquid close to the tube wall.

In Fig. 1, values of ϕ_1 and σ_0 determined in this way are shown plotted against C, the polymer concentration, a broken line being used for the (σ_0, C) curve.

By Oldroyd's Method (3). For the detection and analysis of anomalous behavior near the tube wall in laminar flow, Oldroyd has recommended an examination of the curves obtained by plotting ϕ against $1/\tau$, using smoothed pressure gradient/rate of flow data from experiments in at least two sizes of tube. In the case of a material which behaves isotropically everywhere during deformation there exists a unique relation, $\phi = F(1/\tau)$, and hence all the experimental data will be found to lie on the same curve, enabling η_0, η_1 to be determined directly. Departures of the plotted points from this curve will commence, for each tube, at the value of $1/\tau$ at which R_1, the Reynolds number, attains its critical value, denoting the breakdown of laminar flow. But if, on the other hand, the observed (ϕ, $1/\tau$) curves for different tubes differ at Reynolds numbers below the critical, and if, moreover, the relative displacements of the curves are consistent with the general relation

$$\phi = F(1/\tau) + 4\zeta(\tau)/a, \tag{1}$$

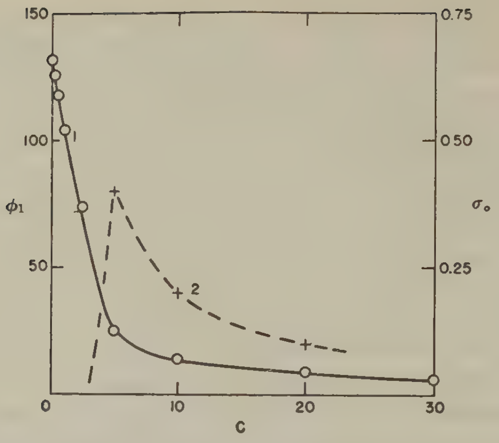

FIG. 1. The relations between (1) ϕ_1 and C, and (2) σ_0 and C.

then it is reasonable to suppose that a thin layer with anisotropic rheological properties exists near the tube wall. In such a case, if the curves are sufficiently well defined by large numbers of consistent readings from different tubes, Eq. (1) can be used to obtain $F(1/\tau)$ and $\zeta(\tau)$. This will enable the curve $\phi = F(1/\tau)$ to be constructed and used, as for a liquid not showing wall effects, to define the stress/rate of strain relationship for the material in an isotropic condition (*i.e.*, remote from boundaries).

The ϕ, $1/\tau$ data for monochlorobenzene are shown graphically in Fig. 2. The value of $1/\tau$ corresponding with $R = 2000$ is indicated for each

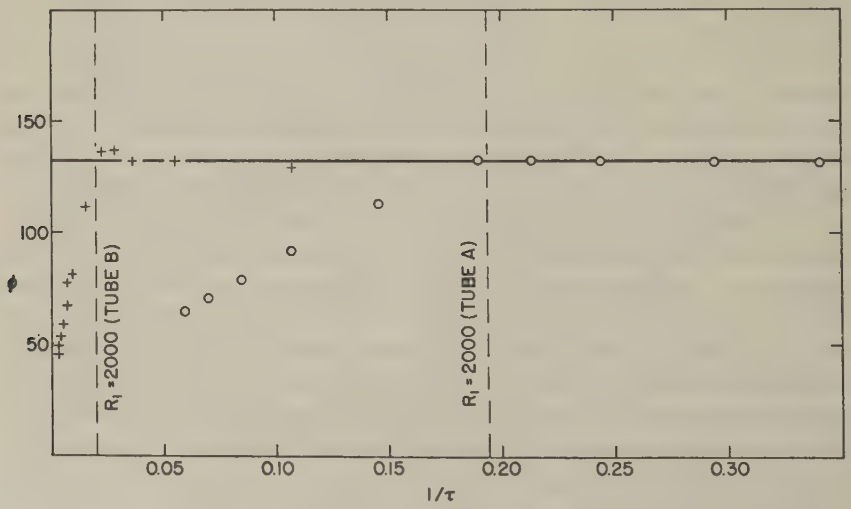

FIG. 2. The relations between ϕ and $1/\tau$ for tube A(⊙) and tube B(+) with $C = 0$.

flow tube: this was the critical Reynolds number, denoting the breakdown of laminar flow, which was deduced from experiments with a "color filament" (5). It can be seen (Fig. 2) that the values of ϕ relating to laminar flow in both tubes lie on a single curve which, as is appropriate to the case of a Newtonian liquid, is a straight line parallel to the $1/\tau$-axis. The value $\phi = 132$ represented by the drawn line, is in excellent agreement with the fluidity of monochlorobenzene determined by means of a standard U-tube viscometer.

With the addition of polymer to the solvent in amounts up to, and including, 2.50 g./l. it was found that, although a single curve could still be drawn through the plotted points (ϕ, $1/\tau$) pertaining to laminar flow in both tubes, this curve was no longer a straight line. Instead, as C increased, a tendency for ϕ to increase with τ grew more pronounced.

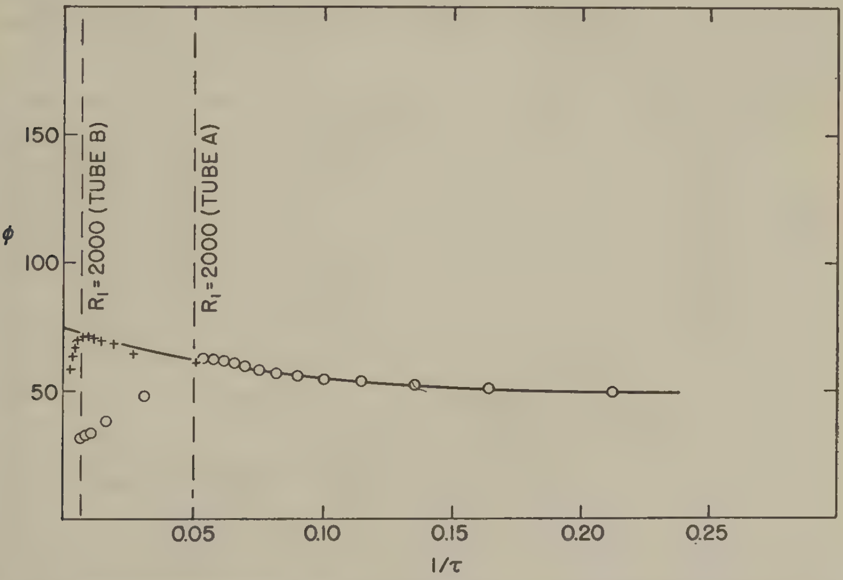

FIG. 3. The relations between ϕ and $1/\tau$ for tube A(⊙) and tube B(+) with $C = 2.50$.

Nevertheless, extrapolation of the curve to $1/\tau = 0$ gave, for each solution having $C \leqslant 2.50$, a value of ϕ_1 which was the same as that found by the method of Schofield and Blair. Moreover, the breakdown of laminar flow was satisfactorily indicated in every case by $R_1 = 2000$. All these features are shown in Fig. 3, wherein the ϕ, $1/\tau$ data for $C = 2.50$ have been plotted.

The failure to detect a wall effect when $C \leqslant 2.50$ is consistent with the finding (*cf.* Fig. 1) that $\sigma_0 = 0$ in each of these liquids, for σ_0 is to be identified with ζ_1 (3). The incidence of a wall effect, of the kind defined by

Oldroyd, was first detected in the flow data for a solution containing 5 g. of polymer/l., and the effect persisted when C was increased to 10 g./l. Unfortunately, the available data for $C = 20$ and $C = 30$ were insufficient for analysis by the present method. In Fig. 4 the ϕ, $1/\tau$ curves for $C = 10.0$ are shown. The separate curves, one for tube A and the other for tube B, that were obtained in laminar flow can clearly be seen, and it will also be observed that a definite departure from the conditions of laminar flow had occurred in experiments at large stresses in tube A but not in tube B. A similar conclusion was reached by plotting the ϕ, $1/\tau$ curves for $C = 5.00$, though in this case, where a less viscous liquid was involved, the transition region was more nearly approached in the experiments with the narrower tube.

Continuing this analysis of data for $C = 5.00$ and $C = 10.0$, there followed next the evaluation of $F(1/\tau)$ and of ζ for selected values of τ. This was accomplished arithmetically using the forms of Eq. (1) appropriate to the two flow tubes.

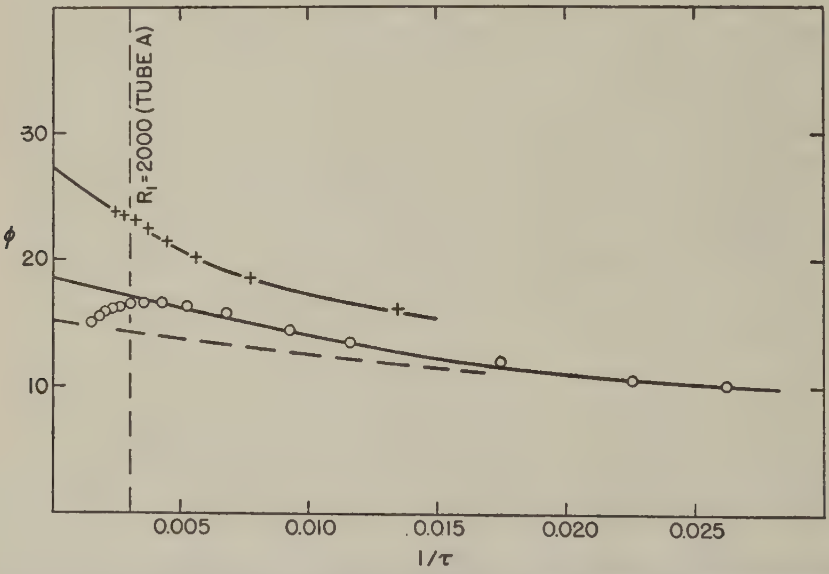

FIG. 4. The relations between ϕ and $1/\tau$ for tube A(⊙) and tube B(+) with $C = 100$. The broken line represents $\phi = F(1/\tau)$.

The curve $\phi = F(1/\tau)$ pertaining to $C = 10.0$ is shown broken in Fig. 4: extrapolation of this curve to $1/\tau = 0$ gave $\phi_1 = 15$, which is very nearly the same as the fluidity of this polymer solution at large rates of strain as was found by the method of Schofield and Blair (Fig. 1). Close agreement between the values of ϕ_1 determined by the two methods was also secured in the case of the solution containing 5.00 g. of polymer/l.

Finally, Fig. 5 comprises the curves relating ζ and τ for $C = 5.00$ and $C = 10.0$. It can be seen that as τ increases from zero, the effective slip coefficient ζ increases very rapidly and attains, over a narrow range of stresses, a value only slightly less than its limiting value ζ_1 when $\tau \to \infty$. The values $\zeta_1 = 0.4$ ($C = 5.00$) and $\zeta_1 = 0.2$ ($C = 10.0$), deduced from Fig. 5, are exactly equal to the corresponding values of σ_0 (Fig. 1). It is confirmed, therefore, that $\zeta_1 = \sigma_0$ in solutions of polymethyl methacrylate. Moreover, since $\zeta_1 > 0$ the effective velocity of slip w_a was not bounded but tended to infinity with the stress at the wall. No definite information could be obtained about the value of ζ at zero stress, but the trend of the curves in Fig. 5 suggests that ζ_0 was small in both polymer solutions.

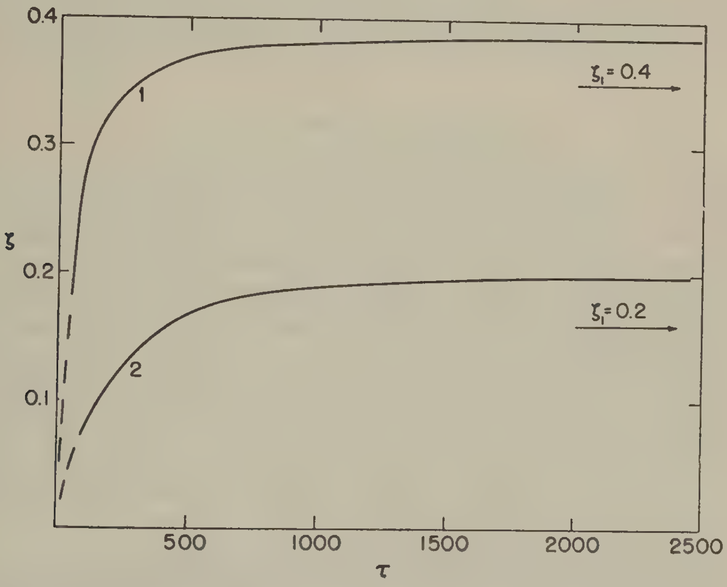

FIG. 5. The relations between ζ and τ with $C = 5.00$ (Curve 1) and $C = 10.0$ (Curve 2).

CONCLUSIONS

Evidence for a Wall Effect in Laminar Flow

The evidence put forward above has established that concordant results are obtained when smoothed pressure gradient/rate of flow data relating to laminar flow in straight tubes are analyzed by the methods which have been proposed by Schofield and Blair (2) and by Oldroyd (3).

While there is no evidence of a wall effect in the pure solvent and the more dilute polymer solutions ($C \leqslant 2.50$), a definite indication of anomalous behavior near the tube wall has been obtained in those cases where

$C \geqslant 5.00$. This wall effect is characterized by an effective velocity of slip (*cf*. Oldroyd (3)), and ζ, the effective coëfficient of slip, attains a limiting value ζ_1 at large stresses. The values of ζ_1 which were obtained for the liquids investigated were identical with the corresponding values of σ_0 determined by the method of Schofield and Blair (2). ζ_0, the counterpart of ζ_1 at small stresses, could not be estimated with certainty, but its value must always have been small compared with ζ_1, and may have been zero for all the liquids examined.

Recalling my earlier work (1), it should be noted that among those solutions for which ζ_1 (or σ_0) is now found to be either zero or very small (*cf*. Fig. 1) are liquids for which striking evidence had been obtained of anomalous behavior near the tube wall *when the mainstream had ceased to be laminar.*

The Breakdown of Laminar Flow

In the case of monochlorobenzene the results obtained by Osborne Reynolds' method show that $R_1 \sim 2000$ is a good criterion for the breakdown of laminar flow in tubes A and B, and also that the change of flow régime occurs quite suddenly. The findings were substantially the same in the cases of the more dilute polymer solutions ($C < 1.00$ g./l.) but as the concentration of polymer was increased, the transition, though no less definitely indicated, appeared to take place more gradually. Thus, instead of vanishing abruptly when the value of R_1 rose above 2000, the colored filament gradually became broader and ever less sharply defined until, eventually, it filled the bore of the flow tube. This trend is reflected in the ϕ, $1/\tau$ curves as can be seen by comparing Figs. 2, 3, and 4 (in that order) and, moreover, it became apparent in the narrow flow tube (B) at smaller values of C than in the wide one (A).

It is not without interest that a critical Reynolds number R_1 has been found for the breakdown of laminar flow in linear polymer solutions, which is not only constant, but is the same, numerically, as in Newtonian liquids, *i.e.*, about 2000. Had the choice been to define R in terms of ϕ_0 (and not ϕ_1), the conclusions would have been different, for it would then have appeared (since $\phi_1/\phi_0 > 1$, even in dilute polymer solutions (6), and the ratio increases with concentration) that there was a critical Reynolds number R_0 peculiar to each solution. Moreover, assuming $C > 0$, it would have been found that $R_0 < 2000$ and its value would have diminished as the concentration of polymer increased. (In the case of the pure solvent, of course, $R_0 = R_1$ since ϕ is constant.) In my view, therefore, R_1 is to be preferred to R_0, but quite apart from making a choice between these parameters, there can be no question that either of them is preferable to a Reynolds number based upon an arbitrary determination of the "apparent fluidity" of a polymer solution.

ACKNOWLEDGMENT

The author was assisted at different times by J. W. G. McLauchlan and (Mrs.) P. M. van Millingen.

REFERENCES

1. TOMS, B. A., *Proc. 1st Intern. Cong. Rheology.* **1948**, Holland.
2. SCHOFIELD, R. K., AND BLAIR, G. W. S., *J. Phys. Chem.* **34**, 248 (1930); **35**, 1212 (1931). See also: BLAIR, G. W. S., Introduction to Industrial Rheology, Chap. IV. Pitman, London, 1938.
3. OLDROYD, J. G., *J. Colloid Sci.* **4**, 333 (1949).
4. ERK, S., *Forschungsarb. Ver. deut. Ing.*, Heft 288 (1927).
5. REYNOLDS, O., *Phil. Trans.* **174**, 935 (1883).
6. *Cf.* STAUDINGER, H., Die hochmolekularen organischen Verbindungen, Springer, Berlin, 1932; DAVIES, C. N., Contribution to Discussion, *Trans. Faraday Soc.* **40**, 274 (1944).

A NOTE ON MIXED SOLVENT EFFECT IN SOLUBILIZATION

Santi R. Palit

Indian Association for the Cultivation of Science, Calcutta 12, India

Received May 27, 1949

Water can be solubilized in nonpolar solvents such as chloroform, benzene, *etc.*, with the help of detergents. It has been shown by Palit and McBain (1) that the amount of water solubilized depends to a large extent on the nature of the medium. This has also been observed lately by Winsor (2), who has also studied the effect of various additives.

It has been observed by the author that a mixture of solvents, say, chloroform and benzene, can solubilize very much more water in presence of a detergent than the individual solvents can alone in presence of the same quantity of the detergent. This behavior is particularly noticeable with pure quarternary ammonium type detergents, but is sometimes masked by the presence of impurities, either added during manufacture or accidentally present in such commercial surface-active agents. A thorough study of the whole phenomenon has been undertaken in this laboratory, and this preliminary note is to draw attention to the existence of this peculiar behavior.

In Fig. 1 is plotted the amount of water solubilized at 30°C./g. of cetyldimethylethylammonium bromide (Eastman Kodak Co.) in a solution of 1 g. of the detergent in 5 cc. of the solvent. The same experimental technique as described previously (1) was used. It will be observed that the solubilizing power of the detergent in chloroform is quite small and is augmented to a great degree by the addition of benzene, although the latter, by itself, has no power to solubilize. A curve is also presented about a similar behavior of carbon tetrachloride-chloroform mixture. In fact, it is observed that almost any hydrocarbon which by itself forms a non-solubilizing medium shows this remarkable property in conjunction with chloroform. It is also observed that chloroform-rich media show a positive temperature coefficient of solubilization, whereas CCl_4-rich media show the reverse behavior. In the figure it will be observed that we have made the solubilizing power of pure benzene or CCl_4 zero but have indicated this by dotted line. This is because the solubility of the detergent is insufficient in these pure solvents to admit of measurement of solubilization at our experimental concentration, but sufficient detergent dissolves on slight warming and the solubilizing power of such a solution is found to be practically zero.

It is currently believed that colloid micelles are responsible for solubilization and so we are led to believe that colloid micelles are being progressively formed and again broken down on gradually increasing the proportion of benzene or carbon tetrachloride. It is however, difficult to imagine how the McBain-Hess micelles accommodate more than 5 times their own weight of water in the interlayer spaces without producing grossly perceptible heterogeneity, particularly as the difference in refractive indices between the nonpolar solvent and water is so high.

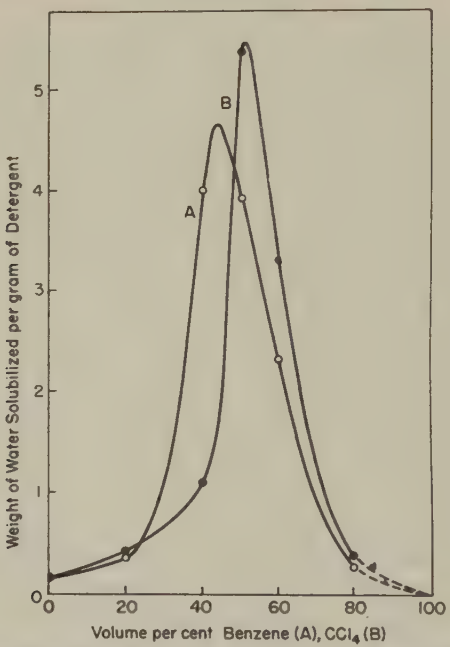

FIG. 1. Solubilization of water by chloroform-benzene mixture (A) and by chloroform-CCl_4 mixture (B) at 30°C.

Causes for the organization of the lamellar micelles on change of composition of the medium are not easy to find, and it seems that this whole idea needs confirmation by other independent evidences such as viscometric, optical, and X-ray investigations. An alternative explanation, that the active spots of the soap molecule which are responsible for solubilization are blocked off by tight coiling up in poor solvents such as benzene or carbon tetrachloride may, however, be also considered, although apparently contradicting the currently accepted idea, in view of the fact that the degree of coiling of polymer molecules in solution has been found to vary with the solvent power of the medium.

REFERENCES

1. PALIT, S. R., AND MCBAIN, J. W., *J. Soc. Chem. Ind., London* **66,** 3 (1947).
2. WINSOR, P. A., *Trans. Faraday Soc.* **44,** 382, 390 (1948).

SEDIMENTATION IN TILTED VESSELS (1)

Koreo Kinosita [1]

From the Department of Applied Physics, Faculty of Engineering,
Nagoya University, Nagoya, Japan

Received June 21, 1949

1. INTRODUCTION

Boycott (2) found, in 1920, that the sedimentation of red blood corpuscles is apparently accelerated when the test tube is tilted (Fig. 1). Many workers, chiefly medical, have studied this curious phenomenon (3), among whom we may mention Nakamura and Kuroda (4) as having produced the standard.

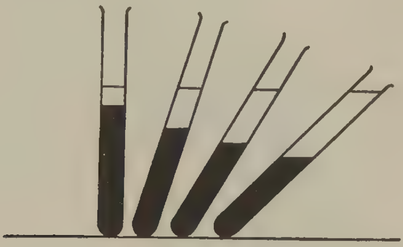

FIG. 1. *Boycott's effect.*

Nakamura's idea is as follows: First, the upper boundary of the suspended phase, which, at time $t = 0$, coincided with the surface of the suspending medium, be at AB at time t (Fig. 2). Now, if the sedimentation velocity of the particles be s (which is considered to be identical with the velocity of descent of the boundary surface when the tube is held vertical), we should primarily expect that the space marked with arrows of length sdt be clarified after the lapse of a short time interval dt. In reality, however, the boundary CD being unstable, the particles in the hatched volume drift to fill up the blank space above CD and form a horizontal boundary FG. The final result to be observed is, thus, nothing more than a descent by dh of the boundary from AB to FG. Nakamura assumes in the above process that the volume $ABGF$ equals the volume of the arrowed space.

---

[1] Now at the Department of Physics and Chemistry, Gakushuin University, Tokyo.

In the case of a rectangular cylinder shown in Fig. 2, we can write[2]

$$\text{the arrowed volume} = \{b \sec\theta + (c - h)\tan\theta\} asdt,$$

and

$$\text{the volume } ABGF = ab \sec\theta \, dh,$$

where a represents the depth of the vessel. Equating these and solving for h, we get

$$h = (c + b \sec\theta)\left(1 - e^{-\frac{st \sin\theta}{b}}\right) \qquad (1)$$

which, for a given value of $t > 0$, is greater than

$$h = st. \qquad (2)$$

For $\theta = 0°$, (1) is reduced to (2).

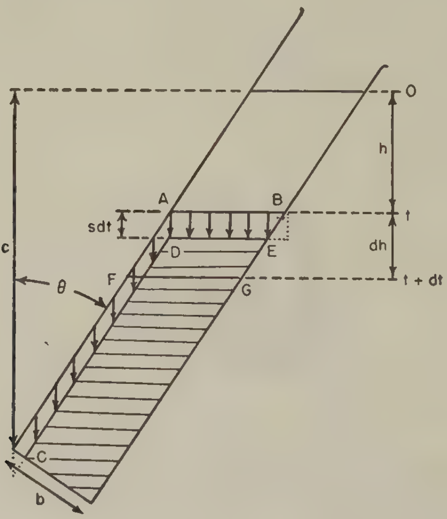

FIG. 2. Illustration of Nakamura's theory.

The relation described above can also be stated in the form that the volume clarified in the lapse of time dt equals the horizontal projection of the upper boundaries of the suspended phase (including the free surface and the ones in contact with the upper walls) multiplied by sdt. The walls beneath the suspension have no essential influence.[3] Hence, the relations illustrated in Fig. 3.

---

[2] Triangular volumes in the corners shown with dotted lines are neglected.

[3] On a horizontal bottom the particles are merely piled up; on an inclined wall some of them adhere and others slide down slowly. In any case, the motion of the suspended particles is not influenced essentially.

Sedimentation velocity, or, strictly speaking, *the descent velocity of the upper boundary of the suspended phase* in any vessel can be calculated according to this simple principle, and the theory seems to explain the experimental data satisfactorily; at least, in Nakamura and Kuroda's experiments on the sedimentation of cattle blood corpuscles, the accord of the theory and the observation is quite splendid.

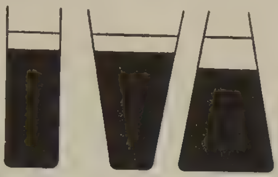

FIG. 3. Effect of upper and lower tilted walls.

Nakamura's theory, however, is phenomenological, and the mechanism of the drift of the particles to form a horizontal boundary—which we call the "*leveling action*" after Katsurai (5)—remains ambiguous. Nakamura employed the term "diffusion"; and some workers are trying theoretical calculations on the basis of this assumption (6, 7). But there is doubt as to whether the *leveling* is actually due to diffusion, which means the drift of particles without any essential mass motion of the suspending medium.

The author understands the sedimentation with a well-marked boundary which we treat here as characteristic of the case where diffusion is negligibly small. Well-known exponential-type concentration distribution will be expected otherwise.

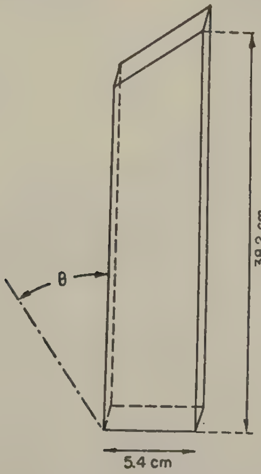

FIG. 4. Vessel of NH_4Cl smoke.

An alternative mechanism to be proposed here is a kind of convection, a hydrodynamic flow in the suspending medium which carries the particles with itself. Our principal interest in the following experiments was in verification of this working hypothesis.

2. Sedimentation of Ammonium Chloride Smoke (8)

Ammonium chloride smoke was prepared by the usual process, poured gently into a vessel[4] illustrated in Fig. 4, and its sedimentation observed in detail.

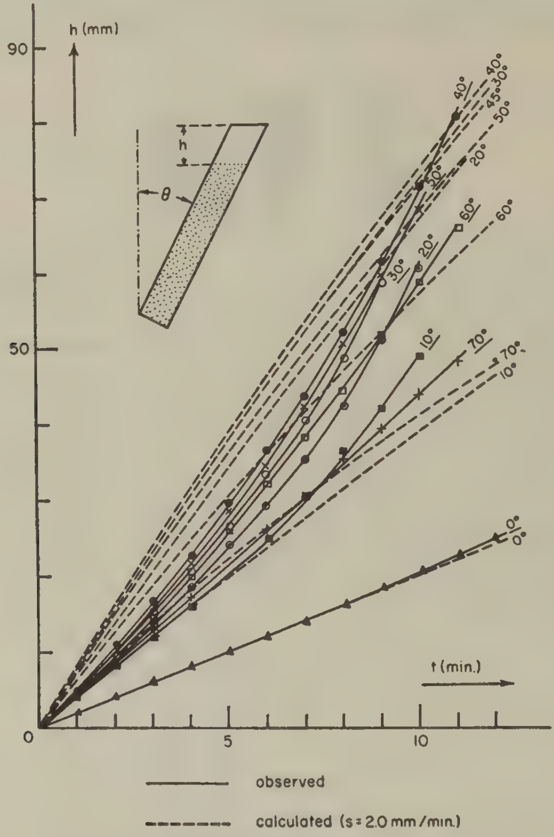

Fig. 5. Relation between the extent of descent of the boundary surface *h* and time *t* (NH_4Cl smoke).

Fig. 5 shows the relation between the descent of the boundary surface *h* and time *t*, observed for various inclination angles θ. Broken lines were calculated after Eq. (1), in which *s* was taken to be equal to 2.0 mm./min., the observed value of the descent velocity of the boundary surface when the cylinder was held vertical ($\theta = 0°$). The smoke was washed by passing through water, dried through desiccative and introduced directly into the

---

[4] We at first used a test tube-type vessel of 3 cm. diam. with ordinary cork, but found it inadequate because the inner side of the cork plays the role of a "tilted wall" and introduces unnecessary complications.

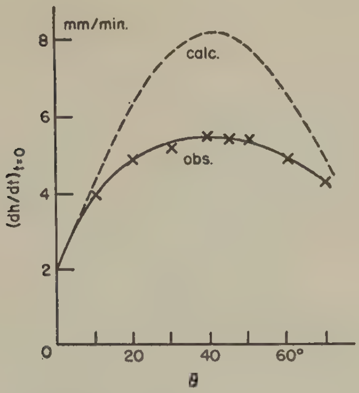

FIG. 6. Initial velocities of descent of the boundary surface for various inclination angles θ (NH_4Cl smoke). Calculated values are derived from Eq. (1).

vessel; hence, the size of the particles was not so uniform,[5] and coagulation occurred soon after beginning the observation. The upward bend of the *h*-*t* curves at $t > 4 \sim 5$ min. may presumably be due to this latter effect. We dare not conclude this because the trend is not clear when $\theta = 0°$, but it would not be unreasonable to suppose that the coagulation is promoted when $\theta > 0°$ by the convection current which, as we shall show later, is the cause of the *leveling action* in this case.

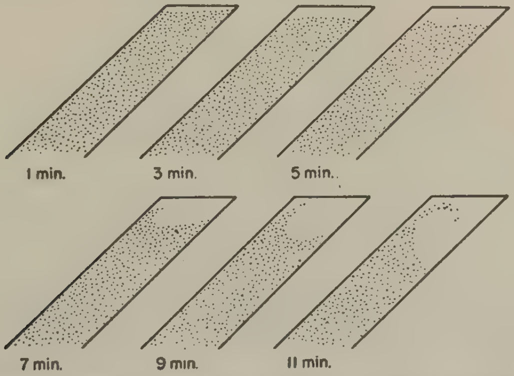

FIG. 7. Change in the appearance of the boundary surface (NH_4Cl smoke).

In Fig. 6 the initial values of the descent velocity of the boundary surface estimated from Fig. 5 are compared with $(dh/dt)_{t=0}$ derived from Eq. (1). The value of θ which makes the latter maximum can be calculated analytically, and is found to be 41° in our case, which is in good agreement with the observed result. Thus, Nakamura's theory explains the experimental results qualitatively very well, but the quantitative values of h or dh/dt calculated from Eq. (1) are not as satisfactory.

---

[5] Mean diameter of the smoke particles was roughly estimated at 8μ.

Fig. 7 illustrates the change in the appearance of the boundary accompanying the progress of sedimentation.[6] These sketches will suffice to show that the *leveling* is mainly due to a current of air (a kind of convection) in the vessel. We shall briefly discuss the mechanism of this convection later (§5), but the situation can be roughly understood if one considers the distribution of the pressure exerted by the suspended system on the medium (in this case, air): the diminution of the concentration of particles in the arrowed space in Fig. 2 will make the magnitude of the component of the gravitational pressure in the wall-direction decrease near the upper tilted wall and increase near the lower one, whose difference is decidedly larger at the bottom than at the upper part of the tube.

3. SEDIMENTATION OF FINE EMERY POWDER (9)

Fine emery powder for optical shop, of nominal size No. 1200, after being homogenized by decantation, was suspended in water, poured gently into vessels like the one shown in Fig. 8, and its sedimentation observed.

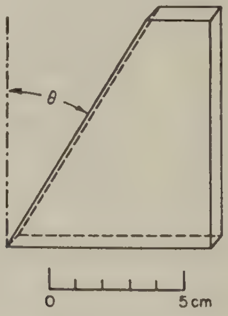

FIG. 8. Vessel of emery powder suspension.

The relations of the extent of descent of the boundary surface h *vs.* t for various inclination angles are plotted in Fig. 9. Broken curves in the figure correspond to the calculated values after Nakamura's theory, putting $s = 2.5$ mm./min. (the observed descent velocity of the boundary when $\theta = 0°$). The dependence of h-t curves on θ is quite different from what was seen in §2 according to the difference in the shape of the vessel. The general tendency of the curves can be explained by Nakamura's theory; especially, the accord between the observed and calculated initial velocities $(dh/dt)_{t=0}$ is excellent, but the observed h values become greater than the calculated ones with the lapse of time.

---

[6] The h values in Fig. 5 were read at the middle of the boundary surface.

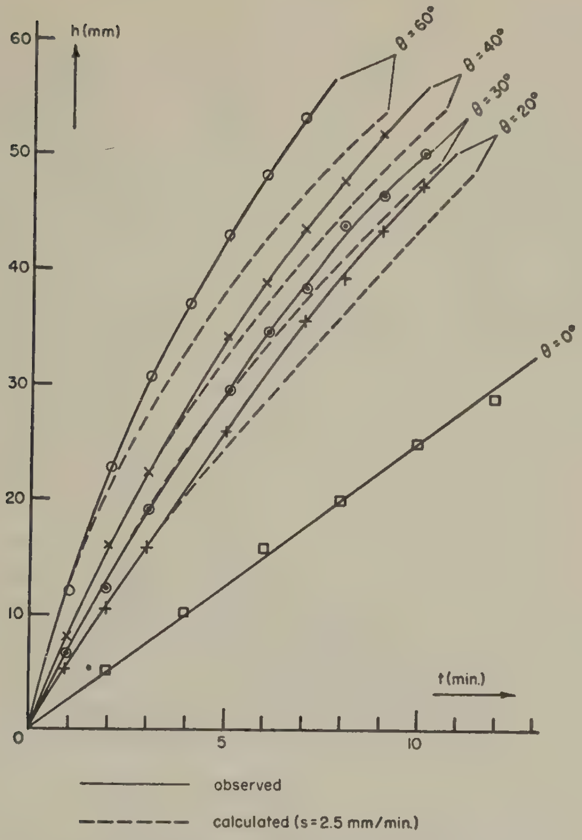

FIG. 9. Relation between the amount of descent of the boundary surface *h* and time *t* (emery powder suspension).

The change in the appearance of the boundary accompanying the advance of sedimentation is as follows: first, a thin wedge-type clarified layer appears just below the tilted wall, which proves the validity of Nakamura's basic ideas (Fig. 10 (a)); convection then takes place to fill up this blank space, and the boundary descends gradually in a form having

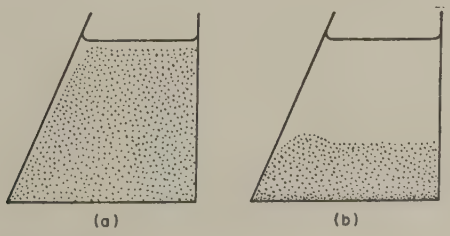

FIG. 10. Change in the appearance of the boundary surface (emery powder suspension).

a protuberance near the tilted wall as shown in Fig. 10 (b). Convection in this type of vessel is not very clear, but, in a test tube-type vessel, the current is so violent that one can hardly make any measurement.

The appearance of the wedge-type clarified layer, which shall be called the *V-layer* hereafter, means that the *leveling* occurs with a time-lag behind the sedimentation, which may be one of the causes of the discrepancy between the actual observation and Nakamura's theory. The *V-layer* was not distinctly recognized in the case of NH_4Cl smoke (presumably because the definition of the boundary was inferior), but we can point out several cases in which we could just perceive it.

Our original purpose of establishing the validity of the hypothesis that the *leveling action* in *Boycott's effect* is not due to diffusion but to a kind of convection current in the suspending medium seems to have been accomplished by these experiments. But it is desirable to confirm this again in the case of erythrocyte sedimentation, because the fact that the sedimentation is much slower in the latter case may aid the diffusion theory.

4. SEDIMENTATION OF RED BLOOD CORPUSCLES

Twenty-five hundredths to 30% of rabbit's blood was dissolved either in physiological saline or in Hayem's solution, and the sedimentation in small glass vessels like the ones used in the preceding section of this solution was observed. Approximate values of the descent velocity of the boundary surface for various inclination angles were 4, 6, 7, and 8.5 mm./hr., respectively, for $\theta = 0°, 25°, 40°$, and $50°$ (in the case of 2.5% solution).

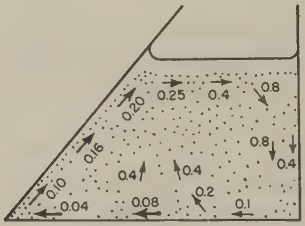

FIG. 11. *Leveling convection* in blood solution (0.5%).

The movement of red blood corpuscles was traced microscopically (100 ×). The microscope was set horizontally, the vessel being placed in the position of the object-glass. No special illumination was needed. The vessel was fixed on a carrier which could be displaced finely in a plane perpendicular to the optical axis in both horizontal and vertical directions, so that we could perform an observation at any desired position.

A thin wedge-type clarified layer (*V-layer*), similar to the one mentioned in the preceding section, appears again in this case. Microscopic observation reveals an upward movement of the blood corpuscles along the edge of this layer. The motion is quite orderly, the boundary with the *V-layer* never being invaded by the corpuscles.

A general idea of the movement of the corpuscles in the whole may be obtained from Fig. 11, but care must be taken as to the interpretation of this illustration. The currents are unstable and are liable to be disturbed by illumination,[7] except the regular currents along the boundary of the *V-layer* and the bottom (especially the left half) of the vessel. Consequently, the directions and the velocities jotted in this figure are, except the ones represented by thick arrows, nothing more than an example showing the general trend. The currents represented by thick arrows are quite stable.

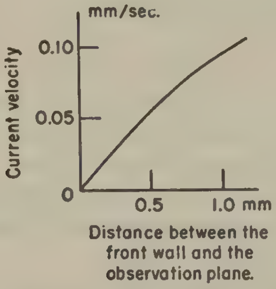

FIG. 12. The diminution of current velocity near the wall due to viscous resistance.

The numerals in the figure represent the velocity (mm./sec.) read with ocular scale. They correspond to the values in a plane near the front wall. The velocities in the central plane are expected to be larger, as can be estimated from Fig. 12, which shows the influence of the viscous resistance near the wall, but actual measurement of them was not possible because of the limitations of the instrument.

A number of complementary observations and experiments would be worth mentioning.

I. Currents in the blood solution caused by sedimentation described above can be visualized by holding a small flake of methyl violet at an appropriate position in the vessel. A colored stream comes out slowly and shows invisible current in the suspension. The general trend estimated by this very simple method agrees with what was illustrated in Fig. 11.

II. As a consequence of the convection in the suspension part, hydrodynamic flow also takes place in the upper, already-clarified, part of the liquid. It is a very slow and not always stationary current, which can be detected by the *methyl violet method* or by the observation of red blood corpuscles remaining in the clarified region. (The concentration of the latter is, of course, very small.)

---

[7] Nakamura emphasizes the unreliability of microscopic observations in reference to these points; but our results are reproducible so far as what we positively maintain are concerned. They are also in accordance with the observations by the *methyl violet method*, which is to be described later.

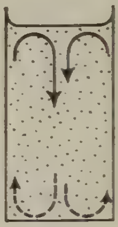

FIG. 13. Convection current liable to take place in a vertical-wall vessel.

III. A weak convection is liable to occur, even in a vessel whose walls are vertical. Unstable as this current is, one can detect it by the *methyl violet method*. The general tendency is sketched in Fig. 13. The current is assuredly due to sedimentation, because if one fills the same vessel with water and tries the *methyl violet method*, nothing more than a straight downward motion of a colored stream can be seen.

5. SUMMARY AND DISCUSSIONS

A. Boycott's effect was observed on the sedimentation of NH_4Cl smoke (in air), fine emery powder (in water), and red blood corpuscles (in diluted blood solution); and it was established that the *leveling action* is not due to diffusion but to a mass motion (a kind of convection) of the suspending medium. The effect of diffusion is very small, if any.

B. The velocity of this convection current is much greater than the descent velocity of the boundary surface of the suspended phase, which is usually regarded as the sedimentation velocity (*cf.* §4). A general idea of the *leveling convection* could be obtained from Fig. 11.

C. Nakamura's theory for the velocity of descent of the boundary surface is qualitatively valid, but not quantitatively satisfactory in all cases.

According to conclusion *A*, it is useless to discuss *Boycott's effect* on the basis of the equation of diffusion.

As was pointed out in *B*, the velocity of the *leveling convection* is some 10^2 times as large as the descent velocity of the boundary surface. Consequently, the author is inclined to picture the sedimentation in tilted vessels with a large horizontal vortex turned up in the suspended phase. The latter, whose upper boundary coincides with the boundary surface which we observe, flattens itself as times goes on, wherein the concentration of the particles in it is kept approximately constant by the excretion downwards of surplus particles (Fig. 14).

The crux is the mechanism of this vortex. It is not difficult to comprehend it qualitatively, as was mentioned before, by considering the uneven distribution, caused by sedimentation, of the pressure which the suspended system exerts on the medium, or, in other words, the nonuniformity of the density of the suspension (*cf.* §1). But if we go any farther to discuss the problem with hydrodynamic equations, we are beset with difficulties. If we wish an attack in the front, our discussions must be based on Navier-Stokes' equations, as the viscosity of the medium plays an important role in this phenomenon. Writing down the fundamental equations is not essentially difficult, if we admit some postulates, but solving them to arrive at a solution of practical value seems almost hopeless. The formulation and the solution of the problem is left to the future.

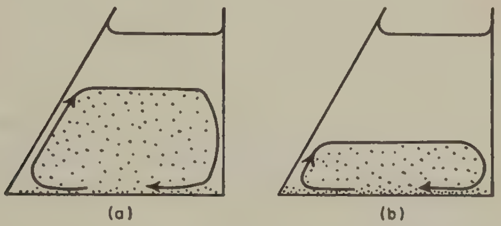

FIG. 14. Vortex model of the *sedimentation in tilted vessels.*

The influence of diffusion was neglected in the above discussions. In reality, however, it does play a role, but of the second or third order. The author expects that a kind of convection in a vertical-wall vessel mentioned at the end of the preceding section could be reasoned if one could have carried out theorectical calculations on the above-stated principle with further corrections for this diffusion effect.

ACKNOWLEDGMENTS

Observations and experiments in each section of this article were carried out with the cooperation of one or more of the students of the Faculty of Engineering, Morihei Hukaya (§2), Eizi Taki (§3), Kozo Isomura (§3), Taizo Tsukada (§§ 3 and 4), and Keizo Murase (§4), to whom the author is very much indebted. I also wish to express my cordial thanks to Mr. Akiya Ookawa and Mr. Nobuhiko Saito of the Kobayashi Institute of Physical Research. The problem was originally suggested by Ookawa, and lively discussions with them stimulated me very much whenever we had the chance to meet. A grateful acknowledgment is due to Dr. Taro Suga, the supervisor of our laboratory, and to Dr. Tominosuke Katsurai of the Scientific Research Institute, Ltd., for their interest throughout the work and for reading the manuscript.

REFERENCES

1. A more detailed report will appear in *Mem. Faculty Engin. Nagoya Univ.* in the near future (in English).
2. BOYCOTT, A. E., *Nature* **104**, 532 (1920).
3. Resumé of these investigations can be found in Ref. (4).
4. NAKAMURA, H., AND KURODA, K., *Keijo J. Med.* **8**, 265 (1937) (in French).
5. KATSURAI, T., Theory of Colloids, 62, Tokyo, 1947 (in Japan.).
6. SAITO, N., AND OKA, S., *Kagaku* (= Science) **18**, 75 (1948) (in Japan.).
7. MIYATAKE, O., An address at a Sectional Meeting of the Physical Society of Japan, Oct., 1948.
8. Of the sedimentation of this aerosol, Tachibana, T., and Terada, H., have observed *Boycott's effect* recently [*J. Chem. Soc. Japan* **68**, 2 (1947) (in Japan.].
9. Similar observations are reported by JOHNSON, R., AND SMYTH, E., *Nature* **160**, 27 (1947) on the sedimentation of *potter's bone* in a conical flask. However, it seems that they were ignorant of the relation to *Boycott's effect.*

LETTER TO THE EDITORS

THE EFFECT OF WATER ON THE SIZE AND SHAPE OF SOAP MICELLES IN BENZENE SOLUTION[1]

Attempts in this laboratory to free solutions of the arylstearate soaps in benzene from adsorbable polar contaminants by percolation over alumina or silica gel have led to the observation that the viscosity of such solutions is critically dependent upon their water content. In the complete absence of water, soaps of good purity swell in benzene to give jelly-like systems, which, on heating or on standing for a day or more, transform to highly viscous liquids showing birefringence of flow. The addition of as little as 0.05% of water to such a system converts this viscous fluid to a mobile liquid having a relative viscosity slightly larger than that predicted for the system by the Einstein equation for suspended spheres (see Fig. 1).

The effect has been observed with solutions of carefully prepared sodium, lithium, and calcium soaps of xylyl- and xenylstearic acids. The quantitative relations for a dilute calcium xenylstearate solution are shown in Fig. 2.

The high viscosity and flow-birefringence of the anhydrous systems suggest that here the soap is present in thread-like aggregates, or micelles, which are analogous to linear polymers. If so, a range of micelle lengths might be expected over which there would be approximate conformity with Staudinger's rule that the molecular weight of linear macromolecules of a given type is proportional to the intrinsic viscosity $[\eta]$. Then, if the concentration of soap is held constant while the average micellar length varies, the number of micelles present will be proportional to the reciprocal of $[\eta]$, or to a quantity such as $c/(\eta_r - 1)$ which in a given dilute solution would be proportional to $1/[\eta]$.

Curve I of Fig. 2 approaches a linear relation between $c/(\eta_r - 1)$ and the water content of the system in the region from 0.1 to 0.7 moles of water per mole of soap; *i.e.*, in this range the number of micelles is proportional to the amount of water added. It is suggested that here the mechanism for the spectacular reduction in the viscosity of the system is the rupture of long polymer-type chains and the stabilization of the shorter units through attachment of water to the free ends.

---

[1] The opinions or assertions contained in this communication are the authors' and are not to be construed as official or reflecting the views of the Navy Department.

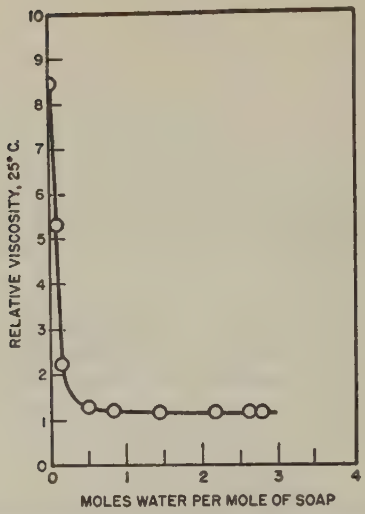

Fig. 1. Effect of water content on the relative viscosity of a solution of calcium xenylstearate in benzene (3.48 g. soap/100 cc.).

This interpretation is supported by observations of the degree of polarization of the fluorescence excited by green light as water was added to a solution of the same soap containing Rhodamine B. This polarization is a function of the average volume of the soap micelles to which the dye molecules are adsorbed (1). Curve II of Fig. 2 shows that, for the solution

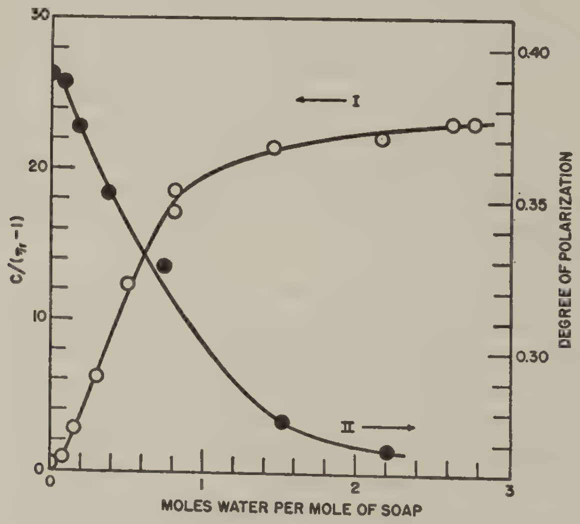

Fig. 2. Plot of $c/(\eta_r - 1)$ and of the degree of polarization of fluorescence from Rhodamine B for a solution of calcium xenylstearate in benzene.

studied, the degree of polarization changes from a value of 0.39, only slightly less than that to be expected for completely immobilized dye molecules (2), to one of 0.27 in the presence of two moles of water per mole of soap. This latter value corresponds to a gram micellar volume of the order of 20,000 cc. The situation in the viscous solutions of low water content is too obscure to justify a calculation of micellar volume in them from Perrin's relation, but the trend of the degree of polarization with increasing water content is in good qualitative agreement with the viscometric data.

On warming, the water-containing solutions increase in relative viscosity in a manner recalling the behavior of benzene dispersions of aluminum soaps (3,4,5). Between 60° and 75°C. the viscosity rises rapidly to that of the original anhydrous solution. It reverts immediately to low values on cooling.

These results establish, for certain soaps of the alkali and alkaline earth metals, a pattern of viscometric behaviour heretofore familiar only in the case of aluminum soaps. They also provide evidence of the existence of two different types of micelle for a given soap in non-aqueous systems, one having an extended structure and the other being approximately isodimensional.

REFERENCES

1. Arkin, L., and Singleterry, C. R., *J. Am. Chem. Soc.* **70**, 3965 (1948).
2. Perrin, F., *J. phys. radium* [6] 7, 390 (1926).
3. McBain, J. W., and Working, E. B., *J. Phys. Colloid Chem.* **51**, 974 (1947).
4. Sheffer, H., *Can. J. Research* **26B**, 481 (1948).
5. Gray, V. R., and Alexander, A. E., *J. Phys. Colloid Chem.* **53**, 9, 23 (1949).

Naval Research Laboratory,
Washington, D. C.

Lorraine Arkin
C. R. Singleterry

Received June 20, 1949

BOOK REVIEW

Principles of High-Polymer Theory and Practice. By Alois X. Schmidt, Assistant Professor in Chemical Engineering, and Charles A. Marlies, Associate Professor in Chemical Engineering, College of the City of New York. McGraw-Hill Book Co., Inc., New York, 1948. xii + 743 pp. Illustrated. Price $7.50.

There is now a book from which polymer chemistry may be taught—and learned. Professors Schmidt and Marlies have written it. Their attention to modern ideas, balanced against lucid factual accounts, is unique in the present literature of the field. With this book, there is no reason to have technologists uninformed of the basic principles in making and using plastics, rubbers, fibers, finishes and adhesives, or to have research investigators ignorant of the general observations of polymer behavior.

The thoughtful and logical planning of the book is striking from the beginning. Chapters 1 and 2 tell the kinds of molecules which polymers are, and how they act together. The examples chosen are usually the best in the field. One is actually surprised that a little of the old confusion between *orientation* and *crystallinity* appears on p. 57, whereas one has learned not be to surprised at this in polymer literature at large.

The next chapters introduce the extraordinary physical properties of polymers. Here is skillfully and valuably preserved the *unity* of polymer science; rubber does have a connection with cellulose, even if we have been told (not by Schmidt and Marlies) that their micelles aren't the same size! Through these chapters (3, 4, 5, and 6), kinetics of polymerization, structures and molecular weight determinations are clearly introduced. One may object that the synthetic polypeptides of 1947 (Leuch—1906) *didn't* have molecular weights in the millions (p. 124), or that the intensity of spots in X-ray fiber diagrams is not so much by itself a sign of amount of crystallinity (p. 167) as of the intrinsic scattering power of the atoms involved (Cl, Br *vs.* C, H, *etc.*). However, there is very little that calls for objections; and that, again, is rare in books on this active field. Also, there are some nice points which the multitude of books on general physical chemistry often miss; for instance, the anisotropy of cubic crystals, such as in their X-ray scattering (p. 177).

Chapters 7–10 treat mechanical and electrical properties, including both "rheology" and "molding"—and do justice to both. While elasticity from van der Waal's forces usually varies exponentially with $1/T$ (instead of being "proportional to $1/T$," p. 282), and will certainly go this way in the 10^8–10^9 modulus range of cellulose and the polyamides (and not "proportional to T" in these non-ideal cases), the basic concepts are clear and authoritative. The treatment of electrical and optical properties is likewise balanced and stimulating, especially for those who spend much time testing polymers, and are curious about the principles involved. Although something more than just oriented polyvinyl alcohol (p. 462) is necessary to make conventional Polaroids, since the intrinsic birefringence of most unmodified polymers is quite low, such factual errors are as rare as the conceptual ones noted earlier.

Chapters 11 through 13 cover fibers and rubbers in interesting descriptive fashion, again with enough of the quantitative aspects brought in to be just right for teaching or casual reference. Finishes (Chap. 14) and adhesives (Chap. 15) are similarly good. Chap. 16 concludes the text on a note of hope—that some day phenolics will be studied scientifically. The several appendices supplement excellent tables throughout the work in listing typical properties and formulas for nearly all technically important polymers.

The book is well made, as one expects in the "Chemical Engineering Series." One wonders why the hyphen in "High-Polymers . . . ," and the conscious use of buta for Buna throughout (buta may well be better for emulsion polymers, if new names are needed). But misprints are few. The bibliography is unusually well chosen.

Professors Schmidt and Marlies have made a notable gift to the field which occupies, as they note, about a third of all chemists and chemical engineers. Those who have learned from this work, and they should include biologists and biochemists, too, will erect the memorial in science and engineering which ever proclaims the only temporal, never spiritual, mortality in Professor Marlies' too-early death.

W. O. Baker, New York, N. Y.

AN IMPROVED PHOTOELECTRONIC COUNTER FOR COLLOIDAL PARTICLES, SUITABLE FOR SIZE-DISTRIBUTION STUDIES[1]

Frank T. Gucker, Jr. and Chester T. O'Konski[2]

From the Chemical Laboratory of Northwestern University, Evanston, Illinois, and Indiana University, Bloomington, Indiana

Received July 18, 1949

INTRODUCTION

Until recently, the tedious methods of determining the concentration and size of colloidal particles have hampered many studies in this field; but the development of photocells and electronic counting devices provides a basis for the development of rapid and convenient instrumental methods. Recently we have described (4,5) an apparatus which automatically counts individual aerosol particles of 0.6 μ (micron) diameter and larger, at rates up to 1000/min. A stream of the very dilute aerosol, flowing at one l./min., and confined by a sheath of air flowing at the same linear rate, passes through a cell, where it is subjected to intense dark-field illumination. The flashes of light scattered by the suspended particles in the near-forward direction fall upon a photosensitive cell, giving rise to electrical pulses which are amplified to actuate a mechanical counter. In this instrument the setting of an electrical discriminator circuit allowed the counting to be limited to particles giving electrical pulses above any selected value, down to a lower limit determined by the background noise of the photosensitive tube. Since the light scattering of similar particles depends upon their size, we suggested that this type of counter might be developed to determine particle size.

The present article describes a new counter in which the optical system has been improved to give more uniform illumination of the aerosol stream with greatly reduced stray light, and the electronic system has been improved to allow the counting of electrical pulses within any predetermined voltage range, as well as those above any desired minimum value. Preliminary experiments show the applicability of the instrument as a counter, and indicate its future usefulness in determining particle-size distribution.

---

[1] Presented before the Division of Physical and Inorganic Chemistry, American Chemical Society, San Francisco, California, April, 1949. This paper is taken from the Ph.D. dissertation submitted by Chester T. O'Konski to Northwestern University in August, 1948. It is based upon work done for Camp Detrick, Frederick, Maryland, under Contracts WA-18-064-CWS-160 with Northwestern University and No. W-18-108-CM-31 with Indiana University.

[2] National Research Council Predoctoral Fellow, 1946–48. Present address: Department of Chemistry, University of California, Berkeley, California.

Apparatus

The present apparatus is similar in principle to the previous instrument, but utilizes an electron-multiplier phototube, chosen for its high sensitivity and excellent frequency response, and a right-angle optical system, especially designed to minimize stray light in order to reduce the phototube noise which limits the sensitivity of the instrument. It also includes an electronic circuit to facilitate the scanning of the pulse-amplitude-distribution spectrum which will allow the determination of the distribution of particle sizes after the relation between pulse height and particle size is established.

The Optical System

The earlier instrument (5) collected the flashes of light scattered in the near-forward direction, rather than at right angles, because, as shown by Lord Rayleigh (1871), its intensity is twice as great for small particles (13) and greater still according to G. Mie (1908) for larger particles (10). However, the limiting factor in such a counter is not the amplification of the signal from the particle, but the ratio of this signal to the background noise in the photomultiplier tube, which is a function of the stray light in the optical system. Our experience with various optical systems (5,6) had shown that the stray light may be reduced to an extremely low level in a properly designed right angle system, while none of the incident light is cut out by the opaque stop necessary in the small angle system, and a greater solid angle of scattered light can be collected. The optical system of the new counter therefore was made for right angle scattering, although it can be adapted for small angle scattering very simply. Incorporation of a carefully designed light trap, the use of achromatic instead of aspheric lenses, and of an illuminated slit instead of the lamp as the light source, sharpened the image in the smoke cell and markedly reduced stray light.

The optical system is drawn to scale in Fig. 1. The metal parts are machined from brass. Joints in the smoke cell are sealed with 0.8 mm. ($\frac{1}{32}$ in.) Garlock gasket material, indicated in each case by an X, which permits rapid removal and interchange of parts. The entire assembly, including the light source and the smoke cell, phototube, and preamplifier, is mounted on an optical bench.[3]

Light from the ribbon-filament tungsten lamp A is collected by a set of achromatic condensing lenses, L_1, L_2, each with a focal length of 78 mm. and diameter of 46 mm. The lenses are held in the auxiliary lens holder B,

---

[3] Catalog No. 85800, Central Scientific Company, Chicago, Illinois.

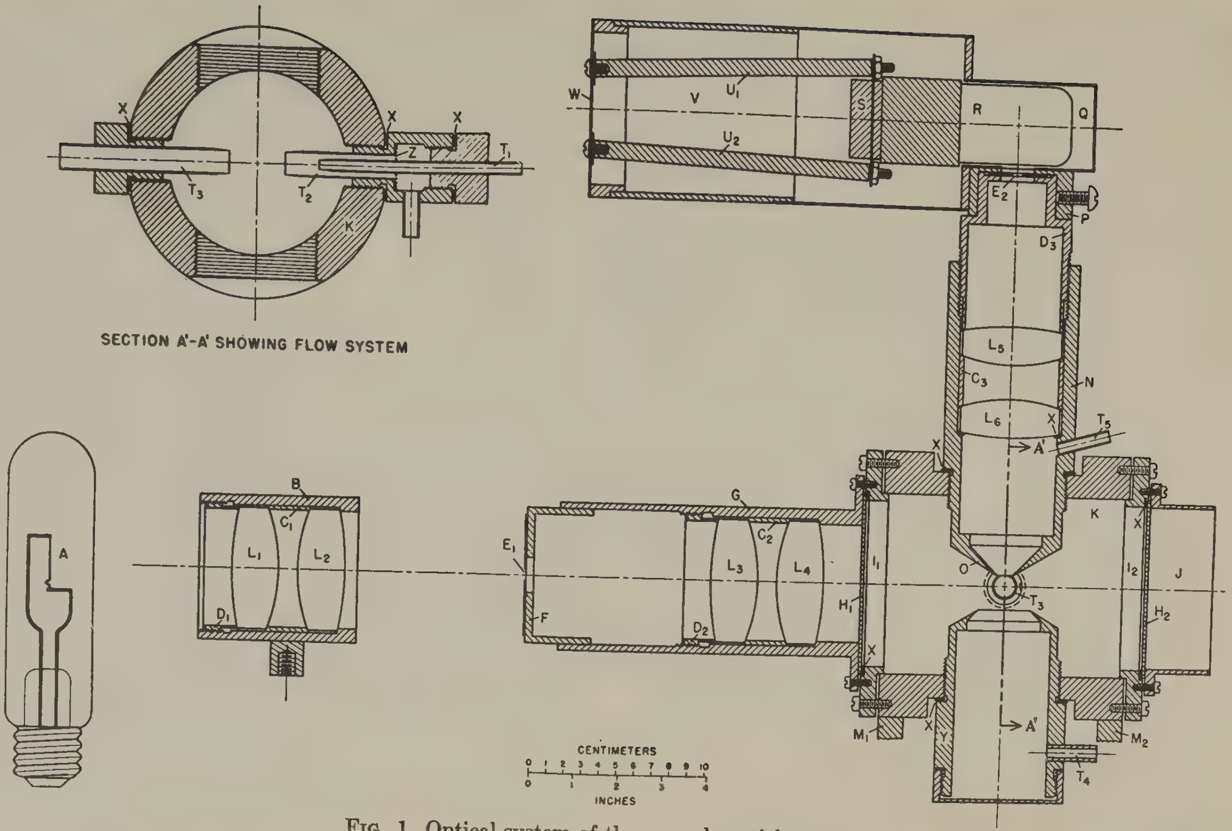

FIG. 1. Optical system of the aerosol-particle counter.

by means of a spacer C_1 and a retaining ring D_1. A full-sized image of the filament is formed in the plane of the source slit E_1, which is made of thin sheet metal to dissipate the heat. The slit holder F telescopes into the lens holder G for adjustment of the position of the source slit along the optical axis. Another identical set of lenses, L_3, L_4, focuses the light in the center of the smoke cell K, on the axis of the smoke tube T_1 (shown in the section $A'A'$), beyond which the beam diverges. The cell is closed with the glass plates H_1, H_2 sealed in with gaskets. The smoke cell assembly is supported on the optical bench in two brass cradle mounts, M_1, M_2, adjustable horizontally and vertically.

The flow system is identical with that in the original counter (5) except that, as shown in section $A'A'$, all of the tubes T_1, T_2, and T_3 are built into individual housings threaded to facilitate replacement, and a baffle screen Z, consisting of three layers of fine wire gauze, helps to smooth the flow of the sheath air. Separate tubes T_4 and T_5, and others suitably located, are connected to a manifold through which filtered air can be blown to flush out the entire system.

Light scattered in the vicinity of 90° is collected by the achromatic viewing lenses L_5, L_6 (with focal lengths of 63 mm. and diameters of 39 mm.) and focused on the viewing slit E_2, mounted in a shallow recess in the end of D_3 to cut out stray light from the knife edge and the interior of the tapered end O of the viewing lens holder.

The phototube housing Q is attached to the cap P so that the optical axis of the viewing system intersects the center of the photosurface of the 931-A photomultiplier tube R when the cap is fastened over the end of the retainer D_3. The phototube socket S is mounted on the brass spacers U_1, U_2, which also support the tube socket and other units of the preamplifier circuit contained in the region V.

The slit pieces E_1, E_2 and the entire interior of the system are painted with optical black paint.[4] A dark background behind the particles is provided by the light trap Y, which is constricted at the top until its knife edge just avoids being visible through the hole in O from any point on the inner surface of L_6. The interiors of the light trap, the smoke cell, and the barrel of the viewing lens holder between the tapered section O and L_6 are lined with velvet-surfaced optical black paper to further decrease stray light.

Light Source

The ideal light source would be intense, stable, and uniform over its entire area. Fluctuations in intensity can lead to spurious counts because of the stray light in the optical system and, together with nonuniformity, preclude the possibility of reliable size-distribution measurements. We

[4] Manufactured by G. J. Nikolas and Company, Chicago, Illinois, and Brooklyn, New York.

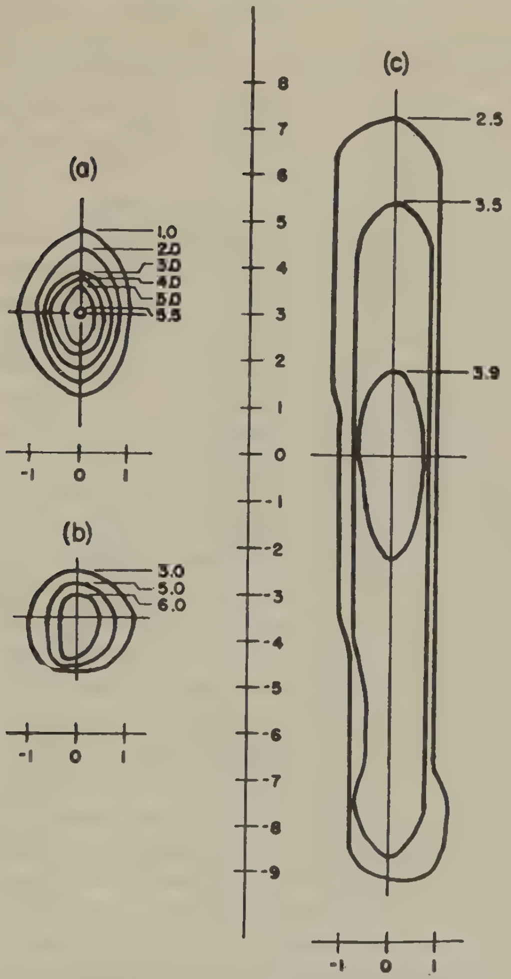

FIG. 2. Intensity contours (in arbitrary units) of images of three light sources: (*a*) 50-w. tungsten lamp and aspheric lens system, (*b*) 100-w. zirconium arc and double achromatic lens system, (*c*) ribbon-filament tungsten lamp and double achromatic lens system. Distances are given in mm.

studied a 50-w. automobile headlight, a 6-v., 18-amp. ribbon-filament tungsten lamp,[5] a 100-w. zirconium concentrated-arc lamp,[6] and a carbon-arc motion-picture projection lamp.[7]

An optical probe was built to explore the image of the various light sources formed by suitable condensing lens systems. It employed an aperture 0.4 mm. in diameter backed by a piece of opal diffusing glass and an RCA 929 vacuum-type phototube which has the same photosurface as the RCA 931-A electron multiplier. The diffusing glass allowed use of a considerable portion of the photosurface, minimized the effects of convergence or divergence of the incident rays, and made the orientation of the aperture plate with respect to the direction of the incident beam less critical. Phototube currents, which are proportional to the light intensity at the aperture, were measured in conventional ways as the aperture was moved across the image by means of a micromanipulator[8] mount.

---

[5] Catalog No. 86606, Central Scientific Company, Chicago, Illinois.

[6] Made by the Western Union Telegraph Company, Water Mill, New York.

[7] Made by Hopkins and Woods, Martinsville, Indiana.

Some of the results, uncorrected for the probe aperture, are presented graphically in Fig. 2, where lines of equal intensity, on an arbitrary scale, are shown at the image plane for different light sources and optical systems. Fig. 2*a* shows the nonuniformity of the light beam in the original counter, using a 50-w. automobile headlight bulb and a pair of aspheric lenses. Fig. 2*b* shows the contour lines obtained for the image of a 100-w. zirconium arc lamp with a double set of achromatic lenses such as used in the revised instrument. The brightness of this image was to be found five times that of the one in the original counter. Fig. 2*c* shows the image of the ribbon-filament lamp obtained with the pair of double achromatic condensing lenses. The optical system of this new counter gave a considerably more uniform image than that of the old. The zirconium-arc source gave a uniform image over a spot of about 1.5 mm. in diameter which, however, moved about, causing variations in intensity near the outer edges. The ribbon-filament lamp, allowing for the aperture of the probe, was found to give an image uniform within ± 10% over an area of 2 × 12 mm. and was ideally suited to the improved counter. The motion-picture projection arc lamp, using copper-coated carbon rods, gave the brightest image of all, even when operated well below its rated capacity of 60 amp. The extreme heat at the focus of the elliptical mirror used with this lamp prevented a complete mapping of the intensity contours. However, preliminary results indicated that the intensity of the center of the image fluctuated about ± 10%, apparently because variations in the rate of burning of the carbons were not completely eliminated by the automatic feed mechanism.

Phototube

Since 931-A electron-multiplier phototubes were found to vary widely in sensitivity and noise, we tested a large number under conditions closely simulating actual experimental conditions of operating voltage, output current, and sensitive area of the photosurface. The phototube was put into position in the instrument, the light was turned on, and the cell was flushed out with filtered air. The high voltage supply of the photomultiplier was adjusted, if possible, to give an average amplified noise (stray-light noise) of 50 mv., as measured on the A. C. electronic voltmeter (see Fig. 3, p. 548). The light then was cut off and the average dark noise was measured on the same voltmeter. In poor tubes this might be equal to or even greater than the average stray-light noise. Finally the light was modulated by a motor-driven sector disk mounted just in front of the source slit E_1 (Fig. 1). The sector was constructed to give stray-light pulses of 1 millisec., equal in duration to those from particles. The amplified pulses were then measured visually on an oscilloscope to about 0.05 v. Data on eleven randomly chosen electron-multiplier tubes, including several of the older 931 type, are shown in Table I. The signal-to-noise ratios were expressed in terms of peak voltage of the signal produced by the intermittent stray light and average stray-light noise. A wide range of values was observed and the best phototube was selected for use in the instrument. In addition to variation in sensitivity from one photomultiplier tube to another, there is also a variation in sensitivity at different points on the photosurface of the same tube, as recent work by Fitz-Hugh Marshall, J. W. Coltman, and A. I. Bennett (1948) has shown (9). In order to obtain electrical pulses from the photomultiplier which are independent of the position of the particle in the aerosol stream, the light pulses must fall on practically the same portion of the photosurface. This is accomplished by using a collecting lens system of sufficient depth and breadth of field, and focusing the image of the particle at E_2 (Fig. 1) some, distance in front of the photosurface, so that the scattered light appears as a diffuse spot on the photosurface, covering a good fraction of the total

---

[8] Made by the Gamma Instrument Company, Inc., New York, New York.

TABLE I

Comparison of Typical Photomultiplier Tubes

Phototube type	High voltage	Av. stray-light noise	Av. dark noise	Peak signal of chopped stray light	Signal-to-noise ratio
	v.	*mv.*	*mv.*	*mv.*	
931-A	550	50	70	100	2.0
931	693	50	50	120	2.4
931-A	657	50	40	250	5.0
931-A	633	50	45	250	5.0
931	655	50	38	300	6.0
931-A	710	50	50	300	6.0
931-A	727	50	32	350	7.0
931-A	795 (max.)	35	30	250	7.1
931-A	795 (max.)	45	25	350	7.8
931	795 (max.)	45	27	400	8.9
931-A	703	50	11	550	11.

area utilized for particles in all possible positions within the illuminated volume. This fraction, which measures the uniformity of response, will approach unity as the cross section of the aerosol stream is decreased.

General Electronic System

The small electronic pulse from each aerosol particle can be amplified without distortion with a wide band-pass amplifier. However, because of the high-frequency components of the noise from the photomultiplier tube, discussed (2) by R. W. Engstrom (1947), the output noise will increase with the band width; hence a wave-filter circuit is advantageous to attenuate the higher frequencies and improve the signal-to-noise ratio. The output voltage still will be proportional to the input for all pulses of the *same duration.* This condition is fulfilled by our optical system in which each particle is illuminated for practically the same length of time, regardless of its position in the aerosol stream.

The block diagram of the complete electronic system is shown in Fig. 3. Since a 60-cycle rejection filter visibly distorted 1-millisec. pulses, it was discarded and the ripple was reduced by shielding all leads and operat-

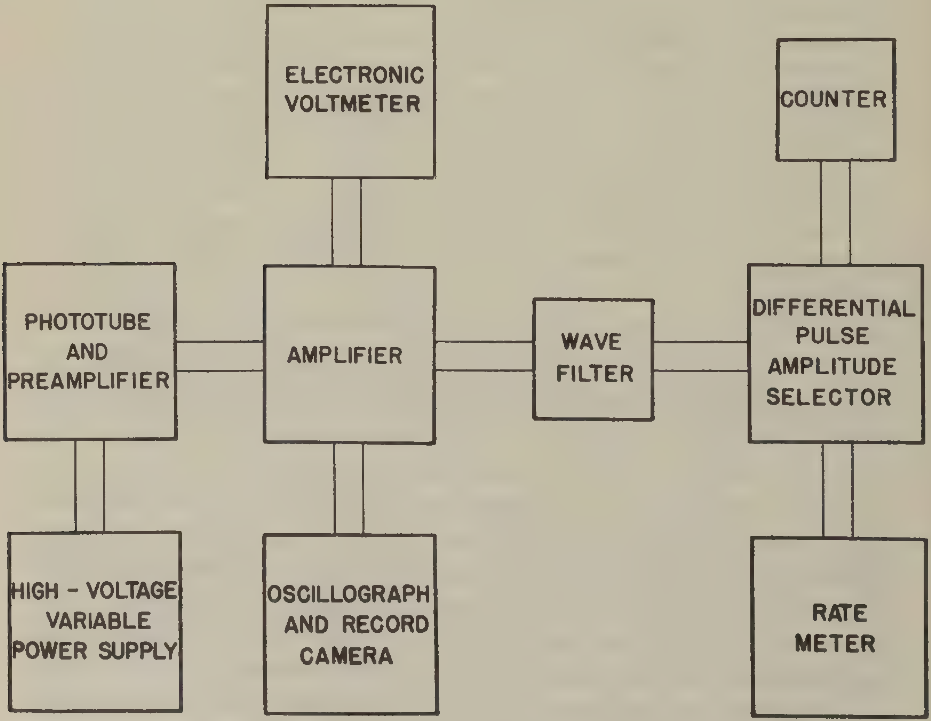
ELECTRONIC VOLTMETER
COUNTER
PHOTOTUBE AND PREAMPLIFIER
AMPLIFIER
WAVE FILTER
DIFFERENTIAL PULSE AMPLITUDE SELECTOR
HIGH - VOLTAGE VARIABLE POWER SUPPLY
OSCILLOGRAPH AND RECORD CAMERA
RATE METER

FIG. 3. Block diagram of electronic circuits.

ing the heater and plate of the preamplifier from batteries. The amplifier,[9] oscillograph,[10] electronic voltmeter,[11] and electronic counter [12] were standard instruments. The rate meter, developed by Don M. Yost (16) and collaborators (1941), was used to provide rapid indication of high counting rates with an accuracy of about 5% when calibrated with uniformly-spaced pulses from Yost's pulse generator.

Preamplifier

The diagram of the photomultiplier and preamplifier circuit is shown in Fig. 4. A regulated power supply, continuously variable from about − 300 to − 800 v., is applied across the 100-K dividing resistors connected to the various dynodes of the photomultiplier. The external connections are made through pin jacks in the cap *W* of the housing of the phototube and preamplifier. The frequency response of the preamplifier is very flat from 200 to 200,000 cycles, as shown in Fig. 5*a*. Here the gain is given in decibels, where 1 db = 20 $\log_{10} A$, and A is the voltage amplification.

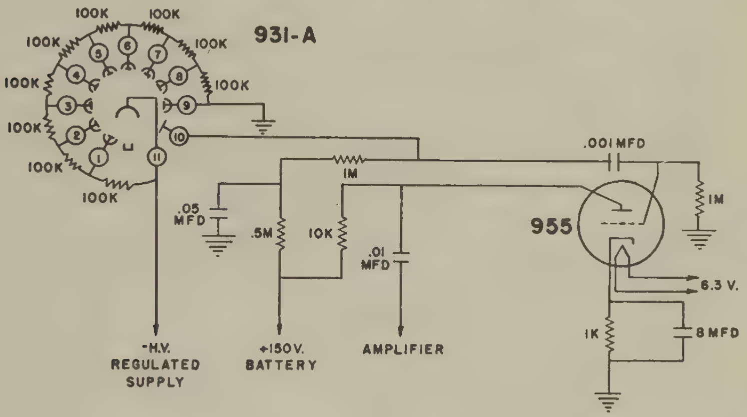

FIG. 4. Photomultiplier and preamplifier curcuit.

Wave Filter

This consisted of a 0.1-megohm resistor in the high side in series with a 0.01-μf. condenser to ground. The output signal from the filter was taken across the condenser. This arrangement, essentially an integrating circuit, attenuated the high-frequency components of the noise considerably more than the pulses due to smoke particles.

[9] Type 450A, Hewlett-Packard Company, Palo Alto, California.

[10] Type 247, Allen B. DuMont Laboratories, Passaic, New Jersey.

[11] Type 400A, Hewlett-Packard Company, Palo Alto, California.

[12] Type 140A, Potter Instrument Company, Flushing, New York.

The Differential Pulse-Amplitude Selector (DPAS) Circuit

This unit, shown in Fig. 6, was designed to give pulse-amplitude-distribution data in conjunction with the rate meter or electronic counter.

The amplified pulses from the counter, about 0.4 v. or more, are fed into the input attenuator (50-K potentiometer), through the 0.02-μf. coupling condenser to the phase-inverter stage *V*1. The switch *SW*2 in the *negative* position sends the pulses from the cathode, and in the *positive* position from the plate, through the 0.02-μf. coupling condenser and the network consisting of the 500-μμf. condenser and two 100-K resistors to the grid of the triode amplifier stage *V*2. The amplification of the combined stages *V*1 and *V*2 at 1000 cycles/sec. is adjusted to 5.0 by means of the 1-K (*adjust gain*) potentiometer which controls the cathode feedback.

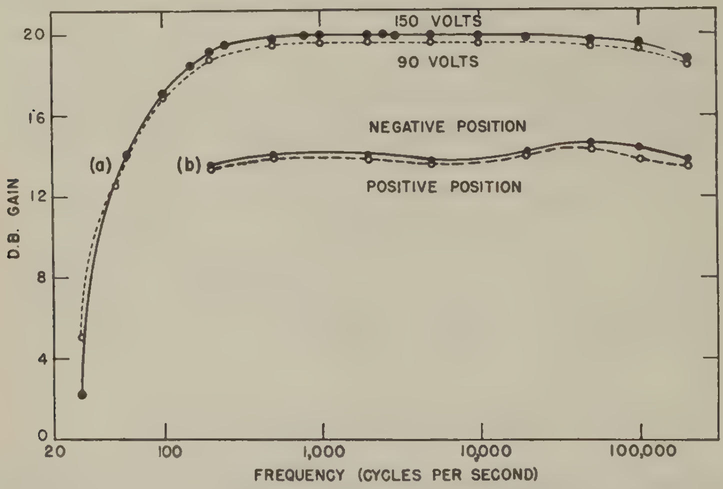

FIG. 5. Response curves: (*a*) photomultiplier preamplifier, (*b*) phase inverter and first amplifier stage, DPAS.

The amplification at the higher frequencies was adjusted to about the same level for both positions of *SW*2 by selecting suitable values of the capacitance between *SW*2 and ground (75-μμf.) and the capacitance (0.006-μf.) and resistance (1-K) shunting the *adjust gain* control. The response curve was flat within ± 1 db from 200 to 200,000 cycles/sec., as shown in Fig. 5*b*.

The amplified pulses from *V*2 are fed to the differential pulse selector circuit, consisting of *V*3 and *V*4, with *SW*3 in the *select* position, or directly to the amplifier stage *V*12 with *SW*3 in the *direct* position. The bias circuit shown in the lower left section of Fig. 6 supplies sufficient negative potential to the grids of the thyratrons *V*3 and *V*4 to prevent

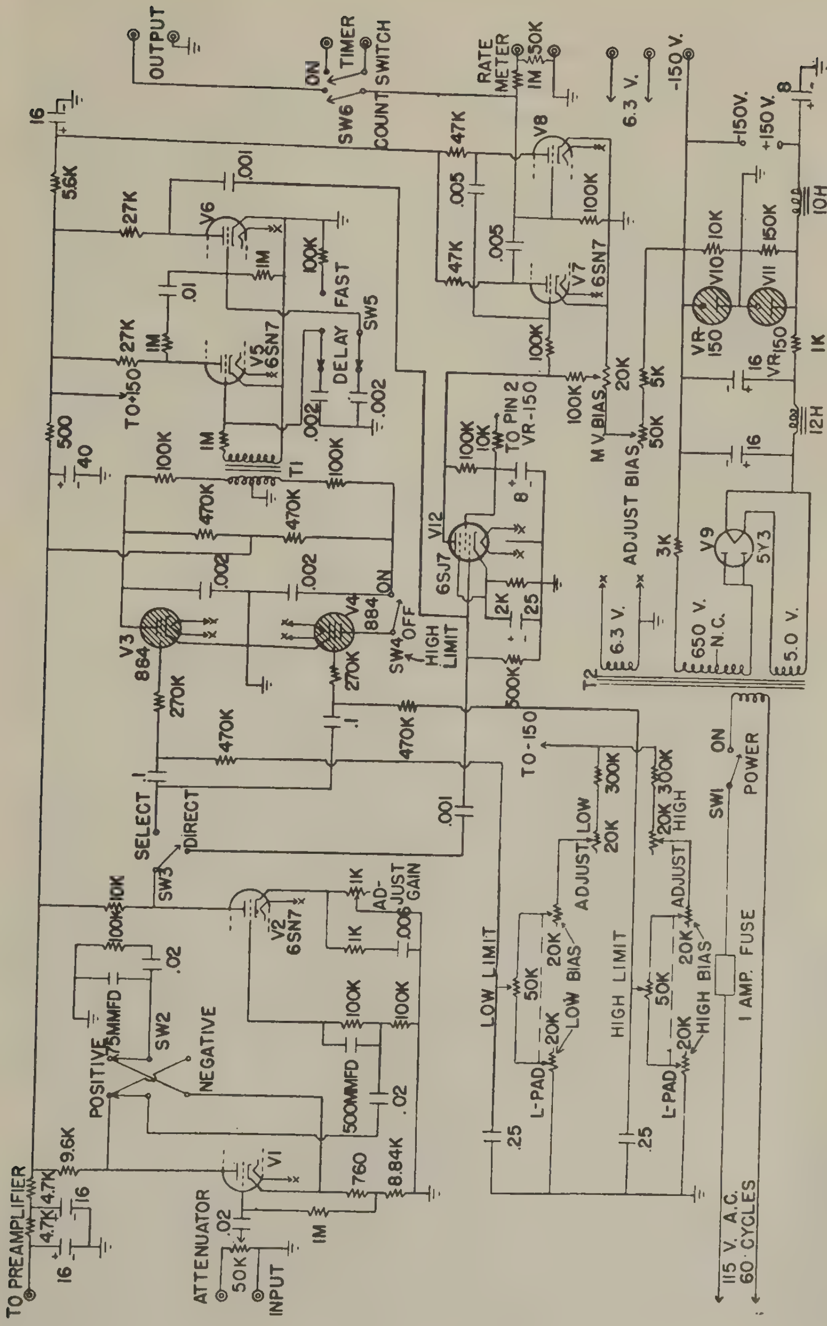

FIG. 6. Differential pulse-amplitude selector circuit. Resistance in ohms unless marked K (kilohm) or M (megohm), capacitance in MFD (microfarads) unless marked MMFD (micromicrofarad).

them from firing. The output circuits of the two tubes are opposed to each other through coupling to the center-tapped 3:1 audio transformer $T1$, as in the differential pulse amplitude circuit (14) of A. Roberts (1940). A pulse firing the low-limit tube $V3$ alone will trigger the multivibrator stage $V7$-$V8$, while a pulse firing both $V3$ and $V4$ almost simultaneously will not trigger the multivibrator. The intermediate stages $V5$, $V6$, and $V12$ amplify the pulse sufficiently to insure positive triggering of the multivibrator. When $SW5$ is in the *delay* position, the R-C combinations, each consisting of a 1-megohm resistor and 0.002 μf. condenser, in the grid and plate circuits of $V5$ delay the peak value of the pulse from the low-limit thyratron $V3$ so that cancellation will be effected even when the high-limit thyratron V4 fires about a half millisecond later.

The bias-control circuit was developed to permit direct reading of the lower and higher voltage limits between which pulses will be counted. $SW5$ was inserted to decrease the resolving time of the selector circuit and might be used in the *fast* position for pulses with very short rise times. Preliminary tests indicated that the resolving time could not be improved significantly, however, and that some revisions might be necessary if the *fast* position is employed.

The *high-limit* switch $SW4$ can be turned *off* to count all pulses firing the low-limit thyratron. With $SW3$ in the *direct* position, the pulses can be fed directly to $V12$, and the 20-K *mv. bias* potentiometer can be used as a low limit discriminator. In this case $SW2$ should be in the negative position in order to obtain a positive pulse from $V12$. The *count switch* $SW6$ simultaneously controls the timer and the output to the counter.

The entire unit is operated from a regulated a.c. line. The VR-stages tend to decrease warmup time and make operation of the circuits independent of the counting rate, which to some extent determines the power requirements. Various R-C filters in the voltage supply lines minimize interaction of the circuits to provide stable operation.

The tests of the DPAS circuit with a pulse generator showed that uniformly-spaced pulses could be counted at rates up to 250/sec. This places the resolving time of the unit at about 4 millisec. With randomly-spaced pulses, the maximum counting rate will be lower, depending upon the coincidence error which can be tolerated.

Experimental Methods

Adjustment of the Optical System

The various units, mounted on the optical bench as shown in Fig. 1, were adjusted to align the centers of the ribbon filament, the auxiliary lens holder B and condensing lens holder G. The source slit E_1, about 1.5 mm. × 4 mm., was then placed at the exact center of the slit holder and the final adjustment was made by moving the lamp along the optical axis until the central section of the image of the ribbon filament was sharply defined upon the source slit. Next, a stream of cigarette smoke was drawn through the smoke tube T_1 at the standard flow rate of one l./min. With an oversize source slit at E_1, the retainer D_3 was cut down to the length shown in the scale drawing, to bring the image of the smoke stream into the plane of the viewing slit.

The adjustment of the slit holder F along the optical axis of the condensing system was made by removing the slit E_2, and viewing the image of the smoke stream from above. With the 3-mm. ($\frac{1}{8}$-in.) smoke tube used in the tests described below, the retainer was moved in and out of the lens holder G to bring the narrowest portion of the image in the center of the bright smoke stream. With a smaller smoke tube, the adjustment can be made to minimize the image dimension normal to the axis of the condensing lens system.

The vertical adjustment of the source slit E_1 was made by placing a circular black stop, about 25 mm. in diameter, on the optical axis just in front of the auxiliary lens holder B to cast a shadow, from which the smoke stream was viewed along the optical axis of the condensing lens system. The slit was readily adjusted to cover the entire smoke stream.

Adjustment of the Electronic Circuits

In connecting the various units together all of the grounds and shields were tied to a common point to prevent a.c. pickup. The amplifier was operated at either 20 db or 40 db.

To adjust the bias control circuit, the dials on *low limit* and *high limit* potentiometers are set to read zero at the low ends of the resistance scales. Then the *adjust low* and *adjust high* controls are turned in succession until 20.0 v. is measured on a high-impedance voltmeter between each of the ground ends and the movable contacts, with the *low limit* and *high limit* potentiometers at dial settings of 10.0. With the *low bias* and *high bias* controls moved all the way to the right, putting the maximum negative bias on the thyratron grids, the *low limit* and *high limit* controls are turned to the left, to read zero. Then, the *bias* controls are set just below the points at which the thyratrons fire. This is conveniently done with an oscilloscope between ground and the grid of $V5$.

When these adjustments are completed, the dials give a reading proportional to the voltage of the pulse required to fire the respective thyratrons. With an amplification of 5.0 in the phase inverter-amplifier stage, and with 20.0 v. across the *low* and *high limit* controls, this corresponds to 4.0 v. at the *input* for the full-scale limit setting of 10.0 when the *attenuator* is also at its full-scale position. With the *attenuator* at some lower setting, the voltage of the input pulse of *positive* or *negative* polarity (determined from the position of $SW2$) which will just fire the corresponding thyratron will be given by the equation:

$$v_p = \frac{\text{limit setting} \times 4.0}{\text{attenuator setting}},$$

where the full-scale setting for both dials is taken as 10.0. This permits selection of a band of pulses within a range between 0.4 and 40 v. before excessive errors arise in reading the dials.

Unless otherwise specified in the tests described below, the DPAS circuit was operated with the *high limit* switch on, $SW2$ on *positive*, $SW3$ on *select*, and the integrator circuit switch $SW5$ on *delay*. In addition the *attenuator* was normally kept at 10.0.

After the light source was turned on, the regulated high-voltage power supply was connected to the 931-A tube, and *in each experiment* the high voltage was adjusted to give a reading of 50 mv. on the electronic voltmeter, connected across the output from the amplifier. This provided a standard operating level for the phototube, which could conveniently be checked with the rotating sector as described under "*Phototube*" above.

Tests of the Improved Counter

Stray Light

The stray light in the optical system appeared at the viewing slit as a faint bluish haze, which could be extinguished by a polaroid oriented at 0° to eliminate the component with the electric vector vibrating normal to the plane of the condensing and viewing lens systems, and reappeared when the polaroid was turned to 90°. This indicated that most of the stray light was caused by scattering from the air molecules within the sensitive volume. When the air was replaced by filtered helium, with a lower refractive index, the stray light decreased noticeably. More careful tests were then made by the method described above for testing phototubes. After measuring the two polarized components with filtered air at atmospheric pressure, the pressure was reduced a known amount and measurements were again made. Results are shown in Table II.

The equation (13) developed by Rayleigh (1871) shows that the intensity of scattering from a fixed volume of air will be proportional to the pressure. Since the pulse voltage is proportional to the total intensity, and the intensity of stray light reflected from the baffles can be regarded

TABLE II

The Effect of Polaroid Setting and Air Pressure on Scattered Light

Air pressure *cm./Hg*	Pulse voltage for polaroid setting 90°	0°
76	2.5	0.25
28	1.3	0.15

as a constant, we may write the relation

$$(2.75 - v_s)/(1.45 - v_s) = 76/28,$$

from which we obtain for v_s, the voltage of the pulse which would be obtained if the system were evacuated, a value of 0.7 v. Thus the stray light from the optical system is *only about one-third the light scattered by the air molecules at atmospheric pressure.*

Distribution of Noise Pulses

A study was made of the voltage distribution of the background counts due to dark current alone and to dark current plus stray light. In each case the amplification of the photomultiplier was adjusted to maintain the *average* noise voltage, read by the electronic voltmeter, at a constant level and the *low-limit* switch of the DPAS was used as a discriminator, with the *high-limit* switch turned off. The voltage distribution of counts is quite different in the two cases, as shown by the second and third columns of Table III. The difference is due to the fact that the photocurrent at the

TABLE III

Counts per Minute for Background and for Aerosols of BG and S, with Standard Amplification[a] and Other Conditions Varied

Low limit voltage	Dark background	Ribbon filament lamp				Carbon arc, BG aerosol
		Background	BG aerosol	BG with polarizer	8-Order S aerosol	
volts						
0.16		5400				
.24	6500	200	1550	1960	4250	2940
.32	2000	1	1140	1290	1580	
.40	1200	0	915	1040	501	2070
.48			680			
.56	540		770		42	1570
.64			650			
.80	100		470	500	5	1320
1.20	8		240			
1.60	0.8		140	213		620
2.00	.03		130			
2.80			50			
3.20			28			350
4.00			20			
6.40						164
12.8						92
20.0						26

[a] Photomultiplier voltage adjusted to give 50 mv. background reading on electronic voltmeter.

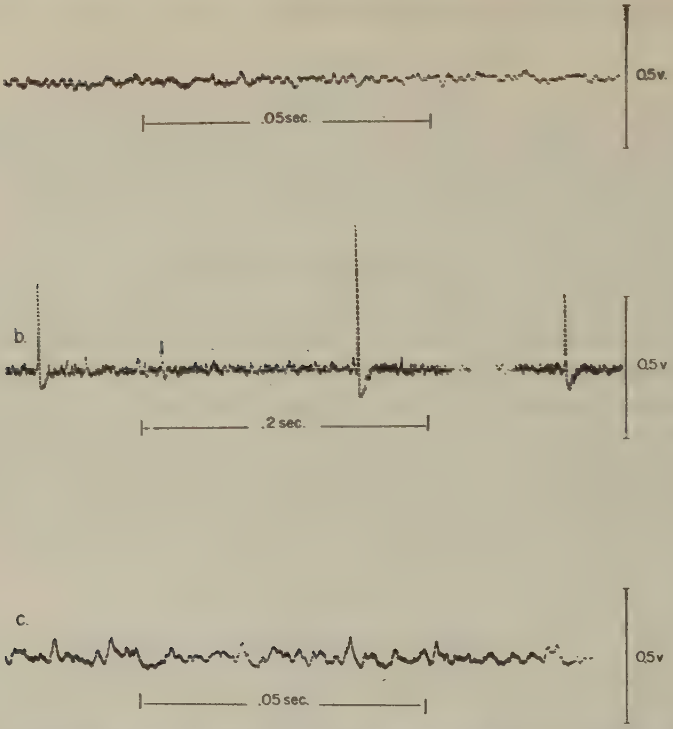

FIG. 7. Oscillograph records of background and particle counts, with average background noise = 50 mv.: (*a*) typical background noise pattern, (*b*) pulses from BG particles, (*c*) pulses from 8-order sulfur particles.

cathode is widely different in the two cases, and with decreased cathode current the statistical fluctuations become relatively more important.

Photographs of the background noise pulses made with a DuMont-Fairchild oscillograph-record camera[13] are shown in Fig. 7*a*.

Tests with BG Smokes

An aerosol of *Bacillus globigii* (BG) spores was set up in the usual way (4,5) from an aqueous suspension containing 1.3×10^9 spores/ml. It was passed through four sheets of fiber-glass paper under constant conditions, to reduce the concentration to a suitable level before it was put through the counter. The amplitude distribution of the pulses then was obtained under the standard conditions of operation as in the case of the background pulses. Repeat counts on the pulses above 0.40 v. during the course of the run were constant within ± 10%. Data are shown in the fourth column of Table III for the count distribution corrected for the background noise counts. An oscillogram of the BG pulses is shown in Fig. 7*b*.

---

[13] Type 314, Allen B. DuMont Laboratories, Inc., Passaic, New Jersey.

In another test with the BG aerosol, an attempt was made to improve the signal-to-noise ratio by using a polarizer to decrease the background light in the optical system. When the phototube high-voltage supply was increased to bring the average background noise to the normal 50 mv. there was a slight increase in the counting rate as shown in the fifth column of Table III.

Test with 8-Order Sulfur Sol

A sulfur sol was prepared following the method of La Mer (1,7,8) and collaborators (1945, 1946) by mixing 0.0005 *M* solutions of HCl and $Na_2S_2O_3$, and allowing them to stand at room temperature for 50 hr. At that time a series of eight red bands was observed in the Tyndall beam, indicating sulfur particles about 1.0μ in diameter. A sample of the sol was transferred to the spray-type generator and an aerosol was put up under the conditions used with the BG above. Data are given in the sixth column of Table III, and an oscillogram of the pulses is shown in Fig. 7*c*. Both the data and the record indicate that the scattering around 90° was less for the 8-order sulfur particles than it was for BG particles under the test conditions.

Test With Carbon-Arc Projection Lamp

The arc-feed unit[7] was adjusted to give an arc about 50% longer than the recommended value. This was found to give maximum brightness with an operating current of 42–46 amp. A metal slit, about 3 mm. × 6 mm., was inserted at the focal plane of the elliptical mirror, which was adjusted to give a speed of *f*: 2.2. This slit was followed by a piece of heat-absorbing glass and the auxiliary lens holder *B* shown in Fig. 1. The system was adjusted until the slit occupied the former position of the ribbon filament. A polarizer in the incident beam was set at 0° to decrease background light in the system and the high-voltage supply was adjusted to give the standard noise level in the usual way with filtered air through the cell. The data obtained for a BG aerosol under the same conditions as in the earlier tests are given in the last column of Table III.

Successful use of the high-intensity carbon arc source is due to the very low level of background illumination in the optical system. Thus, fluctuations which would have caused spurious counts in the original small angle cell were not troublesome here. Comparison of the data in Table III indicates about a threefold increase in signal-to-noise ratio, since aerosols of comparable concentrations were being measured.

DISCUSSION

The intensities of the light scattered at about 90° by individual BG particles and sulfur particles of about equal size can be compared from the data of Table III and Figs. 7*b* and *c*. These show that the average pulse obtained from a BG particle is considerably larger than that from a sulfur particle. The exact scattering functions of the BG particles cannot be calculated because of their irregular shapes, approximate ellipsoids of revolution with a major axis of 1.2 μ and a minor axis of 0.8 μ. The refractive index of bacterial particles is relatively low (12) according to G. Oster (1948), while that of sulfur is high. In general, the scattering intensity is expected to be greater for particles of higher refractive index. The apparent anomaly was first attributed to a surface structure which might increase the scattering from a BG particle. Later, however, it was recalled that the BG particles could not be counted when a dilution apparatus which we had developed was substituted for the filter pad. This indicates that the scattering intensity at 90° was reduced by dilution, which is attributed to further drying in the apparatus. Some previous unpublished data (11) obtained by C. T. O'Konski (1946) with our 90° concentration meter (6) had given similar indications which had led to the adoption of standard flow rates, to keep a constant level of humidity in the aerosol produced in the spray-type generator. Tests of aerosols containing bacterial particles should be carried out under conditions of controlled humidity, since water around aerosol particles will affect the filtering, as well as the light-scattering properties.

The differential pulse amplitude selector was only used as a simple low-limit discriminator in the work described above, but electronic tests showed that the high-limit circuits also functioned satisfactorily. Some differential counts, not presented here, were obtained with the instrument, although the BG and 8-order sulfur particles gave too small a signal-to-noise ratio for optimum application of this feature.

The light scattering from very small particles is proportional to the sixth power of their diameter, as calculated (13) by Lord Rayleigh (1871). Scattering from particles comparable to the wavelength of the light goes through a complicated transition range (7), while that for large particles is proportional to the *square* of the diameter, as calculated (10) by G. Mie (1908) for isotropic spheres. R. C. Tolman (15) and his collaborators (1919), showed experimentally that the intensity of light scattered at about 90° by particles of ground silica, from 2–20 μ in diameter follows this square law. On the basis of results with the 8-order sulfur sol, the square-law scattering relationship, and the measured stability of the ribbon-filament light, it is estimated that this apparatus will classify particles 1μ in diameter and larger into 1-μ size-range groups with a resolution of about 5–10%. For smaller particles, however, the resolution will of course depend upon the signal-to-noise ratio of the instrument.

Since the background light in the optical system was mainly that scattered by the air molecules, it can be decreased considerably by reducing the sensitive volume of the optical system, now about 1.5 × 3.5 × 1.3 mm., or 7 mm.^{3} This easily can be cut down to 1.0 × 1.0 × 0.7 mm. or 1.7 mm.^{3}, if a 0.8-mm. ($\frac{1}{32}$-in.) smoke inlet tube is used. Simultaneous fourfold reduction of the linear flow rate with a corresponding increase of the time constant of the RC wave filter should reduce the output noise level by a factor of about three. This should allow detection of particles 0.6–0.7 μ in diameter and their convenient study up to concentrations of 10^5 particles/l.

Acknowledgment

It is a pleasure to acknowledge our indebtedness to Mr. Jack Baird for the construction of the apparatus here described, to Miss Cheryl Curtis for assistance in tests of the optical system, and to Mr. Donald G. Rose for help in preparation of a number of the illustrations.

Summary

We have described an improved photoelectronic counter employing right angle light scattering, with a new optical system in which stray light has been reduced to an extremely low level. Studies of various light sources show that the ribbon-filament tungsten lamp with its uniformity, stability, and large area, is most suitable for this instrument.

Test of sulfur aerosols made by spraying monodisperse sulfur sols showed that particles of 1.0μ diameter can just be detected. Spores of *Bacillus globigii* (about 0.8 × 1.2 μ) produced by a spray-type generator were easily counted, but lower humidities decreased the intensity of the scattered light until these particles did not register. The effect is attributed to absorption of water by the particles which increases their scattering at high humidities.

Design considerations influencing the determination of particle-size distribution of aerosols with this photoelectronic counter are discussed, and electronic circuits are described, capable of counting those pulses within a predetermined and adjustable size range.

Measurements on the optical system indicate that for larger spherical particles, the pulses will be characteristic of particle diameter within 5–10%. For smaller particles the accuracy is limited by the signal-to-noise ratio.

References

1. Barnes, M. D., and La Mer, V. K., *J. Colloid Sci.* **1**, 79 (1946).
2. Engstrom, R. W., *J. Optical Soc. Am.* **37**, 420 (1947).
3. Gucker, F. T., Jr., *Electronics* **20**, 107 (1947).
4. Gucker, F. T., Jr., O'Konski, Chester T., *Chem. Revs.* **44**, 373 (1949).
5. Gucker, Frank T., Jr., O'Konski, Chester T., Pickard, Hugh B., and Pitts, James N., Jr., *J. Am. Chem. Soc.* **69**, 2422 (1947).
6. Gucker, F. T., Jr., Pickard, H. B., and O'Konski, C. T., *J. Am. Chem. Soc.* **69**, 429 (1947).
7. La Mer, V. K., and Barnes, M. D., *J. Colloid Sci.* **1**, 71 (1946).

8. La Mer, V. K., and Johnson, I., *J. Am. Chem. Soc.* **67**, 2055 (1945).
9. Marshall, Fitz-Hugh, Coltman, J. W., and Bennett, A. I., *Rev. Sci. Instruments* **11**, 744 (1948).
10. Mie, G., *Ann. Physik* **25**, 377 (1908).
11. O'Konski, C. T., M.S. Thesis, Northwestern University (1946).
12. Oster, G., *Chem. Revs.* **43**, 319 (1948).
13. Rayleigh, Lord, *Phil. Mag.* (4), **41**, 107, 274 (1871).
14. Roberts, A., *Rev. Sci. Instruments* **11**, 44 (1940).
15. Tolman, R. C., Gerke, R. H., Brooks, A. P., Herman, A. G., Mulliken, R. S., and Smyth, H. D., *J. Am. Chem. Soc.* **41**, 575 (1919).
16. Yost, Don M., O.S.R.D. Report No. 65, "The Development of Laboratory Methods of Detecting and Analyzing Gases Containing Radioactive Sulfur" (1941) available through Office of Publications Board, U. S. Department of Commerce, as Report No. 16437.

LOSS OF DEVELOPABILITY OF PHOTOGRAPHIC EMULSIONS CAUSED BY WASHING IN WEAK SILVER HALIDE SOLVENTS: A NEW REVERSAL EFFECT[1]

T. H. James

From the Eastman Kodak Research Laboratories, Rochester, N. Y.

Received June 20, 1949

INTRODUCTION

The silver halide solvent, sulfite ion, is always present in practical developing solutions which employ organic developing agents. The conventional solutions contain up to 100 g. of Na_2SO_3/l. The sulfite is added primarily to decrease the rate of loss of developing agent by aerial oxidation and to remove or prevent the formation of the quinone or quinone-like oxidation products of the development reaction, which otherwise would undergo a decomposition-polymerization reaction with the formation of staining material. The solvent action of the sulfite ion, however, has some effect upon the course of development itself under most practical working conditions, and the extent of this effect will vary considerably with the conditions. The solvent action of the sulfite is responsible for the "fine-grain" properties of such slow-working developers as Kodak developers, D-76 and D-25. If the rate of development is very low, the solvent action of the sulfite may prevent direct development from occurring and cause a complete shift to physical development (1). An extreme example of this effect occurs with hydroquinone solutions of pH below 9.0, where the presence of sufficient sulfite can prevent any development from taking place except a small amount of physical development, although normal development is readily attained in the absence of sulfite or in the presence of only small concentrations thereof.

The solvent action of sulfite under some conditions can influence development by uncovering internal latent image and making it available for direct development. The facts that developers containing high sulfite concentrations give considerably less solarization reversal than sulfite-free developers and that the solarization becomes less pronounced as development time is increased in the high sulfite developer stem from the same cause. The sulfite dissolves off the sheath of AgBr which protects the "solarized" latent image from direct attack by the developer.

---

[1] Communication No. 1264 from the Kodak Research Laboratories.

Study of the solvent action of sulfite in the developer is complicated by the simultaneous occurrence of developemnt. In the present investigation, this complication was avoided by the expedient of treating the photographic material with a simple sulfite solution and carrying out development subsequent to this treatment. It was shown that the sulfite can interfere with development by isolating latent-image nuclei from the grain. This action is more pronounced in the high- than in the low-exposure regions. The photographic result is a reversal in the high-exposure regions.

Experimental Procedure

A standard motion-picture positive-type film was employed in most of the work. Strips of this film were exposed on the Eastman IIB Sensitometer, were washed for varying times in the solvent, and were developed under standardized conditions.

The washing was carried out in an apparatus designed as an intermittent batch washer. The wash solution was contained in an earthenware crock of about 70 l. capacity. The temperature of the wash solution was controlled by circulating water of the desired temperature through a stainless-steel coil inside the crock. A tube from the bottom of the crock led into the washing chamber itself. Flow of solution through the tube was controlled by a valve system consisting of a short length of rubber tubing and a pressure clamp which could be operated by air pressure. The clamp closed when the pressure was applied; when the pressure was released, steel springs forced the clamp open. The washing chamber was of stainless steel and held approximately 4 l. of solution. A solenoid-operated dump valve was located at the bottom of the chamber. The washer was controlled by an electric timer which operated on a 3-min. cycle. Approximately 20 sec. were required to empty the chamber through the dump valve. This valve then closed, and the air pressure on the intake valve was released by means of a solenoid-controlled air valve. About 15 sec. were required for the chamber to fill with wash solution. The intake valve then closed. A float operating through an electric relay was used to open the air valve and thus close the liquid intake valve. The wash solution was agitated by means of nitrogen led in through the bottom and discharged through a series of tiny orifices in a tube extending the length of the chamber bottom. The film was held in place on stainless-steel racks.

One bad feature of the batch washer is the time required to empty the chamber and to fill it again. This causes some unevenness of washing between the top and bottom of the film. In the present experiments, the effect of this unevenness was slight but noticeable. Wherever the slight effect was of importance, however, it was minimized by using a directional pair of sensitometer strips and taking the average density point by point as the true value. While this method does not lead to a complete correction, control experiments showed that it was quite adequate for the present purposes.

Experimental Results Obtained with a 2% Sodium Sulfite Solution

The initial experiments with a 2% Na_2SO_3 solution as the washing medium were carried out with the wash solution at 25°C. and development for 2 min. in the Kodak developer, D-16, at 20°C. The film was transferred directly from the wash solution to the developer in most experiments, since preliminary experiments had shown that little or no change was effected by giving the strips an intermediate washing in water.

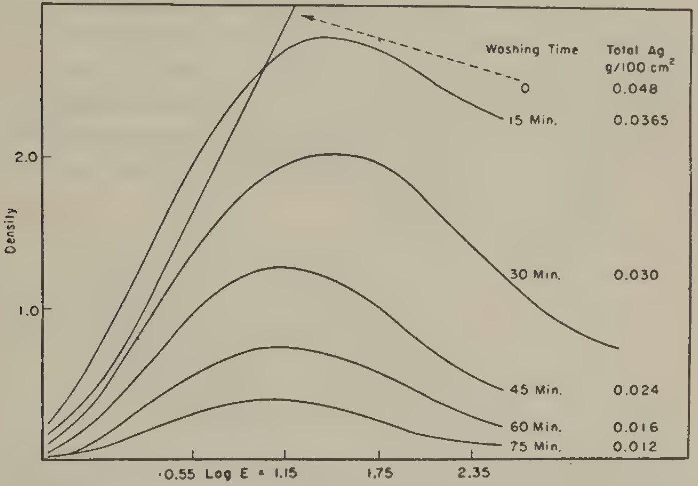

FIG. 1. Characteristic curves for film washed for varying times in 2% Na_2SO_3 solution prior to development.

Strips which had been washed only a few minutes in the sulfite solution showed apparent latensification in the lower exposure regions. At longer washing times, reversal occurred in the shoulder regions. The maximum density decreased with increasing washing times, and the reversal became more pronounced. A family of curves representing a series of washing times is given in Fig. 1. At the heavy-exposure end of the sensitometer strips, the main image area is separated from the halation fringe by a "Mackie line" of lower density than either. Thus, for the 30-min. strip of Fig. 1, the density of the main image area of the highest exposure step is 0.73, the density of the halation fringe is 0.99, and the density of the separating line is 0.62.

As washing proceeds, the total silver halide content of the film decreases almost linearly with time after an initially more rapid decrease in the first few minutes. The data for the silver content at various stages of washing are given on the right-hand side of Fig. 1. The reversal is not associated with a change in the silver halide content of the film from one exposure area to another, insofar as could be detected analytically. Silver values were obtained at various points on a strip of washed film which corresponded closely to the 30-min. strip of Fig. 1. The silver values obtained are as follows (g. Ag/100 cm.^{2}) : 0.0297 g. for log $E = 2.5$; 0.0291 g. for log $E = 1.55$; 0.0297 g. for log $E = 0$; and 0.0296 g. for the unexposed area. All silver determinations were made by D. S. Brooks and T. Davis, of these Laboratories.

The latent-image material itself is affected by the sulfite wash to a much smaller degree than the developability of the silver halide grains. This is shown by experiments on physical development of the washed strips. Fig. 2 shows some results. The strips were fixed 4.5 min. in a solution containing 5% hypo and 0.5% KOH, washed 40 min. in running water, then developed 2 hr. in a *p*-phenylenediamine physical developer (2). Nitrogen agitation was used during the development, which was carried out at 20°C. It is noteworthy that the slufite washing has caused no reversal for physical development.

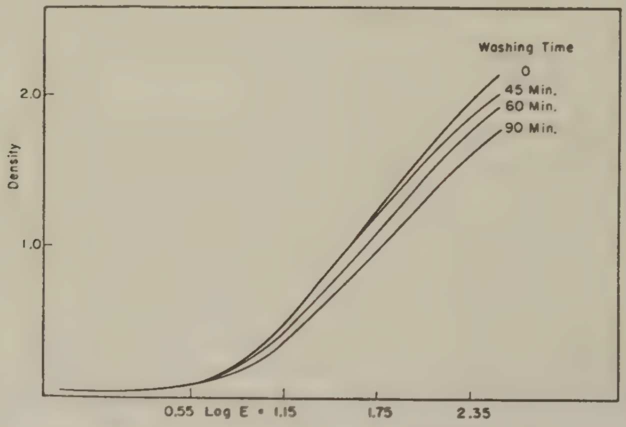

FIG. 2. Physical development of film washed in 2% Na_2SO_3 solution.

The reversal curve bears a striking similarity in appearance to the solarization curve. As already mentioned, however, the usual effect of sulfite is to remove or diminish solarization. Moreover, the reversal obtained by washing the film with sulfite solution does not result from any entombing of the latent-image nuclei. This is shown by the results of experiments on the change in internal image with washing time. Fig. 3 shows the results of 45 min. washing on the internal image. Curve 1 represents the normal internal image of the unwashed film as determined by bleaching the surface image in a solution of 2.5 g. of $K_2Cr_2O_7$ and 1. 33 cc. of H_2SO_4/l. The bleaching time was 3 min. The film, after a water wash, was developed 6 min. in a solution of the Kodak developer, D-19, to which 10 g. hypo/l. had been added. Curve 2 shows the reversal obtained by developing in the D-19 plus hypo solution an unbleached strip which had been washed in 2% sulfite solution for 45 min. Curve 3 represents a similarly treated strip which had been bleached after the washing but before development. The amount of latent image unaffected by the chromic acid bleach after 45 min. wash is quite small.

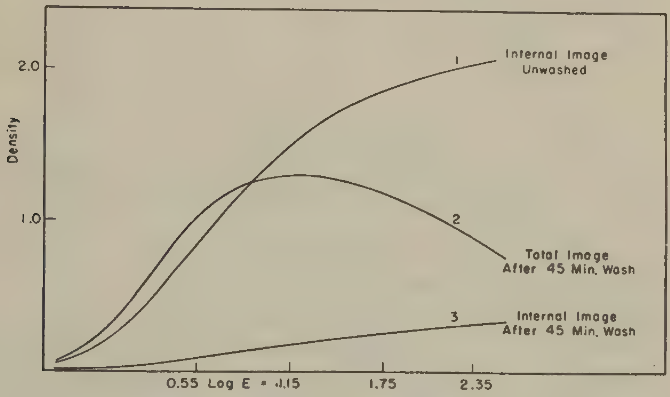

FIG. 3. Effect of washing in 2% Na_2SO_3 solution upon developability of the internal latent image.

Addition of 0.005% lauryl pyridinium *p*-toluenesulfonate to the 2% Na_2SO_3 solution eliminates the reversal. This effect is illustrated by the curves reproduced in Fig. 4. When the film was first washed in 2% sulfite solution and then bathed for 5 min. in the sulfite-pyridinium solution, however, the reversal was as marked as that produced by the sulfite alone, showing that the effect of the quaternary salt was on the solution of silver halide by the sulfite, not on the subsequent development process.

The reversal obtained by washing exposed film in sulfite solution prior to development is not confined to the particular emulsion used. Marked reversals were obtained with two other positive commercial emulsions, one of the "boiled" type, the other of the "ammonia" type (3). Similar reversals were obtained with 2 simple emulsions prepared according to the directions given by Trivelli and Smith (4). One of these was a pure bromide emulsion, the other contained 2.56 *M*-% iodide.

A marked reversal can be obtained by bathing the film in a single solution of Na_2SO_3, provided that sufficient agitation is employed. The curves obtained from the developed strips are almost identical in form

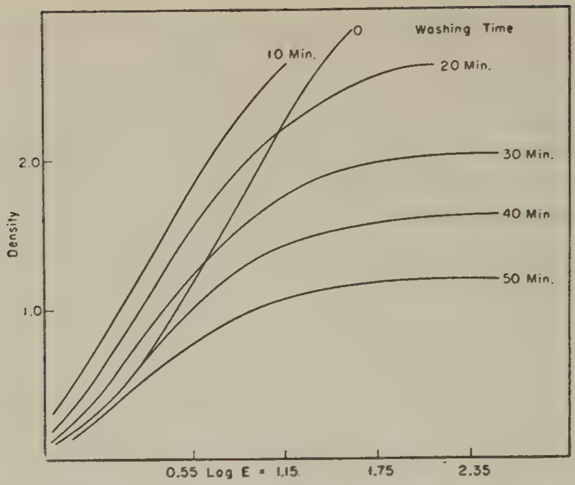

FIG. 4. Characteristic curves for film washed in 2% Na_2SO_3 solution containing 0.005% lauryl pyridinium *p*-toluenesulfonate.

with those obtained by the batch-washing technique, but longer times are required to attain the same loss in density.

All data given thus far have been corrected for fog. The fog values, in general, increased at first with increasing washing time, then passed through a maximum, and decreased. No difference in fog values was noted between film which had been given no treatment except the sulfite wash and film which had been bathed for 3 min. in the acid bichromate solution and then washed. Data are given in Table I.

Gold latensification (2) of the film before the washing operation had only a small effect upon the final result. The gold treatment increased somewhat the rate of loss of density with time of washing and shifted the maximum density towards lower exposures. The general shape of the reversal curve was not changed, however.

TABLE I

Fog Values Obtained for Different Times of Washing in 2% Na_2SO_3 Solution. Development Was for 2 Min. at 20°C.

Time of washing *min.*	Fog for "bleached" film	Fog for "unbleached" film
0	0.02	0.02
6	.07	.07
15	.14	.11
24	.14	.14
30	.19	.16
39	.19	.18
48	.20	.17
60	.19	.15
90	.08	.08

Results with Ammonia Solutions

An ammonia solution wash affects the toe of the characteristic curve in much the same way as the sulfite wash. Short washing times produce an increase in developed density, whereas longer washing times are accompanied by a loss in density. The shoulder of the curve starts to bend over even at quite short washing times, and the maximum density decreases regularly with increasing time of washing. A slight reversal was obtained in some experiments, no reversal in others. Only slight increases in fog were observed. Fig. 5 illustrates the results obtained with 0.6 *M* ammonia used in the batch washer. Similar results were obtained by bathing the film in the developing machine with a single charge of 0.937 *M* ammonia, using paddle agitation. No loss in latent image for post-fixation physical development resulted from the ammonia washing. On the contrary, slight latensification occurred.

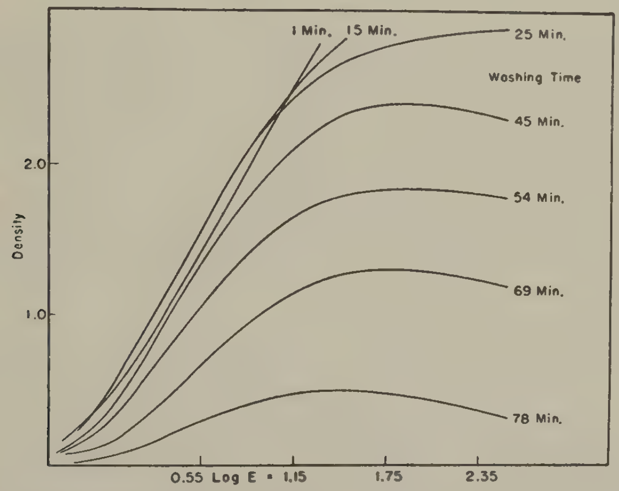

FIG. 5. Characteristic curves for film washed in 0.6 *M* NH_3 solution before development.

Results with Sodium Thiosulfate Solutions

Results similar to those obtained with sulfite were obtained by washing the exposed film in a dilute solution (*e.g.*, 0.18%) of $Na_2S_2O_3$. The reversal, although definite, was not so marked as that obtained with the sulfite treatment. The solvent action of the hypo on the film was, however, quite uneven with respect to depth in the emulsion layer. The image obtained on development was much weaker at the emulsion-solution surface than at the emulsion-support surface. No gradation of this type was noticed when sulfite solution was used as the washing medium.

Discussion

Loss of silver halide on washing in the Na_2SO_3, ammonia, and $Na_2S_2O_3$ solutions can only partially account for the observed loss of developability. It cannot account at all for the reversal obtained with the sulfite or thiosulfate solutions. The solvents evidently isolate some of the latent-image centers from the grains by dissolving silver halide from around them, thus preventing direct development from occurring. Even with the "internal" developer (D-19 plus hypo), little physical development of the isolated nuclei occurs.

The reversal obtained with sulfite and thiosulfate washes probably is a result of a charge effect acting upon the rate of solution of the silver halide. Several writers have suggested that the negative-charge barrier surrounding the silver halide grain is depressed locally at the latent-image centers. Schwarz and Urbach (5) originally suggested that such a depression in the charge barrier constituted the latent image. This extreme form of the charge theory is known to be incorrect, but the possibility remains that a localized depression is associated with the latent-image silver specks.

The sulfite reversal may be attributed in a large degree to such a depression in the charge barrier. Sulfite ion, having a double negative charge, will be repelled by the negative charge of the silver halide surface, and only sulfite ions of higher than average kinetic energy can overcome this repulsion and reach the surface of the grain under ordinary conditions. If a localized depression in the barrier exists in the neighborhood of the latent-image centers, a larger fraction of the sulfite ions will be able to reach the surface at these points than at points distant from the latent-image centers. The rate of solution of silver halide in the neighborhood of the latent-image centers accordingly will be greater than at other points on the silver halide surface.

The magnitude of the charge barrier should be smaller the larger the latent-image speck. Accordingly, the rate of solution of the silver halide around the large silver centers should be higher than that around the small centers. The large centers thus will be isolated from the silver halide grain more quickly than the corresponding smaller centers, and a relative decrease of developability will occur in the higher exposure areas.

The action of lauryl pyridinium *p*-toluenesulfonate in eliminating the reversal is exactly what would be expected if the hypothesis just outlined is the correct explanation of the reversal. The pyridinium salt strongly depresses the charge barrier over all of the grain surface and, thus, should "iron out" completely, or to a large extent, any localized variations in the barrier. The fact that little or no variation in total silver halide content with exposure was detected after washing the film in sulfite solution does not invalidate the preceding speculation. The areas of the latent-image specks are extremely small in comparison with the total area of the grain surface, so that a large variation confined to a very small area would not be detected by the usual analytical methods.

The slight reversal sometimes obtained with ammonia washing evidently cannot be explained in this way. Some tendency favoring preferential isolation of the large specks must exist, apart from a differential charge effect. This is not surprising, however. Simply from space considerations, it might be expected that the silver/silver halide interface would be under a greater strain for the large specks than for the small ones, and the silver may even break away from the silver halide along some portion of the interface. Some of the same factors which cause the silver halide to be more readily reduced by a developer at the silver/silver halide interface may act to make the silver halide dissolve more rapidly at such points.

SUMMARY

The developability of several positive-type photographic emulsions is decreased by washing the exposed film in a 2% Na_2SO_3 solution before development. The maximum density obtained on development decreases regularly with increasing time of washing. Agitation of the washing solution markedly accelerates the effect. The washed film shows a large reversal in the high-exposure areas. The density at the highest exposure used often is less than half of the maximum density. No reversal occurs if lauryl pyridinium *p*-toluenesulfonate is added to the wash solution.

Developability is decreased by washing the exposed film in NH_4OH (0.3 M–1.0 M) and in dilute $Na_2S_2O_3$ solution. No reversal, or at most a slight reversal, was obtained with the film washed in ammonia. Definite reversal was obtained with the film washed in dilute hypo (0.183%), although the reversal was not so marked as that obtained with the sulfite wash.

The washing procedures used do not attack the latent-image material (ammonia), or attack it to only a slight extent (sulfite), as shown by the slight effect of the washing upon subsequent post-fixation physical development. The washing isolates the latent-image nuclei from contact with the grains. The reversal can be explained as primarily a charge effect.

REFERENCES

1. JAMES, T. H., *J. Phys. Chem.* **47**, 597 (1943).
2. JAMES, T. H., VANSELOW, W., AND QUIRK, R. F., *J. Phot. Soc. Am.* **14**, 349 (1948).
3. *Cf.* JAMES, T. H., AND HIGGINS, G. C., Fundamentals of Photographic Theory, pp. 18 and 23. John Wiley and Sons, Inc., New York, 1948.
4. TRIVELLI, A. P. H., AND SMITH, W. F., *Phot. J.* **79**, 330 (1939).
5. SCHWARZ, G., AND URBACH, F., *Z. wiss. Phot.* **31**, 77 (1932).

HYDROPHOBIC MONOLAYERS ADSORBED FROM AQUEOUS SOLUTIONS[1]

Elaine G. Shafrin and W. A. Zisman

From the Naval Research Laboratory, Washington, D. C.

Received May 16, 1949; revised Aug. 3, 1949

INTRODUCTION

The possibility of studying hydrophobic monolayers isolated by adsorption from aqueous solution had been suggested by previous experiments (1,2) in which oleophobic monolayers isolated by adsorption from various organic solvents had been found to be reproducibly hydrophobic. It was hoped that the application of similar techniques to aqueous systems would implement the study of hydrophobic monolayers and allow the comparison of the resultant films with those described earlier. Moreover, a method was desired for investigating many classes of amphipathic polar molecules which, although able to adsorb as monolayers from organic solvents, were not oleophobic. Such compounds could not be isolated from oil solutions by the dipper technique (1) because the dipper emerged from the solution covered by a thick layer of liquid adhering to the underlying monolayer. With the use of either solvent or evaporation techniques to remove this layer there arises the possibility that the monolayer may be damaged by the solvent or that a residue of solute may be left on top of the monolayer as a result of evaporation. When polar molecules can be adsorbed as a film unwetted by the solvent, these difficulties are obviated.

The adsorption of hydrophobic films on solids from aqueous solutions is basic in the formation of water-repellent coatings and corrosion-inhibited and peptized systems. Such films also play an essential part in processes for the flotation separation of a variety of minerals. Wark, Taggart, Gaudin, Cox and others have investigated the formation of hydrophobic films on minerals and the adhesion and wetting phenomena involved in the contact of film-covered solids with bubbles of air, and a valuable survey of fundamental knowledge of the subject up to the beginning of World War II has been given by Wark (3). The close relation between the formation of hydrophobic films on ferrous metals and the property of inhibiting rusting has been remarked for a decade. Recent investigations of this laboratory (4,5) have clarified and extended the subject. But this and numerous other applied problems of surface chemistry require that much more be learned of the structure of hydrophobic films and the kinetics of their formation.

---

[1] The opinions or assertions contained in this paper are the authors' and are not to be construed as official or reflecting the views of the Navy Department.

It may avoid confusion to note that the adsorbed films studied here differ greatly from the Langmuir-Blodgett monolayers and multilayers which are prepared on aqueous substrates *by collecting floating, compressed monolayers of insoluble molecules.* The Langmuir-Blodgett films can be formed only under carefully controlled conditions from a special class of compounds (6). It is evident that the classification of monolayers into hydrophobic and oleophobic types is not the most fundamental, but it is useful.

Experimental Methods

The films were examined after being adsorbed upon "dippers" of carefully selected, scratch-free, commercial platinum foil as in the earlier study (1). Each dipper was cleaned just before use by a brief heating to dull redness in a Bunsen flame. After numerous cycles of heating and cooling a crystalline change often occurred and the platinum became a dull gray. When in that condition the dippers were no longer useful for this type of work (2). The aqueous solutions were made at varying concentrations of polar compounds whose sources and purities have been described earlier (1,2). No precautions were taken to free the amines of CO_2. Distilled water prepared from a "Stokes" still fitted with a solid tin condenser was used throughout. Pyrex glass equipment was used and was always cleaned in chromic-sulfuric acid and rinsed repeatedly with hot distilled water delivered directly from the still.

Measurements of the hydrogen ion concentration were made using a Macbeth Model A pH Meter (line-operated, continuous-reading), fitted with glass and calomel electrodes. The pH of the water was adjusted as needed by the addition of HCl or KOH. The glass electrode was cleaned with chromic acid solution, while the calomel electrode was frequently rinsed and soaked in successive baths of grease-free distilled water. This method of pH measurement was chosen for its convenience and because the results of experiments by Wark and Sutherland (7) revealed that neither dye-indicator nor hydrogen electrode methods of pH measurement were suitable for this type of system. The primary difficulty with such methods is suggested to be the adsorption on the electrodes of a barrier monolayer. Recent studies of ion penetration (4) indicate that, although such a film does not constitute a barrier to the small hydrogen or hydronium ions, it prevents formation of gas bubbles.

All adsorption experiments with the dippers were conducted in a small glass hydrophil tray $4\frac{5}{8}''$ square and $1\frac{1}{8}''$ deep which had a carefully ground and waxed rim $\frac{1}{4}''$ wide. This was filled to overflowing with the aqueous solution and the surface of the water was always scraped clean in the manner customary in trough experiments with several flat, waxed Pyrex barriers 8″ long, $\frac{1}{2}$″ wide and $\frac{1}{4}$″ thick. The unusual depth of the tray permitted adequate immersion of the electrodes of the pH meter for continuous observation of the hydrogen ion concentration and allowed the use of a small, motor-driven, waxed, glass stirrer in order to decrease the time for attaining adsorption equilibrium.

A further experimental precaution was taken to protect the dipper from contacting floating organic material on passing through the air-water interface. A rectangular strip of 0.010″ platinum foil was bent and spot-welded to form a narrow, flat-sided tube open at both ends, to which were welded four strips of platinum foil $\frac{1}{8}$″ in width to form supporting legs. There resulted a narrow chimney of rectangular cross-section just wide enough to permit the passage of the dipper. In use the chimney was first flamed to remove organic contamination, and upon cooling, was immediately placed with its axis vertical in the freshly swept water of the hydrophil tray (see Fig. 1) with the legs adjusted so that the water level reached midway up the chimney. The adsorption experiment was promptly commenced by lowering the clean dipper through the chimney until it was immersed to a depth of over 1 cm. below the surface of the solution. After the proper immersion time the dipper was withdrawn from the solution coated with an adsorbed film.

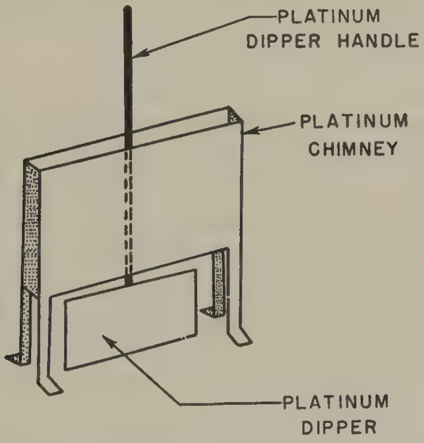

FIG. 1. Platinum chimney in use.

Measurements of the hydrophobic and oleophobic contact angles of the resulting films were obtained using drops of the generating aqueous solution and drops of *n*-hexadecane. The test drops were formed on a flamed platinum loop and then gently lowered onto the dipper surface after which the advancing angles of contact were measured. No attempt was made to study receding contact angles. All measurements were made in room air at temperatures from 25 to 30°C. and at 50 to 70% relative humidity, using the previously described contact angle goniometer (1). In general, water was found to exhibit a higher contact angle against each monolayer than did hexadecane. For example, the maximum contact angle observed for water on a close-packed monolayer was 90° ± 1° ,whereas the maximum angle exhibited by hexadecane was around 40° ± 2°.

MECHANISM OF FILM FORMATION

It was necessary to eliminate confusion as to the origin of the hydrophobic film found on the dipper after withdrawal from the solution. The film could originate by three mechanisms: (A) deposition of a floating monolayer of insoluble polar molecules as in the Langmuir-Blodgett method; (B) exposure to a high concentration of soluble organic material adsorbed at the water-air interface or (C) adsorption on the metal following the diffusion of polar molecules through the bulk solution. Oleophobic monolayer formation from organic solvents had been proved (1,2) to originate according to method (C).

Particles of grease-free talc or sulfur dust were sprinkled on the water near the dipper. Since there was no motion of the powder particles toward the dipper while it passed through the surface, it could be concluded that no continuous carpet of floating molecules had been deposited on the dipper. The use of the narrow platinum chimney is justified, since it limits the surface of the water through which the dipper passes to an area appreciably smaller than the total surface area of the dipper. This restricts the amount of floating film which can be picked up during passage of the dipper through the surface of the water. The total area of the platinum dipper used was 15.6 cm.^{2}, while the restricted area of the water-air interface within the chimney was only 0.8 cm.^{2} This ratio of 20 to 1 is sufficient to eliminate all but a minor amount of contamination of the dipper by the presence of floating, insoluble polar molecules.

There remained the possibility that the floating monolayer within the chimney was being continuously replenished by mechanism (B) as the dipper removed the previously formed film. The speed of motion of the dipper through the interface could, however, be varied from a fraction of a second to a minute without any effect on the film deposited, provided the time of immersion of the dipper below the liquid level of the solution was of sufficient duration. It is reasonable to assume that the organic molecules available for such adsorption at the air-water interface would be drawn from the column of solution enclosed by the chimney. Now a simple calculation using an average area per adsorbed polar molecule of 21 A^2 reveals that with a concentration of 10^{-5} mole/l., all the solute in that column would have to be used to ensure complete coverage of the dipper. But, in experiments carried out with the long chain amines through *n*-hexadecylamine, good hydrophobic films were formed after 30 sec. of contact and a fraction of a second withdrawal speed at concentrations of only 10^{-7} mole/l. Since diffusion from elsewhere could not be so rapid, it is evident that nearly all of the molecules in the film must have originated by adsorption while the dipper was completely immersed.

Where the polar compound has an appreciable solubility in water, the concentration of the solute monolayer adsorbed at the water-air interface can be calculated with the well-known Gibbs adsorption relation. For the dilute solutions of amines described here, only a small surface tension lowering is found. Thus, Ralston *et al.* (8) found that a solution containing 10^{-6} mole/l. of dodecylamine decreased the surface tension by less than 0.4 dyne/cm. at 25°C. Hence, the surface pressure of the adsorbed film on the water will be less than 0.4 dyne/cm. From that the calculated area per molecule adsorbed at the air-water interface is only 700 A^2. If this gaseous film had deposited on the dipper during motion through the interface, there could not have resulted the very hydrophobic film observed. This also leads to the conclusion that mechanism (B) could not be significant here.

Experiments with extremely dilute solutions of amines in water indicated that time of contact of the dipper with the bulk solution was the important factor governing hydrophobic film formation rather than the transit of the dipper through the air-solution interface. Under identical experimental conditions two similar dippers "a" and "b" were simultaneously lowered through the chimney enclosure and contacted with a dilute (1×10^{-6} mole/l.) dodecylamine solution for 30 sec., after which they were quickly withdrawn and examined. Both emerged wet, indicating that the amount of adsorption which had occurred was insufficient for the complete formation of a hydrophobic film. Dipper "a" was flamed, resubmerged through the chimney and kept in continuous contact with the solution. At the end of 4 hr. dipper "b" was flamed and also lowered through the chimney where it was exposed to the bulk solution for 30 sec., after which it was withdrawn and examined and found to be completely wetted. Dipper "a" was then withdrawn and found to be completely hydrophobic as a result of the 4 hr. contact immersion period. This experiment established mechanism (C) beyond any doubt.

Dipper experiments with a series of increasingly more dilute solutions showed that increasing immersion times were necessary to complete the formation of hydrophobic films. Provided that a large enough volume of solution was used for the area of the dipper, the required number of solute molecules were captured after a sufficient length of time, and the dipper became hydrophobic. This led to an informative experiment similar to the earlier one with a non-aqueous solution (2). The polar solute was depleted by repeated adsorption, isolation and destruction of successive hydrophobic films on a clean, polished platinum dipper of known area until the solution had lost its ability to supply hydrophobic films. The average area per adsorbed molecule was estimated from the number of solute molecules available for adsorption and the number of dipper coatings formed. A correction was calculated for adsorption of the solute on non-dipper surfaces. In such calculations, the degree of packing of the molecules in the films was assumed to be constant as long as the hydrophobic contact angle remained constant. This experiment required that a known amount of amine be present in a small volume of dilute solution. *n*-Octylamine was chosen for the test because: (a) films were obtainable from a concentration range which allowed the solutions to be depleted within a reasonable number of dips, and (b) the solubility of the octylamine in water was sufficient to preclude the possibility of formation of insoluble floating monolayers which would increase the uncertainty of the bulk concentration of the solution.

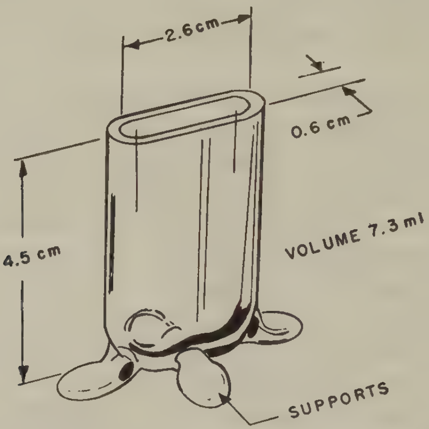

FIG. 2. Dip cell for multiple dipping experiments.

The solution was prepared by adding to 500 ml. of distilled water a single drop of *n*-octylamine, the mass of which was measured by forming it (within the flask neck) from a $\frac{1}{4}$ ml. "Agla" micrometer syringe fitted with a carefully ground, calibrated platinum tip 0.5 mm. in diameter. Two separate determinations were made on different samples of an aqueous solution having a concentration of 1.04×10^{-4} mole/l. ± 2%. A portion of this solution was weighed into a dip cell (Fig. 2) having a capacity of 7.3 ml. and an apparent interior wall area of 30 cm.^{2} Approximate corrections were calculated for the loss of amine due to adsorption of monolayers onto the walls of containing receptacles during the preparation of the solution. A molecular cross-section of 21A^2 was assumed for the adsorbed hydrophobic film and the *apparent surface area* of the film-covered interior walls was used in the calculations. Evaporation losses were minimized by keeping the dip cell in a small, covered glass jar during all dips of 10 min. duration or longer and performing the major portion of experiments within the first 8 consecutive hours. The dipper used had an apparent area of 9.69 cm.^{2} For each dip it was flamed briefly, cooled and quickly lowered into the solution by its platinum wire handle. The time of immersion was manually controlled but the dipper was withdrawn by a 1 r.p.m. synchronous motor geared to retract the dipper completely within 55 sec., during which period any drops of liquid entrained on the dipper were drained back into the solution. The hydrophobic dipper was then transferred to the stage of the contact angle goniometer where measurements were made of the contact angles against drops of distilled water.

TABLE I

Exhaustion of Solute by Repeated Dips

Total no. of dips	Immersion time per dip	Hydrophobic behavior of Pt dipper toward solution	Contact angle against water
1	<1 minute	Completely unwetted	39°
10	<1	Completely unwetted	40°
20	<1	Completely unwetted	37°
30	<1	Completely unwetted	39°
40	<1	Completely unwetted	36°
45	1½	Completely unwetted	28°
47	10	Few small wet patches	23°
50	25	Wet along one edge	14°
51	25	Few small wet patches	13°
52	33	Few small wet patches	13°
53	60	Wet along one edge	27°
54	130	Wet along one edge	29°
55	200	Some wet areas	19°
56	990	Large wet areas	Drop spreads at low angle

Table I lists the results of one experiment. In the second column is given the total immersion time necessary to form a film sufficiently repellent to allow its isolation, in the third column is a description of the appearance of the dipper immediately after withdrawal, and in the fourth column the average hydrophobic contact angle.

Table I shows that for about the first 45 dips it was possible to form uniform monolayers within 1 min. or less of immersion in the solution. Subsequent dips required progressively longer contact with the solution to form a completely hydrophobic film. The dippers emerged progressively less repellent from the 47th and later dips as shown both by the presence of wet patches on the dipper surface and by the decreased contact angle for drops of water measured on the hydrophobic area of the dipper. By the

56th dip an immersion time of 16.5 hr. was not sufficient to form an adequate film. The experiment was stopped at this point because of the difficulty of preventing the removal of the solution. The hydrophobic contact angles for the first 45 dips showed a variation of ± 2°, whereas measurements became less reproducible for subsequent dips as the angle approached zero.

Calculations of the average cross-sectional area per molecule were based on the number of dips which resulted in satisfactory film formation using the apparent area per dipper, and the amount of polar material available originally and at completion of the experiment. Approximately 17 hr. were necessary for film formation on the 56th dip. This is thought to be within 2 or 3 dips of total depletion of the residual organic material. Since the last films are less closely packed, they represent an effective increase of only several per cent in the total area made available for adsorption during the entire experiment.

This experiment on octylamine was repeated later and each time there resulted a cross-sectional area of approximately 14 A^2/molecule. This is to be compared with the value of 20.5 A^2 assigned to the longer chain amines in a compressed film on water (9) and with that of 30 ± 1 A^2 obtained for octadecylamine adsorbed as an oleophobic monolayer on platinum (1). The lower value obtained for the hydrophobic octylamine film is probably due to the deviation of the true surface area of the platinum dipper from the area calculated geometrically, the magnitude of the correction factor being unknown for the particular platinum specimen used. Reference is made, however, to the work of Bowden and Rideal on electrolytic methods of measuring the surface areas of metals in which the ratio of the "accessible area" (available for measurement with the small hydrogen ion) to the "apparent area" is reported to be 2.1 for smooth bright platinum foil (10). Films of the relatively short 8-carbon compounds may conform more closely to the surface irregularities represented by this ratio than would films of long chain compounds which are apparently able to bridge surface asperities, as demonstrated by the work of Bikerman on compounds with 18-carbon chains (11). In that case, the high value of 30 A^2 obtained for the octadecylamine and the low value of 14A^2 for the octylamine may be more readily reconciled. Other experimental errors, such as loss of amine by unavoidable mechanical withdrawal from solution or by evaporation, would also tend to lower the observed area per molecule. Measurements indicated a weight loss of less than 2% due to evaporation in the first 8 hr., during which period completion of the first 52 dips was effected. Since the vapor pressure of octylamine at 30°C. is only about 1 mm. (12), the decrease in weight is considered due primarily to the loss of water, with a comparatively minor loss of amine.

On the basis of the preceding considerations, it is concluded that for water-soluble compounds, such as the primary amines, the mechanism of hydrophobic film formation from dilute aqueous solution during submersion of the dipper is identical with that found earlier for oleophobic films from oil solutions (1,2); that is, the organic molecules diffuse through the solution, eventually reach the solid surface, and there become adsorbed by their polar ends. When a sufficient proportion of the surface has been covered by adsorbed molecules, the packing of the hydrocarbon "tails," which are oriented outward from the adsorbing surface, becomes dense enough to render the surface hydrophobic. To establish and maintain a film of this type, the adsorptive forces must be strong enough to resist the disruptive effects of thermal agitation and solubility. It is evident that the average lifetime of adsorption must be long if the minimum concentration at which a saturated monolayer can form is to be low. As with oleophobic films adsorbed from organic liquids, a very appreciable portion of the energy of adsorption may originate in cohesive forces between the adjacent non-polar portions of the molecule (2).

Influence of Concentration and pH on Hydrophobic Behavior

Some indication of the adsorptivity of the polar solute was obtained by determining the concentration $W_{\min}$, below which there was no formation of hydrophobic films. This was done by observing the film-forming properties of a series of increasingly dilute solutions. Eventually the concentration of the solution was lowered to the point where no hydrophobic film could be formed. To make valid comparisons between solutions of different concentrations, it was essential to work at some standard adjusted value of the hydrogen ion concentration (pH) since the latter varied with the concentration of amine used. The attempt to settle on the most favorable experimental pH value necessitated an examination of the effect of pH on the hydrophobic properties of films formed from a given solution concentration. As in the work of Taggart (13), Wark (3), and others, the adsorptive properties of the primary amines were found to be profoundly influenced by the pH. For low amine concentrations it was possible to progress from complete wetting through a highly non-wetting stage and on to complete wetting again as the pH changed progressively from conditions of high acidity through neutrality and on to high basicity. Thus, for every experimental determination it became necessary to know or control the concentration of amine, the pH of the solution, and the length of time of immersion of the dipper in the solution.

All adsorbed films were prepared with the electrodes of the pH meter immersed in the hydrophil tray. Considerable stirring was used to assure rapid establishment of equilibrium pH conditions after the addition of acid or base, and also to speed up diffusion to the adsorbing surface, with a resultant shortening of the time to attain approximate adsorption equilibrium conditions. For each concentration of solution, dipper observations were made after some fixed time of immersion at intervals over a wide range of pH values. Successively less concentrated solutions were explored until a limiting concentration was reached, at which hydrophobic films were no longer observed, regardless of the pH. This procedure was used to define the minimum concentration $W_{\min}$.

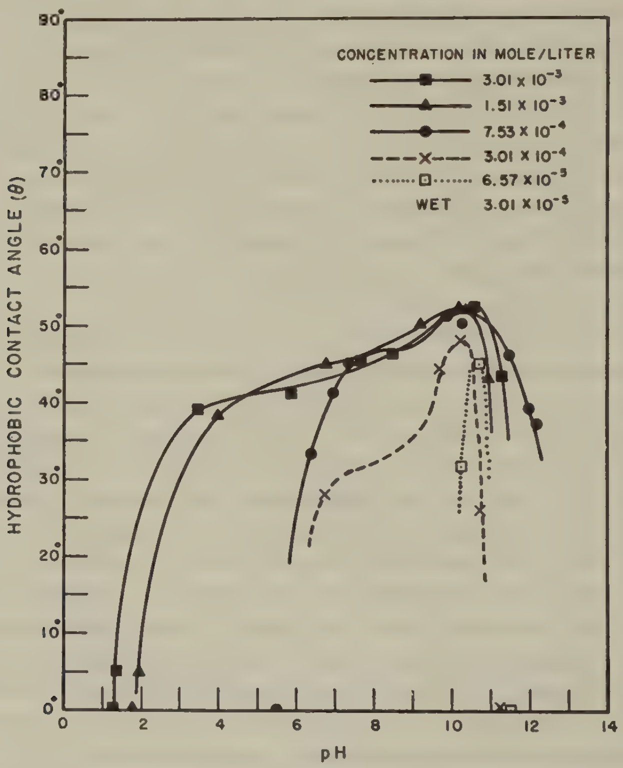

FIG. 3. *n*-Butylamine on platinum from aqueous solution.

The experimental data presented in Figs. 3 through 7 were obtained using a standard immersion time of 30 sec., with considerable stirring of the solution. Changes of the pH were made by the dropwise addition of HCl or KOH. The presence of salts was known, from flotation studies (3), to have a marked influence on the hydrophobic properties of films adsorbed on mineral ores. Since similar salt effects might exist in the present investigation, and since, at the extreme ends of the pH range, solubility effects and colloid formation are important, experiments were made to show the effect of cycling the pH on the reproducibility of the curves within a limited range of pH. Within a pH unit of the critical pH limits to hydrophobic behavior, no effect of cycling was noted for the amines up through the dodecyl compound. For the less soluble long chain amines, where the addition of large amounts of HCl was necessary, two portions of the solution were used, one for the acidic determinations and the other for the alkaline range of determinations; there is no doubt, however, that, for the tetradecyl and higher amines examined, the concentrations of electrolytes were unavoidably of the same order of magnitude as those used in flotation work. It is planned to study later any salt effects on hydrophobic adsorption on metals. Upon withdrawing the dipper from a given solution, measurements were made of the equilibrium contact angles *by using test drops of that aqueous solution* at that same temperature. This eliminated difficulties which could be caused by the dissolving of the underlying monolayer into the test drop during the contact angle measurement. This is essential in studying the more water-soluble solutes such as the lower amines. The nonobservance of this precaution makes it difficult

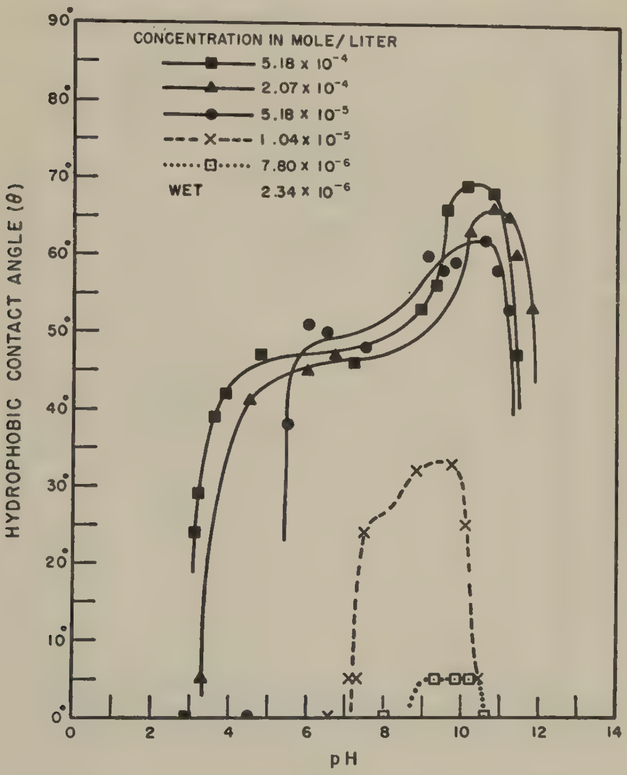

FIG. 4. *n*-Octylamine on platinum from aqueous solution.

to compare much reported in the literature on flotation with that reported here.

The results with several normal alkyl primary amines on the relation of the equilibrium contact angle (θ) and the pH at several concentrations are presented in Figs. 3 through 7, and all are drawn to the same scale. Each curve is the locus of points having the same concentration, while the successive curves are for concentrations commencing just above W_{min} to a value from 10 to 200 times greater than W_{min}. To define sharply the favorable pH ranges, two conventions were adopted. At the limiting pH at which complete wetting occurred, θ was assigned a zero value. Also, θ was assigned a value of 5° at those values of the pH for which any signs of hydrophobic behavior could be detected on the dippers, even though the unwetted areas were too small to test for a measurable contact angle.

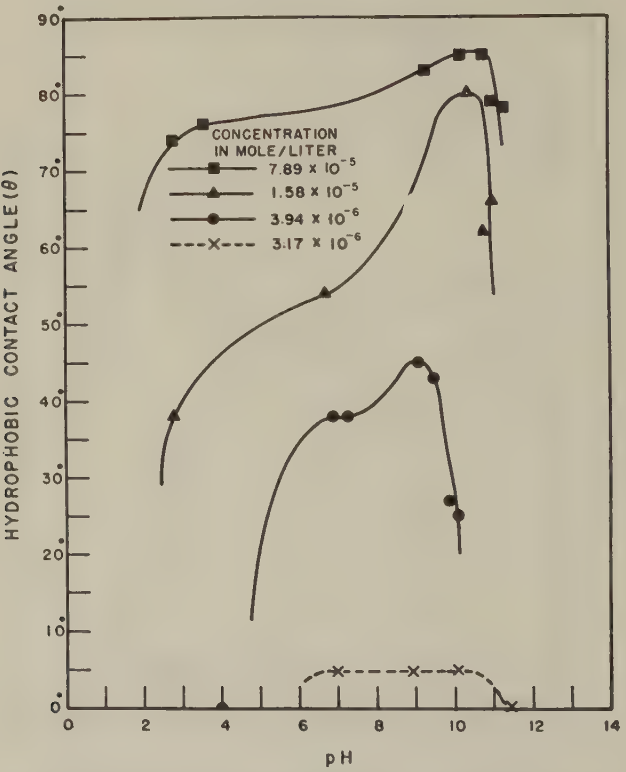

FIG. 5. *n*-Dodecylamine on platinum from aqueous solution.

The general features of the θ *vs.* pH curves follow the same pattern. There is an abrupt rise in the contact angle as soon as a fairly critical pH value is reached, whether approached from the very acid or very alkaline regions. A highest or "peak" contact angle (θ_p) is always obtained over a comparatively limited pH range. Over a portion of the curve, θ is somewhat less than θ_p but tends to remain constant. This "plateau" region occurs unsymmetrically, on the acidic side of the peak region only. Analysis of a series of curves for progressively increasing concentrations reveals: an increase in the acidic pH range favoring hydrophobic film formation; a widening of the "plateau" regions accompanied by an increase in the value of the plateau angle, which results at higher concentrations in materially lessening the difference with the value of θ_p; a widening of the pH range in which the peak contact angle is obtained; and a rapid increase in θ_p with concentration for values of W just above W_{min}, followed by an asymptotic approach of θ_p to some limiting angle (θ_{lim}).

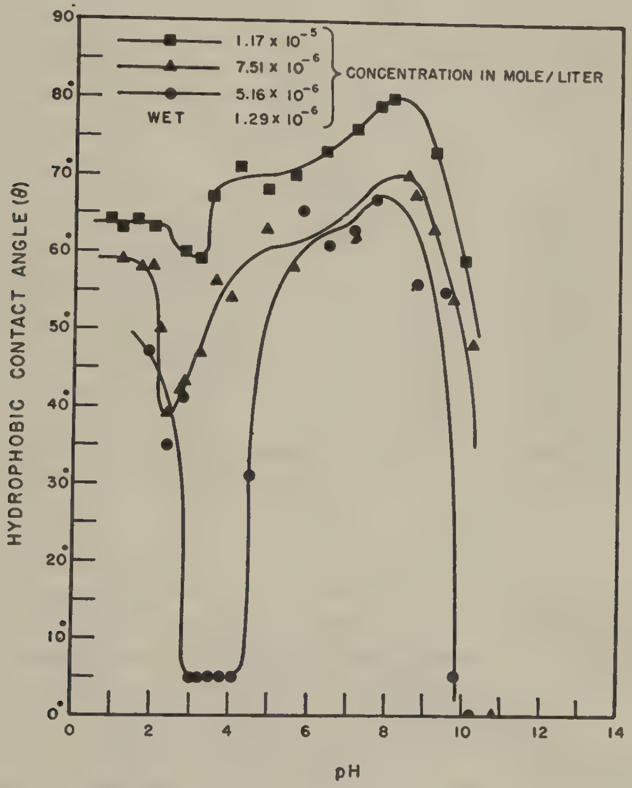

FIG. 6. *n*-Tetradecylamine on platinum from aqueous solution.

Repeated experiments to check the θ *vs.* pH curves showed that θ_p was easily reproducible, as was the general shape and the critical pH limits of the curve. But the height and width of the plateau contact angle region

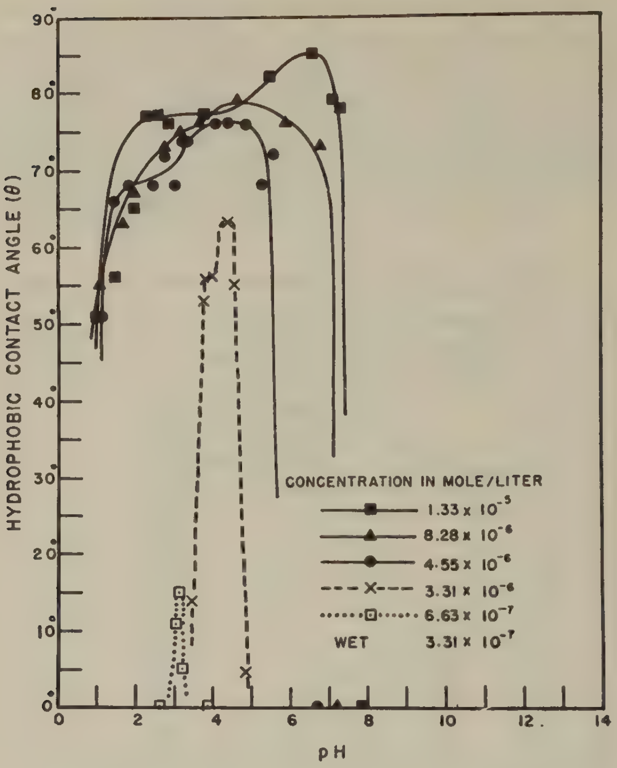

FIG. 7. *n*-Hexadecylamine on platinum from aqueous solution.

could vary considerably from one trial to another. Experiments using longer times of immersion than 30 sec. revealed that, while θ_p was dependent only on the concentration of the solution, the values of θ less than θ_p tended to be increased slightly for the longer contact periods.

EFFECT OF CHAIN LENGTH OF AMINES

Although each of the Figs. from 3 through 7 exhibits the same general characteristics, a comparison of the results for several homologous primary amines reveals pronounced differences with the number of carbon atoms per molecule (N). A plot of θ_p *vs.* log concentration W taken from Figs. 3 through 7 for the several amines is shown in Fig. 8. Attention is called in this figure to three features: (a) the effect of increased chain length in depressing the minimum concentration $W_{\min}$, (b) the progressive increase with chain length in $\theta_{\lim}$ and (c) the asymptotic approach with chain length of $\theta_{\lim}$ to the value of 90°. Fig. 9 is a plot of $\theta_{\lim}$ (estimated from Fig. 8) against N for each amine studied. Evidently $\theta_{\lim}$ approaches 90° as N increases for the various *n*-alkyl primary amines studied, and this maximum value of 90° is attained for values of N in excess of 16. This maximum value of the hydrophobic contact angle is precisely that found for monolayers of the hexadecyl and higher amines when adsorbed as oleophobic films on platinum from such nonpolar solvents as hexadecane, dicyclohexyl and white mineral oil (1).

However, there is one respect in which successive increases in the length of the hydrocarbon chain resulted in a radical alteration in the general pattern of the results. Figs. 3, 4, and 5 show clearly that, for chain lengths of 4, 8, and 12 carbon atoms, the peak angle is found consistently in the alkaline region at a pH of 9–11, and that, for extremely low concentrations, hydrophobic film formation is possible in the alkaline region only. In contrast Fig. 7, presenting the results obtained with the 16-carbon amine, shows the opposite behavior; the occurrence of the peak contact angle and the formation of hydrophobic films is limited to the acidic region. This complete reversal of the effect of pH resulting from a 4-carbon increase in chain length suggested that some intermediate behavior might be expected from the medial 14-carbon amine. This led to the experiments on tetradecylamine, summarized in Fig. 6. Two distinct pH regions favorable for film formation were found, separated by a narrow range of pH values in which only the poorest films were obtainable. The major favorable pH region was shifted from the high alkaline toward the neutral range, while a second favorable range appeared in the highly acidic region. Values of pH between 3 and 5 were found to inhibit highly hydrophobic film formation, with the higher concentrations showing a less pronounced

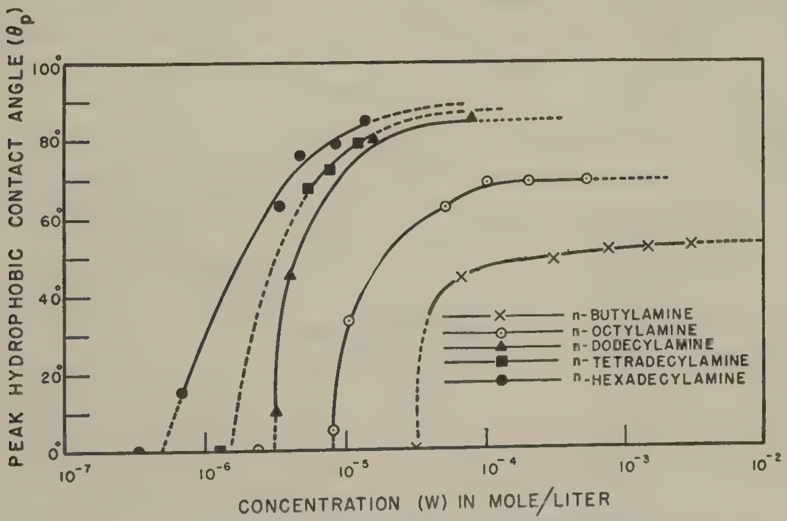

FIG. 8. Correlation of peak hydrophobic contact angle with concentration for homologous family of n-alkyl primary amines from aqueous solution.

depression in the values of the hydrophobic contact angle for the unfavorable region.

Significance of Contact Angles

In Table II are listed the results of contact angle measurements on test drops of water and of hexadecane toward films isolated hydrophobically from aqueous solutions or oleophobically either from the molten amine or from solution in hexadecane. A comparison of the results emphasizes the identity of such films, irrespective of the method of film formation. Thus, evidence adduced in the proof of the structure of oleophobic monolayers is applicable to hydrophobic films of the same compounds.

The smooth gradation of hydrophobic and oleophobic properties with the number of carbon atoms per molecule (N) for the homologous series of amines indicates a uniformity of structure and mechanism of film formation for all members of the family. The contact angle is seen in Fig. 9 to be

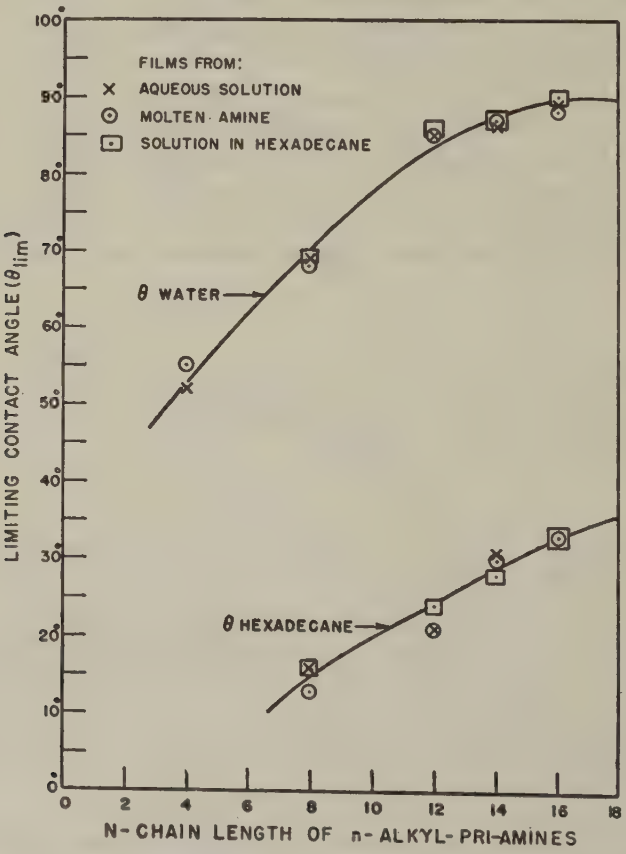

Fig. 9. Effect of chain length on limiting hydrophobic contact angle.

TABLE II

Contact Angle Measurements on Monolayers Adsorbed on a Platinum Dipper[a]

Amine chain length	From aqueous solution		From molten amine		From solution in hexadecane	
	θ_{water}	$\theta_{\text{hexadecane}}$	θ_{water}	$\theta_{\text{hexadecane}}$	θ_{water}	$\theta_{\text{hexadecane}}$
4	52°	0°	55°	0°	—	—
8	69°	16°[b]	68°	13°[b]	69°	16°[b]
12	85°	21°	85°	21°	86°	24°
14	86°	31°	87°	30°	87°	28°
16	89°	33°	88°	33°	90°	33°

[a] Measurements were made at temperature 25° ± 1°C. on a single dipper for all the results listed in this table.

[b] Test drop completely wets underlying monolayer.

a function of N, approaching asymptotically a maximum of 90° for water, and around 40° for hexadecane. In accordance with the explanation advanced in the study of oleophobic monolayers (1) this maximum oleophobic contact angle is characteristic of the closest packing of oriented methyl groups. Similarly, it is concluded from Fig. 9 that there is an analogous maximum hydrophobic angle of 90° characteristic of the same film structure. The difference in magnitude of hydrophobic and oleophobic contact angles for a given film results in the following useful generalizations: (1) Water is a more sensitive agent than organic liquids for testing for the presence of hydrocarbon-type monolayers, particularly those which are not closest packed. (2) Water provides a medium from which a structurally wider variety of hydrocarbon-type adsorbed films can be isolated.

Discussion

The variation of hydrophobic properties with acidity or alkalinity of the generating solution is attributed to solubility effects. The known low solubility of such amines in alkaline solution causes the apparent barrier to hydrophobic film formation noted on the alkaline side of all θ *vs.* pH curves, since there results a reduction in the number of amine molecules available for adsorption from solution down to a concentration below that necessary for hydrophobic film formation. This explanation is consistent with the experimental data, which show virtually no shift in the alkaline limits of the curves for increased amine concentrations. Further confirmation lies in the shift of the barrier to less alkaline pH values with increasing chain length of the amines.

The maximum of the θ *vs.* pH curves just prior to the alkaline limits represents the most favorable equilibrium between the effects of limited solubility and high adsorptivity. The lower "plateau" values for θ are probably due to the increase in the solubility of the amine with decreasing pH. For the amines up through dodecyl, the lack of hydrophobic film formation from acid solutions of low concentration is presumed due to the increased desorptive effects of high solubility. The pronounced shift of the adsorptive boundary to lower pH values with increased concentration further bears this out.

The occurrence of two distinct pH regions favorable for hydrophobic film formation for tetradecylamine (Fig. 6) is considered to result from the ability of a long-chain amine to adsorb either in molecular form (in the alkaline-neutral region) or as ions in the highly acid region. The smoother transition from molecular to ionic adsorption possible at higher concentrations results in the disappearance of the distinctive minimum.

From this it follows that the adsorption of the poorly soluble hexadecylamine is necessarily wholly of the ionic type, since the θ *vs.* pH curve is found exclusively in the highly acidic region (Fig. 7). Independent confirmation of this is gained from the results of previous studies on the effect of dissolved heptadecylamine on the spreading of oil drops on water (14) which demonstrated that appreciable ionization occurred at the water-oil interface beginning at pH 5.8, followed by an S-shaped curve attaining a maximum degree of ionization at pH of 2.5 or less. It is within precisely this pH range where the most satisfactory hydrophobic film formation is found for hexadecylamine.

From these results some general conclusions can be made. The opportunity to obtain monolayers of hydrophilic-hydrophobic polar molecules free from their aqueous solutions provides a convenient experimental approach to the investigation of fundamental relationships involved in adsorption. Monolayers so isolated are available for study as reproducible surfaces which can be characterized by quantitative methods using contact angle measurements. It is planned to extend and apply this method to the study of adsorbed films as regards the effect of: (a) variations in the nature of the polar end group, (b) the introduction of branching in the hydrocarbon portion of the structure, (c) the presence of additional organic radicals on the adsorption group, (d) changes in the nature of the adsorptive surface, (e) changes with temperature, and (f) the presence of salts.

Much has been done in connection with the development of flotation methods (3) in correlating contact angles with floatability for different mineral types as a function of the mineral, activator, solution pH, and temperature of film formation. A recent paper by Taggart and coworkers (13) on the adsorption of laurylamine on metals has emphasized the possibility of the formation of complex coordination compounds which, in the case of platinum, is believed to occur readily at high pH. Since the data presented here were obtained by the use of short periods of contact, the fact that no evidence was found for the formation of such compounds by no means precludes the possibility of their existance. Under experimental conditions more comparable to those of Taggart *et al.*, the present technique may yield corroborative evidence. However, important adsorption factors which do not necessitate chemical reaction of the flotation reagent and the mineral substrate could be investigated by observations on the hydrophobic films physically adsorbed onto a non-reactive polished surface. Thereby, a better appreciation might result of the nature and importance of chemisorption onto the various minerals. Where polished surfaces of each mineral are available, the same types of measurements could be used to study the principles involved in the process of selective adsorption. Similarly, studies of corrosion inhibition and the "pickling" of metals could be made with the object of correlating water repellency with the experimental conditions favorable for film formation, and even the type of pretreatment most effective in preparing surfaces to receive strongly bonded adsorbed films with desirable repellency characteristics.

ACKNOWLEDGMENTS

The authors wish to acknowledge their obligation to Mr. R. L. McCarthy for his assistance in obtaining the data for some of the θ *vs.* pH graphs.

SUMMARY

Experimental methods are described for the preparation and examination of hydrophobic monomolecular films adsorbed and isolated from aqueous solutions of certain types of polar-nonpolar organic compounds. The use of contact angle measurements for the quantitative characterizations of the hydrophobic and oleophobic properties of such films permits the evaluation of the various factors governing their formation, structure, and repellency characteristics. The present paper reports the results of studies on several members of a homologous family of primary amines of the normal alkyl type adsorbed onto platinum surfaces.

The critical limits to hydrophobic film formation and the degree of hydrophobicity are found to be functions of the amine concentration and the pH of the generating solution. A definite correlation is established for the relative effectiveness of these factors and the length of the hydrocarbon chain in the aliphatic portion of the amine molecule. The marked response of hydrophobic film formation to pH and concentration is interpreted as an adsorption-desorption phenomenon in which the equilibrium conditions are determined by the solubility and degree of ionization of the individual amines. The short chain amines (up through dodecyl) are found to be most adsorptive in the alkaline region, whereas film formation of the hexadecylamine is limited to the highly acid regions. The intermediate tetradecylamine evinces a transitional behavior, having two separate pH regions favorable to film formation.

The identity of adsorbed monomolecular films isolated hydrophobically from aqueous solution and oleophobically from the molten amine or from solution in hexadecane is established. The use of water as solvent increases the number of molecular types available for study as reproducible, repellent films.

The method is proposed as a possible approach to the examination of films important in the fields of selective adsorption, mineral flotation, corrosion inhibition, and "pickling" of metals.

REFERENCES

1. BIGELOW, W. C., PICKETT, D. L., AND ZISMAN, W. A., *J. Colloid Sci.* **1**, 513 (1946).
2. BIGELOW, W. C., GLASS, E., AND ZISMAN, W. A., *ibid.* **2**, 563 (1947).
3. WARK, I. W., Principles of Flotation. Australasian Inst. of Mining and Metallurgy, Melbourne, 1938.
4. BAKER, H. R., AND ZISMAN, W. A., *Ind. Eng. Chem.* **40**, 2338 (1948).
5. BAKER, H. R., JONES, D. T., AND ZISMAN, W. A., *ibid.* **41**, 137 (1949).
6. LANGMUIR, I., *Proc. Roy. Soc. London* **170A**, 1 (1939).
7. ROGERS, J., SUTHERLAND, K. L., WARK, E. E., AND WARK, I. W., *AIMME—Mining Technology—Tech. Pub. No. 2022*, Vol. **10** (1946).
8. HOFFMAN, E. J., BOYD, G. E., AND RALSTON, A. W., *J. Am. Chem. Soc.* **64**, 498 (1942).
9. ADAM, N. K., Physics and Chemistry of Surfaces, 3rd ed. Oxford University Press, London, 1941.
10. BOWDEN, F. P., AND RIDEAL, E. K., *Proc. Roy. Soc. London.* **120A**, 80 (1928).
11. BIKERMAN, J. J., *ibid.* **170A**, 130 (1939).
12. RALSTON, A. W., SELBY, W. M., POOL, W. O., AND POTTS, R. H., *Ind. Eng. Chem.* **32**, 1093 (1940).
13. ARBITER, N., KELLOGG, H. H., AND TAGGART, A. F., *AIMME—Mining Technology—Tech. Pub. No. 1581*, Vol. 7 (1943).
14. ZISMAN, W. A., *J. Chem. Phys.* **9**, 534 (1941).

IONIC EFFECTS IN A PARAFFIN-CHAIN SALT SOLUTION AS MEASURED BY THE PRIMARY SALT EFFECT[1]

J. A. Erikson and E. C. Lingafelter

From the Department of Chemistry and Chemical Engineering,
University of Washington, Seattle, Washington

Received July 7, 1949

INTRODUCTION

The existence of colloidal aggregates of paraffin-chain ions has been accepted to account for the many unusual properties of paraffin-chain salt solutions. The interpretations of experimental results leading to explanations of some of these properties have been recently reviewed (14). One point of disagreement in the details regarding the properties of these aggregates or micelles, which is of interest here, concerns the ionic effects of the highly charged micelle.

McBain (16,17,18) has considered that the charges on the surface of the micelle are too widely spaced to exert a mutual influence, and that ionic effects of solutions of micelles would not be much different from those of uni-univalent electrolytes. He gives as evidence for weak interionic effects the similar behavior of paraffin-chain salts compared with uni-univalent electrolytes in regard to freezing-point lowering and conductivities in mixtures of paraffin-chain salts with uni-univalent electrolytes (19).

Hartley (5,6), on the other hand, has assumed that the charges on the micelle act in unison and therefore produce considerable ionic effects. Evidence for strong interionic attractions is given by the behavior of the equivalent conductance of these solutions at high frequencies (21) and at high field strength (1,15).

The dependence of the rate constant of an ionic reaction on the ionic strength of the reaction medium is well known (4,10). It therefore appeared possible to obtain an indication of the ionic effects of an aqueous paraffin-chain salt solution by observing the rate of a suitable ionic reaction in such a solution. Sodium dodecanesulfonate was chosen for the paraffin-chain salt because it is free from hydrolysis (18), and also because its critical concentration, 0.011 molar (24), occurs in the most convenient concentration range. The reaction between the thiosulfate and bromoacetate ions was selected because it has been highly recommended (11) as a means for testing theories on ionic behavior. The reaction is particularly suitable here because both reactants and micelle have a negative charge, and, therefore, the possibility of the micelle adsorbing the reactants and influencing the reaction rate was avoided. It was necessary to use the above compounds as their sodium salts, since the presence of a polyvalent ion with a charge opposite to that of the polyvalent activated complex catalyzes the reaction (11).

---

[1] Taken from a thesis submitted by J. A. Erikson to the University of Washington in partial fulfillment of the requirements for the M.S. degree, June 1949.

EXPERIMENTAL

Sodium Dodecanesulfonate

The sodium dodecanesulfonate was prepared in the normal manner (7,25). The salt was recrystallized from alcohol four times and dried in an oven at 50°C. A water analysis using a vacuum oven at 135°C. gave 0.15 moles of water per mole of sodium dodecanesulfonate.

Sodium Bromoacetate

The sodium bromoacetate was prepared by mixing an alcoholic solution of sodium hydroxide with an alcoholic solution of bromoacetic acid (8) which had been purified by two recrystallizations from benzene (22). This method was used because it was not desired to introduce any internal indicator (11) to determine when an equivalent amount of sodium hydroxide had been added. The crystals were dried *in vacuo* at room temperature over concentrated sulfuric acid (9). Tests made concurrently with the rate determinations using a 3 or 4 to 1 excess of standard sodium thiosulfate solution showed 0.989–0.980, 0.975–0.967, and 0.970–0.960 equivalents of thiosulfate consumed for every equivalent of bromoacetate.

Sodium Thiosulfate

The sodium thiosulfate solutions were prepared by adding boiling distilled water to a C. P. grade of sodium thiosulfate pentahydrate in previously sterilized Pyrex bottles. This procedure yielded solutions that were quite stable, and was adopted instead of using a preservative because of the possibility of the preservative influencing the results. No solution was ever retained for more than five days.

Iodine

A C. P. grade of iodine was used. Solutions contained 4% potassium iodide.

Arsenious Acid

A C. P. grade of arsenious oxide was used as the primary standard.

Procedure

Runs were carried out using solutions containing various concentrations of the sodium dodecanesulfonate ranging from 0–0.02 *M*. The reaction was carried out at 40 ± 0.01°C. in a thermostated water bath, because of the small solubility of sodium dodecanesulfonate (23) at room temperature. The concentrations of the bromoacetate and thiosulfate ions were equal, thus simplifying the calculations; they were adjusted to a predetermined concentration, depending upon the concentration of the sodium dodecanesulfonate, so that the ionic strength of all the runs would be the same, 0.022 *M*, assuming the sodium dodecanesulfonate to behave as a simple uni-univalent electrolyte. Accordingly, two solutions were prepared at 40°C., one containing the appropriate concentrations of sodium dodecanesulfonate and sodium thiosulfate, and the other containing the appropriate concentration of sodium bromoacetate. These solutions were mixed at 40°C. by adding an aliquot of the second solution to an equal aliquot of the first solution. The time at the start of the addition was taken as the starting time of the reaction. The reaction was stopped by rapidly adding from a buret a calculated amount of standard iodine solution which was just insufficient to combine with the thiosulfate present. The time that the initial iodine was added was taken as the stopping time of the reaction. The reaction was then cooled externally with tap water at 5°C. in order to sharpen the end point (13) and to prevent the solution from frothing. Starch solution was then added and the titration completed.

The burets and pipets used were calibrated. All volumetric flasks were retested. Time was recorded with a stop watch which on comparison with an electric clock showed a gain of 18 sec. in 18 hr. or a relative error of 0.03%.

Blank corrections were applied in all cases. This was important since the color of the starch-iodine complex at the end point in the presence of the paraffin-chain salt was a pale yellow instead of the usual blue. Tests using identical amounts of thiosulfate in identical total volumes with and without the presence of the paraffin-chain salt, showed that the end point in the presence of the paraffin-chain salt occurred slightly later.

The rate constants were calculated from the slopes of plots of the reciprocal of the volume of standard iodine required against the time.

Presentation and Discussion of the Results

The observed rate constants for twelve runs in which the paraffin-chain salt concentration was increased from 0–0.02 *M* are given in Table I. Since the utmost of strict precautions were not taken, a high accuracy cannot be claimed for the results, although it is believed that any error involved was systematic and that the results could be reporduced using the same technique within an error of ± 0.03 min.^{-1}. Errors such as evaporation losses from the solution and unintentional presence of foreign ions both would tend to give larger rate constants.

No direct measurement of the rate constant at 40°C. could be found in the literature. La Mer and Kamner (12) have determined the rate constant at an ionic strength of 0.02 *M* for 0, 12.5, 25, and 37.5°C., and Davis and La Mer (3) have determined the rate constant at 45°C. for various ionic strengths. From these data the rate constant at an ionic strength of 0.022 *M* was calculated to be 1.52 min.^{-1}.

To demonstrate the effect of the paraffin-chain salt on the rate constant, the results are plotted in Fig. 1. It is seen that the rate constant remains constant within the limits of experimental error up to a certain point and then increases rapidly. The "break" in the curve occurs near the critical concentration of the paraffin-chain salt. It is well known that the presence of electrolytes lowers the critical concentration of a paraffin-chain salt. It is estimated that the critical concentration here, in the presence of the reactants, is about 0.0074 *M*. This was obtained from data (24) on the lowering of the critical concentration of sodium dodecanesulfonate by sodium chloride using the fact brought out by Corrin and Harkins (2) that the logarithm of the critical concentration varies linearly with the logarithm of the sodium-ion concentration.

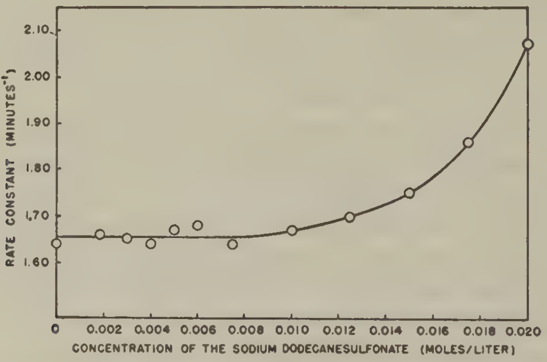

FIG. 1. Variation of the rate constant of the thiosulfate-bromoacetate reaction at 40°C. with the concentration of the sodium dodecanesulfonate.

The fact that the rate constant remains constant, within the limits of experimental error, below the critical concentration is in accord with the principle of the primary salt effect. The rate constant is constant because the ionic strength is constant.

It seems logical to interpret the increasing values of the rate constants in solutions above the critical concentration as being due to an increasing ionic strength of the solutions. If the micelle behaved as a uni-univalent electrolyte, then a decrease in the rate constant should occur, since the formation of micelles removes a large percentage of simple ions from the solution. The ionic effect of the micelle, therefore, not only compensates for this decrease in ionic effect due to the decrease in simple ion concentration, but contributes an excess to the solution.

It is possible to calculate an effective ionic strength by means of the dependence of the rate constant on ionic strength. This was done from the data mentioned before (3,12), and the calculated effective ionic strengths are given in Table I. While the effect is not as great as Hartley's estimates, it is in the most concentrated paraffin-chain salt solutions at least three times as large as the effect of a uni-univalent electrolyte.

TABLE I

Effect of Sodium Dodecanesulfonate on the Reaction Rate Constant of the Bromoacetate-Thiosulfate Reaction and Corresponding Effective Ionic Strengths

c_p	μ	k	μ^*
—	0.0220	1.64 ± 0.05	0.0220
0.00182	0.0218	1.66 ± 0.04	0.0220
0.00300	0.0220	1.65 ± 0.02	0.0220
0.00400	0.0219	1.64 ± 0.02	0.0220
0.00500	0.0220	1.67 ± 0.01	0.0220
0.00600	0.0220	1.68 ± 0.01	0.0220
0.00750	0.0219	1.64 ± 0.03	0.0220
0.0100	0.0219	1.67 ± 0.02	0.0230
0.0125	0.0219	1.70 ± 0.02	0.0250
0.0150	0.0220	1.75 ± 0.02	0.0295
0.0175	0.0218	1.86 ± 0.06	0.0397
0.0200	0.0220	2.07 ± 0.11	0.0620

c_p is the concentration of the sodium dodecanesulfonate present.

μ is the hypothetical ionic strength assuming the sodium dodecanesulfonate to behave as a simple uni-univalent electrolyte.

k is the rate constant in min.^{-1} l./mole at 40°C.

μ^* is the effective ionic strength corresponding to the observed rate constant.

This increase in rate constant also seems to be in disagreement with the recent observations of Olson and Simonson (20) that the rate of an ionic reaction does not depend upon the ionic strength of the solution, but only upon the concentration of ions of charge opposite to that of the charge on the activated complex. While it is true that the stoichiometric concentration of sodium ion here is steadily increasing as the concentration of the paraffin-chain salt is increasing, it seems very likely that the actual concentration of sodium ions decreases above the critical concentration. This is because the formation of a micelle requires a considerable number of counter ions as part of its constitution (14). In any event the sodium-ion concentration certainly is not increasing as much here as below the critical concentration, and, therefore, it would seem that the increasing rate constant above the critical cannot be ascribed to the variation in sodium-ion concentration.

Lack of quantitative data on the number of simple units in the micelle, on the equilibrium relationship between the micelle and simple ions, and on the effect of multivalent ions on ionic strength, prevents a quantitative explanation of this observed increase of the reaction rate constant.

One might also discuss the observed increase in rate constant on the basis of an increase in the effective concentration of the reactants. This could be visualized by supposing that the highly charged negative micelles repel the negatively charged reactants, forcing them out of the vicinity of the micelles, and thus effectively decreasing the free volume available to the reactants. Neglecting ionic strength effects and ascribing the increase in rate constant solely to this decrease in volume, one can calculate an effective volume which is void of the reactants.

Using one liter of solution as a basis for the calculation, one has:

$$\text{Rate of reaction} = k_{\text{obs}}\left(\frac{\text{moles } S_2O_3^{=}}{1000}\right)\left(\frac{\text{moles BrAcO}^{-}}{1000}\right)$$
$$= k_{\text{theo}}\left(\frac{\text{moles } S_2O_3^{=}}{\text{eff. vol.}}\right)\left(\frac{\text{moles BrAcO}^{-}}{\text{eff. vol.}}\right)$$

where k_{theo} is the rate constant observed below the critical concentration. The repulsion between the micelle and divalent ions will be greater than that between the micelle and univalent ions; however, the counter-repulsion from the surroundings toward the micelle likewise will be greater for the divalent ions and it will be assumed that the displacements of the negative divalent and univalent ions from the micelle are the same. Since the number of thiosulfate ions is the same as the number of bromoacetate ions, the above expression reduces to

$$V = \text{eff. vol.} = 1000\sqrt{\frac{k_{\text{theo}}}{k_{\text{obs}}}}$$

From an estimation of the number of micelles in the solution, the volume or effective void per micelle and the radius of the void, assuming it to be spherical around the micelle, can be calculated. The concentrations of simple paraffin-chain ions in the solutions are assumed to be equal to the concentrations at the critical concentrations which are estimated for each solution as before. The number of simple ions in the micelle is estimated, on the basis of a Hartley micelle, using densities of liquid paraffins, to be 54 simple ions/micelle. The concentration of micelles is then given by

$$c_M = \frac{c_p - cmc}{54}$$

and the radius of effective void is given by

$$10^{-8}\sqrt[3]{\frac{(1000 - V)\quad(3)}{c_M\,(6.02 \times 10^{23})\,(4\pi)}}\ \text{A}$$

TABLE II

Effective Sphere Void of Reactants

c_p	0.0100	0.0125	0.0150	0.0175	0.0200
Effective volume per liter (ml.)	994.0	985.2	971.0	941.9	893.0
Effective volume void of reactants (ml.)	6.0	14.8	29.0	58.1	107
Radius of sphere void of reactants (A)	39	43	47	54	62

The estimated radii of the effective spheres void of reactants are given in Table II. These values are not unreasonable when it is considered that the radius of a Hartley micelle for a dodecanesulfonate is about 20–25 A.

SUMMARY

The ionic effect of sodium dodecanesulfonate has been measured by studying its influence on the rate constant of the reaction between thiosulfate and bromoacetate ions. Below the critical concentration of the sodium dodecanesulfonate the rate constant is constant as required by the primary salt effect. Above the critical concentration the rate constant increases, indicating that the ionic effect of paraffin-chain salt micelles is greater than that of a uni-univalent electrolyte. The increase in rate constant is also evidence which appears to be in disagreement with a recent suggestion that the rate constant of an ionic reaction does not depend upon the ionic strength of the medium.

REFERENCES

1. ADCOCK, Ph.D. Thesis, Brown University, 1948.
2. CORRIN, M. L., AND HARKINS, W. D., *J. Am. Chem. Soc.* **69**, 638 (1947).
3. DAVIS, H. G., AND LAMER, V. K., *J. Chem. Phys.* **10**, 585 (1942).
4. GLASSTONE, S., LAIDLER, K. J., AND EYRING, H., The Theory of Rate Processes, 1st Ed., p. 423–430. McGraw-Hill Book Company, Inc., New York and London, 1941.
5. HARTLEY, G. S., Aqueous Solutions of Paraffin-chain Salts. Hermann et Cie, Paris, 1939.
6. HARTLEY, G. S., *Trans. Faraday Soc.* **31**, 31 (1935).
7. HOULTON, H. G., AND TARTAR, H. V., *J. Am. Chem. Soc.* **60**, 544 (1938).
8. KASTLE, J. H., AND KEISER, B. C., *Am. Chem. J.* **15**, 471–493 (1893).
9. KRAPIVIN, S., *Z. physik. Chem.* **82**, 439 (1913).
10. LA MER, V. K., *Chem. Revs.* **10**, 179 (1932).
11. LA MER, V. K., *J. Am. Chem. Soc.* **51**, 3341 (1929).
12. LA MER, V. K., AND KAMNER, M. E., *J. Am. Chem. Soc.* **57**, 2662–8 (1935).
13. LA MER, V. K., AND KAMNER, M. E., *J. Am. Chem. Soc.* **57**, 2670 (1935).
14. LINGAFELTER, E. C., *Chem. Revs.* **44**, 135 (1949).
15. MALSCH, J., AND HARTLEY, G. S., *Z. physik. Chem.* **A170**, 321 (1934).
16. MCBAIN, J. W., *J. Am. Chem. Soc.* **50**, 1639 (1928).
17. MCBAIN, J. W., Advances in Colloid Science, Vol. I, p. 123. Interscience Publishers, New York, 1942.

18. McBain, J. W., and Betz, M. D., *J. Am. Chem. Soc.* **57**, 1905 (1935).
19. McBain, J. W., and Searles, J., *J. Phys. Chem.* **40**, 493 (1936).
20. Olson, A. R., and Simonson, T. R., *J. Chem. Phys.* **17**, 348 (1949).
21. Schmid, H. G., and Larsen, E. C., *Z. Elektrochem.* **44**, 651 (1938).
22. Senter, G., *J. Chem. Soc.* **107**, 1072 (1915).
23. Tartar, H. V., and Wright, K. A., *J. Am. Chem. Soc.* **61**, 539 (1939).
24. Wright, K. A., Abbott, A. D., Sivertz, V., and Tartar, H. V., *J. Am. Chem. Soc.* **61**, 549 (1939).
25. Zuffanti, S., *J. Am. Chem. Soc.* **62**, 1044 (1940).

A NOTE ON THE DIRECT DETERMINATION OF ADSORPTION FROM SOLUTION[1]

In recent years doubt has been cast on the validity of the Gibbs adsorption theory in the light of the so-called Type III surface tension-concentration curves, exhibiting minima which at first glance indicate that no material is adsorbed on the surface of aqueous solutions at the concentrations corresponding to the minima (1).

Investigations by Shedlovsky and coworkers (2), later confirmed by the author (3), have shown that, in certain "anomalous" cases, the minima are due to the presence of small traces of impurity in the surface-active compounds studied, and it appears probable that this explanation has general validity.

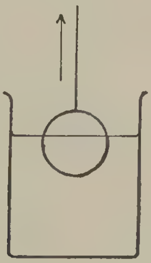

FIG. 1.

In the case of sodium dodecyl sulfate an experimental determination of the quantity of solute adsorbed on aqueous solutions has been made by use of a radioactive tracer technique which is thought to be of general interest and value. Radioactive sodium, Na^{22}, was exchanged with some of the normal sodium in a pure sample of the detergent from which the aqueous solutions were prepared. Platinum wire of about 0.5 mm. diameter was bent into the shape of a circle provided with a stirrup for convenience in handling. The ring was immersed, after gentle flaming, into a solution of the radioactive detergent, and then carefully raised through the surface as shown in Fig. 1, so that a film of the solution was formed on the ring. Once free of the surface of the solution the ring plus film was rapidly transferred to a weighing bottle and the weight of the solution in the film determined. This transfer must be carried out rapidly but carefully to avoid rupture of the film. The contents of the weighing bottle were rinsed out and the quantity of radiosodium in the rinsings determined by radioassay in the conventional way.

---

[1] Research done at the Brookhaven National Laboratory under the auspices of the Atomic Energy Commission.

By comparing the count of the film material with an equal weight of the solution *drawn from the interior of the bulk solution* the excess sodium present in the surface of the film was readily determined.

If it is assumed that the number of sodium ions adsorbed on the surface of the film is exactly the same as the number of dodecyl sulfate ions, as seems reasonable, the quantity of sodium dodecyl sulfate adsorbed per unit area may be calculated.

The observed values for the surface concentration of the detergent Γ_d are given in Table I together with corresponding values calculated from

TABLE I

Concentration of detergent moles/liter	Γ_d obsd. moles/cm.^{2} $\times 10^{-10}$	Γ_d calc. moles/cm.^{2} $\times 10^{-10}$
4.9×10^{-3}	9.5 ± 2	6.1
2.4×10^{-3}	5.7 ± 1.6	4.5
1.0×10^{-3}	1.1 ± 0.5	1.8

the following form of the Gibbs equation (4)

$$\Gamma_d = -\frac{N_d}{N_o}\frac{T_o^2}{L \cdot T} \cdot \frac{\partial \sigma}{\partial \theta}. \tag{1}$$

It will be seen that the agreement is reasonably good, but is much less than that attainable by the "microtome" method of McBain and Swain (5). Agreement between individual results at a given concentration was of the order ± 35%. Such agreement is much less than that obtainable in the radioactive assay, and it must be concluded that the variations arise from differences in the rate of withdrawal of the ring from the surface. Whether the rate of withdrawal affects the attainment of equilibrium or drainage of solution in the film cannot at present be determined, although on theoretical grounds failure to attain complete equilibrium would seem to be the more likely explanation.

Experiments were also carried out on a solution containing 7×10^{-3} moles per liter of sodium dodecyl sulfate contaminated with 0.1% dodecanol. This concentration was shown by Miles and Shedlovsky (2) to be near to the minimum of the surface tension curve for the contaminated material, and Γ_d should be zero at this concentration if the solution is treated as a 2-component system. The results varied among themselves by about 40% but gave a mean value of $0.83 \pm 0.30 \times 10^{-10}$ moles of sodium dodecyl sulfate/cm.^{2} There is no theoretical value with which this can be compared, since osmotic data for the solution containing both solutes are not obtainable, and to assume ideality in the solution is clearly inadmissible, since even the detergent alone at this concentration is far removed from ideality. Hence, although for this particular system no check between theory and observation is possible, the experiment demonstrates the fallacies in treating the system as a 2-component system.

Further experiments were carried out on solutions of lauryl pyridinium chloride in which some of the chloride ion was exchanged with radiobromine. Positive values of Γ_d were obtained, but without information on the equilibrium governing the exchange of the bromide and chloride ions the results are only semiquantitative, and are not quoted here. These experiments are part of an extensive investigation of the application of the Gibbs equation to complex systems.

The author has great pleasure in acknowledging his gratitude to the many colleagues at the Brookhaven National Laboratory whose cooperation facilitated these exploratory investigations.

REFERENCES

1. McBain, J. W., and Mills, G. T., *Repts. Progress in Phys.* **5**, 30 (1939).
2. Miles, G. D., and Shedlovsky, L., *J. Phys. Chem.* **48**, 57 (1944); Shedlovsky, L., and Ross, J., *J. Colloid Sci.* **4**, 25 (1949).
3. Hutchinson, E., *ibid.* **3**, 413 (1948).
4. Hutchinson, E., *ibid.* **3**, 219, 531 (1948).
5. McBain, J. W., and Swain, R. C., *Proc. Roy. Soc. London* **154A**, 608 (1936).

Eric Hutchinson

Brookhaven National Laboratory,
Associated Universities, Inc.,
Upton, Long Island.

Department of Chemistry,
Fordham University,
New York 58, N. Y.

Received June 10, 1949

BOOK REVIEWS

Elastomers and Plastomers, Their Chemistry, Physics and Technology. Volume III. Testing and Analysis; Tabulation of Properties. Edited by R. Houwink. Elsevier Publishing Co., Inc. New York and Amsterdam, 1948. 174 pp. Price $4.50.

This volume consists of the following five chapters: 1. Introduction, by R. Houwink. 2. Methods of Testing, by J. H. Teeple. 3. The Chemical Analysis of Polymers, by A. G. Epprecht. 4. Properties of Elastomers, by B. B. S. T. Boonstra. 5. Properties of Plastomers, by W. F. Van'T Wout and R. Houwink.

It is an extremely useful book which packs into approximately 170 pages the major part of all the available information on the chemical and physical properties of most polymeric materials.

In his *Introduction*, Dr. Houwink states the point of view from which the contents of the volume have been collected: the methods of testing. This explains the separate treatment of elastomers and plastomers. The theoretical analysis of properties is the subject matter of a different volume of the series. The use of units, the spread of values for a given property, and the method of rounding off numerical values to significant figures is mentioned. The approach is fully sound and it is refreshing to be promised data in truly usable form where formerly, in most cases, only an unsystematic mess was available. Let it be said in anticipation, that Dr. Houwink's promise is fulfilled.

Dr. Teeple's *Methods of Testing* is introduced by a sampling of the lack of standardization of testing methods. He then proceeds to discuss the conditions which affect test results; moisture, temperature, size and skin effect, speed of testing, and specimen preparation. A short paragraph on the very important question of the dependence on *Casting and Molding* properties of the measurement is followed by the paragraph on *Mechanical Properties*. In this, first, the measurement of tensile properties—tensile strength, modulus, creep, and hysteresis—is thoroughly treated. Methods of measuring and reporting compressive properties, flexural properties, impact strength, hardness, abrasion, and fatigue follow. Under the heading *Thermal Properties*, the determination of thermal expansion, softening temperature, and flammability, are discussed. The measurement of haze and birefringence comprise the paragraph on *Optical Properties*. Under *Chemical Properties*, the testing of resistance to chemical reagents in general is followed by the discussion of water absorption, moisture vapor permeability, and resistance to weathering and aging. Finally, dielectric strength, electrical resistance, dielectric constant, and power factor and arc resistance are treated under the heading *Electrical Tests*. All the above is successfully concentrated in approximately 55 pages.

Dr. Epprecht's *Chemical Analysis of Polymers* deserves equal praise. An introduction outlining the difficulties of the analysis of polymers is followed by a paragraph on preparation for analysis and one on preliminary examination. In this latter, the specific tests are described under a number of headings, whereas in the paragraph on systematic analysis 36 steps are listed, indicating from which step the one described follows, and also what the outcome of the test indicates as to the nature of the polymer. A typical example: "step 1—the plastic is soluble in cold water . . . ; step 2—the aqueous solution of the plastic coagulates to a gel on warming, *Methyl cellulose*. The aqueous solution does not coagulate, *Polyvinyl alcohol*." Under further specific tests the behavior of the plastic or resin in the Bunsen flame, fluorescence of polymer, *etc.*, are listed. A scheme for the qualitative analysis of the more common plastics, based on their solubilities in organic solvents, is given in the form of a table. Similarly collected in a table are the resistance to chemicals of polymers. A paragraph deals with an example of a qualitative analysis of a plastic, carrying it through all steps. The last paragraph of the chapter deals with the quantitative analysis of the most important polymers.

The last two chapters contain a tabulation of properties of elastomers collected by Dr. Boonstra, and properties of plastomers collected by Van'T Wout and Dr. Houwink, in addition to a short introduction on standardization. It is impossible to do justice to those tables otherwise than by reproducing their contents, which is manifestly impossible. Suffice it to state that they are as complete as can be expected by the severest critic.

In summarizing, be it said that Dr. Houwink and his collaborators deserve the gratitude of every person dealing with macromolecules, be it from the point of view of fundamental research at one extreme, to that of the businessman at the other extreme. Incidentally, the volume seems to t he reviewer as well suited for the classroom and school laboratory use (if appropriately supplemented by fundamental texts) as it is valuable for the research investigator.

George Goldfinger, Buffalo, New York

Neue Verfahren in der Technik der chemischen Veredlung der Textilfasern (Hilfsmittel in der Textilindustrie). Vol. I. By Louis Diserens. Published by Verlag Birkhäuser, Basle, Switzerland, 1948. Price 87.50 Swiss francs.

The work of Dr. Diserens was originally published in French between 1937 and 1940. The first German edition was published in 1941. The second German edition is entitled "Recent Developments and Processes in the Chemical Technology of Textiles." The first part of this is entitled "Recent Developments in the Application of Dyes," the second part "New Processes in the Technique of Textile Finishing." The book to be reviewed here is the first volume of this second part and consists of the following chapters: 1. Pretreatment of vegetable fibers. 2. Pretreatment of animal fibers. 3. Treatment of silk. 4. Bleaching of textile fibers. 5. The action of caustic on cellulose fibers. 6. The action of acids on vegetable fibers.

The book contains an unusually great deal of useful information. It is neither a textbook nor a comprehensive survey of present technique but rather a systematic compilation of patent literature. The text of nearly 700 pages makes reference to approximately 2000 patents, about one third of these being U. S. patents. This is by itself an enormous help to the research workers frequently trapped in the maze of patents in this field. The book would have gained in usefulness if the author would have exerted more effort to critically evaluate the relative merits of the patented processes. Of particular value are the numerous tables of textile finishing compounds, listing product, producer, chemical nature, properties, literature, and application. In this type of work minor errors are almost unavoidable, and while their number in the present work appears to be rather low, they warrant a certain caution in use of the tables. Since the text was written in 1944 and 1945, only limited use could have been made in the proofs of the reports on the German industry, published by the Allied military authorities, which contain much information unavailable before.

In spite of its shortcomings, the work of Dr. Diserens is a valuable addition to the literature of modern textile technology which will be highly welcomed by textile research men and textile technologists everywhere.

Emery I. Valko, Mountain Lakes, N. J.

Surface Chemistry. Papers presented for a Discussion at a joint meeting of the Société de Chimie Physique and the Faraday Society held at Bordeaux from 5 to 9 October 1947 in honour of Professor Henri Devaux, published as a Special Supplement to *Research*, A Journal of Science and its Applications. Published by Butterworths Scientific Publications, London, and Interscience Publishers, Inc., New York, 1949. 334 pp., $9\frac{3}{4} \times 7\frac{1}{4}$ in. Price $6.00.

This excellent collection of papers embodying recent investigations in the science of Interfaces is now available in book form, under the Editorship of the Faraday Society. It opens with the Presidential address by H. Devaux on the "Hygroscopicity of Monolayers." "Theoretical Aspects of Interfaces" are treated by E. A. Guggenheim, D. J. Crisp, M. Joly, and D. G. Dervichian, pp. 11–52; "Physical Chemistry" by A. F. H. Ward, D. J. Crisp, R. C. Palmer, J. F. Danielli, J. T. Davies, J. Guastalla, K. G. A. Pankhurst, J. Pouradier, A. Dubois, A. E. Alexander, J. Michel, M. Abribat, M. Joly, F. Lachampt, C. R. Clark, J. Degont, L. Denard, D. G. Dervichian, M. Raison, and R. Matalon, pp. 55–201; "Films on Solid Surfaces" by S. J. Gregg, D. Tabor, E. D. Tingle, M. A. Marcelin, and P. Cotton, pp. 205–238; "Biophysical Chemistry" by A. C. Frazer, A. Dognon, L. Gougerot, J. H. Schulman, W. M. Armstrong, J. Elkes, J. B. Finean, J. Remy, A. E. Alexander, A. I. McMullen, A. J. H. Tomlinson, F. Tayeau, and P. Blanquet, pp. 241–334.

This is an imposing list of experts of standing in this field. In several cases, the papers are in both French and English, and in all cases a summary in the other language is given.

The printing, format, paper, and reproduction of the figures and photographs are of a high quality. The physical appearance of the book is far above the average of those appearing at the present time.

The publishers are to be commended for making a book of this size available at what is today a modest price.

VICTOR K. LA MER, New York, N. Y.

AUTHOR INDEX

A

ALFREY, TURNER, JR., WIEDERHORN, NORMAN, STEIN, RICHARD, AND TOBOLSKY, ARTHUR. Some studies of plasticized polyvinyl chloride, 211
And RODEWALD, CHARLES W. An experimental study of thixotrophy in bentonite suspensions, 283

ARKIN, LORRAINE, AND SINGLETERRY, C. R. The effect of water on the size and shape of soap micelles in benzene solution, 537

B

BECHTEL, WELKER G., AND FISCHER, EARL K. The measurement of starch paste viscosity, 265

BRADY, A. P. Surface films of soluble detergents, 417

BRICE, B. A. See Halwer, 439

BUCHANAN, A. S., AND HEYMANN, E. The electrokinetic potential of sparingly soluble sulfates. I., 137
Electrokinetic potential and reversible electrode potential of sparingly soluble sulfates. II., 151
Determination of electrokinetic potentials in concentrated solutions by the streaming current method, 157

C

COLLINS, FRANK C., AND KIMBALL, GEORGE E. Diffusion-controlled reaction rates, 425

CORRIN, M. L., LIND, E. L., ROGINSKY, ADELLE, AND HARKINS, WILLIAM D. Adsorption of long-chain electrolytes from aqueous solution on graphite of known area and on polystyrene, 485

D

DAVIS, W. E., AND ELLIOTT, J. H. Present status of the intrinsic viscosity determination, 313

DIENES, G. J. Flow properties of phenolic resins, 257

DILLON, J. H. Introduction of Melvin Mooney as E. C. Bingham Medalist, 187

DILLON, R. E. See Spencer, 241

DOSS, K. D. VENKATESHA. See Prasad, 349

DRUCKER, D. C. The significance of the criterion for additional plastic deformation of metals, 299

E

EIRICH, F. R. Impressions from the International Rheological Congress, Scheveningen. 1948, 189

ELLIOTT, J. H. See Davis, 313
See Stow, 321

ERIKSON, J. A., AND LINGAFELTER, E. C. Ionic effects in a paraffin-chain salt solution as measured by the primary salt effect, 591

F

FISCHER, EARL K. See Bechtel, 265

FRIEND, J. A. See Schulman, 497

G

GOETTE, ERNST K. Theoretical considerations of detergency, 459

GUCKER, FRANK T., JR., AND O'KONSKI, CHESTER T. An improved photoelectric counter for colloidal particles suitable for size-distribution studies, 541

H

HALWER, M., AND BRICE, B. A. Molecular weight of β-lactoglobulin as determined by light-scattering measurements, 439

HARKINS, WILLIAM D, AND MITTELMANN, ROSE. X-ray investigations of the structure of colloidal electrolytes. IV. A new type of micelle formed by film penetration, 367
See Corrin, 485

HATTIANGDI, GOPAL S. See Vold, 93

HAVENS, C. B. Plasticizing linear polymers, 347

HERRMANN, R. G. See Landahl, 103

HEYMANN, E. See Buchanan, 137, 151, 157
And O'DONNELL, I. J. Physicochemical investigation of a cation exchange resin (Amberlite IR100). I. Resin equilibria, 395
II. Resin conductance, 405
HOROWITZ, K. H. See Stow, 321
HUFF, HARRIETTE M. See McBain, 383
HUTCHINSON, ERIC. A note on the direct determination of adsorption from solution, 599

I

ISIHARA, AKIRA. See Sokai, 71

J

JAKOB, CONRAD W. See Shedlovsky, 25
JAMES, T. H. Loss of developability of photographic emulsions caused by washing in weak silver halide solvents: A new reversal effect, 561

K

KENYON, ALLEN S., AND LA MER, VICTOR K. Light scattering properties of monodispersed sulfur sols. I. Monochromatic ultraviolet angular scattering. II. Effect of the complex index of refraction upon transmittance, 163
KIMBALL, GEORGE E. See Collins, 425
KING, G., AND MEDLEY, J. A. D. C. conduction in swollen polar polymers. I. Electrolysis of the keratin-water system, 1
II. The influence of temperature and adsorbed salts on the D. C. conductivity of polar polymer absorbate systems, 9
KINOSITA, KOREO. Sedimentation in tilted vessels. I., 525
KRATKY, O., AND POROD, G. Diffuse small-angle scattering of X-rays in colloid systems, 35

L

LA MER, VICTOR K. See Kenyon, 163
LANDAHL, H. D., AND HERRMANN, R. G. Sampling of liquid aerosols by wires, cylinders, and slides, and the efficiency of impaction of the droplets, 103
LEADERMAN, HERBERT. Proposed nomenclature for elastic and inelastic behavior of high polymers, 193
LIND, E. L. See Corrin, 485
LINGAFELTER, E. C. See Erikson, 591
LIVINGSTONE, H. K. The cross-sectional areas of molecules adsorbed on solid surfaces, 447

M

MATALON, R., AND SCHULMAN, J. H. A new method of studying mechanical properties of penetrated monolayers, 89
McBAIN, J. W., AND HUFF, HARRIETTE M. Changes in solubilizing power with concentration for various detergents, 383
MITTELMANN, ROSE. See Harkins, 367
MOONEY, M. Speech of acceptance, 188
MACK, CHARLES. A theory of anomalous viscosity and elasticity, 343
MARKWOOD, W. H. JR. The Bingham Medal- Society of Rheology, 1948, 185
MEDLEY, J. A. See King, 1,9

O

O'DONNELL, I. J. See Heymann, 395, 405
O'KONSKI, CHESTER T. See Gucker, 541
OLDROYD, J. G. The interpretation of observed pressure gradients in laminar flow of non-Newtonian liquids through tubes, 333

P

PALIT, SANTI R. A note on mixed solvent effect in solubilization, 523
POLLACK, HANS L. See Seifriz, 19
POROD, G. See Kratky, 35
PRASAD, MATA, AND DOSS, K. D. VENKATESHA. Scattering of light during the process of gel formation, 349

R

RODEWALD, CHARLES, W. See Alfrey, 283
ROGINSKY, ADELLE. See Corrin, 485
ROSS, JOHN. See Shedlovsky, 25

S

SAKAI, TAKUZO, AND ISIHARA, AKIRA. On the statistical theory of rubber-like elasticity, 71

SCHULMAN, J. H. See Matalon, 89
And FRIEND, J. A. Light scattering investigations of the structure of transparent oil-water disperse systems. II., 497
SHEDLOVSKY, LEO, ROSS, JOHN, AND KAKOB, CONRAD W. The effect of certain impurities on the surface and interfacial tension of aqueous solutions of sodium dodecyl sulfonate, 25
SEIFRIZ, WILLIAM AND POLLACK, HANS L. A colloidal interpretation of biological stimulation and depression, 19
SHAFRIN, ELAINE G., AND ZISMAN, W. A. Hydrophobic monolayers adsorbed from aqueous solutions, 571
SINGLETERRY, C. R. See Arkin, 537
SPENCER, R. S. Volume-temperature-time relationships for polystyrene, 229
And DILLON, R. E. The viscous flow of molten polystyrene. II., 241
STEIN, RICHARD. See Alfrey, 211
STOW, F. S., JR., HOROWITZ, K. H., AND ELLIOTT, J. H. Application of the rising-column capillary viscometer to the high-viscosity range, 321

T

TOBOLSKY, ARTHUR. See Alfrey, 211
TOMS, B. A. Detection of a wall effect in laminar flow of solutions of a linear polymer, 511

V

VAN DE HULST, H. C. Scattering of light by colloidal solutions. Interpolation of the oscillatory functions, 79
VOLD, MARJORIE J., HATTIANGDI, GOPAL S., AND VOLD, ROBERT D. Crystal forms of anhydrous calcium stearate derivable from calcium stearate monohydrate, 93
VOLD, ROBERT D. See Vold, 93

W

WIEDERHORN, NORMAN. See Alfrey, 211

Z

ZISMAN, W. A. See Shafrin, 571

SUBJECT INDEX

A

Adsorption, polar polymer adsorbate systems and adsorbed salts, King and Medley, 9; cross-sectional areas of molecules adsorbed on solid surfaces, Livingston, 447; — of long-chain electrolytes from aqueous solution on graphite of known area and on polystyrene, Corrin, Lind, Roginsky and Harkins, 485; hydrophobic monolayers adsorbed from aqueous solutions, Shafrin and Zisman, 571; direct determination of — from solution, Hutchinson, 599

Aerosols, sampling of liquid — by wires, cylinders, and slides, and the efficiency of impaction of the droplets, Landahl and Herrmann, 103

Amberlite, cation exchange resin (I), —, Heymann and O'Donnell, 395; (II) resin conductance, Heymann and O'Donnell, 405

B

Bentonite, thixotropy in — suspensions, Alfrey and Rodewald, 283

Benzene, effect of water on soap micelles in — solution, Arkin and Singleterry, 537

Bingham Medal-Society of Rheology, Markwood, 185

C

Cation, — exchange resin (I), Heymann and O'Donnell, 395; (II), Heymann and O'Donnell, 405

Colloidal particles, photoelectronic counter for — —, Gucker and O'Konski, 541

Colloids, colloidal interpretation of biological stimulation and depression, Seifriz and Pollack, 19; diffuse small-angle scattering of X-rays in colloid systems, Kratky and Porod, 35; scattering of light by colloidal solutions, oscillatory functions, van de Hulst, 79; light scattering properties of monodispersed sulfur sols: (I), monochromatic ultraviolet angular scattering; (II), effect of the complex index of refraction upon transmittance, Kenyon and La Mer, 163; X-rays on colloidal electrolytes (IV), new micelle by film penetration, Harkins and Mittelmann, 367

Conductance, resin —, Heymann and O'Donnell, 405

Conductivity, of polar polymers, King and Medley, (I), 1, (II), 9

Counter, photoelectronic — for colloidal particles for size-distribution studies, Gucker and O'Konski, 541

Crystals, anhydrous calcium stearate —, Vold, Hattiangdi and Vold, 93

Cylinders, sampling of liquid aerosols by —, Landahl and Herrmann, 103

D

D. C. conductivity, — of polar polymers, King and Medley, (I) 1, (II), 9

Deformation, plastic — of metals, Drucker, 299

Depression, colloid interpretation of biological —, Seifriz and Pollack, 19

Detergents (see also *Soap*), changes in solubilizing power with concentration for various —, McBain and Huff, 383; surface films of soluble —, Brady, 417; theoretical considerations of detergency, Goette, 459

Developability, loss of — of photographic emulsions, James, 561

Diffusion, — controlled reaction rates, Collins and Kimball, 425

Disperse systems, light scattering investigation of oil-water — — (II), Schulman and Friend, 497

Distribution, photoelectronic counter for colloidal particles for size — studies, Gucker and O'Konski, 541

Dodecyl sulfonate, surface tension of

aqueous solutions of sodium — —, Shedlovsky, Ross and Jakob, 25

E

Elasticity, statistical theory of rubber-like —, Sakai and Isihara, 71; theory of anomalous viscosity and —, Mack, 343

Electrokinetic potential(s), — — of sparingly soluble sulfates (I), Buchanan and Heymann, 137; — — and reversible electrode potential of sparingly soluble sulfates (II), Buchanan and Heymann, 151; determination of — — in concentrated solutions by the streaming current method, Buchanan and Heymann, 157

Electrolysis, — of the keratin-water system, King and Medley, 1

Electrolytes, X-rays on colloidal — (IV), new micelle by film penetration, Harkins and Mittelmann, 367; adsorption of long-chain — from aqueous solution on graphite and on polystyrene, Corrin, Lind, Roginsky and Harkins, 485

Emulsions, loss of developability of photographic —, James, 561

Exchange, cation — resin (I), Heymann and O'Donnell, 395; (II), Heymann and O'Donnell, 405

F

Films, surface — of soluble detergents, Brady, 417

Flow, viscous — of molten polystyrene (II), Spencer and Dillon, 241; — properties of phenolic resins, Dienes, 257; wall effect in laminar — of solutions of a linear polymer, Toms, 511

G

Gel, scattering of light during — formation, Prasad and Doss, 349

Graphite, adsorption of electrolytes on —, Corrin, Lind, Roginsky and Harkins, 485

H

Hydrophobic, — monolayers adsorbed from aqueous solutions, Shafrin and Zisman, 571

I

Impaction, sampling of aerosols and — of the droplets, Landahl and Herrmann, 103

International rheological congress, Eirich, 189

Ions, ionic effects in a paraffin-chain salt solution as measured by the primary salt effect, Erikson and Lingafelter, 591

K

Keratin, D. C. conduction in swollen polar polymers (I), electrolysis of the — water system, King and Medley, 1

L

Lactoglobulin, molecular weight of β- — determined by light-scattering measurements, Halwer and Brice, 439

Light see also *X-rays*

Light scattering, — by colloidal solutions, oscillatory functions, van de Hulst, 79; — properties of monodispersed sulfur sols: (I), monochromatic ultraviolet angular scattering; (II), effect of the complex index of refraction upon transmittance, Kenyon and LaMer, 163; — during the process of gel formation, Prasad and Doss, 349; — investigation of the structure of transparent oil-water disperse systems (II), Schulman and Friend, 497

Liquids, pressure gradients in laminar flow of non-Newtonian — through tubes, Oldroyd, 333

M

Metals, plastic deformation, Drucker, 299

Micelle, colloidal electrolytes (IV), new — by film penetration, Harkins and Mittelmann, 367

Monolayers, mechanical properties of penetrated —, Matalon and Schulman, 89; hydrophobic — adsorbed from aqueous solutions, Shafrin and Zisman, 571

Mooney, M., as Bingham Medalist, Dillon, 187

N

Nomenclature, — for elastic and inelastic behavior of high polymers, LEADERMAN, 193

O

Oil, light scattering investigation of — -water disperse systems, SCHULMAN AND FRIEND, 497

P

Paraffin, ionic effects in a — -chain salt solution, ERIKSON AND LINGAFELTER, 591

Particles, photoelectronic counter for colloidal — for size-distribution studies, GUCKER AND O'KONSKI, 541

Penetration, properties of penetrated monolayers, MATALON AND SCHULMAN, 89; colloidal electrolytes (IV), new micelle by film —, HARKINS AND MITTELMANN, 367

Phenolic resins, flow properties of — —, DIENES, 257

Photoelectronic counter, improved — — for colloidal particles for size-distribution studies, GUCKER AND O'KONSKI, 541

Photographic emulsions, loss of developability, JAMES, 561

Plasticizers (see also *Polyvinyl chloride*); plasticizing linear polymers, HAVENS, 347

Plasticity, plastic deformation of metals, DRUCKER, 299

Plastic systems, theory of anomalous viscosity and elasticity, MACK, 343

Polymer(s), D. C. conduction in — KING AND MEDLEY, (I) 1, (II) 9; nomenclature for elastic and inelastic behavior of high —, LEADERMAN, 193; plasticizing linear —, HAVENS, 347; wall effect in laminar flow of solutions of a linear —, TOMS, 511

Polystyrene, volume-temperature-time relationships for —, SPENCER, 229; viscous flow of molten — (II), SPENCER AND DILLON, 241; adsorption of electrolytes on —, CORRIN, LIND, ROGINSKY AND HARKINS, 485

Polyvinyl chloride, plasticized — —, ALFREY, WIEDERHORN, STEIN AND TOBOLSKY, 211

Potential(s), electrokinetic — of sparingly soluble sulfates (I), BUCHANAN AND HEYMANN, 137; electrokinetic — and reversible electrode — of sparingly soluble sulfates (II), BUCHANAN AND HEYMANN, 151; determination of electro-kinetic — in concentrated solutions by the streaming current method, BUCHANAN AND HEYMANN, 157

Pressure, interpretation of observed — gradients in laminar flow of non-Newtonian liquids through tubes, OLDROYD, 333

R

Reaction, diffusion-controlled — rates, COLLINS AND KIMBALL, 425

Resin(s), flow properties of phenolic —, DIENES, 257; cation exchange — (I), — equilibria, HEYMANN AND O'DONNELL, 395; (II), — conductance, HEYMANN AND O'DONNELL, 405

Reversal, loss of developability of photographic emulsions, a new — effect, JAMES, 561

Rheology, — 185–347; the Bingham Medal-Society of —, MARKWOOD, 185; international rheological congress, Scheveningen, EIRICH, 189

Rising-column capillary viscosimeter, STOW, HOROWITZ AND ELLIOTT, 321

Rubber, statistical theory of — -like elasticity, SAKAI AND ISIHARA, 71

S

Salt, ionic effects in a paraffin-chain — solution as measured by the primary — effect, ERIKSON AND LINGAFELTER, 591

Sedimentation, — in tilted vessels, KINOSITA, 525

Silver halide, loss of developability of photographic emulsions caused by washing in weak — — solvents, JAMES, 561

Size, photoelectronic counter for colloidal particles for — -distribution studies, GUCKER AND O'KONSKI, 541

Soap (see also *Detergent*), detergent action, GOETTE, 459; effect of water on — micelles in benzene solution, ARKIN AND SINGLETERRY, 537

Solubilization, solubilizing power, changes with concentration for various deter-

gents, McBAIN AND HUFF, 383; mixed solvent effect in —, PALIT, 523
Starch, paste viscosity, BECHTEL AND FISCHER, 265
Statistics, — and elasticity, SAKAI AND ISIHARA, 71
Stearate, crystal forms of anhydrous calcium — derivable from calcium — monohydrate, VOLD, HATTIANGDI AND VOLD, 93
Stimulation, colloidal interpretation of biological — and depression, SEIFRIZ AND POLLACK, 19
Streaming current, determination of electrokinetic potentials by the — — method, BUCHANAN AND HEYMANN, 157
Sulfates, electrokinetic potential of sparingly soluble — (I), BUCHANAN AND HEYMANN, 137; electrokinetic potential and reversible electrode potential of sparingly soluble — (II), BUCHANAN AND HEYMANN, 151
Sulfur, light scattering properties of monodispersed — sols, KENYON AND LAMER, 163
Surface(s), — tension of aqueous solutions of sodium dodecyl sulfonate, SHEDLOVSKY, ROSS AND JAKOB, 25; — films of soluble detergents, BRADY, 417; cross-sectional areas of molecules adsorbed on solid —, LIVINGSTON, 447

T

Thixotropy, — in bentonite suspensions, ALFREY AND RODEWALD, 283
Tilted vessels, sedimentation in —, KINOSITA, 525
Tubes, pressure gradients in laminar flow of non-Newtonian liquids through —, OLDROYD, 333

V

Viscosity, starch paste —, BECHTEL AND FISCHER, 265; intrinsic determination, DAVIS AND ELLIOTT, 313; application of the rising-column capillary viscosimeter to the high- — range, STOW, HOROWITZ AND ELLIOTT, 321; theory of anomalous — and elasticity, MACK, 343

W

Wall effect, — — in laminar flow of solutions of a linear polymer, TOMS, 511
Water, electrolysis of the keratin- — system, KING AND MEDLEY, 1; light scattering investigation of oil- — disperse systems, SCHULMAN AND FRIEND, 497; effect on soap micelles in benzene solution, ARKIN AND SINGLETERRY, 537; hydrophobic monolayers adsorbed from aqueous solutions, SHAFRIN AND ZISMAN, 571
Wires, sampling of liquid aerosols by —, cylinders, and slides, LANDAHL AND HERRMANN, 103

X

X-rays (see also *Light*), diffuse small-angle scattering of — in colloids, KRATKY AND POROD, 35; — investigations of the structure of colloidal electrolyte (IV), new type of micelle formed by film penetration, HARKINS AND MITTELMANN, 367

INDEX OF BOOK REVIEWS

DISERENS, L., Neue Verfahren in der Technik der chemischen Veredlung der Textilfasern (Hilfsmittel in der Textilindustrie). Vol. I (*Valko, E. I.*), 604
FARADAY SOCIETY (ed.), Surface Chemistry (*LaMer, V. K.*), 605
FREY-WYSSLING, A., Submicroscopic Morphology of Protoplasm and Its Derivatives (trans. by HERMANS, J. J., AND HOLLANDER, M.) (*Seifriz, W.*), 441
GABOR, D., The Electron Microscope, Its Development, Present Performance, and Future Possibilities (*LaMer, V. K.*), 91
HOUWINK, R. (ed.), Elastomers and Plastomers, Their Chemistry, Physics and Technology. Vol. III. Testing and Analysis; Tabulation of Properties (*Goldfinger, G.*), 603
NIJBOER, L. W., Plasticity as a Factor in the Design of Dense Bituminous Road Carpets (*Traxler, R. N.*), 444
SCHMIDT, A. X., AND MARLIES, C. A., Principles of High-Polymer Theory and Practice (*Baker, W. O.*), 540